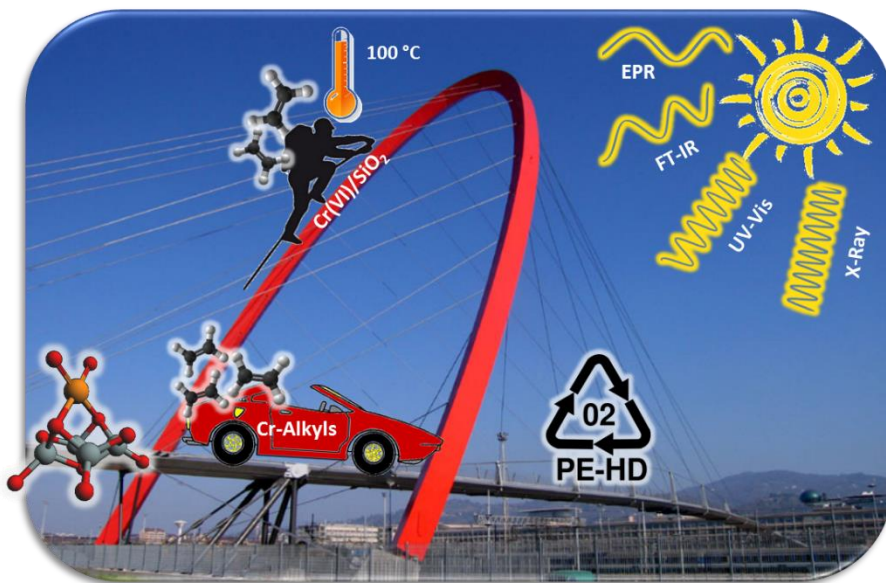**Università degli Studi di Torino**

Doctoral School of Sciences and Innovative Technologies

PhD Programme in Chemical and Materials Sciences XXXI Cycle

Cr-Alkyl sites in ethylene polymerization

Giorgia Antonina Martino

Supervisor:
Prof. Elena Groppo

Università degli Studi di Torino

Doctoral School of Sciences and Innovative Technologies

PhD Programme in Chemical and Materials Sciences XXXI cycle

Cr-Alkyl sites in ethylene polymerization

Candidate: **Giorgia Antonina Martino**

Supervisor: Prof. **Elena Groppo**

Jury Members: Prof. **Angelika Brückner**
                Universität Rostock
                Leibniz-Institut für Katalyse (LIKAT)

                Prof. **Timothy McKenna**
                École supérieure chimie physique électronique de Lyon
                C2P2

                Prof. **Mario Chiesa**
                Università di Torino
                Dipartimento di Chimica

Head of the Doctoral School: Prof. Massimo Maffei
PhD Programme Coordinator: Prof. Mario Chiesa

Torino, 2018

A Nonna Carmela che ha sempre pregato per me e

a Nonno Nicolò che mi chiamava la "scienziata"…

Index

Chapter 2

Experimental methods 25

Chapter 3

The unmodified Phillips catalyst 35

Chapter 4

Modification of Cr(II)/SiO$_2$ with Al-alkyls　　　57

Chapter 5

Modification of Cr(VI)/SiO$_2$ with Al-alkyls.   83

Chapter 6

SiO$_2$-supported Cr[CH(SiMe$_3$)$_2$]$_3$ catalysts   107

Chapter 1

The Phillips catalyst and its modifications.

"I wanna say just one word to you, just one word […] PLASTICS. […] There's a great future in plastics…think about it", this particular advice disoriented a young graduated Dustin Hoffman in the movie "The Graduate" (1967). I decided to report this sentence to testify the impact that these materials had on common life since their discovery, just sixty years ago. Actually, our century can be considered as the Century of plastics; their discovery, made only after the Second World War, started from polystyrene, passed through polyvinylchloride and arrived finally to the polyethylene and polypropylene [1, 2]. Among all, polyolefins are the most worthwhile and produced polymers and their demand is in continue growth as clearly shown in Figure 1. 1 [2-4], that reports the incessant increase of the production of polyolefins (and in particular of polyethylene) with respect to other polymers year after year.
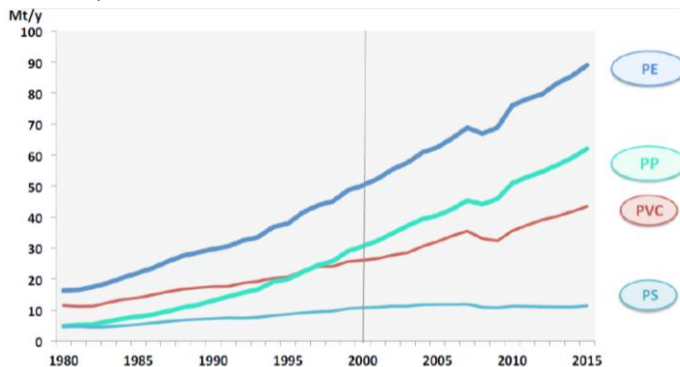
Figure 1. 1 Trend of the production of the most diffuse polymers in the last decades [4].

1.1 Introduction

1.1.1 Properties of polyethylene

The reason of the success of polyethylene (PE) lies in the peculiar properties of this polymer. *"The principal value of polyethylene lies in its desirable balance of physical properties in the solid state and its chemical inertness"* [1]. The wide use of polyethylene is related to economic and environmental reasons (low cost, broad availability of the monomers, non-toxicity, easy to recycle), as well as to its excellent physical and chemical properties, i.e. the resistance to chemical agents, (as water, acids and bases, alcohols and saline solutions - it is only corroded by oxidizing acids, such as nitric or sulfuric), the abrasion resistance, the high impact strength, and the wide temperature range of use from -40 to +80 °C [1, 5].

Although it is the polymer with the simplest composition $(-CH_2-)_n$, hundreds of specialized PE exist, differing to each other's for the amount and the length of branching, for the density, and for the molecular weight (MW) distribution. Commonly PEs are divided in three categories, as illustrated in Figure 1. 2:

1) HDPE (high-density polyethylene), characterized by long chains with a very small amount of short ramifications. This feature gives higher density, higher crystallization grade and higher melting point compared to the other types of polyethylene.

2) LLDPE (linear low-density polyethylene), characterized by chains with a huge amount of short branches, hence the density of this polymer is lower than HDPE.

3) LDPE (low-density polyethylene), characterized by short and long chains connected to each others, forming a branched structure; this polymer has the lowest density and melting point.

Figure 1. 2 The three types of commercial polyethylenes.

These three categories of PE are also produced in different ways: LDPE is obtained through radical processes at high temperature (above 300 °C) and at high pressure (in the 500-3000 atm range), while HDPE and LLDPE are obtained using heterogeneous or homogeneous catalysts at low temperature (below 150 °C) and pressure (below 50 atm) [5].

1.2 A brief historical excursus of the polymerization catalysts

The polyethylene industry has undergone a rapid development, starting to produce tons of materials, since the discovery of the proper catalysts in the 1950s. Such heterogeneous catalysts were discovered almost simultaneously in two different locations, and, as it often happens, their discovery was accidental. Chronologically:

1) Paul Hogan and Robert Banks discovered the first catalytic system in 1951. Since they were working in the Phillips research laboratories in Oklahoma, that catalyst went down in the history with the name of Phillips catalyst. It is composed by grafted chromium centers on an amorphous support, commonly silica [6-8].

2) A few years later, in 1953 in Germany Karl Ziegler accidentally discovered a new catalyst for olefin polymerization, consisted of titanium chloride activated by aluminum alkyls; the same catalyst was used the following year by Giulio Natta in Italy to produce the different stereoisomers of polypropylene. Therefore, that catalyst is commonly known as Ziegler-Natta catalyst, although technically the latter name is used only for the polymerization of the propylene, while for the production of the polyethylene it should be named just Ziegler catalyst.

3) Afterwards, the story of olefin polymerization catalysts has to wait up 1977 for the discovery of a homogeneous catalyst able to polymerize ethylene. In that year, Walter Kaminsky discovered the single-site metallocene catalysts, activated by methylaluminoxane (MAO) [1, 5].
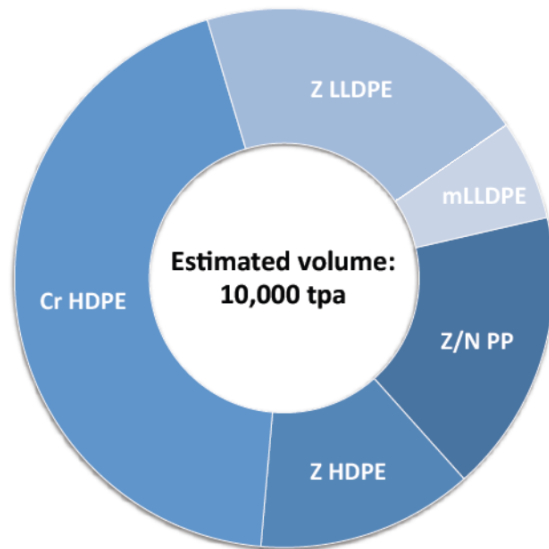
Figure 1. 3 Global market of polyolefins in 2015 as a function of the adopted catalysts. Cr stands for the Phillips catalyst, Z and Z/N for the Ziegler-Natta catalysts applied respectively to ethylene and propylene polymerization, m for the homogeneous molecular catalysts [2].

Figure 1. 3 displays the volume of the polyolefins produced in the World by each class of catalysts. On one side, the predominance of the heterogeneous catalysts is due to their cheapness and easy handling, together with the capability to control the shape of the particles of the produced polymer as a replication of the catalyst particles [5]. On the other side, the homogeneous catalysis finds application especially for the production of particularly tailored polymers, thanks to the incredibly high levels reached in the design of the catalysts, which competes even with some natural enzymes [9]. Interestingly, in order to promote their industrial use, they have been gradually undergoing a heterogenization process, allowing the exploitation of the widespread industrial technology for supported catalysts [10-13]. The three classes of catalysts satisfy different needs of the market, and hence they should be considered complementary, rather than competitors.

1.3 A short description of the Phillips catalyst

The Phillips catalyst is a heterogeneous catalyst consisting of a porous support, traditionally amorphous silica, on which chromium ions are grafted. Despite being industrially employed and studied from a scientific point of view since its discovery, it is yet a controversial system. Nowadays, there are still some open questions about the structure of the active site and the exact

4

initiation/polymerization mechanism. Unlike Ziegler-Natta catalysts, on the Phillips catalyst the polymerization proceeds without any activators. The precursor of the active site contains neither an alkyl ligand nor a hydride ligand in its coordination sphere: ethylene itself is able to create an alkyl-type active species [14].

One of the main problems in the characterization of the actives sites is the high dilution of the catalytic centres on the support. In this respect, McDaniel said: ***"One of the historical difficulties of investigating it has been the large number of available chromium valence states, and the low number of active sites, which are only a small minority of the total chromium population in these catalysts. These limitations have sometimes rendered spectroscopic techniques, however sophisticated, inadequate, and some spectra were even misleading"*** [5].

The Phillips catalyst is traditionally prepared by impregnation of the silica support with a chromium compound. Chromic anhydride (CrO_3) is often used for its solubility in water, leading to the formation of the chromic acid H_2CrO_4 [5, 14]. The anchoring process occurs through the surface OH groups, weakly acidic, which react with chromic acid to form grafted chromates (monochromates, dichromates or polychromates). In this esterification reaction, OH groups are consumed and new bonds are formed between the chromium species and the support through oxygen linkages [14-17].
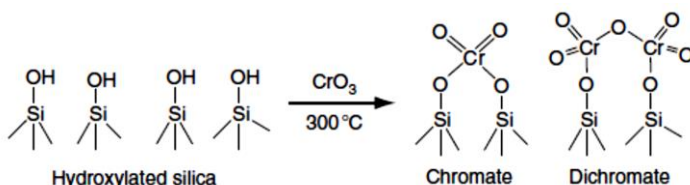
Figure 1. 4 Anchoring reaction of chromates on hydroxylated silica to form monochromate and dichromate species [5].

The molecular structure of the anchored Cr(VI) was object of discussion in the past, and several molecular structures (mono-, di- or polychromates) were proposed. The presence of these different species can be controlled through the hydroxyl concentration on silica surface during the anchoring process; as a matter of fact, monochromates react with two vicinal hydroxyls per chromium, while dichromate involve more distant hydroxyls (displacing only one per chromium), as illustrated in Figure 1. 4. After the impregnation, a calcination process fixes the chromium species on silica.
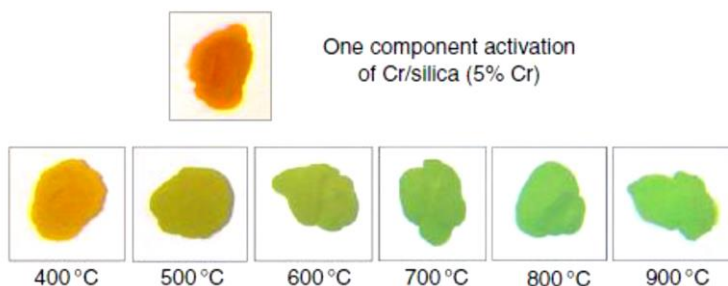
Figure 1. 5 The progression from orange to green indicates the saturation of the support by Cr(VI) and the subsequent decomposition to Cr(III). The amount of Cr(III) increases with increasing activation temperature: when the temperature reaches 900 °C, almost 80% of the chromium is trivalent [5].

At low chromium loading the majority of the Cr(VI) sites are monochromates with a dioxochromate structure, although the relative importance of dichromates and polychromates increases at high chromium loadings and activation temperature [14, 16, 18, 19]. The thermal stability of the grafted hexavalent chromium is also influenced by the presence of gas stream of oxygen and of water, which can hydrolyse the Si-O-Cr bonds. Indeed, there is a dynamic equilibrium during calcination in which the chromium shuttles from attached Cr(VI) to unattached Cr(III) and O_2. The segregation of trivalent α-chromia increases with increasing the chromium loading. Actually, at the lowest chromium loading, all the chromium remains hexavalent, even at a temperature as high as 900 °C [20-23]. Upon increasing the chromium loading, the silica surface is gradually saturated, with the concurrent formation of trivalent α-chromia. This phenomenon is easily recognizable by looking to the colour of the catalyst: the catalyst is orange when chromium is stabilized as Cr(VI), while it turns to green when segregation of Cr(III) occurs (Figure 1. 5).

Cr(VI) is not the active site, as the early workers quickly recognized. Ethylene itself reduces the Cr(VI) sites to a lower valence oxidation state during the induction time. In this step, the coordination sphere of the chromium sites expands, because most of the lower-valent chromium sites can accept or even prefer octahedral coordination. As a result, in the absence of basic ligands, vacancies are created and those are the sites on which polymerization can occur. The identity of this unknown lower-valent chromium species has been a matter of controversy in the literature for more than 50 years [5, 24-27]. All the possible chromium valent states have been proposed as the active ones, either alone or in combination. Oscillation between two valence states, such as Cr(II) and Cr(IV), has

6

been proposed [5], and it is also conceivable that more than one oxidation state might simultaneously be active. Adding a certain degree of confusion, **the term "active valence'' has been used by some authors to refer to the site during polymerization, whereas others have applied the same term to the precursor state that immediately precedes the beginning of ethylene polymerization.**

1.4 Modification of the Phillips catalyst

More so than other catalysts, the Phillips catalyst is extremely sensitive to minor changes, not only in the silica preparation or in the calcination treatment, but also to the introduction of external agents used for changing the productivity of this system. The active sites no doubt respond to the local electronic environment and spatial surroundings. Thus, **small changes in the Cr environment can have major consequences for the polymerization activity and the properties of the resultant polymer**. It is not a surprise, then, that the catalyst is highly sensitive to changes in the composition. Therefore, replacing the air-activated Cr/silica with another support or with other activation procedures can have profound consequences for the polymer. Many catalyst modifications have been developed to produce different polymer grades for the dozens of various commercial applications [28].

1.4.1 Modifications on the support

The most used support material is silica, which can show up in several structures (with different mechanical and morphological properties), depending on the assembly of the rigid tetrahedron SiO_4 building blocks, thanks to the mobility of the Si-O-Si angle. However, also other oxides have been used to specifically modify the properties of the Phillips catalyst. Depending on the choice of support, chromium catalysts can produce a huge variety of compounds, from liquid oligomers and low-MW waxes to the bullet-stopping ultrahigh-MW grades (UHMW PE).

1.4.1.1 The Cr/silica-titania case.

After silica, the most commonly used commercial support is silica–titania. Although titania alone is poorly effective as a support for the Phillips catalysts, when a few percent of titania is added to Cr/silica it serves as a strong promoter for the supported chromium, increasing its activity and lowering the polymer MW (which is usually considered as a desirable outcome) [24, 29-37]. It is known that the addition of titania to silica enhances the Brønsted acidity of the surface [5], making the Cr species bound to these acidic sites more electron deficient and

hence more reactive with olefins [36, 37]. Curiously, Cr/titania produces extremely high MW polymer, whereas when incorporated into Cr/silica catalysts, titania contributes to the lower fraction of the MW distribution. This may indicate that the Si−Ti combination is the key of such activity. That is, the capability of titania to influence polymerization may derive from an ability of Ti(IV) to assume a tetrahedral coordination and fit in with the silica lattice, increasing the acidity of Brønsted sites where Cr(VI) is grafted [38].

The presence of titania in small amounts on Cr/silica catalysts has a strong promotional effect on chromium, for both the activity and the termination rate [39-45]. Many experiments suggest that this promotional effect is due to the formation of Cr sites closely associated with Ti, perhaps through Ti−O−Cr linkages, depending on subtle variations in the catalyst preparation. At present, titania seems to be fairly unique. Indeed, even if many other oxide additives are also known to enhance the acidity (zirconia, for example), they do not produce the same dramatic result on Phillips catalysis [46-48]. This is probably because the Cr(VI) is not as thermally stable when attached to these supports and it migrates back to the silica as the activation temperature is raised.

1.4.1.2 The Cr/Al$_2$O$_3$ case.

In principle, many metal oxides can be used as carriers for Cr species through the reaction with the surface hydroxyl groups, but, unlike silica, most of these materials do not provide adequate porosity for polymerization. An exception is alumina. The surface properties of all kinds of alumina are mostly influenced by the Lewis acid character of the exposed Al(III) sites, which depends on many factors (bulk structure, sample morphology, cations and cation vacancies distribution). This very high Lewis acidity of Al(III) cations is the fundamental reason for high hydroxylation of the surface with desorption of water only at high temperature. The presence of a larger amount of OH groups at the surface of alumina allows more possibilities for reaction with CrO$_3$, with respect to what observed for silica.

Concerning the properties of the grafted oxidized chromium sites, several studies explained that Cr(VI) on alumina exists primarily (or even exclusively) as monochromate species, with a few (or none) dichromate species detected [5, 15-17, 19, 49]. In fact, Cr/aluminas appear yellow after activation, even at high temperature, whereas Cr/silica usually exhibits a dark orange color, especially upon increasing the activation temperatures.

Interestingly, **Cr/alumina exhibits a "fast" kinetics profile, quite different from that of Cr/silica** [5]. The polymerization rate rises quickly when ethylene is added, but later it tends to decay quite soon. The rapid initial rise indicates that reduction of Cr(VI) and/or its alkylation may be more simple on alumina than on silica. The reasons for this "fast" kinetics profile was recently attributed to both the higher ionicity of the Cr-O-Al bond with respect to the Cr-O-Si one and the presence of different ligands around the Cr sites (i.e., beside the strained Al-O-Al bridges, carbonates are found in the CO-reduced Cr/Al_2O_3) [50].

An interesting aspect of this catalyst is that **the polymer produced by Cr/alumina**, at 90-100 °C in the absence of H_2**, has an extremely high molecular weight, reaching the ultra-high molecular weight polyethylene (UHMWPE)** [5, 51]. This property was attributed to the fact that β-hydride elimination occurs on Cr/Al_2O_3 more reluctantly that on Cr/SiO_2. Indeed, an increase in the electron density on the chromium sites is expected to diminish the tendency to agostic β-hydride coordination, which is needed for chain termination. Furthermore, Cr/alumina produces an extremely broad molecular weight distribution, which allows the molten polymer to flow at high rates when under pressure, in spite of the high molecular weight. It can be thought that the shortest chains act as "lubricating" for the flow of the longest chains. A typical molecular weight distribution of the polymer produced by Cr/alumina is shown in Figure 1. 6. Polymers made under the same conditions by Cr/silica and $Cr/AlPO_4$ (0.9 P/Al) are also shown for comparison. The MW distribution of polymer from Cr/alumina extends over the entire molecular weight range, with a strong preference for the high-MW side (about one third of the polymer had MW > 1 million g/mol) [5, 51].
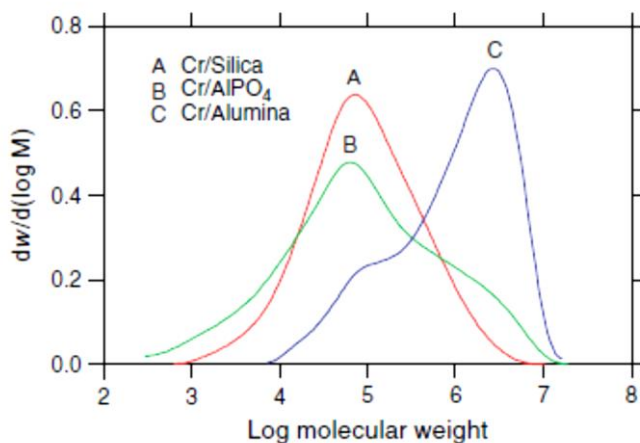
Figure 1. 6 Molecular weight distribution of polyethylene produced by Cr/silica, $Cr/AlPO_4$ and Cr/alumina catalysts, all of them activated at 700 °C [51].

1.4.2 The use of co-catalysts

Since its discovery in 1951, the Cr/SiO_2 Phillips catalyst has been tailored and upgraded mainly following trial-and error approaches or serendipitous discoveries. An explicative example is the epiphany that pushed the research in investigating the use of co-catalysts on the Phillips catalyst (including this PhD project), which originated from a fortuitous event. Indeed, the idea of modifying the Phillips catalyst with aluminium alkyls emerged in an industrial plant because of an accidental contamination coming from a polymerization line close by, that was running a Ziegler-Natta (ZN) catalyst [52, 53], where metal alkyls are necessary for developing the reactivity towards olefins conversion. **That "mistake" in the Cr/SiO_2 line resulted in a catalyst displaying lower induction time, higher sensitivity to H_2 and producing a more branched polyethylene (without adding any α-olefin co-monomers to the system).** Since then, Al-alkyls are used in the industrial practice to influence the activity of the Phillips catalyst, to modify the active sites distribution, to promote in situ branching, and to enhance the sensitivity to H_2 for molecular-weight regulation [5]. This latter aspect is one of the most interesting because the un-modified Phillips catalyst is not sensitive to the presence of hydrogen during the polymerization process.

The drastic decrease of the induction time is due to the fact that Al-alkyls are reducing agents, so that Cr sites after reacting with them have already a lower oxidation state and some coordinative unsaturations (as discussed above, these are the necessary conditions for ethylene polymerization on Phillips catalysts). Most of the authors attribute the polymerisation-active sites to Cr(II) species [54-57] although other species of higher valences, i.e. Cr(III), Cr(IV) and Cr(V), should still be taken into consideration [15, 58-61], especially in view of the recent work of the group of Copéret [62-64].

Metal alkyl co-catalysts can improve the polymerisation rate also by alkylating the Cr sites, thus promoting a chain initiation similar to Ziegler–Natta catalysis. Moreover, as highly reactive compounds, metal alkyls can degrade the adventitious poisons present in the reactor, such as moistures or the by-products formed during the initiation stages of the reaction. Finally, **it is possible that some new sites active in ethylene polymerization are formed only in the presence of the co-catalysts and not during the "classical" process** (i.e., upon reaction of ethylene on Cr(VI)/SiO$_2$ at 100 °C).

Different Al-alkyls behave in different ways. Many metal alkyls can function as cocatalysts, provided that they contain at least one M–R bond. Among the compounds most commonly used in commercial practice there are $AlEt_3$, BEt_3,

ZnEt$_2$, Al(i-Bu)$_3$, Et$_2$AlOEt, MgBuOct, Al(i-Bu)$_2$H, and LiBu. Mixtures of these compounds have also been used and claimed to have advantages (e.g., ZnEt$_2$ with BEt$_3$, or AlEt$_3$ with BEt$_3$).

The exact effect, at a molecular level, of Al-alkyls on the Cr sites is still unknown. The scientific literature in this field is very poor, with just a few articles and a few research groups working on these systems [58, 65-71]. Figure 1. 7 resumes the possible effects of metal alkyls on the Phillips catalysts:

1) **Reduction:** they can reduce Cr(VI) to the lower-valent active species, thus accelerating the development of polymerization.

2) **Alkylation**: in some cases, they can alkylate the chromium to initiate the first chain, and this action is similar to the role of the cocatalyst in Ziegler catalysis.

3) **Scavenger**: they can react with and remove any poisons present at trace levels in the feed streams, particularly oxygen, water, and redox by-products.

4) **Modification:** metal alkyls can react with the chromium site itself, or with neighbouring OH or oxide groups, to modify or become part of the environment of the site, thus influencing its behaviour.

5) **Attack**: depending on the type of cocatalyst, there is an optimal amount expressed as the metal-to-Cr ratio, which gives the highest catalytic activity. A further increase of the cocatalyst amount can deteriorate the polymerisation rate or even destroy the catalyst due to the attack on the Cr–support bonds, thus initially converting di-attached chromium species into mono-attached ones, and eventually completely detaching the sites from the surface and causing a loss of activity.

6) **Exchange:** there is evidence that some metal alkyls can exchange alkyl groups with the active site, thus providing a different mechanism of chain transfer.
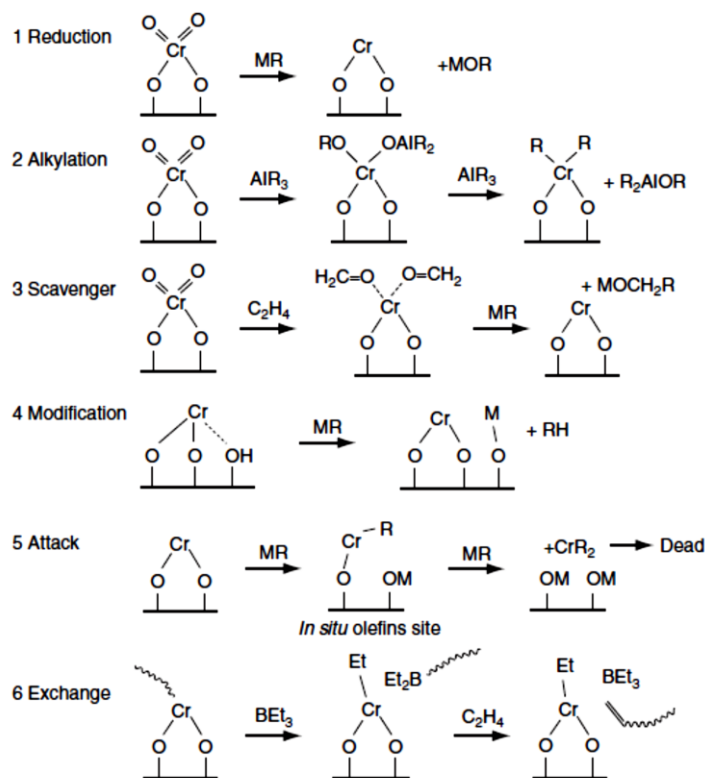
Figure 1. 7 Six ways in which the cocatalyst might influence the Cr active-site behaviour. For each effect a plausible illustration is offered, although the details of such reactions are not necessarily known [5].

The various metal alkyls probably act in each of these ways to different extents, thus resulting in the many subtle distinctions among the modified catalysts. There is also some evidences that different Cr sites on the catalyst can respond to the cocatalyst in widely divergent ways.

Cocatalysts influence also the polymer properties [72-85]. This influence can be explained primarily by the change in the active site distribution. Some sites become active more rapidly in the presence, rather than in the absence, of cocatalyst, thus increasing their contribution to the final MW distribution of the polymer. Still other sites can be activated only in the presence of a cocatalyst, and McDaniel claims that these particular sites produce higher-MW polymer [5, 27, 86]. Therefore, the addition of cocatalyst often tends to introduce a high-MW tail in the MW distribution. Consequently, cocatalysts can provide convenient ways of tailoring the polymer characteristics, and numerous variations are possible.

Mc Daniel reports [5, 86] an explicative example: a Cr/silica-titania catalyst was tested for ethylene polymerization activity, first alone and then with AlEt$_3$ or BEt$_3$ cocatalyst added to the reactor. The MW distributions of the resultant polymers are shown in the Figure 1. 8. Both cocatalysts added a high-MW tail to the MW distribution, because of the creation of new sites. However, BEt$_3$ also broadened the MW distribution on the low-MW side. Some of this contribution may have resulted from alkyl exchange, as described above. The lower part of Figure 1. 8 shows the difference curves, i.e. the MW distribution with the cocatalysts after subtracting the MW distribution without them. Hence, this datum shows how cocatalysts contribute to the MW distribution of the produced polymers. While triethylboron spreads the low-MW portion probably because of the alkyl exchange reaction, triethylaluminum contributes mostly to the high-MW polymer, which suggests the awakening of sites that would not otherwise have been active (without undergoing the alkyl exchange reaction).
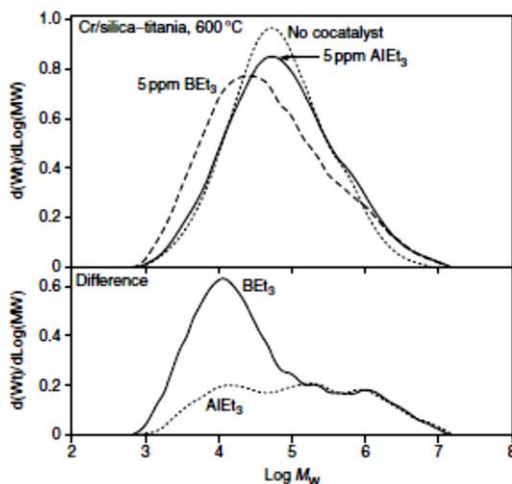
Figure 1. 8 Influence of AlEt$_3$ and BEt$_3$ cocatalysts on the MW distribution of PE made with Cr/silica–titania catalyst activated at 600°C [5].

It is not clear why but when contacted with some cocatalysts, especially aluminium alkyls, the catalysts then become highly sensitive to H$_2$. The data reported in the MW curves in Figure 1. 9 show clearly the effect of the H$_2$ on both the bare and the modified catalysts. There is a huge shift in low region of MW distribution, when a reduced Cr/Silica catalyst is contacted with TEA and H$_2$.

The reasons behind all the cocatalysts effects at a molecular level are still unknown, although an hypothesis proposed by McDaniel is linked to the presence of the so-called "mono-attached organochromium species"[5]. However it is

unequivocal that the addition of cocatalyst can be a valuable commercial tool for controlling the properties of the produced polymers.
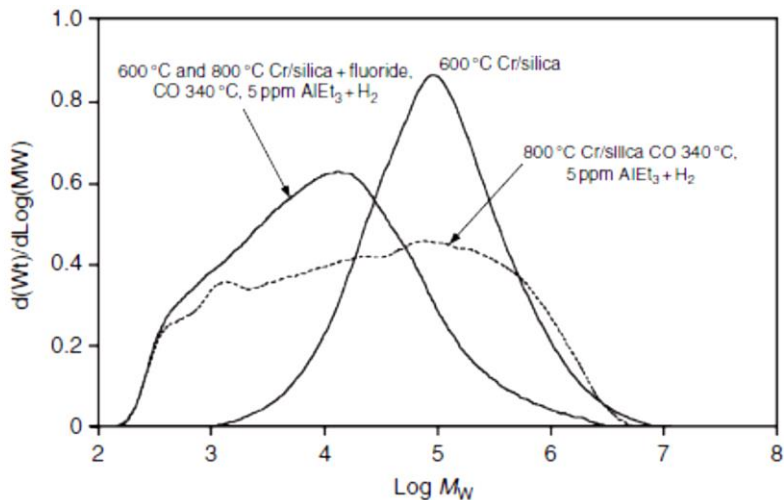
Figure 1. 9 MW distributions of polymers made with reduced Cr/silica catalysts that were treated to produce extreme sensitivity to H_2[5].

1.4.3 Organochromium catalysts

In some specific applications of PEs it is desirable to have a certain amount of short chain branches to ease the processability of the polymer. With this aim, several Phillips-like catalysts were synthetized for highly selective ethylene conversion, constituted by silica-supported chromium complexed. Nowadays, the so-called organochromium compounds are intensively used to form highly active polymerization catalysts. These systems are usually dispersed onto an already calcined oxide carrier, which plays an essential role, because without it such compounds rarely exhibit any activity. Examples of organochromium compounds which form active catalysts include all the possible formal chromium valences from Cr(0) to Cr(IV), but the oxidation state does not seem to make a major difference in the catalytic performances.

An early example of organochromium compound came from workers at Union Carbide [84, 87-93], who developed chromocene on silica as a commercial catalyst, which became a well-studied example of an active divalent compound. The so-called ''open ring'' chromocene, bis(2,4-dimethylpentadiene)chromium(II), is another example [94-96]. Other examples include Cr(allyl)$_2$ and Cr(allyl)$_3$ [89, 97-102], and the β-stabilized alkyls of Cr(II) and Cr(IV), such as the trimethylsilylmethyl derivative [39, 40, 95, 98-100, 103-111]. Still others organochromium catalysts were obtained by reacting Cr(III)(acetylacetonate)$_3$ with Al-alkyl reducing agents

[112]. Most of these organochromium compounds have minimal or no activity for ethylene polymerization until they are grafted onto a calcined oxide support. A possible reason for their inactivity in the absence of a support can be the fact that some of them exist in solution as dimers or even tetramers [39, 40, 95]. Anchoring these compounds onto a support may immobilize the chromium as stable monomers, thus preventing their decomposition. Another possible reason for the necessity of a support is the electron-withdrawing character of the support itself, which induces a stronger positive charge on the chromium.

Organochromium compounds are thought to bind to the support by reaction with one (usually) or more surface hydroxyl groups, often losing by hydrolysis one or more organic ligands in the process, as shown in Figure 1. 10. Despite many molecular differences between chromium oxide catalysts and the organochromium catalysts, they usually display a similar activity, although the latter have a much higher response to the treatment conditions than the former, with macroscopic consequences on the properties of the produced polymer. For example, the MW of the polymer produced with organochromium catalysts usually decreased as the support calcination temperature was raised [5, 24, 27, 86].

Structurally, the main differences in the organochromium catalysts are the presence of the remaining organic ligands (not consumed upon grafting on the support surface) and the possibility to be stabilized in several possible geometries. The catalytic yield is very similar between chromium oxide and organochromium catalysts, despite displaying different kinetics profiles: on the oxide catalyst the polymerization rate usually increases along with the whole reaction time, whereas **the organochromium catalysts become active very rapidly, if not instantaneously, upon exposure to ethylene.** They tend to make polymer having very broad MW distributions, often broader than those of the corresponding polymers made with chromium oxide catalysts. **These organochromium catalysts produce polymer in which a significant portion of the MW distribution is often low-MW oligomers, including 1-butene, 1-hexene and 1-octene.** Copolymerization of α-olefin is easily accomplished, and these in situ produced a-olefins also become incorporated into the polymer, resulting in branched polyethylene even when ethylene is the only olefin in the feedstock.

It is significant that so many diverse organochromium compounds should behave so much alike. Possible reasons for the similarity can be the fact that in all these organochromium catalysts prevails either the nature of the Cr-alkyl bond (trimethylsilylmethyl, neopentyl, benzyl, etc.), or the capability of assuming a

mono-hapto form (allyl or 2,4-dimethylpentadienyl), or of becoming hydrides (arene Cr(0) compounds). More generally speaking, the structures of these complexes appear to be quite similar to each other when grafted on a support and in the presence of ethylene. In many (or perhaps all) of these cases, **the chromium may be considered as already alkylated, and therefore the ligand may become the end-group of the first polymer chain produced. In most cases, there is no induction time, because the chromium is already reduced and alkylated before the contact with ethylene.** Polymerization usually starts immediately on contact with ethylene, and the rate either remains constant or slowly declines in the first hour of polymerization.
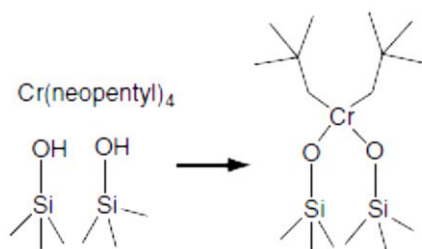
Figure 1. 10 An example the anchoring process of an organochromium compound [5, 86].

1.5 Goal and structure of the thesis

1.5.1 Goal

As reported above, the modification of the existing, highly efficient Phillips catalysts for ethylene polymerization is a common practice in industry and it is object of intense industrial researches, because it may lead to new varieties of polyethylene. However, a clear picture of the changes occurring at a molecular level around the active metal sites upon modification is still missing and it is the object of an intense debate, picking up disparate contributions, from the direct investigation of the catalysts to the theoretical simulations. Answering this question can disclose the way for a real rational design of the Phillips catalysts, improving the reaction yield and selectively changing the properties of the products.

The ambitious goal of this thesis was to investigate the Cr active sites in the Cr/SiO$_2$ Phillips catalyst in three different conditions.

1) During the reaction with ethylene;

2) After the modification with different co-catalysts. Two alkylating agents were introduced after the "classical" procedure of synthesis and activation of the Phillips catalyst [14]. In particular, we used AlEt$_3$, triethylaluminum (TEA) and Et$_2$AlOEt diethylaluminoethoxide (DEALE) (Figure 1. 11). The two compounds are very similar to each other (the only difference is formally an oxygen atom) and have several similar functions as reducing agents, alkylating agents, scavengers and modifying agents, but they present a remarkable difference in promoting the H$_2$ sensitivity of the catalyst (just a little effect for TEA, while DEALE has a very pronounced influence). The investigation of the effect of these two Al-alkyls was a very challenging task, because the modifications induced a further increase of the complexity of the catalyst, not only changing the oxidation state of the chromium sites, but also modifying its structures and adding other ligands and by-products on the surface.
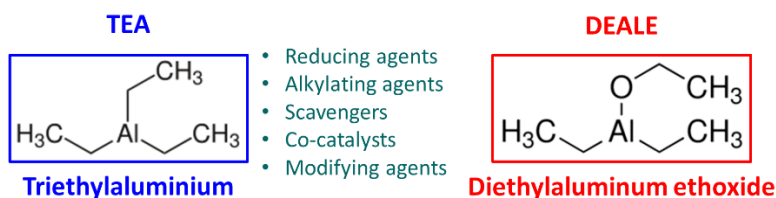
Figure 1. 11 Structure and properties of TEA (in blue) and DEALE (in red).

3) In an organo-chromium catalyst. In particular, we investigated the structure of the chromium sites in silica-supported $Cr[CH(SiMe_3)_2]_3$ catalysts as a function of the chromium loading, with t**he final goal to correlate the catalyst's structure with the catalytic performances.** In fact, according to the industrial reports, by keeping constant the silica activation temperature an increase in the Cr loading causes a decrease of the polymer density.

The final aim was to find a correlation between the structure of the active sites and the properties of the produced polymers. Both points 2) and 3) have been prompted by a stimulating collaboration with Dr. Takashi Monoi (JPE/JPC). In all the three cases, the combination of several, highly sensitive, spectroscopic techniques was a mandatory condition in order to get information about the coordination and oxidation state of the Cr centres, the functional groups at the surface of the catalysts, and the mutual interactions among all the components [113].

1.5.2 The use of the spectroscopic techniques for the characterization of Phillips catalyst.

The above-described goal of the thesis can be achieved only through the direct experimental observation of the working centres, as well as reaction intermediates. The need for suitable characterization techniques directly follows. Among all the techniques, vibrational, electronic and paramagnetic spectroscopies are well-known powerful techniques to provide information at the molecular level, also for highly diluted surface species.

In particular, the vibrational spectra are sensitive to the molecular properties of the investigated samples, such as type of atoms, chemical bonding, geometry, and intra/intermolecular interactions, discriminating between different species that may simultaneously be present in the investigated systems. Moreover, the vibrational spectroscopy of adsorbed probe molecules was largely employed in the past to get indirect information about the surface properties of the catalytic materials.

On the other hand, the electronic properties of the metal centers in heterogeneous catalysts, such as the oxidation state and the coordination geometry, were directly explored by UV-Vis (in diffuse reflectance mode, DR) and XANES spectroscopy, together with a few remarkable examples of XPS analysis.

Finally, EPR spectroscopy was successfully applied to detect and characterize Cr species with specific oxidation states. As a matter of fact, EPR is a really sensible technique and provides an incontrovertible proof for the presence of such species.

It clearly appears how the best approach to face the analysis of intrinsically complex multicomponent catalysts (as the Phillips one) is to carefully combine the data obtained with different spectroscopic methods, in order to have a complete picture of the topic.

1.5.3 Structure of the Thesis

This PhD thesis is constructed into seven chapters.

Chapter 2 is devoted to the description of the experimental details. The first part of the chapter provides the list of the investigated catalysts and of the activation procedures. Secondly, all the modification agents employed in the work are listed, describing in details the optimized conditions to successfully modify the catalysts. Finally, a brief description of the adopted experimental set-ups is provided for each characterization technique.

Chapter 3 contains all the recent experimental results obtained by investigating the classical Cr/SiO_2 Phillips catalysts during ethylene polymerization, both for the CO-reduced $Cr(II)/SiO_2$ and the oxidized $Cr(VI)/SiO_2$ forms.

Chapters 4 and 5 contain the most relevant results obtained on both the $Cr(II)/SiO_2$ and $Cr(VI)/SiO_2$ catalysts modified with TEA and DEALE. More in details, Chapter 4 discusses the modification of the $Cr(II)/SiO_2$ catalyst, whereas Chapter 5 the modification of the oxidized $Cr(VI)/SiO_2$ one. This section includes the experiments performed during a visiting period at the group of Magnetic resonance and X-ray methods of Rostock University, under the supervision of Professor Angelika Brückner.

Chapter 6 shows the most interesting results obtained for the silica-supported $Cr[CH(SiMe_3)_2]_3$ organochromium catalysts, which were the main object of the collaboration with Dr. Takashi Monoi from the Japan Polychem Corporation (JPC).

Chapter 7 is dedicated to conclusions and perspectives.

References

[1] Peacock, A.J., Handbook of Polyethylene. Structures, properties and applications. , New York Basel 2000.

[2] Jansz, J., Global PO&E News Analysis, 2015.

[3] Nowlin, T.E., Business and Technology of the Global Polyethylene Industry, Wiley-Scrivener, New York, 2014.

[4] Ellen MacArthur Foundation, The New Plastics Economy: Rethinking the Future of Plastics, McKinsey & Company, 2016.

[5] McDaniel, M.P.,Adv. Catal., 53 (2010) 123-606.

[6] Hogan, J.P.,J. Polym. Sci., 8 (1970) 2637-2652.

[7] Hogan, J.P., Chapter 6 - Catalysis of the Phillips Petroleum Company Polyethylene Process in: Applied Industrial Catalysis, Academic Press, New York, 1983, pp. 149-176.

[8] Hogan, J.P., Banks, R.L., US. Patent 2.825.721, in, 1958.

[9] Robert, C., Thomas, C.M.,Chem. Soc. Rev., 42 (2013) 9392-9402.

[10] Kaminsky, W.,Macromol. Chem. Phys., 197 (1996) 3907-3945.

[11] Fink, G., Steinmetz, B., Zechlin, J., Przybyla, C., Tesche, B.,Chem. Rev., 100 (2000) 1377-1390.

[12] Olabisi, O., Atiqullah, M., Kaminsky, W.,J. Macromol. Sci., Rev. Macromol. Chem. Phys., 37 (1997) 519-554.

[13] Tisse, V.F., Boisson, C., McKenna, T.F.L.,Macrom. Chem. Phys., 215 (2014) 1358-1369.

[14] Groppo, E., Lamberti, C., Bordiga, S., Spoto, G., Zecchina, A.,Chem. Rev., 105 (2005) 115-183.

[15] Weckhuysen, B.M., Deridder, L.M., Schoonheydt, R.A.,J. Phys. Chem., 97 (1993) 4756-4763.

[16] Weckhuysen, B.M., Schoofs, B., Schoonheydt, R.A.,J Chem Soc Faraday T, 93 (1997) 2117-2120.

[17] Weckhuysen, B.M., Wachs, I.E., Shoonheydt, R.A.,Chem. Rev., 96 (1996) 3327-3349.

[18] Weckhuysen, B.M., Schoonheydt, R.A.,Catal. Today, 49 (1999) 441-451.

[19] Weckhuysen, B.M., Schoonheydt, R.A., Jehng, J.M., Wachs, I.E., Cho, S.J., Ryoo, R., Kijlstra, S., Poels, E.,J Chem Soc Faraday T, 91 (1995) 3245-3253.

[20] McDaniel, M.P.,J. Catal., 67 (1981) 71-76.

[21] McDaniel, M.P.,J. Catal., 76 (1982) 29-36.

[22] McDaniel, M.P.,J. Catal., 76 (1982) 37-47.

[23] McDaniel, M.P.,J. Catal., 76 (1982) 17-28.

[24] McDaniel, M.P.,Adv. Catal., 33 (1985) 47-98.

[25] Zecchina, A., Groppo, E.,Proc. R. Soc. A-Math. Phys. Eng. Sci., 468 (2012) 2087-2098.

[26] Chakrabarti, A., Gierada, M., Handzlik, J., Wachs, I.E.,Top. Catal., 59 (2016) 725-739.

[27] McDaniel, M.,MRS Bull., 38 (2013) 234-238.

[28] Marsden, C.E.,Plast. Rubb. Compos. Process. Appl., 21 (1994) 193-200.

[29] McDaniel, M., Welch, M.B., Dreiling, M.J.,J. Catal., 82 (1983) 118-126.

[30] Pullukat, T.J., Hoff, R.E., Shida, M.,J. Polym. Sci,: Polym. Chem. Ed., 18 (1980) 2857-2866.

[31] Conway, S.J., Falconer, J.W., Rochester, C.H., Dows, G.W.,J Chem Soc Faraday T, 85 (1989) 71-78.

[32] Conway, S.J., Falconer, J.W., Rochester, C.H., Dows, G.W.,J Chem Soc Faraday T, 85 (1989) 79-90.

[33] Conway, S.J., Falconer, J.W., Rochester, C.H., Dows, G.W.,J Chem Soc Faraday T, 85 (1989) 1841-1851.

[34] Rebenstorf, B., Sheng, T.C.,Langmuir, 7 (1991) 2160-2165.

[35] Hogan, J.P., Witt, D.R., U.S. Patent 3, 622, 521, in, 1971.

[36] Ellison, A., Overton, T.L.,J. Mol. Catal., 90 (1994) 81-86.

[37] Ellison, A., Overton, T.L., Bencze, L.,J Chem Soc Faraday T, 89 (1993) 843-849.

[38] Hogan, J.P., Copolymerization, Chap. 3. , Interscience/Wiley, New York, 1964.

[39] McDaniel, M.P., Smith, P.D., U.S. Patent 5,075,394, in, 1991.

[40] McDaniel, M.P., Smith, P.D., U.S. Patent 5,200,379, in, 1993.

[41] Zhu, Z.D., Chang, Z.X., Kevan, L.,J. Phys. Chem. B, 103 (1999) 2680-2688.

[42] Rao, R.R., Weckhuysen, B.M., Schoonheydt, R.A.,Chem. Commun., (1999) 445-446.

[43] Bade, O.M., Blom, R., Dahl, I.M., Karlsson, A.,J. Catal., 173 (1998) 460-469.

[44] Aguado, J., Calleja, G., Carrero, A., Moreno, J.,Chem. Eng. J., 137 (2008) 443-452.

[45] Mokaya, R., Jones, W.,Chem. Comm., (1997) 2185-2186.

[46] McDaniel, M.P., Benham, E.A., Collins, K.S., Eaton, A.P., Jensen, M.D., Martin, J.L., Hawley, G.R., U.S. Patent 6,613,852, in, 2003.

[47] McDaniel, M.P., Benham, E.A., Martin, S.J., Collins, K.S., Smith, J.L., Hawley, G.R., Wittner, C.E., Jensen, M.D., U.S. Patent 6,300,271, in, 2001.

[48] Grayson, M.E., McDaniel, M.P.,J. Mol. Catal. , 65 (1991) 139-144.

[49] Weckhuysen, B.M., Deridder, L.M., Grobet, P.J., Schoonheydt, R.A.,J. Phys. Chem., 99 (1995) 320-326.

[50] Martino, G.A., Barzan, C., Piovano, A., Budnyk, A., Groppo, E.,J. Catal., 357 (2018) 206-212.

[51] McDaniel, M.P., Handbook of heterogeneous catalysis, in: G. Ertl, H. Knözinger, J. Weitkamp (Eds.) Handbook of heterogeneous catalysis, VHC, Weinheim, 1997, pp. 2400.

[52] Böhm, L.L.,Angew. Chem., Int. Ed.,, 42 (2003) 5010-5030.

[53] Wilke, G.,Angew. Chem. - Int. Ed., 42(41) (2003) 5000-5008.

[54] Groppo, E., Estephane, J., Lamberti, C., Spoto, G., Zecchina, A.,Catal. Today, 126 (2007) 228-234.

[55] Ghiotti, G., Garrone, E., Zecchina, A.,J. Mol. Catal., 46 (1988) 61-77.

[56] Myers, D.L., Lunsford, J.H.,J. Catal., 99 (1986) 140-148.

[57] Weckhuysen, B.M., Schoonheydt, R.A.,Zeolites, 14 (1994) 360-366.

[58] Liu, B., Šindelář, P., Fang, Y., Hasebe, K., Terano, M.,J Mol Catal A Chem, 238 (2005) 142-150.

[59] Weckhuysen, B.M., Wachs, I.E.,J Chem Soc Faraday T, 92 (1996) 1969-1973.

[60] Jehng, J.M., Wachs, I.E., Weckhuysen, B.M., Schoonheydt, R.A.,J Chem Soc Faraday T, 91 (1995) 953-961.

[61] Beck, D.D., Lunsford, J.H.,J. Catal., 68 (1981) 121-131.

[62] Conley, M.P., Delley, M.F., Siddiqi, G., Lapadula, G., Norsic, S., Monteil, V., Safonova, O.V., Copéret, C.,Angew. Chem. Int. Ed., 53 (2014) 1872-1876.

[63] Delley, M.F., Conley, M.P., Copéret, C.,Catal Lett, 144 (2014) 805-808.

[64] Delley, M.F., Núñez-Zarur, F., Conley, M.P., Comas-Vives, A., Siddiqi, G., Norsic, S., Monteil, V., Safonova, O.V., Copéret, C.,Proc. Natl. Acad. Sci. U. S. A., 111 (2014) 11624-11629.

[65] Cicmil, D., Meeuwissen, J., Vantomme, A., Wang, J., van Ravenhorst, I.K., van der Bij, H.E., Munoz-Murillo, A., Weckhuysen, B.M.,Angew. Chem., 54 (2015) 13073-13079.

[66] Cicmil, D., Meeuwissen, J., Vantomme, A., Weckhuysen, B.M.,ChemCatChem, 8 (2016) 1937-1944.

[67] Cicmil, D., van Ravenhorst, I.K., Meeuwissen, J., Vantomme, A., Weckhuysen, B.M.,Catal Sci Technol, 6 (2016) 731-743.

[68] Li, J.H., DiVerdi, J.A., Maciel, G.E.,J. Am. Chem. Soc., 128 (2006) 17093-17101.

[69] Barzan, C., Gianolio, D., Groppo, E., Lamberti, C., Monteil, V., Quadrelli, E.A., Bordiga, S.,Chem. Eur. J., 19 (2013) 17277-17282.

[70] Barzan, C., Groppo, E., Quadrelli, E.A., Monteil, V., Bordiga, S.,Phys.Chem.Chem.Phys., 14 (2012) 2239–2245.

[71] Basset, J.M., Lefebvre, F., Santini, C.,Coord. Chem. Rev., 180 (1998) 1703-1723.

[72] Hogan, J.P., U.S. Patent 3,959,178, in, 1974.

[73] Hogan, J.P., U.S. Patent 3,878,179, in, 1975.

[74] Hogan, J.P., U.S. Patent 3,956,257, in, 1976.

[75] Hogan, J.P., U.S. Patent 4,025,707, in, 1977.

[76] Witt, D.R., U.S. Patent 3,947,433, in, 1976.

[77] Bergmeister, J.J., Wolfe, A.R., Secora, S.J., Benham, E.A., Coutant, W.R., McDaniel, M.P., U.S. Patent 6,174,981,, in, 2001.

[78] Sukhadia, A.M., Benham, E.A., Bergmeister, J.J., Bobsein, R.L., Guenther, G., Hsieh, E.T., McDaniel, M.P., Secora, S.J., Shveima, J.S., Stewart, J.D., U.S. Patent 6,617,403, in, 2003.

[79] Bergmeister, J.J., Secora, S.J., Benham, E.A., McDaniel, M.P., U.S. Patents 6,569,960, in, 2003.

[80] Bergmeister, J.J., Secora, S.J., Benham, E.A., McDaniel, M.P., U.S. Patent 6,855,781, in, 2005.

[81] Bergmeister, J.J., Secora, S.J., Guenther, G., Benham, E.A., McDaniel, M.P., U.S. Patents 6,201,077, in, 2001.

[82] Bergmeister, J.J., Secora, S.J., Guenther, G., Benham, E.A., McDaniel, M.P., U.S. Patent 6,204,346, in, 2001.

[83] Bergmeister, J.J., Secora, S.J., Guenther, G., Benham, E.A., McDaniel, M.P., U.S. Patent 6,642,324, in, 2003.

[84] McDaniel, M.P., Short, J.N., U.S. Patent 4,803,253, in, 1989.

[85] McDaniel, M.P., Short, J.N., U.S. Patent 4,877,763, in, 1989.

[86] McDaniel, M.P., A review of the Phillips Chromium Catalyst for Ethylene Polymerization, in: Handbook of Transition Metal Polymerization Catalysts: Second Edition, 2018, pp. 401-571.

[87] Karol, F.J.,Catal. Rev., 26 (1984) 557-595.

[88] Karol, F.J., Brown, G.L., Davison, J.M.,J. Polym. Sci. A, 11 (1973) 413 - 424.

[89] Karol, F.J., Johnson, R.N.,J. Polym. Sci. Polym. Chem. Ed., 13 (1975) 1607-1617.

[90] Rebenstorf, B.,J. Mol. Catal., 66 (1991) 59-71.

[91] Rebenstorf, B., Lindblad, T.,Acta Chem. Scand., 44 (1990) 789-792.

[92] McDaniel, M.P., J.N., S., U.S. Patent 4,424,139, in, 1984.

[93] McDaniel, M.P., J.N., S., U.S. Patent 4,690,990, in, 1987.

[94] Newbound, T.D., Freeman, J.W., Wilson, D.R., Kralik, M.S., Patton, A.T., Campana, C.F., Ernst, R.D.,Organometal., 6 (1987) 2432-2437.

[95] Smith, P.D., McDaniel, M.P.,J. Polym. Sci. A Polym. Chem., 27 (1989) 2695-2710.

[96] McDaniel, M.P.,Ind. Eng. Chem. Res., 27 (1988) 1559-1564.

[97] Bade, O.M., Blom, R., Ystenes, M.,Organometallics, 17 (1998) 2524-2533.

[98] Ballard, D.G.H.,Adv. Catal., 23 (1973) 263-325.

[99] Ballard, D.G.H., Jones, E., Pioli, A.J.P., Robinson, P.A., Wyatt, R.J., U.S. Patent 3,840,508,, in, 1974.

[100] Ballard, D.G.H., Parkins, A.W., Robinson, P.A., Ibekwe, S.D., Lappert, M.F., Pearce, R., U.S. Patent 3,969,386,, in, 1976.

[101] Yermakov, Y., Zakharov, V.,Adv. Catal. , 24 (1975) 173-219.

[102] Yermakov, Y.I.,Catal. Rev., 13 (1976) 77-120.

[103] Monoi, T., Sasaki, Y.,J. Mol. Catal. A-Chem. , 187 (2002) 135-141.

[104] Ikeda, H., Monoi, T., Sasaki, Y.,J. Polym. Sci.: Part A: Polym. Chem., 41 (2003) 413-419.

[105] Monoi, T., Ikeda, H., Sasaki, Y., Matsumoto, Y.,Polym. J., 35 (2003) 608-611.

[106] Amor Nait Ajjou, J., Rice, G.L., Scott, S.L.,J. Am. Chem. Soc., 120 (1998) 13436-13443.

[107] Amor Nait Ajjou, J., Scott, S.L.,Organometallics, 16 (1997) 86-92.

[108] Amor Nait Ajjou, J., Scott, S.L., Paquet, V.,J. Am. Chem. Soc., 120 (1998) 415-416.

[109] Amor Nait Ajjou, J., Scott, S.L.,J. Am. Chem. Soc., 122 (2000) 8968-8976.

[110] Scott, S.L., Amor Nait Ajjou, J.,Chem. Eng. Sci., 56 (2001) 4155-4168.

[111] Scott, S.L., Fu, A., MacAdams, L.A.,Inorg. Chim. Acta, 361 (2008) 3315-3321.
[112] Henrici-Olivé, G., Olivé, S.,Angew. Chem., 10 (1971) 776-786.
[113] Groppo, E., Seenivasan, K., Barzan, C.,Catal. Sci. Technol., 3 (2013) 858-878.

Chapter 2

Experimental methods.

In this Chapter we provide the details of all the catalysts investigated in this thesis, their synthesis procedure and the characterization techniques. Because of the high air-sensitivity of all the Cr catalysts, as well as of the Al-Alkyls, a dedicated glove-box and specifically dedicated vacuum lines (Figure 2. 1) were extensively used for both the storage and the handling of the samples.
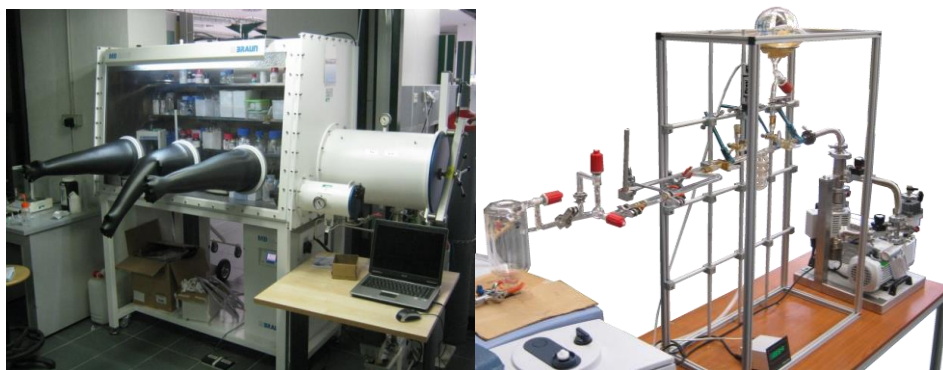
Figure 2. 1 Left): The glove-box and the vacuum line used for storing and manipulating the samples under nitrogen atmosphere or under vacuum.

2.1 Samples preparation

2.1.1 Synthesis and activation of Cr/SiO$_2$

The Phillips catalysts were prepared through a wet-impregnation of the silica support with an aqueous solution of Cr(VI). The silica used as a support is a silica-aerosil (surface area 380 m^2/g). As a precursor of chromium, chromic anhydride was used. Two different batches of samples were prepared, characterized by a chromium loading of 0.5 wt% and 1.0 wt%, respectively: the former was used for the DR-UV-Vis-NIR measurements and the latter for FT-IR and kinetics experiments. The choice was done to optimize the spectral quality. Cross-checking experiments demonstrated that the spectroscopic properties are the same irrespective of the Cr loading, as already demonstrated in the past [1].

The activation procedure, optimized along more than 15 years of research in the Torino's group, involves the following steps: i) evacuation at 973 K followed by calcination in O$_2$ at the same temperature for 1 hour; ii) reduction in CO at 623 K for 1 hour followed by evacuation at the same temperature; and iii) cooling down to room temperature in dynamic vacuum. It was previously demonstrated (by coupling DR UV-Vis with Raman measurements) that step i provides Cr sites in a hexavalent state having a mono-chromate structure, which are stoichiometrically and cleanly reduced to Cr(II) by CO [1]. In the following we will call the two form of the catalyst Cr(VI)/SiO$_2$ and Cr(II)/SiO$_2$, respectively.

2.1.2 Modification of Cr/SiO$_2$ by AlR$_3$

Both Cr(VI)/SiO$_2$ and Cr(II)/SiO$_2$ have been subjected to modification by AlEt$_3$ (TEA) or Al(OEt)Et$_2$ (DEALE). The modification was achieved following two methods.

Method A: vapor deposition. A small balloon containing the alkylating agent was filled in the glovebox, and successively connected to a vacuum line. The vapors of TEA (or DEALE) were sent directly on the activated catalyst. This method has the advantage to allow the investigation of the activation process in real time by means of spectroscopic methods. However, it is susceptible of contamination by moisture, enhanced by the low vapor tension of TEA and DEALE, which take time to reach the sample. Moreover, the main disadvantage of that method is that it is not possible to quantify the amount of dosed Al-Alkyls, that means the Al/Cr stoichiometry.

Method B: impregnation. The activated samples were impregnated directly in the glovebox with a stoichiometric amount of Al-alkyl, corresponding to Al:Cr = 2:1 or 4:1, as reported in the literature [2-6]. Figure 2. 2 shows a detail of the impregnation procedure. Briefly, the sample is weighted, the molar content of Cr determined, and the exact amount of Al-alkyl necessary to reach the desired Al:Cr concentration is diluted in hexane. Due to the small amount of liquid, the impregnation is performed by using a micropipette. Hexane rapidly evaporates during the successive degassing step.

Figure 2. 2 Impregnation procedure made in glove box.

The resulting catalysts are labelled throughout the text with a nomenclature that contains, in the order: the form of the starting catalyst (oxidized or reduced), the name of the Al-alkyl used for the modification (TEA or DEALE) and its concentration expressed as Al:Cr ratio (as done conventionally in the literature). For example, the nomenclature $Cr(II)/SiO_2+TEA(2:1)$ indicates a $Cr(II)/SiO_2$ catalyst modified by TEA at a concentration of Al:Cr =2:1. The whole list of samples investigated during this thesis work is reported in Table 1.

Table 1 List of the Cr[CH(SiMe$_3$)$_2$]$_3$/SiO$_2$ catalysts received by JPE.

Label	Oxidation	Reduction	Modification	
			Al-Alkyl	Al:Cr
Cr(VI)/SiO$_2$	O$_2$, 650 °C	-		
Cr(VI)/SiO$_2$+TEA(2:1)	O$_2$, 650 °C	-	TEA	2:1
Cr(VI)/SiO$_2$+TEA(4:1)	O$_2$, 650 °C	-	TEA	4:1
Cr(VI)/SiO$_2$+DEALE(2:1)	O$_2$, 650 °C	-	DEALE	2:1
Cr(VI)/SiO$_2$+DEALE(4:1)	O$_2$, 650 °C	-	DEALE	4:1
Cr(II)/SiO$_2$	O$_2$, 650 °C	CO, 350 °C		
Cr(II)/SiO$_2$+TEA(2:1)	O$_2$, 650 °C	CO, 350 °C	TEA	2:1
Cr(II)/SiO$_2$+TEA(4:1)	O$_2$, 650 °C	CO, 350 °C	TEA	4:1
Cr(II)/SiO$_2$+DEALE(2:1)	O$_2$, 650 °C	CO, 350 °C	DEALE	2:1
Cr(II)/SiO$_2$+DEALE(4:1)	O$_2$, 650 °C	CO, 350 °C	DEALE	4:1

2.1.3 Silica-supported Cr[CH(SiMe$_3$)$_2$]$_3$ catalysts

The nCr[CH(SiMe$_3$)$_2$]$_3$/SiO$_{2-600}$ catalysts were provided by Dr. Takashi Monoi (JPE/JPC) in the frame of a Confidentiality Agreement. The synthesis procedure was as follows. The Cr[CH(SiMe$_3$)$_2$]$_3$ complex, shown in Figure 2. 3, was synthesized from (Me$_3$Si)$_2$CHCl and CrCl$_3$ as dark green crystals. A 0.2M stock solution of Cr[CH(SiMe$_3$)$_2$]$_3$ in hexane was prepared.
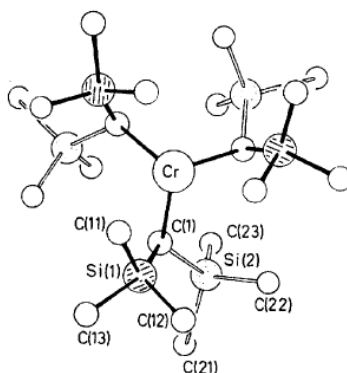
Figure 2. 3 Molecular structure of Cr[CH(SiMe$_3$)$_2$]$_3$ with hydrogen atoms omitted for clarity [7].

Two different batches of silica Sylpol952 (Grace, surface area = 300 m^2/g, pore volume = 1.6 cm^3/g) were calcined in quartz tubes by fluidization with a stream of dry nitrogen at 600 °C (hereafter SiO$_{2-600}$) for 24 h, respectively. The silica was placed in a 100-mL round-bottom flask, and 40 mL of dry hexane were added. After stirring and warming to 40 °C, the hexane solution of Cr[CH(SiMe$_3$)$_2$]$_3$ was

added and stirred at 40 °C. Different chromium loadings were employed. Hereafter we will indicate the Cr loading before the name of the sample. For example, $0.5Cr[CH(SiMe_3)_2]_3/SiO_{2-600}$ indicates a Cr content of 0.5 wt% on a SiO_{2-600}. After 1 h of stirring, the hexane was removed in vacuum at 40 °C until no volatiles appeared.

Table 2 List of the $Cr[CH(SiMe_3)_2]_3/SiO_2$ catalysts received by JPE. The $0.1Cr[CH(SiMe_3)_2]_3/SiO_{2-600}$ revealed to be too much sensitive to moisture, and was not investigated in details.

Label	SiO₂ Act. T (°C)	Cr loading (wt%)	Picture
SiO_{2-600}	600	-	
$0.1Cr[CH(SiMe_3)_2]_3/SiO_{2-600}$	600	0.1	
$0.2Cr[CH(SiMe_3)_2]_3/SiO_{2-600}$	600	0.2	
$0.3Cr[CH(SiMe_3)_2]_3/SiO_{2-600}$	600	0.3	
$0.4Cr[CH(SiMe_3)_2]_3/SiO_{2-600}$	600	0.4	
$0.5Cr[CH(SiMe_3)_2]_3/SiO_{2-600}$	600	0.5	

A picture of the $Cr[CH(SiMe_3)_2]_3/SiO_2$ samples, of the starting silica powders and a complete list of the investigated samples is reported in Table 2.

2.2 Ethylene polymerization tests

All the Cr catalysts were tested in gaseous ethylene polymerization in mild conditions (room temperature, ca. 100-200 mbar). In all the cases the reaction was performed directly into the activation/measurement cell. Information on the polymerization reaction were obtained following two different approaches:

A. Spectroscopic approach. C_2H_4 (ca. 100 mbar) was dosed in the reaction cell and the spectroscopic manifestations of the growing polymer, as well as of the active catalyst, were recorded at different time resolution depending on the technique. FT-IR spectra during ethylene polymerization were recorded every 30 seconds, while DR UV-Vis spectra during ethylene polymerization were collected every 2 minutes. For EPR, ethylene was sent on the catalyst and the polymerization was quenched by liquid nitrogen after a few minutes, followed by the collection of the EPR spectrum.

B. Kinetic approach. In most of the cases, the ethylene polymerization rate was evaluated by monitoring the decrease in ethylene pressure as a function of time, by means of a capacitive pressure gauge. In a standard experiment, a starting

pressure of ca. 200 mbar was adopted and the ethylene pressure was recorded every 5 seconds within the first minute of reaction, every 10 seconds until two minutes and every 30 seconds until reaching the tenth minute. This approach offers the possibility to evaluate the constants of ethylene polymerization kinetics, and to compare quantitatively the performances of different catalysts.

2.3 Characterization techniques

2.3.1. FT-IR spectroscopy

FT-IR spectra in transmission mode were collected by using a Bruker Vertex70 instrument equipped with a MCT detector, at a resolution of 2 cm^{-1}. Each sample was prepared in the form of a thin pellet (surface density ca. 30 mg cm^{-2}) and put into a gold envelope within a quartz cell equipped with two KBr windows, as shown in Figure 2. 4 (part a), which allows performing the activation procedure through the use of thermal treatment vacuum line (part b of Figure 2. 4) and measurements in presence of gases. In order to monitor *in situ* the evolution of the spectra in the presence of molecular probes and/or during the reactions, the quartz cell containing the sample was connected to a devoted vacuum line and interfaced with the spectrophotometer (part b of Figure 2. 1).
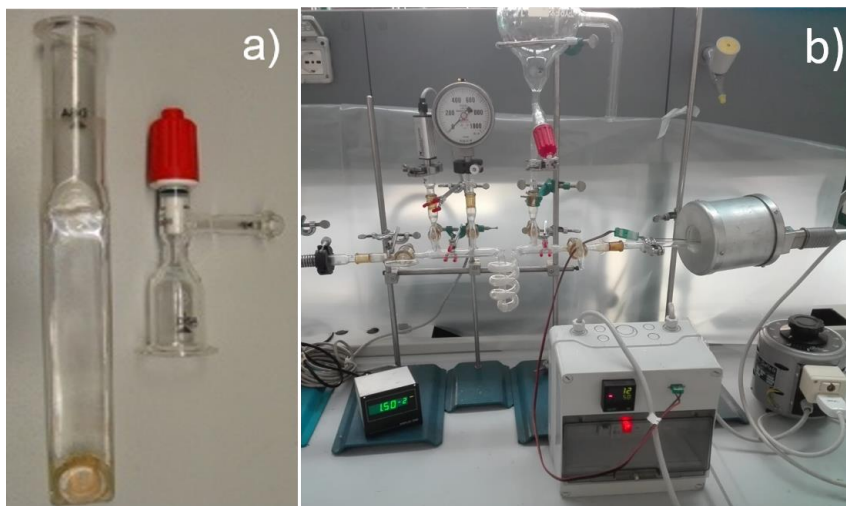
Figure 2. 4 Part a) Room temperature IR cell allowing transmission measurements. Part b) thermal treatment vacuum line.

ATR-IR spectra of liquid and powder samples were collected with a Bruker Alpha instrument with a diamond crystal placed inside the glove box.

2.3.2 DR UV-Vis-NIR spectroscopy

The UV-Vis-NIR spectra were collected in diffuse reflectance mode (DR), using a Varian Cary5000 spectrophotometer, equipped with a reflectance sphere. The samples were placed inside a quartz cell with an optical quartz window ("Suprasil"). Two different geometries for the optical window were available, as a compromise between the spectroscopic response and the adjustment to the sample form: a bulb-shaped window for powder samples and a flat window for samples prepared as thick pellets (surface density ca. 300 mg cm^{-2}) as shown respectively in Figure 2. 5. The spectra were collected in reflectance and successively converted into Kubelka-Munk.
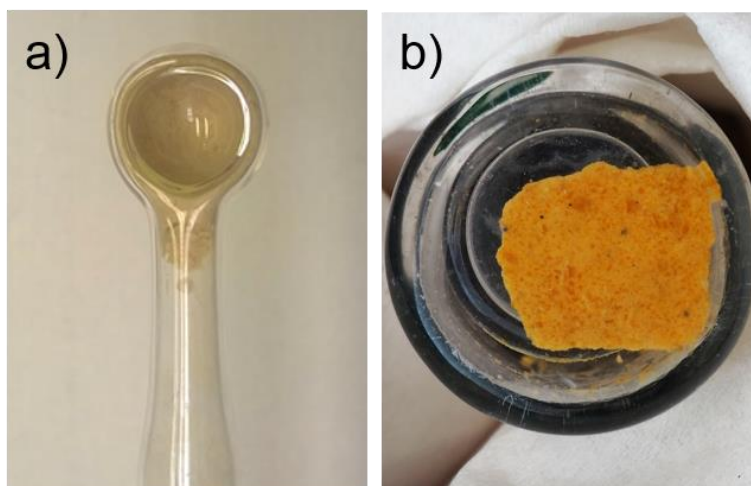
Figure 2. 5 Cells in optical quartz used for diffuse reflectance, part a) in the bulb-shaped window, part b) in the flat window.

2.3.3 EPR spectroscopy

The EPR experiments were conducted in two different laboratories. Those reported in Chapter 3 and Chapter 6 were performed at the Department of Chemistry at UniTO (under the supervision of Prof. Mario Chiesa). X-band (microwave frequency 9.76 GHz) and Q-band (microwave frequency 33.7 GHz) CW-EPR experiments were carried out on a Bruker ELEXYS 580 EPR spectrometer, equipped with a SHQ cavity (X-band) and a flexline dielectric ring Q-band EPR and ENDOR resonator (Bruker EN 5107D2). X-band measurements at 77 K were performed using a finger dewar, filled with liquid nitrogen. The magnetic field was measured with a Bruker ER035 M NMR gaussmeter. All simulations of the EPR spectra were done using Easyspin.

The EPR experiments reported in Chapter 5 were performed at the Leibniz-Institut für Katalyse e.V. an der Universität Rostock (LIKAT), in the frame of the three months internship I spent there. EPR spectra were recorded on an ELEXSYS 500-10/12 X band cw-spectrometer (Bruker) with a microwave power of 6.3 mW, a modulation frequency of 100 kHz an modulation amplitude of 5 G. The spectra were collected at 100 K.

2.3.4 XPS measurements

During my internship at the Leibniz-Institut für Katalyse e.V. an der Universität Rostock (LIKAT), I also attempted to perform some X-ray Photoelectron Spectroscopy (XPS) experiments. The XPS measurements were performed with a VG ESCALAB220iXL instrument, using a monochromatic Al K_α radiation (E = 1486.6 eV). In order to preserve the samples from the air and the moisture, a glove bag filled with nitrogen was set around the entrance chamber of the instrument as shown in Figure 2. 6.
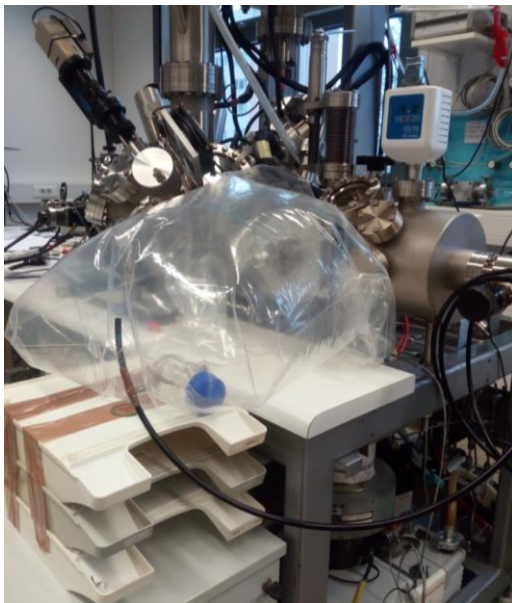
Figure 2. 6 The glove-bag set around the entrance chamber of the XPS instrument at LIKAT.

Unfortunately, despite the numerous attempts, no reliable results were obtained by XPS, for two main reasons.

1) Despite the precautions used to insert the samples in the pre-measurement chamber, they appear all contaminated by moisture. This is not strange, since

it is known that Cr/SiO$_2$ catalysts are extremely sensitive. If additional trials have to be made in the future, some efforts are necessary to equip the instrument with the possibility to introduce air-sensitive samples without exposure to moisture.

2) Only a very weak and broad signal in the Cr 2p region was detected, due to the low Cr loading. The consequent signal to noise ratio was very poor, and did not allow to perform a reliable deconvolution of the peaks, which is mandatory for the interpretation of the spectra.

2.3.4 Differential scanning calorimetry (DSC)

DSC measurements on the obtained polymers were performed with a TA Q200 instrument at a heating rate of 2°C/min, with two consecutive heating and cooling temperature ramps in the 50-150°C range. The values for polymer melting temperature (T_m) and crystallization temperature (T_c) were taken from the second heating ramp, so that the measures were not affected by the thermal history of the polymer.

References

[1] Groppo, E., Lamberti, C., Bordiga, S., Spoto, G., Zecchina, A.,Chem. Rev., 105 (2005) 115-183.

[2] Cicmil, D., Meeuwissen, J., Vantomme, A., Wang, J., van Ravenhorst, I.K., van der Bij, H.E., Munoz-Murillo, A., Weckhuysen, B.M.,Angew. Chem., 54 (2015) 13073-13079.

[3] Cicmil, D., van Ravenhorst, I.K., Meeuwissen, J., Vantomme, A., Weckhuysen, B.M.,Catal Sci Technol, 6 (2016) 731-743.

[4] Cicmil, D., Meeuwissen, J., Vantomme, A., Weckhuysen, B.M.,ChemCatChem, 8 (2016) 1937-1944.

[5] McDaniel, M.P.,Adv. Catal., 53 (2010) 123-606.

[6] Liu, B., Šindelář, P., Fang, Y., Hasebe, K., Terano, M.,J Mol Catal A Chem, 238 (2005) 142-150.

[7] F., B.G.K.a.L.M.,Journal of the Chemical Society, Dalton Transactions, (1978) 734-740.

Chapter 3
The unmodified Phillips catalyst.

The Phillips catalyst employed nowadays in the industrial process is essentially the same as the one discovered in 1951, and this is due to its rather simple synthesis procedure: the impregnation of a chromium precursor (typically CrO_3) on a high surface area material (traditionally an amorphous silica). The catalyst is first activated in an oxidative atmosphere at a temperature higher than 600 °C. This procedure leads to the dihydroxylation of the support and to the grafting of Cr in the form of chromates species. Ethylene is then put in contact directly with the activated pre-catalyst at temperatures from 80 to 120°C. At this point, after an induction time that can vary from minutes to hours, ethylene slowly reduces the Cr(VI) sites initially present in the pre-catalyst to low valent chromium sites, with the concomitant formation of oxygenated by-products. The study of the real actives sites is very challenging to perform in this situation, considering that once the reduced Cr sites are formed, they immediately react with ethylene. For this reason, in last seventy years, the investigation of Cr reduced sites was performed on model catalysts obtained by several alternatives that have been used to produce supported chromium already in a reduced state. One of the most successful method was the thermal reduction of the catalyst at 350°C by means of CO. The pre-reduced catalyst is able to polymerize ethylene already at room temperature without induction periods, and it turned out to be a more facilitated system to be studied from a spectroscopic point of view.

3.1 The Phillips catalyst in its oxidized form: Cr(VI)/SiO$_2$

About the oxidation state of the chromium species formed during the induction time, there is a general consensus on that Cr(II) sites are mainly formed during this step[1-7]. Concerning the oxygenated by-products, formaldehyde has been long claimed as the most probable one[8-13], but recent experiments performed in *operando* conditions pointed out that more complex species (such as ketones, carboxylic acids, or esters) are actually formed and, more important, retained on the chromium sites (and likely also at the silica surface), at least during the initiation of the ethylene polymerization reaction [14, 15].

One of the most debated question concerns the mechanism through which ethylene at first reduces the Cr sites and then initiates the polymerization. Several proposals in literature have been formulated, most of them involving reduced Cr sites (either Cr(II) sites or Cr(III) sites [1, 6, 16]), but nowadays there are no unequivocal experimental proofs to support a thesis or the others. From a practical point of view, the most difficult step to overcome is distinguishing between the chromates reduction and the starting of the polymerization. For this reason, the easiest way explored by researchers in the past was to separate the formation of the active sites from the ethylene polymerization, either by pre-activating the chromate precursor with an external reducing agent before the ethylene injection[1-5], or by starting from ad-hoc synthesized organometallic systems in a well-defined reduced oxidation state[1, 16, 17].The approaches made separating the two steps of the formation of the actives sites and the sites involved in the ethylene polymerization, although useful for a fundamental understanding, lead to the production of different polyethylene grades with respect to the traditional Phillips catalyst, suggesting that the structure of the Cr sites is not the same in all the cases and strongly depends on the preparation process. The only way to have a complete vision of the active sites in the ethylene-reduced Cr/SiO$_2$ catalyst is to observe it under the real reaction conditions, exploiting the by now mature technology of advanced *operando* spectroscopies [1, 5, 18-20].

3.1.1 The reaction of Cr(VI)/SiO$_2$ with ethylene: the question of the Cr oxidation state addressed by DR UV-Vis and EPR spectroscopies.

DR UV-Vis and EPR spectroscopies are probably two of the most powerful techniques to determine the oxidation state of the chromium sites and their

coordination geometry. However, both techniques present some "risks". As far as DR UV-Vis spectroscopy is concerned, the following two arguments are often criticized: i) the electronic transitions give rise to broad and overlapping bands, ii) whose positions depend on both the oxidation state and the coordination geometry of the chromium sites, which are difficult to disentangle[21]. On the other hand, the EPR spectroscopy of Cr/SiO$_2$ Phillips catalysts is particularly delicate because of the possible co-presence of several Cr oxidation and spin states, not always detectable at conventional frequencies and temperatures. Cr(III) (d^3, S=3/2) and Cr(V) (d^1 S=1/2) species are the typical EPR active species observed[22, 23].

Figure 3. 1 shows the pictures of the Cr(VI)/SiO$_2$ catalyst prepared in form of thick pellet before the ethylene dosage (part a), after the induction time (part b) and after ethylene polymerization (part c). Clearly, some color changes are observable, even visually. In fact, at each step, the catalyst is characterized by a specific color, which is linked to the different oxidation states of the Cr sites and can be investigated more in details by DR UV-Vis spectroscopy.

Cr^{VI}/SiO_2 Cr/SiO_2 red $Cr/SiO_2 + PE$
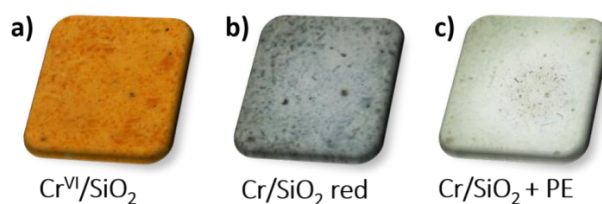
Figure 3. 1 Pictures of the Cr^{VI}/SiO$_2$ catalyst a) before the ethylene dosage, b) after the reduction by ethylene and c) after the complete ethylene polymerization.

The spectrum of the oxidized Cr^{VI}/SiO$_2$ catalyst (spectrum 1 in Figure 3. 1a) displays three intense bands at about 21500, 29000 and 39500 cm^{-1}, which are assigned to the charge-transfer transitions of grafted mono-chromate species, while no absorptions are observed in the region of the d-d transitions, because Cr(VI) is a d^0 transition metal[23-25]. In particular, the absorption band at 21500 cm^{-1} which gives the distinctive orange color (Figure 3. 1a), was attributed to the O → Cr^{VI} charge-transfer transition of the Cr^{VI}(=O)$_2$ moiety and was assumed as the fingerprint of highly diluted mono-chromate species.

Figure 3. 2a shows the evolution of the DR UV-Vis-NIR spectra during the reduction of Cr^{VI}/SiO$_2$ in presence of ethylene at about 150 °C, and before the onset of ethylene polymerization. The reaction temperature is slightly higher with respect to that employed in industrial conditions, and was chosen to compensate the low ethylene pressure. During the reaction all the absorption bands ascribed

to chromates gradually decrease in intensity (especially the one at 21500 cm^{-1}), in favor of two weaker bands at lower frequencies in the d-d region (at ca. 9500 and 16700 cm^{-1}, with a shoulder at 15000 cm^{-1}), attributable to reduced chromium species[6, 26]. At the end of this step, the color of the sample is bluish (Figure 3. 1b).
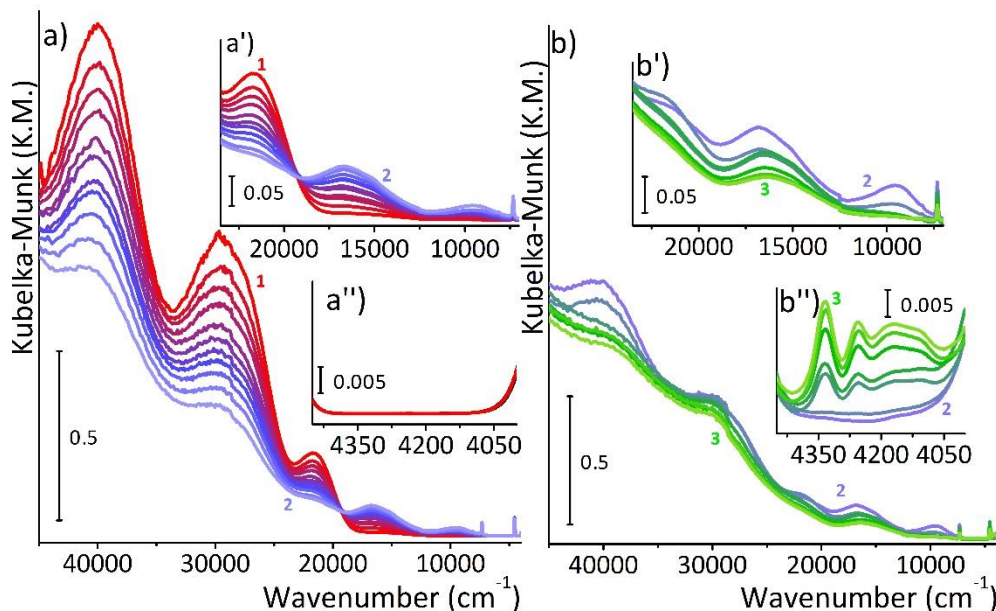
Figure 3. 2 Evolution of the DR UV-Vis-NIR spectra upon ethylene reaction at 150 °C (gas flow of 20 mL/min) on the Cr^{VI}/SiO$_2$ catalyst, both during the induction period (from spectrum 1 to spectrum 2 in part a) and during ethylene polymerization (from spectrum 2 to spectrum 3 in part b). The part a') and b') show a magnification of the d-d region, and the parts a'') and b'') a magnification of the NIR region.

The assignment of the bands in spectrum 2 is not straightforward, because they are the result of several contributions, including some still unreduced Cr^{VI} species (as testified by the residues of the band at 21500 cm^{-1}). In particular, the bands at 9500 and 16700 cm^{-1} could be assigned both to Cr(II) or Cr(III) reduced species. As a matter of fact, low-spin Cr(II) complexes in a perfect octahedral environment present a single $^5E_g \rightarrow ^5T_{2g}$ transition band in the 20000-10000 cm^{-1} range (e.g. at 14000 cm^{-1} for Cr^{2+}(H$_2$O)$_6$). Such band is split into two components when these complexes undergo a tetragonal distortion (from O$_h$ to D$_{4h}$ symmetry), a contribution in the visible and another one in the near-infrared region (extending downwards up to 10000 cm^{-1} in some cases)[21, 27, 28]. On the contrary, the salts of trivalent chromium usually give in water light green solutions, with two intense bands at 17000 cm^{-1} and 24000 cm^{-1} due to the transitions from the $^4A_{2g}$ ground term to the ^4T_g terms. In particular, the band at 17000 cm^{-1} is due to the $^4A_{2g} \rightarrow ^4T_{2g}$

transition and the 24000 cm^{-1} to the $^4A_{2g} \rightarrow {}^4T_{1g}$ transition[21]. On these basis, the band at ca. 9500 cm^{-1} supports the presence of Cr(II) species, being too low in energy to be attributed to Cr(III) ones. This assignment is validated by the similarity of spectrum 2 in Figure 3. 2a with the spectrum of Cr(VI)/SiO$_2$ reduced by cyclohexene, for which the presence of 6-fold Cr(II) species in interaction with an ester was demonstrated by independent techniques[29]. Hence, at the end of the induction period, Cr(VI) sites are reduced mainly to Cr(II) species in a distorted octahedral coordination, although the co-presence of a minor fraction of Cr(III) species cannot be excluded.

After an induction time of about 40 minutes, the polymerization starts. The polymer growth is outlined by the appearance of the typical absorption bands in the NIR region (inset in Figure 3. 2b), where the overtones and combination of stretching and bending modes of the CH$_2$ moieties belonging to the polyethylene are visible. At the same time, the bands in the d-d region attributed to the Cr(II) species decrease in intensity and no new bands are observable during the reaction. The first observation clearly indicates that the Cr(II) species are involved in ethylene polymerization. Concerning the reason why no new bands are observed in the DR UV-Vis spectra, this was ascribed to the fact that, as soon as the Cr sites begin to work, they are shielded by the growing polyethylene and rapidly become invisible to the spectrophotometer. And this is also the reason why at the end of the polymerization process, the whole spectrum (spectrum 3 in Figure 3. 2b) is characterized by a general loss of intensity, because the layer of polyethylene around the catalyst particles changes their scattering properties. This effect is macroscopically visible, since the sample appears white after the polymerization (Figure 3. 1c). The spectrum at the end of the ethylene polymerization reaction still shows two very weak bands in the d-d region that can be ascribed to reduced chromium sites not involved in the polymerization (compatible with both Cr(II) and Cr(III) in 6-fold coordination), and a band linked to unreacted chromates. Hence, ethylene polymerization takes place in presence of some residual chromates, that could have an influence on the activity of the catalyst, maybe enhancing the strain at the silica surface and modifying the chemical environment around the active species (i.e., the bond Cr-O of the chromates is shorter respect to the reduced chromium sites) [11, 30, 31].

As a complementary experiment, we performed a detailed X- band EPR investigation, aimed at establishing the Cr oxidation and spin states before and after reaction with ethylene. In this case the occurrence of the polymerization was testified by the decrease in ethylene pressure and univocally proven at the end of

the experiment by the whitish coverage around the catalyst particles and by FT-IR spectroscopy in ATR mode (Figure 3. 3c). The EPR results are reported in Figure 3. 3. Before the introduction of ethylene, the Cr^{VI}/SiO_2 is characterized by pseudo axial resonances in the g region 1.895-1.979 (spectrum 1 in Figure 3. 3Figure 3. 1a), which is due to residual Cr(V) species, detected in the X-band EPR spectrum of Cr^{VI}/SiO_2 since the early 1990s[32-35], and usually considered as spectators.

Upon reaction with ethylene, a marked change in the EPR spectrum occurs in both the low-field (100-225 mT, Figure 3. 3a') and mid-field (320-370 mT, Figure 3. 3a'') spectral regions. After 10 minutes of reaction with ethylene the EPR signals associated to Cr(V) species decrease in intensity. After 30 min of reaction a further decrease in intensity, accompanied by a g shift and a change in the spectral profile in the g_e region, is observed, together with the appearance of a new complex signal in the low field region (Figure 3. 3a') at $g \approx 4.3$. This signal is the fingerprint of Cr(III) (d^3, S=3/2) species and further increases in intensity for prolonged reaction times.
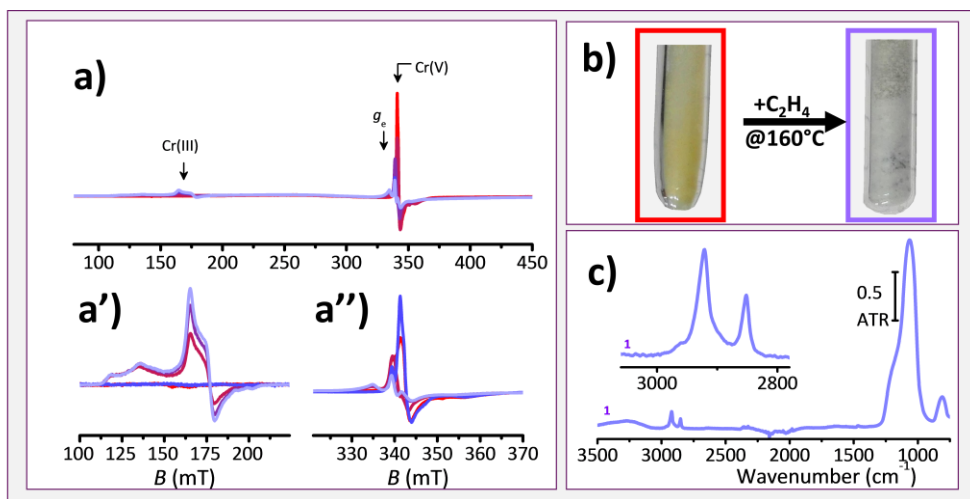
Figure 3. 3 a) X-band CW-EPR spectra of Cr(VI)/SiO₂ (red trace) and upon reaction with ethylene at 150 °C for 10 min, 30 min, 1 h and 2 h (violet trace). Panels a') and a'') show the enlargements of the low- and mid-field spectral regions. The spectra were recorded at T = 77 K, with microwave power of 1 mW. b) Pictures of the Cr(VI)/SiO₂ before and after reaction with C₂H₄; c) ATR FT-IR spectrum of the Cr/SiO₂ catalyst after ethylene polymerization.

Simulation of the spectra taken at different reaction steps (before reaction, after 30 min, and after 2 h of reaction with ethylene) allows estimating the relative contribution of the different species as a function of the reaction evolution (Figure 3. 4). The overall contribution of Cr(V) is found to decrease from 99 ± 1% to 13 ±

2% after 30 min of reaction to 4 ± 3% at the end of the reaction, while the corresponding contribution of the overall Cr(III) species is found to increase from 1 ± 1% up to 96 ± 3% [36]. Although it is not possible to exclude that a fraction of these Cr(III) sites derive from the reduction of Cr(VI), the correlation with the disappearance of the Cr(V) signal suggests that most of the detected Cr(III) species originate from the reduction of Cr(V).
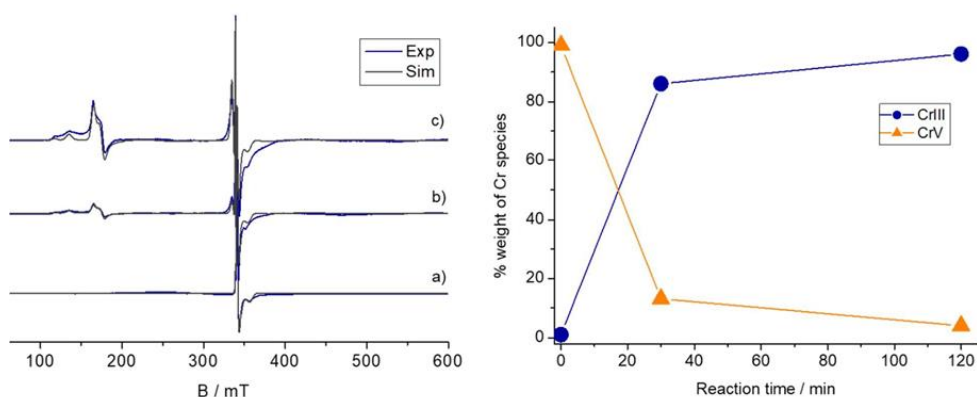
Figure 3. 4 Experimental (blue) and simulated (grey) X-band EPR spectra of the Cr(VI)/SiO$_2$ sample at different stages of reaction with ethylene. a) oxidized sample before reaction; b) after reaction with ethylene at 150 °C for 30 min, c) after reaction with ethylene for 2h. All spectra were recorded at 77K. The simulation was carried out using the same spin Hamiltonian parameters reported in Table 1 of the main text and varying the relative abundance of the different species. The % of the total Cr(III) and Cr(V) species at the different stages of reaction is plotted on the right hand side of the figure.

Although it is not possible to exclude that a fraction of these Cr(III) sites derive from the reduction of Cr(VI), the correlation with the disappearance of the Cr(V) signal suggests that most of the detected Cr(III) species originate from the reduction of Cr(V).

3.1.2 The reaction of Cr(VI)/SiO$_2$ with ethylene: detection of the oxidized by-products by operando FT-IR spectroscopy.

In order to achieve more information about the reaction between ethylene and Cr(VI)/SiO$_2$, we analysed the output stream from the reactor with an online mass spectrometer during all the reaction, aimed at detecting eventual volatile oxidized by-products. However, only a few traces of masses diverse from ethylene were detected, and in particular a few traces of formaldehyde. This implicates that most of the by-products are not volatile, and retained on the catalyst surface.

For this reason, we investigated the same reaction by *operando* FT-IR spectroscopy. The evolution of the FT-IR spectra of Cr(VI)/SiO$_2$ recorded in

presence of ethylene at 150 °C is shown in Figure 3. 5a. Spectrum 1 shows the well-known features of a dehydroxylated silica, with the characteristic band of the free silanol at 3748 cm^{-1} and the silica overtone in the 2100-1500 cm^{-1} range. The presence of the chromates at the silica surface is revealed by the very weak band around 1980 cm^{-1}, which was attributed to the first overtone of the ν(Cr=O) vibrational mode[6, 37, 38]. In presence of ethylene at 150 °C a few IR absorption bands gradually grow at 2892 and 2865 cm^{-1} (typical IR region for ν(CH$_x$) modes), along with two more intense bands at 1617 and 1573 cm^{-1}. Despite several functional group can present a manifestation in that spectral region, the assignment of these bands to vibrations involving oxygenated species is straightforward due to their extremely high intensity with respect to the ν(CH$_x$) modes. Indeed, only chemical groups with high extinction coefficients (such as organic carbonyls, formates and others) can result in such intense manifestations[39-42], while the ν(C=C) modes, although compatible in terms of position, would give much weaker absorption bands[43-46].
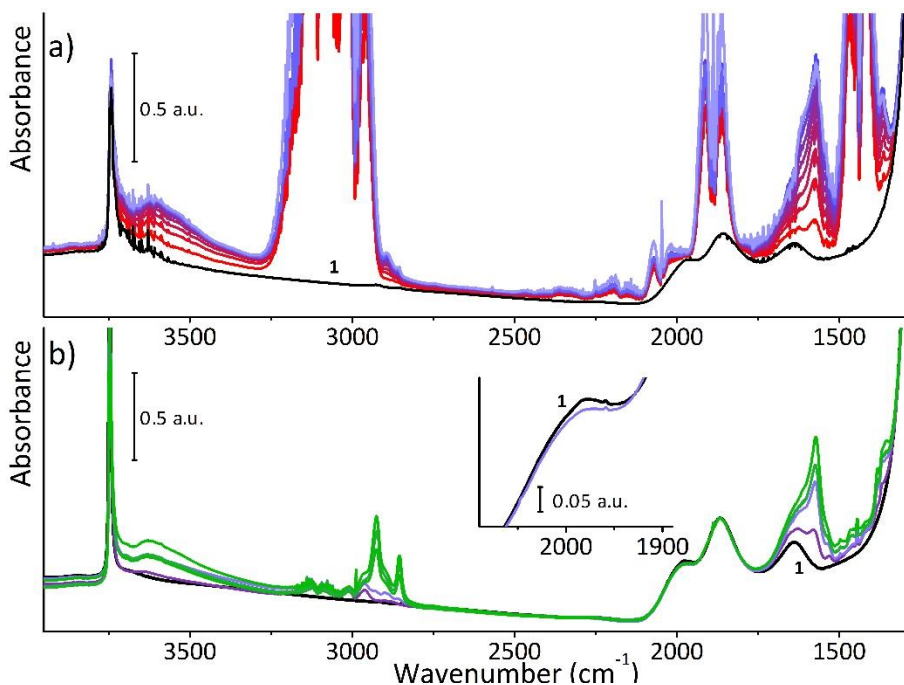
Figure 3. 5 Time evolution of the spectra for the Cr^{VI}/SiO$_2$ catalyst (bold black) during reduction with ethylene (from black to bold violet) and during ethylene polymerization at 150 °C (from violet to bold green). Part (a): Operando FT-IR spectra. Part (b): FT-IR spectra collected in static conditions. In the inset a magnification of the chromate region.

A clear and complete analysis of the adsorbed species can be achieved analysing the Mid-IR spectral region in its totality. As soon as ethylene is flowed into the reaction cell, all the FT-IR spectra are dominated by the absorption bands of the gaseous ethylene (Figure 3. 5a). This greatly limits the observation of the oxidized by-products. In order to overcome this spectroscopic problem, a FT-IR experiment in static condition was designed (150 °C, PC_2H_4 = 100 mbar, Figure 3. 5b). This experiment allowed us observing: 1) the chromate reduction, because the band at 1980 cm^{-1} (inset in Figure 3. 5b) gradually decreases in intensity; 2) the formation of the oxidized by-products, characterized by absorption bands at 2955, 2892, 2865, 2747, 1617, 1573, 1455, 1383 and 1369 cm^{-1}, before the onset of ethylene polymerization.

Although formaldehyde has been claimed for a long time as the main by-product of the reaction between Cr^{VI}/SiO_2 and ethylene, the observed bands cannot be assigned to formaldehyde as such, but rather to some oxygenated molecules derived from a rearrangement of formaldehyde on the Cr(II) sites. In particular, our most accredited species is methylformate, which is formed by disproportionation of two formaldehyde molecules at the same Cr(II) site, through the so called Tischenko reaction [29, 47-52]. A complete assignment of all the absorption bands associated to the by-products is reported in Table 1.

Table 1. Position (in wavenumbers, cm^{-1}) and relative intensity (vs = very strong, s = strong, m = medium, w = weak) of the IR absorption bands attributed to ethylene oxidation products in interaction with the ethylene reduced Cr^{VI}/SiO_2 catalyst

Observed bands (cm^{-1})	Assignment
2955 (s)	$\nu_{asymm}(OCO) + \delta(CH)$ $\nu_{asymm}(CH_3)$
2892 (s)	$\nu_{symm}(CH3)$
2865 (s)	$\nu(CH)$
2747 (w)	$\nu_{symm}(OCO) + \delta(CH)$
1617, 1573 (vs)	$\nu_{asymm}(OCO)$
1455 (m)	$\delta(CH_3)$
1383 (s)	$\delta(CH)$
1369 (vs)	$\nu_{symm}(OCO)$

A possible reaction pathway is shown in Scheme 1, wherein ethylene reduces a chromate forming two molecules of formaldehyde (as proposed in the literature), which immediately rearrange on the Cr(II) sites, to give a methylformate molecule.
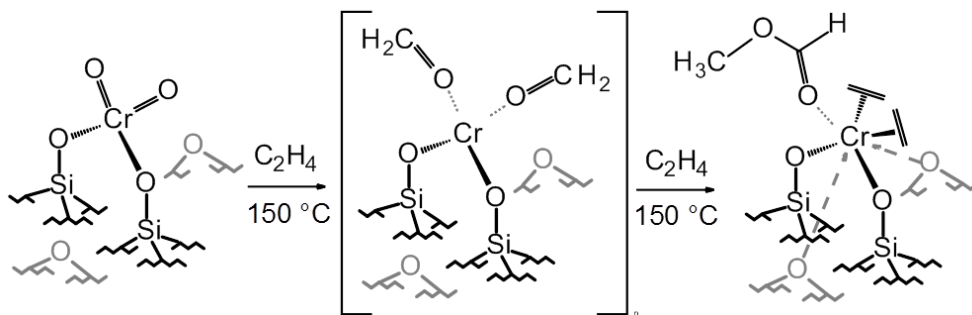
Scheme 1 Possible reaction pathway for the reaction between ethylene on the Cr^{VI}/SiO_2 catalyst at 150 °C, during the induction period.

3.1.3 The reaction of Cr(VI)/SiO$_2$ with ethylene: a kinetic study.

The ethylene polymerization activity of Cr(VI)/SiO$_2$ in our experimental conditions was determined by measuring with a capacitive pressure gauge the decrease of ethylene pressure as a function of the time. A starting ethylene pressure of 200 mbar was dosed on the catalyst at 150 °C, and the ethylene pressure was registered every 10 minutes during the induction time, and every 30 seconds when the polymerization started, as reported in Figure 3. 6. During the first 40 minutes, almost no changes are observable in the pressure value. This corresponds to the induction time, during which the chromates are reduced by ethylene. After this time, the ethylene pressure progressively decreases with an almost linear trend and only at the end of the reaction a change in the slope is observed, likely because the ethylene pressure becomes too low.

The polymerization rate was evaluated by excluding the induction time and considering the reaction as a first order reaction, as proposed in the literature [53-55]. The rate law for polymerization at low ethylene pressure is as follows:

$$\frac{dP(C_2H_4)}{dt} = -kP(C_2H_4)$$

Hence, by plotting the $lnP(C_2H_4)$ versus time during the first ten minutes of the polymerization, it is possible to estimate the rate constant k as the slope of the linear trend. A value of k = 7.7 s^{-1}molCr^{-1} was obtained.
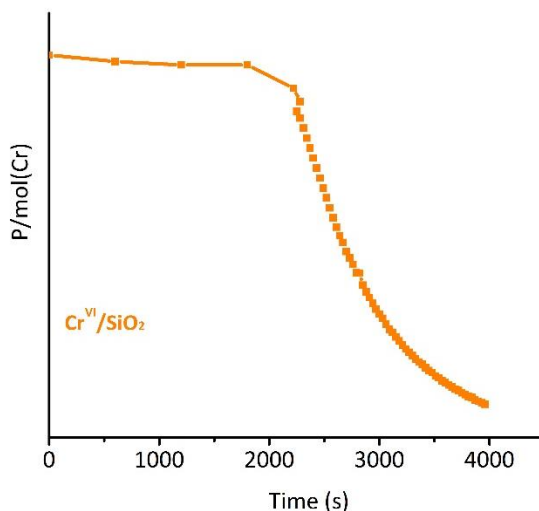
Figure 3. 6 Kinetics of ethylene polymerisation on Cr^{VI}/SiO_2 catalyst, obtained by recording ethylene pressure as a function of time at 150 °C degrees.

3.1.4 The reaction of Cr(VI)/SiO$_2$ with ethylene: the emerging picture.

The accurate analysis of all the spectroscopic data discussed above led to the following conclusions:

1. During the induction time, the chromates species are reduced mainly to Cr(II) species in interaction with oxidized by-products (such as methylformate), and other reduced species not clearly identifiable (either 6-fold Cr(III) or 6-fold Cr(II) species) that do not participate to the polymerization reaction.
2. Ethylene polymerization starts and proceeds in the presence of residual, slowly reducible, chromates.
3. The oxidized by-products (such as methylformate) remain in the coordination sphere of the Cr sites also during the initial steps of ethylene polymerization, and have to be considered as important participants in the catalysis.

It is clear that the old vision of "naked" chromium sites is exceeded and cannot be anymore considered as a reliable model for the industrial catalyst. Hence, in designing new variants of the Phillips catalyst, one should always take into account not only the oxidation state, but also the ligands sphere of the Cr sites.

45

3.2 The Phillips catalyst in its reduced form: Cr(II)/SiO₂

The reduced Cr^{II}/SiO$_2$ catalyst is obtained using as reducing agent CO at 350 °C: this treatment converts all the Cr(VI) sites into "naked" Cr(II), since the CO$_2$ by-product is easily removed from the surface at 350°C[1-3, 6, 18, 56]. When ethylene is dosed on Cr^{II}/SiO$_2$, the polymerization starts immediately without any induction time. This is the reason why the CO-reduced Phillips catalyst has been widely adopted as a model system to investigate the initiation mechanism. Nevertheless, the polyethylene produced on the reduced catalyst is slightly different from the one produced on the oxidized catalyst, displaying a slightly higher M$_W$ and a better co-monomer incorporation efficiency [1, 57]. These differences imply that the precursors of the active sites are different in the two cases. In this respect, it is useful to recall here the most important spectroscopic details on Cr(II)/SiO$_2$.

3.2.1 Properties of Cr(II)/SiO₂ as determined by multiple spectroscopic methods

Upon reduction of Cr(VI)/SiO$_2$ in CO at 350 °C, the colour of the catalyst changes from orange to light-blue (Figure 3. 7d). Correspondingly, the DR UV-Vis spectrum (curve 2 in Figure 3. 7a) greatly changes. In particular: 1) a strong band appears at 30000 cm^{-1}, straightforwardly assigned to an oxygen to chromium (O $\rightarrow$ Cr) charge transfer transition; 2) the band at about 21500 cm^{-1}, previously assigned to the charge transfer transition of grafted mono-chromate species, disappears; and 3) two broad bands at 7500 and 12000 cm^{-1} appear, which are assigned to d-d transitions of 4-fold coordinated Cr$^{2+}_{4c}$ species [5, 24, 25, 58-60]. Cr(II) species are characterized by a non-Kramer spin state (S=2), and hence are EPR silent at conventional frequency-field conditions. This is why EPR at X-band (spectrum 2 in Figure 3. 7b) monitors only the disappearance of the Cr(V) signal and no new signals became visible after the reduction. It is important to notice that, when the activation procedure is correctly performed, no Cr(III) species are detected.
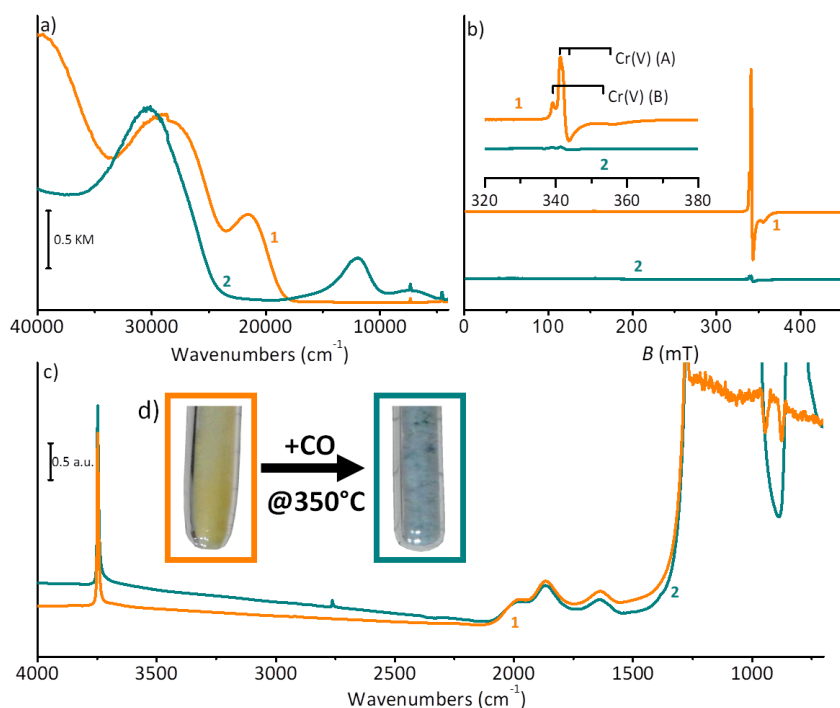
Figure 3. 7 Part a) DR UV-Vis-NIR, Part b) X-band CW-EPR, part C) FT-IR, spectra of the oxidized (spectrum 1) and reduced (spectrum 2) Cr/SiO₂ catalyst. The inset shows the enlargement of the mid-field region. Part d) the pictures of the oxidized and reduced catalyst.

In the FT-IR spectra, the most evident change observed after CO reduction is the disappearance of a band at about 910 cm^{-1}, in the so-called "window of transparency of silica". This band, observed in the spectrum of Cr(VI)/SiO₂, (spectrum 1 in Figure 3. 7c) is due to the perturbation of the SiO₂ vibration modes induced by the presence of chromates. In addition, the very weak band around 1980 cm^{-1}, which was attributed to the first overtone of v(Cr=O₂), after the reduction disappears. It is interesting to observe that a very weak band at 1596 cm^{-1} is always observed in the spectrum of Cr(II)/SiO₂. This band was never assigned in the literature, but we have evidences that it is connected with some surface modes of Cr(II)/SiO₂. As a matter of fact, the band is sensitive to the adsorption of molecules on the Cr(II) sites.

The accessibility of the Cr(II) has been traditionally scrutinized by using FT-IR spectroscopy of adsorbed CO. Figure 3. 8 shows the evolution of the DR UV-Vis-NIR (part a) and FT-IR (part b) spectra of Cr^{II}/SiO₂ catalyst as a function of the CO coverage at room temperature.
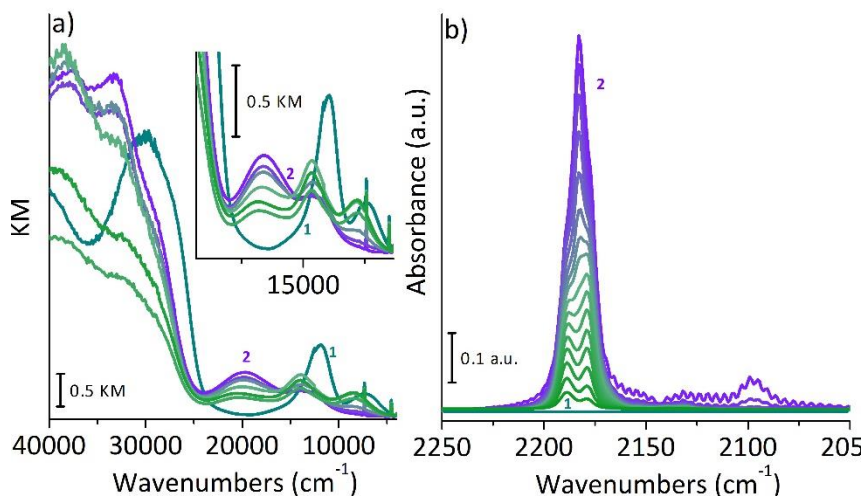
Figure 3. 8 Part a) DR UV-Vis-NIR in the presence of CO (P_{CO} = 100 mbar) at room temperature (spectrum 2). Green spectra show the effect of gradual CO desorption at room temperature. The inset shows a magnification of the d-d region. Part b) Evolution of the FT-IR spectra (magnification of the v(CO) region) upon CO adsorption at room temperature as a function of P_{CO} coverage, from P_{CO} = 100 mbar (spectrum 2) to zero (spectrum 1).

Starting from DR UV-Vis spectroscopy, the d-d bands characteristic of the Cr(II) sites are perturbed by CO adsorption, as a consequence of the increased ligand field [6, 18, 43].In particular, at low CO pressure the bands at 12000 and 7500 cm^{-1} shift at 14000 and 8600 cm^{-1}, because of the formation of mono-carbonyl Cr(II) adducts. At higher CO pressure, the band at 12000 cm^{-1} further shifts up to 20000 cm^{-1}, due to the formation of dicarbonyl Cr(II) species [6]. Analogously, in the CT region, the band centred at ca. 30000 cm^{-1} decreases in intensity, and a new intense band appears at 37000 cm^{-1}, as a consequence of the electron donor properties of CO [6].

Figure 3. 8b shows the FT-IR spectra, in the v(CO) region, of CO adsorbed on Cr(II)/SiO$_2$ as a function of the CO coverage. The spectrum at the maximum CO coverage (violet) presents a characteristic triplet of bands (at 2191, 2184 and 2178 cm^{-1}), which evolves in a doublet at low CO pressures (at 2180 and 2191 cm^{-1}). These spectra have been in terms of two families of Cr(II) sites (Cr$_A$ and Cr$_B$), differing in the number of coordination vacancies available for CO insertion: Cr$_A$ coordinates up to two CO molecules, while Cr$_B$ can coordinate only one CO molecule at room temperature[6]. The evolution of the FT-IR spectra upon decreasing the CO coverage was explained in terms of transformation of a dicarbonyl species on the Cr$_A$ site (bands at 2184 and 2178 cm^{-1}) into a

monocarbonyl (at 2180 cm^{-1}), whereas on the Cr$_B$ site only a monocarbonyl species can be formed even at high CO coverage (band at 2191 cm^{-1}).

3.2.2 The reaction of Cr(II)/SiO$_2$ with ethylene: a kinetic study.

The activity of Cr(II)/SiO$_2$ in ethylene polymerization in our experimental conditions was evaluated by means of a kinetic experiment similar to that discussed for Cr(VI)/SiO$_2$, as reported in Figure 3. 9. The reaction starts immediately, without any induction time, and the ethylene pressure decreases in a perfect linear way, indicating that the reaction is of the first order, as proposed by Ajjou et al [54]. By plotting the $lnP(C_2H_4)$ versus time, a rate constant k = 14 s$^-$^{1}molCr^{-1} was determined, which is almost the double of that observed for ethylene polymerization on Cr(VI)/SiO$_2$.

This difference could be due to several factors: 1) in Cr(VI)/SiO$_2$ the polymerization starts in the presence of a fraction of still unreduced Cr(VI) species, and 2) in Cr(VI)/SiO$_2$ the precursors of the actives sites do have in the coordination sphere the oxidized by-products.
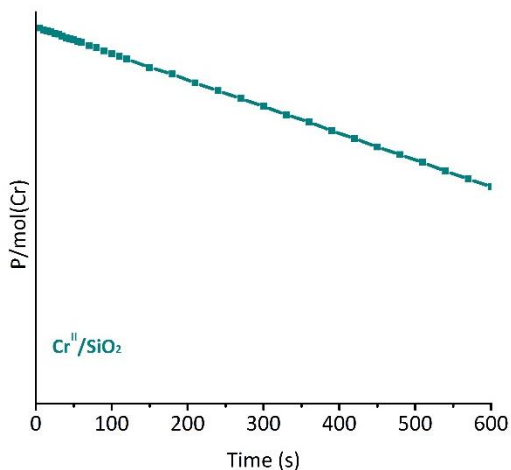
Figure 3. 9 Kinetics of ethylene polymerisation on Cr^{II}/SiO$_2$ catalysts, obtained by recording ethylene pressure as a function of time.

3.2.3 The reaction of Cr(II)/SiO$_2$ with ethylene: a spectroscopic study.

Ethylene polymerization on Cr(II)/SiO$_2$ was monitored by means of DR UV-Vis, EPR and FT-IR spectroscopies, as summarized in Figure 3. 10. Upon ethylene dosage, the DR UV-Vis spectrum of Cr(II)/SiO$_2$ (part a) immediately changes: the d-d bands previously ascribed to Cr$^{2+}_{4c}$ sites are gradually eroded and shifted to 16500 and 13500 cm^{-1}, while the intense CT band shifts at 35000 cm^{-1}. These changes are very similar to those observed in the presence of CO, and simply reveal that all the Cr(II)

sites got in contact with ethylene. Meanwhile, weak bands grow in the 4500-4000 cm^{-1} region, where overtones and combinations of the stretching and bending vibrational modes of polyethylene are located (inset in Figure 3. 10a). These results provide a strong evidence that the Cr^{2+}_{4c} sites are those involved in ethylene polymerization. However, the disappearance of the spectroscopic fingerprints of Cr^{2+}_{4c} is not accompanied by the appearance of any additional band that could reveal the destiny of the active sites. Likely, the Cr active sites remain buried into a layer of polyethylene and become rapidly invisible to DR UV-Vis-NIR. This is macroscopically visible in the aspect of the sample that progressively becomes white.
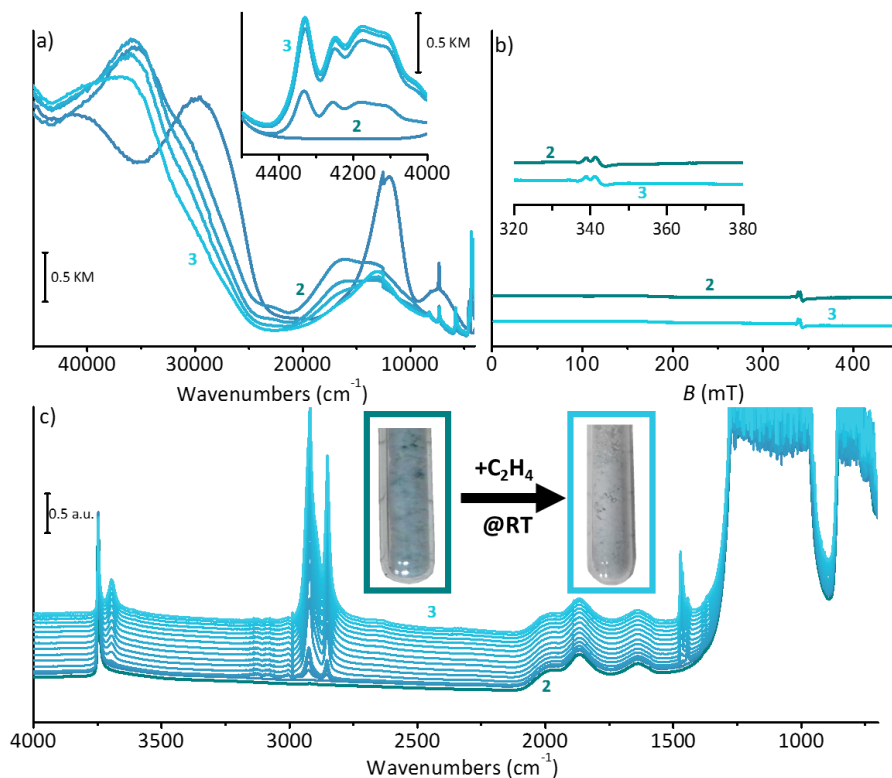
Figure 3. 10 Part a) Evolution of the DR UV-Vis-NIR spectra upon ethylene reaction at room temperature on the $Cr(II)/SiO_2$ catalyst (from spectrum 2 to spectrum 3). The inset shows a magnification of the NIR region. Part b) X-band CW-EPR spectra of the $Cr(II)/SiO_2$ before (spectrum 2) and after reaction with ethylene at room temperature (spectrum 3). The inset shows the enlargement of the mid-field region. Part c) Time evolution of FT-IR spectra for the Cr^{II}/SiO_2 catalyst during ethylene polymerization (from spectrum 2 to spectrum 3). In the inset the pictures of the catalyst before and after the polymerization.

This does not mean that UV-Vis spectroscopy is not useful in the investigation of these systems, but that the results must be interpreted with caution and in combination with other methods. For this reason, we monitored the same experiment by EPR spectroscopy, recording at the end of the reaction an ATR spectrum of the sample, in order to confirm *a posteriori* the presence of the polymer. Ethylene (P = 100 mbar) was admitted on the sample at room temperature and after 10 minutes the reaction was quenched with liquid nitrogen and an EPR spectrum was collected (spectrum 3 in Figure 3. 10b). We do not observe any change in the EPR spectra before and after ethylene polymerization. These results indicate that, under these experimental conditions, the active Cr sites originated by reacting Cr(II)/SiO$_2$ with ethylene at room temperature are not EPR active.

Finally, Figure 3. 10 shows the time-resolved FT-IR spectra collected during ethylene polymerization on Cr(II)/SiO$_2$, at P_{C2H4} = 100 mbar and room temperature. The occurrence of ethylene polymerization is indicated by the growth of the IR absorption bands characteristic of polyethylene: two bands at 2920 and 2851 cm^{-1}, growing with time at nearly constant rates, which are readily assigned to the asymmetric and symmetric stretching vibrations of CH$_2$ groups of living polymeric chains. Other two bands are formed at 1472 and 1463 cm^{-1}. They have been assigned to the bending modes of CH$_2$, the former typical of crystalline PE, the latter in common to both the crystalline and the molten phase. Their relative intensity indicates that the produced polyethylene is highly crystalline also at short polymerization time, as evidenced by the predominance of the band at 1472 cm^{-1} [61]. Finally at long polymerization time, i.e. for high polyethylene content, also the ν(OH) bands are perturbed, as a consequence of the interaction of the surface silanol groups with the polyethylene chains [8].

3.2.4 Before going on: a short summary on the properties of the unmodified Cr^{II}/SiO$_2$ Phillips catalyst.

Before going on with the "story" of the modified Al-alkyls systems (which have a greater degree of complexity) a short summary on the Cr(II)/SiO$_2$ sample is request, with a little help of some pictures.

1. The support plays an important role in determining the properties of the chromium sites.
2. On Cr(II)/SiO$_2$, the Cr(II) sites are isolated, in a divalent state and highly uncoordinated, as shown in Scheme 2.
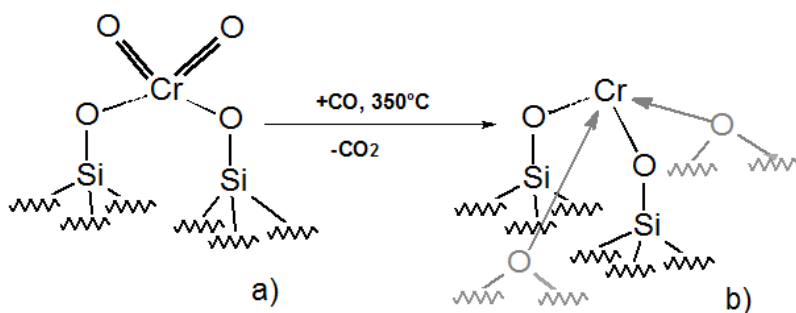
Scheme 2 Schematic representation of the structure of the oxidized (a) and reduced (b) forms of Cr/SiO$_2$ catalyst.

3. Due to the amorphous character of the support, different families of Cr(II) structures are present on the silica surface, which can be identified via accurate spectroscopic methods and classified into three distinct families (Cr$_A$, Cr$_B$, and Cr$_C$), depending on the number of coordination vacancies available at room temperature, as shown in Scheme 3.
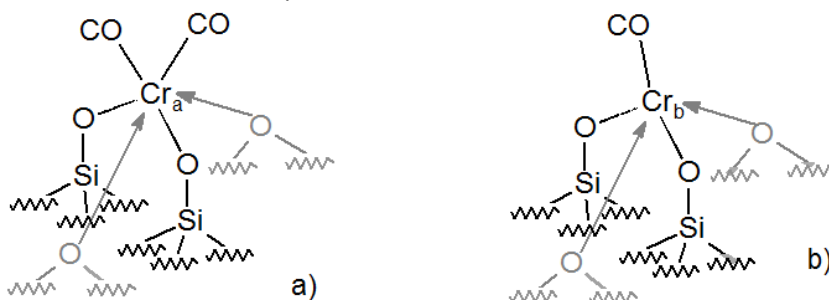
Scheme 3 Schematic Picture of CO adsorption to isolated Cr$_a$ sites (a) and to Cr$_b$ sites (b).

4. The synergic use of different and complementary spectroscopic techniques is mandatory for obtaining detailed information on the molecular-level structure of the chromium sites.

References

[1] M.P. McDaniel, Adv. Catal., 53 (2010) 123-606.

[2] v.H.L. Krauss, H. Stach, Inorg. Nucl. Chem. Lett., 4 (1968) 393-397.

[3] H.L. Krauss, H. Stach, Z. Anorg. Allg. Chem., 366 (1969) 34-42.

[4] J.N. Finch, J. Catal., 43 (1976) 111.

[5] A. Zecchina, E. Garrone, G. Ghiotti, C. Morterra, E. Borello, J. Phys. Chem., 79 (1975) 966-972.

[6] E. Groppo, C. Lamberti, S. Bordiga, G. Spoto, A. Zecchina, Chem. Rev., 105 (2005) 115-183.

[7] C. Brown, J. Krzystek, R. Achey, A. Lita, R. Fu, R.W. Meulenberg, M. Polinski, N. Peek, Y. Wang, L.J. Van De Burgt, S. Profeta, A.E. Stiegman, S.L. Scott, ACS Catal., 5 (2015) 5574-5583.

[8] R. Cheng, Z. Liu, L. Zhong, X. He, P. Qiu, M. Terano, M.S. Eisen, S.L. Scott, B. Liu, Adv. Polym. Sci., 257 (2013) 135-202.

[9] Z. Liu, X. He, R. Cheng, M.S. Eisen, M. Terano, S.L. Scott, B. Liu, Chromium catalysts for ethylene polymerization and oligomerization, in: Adv. Chem. Eng., 2014, pp. 126-191.

[10] B. Liu, H. Nakatani, M. Terano, J Mol Catal a-Chem, 184 (2002) 387-398.

[11] B.P. Liu, H. Nakatani, M. Terano, J Mol Catal a-Chem, 201 (2003) 189-197.

[12] W. Xia, B. Liu, Y. Fang, K. Hasebe, M. Terano, J. Mol. Cat. A, 256 (2006) 301-308.

[13] L. Zhong, Z. Liu, R. Cheng, S. Tang, P. Qiu, X. He, M. Terano, B. Liu, Chemcatchem, (2012).

[14] K.C. Potter, C.W. Beckerle, F.C. Jentoft, E. Schwerdtfeger, M.P. McDaniel, J. Catal., 344 (2016) 657-668.

[15] C. Barzan, A. Piovano, L. Braglia, G.A. Martino, C. Lamberti, S. Bordiga, E. Groppo, JACS, 139 (2017) 17064-17073.

[16] C. Coperet, M. Chabanas, R.P. Saint-Arroman, J.M. Basset, Angew. Chem.-Int. Edit., 42 (2003) 156-181 and references therein.

[17] C. Coperet, J.M. Basset, Adv. Synth. Catal., 349 (2007) 78-92.

[18] A. Zecchina, E. Garrone, G. Ghiotti, S. Coluccia, J. Phys. Chem., 79 (1975) 972-978.

[19] A. Zecchina, E. Garrone, C. Morterra, S. Coluccia, J. Phys. Chem., 79 (1975) 978-983.

[20] B.M. Weckhuysen, PCCP, 5 (2003) 4351-4360.

[21] B.N. Figgis, Introduction to ligand fields, John Wiley & Sons, New York, 1966.

[22] B.M. Weckhuysen, R.A. Schoonheydt, F.E. Mabbs, D. Collison, J Chem Soc Faraday T, 92 (1996) 2431-2436.

[23] B.M. Weckhuysen, L.M. Deridder, P.J. Grobet, R.A. Schoonheydt, J. Phys. Chem., 99 (1995) 320-326.

[24] B.M. Weckhuysen, L.M. Deridder, R.A. Schoonheydt, J. Phys. Chem., 97 (1993) 4756-4763.

[25] B.M. Weckhuysen, R.A. Schoonheydt, J.M. Jehng, I.E. Wachs, S.J. Cho, R. Ryoo, S. Kijlstra, E. Poels, J Chem Soc Faraday T, 91 (1995) 3245-3253.

[26] B.M. Weckhuysen, I.E. Wachs, R.A. Shoonheydt, Chem. Rev., 96 (1996) 3327-3349.

[27] R.J.H. Clark, J. Chem. Soc., (1964) 417-425.

[28] G.L. Miessler, D.A. Tarr, Inorganic Chemistry, St. Olaf College Northfield, Minnesota.

[29] C. Barzan, A.A. Damin, A. Budnyk, A. Zecchina, S. Bordiga, E. Groppo, J. Catal., 337 (2016) 45-51.

[30] R.H. Cheng, C. Xu, Z. Liu, Q. Dong, X.L. He, Y.W. Fang, M. Terano, Y.T. Hu, T.J. Pullukat, B.P. Liu, J. Catal., 273 (2010) 103-115.

[31] D. Gianolio, E. Groppo, J.G. Vitillo, A. Damin, S. Bordiga, A. Zecchina, C. Lamberti, Chem. Commun., 46 (2010) 976–978.

[32] D. Cordischi, V. Indovina, M. Occhiuzzi, J Chem Soc Faraday T, 87 (1991) 3443-3447.

[33] D. Cordischi, V. Indovina, M. Occhiuzzi, Appl Surf Sci, 55 (1992) 233-237.

[34] D. Cordischi, M.C. Campa, V. Indovina, M. Occhiuzzi, J Chem Soc Faraday T, 90 (1994) 207-212.

[35] C. Groeneveld, P.P.M.M. Wittgen, A.M. Kersbergen van, P.L.M. Hestrom, C.E. Nuijten, G.C.A. Schuit, J. Catal., 59 (1979) 153.

[36] E. Morra, G.A. Martino, A. Piovano, C. Barzan, E. Groppo, M. Chiesa, Journal of Physical Chemistry C, 122 (2018) 21531-21536.

[37] C.A. Demmelmaier, R.E. White, J.A. van Bokhoven, S.L. Scott, J. Catal., 262 (2009) 44-56.

[38] C.A. Demmelmaier, R.E. White, J.A. van Bokhoven, S.L. Scottt, Journal of Physical Chemistry C, 112 (2008) 6439-6449.

[39] G. Busca, V. Lorenzelli, J. Catal., 66 (1980) 155-161.

[40] G. Busca, J. Lamotte, J.C. Lavalley, V. Lorenzelli, J. Am. Chem. Soc. , 109 (1987) 5197-5202.

[41] G. Busca, Catal. Today, 27 (1996) 457-496.

[42] M. Vijayaraj, C.S. Gopinath, J. Catal., 226 (2004) 230-234.

[43] E. Groppo, C. Lamberti, S. Bordiga, G. Spoto, A. Zecchina, J. Phys. Chem. B, 109 (2005) 15024-15031.

[44] C. Barzan, E. Groppo, E.A. Quadrelli, V. Monteil, S. Bordiga, Phys.Chem.Chem.Phys., 14 (2012) 2239–2245.

[45] G. Spoto, S. Bordiga, G. Ricchiardi, D. Scarano, A. Zecchina, E. Borello, J Chem Soc Faraday T, 90 (1994) 2827-2835.

[46] E. Groppo, J. Estephane, C. Lamberti, G. Spoto, A. Zecchina, Catal. Today, 126 (2007) 228-234.

[47] V. Crocellà, G. Cerrato, G. Magnacca, C. Morterra, F. Cavani, L. Maselli, S. Passeri, Dalt.Trans., 39 (2010) 8527-8537.

[48] T. Ooi, T. Miura, Y. Itagaki, H. Ichikawa, K. Maruoka, Synthesis, (2002) 279-291.

[49] M.M. Mojtahedi, E. Akbarzadeh, R. Sharifi, M.S. Abaee, Org. Lett., 9 (2007) 2791-2793.

[50] V. Gnanadesikan, Y. Horiuchi, T. Ohshima, M. Shibasaki, J. Am. Chem. Soc., 126 (2004) 7782-7783.

[51] Y. Hoshimoto, M. Ohashi, S. Ogoshi, J. Am. Chem. Soc., 133 (2011) 4668-4671.

[52] S.P. Curran, S.J. Connon, Angew. Chem. - Int. Ed., 51 (2012) 10866-10870.

[53] S.L. Scott, J. Amor Nait Ajjou, Chem. Eng. Sci., 56 (2001) 4155-4168.

[54] J. Amor Nait Ajjou, S.L. Scott, J. Am. Chem. Soc., 122 (2000) 8968-8976.

[55] J. Amor Nait Ajjou, G.L. Rice, S.L. Scott, J. Am. Chem. Soc., 120 (1998) 13436-13443.

[56] M.P. McDaniel, Adv. Catal., 33 (1985) 47-98.

[57] M. McDaniel, Appl. Catal. A, 542 (2017) 392-410.

[58] H.-L. Krauss, H. Stach, Z. Anorg. Allg. Chem., 414 (1975) 97-108.

[59] B. Fubini, G. Ghiotti, L. Stradella, E. Garrone, C. Morterra, J. Catal., 66 (1980) 200-213.

[60] G. Ghiotti, E. Garrone, G. Della Gatta, B. Fubini, E. Giamello, J. Catal., 80 (1983) 249-262.

[61] D. Chelazzi, M. Ceppatelli, M. Santoro, R. Bini, V. Schettino, Nat. Mater., 3 (2004) 470-475.

Chapter 4
Modification of Cr(II)/SiO$_2$ with Al-alkyls.

This Chapter is devoted to investigate the effect, at a molecular level, of Al-Alkyls on the Cr(II)/SiO$_2$ catalyst. Although Al-alkyls are not necessary to develop the activity, they can be used to enhance it: in the modified systems, the induction time is almost eliminated and the polymerization rate rises to its maximum more quickly [1]. However, the exact basics of the Cr sites modifications by Al-alkyls are still unknown. The scientific literature in this field is very poor, with just a few articles and a few research groups working on these systems [2-11]. Considering these lacunae in the literature, we started working on the well-known Cr(II)/SiO$_2$ catalyst, that has a lower "number of variables" that can influence the interpretation of the data with respect to the industrial catalyst. At first, the chromium sites are "naked" (i.e. highly uncoordinated) and well dispersed on the silica surface without any by-products around (as already discussed in the previous Chapters) [12]. Furthermore, the chromium oxidation state has to be considered always the same upon the catalytic process, because an oxidation reaction is very improbable (Al-alkyls are reducing agents), as well as an over-reduction reaction (the presence of a Cr^I was discarded) [1]. This approach allowed us to create a reference dataset to subsequently study the modification of the more complex Cr(VI)/SiO$_2$ catalyst.

4.1 The reactivity of the Cr(II)/SiO$_2$ with TEA and DEALE

4.1.1 Electronic properties of Cr(II)/SiO$_2$ modified by TEA and DEALE

Figure 4. 1 shows the evolution of the DR UV-Vis-NIR spectra of Cr(II)/SiO$_2$ upon the interaction with TEA (part a) and DEALE (part b), in the stoichiometric ratio of Al:Cr=2:1 (spectra 2) and Al:Cr=4:1 (spectra 3). The spectrum of Cr(II)/SiO$_2$ (spectra 1) has been already discussed in the previous Chapter (Figure 3.6). It would be expected that an amount of TEA (and DEALE) corresponding to two/four times the amount of Cr should be sufficient to modify all the Cr(II) sites, as it was reported in literature [4, 5]. In contrast, the DR UV-Vis-NIR spectra clearly indicate that the effect of TEA on Cr(II)/SiO$_2$ is modest (spectra 2 and 3 in Figure 4. 1a). In particular, while the intense band at about 29000 cm^{-1} decreases abruptly, the two bands in the d-d region at ca. 12000 and 7000 cm^{-1} are only slightly affected in intensity, and a modest shift at higher wavenumbers is observed. These changes suggest that **a fraction of the Cr(II) sites is now characterized by an increased number of ligands** (as described for Cr(II) in interaction with probe molecules, such as CO).
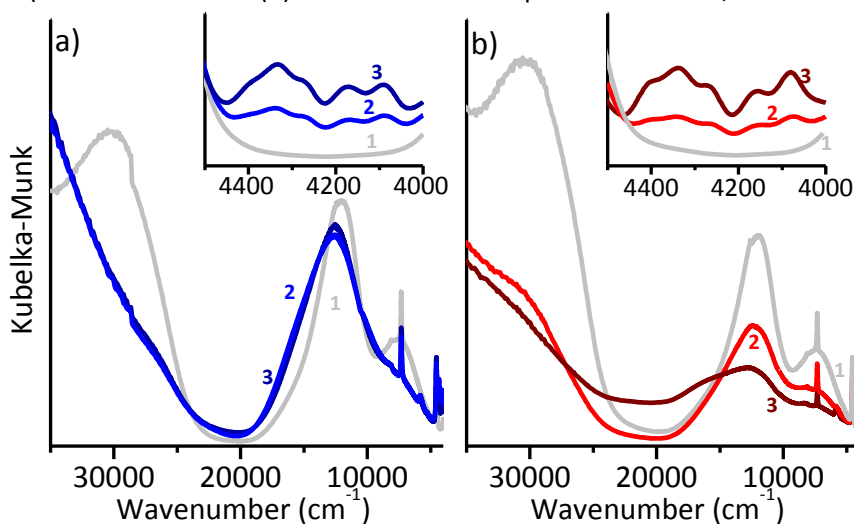
Figure 4. 1. Part a): DR UV-Vis-NIR spectra of Cr(II)/SiO$_2$ (spectrum 1), Cr(II) /SiO$_2$+TEA(2:1) (spectrum 2), and Cr(II) /SiO$_2$+TEA(4:1) (spectrum 3). The inset shows a magnification of the NIR region. Part b): the same of part a, but with DEALE.

The fraction of Cr(II) sites involved by reaction/interaction with TEA does not change upon increasing the amount of TEA (compare spectrum 2 with spectrum 3 in Figure 4. 1a). The only relevant change is detected in the NIR region (in the inset), where a complex series of bands appear, assigned to the overtones and the combinations of the $\nu(CH_x)$ and $\delta(CH_x)$ vibrational modes of the alkyl

groups. The intensity of these bands is directly proportional to the amount of Al-Alkyls used. These data clearly indicate that **TEA reacts not only with the Cr(II) sites, but also with the silica surface**.

The effect of DEALE on the DR UV-Vis-NIR spectrum of Cr(II)/SiO$_2$ is more pronounced (Figure 4. 1b) than that of TEA. In Cr(II)+DEALE(2:1), the bands characteristic of the Cr(II) sites decrease in intensity, while new bands appear in the 4500 – 4000 cm^{-1} region due to the overtones of the vibrational modes of the alkyl species. Also in this case, however, the fraction of Cr(II) sites involved by the reaction/interaction with DEALE is much smaller than expected. The two bands at 12000 and 7500 cm^{-1} characteristic of Cr(II) sites decrease of ca. 30% in intensity. At the same time, no specific features associable with the modified Cr sites are observed. The absence of peculiar spectroscopic fingerprints makes it difficult to unravel their molecular structure. Nevertheless, the observation that the modified Cr sites are almost invisible by UV-Vis spectroscopy might suggest that they have prevalently an octahedral coordination. Indeed, d-d transitions are formally Laporte forbidden for transition metals in octahedral symmetry. Hence, the corresponding bands are expected to have a very low intensity compared to those of the unmodified Cr(II) sites.

In the Cr(II)+DEALE (4:1) catalyst, an additional change is observed in the DR UV-Vis spectrum (spectrum 3 of Figure 4. 1b). The d-d bands characteristic of Cr(II) slightly decrease in intensity, and a new broad band is observed centred at 20000 cm^{-1}. Such a perturbation is typical, as was observed for CO adsorption on the unmodified Cr(II)/SiO$_2$ system, of the increased ligand sphere of the metal in a distorted octahedral geometry[12].

4.1.2 Reactivity of TEA and DEALE with SiO₂ as monitored by FT-IR spectroscopy

Successively, we investigated the effect of TEA and DEALE on pure silica activated at 650 °C, by means of FT-IR spectroscopy, in order to discriminate between the effect of the Al-Alkyls on the silica surface and their effect on the chromium sites. The results are summarized in Figure 4. 2.
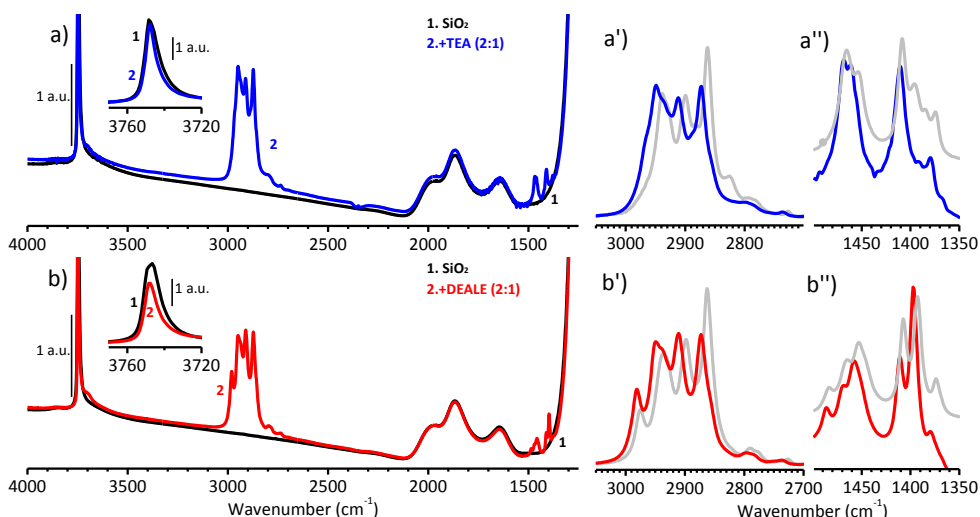
Figure 4. 2 FT-IR spectra of the silica support before (spectrum 1) and after the interaction (spectrum 2) with TEA(2:1) (part a) and DEALE(2:1) (part b). The insets in parts a and b show a magnification of the Si-OH stretching. Parts a' and a'' report a magnification of spectrum 2 after subtraction of spectrum 1, in the CH stretching and bending regions, compared to the spectrum of pure TEA (grey spectrum). Parts b' and b'' are the same for DEALE.

Spectra 1 in Figure 4. 2 are those typical of a highly dehydroxylated silica [12, 13]. After dosing the same amount of TEA corresponding to a Al:Cr=2:1 ratio in the experiments with Cr(II)/SiO₂ (spectrum 2 in Figure 4. 2a), new bands appear in the FT-IR spectrum in the 3000-2800 cm⁻¹ and 1500-1300 cm⁻¹ regions. These bands are attributed to the stretching and bending modes of the CH_x groups, and are very similar to those of pure TEA (grey spectrum in insets a' and a'') [14], except for a slight shift in wavenumbers which is likely due to the fact that in the liquid phase TEA is mainly present in the dimeric form. At the same time, the absorption band at ca. 3750 cm⁻¹ due to the surface OH groups is only slightly affected in intensity, demonstrating that **TEA reacts preferentially with the siloxane bridges at the silica surface** (paths 2 and 3 in Scheme 1), **more than with the OH groups** (path 1 in Scheme 1). According to the literature, reaction of Al-alkyls with a strained siloxane group might lead to the formation of a mono

grafted –O-AlR$_2$ species (path 2) that, upon further reaction with a vicinal siloxane group (path 3), would lead to the formation of a bis-grafted (–O)$_2$-AlR species [15-17].
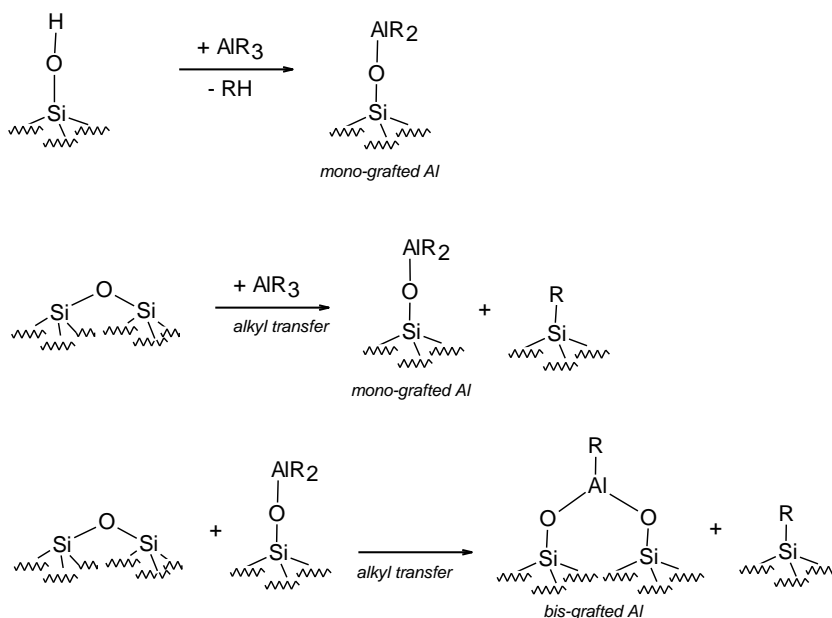
Scheme 1 Some of the surface structures that can be formed upon reaction of monomeric TEA with the silica surface.

The effect of DEALE on SiO$_2$ (Spectrum 2 in Figure 4. 2b) is similar to that of TEA. The absorption bands observed the IR spectrum are very similar, except for the absorption band at 2980 cm^{-1} which is peculiar of the –OR ligand [18]. In this case, the absorption band ascribed to the free silanols is more consumed than in the case of TEA, demonstrating that DEALE has a slightly greater preference for the OH species than TEA.

4.1.3 Reactivity of TEA and DEALE with Cr(II)/SiO$_2$ as monitored by FT-IR spectroscopy

The reactivity of TEA and DEALE with Cr(II)/SiO$_2$ was investigated by FT-IR spectroscopy following the same procedure as for the DR UV-Vis-NIR experiment. The results are shown in Figure 4. 3. The spectrum of Cr(II)/SiO$_2$ (spectrum 1) is the same as that described in Figure 3.6. Upon reaction with TEA (spectra 2 and 3, Figure 4. 3a) new absorption bands appear in the spectrum, due to the ν(CH$_x$) and δ(CH$_x$) vibrations, very much similar to those observed in the spectrum of SiO$_2$ reacted with TEA. The intensity of these bands is roughly proportional to the

amount of TEA. Also in this case, the absorption band due to the free silanols decreases in intensity, proportionally to the amount of TEA. Similar results have been obtained in the case of DEALE (Figure 4. 3b). Hence, we must conclude that **FT-IR spectroscopy does not allow distinguishing among the alkylated Cr sites, the Al(OR)$_x$R$_y$ by-products, and the AlR$_x$ grafted on silica** [15].
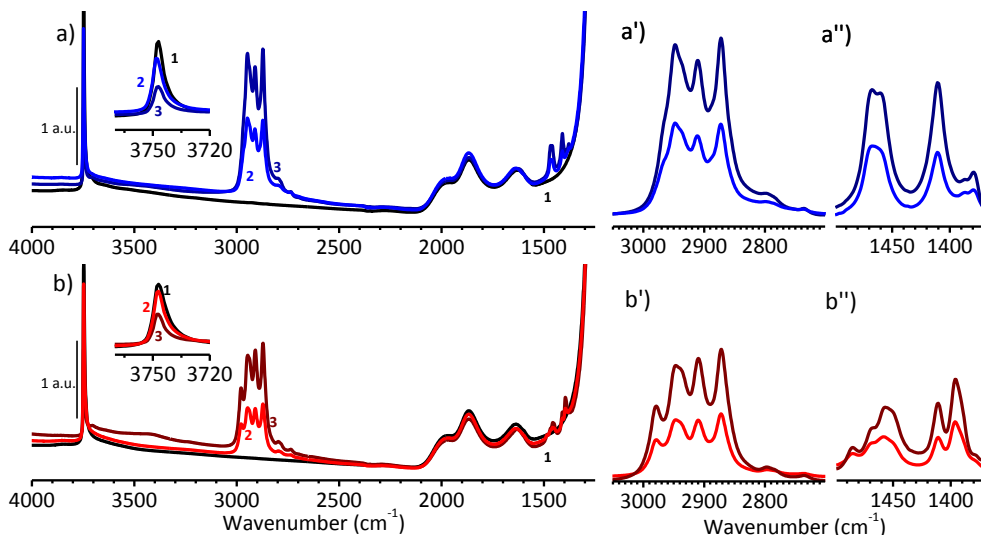
Figure 4. 3 Part a) FT-IR spectra of Cr(II)/SiO$_2$ before (spectrum 1), and after modification with TEA in a stoichiometric amount equal to Al:Cr = 2:1 (spectrum 2) and Al:Cr = 4:1 (spectrum 3). The inset in part a shows a magnification of the Si-OH stretching region. Parts a' and a'' report a magnification of spectra 2 and 3 after subtraction of spectrum 1, in the CH stretching and bending regions. Parts b, b' and b'' are the same for DEALE.

4.2 The accessibility of the Cr sites modified by TEA and DEALE.

Successively, the accessibility of the Cr sites in the modified $Cr(II)/SiO_2$ catalyst was investigated by means of FT-IR spectroscopy of adsorbed probe molecules. CO and CD_3CN were selected as suitable probes since they interact in a different way with the metal sites, thus giving complementary information.

Generally speaking, interaction of CO with a metal site can be dominated by an electrostatic, a covalent σ dative, or a π back-donation contribution, depending on the type and on the coordination of the metal site. Both the electrostatic polarization and the σ-dative contribution cause a blue shift of ν(CO) with respect to the frequency of the free gas (2143 cm^{-1}), while the π back-donation causes a red-shift. The adsorption of CO onto the $Cr(II)/SiO_2$ Phillips catalyst has been used since decades [8, 19-23], and it has been demonstrated that it is among the experimental methods most sensitive to the local geometry of the Cr(II) sites.

In contrast, CD_3CN was never reported as a probe for Cr(II) sites, while it has been often used as a probe for the characterization of acid or basic sites due to its ability to give different types of interaction: as a soft Lewis base, it can interact through the nitrogen lone pair, whereas as a weak Brønsted acid, it can interact with surface basic sites of oxides [24, 25].

4.2.1 Probing the accessible Cr sites with CO

Figure 4. 4 shows the FT-IR spectra, in the ν(CO) region, of CO adsorbed at room temperature on the unmodified $Cr(II)/SiO_2$ catalyst (Figure 4. 4a), and on the TEA/DEALE-modified $Cr(II)/SiO_2$ catalysts (Al:Cr=2:1, Figure 4. 4b and b', and Al:Cr=4:1, Figure 4. 4c and c'). The evolution of the spectra as a function of the CO coverage is also reported. Note that all the spectra are reported after subtraction of the spectrum prior CO dosage, and are normalized for the optical thickness of the sample. Hence, the absolute intensities are comparable and quantitative information can be extracted. Irrespective of the TEA concentration, the spectra collected at the maximum CO coverage (spectra 2) on the TEA-modified $Cr(II)/SiO_2$ catalysts (Figure 4. 4b and c) show some absorption bands in two distinct spectral regions, one centred at about 2190 cm^{-1} and the other one at about 1990 cm^{-1}. Notably, when the same experiment is conducted on SiO_2+TEA, no absorption bands are observed in the whole spectral region, but only the roto-vibrational spectrum of gaseous CO. Hence, the above mentioned absorption bands are all due to CO interacting with the Cr sites.

In the first region, a triplet of bands is observed at 2191, 2184 and 2178 cm^{-1}, exactly the same as observed for CO adsorbed on the unmodified Cr(II)/SiO$_2$ (Figure 4. 4a) and described in the previous Chapter, but with a lower intensity. This evidence unequivocally demonstrates that, **even at a Al:Cr ratio equal to 4:1, TEA does not modify all the Cr(II) sites, but only a fraction of them**.
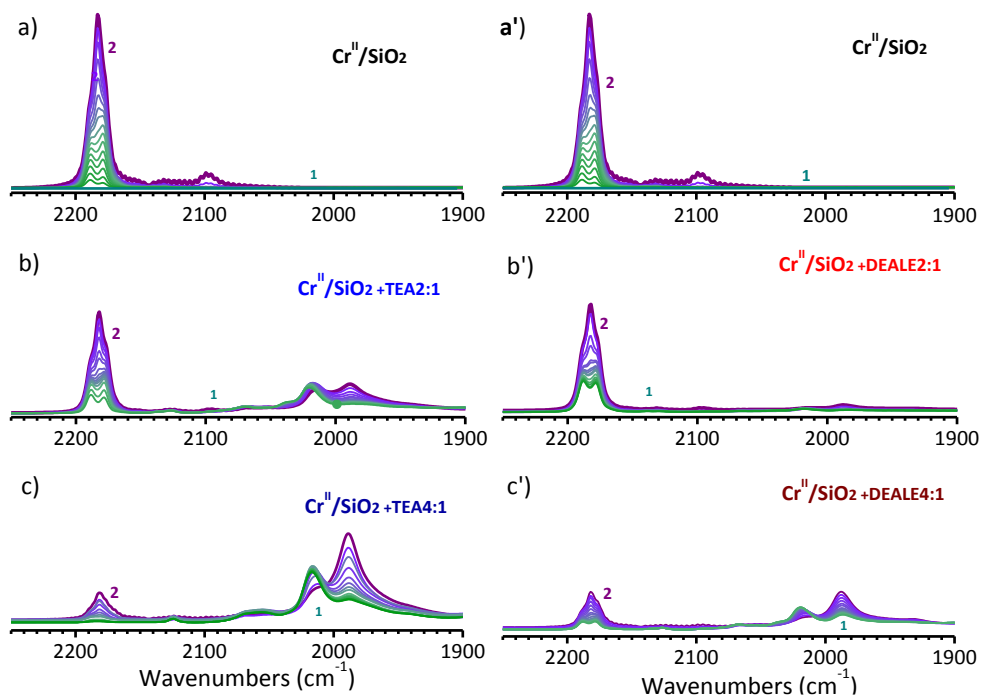
Figure 4. 4 Evolution of the FT-IR spectra, in the $\tilde{\nu}$(CO) region, for CO adsorbed at room temperature from P$_{CO}$ = 100 mbar (spectrum 2) to zero (spectrum 1) on unmodified Cr(II)/SiO$_2$ (part a), compared to the same sequence of spectra collected on Cr(II)/SiO$_2$ modified with TEA/DEALE in the Al:Cr=2:1 ratio (parts b and b') and in the Al:Cr=4:1 ratio (parts c and c'). All the spectra are reported after subtraction of that collected before CO dosing, and normalized for the optical thickness of the pellet.

The other set of bands in the second region (around 2100-1900 cm^{-1}) indicates the formation of classical Cr carbonyls (i.e. of carbonyls where the prevalent contribution is the Cr→CO π back-donation) [12, 26-28]. In particular, at the maximum CO coverage the main absorption band is centred at 1988 cm^{-1}, with a shoulder at 2014 cm^{-1}. Upon decreasing the CO pressure, the former gradually diminishes in intensity and the latter shifts at 2017 cm^{-1} (green spectrum). The intensity of these bands is roughly proportional to the amount of TEA. While classical carbonyls are typically formed on homogeneous Cr complexes [12, 29-33], they are much more rare for Cr species grafted on supports. One of the very few

examples reported in the literature for classical Cr carbonyls on heterogeneous Cr-based systems is represented by CO adsorption on the CO-reduced $Cr(II)/SiO_2$ catalyst modified by hydrosilanes (SiH_4 or R_3SiH) [7, 8]. In that case, the modifying agents were demonstrated to transform more than 80% of the Cr(II) sites into mono-grafted [≡Si-O-Cr(II)-$OSiR_3$] sites, having a character similar to that of homogeneous Cr complexes, and forming prevalently di-carbonyl species in the presence of CO. The spectral behaviour observed upon decreasing the CO coverage was explained in terms of transition from a dicarbonyl Cr species (characterized by a wide angle between the two CO molecules [34-36]) to a mono-carbonyl Cr species. The FT-IR spectra of CO adsorbed on $Cr(II)/SiO_2$+TEA are very close to those reported for CO adsorbed on $Cr(II)/SiO_2$+hydrosilanes. Hence, we can conclude that **the modified Cr(II) sites are structurally similar, and can be described as mono-grafted [≡Si-O-Cr(II)-L] sites**, where L = R (in agreement with the hypothesis reported in the literature).

The same experiment was performed for the DEALE-modified $Cr(II)/SiO_2$ catalyst, as reported in Figure 4. 4b' and c'. The results are very similar, except for the absolute intensities of the $\tilde{v}$(CO) bands.

The fraction of the unmodified Cr(II) sites in each experiment was quantified by calculating the integrated absorbance of the v(CO) "triplet" centred at ca. 2190 cm^{-1} (Triplet Int. Area in Table 4. 1) and comparing it to the value obtained for CO on $Cr(II)/SiO_2$, which corresponds to 100% of the total Cr(II) sites accessible to CO. The results are reported in Table 4. 1 (first two columns) and Figure 4. 5 (grey bars). Interestingly, **by keeping constant the Al-alkyl concentration, the fraction of unmodified Cr(II) sites (Cr(II)^{unmodif}) is almost the same irrespective of the type of Al-alkyl**. For Al:Cr=2:1, roughly 65% of the original Cr(II) sites remain not modified by both TEA and DEALE, while this fraction decreases to ca. 22% when Al:Cr=4:1. In the other way around, about 35% of the total Cr(II) sites are modified by Al-alkyls at Al:Cr=2:1 concentration, and this fraction increases to ca. 78% at Al:Cr=4:1 (Cr(II)^{modif} in Table 4. 1).

The same approach applied to the v(CO) absorption band at 1988 cm^{-1} gives an estimation of the fraction of modified Cr(II) sites accessible by CO, which are described as mono-grafted [≡Si-O-Cr(II)-L] sites (see above). We considered as a reference the spectrum of CO adsorbed on $Cr(II)/SiO_2$+TES (TES = triethylsilane), where the 80% of the sites were transformed into mono-grafted ones. Hence, for each experiment we calculated the integrated absorbance of the v(CO) band at 1988 cm^{-1} (classic carbonyls Int. Area in Table 4. 1) and we compared the obtained values with that obtained for CO on $Cr(II)/SiO_2$+TES. The results are

reported in Table 4. 1 (last three columns), and better visualized in Figure 4. 5 (light blue bars). From this analysis it clearly emerges that **only a fraction of the modified Cr(II) sites are accessible to CO (Cr(II)$_{vis}^{modif}$). In general, this fraction is larger for Cr(II)/SiO$_2$+TEA than for Cr(II)/SiO$_2$+DEALE, and increases at higher Al:Cr ratio.**

The difference Cr(II)^{modif} − Cr(II)$_{vis}^{modif}$ gives the fraction of Cr(II) modified by Al-alkyls but not visible by CO (Cr(II)$_{novis}^{modif}$ in Table 4. 1 and dark blue bars in Figure 4. 5). **It is evident that a fraction of the modified chromium sites remains not accessible to the CO probe, probably because shielded by sterically encumbering ligands nearby.** In this respect it is worth mentioning that most of the Al-alkyls have the tendency to dimerize [34].

Table 4. 1 Quantification of the fraction of Cr sites (with respect to the total) visible by CO in Cr(II)/SiO$_2$, Cr(II)/SiO$_2$+TEA and Cr(II)/SiO$_2$+DEALE, as determined by analysing the FT-IR spectra of CO adsorbed at room temperature (details in the text).

	System	ratio	"Triplet" int. Area	Cr(II)^{unmodif} (%)	Cr(II)^{modif} (%)	1988 cm^{-1} int. Area	Cr(II)$_{vis}^{modif}$ (%)	Cr(II)$_{novis}^{modif}$ (%)
Cr(II)/SiO$_2$	bare	0	28,0	100,0				
	TEA(2:1)	2	18,4	65,7	34,3	25,0	34,2	0,1
	TEA(4:1)	4	6,1	21,8	78,2	44,7	61,1	17,1
	DEALE(2:1)	2	18,4	65,7	34,3	8,0	10,9	23,3
	DEALE(4:1)	4	6,2	22,1	77,9	12,0	16,4	61,4
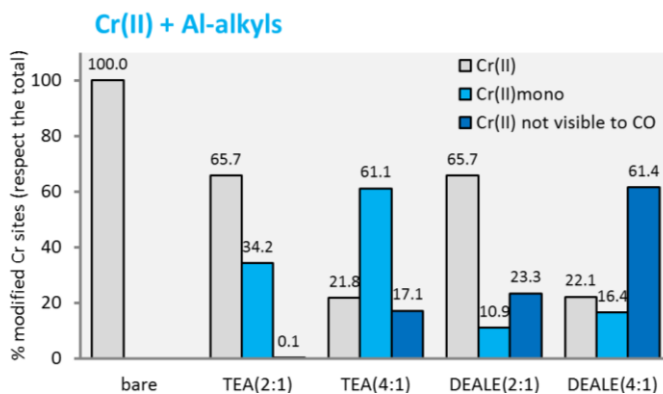
Figure 4. 5 Quantitative determination of the fraction of Cr(II) sites unmodified and modified by TEA and DEALE at different Al:Cr ratios, as determined by analysing the FT-IR spectra of CO adsorbed at room temperature on Cr(II)/SiO$_2$+TEA and Cr(II)/SiO$_2$+DEALE. The fraction of unmodified Cr(II) sites (grey bars) has been determined from the integrated intensity of the ν(CO) "triplet" centred at ca. 2190 cm^{-1}. The fraction of modified Cr(II) accessible to CO (light blue bars), which have a mono-grafted [≡Si-O-Cr(II)-L] structure, has been estimated from the integrated intensity of the ν(C≡O) band at 1988 cm^{-1}.

4.2.2 Probing the accessible Cr sites with CD₃CN

To obtain a more complete description of the modified Cr(II)/SiO₂ systems, the accessibility of the Cr sites was successively probed by the adsorption of CD₃CN at room temperature. While this molecule has been largely employed to probe both acid and basic sites on metal oxides and zeolites [24, 25, 35-42], it was curiously never used in the characterization of the Phillips catalyst. Since both Cr(II) and Al(III) sites are Lewis acids (i.e. prone to accept electrons), acetonitrile is expected to interact with both of them as a soft Lewis base by sharing the nitrogen lone-pair, according to equation (1):

CD₃CN: + M(surf) → [CD₃CN:···M(surf)]ₐds   (1)
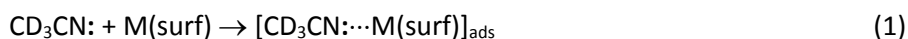
where M(surf) = Cr(II) or Al(III).

Because of this interaction, the $\tilde{v}$(C≡N) vibrational frequency is expected to increase, proportionally to the strength of the Lewis acid-base couple. In general, d-acetonitrile is employed to avoid the occurrence of an annoying Fermi resonance effect [43].

At first, we decided to perform the experiment on the two systems taken as references: 1) the Cr(II)/SiO₂ catalyst, on which there is a general consensus about the presence of bis-grafted "naked" Cr(II) sites (whereby "naked" indicates largely uncoordinated species); and 2) the Cr(II)/SiO₂+TES catalyst, for which we have previously demonstrated that more than 80% of the Cr(II) sites are transformed into mono-grafted [≡Si-O-Cr(II)-OSiR₃] sites [8]. The results are summarized in Figure 4. 6, that shows the evolution of the background subtracted FT-IR spectra in the $\tilde{v}$(C≡N) region for d-acetonitrile adsorbed at room temperature on Cr(II)/SiO₂+TES(part a), and Cr(II)/SiO₂ (part b) ,as a function of the CD₃CN coverage. Three bands are observed in the $\tilde{v}$(C≡N) region in both cases, at 2275 cm⁻¹, 2265 cm⁻¹ and 2306 cm⁻¹. The two bands at 2275 cm⁻¹ and 2265 cm⁻¹ are assigned to CD₃CN adsorbed on the surface OH groups and to liquid-like (physisorbed) acetonitrile, respectively [24, 25, 36, 42]. Both bands decrease rapidly in intensity upon decreasing the acetonitrile coverage up to disappear, indicating that the interaction of d-acetonitrile with the silica surface is weak and fully reversible. The band at 2306 cm⁻¹ is straightforwardly ascribed to CD₃CN in interaction with the Cr(II) sites. This band is only slightly affected by degassing, indicating that the interaction is very strong and not reversible at room temperature.
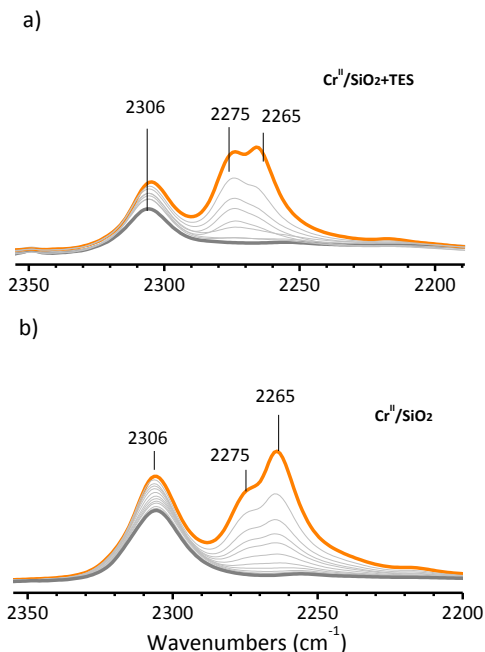
Figure 4. 6 Evolution of the FT-IR spectra, in the $\tilde{\nu}(C\equiv N)$ region, for CD$_3$CN adsorbed at room temperature on Cr(II)/SiO$_2$+TES as a function of the CD$_3$CN coverage (part a), compared to the same sequence of spectra collected for CD$_3$CN adsorbed on unmodified Cr(II)/SiO$_2$ (part b). All the spectra are reported after subtraction of that collected before CD$_3$CN dosing, and normalized for the optical thickness of the pellet. Orange spectra: maximum CD$_3$CN coverage; bold grey spectra: irreversible fraction of adsorbed CD$_3$CN.

Curiously, **CD$_3$CN does not differentiate between bis-grafted "naked" Cr(II) sites and mono-grafted [≡Si-O-Cr(II)-OSiR$_3$] sites, while CO does**. This is a nice example of the complementarity of different probe molecules. CD$_3$CN probes the "electronic environment" of the Cr(II) sites, that means their Lewis acidity, but is not sensitive to the molecular structure of the Cr(II) sites. From an electronic point of view, the bis-grafted "naked" Cr(II) sites are very similar to the mono-grafted [≡Si-O-Cr(II)-OSiR$_3$] sites, as demonstrated also by DR UV-Vis spectroscopy. In contrast, CO is sensitive to the molecular structure, that in turns influences the exposed molecular orbitals. Hence, **CO gives a description of the molecular structure of the Cr(II) sites on the silica surface, while CD$_3$CN discriminates between sites with different Lewis acidity**.
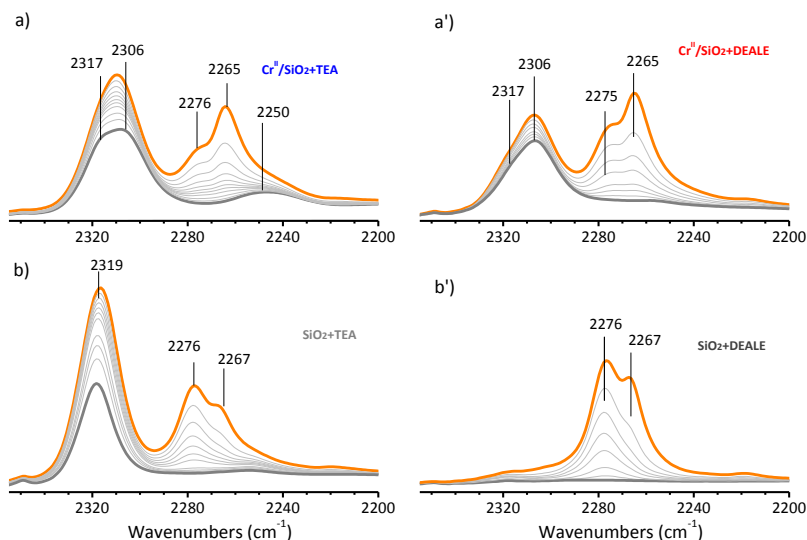
Figure 4. 7 Evolution of the FT-IR spectra, in the $\tilde{v}(C\equiv N)$ region, for CD_3CN adsorbed at room temperature on $Cr(II)/SiO_2+TEA(2:1)$ as a function of the CD_3CN coverage (part a), compared to the same sequence of spectra collected for CD_3CN adsorbed on $SiO_2+TEA(2:1)$ (part b). All the spectra are reported after subtraction of that collected before CD_3CN dosing, and normalized for the optical thickness of the pellet. Orange spectra: maximum CD_3CN coverage; bold grey spectra: irreversible fraction of adsorbed CD_3CN. Parts a' and b': the same as parts a and b, for DEALE.

Figure 4. 7 shows the evolution of the background subtracted FT-IR spectra in the $\tilde{v}(C\equiv N)$ region for CD_3CN adsorbed at room temperature on $Cr(II)/SiO_2+TEA$ (part a) and SiO_2+TEA (part b), as a function of the CD_3CN coverage. The spectra of CD_3CN adsorbed on SiO_2+TEA show the same two bands at 2275 and 2265 cm^{-1} described above, and attributed to CD_3CN adsorbed on the surface OH groups and to liquid-like (physisorbed) acetonitrile. An additional band is observed at 2319 cm^{-1}, which is quite resistant to degassing, and is assigned to CD_3CN in interaction with the Al(III) species [36]. This means that **at least a fraction of the AlR_xO_y species derived from reaction of TEA with the silica surface are accessible by CD_3CN.**

The spectra of CD_3CN adsorbed on $Cr(II)/SiO_2+TEA(2:1)$ (Figure 4. 7a) look like a mixture of those collected on $Cr(II)/SiO_2$ and on SiO_2+TEA. In particular, the absorption band centred at ca. 2315 cm^{-1} is clearly asymmetric and constituted by two overlapping bands at 2306 cm^{-1} and 2317 cm^{-1}. A third weak band is clearly present at 2250 cm^{-1}, more evident at low CD_3CN coverage. In accordance with the considerations made before, acetonitrile discriminates between sites with different Lewis acidity. We attribute the band at 2306 cm^{-1} to CD_3CN adsorbed on weaker Lewis acid sites (hereafter W-LA), that could be either mono-grafted Cr(II)

69

sites or bis-grafted Cr(II) sites, or both. The band at 2317 cm^{-1} is attributed instead to CD$_3$CN adsorbed on stronger Lewis sites (hereafter S-LA). At least in part, the Al(III) species deriving from the reaction of TEA with silica contribute to this band too. Finally, the band at 2250 cm^{-1} is tentatively ascribed to CD$_3$CN bridged in between Cr(II) and Al(III), which indicates the presence of Cr(II)-Al(III) couples simultaneously probed by the same CD$_3$CN molecule (hereafter Cr-Al).

Table 4. 2 . Quantification of the amount of weak Lewis acid sites (W-LA) and strong Lewis acid sites (S-LA) visible by CD$_3$CN in the Cr(II)/SiO$_2$, Cr(II)/SiO$_2$+TEA, Cr(II)/SiO$_2$+DEALE, SiO$_2$+TEA and SiO$_2$+DEALE expressed in percentage with respect to the total amount of Cr sites. These values have been determined by analysing the FT-IR spectra of CD$_3$CN adsorbed at room temperature on all the systems (see text for details).

	System	ratio	W-LA (Int. Area 2306 cm-1)	S-LA (Int. Area 2317 cm-1)	W-LA (%)	S-LA (%)
Cr(II)/SiO$_2$	bare	0	11.5	0.0	100.0	0.0
	TEA(2:1)	2	11.4	5.4	98.7	46.6
	DEALE(2:1)	2	5.9	1.8	51.1	15.7
	SiO2+TEA	2	0.0	11.0	0.0	95.4
	SiO2+DEALE	2	0.0	0.0	0.0	0.0
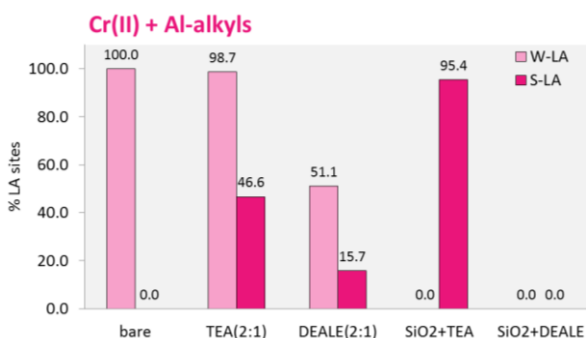
Figure 4. 8 Quantitative determination of the fraction of Cr(II) sites unmodified and modified by TEA and DEALE, as determined by analysing the FT-IR spectra of CD$_3$CN adsorbed at room temperature on the Cr(II)/SiO$_2$, on the Cr(II)/SiO$_2$+TEA and Cr(II)/SiO$_2$+DEALE. In addition, it is reported also the quantification of the Al(III) sites in the SiO$_2$+TEA, and in the SiO$_2$+DEALE.

The relative fraction of the W-LA and S-LA sites can be qualitatively estimated by calculating the integrated areas of the bands at 2317 and 2306 cm^{-1}, as determined by a deconvolution process of the spectra at the minimum coverage. These values have been compared to the integrated area of the band at 2306 cm^{-1} for CD$_3$CN adsorbed on Cr(II)/SiO$_2$ (where the totality of the Cr(II) sites are accessible and behave as W-LA sites), in the approximation of a constant molar extinction coefficient. This approximation is reasonable by considering a narrow spectral range, while it cannot be used for the band at 2250 cm^{-1}. The results of this analysis are summarized in Table 4. 2 and visualized in Figure 4. 8. It is worth

noticing that the sum of the W-LA and S-LA sites might exceed 100%, since also the Al(III) sites are potentially probed by CD₃CN as S-LA sites. We anticipate here that both the unmodified Cr(II) sites and a fraction of mono-grafted [≡Si-O-Cr(II)-L] sites display W-LA properties. However, the mono-grafted [≡Si-O-Cr(II)-L] sites could become more acidic (S-LA sites) when they are in proximity of an Al(III) site, as reported in Scheme 2. **These modified Cr(II) sites are partially detached from the silica surface (hence, the classical behaviour of the di-carbonyl complexes), stabilized by some ancillary ligands nearby (hence, they appear as highly coordinated in the DR UV-Vis spectrum) and with a strong Lewis acidity due to the proximity of the Al(III) sites.**
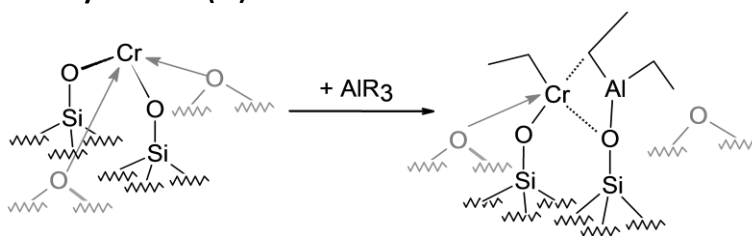
Scheme 2 Proposed mechanism to explain the formation of the mono-grafted Cr(II) sites from reaction of Cr(II)/SiO₂ with AlR₃.

The same experiment was repeated for Cr(II)/SiO₂+DEALE (2:1). Figure 4. 7a' shows the evolution of the background subtracted FT-IR spectra in the $\tilde{v}$(C≡N) region for CD₃CN adsorbed at room temperature on the DEALE-modified Cr(II)/SiO₂ catalyst, compared to SiO₂+DEALE (part b'), as a function of the CD₃CN coverage. When dosed on SiO₂+DEALE, acetonitrile interacts with the silica surface, but not with the Al(III) sites. Indeed, only a minor band is hardly observable at ca. 2318 cm⁻¹, differently from what observed on SiO₂+TEA. This means that **the majority of the Al(III) sites derived from reaction of DEALE with the silica surface are inaccessible to CD₃CN, probably because of steric reasons**.

The spectra of CD₃CN adsorbed on Cr(II)/SiO₂+DEALE (Figure 4. 7a') are very similar to those of CD₃CN adsorbed on Cr(II)/SiO₂ (Figure 4. 6b), except that the absorption band ascribed to CD₃CN in interaction with the Cr(II) sites is clearly asymmetric and with an evident shoulder at ca. 2317 cm⁻¹. No bands are noticed at 2250 cm⁻¹. By deconvolving the absorption band at ca. 2315 cm⁻¹ two contributions can be found, the first centred at 2306 cm⁻¹ (W-LA sites), and the second at 2316 cm⁻¹ (S-LA sites). The relative fraction of the W-LA and S-LA sites was determined following the same protocol discussed above, and is summarized in Table 4. 2 and in Figure 4. 8.

4.2.3 A summary on the accessibility of the Cr sites in the Al-alkyl modified Cr(II)/SiO$_2$ catalysts

The experiments performed by using CO and CD$_3$CN as molecular probes, let us reaching the following conclusions.

1) Also in large excess of Al-alkyls (Al:Cr=4:1), a substantial amount of Cr(II) sites are not modified.

2) Not all the modified Cr(II) sites are accessible to CO. The fraction of modified sites not accessible to CO (blue bars in Figure 4. 5) increases upon increasing the Al:Cr ratio, and by going from TEA to DEALE. For example, for TEA(2:1) all the modified sites are accessible to CO, while for TEA(4:1) ca. 17% of the modified sites are not accessible. The steric encumbrance of DEALE is larger than that of TEA (or, in other words, DEALE has a larger shielding ability for the Cr(II) sites, likely due to the presence of the alkoxy group, due to the oxophylicity of the Cr sites). Hence, **upon increasing the Al:Cr ratio we increase the fraction of modified sites, but also the amount of those which are sterically hindered**.

3) CD$_3$CN is a stronger acidic probe than CO and it is able to detect a larger fraction of modified Cr(II) sites. **CO discriminates between mono- or bis-grafted Cr(II) sites, while CD$_3$CN discriminates sites with different Lewis acidity.**

4) Cr(II) sites having a different local structure (mono- or bis-grafted) may have the same acidity, whereas Cr(II) sites having the same local structure (mono-grafted) may display a different acidity depending on the type and proximity of ligands with a Lewis acidic character. In comparison to CO, CD$_3$CN is able to distinguish between mono-grafted [≡Si-O-Cr(II)-L] sites having different ligands nearby. **Those Cr(II) sites in close proximity of an Al(III) sites on the silica surface are more acidic**. The fraction of S-LA sites is higher for the TEA-modified catalyst than for the DEALE-modified one.

4.3. Ethylene polymerization over the Al-alkyl modified Cr(II)/SiO$_2$

4.3.1 A kinetic study

Kinetic experiments were performed to evaluate at a lab scale the ethylene polymerization rate on the TEA- and DEALE-modified Cr(II)/SiO$_2$ catalysts, at two different concentrations, in comparison with the Cr(II)/SiO$_2$ catalyst. Figure 4. 9 shows the decrease of ethylene pressure as a function of time for the TEA/DEALE-modified catalysts, monitored in the same experimental conditions and at a constant Cr loading. The data clearly demonstrate that Cr(II)/SiO$_2$+TEA and Cr(II)/SiO$_2$+DEALE in both concentrations are much faster than the unmodified Cr(II)/SiO$_2$ catalyst, although in all the cases the reaction rate drastically decreases after the first two minutes of reaction. This phenomenon might be explained at least in three ways: 1) it must be noticed that the silica adopted as support does not fragment; 2), when PE starts growing around the catalyst particles it creates a layer that limits the diffusion of ethylene and 3) there could be catalyst deactivation problems.

For this reason, the reaction constants were calculated on the basis of the first order law reported in Chapter 3, but considering only the first minute of reaction. The values of the kinetic constants are reported in Table 4. 3

Table 4. 3 Kinetic constants for ethylene polymerization reaction conducted at room temperature on Cr(II)/SiO$_2$ and on the TEA- and DEALE-modified versions, at two different Al:Cr ratios.

Kinetic constants (s^{-1} molCr^{-1})			
Catalyst	**No Al-alkyls**	**Al:Cr=2:1**	**Al:Cr=4:1**
Cr(II)/SiO$_2$	14	-	-
Cr(II)/SiO$_2$+TEA	-	202	230
Cr(II)/SiO$_2$+DEALE	-	270	237

All the modified catalysts are faster than the Cr(II)/SiO$_2$ catalyst. **This means that the modified Cr(II) sites are intrinsically much faster than the unmodified ones**, since they are just a fraction of the total Cr loading. For instance, values of 202 s^{-1} molCr^{-1} and 230 s^{-1} molCr^{-1} were estimated for the TEA-modified systems (Al:Cr=2:1 and Al:Cr=4:1, respectively), which are ca. 14 and 17 times higher than that obtained for the unmodified system (14 s^{-1} molCr^{-1}). Remarkably, **the kinetic constant is not proportional to the amount of TEA**, despite slightly increasing.
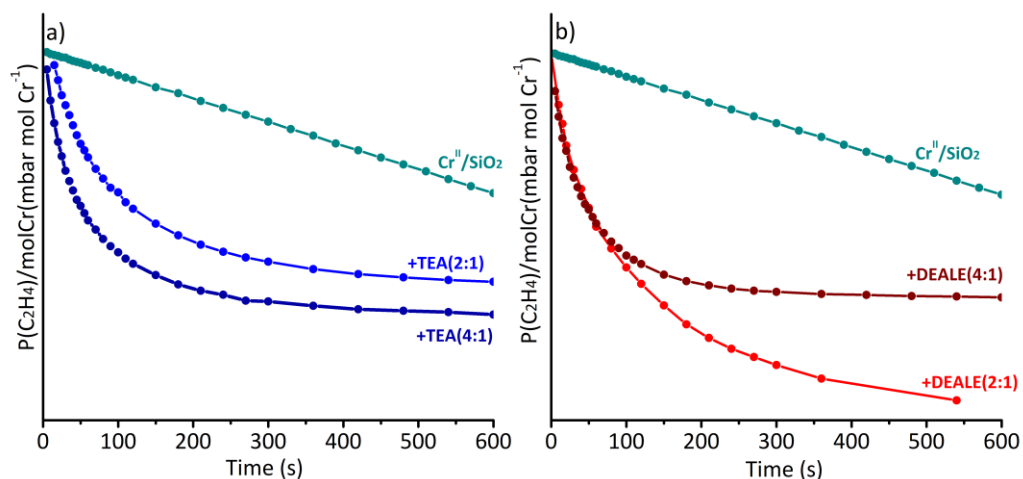
Figure 4. 9 Part a) Kinetics of ethylene polymerisation on the Cr(II)/SiO$_2$ catalyst (cyan curve) in comparison to that on TEA-modified Cr(II)/SiO$_2$ catalyst (at two different Al:Cr ratio), obtained by recording the ethylene equilibrium pressure as a function of time. Part b) the same as part a for DEALE-modified Cr(II)/SiO$_2$ catalyst.

Overall, **the faster catalyst is Cr(II)/SiO$_2$+DEALE(2:1)**: its kinetic constants is 270 s^{-1} molCr^{-1} , about 20 times higher with respect to the unmodified catalyst, while this value decreases to 237 s^{-1} molCr^{-1} for the DEALE (4:1) modified catalyst. It is clear that in presence of a higher amount of the Al-Alkyls, the catalysts seem to be less active respect to the catalyst modified with a Al:Cr=2:1 amount. This is in agreement with McDaniel [44], who reports that an excess of Al-Alkyls deactivates the catalyst (Figure 1.9).

4.3.2 A spectroscopic study.

Ethylene polymerization on the modified Cr(II)/SiO$_2$ catalysts was monitored by means of DR UV-Vis and FT-IR spectroscopies, as summarized respectively in Figure 4. 10 and in Figure 4. 11. Upon ethylene dosage, the DR UV-Vis spectra of both Cr(II)/SiO$_2$+TEA(2:1) and Cr(II)/SiO$_2$+DEALE(2:1) immediately change: the d-d bands are slightly eroded and shifted at higher frequencies (about at 16500 cm^{-1}). This change simply reveals that the modified Cr(II) sites got in contact with ethylene, further expanding their coordination. Meanwhile, weak bands grow in the 4500-4000 cm^{-1} region, where overtones and combinations of the stretching and bending vibrational modes of polyethylene are located (insets in Figure 4. 10). Also in this case, no new bands are observed during the polymerization that could

reveal the destiny of the active sites. Indeed, the Cr active sites likely remain buried into a layer of polyethylene and become rapidly invisible to DR UV-Vis-NIR.
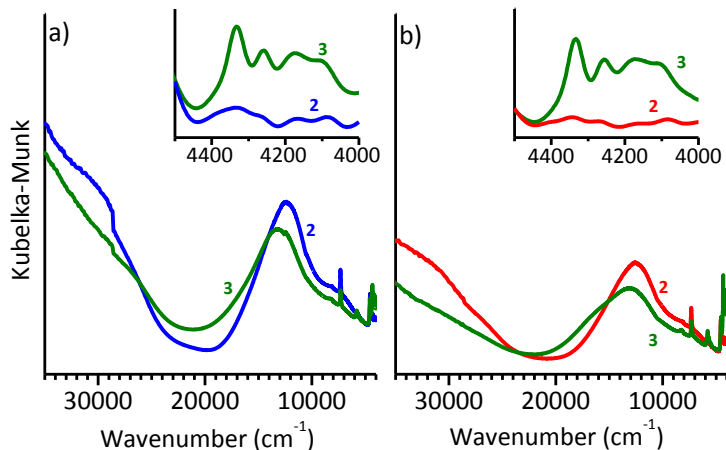
Figure 4. 10 Part a) Evolution of the DR UV-Vis-NIR spectrum upon ethylene reaction at room temperature on the Cr(II)/SiO$_2$+TEA(2:1) catalyst (from spectrum 2 to spectrum 3). The inset shows a magnification of the NIR region. Part b) The same of part a but for Cr(II)/SiO$_2$+DEALE(2:1).

Figure 4. 11 shows the time-resolved FT-IR spectra collected during ethylene polymerization on Cr(II)/SiO$_2$+TEA(2:1) (part a) and Cr(II)/SiO$_2$+DEALE(2:1) (part b), at P_{C2H4} = 100 mbar and room temperature. The spectra are reported after subtraction of the spectrum collected before ethylene admission, in the region of interest for PE. In both cases, the occurrence of ethylene polymerization is indicated by the fast growth of the IR absorption bands characteristic of polyethylene: two bands at 2920 and 2851 cm^{-1}, growing in time at nearly constant rates, which are readily assigned to the asymmetric and symmetric stretching vibrations of CH$_2$ groups of the polymeric chains, and the two bands at 1472 and 1463 cm^{-1} assigned to the bending mode of the CH$_2$ groups (inset in Figure 4. 11).
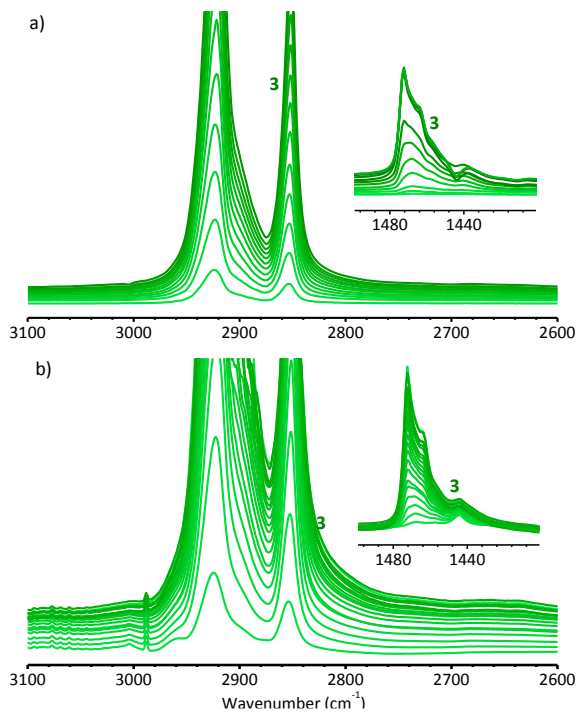
Figure 4. 11 Part a) Time evolution of the background subtracted FT-IR spectra, in the $\tilde{v}(CH_x)$ region, collected during ethylene polymerization on $Cr(II)/SiO_2+TEA(2:1)$. In the inset the same sequence of spectra but in the in the $\delta(CH_x)$ region. Part b) The same as part a for $Cr(II)/SiO_2+DEALE(2:1)$.

4.4 A short summary on the properties of the unmodified Cr(II)/SiO₂ Phillips catalyst and some hypothesis on the structure of the modified Cr sites.

The present paragraph summarizes the main results achieved by applying several complementary spectroscopic techniques to investigate the TEA- and DEALE-modified Cr(II)/SiO₂ catalysts. Some hypothesis on the molecular structures of the modified Cr sites are also proposed.

4.4.1 Fraction of modified Cr sites and their oxidation state

Only a fraction of the Cr(II) sites are modified by the Al-alkyls, even at an Al:Cr ratio equal to 4:1. The fraction of the modified Cr(II) sites can be easily determined by means of FT-IR spectroscopy of CO adsorbed at room temperature. Indeed, CO adsorbed on the original "naked" Cr(II) sites gives a well-known triplet of absorption bands centred at ca. 2180 cm^{-1}, which decreases in intensity as soon as the Cr(II) sites are modified. It was found that, at constant Al-alkyl concentration, **the fraction of modified Cr(II) sites is almost the same irrespective of the type of Al-alkyl**. For Al:Cr=2:1, about 35% of the total Cr(II) sites are modified by Al-alkyls, and this fraction increases to ca. 78% at Al:Cr=4:1.

The remaining **Al-alkyls must react with the silica surface, either with the siloxane bridges and/or with the silanol groups, to give –AlR$_x$ (or AlR$_x$O$_y$) species.** This means that any realistic representation of the structures of the modified Cr sites should consider the presence of AlR$_x$O$_y$ moieties in the proximity of the Cr sites.

As far as the oxidation state of the modified Cr sites is concerned, the DR UV-Vis results clearly demonstrated that after the interaction with the Al-Alkyls, **it remains Cr(II).** This is intuitive, since an oxidation of the Cr(II) sites in the presence of reducing agents is unlikely, and further reduction to Cr(I) is not favoured due to the instability of the Cr(I) species. However, the UV-Vis spectra indicate that most of the Cr(II) sites **increase their coordination**. This is also reasonable, since the number of ligands surrounding the Cr(II) sites is clearly greater in the presence of TEA/DEALE and their by-products.

4.4.2 Accessibility of the modified Cr sites, local structure and acid properties

The unmodified Cr(II) sites (species **1** in Scheme 3) are, obviously, accessible by CO and behave as W-LA sites. Not all the modified Cr(II) are accessible by CO, but

those which are accessible are univocally described as **mono-grafted Cr(II) sites, of the type ≡SiOCr(II)-L (where L = R or OR), partially detached from the silica surface** (hence, the classical behaviour of the di-carbonyl complexes). All of them are **stabilized by some ancillary ligands nearby** (hence, they appear as highly coordinated in the DR UV-Vis spectrum). Among the ancillary ligands there would be the ≡SiO–AlR$_2$ and/or ≡SiO–AlROR species obtained from the rupture of one Cr-O bond (see Scheme 2) and the ≡SiO–AlR$_2$, ≡SiO–AlROR, or ≡SiO–R species deriving from the direct reaction of the Al-alkyl with the silica surface.
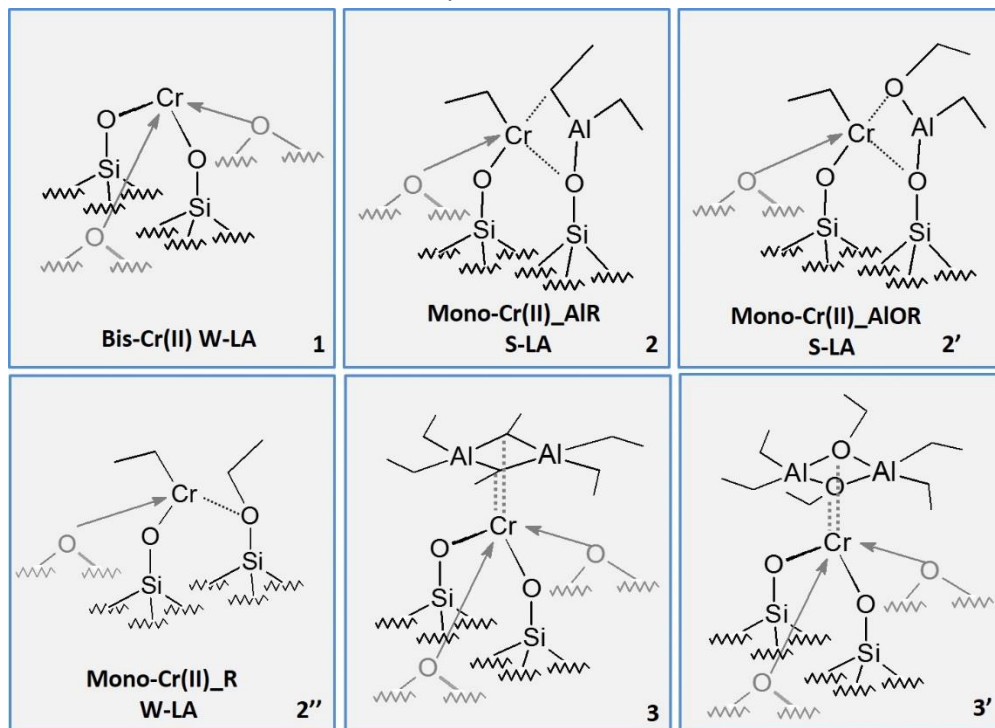
Scheme 3. Hypothetical structures (at a molecular level) for the chromium sites in the Cr(II)/SiO$_2$ +Al-Alkyls catalysts.

The overall accessibility and, more important, **the acidic nature of the mono-grafted Cr(II) sites strongly depend on the number and the type of the ancillary ligands.** In the presence of an AlR$_x$O$_y$ fragment (species **2** in Scheme 3), the ≡SiOCr(II)-L sites display a stronger Lewis acid character than the ≡SiOCr(II)-L sites closed to a SiO–R species (species **2"** in Scheme 3). The S-LA sites are less accessible when the AlR$_x$O$_y$ fragment contains more OR ligands (species **2'** in Scheme 3). The relative proportion of these strong and weak Lewis acid sites depends on the type of the Al-alkyl and on its concentration. In general, the

formation of S-LA sites is favoured in the presence of TEA and at high concentration. In these cases, a fraction of the mono-grafted ≡SiOCr(II)-L sites is in such a close proximity with the AlR$_x$O$_y$ fragment, that CD$_3$CN can be shared between the Cr(II) and the Al(III) cations in a bridged fashion. Scheme 3 shows a collection of the possible Cr species that can co-exist on Cr(II)/SiO$_2$+TEA/DEALE.

The fraction of Cr(II) sites not accessible by CO is much higher in the presence of DEALE than in the presence of TEA. Considering the tendency of the Al-Alkyls to form dimers, we advance the hypothesis that at least **a fraction of the inaccessible sites have the structure of bis-grafted Cr(II) in interaction with Al-Alkyls dimers** (Structures **3** and **3'** in Scheme 3).

4.4.3 Role of the modified Cr sites in ethylene polymerization

Plausibly all the Cr sites described in the previous scheme play a role in ethylene polymerization, although at present it is difficult to define the exact role of each of them. In terms of reaction rate, Cr(II)/SiO$_2$+DEALE(2:1) seems the most performant catalyst, although the fraction of Cr(II) sites accessible by probe molecules (CO and CD$_3$CN) is much lower than for Cr(II)/SiO$_2$+TEA(2:1). This observation indicates that **also those sites which are not accessible by CO and CD$_3$CN might be accessible to ethylene, and hence active in ethylene polymerization**. This should not look strange. In our experience, ethylene is able to access also hindered Cr sites not accessible by other probes, provided that the coordinating ligands are flexible enough to allow it to enter.

As far as the mono-grafted ≡SiOCr(II)-L sites are concerned, their behaviour is strongly influenced by their acidic nature. Mono-grafted ≡SiOCr(II)-OSiR$_3$ sites generated by reacting Cr(II)/SiO$_2$ with hydrosilanes, which are W-LA sites, have been demonstrated to be responsible of ethylene oligomerization to 1-hexene [7]. Similarly, we might hypothesize that **the fraction of ≡SiOCr(II)-L sites having a W-LA character** (species **2"** in Scheme 3) **generate prevalently α-olefins through ethylene oligomerization, and hence contribute to the formation of low molecular weight PE. In contrast, the ≡SiOCr(II)-L sites having a S-LA character** (species **2** and **2'** in Scheme 3) **might contribute to the formation of a high molecular weight PE, in close analogy to the behaviour of the Cr(II) sites on Al$_2$O$_3$** [45].

References

[1] McDaniel, M.P.,Adv. Catal., 53 (2010) 123-606.

[2] Liu, B.P., Fang, Y.W., Terano, M.,J. Mol. Catal. A-Chem., 219 (2004) 165-173.

[3] Liu, Z., He, X., Cheng, R., Eisen, M.S., Terano, M., Scott, S.L., Liu, B., Chromium catalysts for ethylene polymerization and oligomerization, in: Adv. Chem. Eng., 2014, pp. 126-191.

[4] Cicmil, D., Meeuwissen, J., Vantomme, A., Wang, J., van Ravenhorst, I.K., van der Bij, H.E., Munoz-Murillo, A., Weckhuysen, B.M.,Angew. Chem., 54 (2015) 13073-13079.

[5] Cicmil, D., Meeuwissen, J., Vantomme, A., Weckhuysen, B.M.,ChemCatChem, 8 (2016) 1937-1944.

[6] Cicmil, D., van Ravenhorst, I.K., Meeuwissen, J., Vantomme, A., Weckhuysen, B.M.,Catal Sci Technol, 6 (2016) 731-743.

[7] Barzan, C., Groppo, E., Quadrelli, E.A., Monteil, V., Bordiga, S.,Phys.Chem.Chem.Phys., 14 (2012) 2239–2245.

[8] Barzan, C., Gianolio, D., Groppo, E., Lamberti, C., Monteil, V., Quadrelli, E.A., Bordiga, S.,Chem. Eur. J., 19 (2013) 17277-17282.

[9] Barzan, C., Bordiga, S., Quadrelli, E.A., Groppo, E.,Top. Catal., 59 (2016) 1732-1739.

[10] Brückner, A.,Phys. Chem. Chem. Phys., 5 (2003) 4461-4472.

[11] Brückner, A., Jabor, J.K., McConnell, A.E.C., Webb, P.B.,Organometallics, 27 (2008) 3849-3856.

[12] Groppo, E., Lamberti, C., Bordiga, S., Spoto, G., Zecchina, A.,Chem. Rev., 105 (2005) 115-183.

[13] Borello, E., Zecchina, A., Morterra, C.,J. Phys. Chem., 71 (1967) 2938-2945.

[14] Kvisle, S., Rytter, E.,Spectrochim. Act. A, 40 (1984) 939-951.

[15] Kerber, R.N., Kermagoret, A., Callens, E., Florian, P., Massiot, D., Lesage, A., Coperet, C., Delbecq, F., Rozanska, X., Sautet, P.,J. Am. Chem. Soc., 134 (2012) 6767-6775.

[16] Li, J.H., DiVerdi, J.A., Maciel, G.E.,J. Am. Chem. Soc., 128 (2006) 17093-17101.

[17] Pelletier, J., Espinas, J., Vu, N., Norsic, S., Baudouin, A., Delevoye, L., Trébosc, J., Le Roux, E., Santini, C., Basset, J.M., Gauvin, R.M., Taoufik, M.,Chem Commun., 47 (2011) 2979-2981.

[18] Ryokichi, T.,Bulletin of Chemica Society of Japan, 39 (1966) 2126-2132.

[19] Ghiotti, G., Garrone, E., Della Gatta, G., Fubini, B., Giamello, E.,J. Catal., 80 (1983) 249-262.

[20] Ghiotti, G., Garrone, E., Zecchina, A.,J. Mol. Catal., 46 (1988) 61-77.

[21] Ghiotti, G., Garrone, E., Zecchina, A.,J. Mol. Catal., 65 (1991) 73-83.

[22] Zecchina, A., Spoto, G., Ghiotti, G., Garrone, E.,J. Mol. Catal., 86 (1994) 423-446.

[23] Rebenstorf, B.,Acta Chem. Scand. A, 43 (1989) 413.

[24] Morterra, C., Cerrato, G., Novarino, E., Mentruit, M.P.,Langmuir, 19 (2003) 5708-5721.

[25] Morterra, C., Mentruit, M.P., Cerrato, G.,PCCP, 4 (2002) 676-687.

[26] Lupinetti, A.J., Frenking, G., Strauss, S.H.,Angew. Chem. -Int. Edit., 37 (1998) 2113-2116.

[27] Lupinetti, A.J., Strauss, S.H., Frenking, G.,Progr. Inorg. Chem., 49 (2001) 1-112.

[28] Xia, W., Tonosaki, K., Taniike, T., Terano, M., Fujitani, T., Liu, B.P.,J. Appl. Polym. Sci., 111 (2009) 1869–1877.

[29] Braterman, P.S., Metal Carbonyl Spectra, Academic Press, London, 1975.

[30] Zhou, M.F., Andrews, L., Bauschlicher, C.W.,Chem. Rev., 101 (2001) 1931-1961.

[31] Estephane, J., Groppo, E., Vitillo, J.G., Damin, A., Gianolio, D., Lamberti, C., Bordiga, S., Quadrelli, E.A., Basset, J.M., Kervern, G., Emsley, L., Pintacuda, G., Zecchina, A.,J. Phys. Chem. C, 114 (2010) 4451-4458.

[32] Estephane, J., Groppo, E., Vitillo, J.G., Damin, A., Lamberti, C., Bordiga, S., Zecchina, A.,Phys.Chem.Chem.Phys., 11 (2009) 2218-2227.

[33] Groppo, E., Damin, A., Otero Arean, C., Zecchina, A.,Chem. Eur. J., 17 (2011) 11110 – 11114.

[34] Jeffery, E.A., Mole, T.,Aust J Chem, 21 (1968) 2683-2686.

[35] Cerruti, M., Morterra, C., Ugliengo, P.,Chemistry of Materials, 17 (2005) 1416-1423.

[36] Platero, E.E., Mentruit, M.P., Morterra, C.,Langmuir, 15 (1999) 5079-5087.

[37] Arean, C.O., Platero, E.E., Mentruit, M.P., Delgado, M.R., Xamena, F., Garcia-Raso, A., Morterra, C.,Micropor Mesopor Mat, 34 (2000) 55-60.

[38] Sempels, R.E., Rouxhet, P.G.,J Colloid Interface Sci, 55 (1976) 263-273.

[39] Pelmenschikov, A.G., Van Santen, R.A., Jänchen, J., Meijer, E.,J.Phys.Chem. , 97 (1993) 11071-11074.

[40] Chen, J., Thomas, J.M., Sankar, G.,J. Chem. Soc., Faraday Trans., 90 (1994) 3455-3459.

[41] Aboulayt, A., Binet, C., Lavalley, J.,J. Chem. Soc., Faraday Trans., 91 (1995) 2913-2920.

[42] Cerruti, M., Bolis, V., Magnacca, G., Morterra, C.,PCCP, 6 (2004) 2468-2479.

[43] Knoezinger, H., Krietenbrink, H.,J. Chem. Soc., Faraday Trans. 1,, 71 (1975) 2421-2430.

[44] Classification of Adsorption Behavior: Simple Fluids in Pores of Slit-shaped Geometry," Perla B. Balbuena and Keith E. Gubbins, Fluid Phase Equilibria, 76, 21-35, Elsevier Science Publishers, B.V., Amsterdam (1992).

[45] Martino, G.A., Barzan, C., Piovano, A., Budnyk, A., Groppo, E.,J. Catal., 357 (2018) 206-212.

Chapter 5
Modification of Cr(VI)/SiO₂ with Al-alkyls.

In this chapter we will discuss the effect of Al-alkyls on the Cr(VI)/SiO$_2$ system. As starting point, the oxidized catalyst presents further levels of complexity with respect to the reduced one. The major one is the possible co-existence of Cr sites in different oxidation states after the reaction with Al-alkyls: Cr(VI), Cr(V), Cr(IV), Cr(III), Cr(II), are all possible (and why not, also Cr(I)). Moreover, different types of by-products can be formed during the reaction of Al-alkyls with the chromates, as well as with the silica surface.

5.1 The reactivity of the Cr(VI)/SiO₂ with TEA and DEALE

5.1.1 Electronic and paramagnetic properties of Cr(VI)/SiO₂ modified by TEA and DEALE

Figure 5. 1 shows the evolution of the DR UV-Vis spectra of Cr(VI)/SiO₂ upon the interaction with TEA (part a) and DEALE (part b). The characteristic features of the Phillips catalyst in its oxidized form (spectra 1) have been already discussed in Figure 3.2. Upon interaction with the alkylating agents in the Al:Cr=2:1 ratio (spectra 2), the colour of the catalyst changes from orange-yellow to brown-greenish, and the colour becomes darker for Al:Cr=4:1 (spectra 3). Correspondingly, the DR UV-Vis spectra change. In particular, for both systems the intense bands at about 29000 cm^{-1} and 39500 cm^{-1} decrease in intensity, accompanied by the appearance of a broad band covering the whole 8000-20000 cm^{-1} range, due to a multitude of d-d transitions of reduced chromium species, and of a complex envelope of bands in the NIR region (insets in Figure 5. 1).
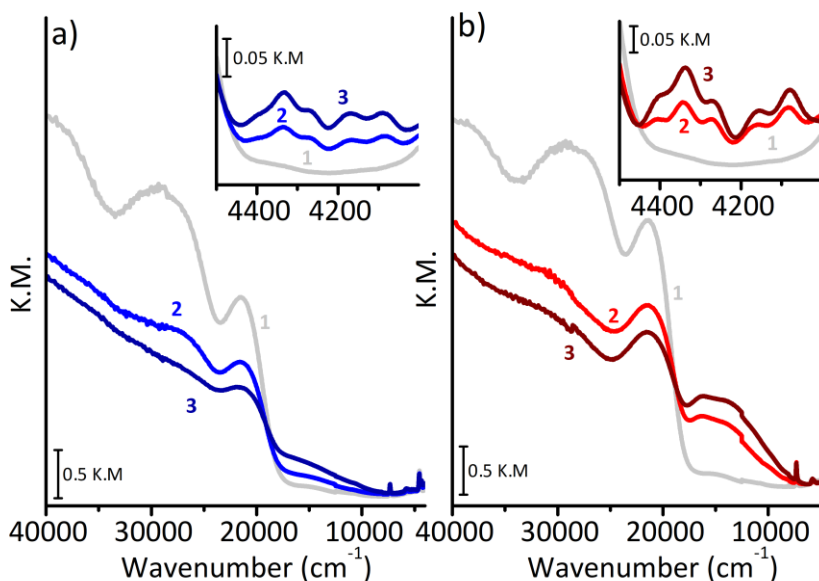
Figure 5. 1 DR UV-Vis-NIR spectra of part a) Cr(VI)/SiO₂ (spectrum 1), of the Cr(VI) /SiO₂+TEA(2:1) (spectrum 2), and of Cr(VI) /SiO₂+TEA(4:1) (spectrum 3) systems. The inset shows a magnification of the NIR region. Part b) the same of part a, but with DEALE.

While the latter bands are easily assigned to the overtones and the combinations of the ν(CH$_x$) and δ(CH$_x$) vibrational modes of the alkyl groups deriving from TEA and DEALE (proportional to the amount of Al-Alkyls added), the assignment of the very broad band in the d-d region is less straightforward. The following observation can be done:

1. The band at 21500 cm^{-1} (attributed to the monochromates) decreases in intensity proportionally to the amount of the alkylating agent. In the meanwhile, the bands in the d-d region increase in intensity with the same trend.

2. In the presence of a Al:Cr=2:1 amount of TEA and DEALE, only a fraction of the Cr(VI) sites are reduced, although in principle this amount should be enough for the reduction of all the chromium sites (in the literature it is considered as the stoichiometric ratio) [1, 2]. The amount of Cr(VI) reduced by TEA and DEALE increases when Al:Cr=4:1, but this is still not enough for a complete reduction. This observation is in agreement with the quantitative speciation measured with XPS by Liu et al. [3], and it means that only a fraction of the Al-Alkyls molecules are involved in the reaction with the Cr(VI) sites, while the others are likely involved in other reactions at the silica surface, as reported in literature (vide infra) [4, 5].

3. The fraction of modified Cr sites, evaluated in terms of decrease of the band at 21500 cm^{-1}, is similar in the two cases. However, the d-d bands are more intense for Cr(VI)/SiO$_2$+DEALE than for Cr(VI)/SiO$_2$+TEA, suggesting that in the latter case the reduced Cr species are more symmetric.
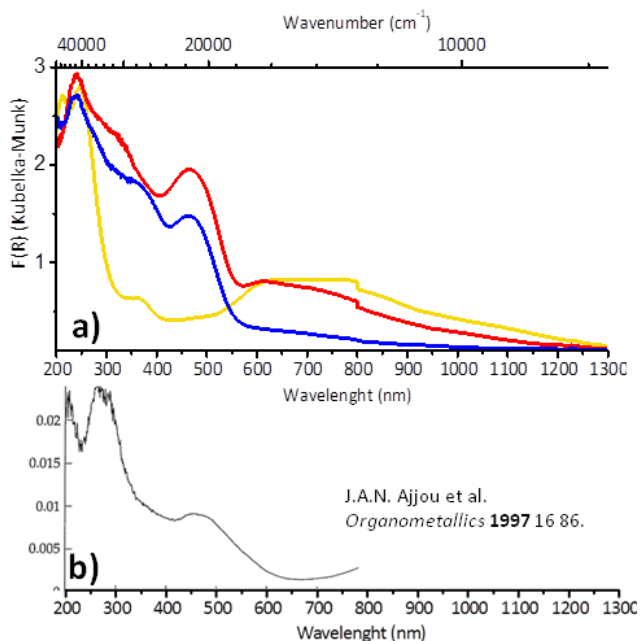
Figure 5. 2 Part a): DR UV-Vis spectra of Cr(VI) /SiO$_2$+TEA(2:1) (blue), Cr(VI) /SiO$_2$+DEALE(2:1) (red) and that of Cr(II)/SiO$_2$ in interaction with N$_2$O (yellow), taken here as a reference for Cr(II) sites highly coordinated by O-containing ligands. Part b): DR UV-Vis spectrum of a SiO$_{2-500}$ modified with Cr(CH$_2$C(CH$_3$)$_3$)$_4$, reproduced from Ref. [6].

The determination of the oxidation state for the modified Cr sites is not unambiguous, especially because the UV-Vis spectra still contain some signals from a residual amount of Cr(VI) sites. A possible interpretation of these spectra can be done on the basis of UV–Vis spectra of reference compounds. In Figure 5. 2 we compared the spectra of the Cr(VI)/SiO$_2$+TEA(2:1) and Cr(VI)/SiO$_2$+DEALE(2:1) with those of two references: a) Cr(II)/SiO$_2$ in interaction with the N$_2$O probe molecule (spectrum yellow), considered as a reference of Cr(II) sites highly coordinated by O-containing ligands; b) Cr(CH$_2$C(CH$_3$)$_3$)$_4$ grafted on silica (Figure 5. 2b), where the presence of only Cr(IV) alkylated sites was claimed by EPR analysis [6]. For sake of comparison the spectra are reproduced in the same scale, although unfortunately a limited wavelength region is reported by Ajjou group, which does not allow a full comparison.

The spectra of Cr(VI)/SiO$_2$+TEA(2:1) and Cr(VI)/SiO$_2$+DEALE(2:1) catalysts display some features in common with both the reference spectra. In the d-d region the spectra of the modified catalysts are very similar to that of Cr(II)/SiO$_2$ in interaction with N$_2$O, where the Cr(II) sites expand their coordination environment due to the coordination of two N$_2$O molecules. This suggests that Cr(II) sites might be formed from the interaction of Cr(VI)/SiO$_2$ with TEA and DEALE, but also that the AlO$_x$R$_y$ by-products or other AlR$_x$ species grafted nearby must stay in interaction with the Cr(II) sites. Nevertheless, the spectra of Cr(VI)/SiO$_2$+TEA(2:1) and Cr(VI)/SiO$_2$+DEALE(2:1) differ from that of Cr(II)/SiO$_2$+N$_2$O in the 400-500 nm region (at around 25000-20000 cm^{-1}). At least in part, the difference is due to the presence of residual Cr(VI) species, as discussed above. However, it must be noticed that the spectrum of alkylated Cr(IV) species also contains an intense band at ca. 21500 cm^{-1}.

Overall, the spectra of Cr(VI)/SiO$_2$+TEA(2:1) and Cr(VI)/SiO$_2$+DEALE(2:1) suggest that, after interaction of Cr(VI)/SiO$_2$ with TEA and DEALE, a fraction of the Cr(VI) sites is reduced to highly coordinated Cr(II) species, and another to alkylated Cr(IV) species. It is worth noticing that the formation of alkylated Cr(IV) species has been postulated as one of the possible mechanism of alkylation [7] (see paragraph 1.4.3). These observations are only partially in agreement with the pioneering works of Cicmil et al.[1, 2, 8]. Indeed, in these works two different contributions were tentatively pointed out in the d-d transition region: i) a band at ca. 10000 cm^{-1}, attributed to the $^5E_g \rightarrow ^5T_{2g}$ transition of a 6-fold coordinated Cr(II) species; ii) a band around 16000 cm^{-1}, assigned to the $^4A_{2g} \rightarrow ^4T_{2g}$ transition of a 6-fold coordinated Cr(III) species [2].

Complementary information on the oxidation state of the modified Cr sites can be obtained by X-band EPR experiments. Figure 5. 3 shows the X-band EPR spectra of Cr(VI)/SiO$_2$ before (spectra 1) and after reaction with TEA and DEALE at the two concentrations (spectra 2 and 3). After the oxidative treatment at 650 °C, most of the Cr sites are in the form of diamagnetic Cr(VI) monochromates, hence EPR inactive, as already discussed in Chapter 3. As previously discussed, the signal observable in the EPR spectra at *g* = 1.969 is due to a small fraction of Cr(V) species, always present but considered as spectators [7, 9, 10]. The amount of Cr(V) is typically lower than 2% of the total Cr sites [9].
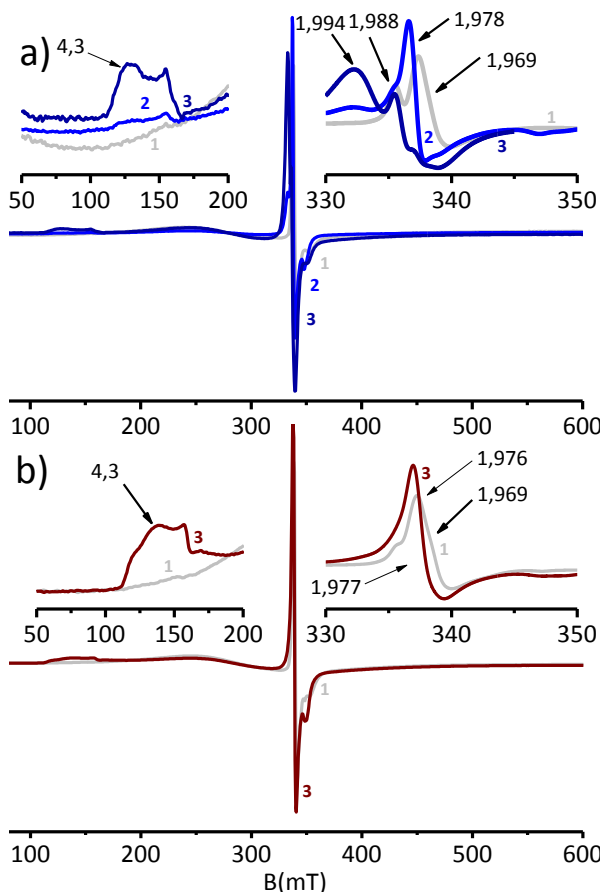
Figure 5. 3 Part a) X-band CW-EPR spectra of oxidized Cr(VI)/SiO$_2$ (spectrum 1), of Cr(VI) /SiO$_2$+TEA(2:1) (spectrum 2) and of Cr(VI) /SiO$_2$+TEA(4:1) (spectrum 3). The enlargements of the mid-field and of the low-field regions are shown in the inset. The spectra were recorded at T = 100 K. Part b) The same of part a but with DEALE.

After reaction with the Al-alkyls, some changes are observed in the EPR spectra. Starting with Cr(VI)/SiO$_2$+TEA(2:1) (Figure 5. 3a, spectrum 2), the signal of

Cr(V) becomes sharper and slightly shifts at $g = 1.978$. This is likely a consequence of the proximity of TEA (or its reaction by-products) to the Cr(V) sites, that causes a modification of their symmetry. No additional bands are observed in the spectrum, but only an extremely weak signal at $g = 4.3$, that indicates the presence of a tiny amount of isolated Cr(III). This means that **the majority of the Cr(VI) sites reduced by TEA are transformed into reduced Cr species which are EPR silent (either Cr(IV) or Cr(II)).** This result is in very good agreement with the DR UV-Vis results discussed above, which indicate the formation of Cr(IV) and highly coordinated Cr(II) sites. The EPR spectrum of Cr(VI)/SiO$_2$+TEA(4:1) (Figure 5. 3a, spectrum 3) further changes. This time the signal of Cr(V) drastically decreases in intensity, and simultaneously a new signal at $g = 1.994$ appears. Simultaneously, the signal at $g = 4.3$ becomes much more intense. While the signal at $g = 4.3$ is straightforwardly associated to isolated Cr(III) species [11], that at $g = 1.994$ is related to Cr(III) in small clusters (α-Cr$_2$O$_3$). Both signals seem correlated to the disappearance of the Cr(V) signal.

The evolution of the EPR spectra is slightly different in the presence of DEALE. In the spectrum of Cr(VI)/SiO$_2$+DEALE(4:1) (spectrum 3) we observe the formation of two new signals at $g = 1.976$ and at $g = 4.3$. The latter signal indicates that, as for TEA, an excess of DEALE causes the formation of a small portion of isolated Cr(III), while in this case no Cr(III) clusters are noticed. This behaviour could be related to the less reducing power of DEALE respect to TEA.

5.1.2 Reactivity of TEA and DEALE with Cr(VI)/SiO$_2$ as monitored by FT-IR spectroscopy

The reaction of Cr(VI)/SiO$_2$ with both Al-Alkyls was monitored by FT-IR spectroscopy, as reported in Figure 5. 4. The spectrum of the oxidized catalyst (spectrum 1) is the same as that previously described in Figure 3.4. The reaction of Cr(VI)/SiO$_2$ with TEA and DEALE (spectra 2) is demonstrated by the appearance of the absorption bands related to the alkyl groups, as described in the previous chapter. Also in this case, it is not possible to distinguish among the alkylated Cr sites, the Al(OR)$_x$R$_y$ by-products, and the AlR$_x$ species grafted on silica [5]. The main difference with respect to the reactivity of Cr(II)/SiO$_2$ with TEA and DEALE, is the fact that the intensity of these bands is almost the same when Al:Cr = 2:1 (spectrum 2) and when Al:Cr = 4:1 (spectrum 3). In other words, **the Al:Cr = 2:1 ratio seems to be the maximum amount of Al-alkyl that can react with Cr(VI)/SiO$_2$.** This is quite curious, since we know from the other techniques (*vide supra* DR UV-Vis) that a fraction of Cr(VI) sites remains unmodified even in the presence of a Al:Cr = 4:1 ratio. Moreover, only a small fraction of the OH groups reacts with TEA and DEALE and this amount seems independent on the Al:Cr ratio.
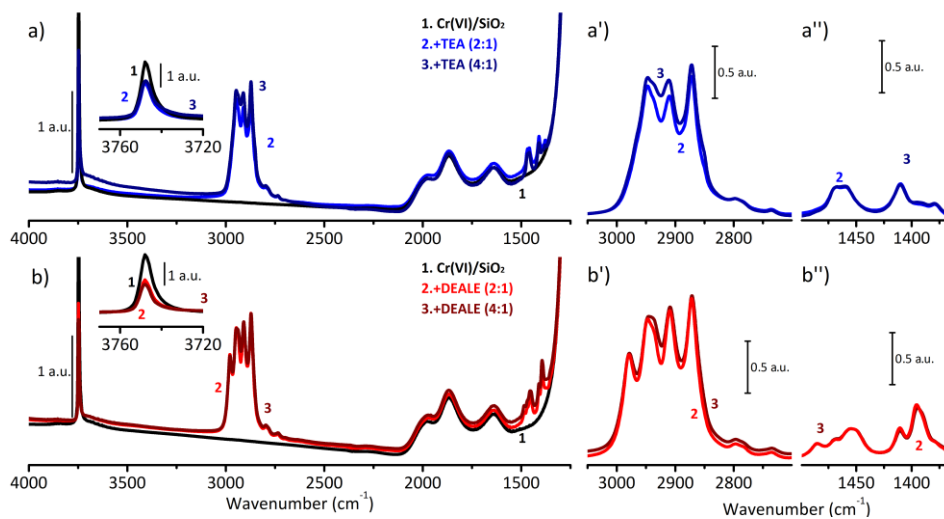
Figure 5. 4 Part a) FT-IR spectra of Cr(VI)/SiO$_2$ before (spectrum 1), and after modification with TEA in an amount equal to Al:Cr = 2:1 (spectrum 2) and Al:Cr = 4:1 (spectrum 3). The inset in part a shows a magnification of the Si-OH region. Parts a' and a'' report a magnification of spectra 2 and 3 after subtraction of spectrum 1, in the CH stretching and bending regions. Parts b) b') and b'') the same of part a), a') and a'') for DEALE.

5.2 The accessibility of the Cr sites modified by TEA and DEALE.

Successively, the accessibility of the Cr sites in the modified $Cr(VI)/SiO_2$ catalysts was investigated by means of FT-IR spectroscopy of adsorbed probe molecules.

5.2.1 Probing the Cr sites with CO

Figure 5. 5 shows the FT-IR spectra, in the v(CO) region, of CO adsorbed at room temperature on the TEA/DEALE-modified $Cr(VI)/SiO_2$ catalysts (Al:Cr=2:1, Figure 5. 5a-a', and Al:Cr=4:1, Figure 5. 5b-b'). All the spectra were normalized for the thickness of the pellet and hence the absolute intensities are comparable and quantitative information can be extracted.
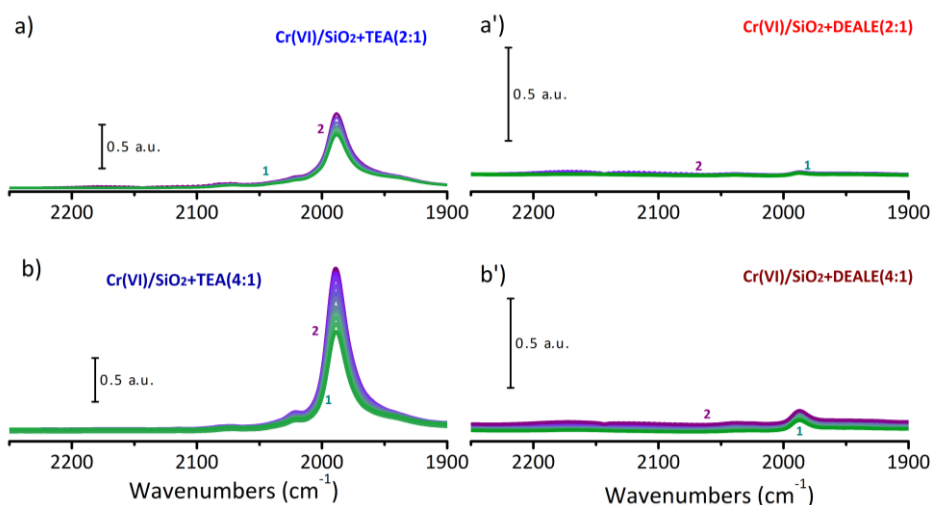
Figure 5. 5 Part a) Evolution of the background subtracted FT-IR spectra, in the $\tilde{v}$(CO) region, for CO adsorbed at room temperature on the $Cr(VI)/SiO_2$+TEA(2:1) catalyst (part a), from P_{CO} = 100 mbar (spectrum 2) to zero (spectrum 1). Part b): the same for $Cr(VI)/SiO_2$+TEA(4:1). Parts a') and b') the same of parts a) and b) but for the DEALE. All the spectra are reported after subtraction of that collected before CO dosing.

The spectra collected at the maximum CO coverage (spectra 2) on the $Cr(VI)/SiO_2$+TEA catalysts (Figure 5. 5a-b) are dominated by a single absorption band centred at about 1988 cm^{-1}, with a shoulder at 2022 cm^{-1} that becomes more evident for $Cr(VI)/SiO_2$+TEA(4:1). No other bands are detected. Interestingly, the shape and the position of these bands are similar not only to those of CO adsorbed on $Cr(II)/SiO_2$+TEA, Interestingly, the shape and position of these bands are similar to those observed in the spectrum of CO adsorbed on the $Cr(II)/SiO2$ catalyst modified with triethylsilane (TES), analogously to what already discussed for CO adsorbed on $Cr(II)SiO2$+TEA [12, 13]. For sake of comparison, Figure 5. 6 shows the FT-IR spectrum of CO adsorbed at the maximum coverage on: the unmodified

Cr(II)/SiO$_2$ (spectrum 1), Cr(VI)/SiO$_2$+TEA(2:1) (spectrum 2), Cr(VI)/SiO$_2$+TEA(4:1) (spectrum 3), and Cr(II)/SiO$_2$+TES (spectrum 4). For Cr(II)/SiO$_2$+TES some of us previously demonstrated that more than 80% of the Cr(II) sites were transformed into mono-grafted [≡Si-O-Cr(II)-OSiR$_3$] sites [12]. For this reason, we conclude that **at least a fraction of the Cr(VI) sites in Cr(VI)/SiO$_2$+TEA have been transformed into mono-grafted Cr(II) species, stabilized by some ligands nearby**. This result is again in very good agreement with the DR UV-Vis results discussed above.
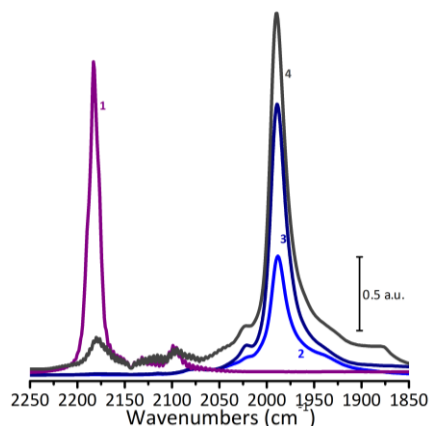
Figure 5. 6 FT-IR spectra, in the ṽ(CO) region, of the maximum coverage of CO adsorbed at room temperature on unmodified Cr(II)/SiO$_2$ (spectrum 1), on Cr(VI)/SiO$_2$+TEA(2:1) (spectrum2), on Cr(VI)/SiO$_2$+TEA(4:1) (spectrum 3) and on Cr(II)/SiO$_2$+TES (spectrum 4). All the spectra are reported after subtraction of that collected before CO dosing. All the spectra were normalized for the thickness of the pellet and hence the absolute intensities are comparable and quantitative information can be extracted.

In order to better assign the band at 1988 cm^{-1}, we performed an analogous experiment with a 1:1 mixture of ^{12}CO:^{13}CO. The use of isotopic mixtures is a widely employed method for assigning complex IR spectra [12]. The results are summarized in Figure 5. 7, and compared to those published for the similar Cr(II)/SiO$_2$+TES [12]. The analogy between the two systems is immediately clear. The IR absorption pattern is typical of dicarbonyl species. Hence, we can conclude that **in Cr(VI)/SiO$_2$+TEA catalysts the modified Cr sites accessible to CO are Cr(II) species mono-grafted to silica, and are characterized by at least two coordination vacancies**.
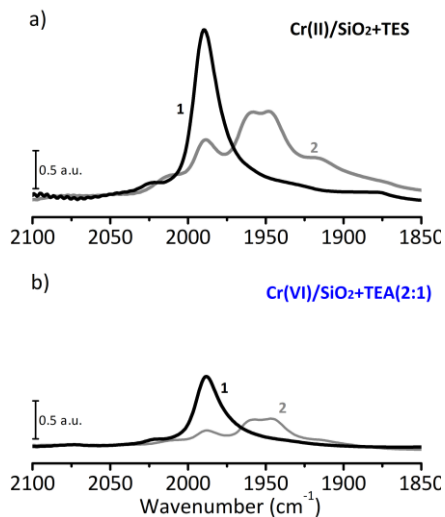
Figure 5. 7. Part a): FT-IR spectra, in the $\tilde{v}(CO)$ region, of ^{12}CO (black) and a mixture of $^{12}CO{:}^{13}CO =$ 1:1 (grey) adsorbed on Cr(II)/SiO$_2$+TES. Part b): the same experiment for Cr(VI)/SiO$_2$+TEA(2:1). All the spectra were normalized for the thickness of the pellet and hence the absolute intensities are comparable and quantitative information can be extracted.

For Cr(VI)/SiO$_2$+DEALE the spectra of CO adsorbed at room temperature (Figure 5. 5 b' and c') contain almost no bands. Only for CO adsorbed on Cr(VI)/SiO$_2$+DEALE(4:1) a very weak band is observed, which is a reminiscence of those detected for the Cr(VI)/SiO$_2$+TEA systems. The logical conclusion from these results is that **the modified chromium sites in Cr(VI)/SiO$_2$+DEALE are more sterically hindered and for this reason mostly not accessible to CO.** It is worth anticipating here that this does not means that the same sites are not accessible by stronger probes, including ethylene.

A quantification of the modified Cr(VI) sites in Cr(VI)/SiO$_2$+TEA and Cr(VI)/SiO$_2$+DEALE is less easy than for Cr(II)/SiO$_2$+TEA/DEALE. Indeed, we cannot estimate the total amount of modified Cr sites in this case, but only those that are accessible by CO. However, we can measure the integrated area of the band at 1988 cm^{-1} and compare it to the value obtained for CO on Cr(II)/SiO$_2$+TES, which corresponds to 80% of the total Cr sites [12]. The results of the calculation are reported in Table 5. 1, and better visualized in Figure 5. 8. As already discussed for Cr(II)/SiO$_2$+TEA/DEALE, **only a fraction of the total Cr sites is modified and accessible to CO. In general, this fraction is larger for Cr(VI)/SiO$_2$+TEA than for Cr(VI)/SiO$_2$+DEALE, and increases at higher Al:Cr ratio.** It is worth noticing that the fraction of Cr sites modified by DEALE and accessible to CO is very small in this case.

Table 5. 1 Quantification of the fraction of the Cr sites (with respect to the total) visible by CO in Cr(VI)/SiO$_2$+TEA and Cr(VI)/SiO$_2$+DEALE, as determined by analysing the FT-IR spectra of CO adsorbed at room temperature on Cr(VI)/SiO$_2$+TEA and Cr(VI)/SiO$_2$+DEALE. These sites are likely mono-grafted Cr(II) species, very similar to those formed in Cr(II)/SiO$_2$+TEA and Cr(II)/SiO$_2$+DEALE.

	System	ratio	classic carbonyls int. Area	Cr(II)$^{modif}_{vis}$ (%)
Cr(VI)/SiO$_2$	bare	0		
	TEA 2:1	2	23	31.5
	TEA 4:1	4	47.4	64.8
	DEALE 2:1	2	0.4	0.5
	DEALE 4:1	4	1.5	2.1
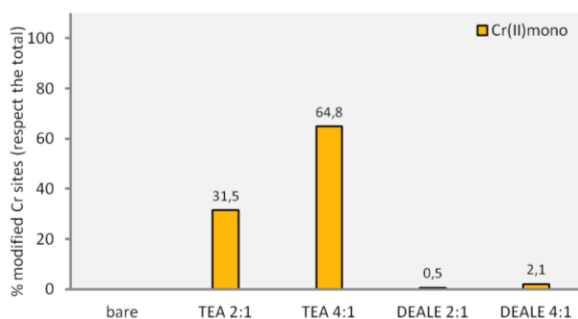
Figure 5. 8 Quantitative determination of the fraction of Cr(VI) sites reduced and modified by TEA and DEALE in different Al:Cr ratio, as determined by analysing the FT-IR spectra of CO adsorbed at room temperature on Cr(VI)/SiO$_2$+TEA and Cr(VI)/SiO$_2$+DEALE. This fraction has been estimated from the integrated intensity of the ν(C≡O) band at 1988 cm^{-1}. The position of the band indicate that the sites accessible to CO are Cr(II) species mono-grafted to the silica surface.

5.2.2 Probing the Cr sites with CD$_3$CN

Successively, we performed a series of FT-IR experiments using CD$_3$CN as probe molecule. As already discussed in the previous chapter, CD$_3$CN is a stronger probe than CO and hence has the capability to probe also the sites more hindered; moreover, it has a stronger basic character, and hence it is more sensible to the acidic strength. The experiments have been performed in the presence of an Al:Cr ratio of 2:1. Figure 5. 9 shows the evolution of the background subtracted FT-IR spectra in the $\tilde{v}$(C≡N) region for d-acetonitrile adsorbed at room temperature on Cr(VI)/SiO$_2$+TEA(2:1) (part a), Cr(VI)/SiO$_2$+DEALE(2:1) (part a'), Cr(VI)/SiO$_2$ (part b and b'), SiO$_2$+TEA (part c) and SiO$_2$+DEALE (part c'), as a function of the CD$_3$CN coverage. The spectra of SiO$_2$+TEA (part c) and of SiO$_2$+DEALE (part c') were already described at Chapter 4.2.2.
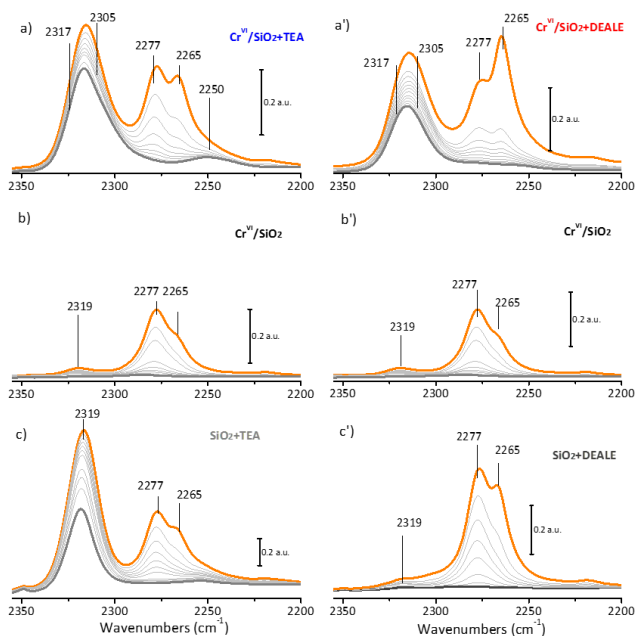
Figure 5. 9 Evolution of the background subtracted FT-IR spectra, in the $\tilde{\nu}(C\equiv N)$ region, for CD_3CN adsorbed at room temperature on Cr(VI)/SiO$_2$+TEA(2:1) catalyst as a function of the CD_3CN coverage (part a), compared to the same sequence of spectra collected for CD_3CN adsorbed on unmodified Cr(VI)/SiO$_2$ (part b), and on SiO$_2$+TEA(2:1) (part c). All the spectra are reported after subtraction of that collected before CD_3CN dosing. The spectra are all normalized for the optical thickness of the pellet. Orange spectra: maximum CD_3CN coverage; bold grey spectra: irreversible fraction of adsorbed CD_3CN. Parts a' and c': the same as parts a and c, for DEALE.

Upon CD_3CN adsorption on the Cr(VI)/SiO$_2$ catalyst (part b and b') the only observed bands are those associated to CD_3CN adsorbed on the surface OH groups (at 2277 cm^{-1}) and the physisorbed CD_3CN (at 2265 cm^{-1}), as previously described in Chapter 4 [14-17]. The absolute intensity of these bands is lower with respect to those observed in the spectrum of CD_3CN on Cr(II)/SiO$_2$, and their relative intensity is inverted. This indicates that Cr(II)/SiO$_2$ is more dehydroxylated than Cr(VI)/SiO$_2$. A very weak band is also observed at 2319 cm^{-1}, which is due to d-acetonitrile in interaction with a minor amount of Cr(VI) species. The intensity of this band, however, is negligible with respect to all the other bands and will be neglected in the following discussion. Upon degassing, all these bands rapidly decrease in intensity up to disappear, indicating that the interaction is quite weak and fully reversible.

Besides the two bands at 2277 and 2265 cm^{-1} already described, the spectra of CD_3CN adsorbed on Cr(VI)/SiO$_2$+TEA(2:1) (Figure 5. 9a) are characterized by two additional contribution, much more resistant to degassing and the same as those already discussed for Cr(II)/SiO$_2$+TEA(2:1):

1) a very broad absorption band centred at 2315 cm^{-1}, which is evidently the overlap of at least two different contributions: the first one, at ca. 2305 cm^{-1}, is attributed to weak Lewis acid sites (W-LA), while the second, at ca. 2317 cm^{-1}, is due to strong Lewis acid sites (S-LA). At least in part, the Al(III) species deriving from TEA contribute to this second band.

2) a band at ca. 2250 cm^{-1}, already observed for CD_3CN adsorbed on Cr(II)/SiO$_2$+TEA(2:1), and previously assigned to CD_3CN bridged in between Cr and Al, that provides evidence for the presence of Cr-Al couples.

The spectrum of CD_3CN adsorbed on Cr(VI)/SiO$_2$+TEA(2:1) at the minimum coverage was subjected to a deconvolution process, and the integrated areas of the bands at 2317, 2305 and 2250 cm^{-1} were determined. The fraction of accessible W-LA, S-LA and Cr-Al couples were then estimated in relation to the total amount of Cr sites (i.e. the Cr(II) sites accessible to CD_3CN in Cr(II)/SiO$_2$), and in the approximation of a constant molar extinction coefficient in the whole spectral range. It is worth noticing that the sum of the W-LA, S-LA and Cr-Al species might exceed 100%, since also the Al(III) sites are potentially probed by CD_3CN. The results are summarized in Table 5. 2 and in Figure 5. 10.

Table 5. 2. Quantification of the amount of weak Lewis acid sites (W-LA), strong Lewis acid sites (S-LA) and Cr-Al couples (Cr-Al) visible by CD_3CN in Cr(VI)/SiO$_2$+TEA and Cr(VI)/SiO$_2$+DEALE, expressed in percentage with respect to the total amount of Cr sites. These values have been determined by analysing the FT-IR spectra of CD_3CN adsorbed at room temperature on Cr(VI)/SiO$_2$+TEA and Cr(VI)/SiO$_2$+DEALE.

Cr(VI)/SiO$_2$ System	ratio	W-LA (Int. Area 2305 cm-1)	S-LA (Int. Area 2317 cm-1)	Cr-Al (Int. Area 2250-2270 cm-1)	W-LA (%)	S-LA (%)	Cr-Al (%)
bare	0						
TEA(2:1)	2	4.0	4.6	1.7	34.6	39.8	14.6
DEALE(2:1)	2	1.1	3.7		9.8	32.0	0.0
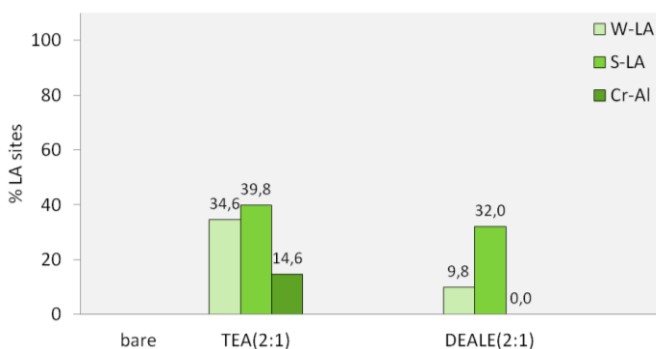
Figure 5. 10 Quantitative determination of the fraction of weak Lewis acid sites (W-LA), strong Lewis acid sites (S-LA) and Cr-Al couples (Cr-Al), as determined by analysing the FT-IR spectra of CD_3CN adsorbed at room temperature on Cr(VI)/SiO$_2$+TEA and Cr(VI)/SiO$_2$+DEALE.

Overall, the analysis of the spectra shown in Figure 5. 9 indicates that, **in Cr(VI)/SiO$_2$+TEA(2:1), CD$_3$CN probes ca. 35% of W-LA, ca. 40% of S-LA and ca. 15% of Cr-Al couple** (where the fractions have been estimated in relation to the total amount of Cr sites). **It is worth noticing that the amount of W-LA sites probed by CD$_3$CN is very close to the 32% of mono-grafted Cr(II) sites probed by CO**.

The same experiment was repeated for Cr(VI)/SiO$_2$+DEALE(2:1), as reported in Figure 5. 9a'. Contrarily to what happens with CO, d-acetonitrile interacts with a substantial fraction of Lewis acid sites, giving origin to a broad band centred at ca. 2317 cm^{-1}, as already discussed for Cr(VI)/SiO$_2$+TEA(2:1). The spectrum at the lowest coverage was analysed following the same protocol discussed above and the results are reported in Table 5. 2 and Figure 5. 10. The W-LA sites accessible to CD$_3$CN account for ca. 10% of the total Cr sites, whereas the S-LA account for ca. 32%. This latter contribution should not include any accessible Al(III) sites. Indeed, the blank experiment performed on SiO$_2$+DEALE(2:1) demonstrates that the DEALE-derived Al species are not accessible to CD$_3$CN (Figure 5. 9c'). **Hence, these data indicate that ca. 42% of the Cr(VI) in Cr(VI)/SiO$_2$+DEALE(2:1) are reduced to Cr(II), although CO is not able to probe any of them.** Finally, similarly to the case of Cr(II)/SiO$_2$+DEALE(2:1) (Chapter 4) and contrarily to Cr(VI)/SiO$_2$+TEA(2:1) (Figure 5. 9a), no bands are noticed at 2250 cm^{-1} that could be linked to CD$_3$CN in interaction with Al-Cr couples.

5.2.3 A summary on the accessibility of the Cr sites in the Al-alkyl modified Cr(VI)/SiO$_2$ catalysts.

The experiments performed by using CO and CD$_3$CN as molecular probes are compared and summarized in the following. For Cr(VI)/SiO$_2$+TEA(2:1), ca. 32% of the total Cr(VI) sites are reduced to Cr(II) mono-grafted to silica, as probed by CO. This fraction is very similar to the amount of W-LA sites probed by CD$_3$CN (ca. 35% of the total Cr sites). Hence, it is very likely that the mono-grafted Cr(II) sites detectable by CO behave like W-LA sites. In addition, CD$_3$CN reveals the presence of: 1) ca. 40 % of S-LA sites, among which a fraction might be due to the Al(III) sites derived from the reaction of TEA with silica and/or the Cr sites; and 2) ca. 15% of Cr-Al couples able to coordinate CD$_3$CN in a bridged way. Both the S-LA and the Cr-Al sites are not probed by CO, and hence should be shielded by TEA in excess and/or its by-products.

For Cr(VI)/SiO$_2$+DEALE, almost no reduced Cr sites are probed by CO. This indicates that, if present, the mono-grafted Cr(II) sites are much more shielded than those present in Cr(VI)/SiO$_2$+TEA. In contrast, CD$_3$CN, being a stronger probe,

is able to probe at least part of them. In Cr(VI)/SiO$_2$+DEALE(2:1) CD$_3$CN reveals the presence of ca. 10% of W-LA (probably Cr(II) sites mono-grafted to silica), and ca. 34% of S-LA sites. It is evident that a much larger amount of the Cr sites in the Cr(VI)/SiO$_2$+DEALE catalyst are not accessible to both probes. This implies that the modified sites are more hindered and/or that a larger amount of Cr(IV)-alkylated sites are present.

5.3. Ethylene polymerization over the Al-alkyl modified Cr(VI)/SiO$_2$

5.3.1 A kinetic study

Kinetic experiments were performed to evaluate the gas-phase ethylene polymerization rate on the TEA-modified and the DEALE-modified Cr(VI)/SiO$_2$ catalysts, at two different concentrations, in comparison with the Cr(VI)/SiO$_2$ catalyst. Taking into account that the Cr(VI)/SiO$_2$ catalyst shows a long induction time, we decided to show in Figure 5. 11 all the data recorded in order to demonstrate how the modification made with the Al-alkyls influences the kinetic of the polymerization. In practice, as already claimed in literature [7], no induction time is recorded for the modified catalysts. In addition, all the modified catalysts show the same trend observed before for the pre-reduced Cr(II)/SiO$_2$+TEA and Cr(II)/SiO$_2$+DEALE catalysts.
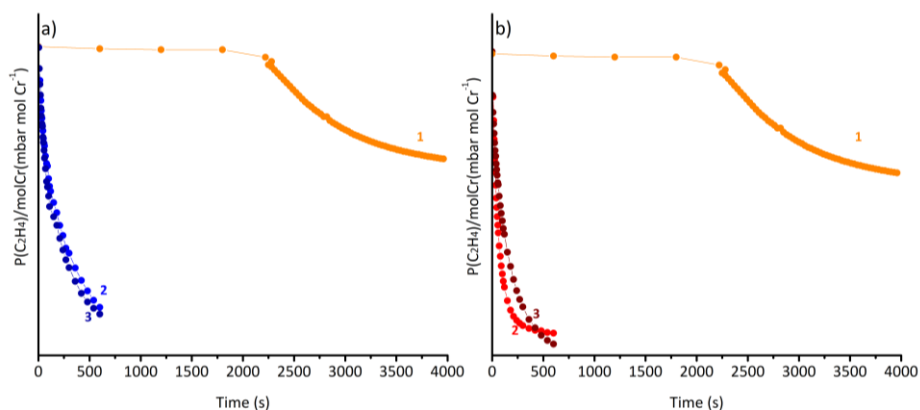
Figure 5. 11 Part a): Kinetics of the gas-phase ethylene polymerisation on the Cr(VI)/SiO$_2$ catalyst (curve 1) in comparison to that on Cr(VI)/SiO$_2$+TEA(2:1) (curve 2), and on Cr(VI)/SiO$_2$+TEA(4:1) (curve 3). The measurements were performed at room temperature, by recording the ethylene pressure as a function of time. Part b): the same as part a for the DEALE-modified Cr(VI)/SiO$_2$ catalyst.

In all the cases, the reaction rate decreases rapidly after the first minutes of reaction. This behaviour could be explained because of the type of silica used (that does not fragment), ethylene diffusion problems, and deactivation of the

catalyst, as already discussed in Chapter 4.3.1. For these reasons, the reaction rate constants were calculated taking into account only the first minute of the reaction, on the basis of the first order law already discussed in Chapter 3. The values obtained are shown in Table 5. 3.

Table 5. 3 Kinetic constants for ethylene polymerization reaction conducted at room temperature on Cr(VI)/SiO$_2$ and on the TEA- and DEALE-modified versions, at two different Al:Cr ratios.

Kinetic constants (s^{-1} molCr^{-1})			
Catalyst	No Al-alkyls	Al:Cr=2:1	Al:Cr=4:1
Cr(VI)/SiO$_2$	8	-	-
Cr(VI)/SiO$_2$+TEA	-	140	150
Cr(VI)/SiO$_2$+DEALE	-	390	100

The reaction rates of the modified catalysts are much higher than that of Cr(VI)/SiO$_2$, and this makes clear the reason why Al-alkyls are industrially interesting. Some analogies can be found with the kinetic constants calculated for the modified Cr(II)/SiO$_2$ catalysts. Indeed, once again **the Cr(VI)/SiO$_2$ +TEA(4:1) is faster that the Cr(VI)/SiO$_2$ +TEA(2:1), although the kinetic constant is not proportional to the amount of TEA** (for both catalyst the reaction is about 20 times faster). Curiously, whether starting from the oxidized Cr(VI)/SiO$_2$ catalyst or from the reduced Cr(II)/SiO$_2$ one, **the fastest system results to be the DEALE(2:1) modified one** (50 times faster). While the value for the Cr(VI)/SiO$_2$ +DEALE(4:1) catalyst drastically decreases (13 times faster), implying a partial deactivation of the catalyst, as it was already suggested [7].

5.3.2 A spectroscopic study

Ethylene polymerization on the Cr(VI)/SiO$_2$+TEA(4:1) catalyst was monitored by means of DR UV-Vis, EPR and FT-IR spectroscopies, as summarized in Figure 5. 12. Upon ethylene dosage, the DR UV-Vis spectrum of Cr(VI)/SiO$_2$+TEA(4:1) immediately changes (Figure 5. 12a). A drastic decrease of the intensity is observed in the entire spectral region. This effect is due to the layer of polyethylene that grows around the Cr actives sites, making the sites rapidly invisible to DR UV-Vis-NIR. Meanwhile, weak bands grow in the 4500-4000 cm^{-1} region, where overtones and combinations of the stretching and bending vibrational modes of polyethylene became visible (inset in Figure 5. 12a). Although the change in the scattering properties of the powder prevents any definitive conclusion on the nature of the Cr sites involved in ethylene polymerization, nevertheless it must be noticed that the band at 21500 cm^{-1} is the most affected

one, while the d-d bands remain almost unaffected. As suggested in section 5.2.1, at least part of this signal might be due to alkylated Cr(IV) sites. Hence, **the DR UV-Vis data seem to suggest that alkylated Cr(IV) sites are those faster in the initiation of the ethylene polymerization reaction**.
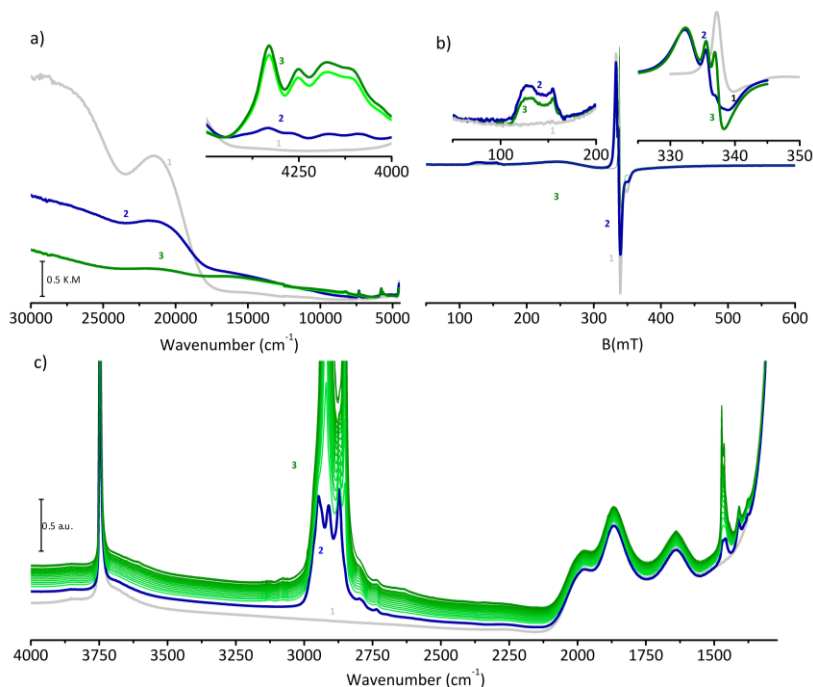
Figure 5. 12 Part a) Evolution of the DR UV-Vis-NIR spectra upon ethylene reaction at room temperature on the Cr(VI)/SiO$_2$+TEA(4:1)catalyst (from spectrum 2 to spectrum 3). The inset shows a magnification of the NIR region. Part b) X-band CW-EPR spectra of the Cr(VI)/SiO$_2$+TEA(4:1) before (spectrum 2) and after reaction with ethylene at room temperature (spectrum 3). The inset shows the enlargement of the low field and of the mid-field region. Part c) Time evolution of the FT-IR spectra for the Cr(VI)/SiO$_2$+TEA(4:1) catalyst during ethylene polymerization (from spectrum 2 to spectrum 3).

The same experiment was followed by EPR spectroscopy. Ethylene was admitted on the sample at room temperature and after 2 minutes the reaction was quenched with liquid nitrogen and an EPR spectrum was collected at 100 K (spectrum 3 in Figure 5. 12b). At the end of the EPR measurement, an ATR spectrum of the sample was collected, in order to confirm *a posteriori* the presence of the polymer. In the spectrum recorded after ethylene polymerization (spectrum 3 in Figure 5. 12b), the signal of isolated Cr(III) sites at g = 4.3 decreases and the narrow signal at g = 1.98 assigned to Cr(V) increases. This could be due to oxidative addition of ethylene to Cr(III) single sites. The signal of small clusters at g = 1.994 does not change at all, suggesting that these sites do not participate in the reaction.

Finally, Figure 5. 12c shows the time-resolved FT-IR spectra collected during ethylene polymerization on $Cr(VI)/SiO_2$ +TEA(4:1) at room temperature. The occurrence of ethylene polymerization is indicated by the growth of the characteristic IR absorption bands, both in the stretching and in the bending regions, as described previously.
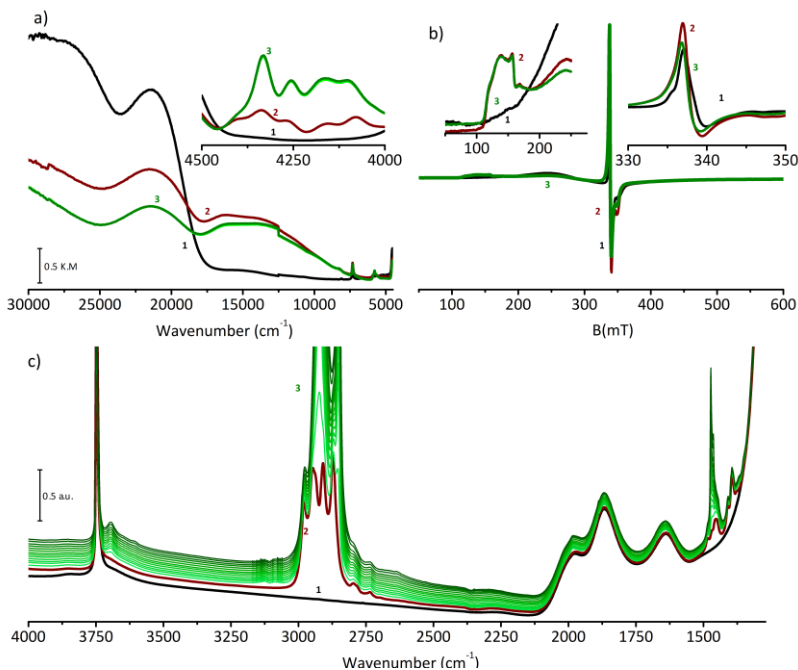
Figure 5. 13 Part a) Evolution of the DR UV-Vis-NIR spectra upon ethylene reaction at room temperature on the $Cr(VI)/SiO_2+DEALE(4:1)$ catalyst (from spectrum 2 to spectrum 3). The inset shows a magnification of the NIR region. Part b) X-band CW-EPR spectra of the $Cr(VI)/SiO_2+DEALE(4:1)$ before (spectrum 2) and after reaction with ethylene at room temperature (spectrum 3). The inset shows the enlargement of the low field and of the mid-field region. Part c) Time evolution of the FT-IR spectra for the $Cr(VI)/SiO_2+DEALE(4:1)$ catalyst during ethylene polymerization (from spectrum 2 to spectrum 3).

The same experiments were conducted for the $Cr(VI)/SiO_2+DEALE(4:1)$ catalysts, with similar results. The main differences are observed in the EPR spectra (Figure 5.13b). Indeed, this time we did not observe any change in the EPR spectra of the $Cr(VI)/SiO_2+DEALE(4:1)$ catalyst before and after ethylene polymerization, just a slightly decrease of the intensity of the signals attributed to the Cr(V) species. These results indicate that, **under these experimental conditions, the active Cr sites originated by reacting $Cr(VI)/SiO_2+DEALE(4:1)$ with ethylene at room temperature are not EPR active**.

5.4 A short summary on the properties of the modified Cr(VI)/SiO₂ Phillips catalyst and some hypothesis on the structure of the modified Cr sites.

The present paragraph summarizes the main results achieved by applying several complementary spectroscopic techniques to the investigation of the TEA- and DEALE-modified Cr(VI)/SiO₂ catalysts. Some hypothesis on the molecular structure of the modified Cr sites are also proposed.

5.4.1 Reducibility of the Cr(VI) sites and oxidation state of the modified Cr sites

Only a fraction of the Cr(VI) sites are reduced by the Al-alkyls. The DR UV-Vis results clearly demonstrated that, also with an Al:Cr=4:1 ratio, a fraction of Cr(VI) sites are still present, in accordance with the literature [3, 7, 18].Hence, a fraction of the Al-alkyls must react with the silica surface (either with the siloxane bridges and/or with silanol groups), to give $-AlR_x$ (or AlR_xO_y) species.

The oxidation state of the reduced Cr species cannot be straightforwardly attributed. However, the DR UV-Vis spectra suggest the **presence of highly coordinated Cr(II) species and alkylated Cr(IV) species**, both of them postulated in the alkylation mechanisms proposed in the literature [7]. Both these species are not active in EPR. Indeed, for an Al:Cr=2:1 ratio, EPR reveals the presence of residual Cr(V) only (which are ubiquitous in Cr(VI)/SiO₂ catalysts), and indicates that **only a negligible amount of isolated Cr(III) species are formed** (not detectable by DR UV-Vis). The amount of isolated Cr(III) species increases for an Al:Cr ratio equal to 4:1, likely as a consequence of the 2-electron reduction of the residual Cr(V) species.

A possible mechanism to explain the formation of Cr(IV) sites is shown in Scheme 1 (first two steps of reaction). According to this mechanism, starting from one Cr(VI) and two TEA molecules, a bis-alkylated Cr(IV) species ($\equiv SiO)_2Cr(IV)R_2$ is obtained, as well as a by-product which resembles an alkyl-alumoxane fragment (omitted in the scheme for simplicity). When DEALE is used instead of TEA, the by-product contains more –OR groups. The by-product must reside close to the Cr site that originated it, and the interaction strength surely increases with the number of –OR groups, being Cr notoriously an oxophilic species. Cr(II) sites can be formed from the over-reduction of the bis-alkylated Cr(IV) sites (Scheme 1, last step), as already proposed in the literature [7]. According to this mechanism, a mono-

grafted ≡SiOCr(II)-R species would be formed, together with a surface ≡SiO-R species nearby.
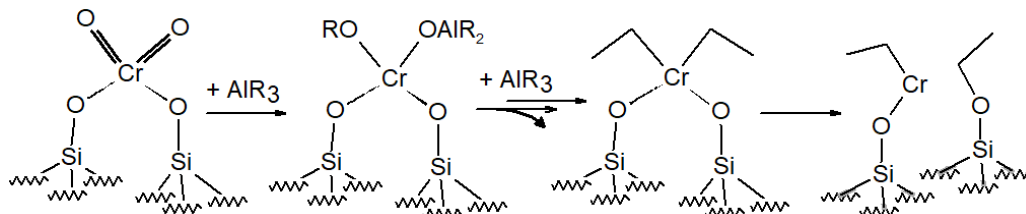
Scheme 1 Proposed mechanism to explain the formation of bis-alkylated Cr(IV) sites and mono-grafted Cr(II) sites from reaction of Cr(VI)/SiO$_2$ with AlR$_3$. The Al-alkyl by-products (R$_2$Al-O-AlROR) are omitted for simplicity. The reaction with DEALE may proceeds in the same way, but the by-product will have a greater number of OR groups.

5.4.2 Accessibility of the modified Cr sites, local structure and acid properties

The bis-grafted and bis-alkylated Cr(IV) species (species **2** in Scheme 2) **are not probed** neither by CO nor by CD$_3$CN. In contrast, the Cr(II) sites are partially probed by both molecules, in a relative proportion that depends on the type of the Al-alkyl and on its concentration. Generally speaking, CO probes a lower amount of Cr(II) sites with respect to CD$_3$CN, as expected because of its weaker interaction energy. All the Cr(II) sites accessible to CO are univocally described as **mono-grafted Cr(II) sites, of the type ≡SiOCr(II)-L (where L = R or OR), partially detached from the silica surface** (hence, the classical behaviour of the di-carbonyl complexes). All of them are **stabilized by some ancillary ligands nearby** (hence, they appear as highly coordinated in the DR UV-Vis spectrum). Among the ancillary ligands there would be the alkyl-alumoxane by-products, the ≡SiO–R species obtained from the rupture of one Cr-O bond (see Scheme 1) and the ≡SiO–AlR$_2$, ≡SiO–AlROR, or ≡SiO–R species deriving from the direct reaction of the Al-alkyl with the silica surface.

The overall accessibility and, more important, **the acidic nature of the mono-grafted Cr(II) sites strongly depend on the number and the type of the ancillary ligands.** In the presence of an AlR$_x$O$_y$ fragment (species **4** in Scheme 2), the ≡SiOCr(II)-L sites display a stronger Lewis acid character than the ≡SiOCr(II)-L sites close to a SiO–R species (species **3** in Scheme 2). The S-LA sites are less accessible when the AlR$_x$O$_y$ fragment contains more OR ligands (species **4'** in Scheme 2). The relative proportion of these strong and weak Lewis acid sites depends on the type of the Al-alkyl and on its concentration. In general, the formation of S-LA sites is favoured in the presence of TEA and at high concentration. That is, **upon increasing the reduction power of the Al-alkyl a**

larger fraction of the original Cr(VI) sites is over-reduced to give mono-grafted ≡SiOCr(II)-L sites having a strong Lewis acid character. In these cases, a fraction of the mono-grafted ≡SiOCr(II)-L sites is in such a close proximity with the AlR_xO_y fragment, that CD_3CN can be shared between the Cr(II) and the Al(III) cations in a bridged fashion. Scheme 2 shows a collection of the possible Cr species that can co-exist on $Cr(VI)/SiO_2+TEA/DEALE$.
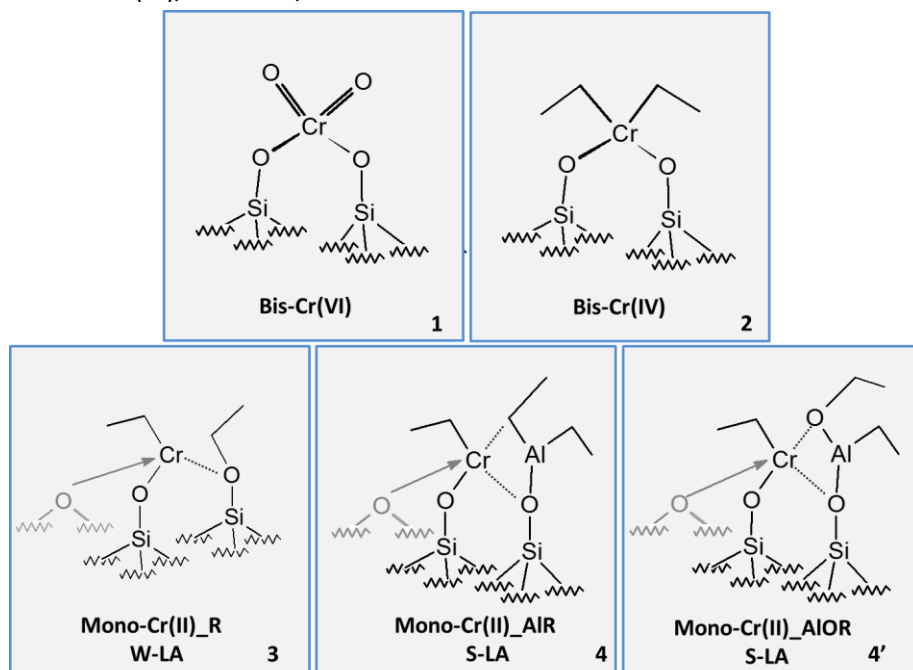
Scheme 2. Hypothetical structures (at a molecular level) for the chromium sites in the $Cr(VI)/SiO_2$ +Al-Alkyls catalysts.

5.4.3 Role of the modified Cr sites in ethylene polymerization

Plausibly all the Cr sites described in the previous scheme play a role in ethylene polymerization, although at present it is difficult to define the exact role of each of them. In terms of reaction rate, $Cr(VI)/SiO_2+DEALE(2:1)$ seems the most performant catalyst. All the results discussed so far converge in concluding that this is probably the less reduced catalyst, i.e. the system containing the larger amount of bis-alkylated $(\equiv SiO)_2Cr(IV)R_2$ sites (species **2** in Scheme 2). Hence, we might argue that **the bis- alkylated $(\equiv SiO)_2Cr(IV)R_2$ sites are the major protagonist in ethylene polymerization**. This conclusion suggests that a similar site might be the propagating site generated in situ by ethylene starting from both $Cr(VI)/SiO_2$ and $Cr(II)/SiO_2$.

As far as the mono-grafted $\equiv$SiOCr(II)-L sites are concerned, their behaviour is strongly influenced by their acidic nature. Mono-grafted $\equiv$SiOCr(II)-OSiR$_3$ sites generated by reacting Cr(II)/SiO$_2$ with hydrosilanes, which are W-LA sites, have been demonstrated to be responsible of ethylene oligomerization to 1-hexene [13]. Similarly, we might hypothesize that **the fraction of $\equiv$SiOCr(II)-L sites having a W-LA character** (species **3** in Scheme 2) **generate prevalently α-olefins through ethylene oligomerization, and hence contribute to the formation of low molecular weight PE. In contrast, the $\equiv$SiOCr(II)-L sites having a S-LA character** (species **4** and **4'** in Scheme 2) **might contribute to the formation of a high molecular weight PE, in close analogy to the behaviour of the Cr(II) sites on Al$_2$O$_3$** [19].

Finally, according to the literature, Cr(VI)/SiO$_2$ modified by TEA and DEALE display a more pronounced hydrogen response with respect to the standard Phillips catalyst. This implies that at least some of the modified sites should be able to activate H$_2$. According to our previous work on Cr(II)/SiO$_2$ modified by hydrosilanes, mono-grafted $\equiv$SiOCr(II)-OSiR$_3$ sites having a W-LA character are able to activate molecular H$_2$. This strongly suggests that the mono-grafted, W-LA, $\equiv$SiOCr(II)-L sites are the responsible of hydrogen response also in the present case.

References

[1] Cicmil, D., Meeuwissen, J., Vantomme, A., Weckhuysen, B.M.,ChemCatChem, 8 (2016) 1937-1944.

[2] Cicmil, D., van Ravenhorst, I.K., Meeuwissen, J., Vantomme, A., Weckhuysen, B.M.,Catal Sci Technol, 6 (2016) 731-743.

[3] Liu, B., Šindelář, P., Fang, Y., Hasebe, K., Terano, M.,J Mol Catal A Chem, 238 (2005) 142-150.

[4] Pelletier J. , Espinas J., Vu N. , Norsic S. , Baudouin A., Delevoye L. , Trebosc J. , Le Roux E., Santini C. , Basset J.-M. , Gauvin R. M., Taoufik M.,Chem. Commun., 47,2979. (2011).

[5] Kerber, R.N., Kermagoret, A., Callens, E., Florian, P., Massiot, D., Lesage, A., Coperet, C., Delbecq, F., Rozanska, X., Sautet, P.,J. Am. Chem. Soc., 134 (2012) 6767-6775.

[6] Amor Nait Ajjou, J., Scott, S.L.,Organometallics, 16 (1997) 86-92.

[7] McDaniel, M.P.,Adv. Catal., 53 (2010) 123-606.

[8] Cicmil, D., Meeuwissen, J., Vantomme, A., Wang, J., van Ravenhorst, I.K., van der Bij, H.E., Munoz-Murillo, A., Weckhuysen, B.M.,Angew. Chem., 54 (2015) 13073-13079.

[9] Weckhuysen, B.M., Schoonheydt, R.A., Mabbs, F.E., Collison, D.,J. Chem. Soc. Faraday Trans., 92 (1996) 2431-2436.

[10] Weckhuysen, B.M., Deridder, L.M., Grobet, P.J., Schoonheydt, R.A.,J. Phys. Chem., 99 (1995) 320-326.

[11] Morra, E., Martino, G.A., Piovano, A., Barzan, C., Groppo, E., Chiesa, M.,J. Phys. Chem. C, 122 (2018) 21531-21536.

[12] Barzan, C., Gianolio, D., Groppo, E., Lamberti, C., Monteil, V., Quadrelli, E.A., Bordiga, S.,Chem. Eur. J., 19 (2013) 17277-17282.

[13] Barzan, C., Groppo, E., Quadrelli, E.A., Monteil, V., Bordiga, S.,Phys.Chem.Chem.Phys., 14 (2012) 2239–2245.

[14] Morterra, C., Mentruit, M.P., Cerrato, G.,PCCP, 4 (2002) 676-687.

[15] Morterra, C., Cerrato, G., Novarino, E., Mentruit, M.P.,Langmuir, 19 (2003) 5708-5721.

[16] Platero, E.E., Mentruit, M.P., Morterra, C.,Langmuir, 15 (1999) 5079-5087.

[17] Cerruti, M., Morterra, C., Ugliengo, P.,Chemistry of Materials, 17 (2005) 1416-1423.

[18] Liu, B.P., Fang, Y.W., Terano, M.,J. Mol. Catal. A-Chem., 219 (2004) 165-173.

[19] Martino, G.A., Barzan, C., Piovano, A., Budnyk, A., Groppo, E.,J. Catal., 357 (2018) 206-212.

Chapter 6
SiO$_2$-supported Cr[CH(SiMe$_3$)$_2$]$_3$ catalysts

The main goal of this research Chapter was to investigate the structure of the chromium sites in silica-supported Cr[CH(SiMe$_3$)$_2$]$_3$ catalysts as a function of the chromium loading, and to correlate it with the catalytic performances. This activity was stimulated by the interaction with Dr. Takashi Monoi at JPE/JPC, in the frame of a Confidentiality Agreement.

6.1 Why Cr[CH(SiMe₃)₂]₃/SiO₂ catalysts?

According to the seminal works of Monoi et al.[1-3], heterogeneous catalysts prepared by supporting tris[bis(trimethylsilyl)methyl]chromium(III), Cr[CH(SiMe₃)₂]₃, on a silica pre-calcined at high temperature, have a high activity towards ethylene polymerization, even without using any organo-aluminum compounds as co-catalysts or scavengers. These catalysts display characteristics similar to those of the Phillips catalyst (in terms of molecular weight, molecular weight distribution, copolymerization ability, and presence of LCB), prompting the conclusion that the active sites in the Phillips catalyst should resemble the active sites in the Cr[CH(SiMe₃)₂]₃/SiO₂ catalysts. The only difference between the Cr[CH(SiMe₃)₂]₃/SiO₂ catalysts and the Phillips catalyst is that the former are sensitive to the addition of hydrogen during ethylene polymerization, while the latter is not.
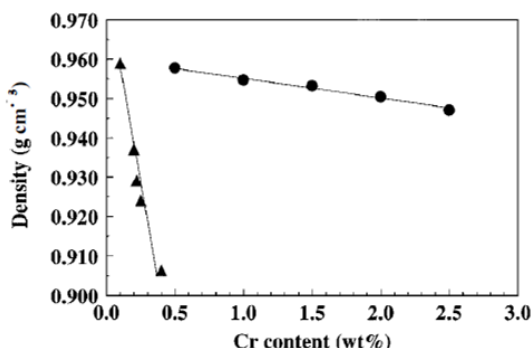
Figure 6. 1 Effect of Cr loading on the density of the polymer obtained with Cr[CH(SiMe₃)₂]₃/SiO₂ catalysts. Circles: silica calcination temperature = 200 °C; triangles: silica calcination temperature = 600 °C [1].

Nevertheless, the situation is more complex than that described above. Indeed, the performances of the Cr[CH(SiMe₃)₂]₃/SiO₂ catalysts strongly depend on the Cr loading. Figure 6. 1 shows the density of the polyethylene produced with these Cr[CH(SiMe₃)₂]₃/SiO₂ catalysts, as a function of the Cr loading and of the silica activation temperature [1]. By keeping constant the silica activation temperature, an increase in the Cr loading causes a decrease of the polymer density. Such effect is more drastic for the catalysts supported on a silica activated at higher temperature. In this case, a slight increase of Cr content from 0.1 to 0.4 wt% decreases the density from 0.9590 to 0.9065 g/cm³. Such a drastic decrease of density is the result of the formation of short-chain branching (SCB), as demonstrated by ¹³C NMR [1, 3]. The presence of SCB indicates the occurrence of

108

ethylene trimerization. Monoi et al. [2, 3] also found that the activity per Cr decreases with an increase of Cr content. All together, these results suggested that **two types of Cr sites co-exist in these catalysts, those active in ethylene polymerization (that dominate at low Cr loading) and those active in ethylene trimerization (whose fraction increases at high Cr loading)**.

From this short introduction it appears clear that the $Cr[CH(SiMe_3)_2]_3/SiO_2$ catalysts are intriguing systems at least for two reasons. The first is that **the Cr sites active in ethylene polymerization might resemble the active sites in the Phillips catalyst**. The second is that they are **actually tandem catalysts, whereby at least two types of Cr active sites co-exist, whose relative concentration is a function of the Cr loading**. With that in mind, we applied several in situ spectroscopic techniques aimed at highlighting the properties of the Cr sites.

6.2 The Cr[CH(SiMe₃)₂]₃ precursor

Figure 6. 2 shows the transmission UV-Vis, the EPR and the ATR-IR spectra of the Cr[CH(SiMe₃)₂]₃ precursor. The transmission UV-Vis spectrum of the compound in hexane solution (Figure 6. 2a) shows two very intense bands at about 30000 and 25000 cm^{-1} having a charge-transfer nature, and two weak and broad bands in the d-d region at about 14000 and 11000 cm^{-1}. The spectrum is very similar to that reported in the literature for the analogous trigonal complex tris(bistrimethylsilylamido) Cr(III), which has been interpreted on account of its geometry (D_{3h} symmetry) [4-7]. According to this assignment, the band at 11000 cm^{-1} is attributed to the transition $^4A'_2 \rightarrow (^4A''_1, {}^4A''_2)$ and the band at 14000 cm^{-1} is attributed to the $^4A'_2 \rightarrow {}^4E$ transition [4].
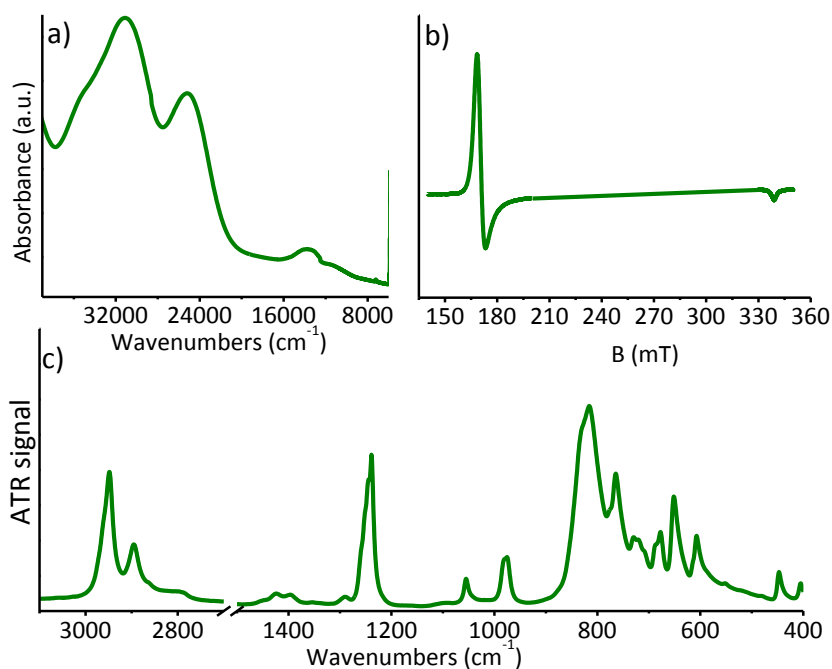
Figure 6. 2 Transmission UV-Vis (part a), EPR (part b), and ATR-IR (part c) spectra of the Cr[CH(SiMe₃)₂]₃ compound. The UV-Vis and EPR spectra were collected in hexane solution, while the ATR-IR spectrum was collected on the sample in the powder form. All the measurements have been performed avoiding any contact with air.

Based on this model, also the interpretation of the EPR spectrum (in hexane solution at 77 K) could be made. The complex gave a very sharp and intense signal at g-values of $g_⊥ = 4$ and another low signal at $g_{\parallel}=2$ (Figure 6. 2b).

These signals are typical of a Cr(III) species in a very low symmetry (that means far from the octahedral O_h situation) like the D_{3h} geometry of our complex [5].

Finally, Figure 6. 2c shows the ATR FT-IR spectrum of the $Cr[CH(SiMe_3)_2]_3$ complex. In the high frequency region, the spectrum is dominated by two sharp absorption bands at 2950 and 2895 cm^{-1} region, that are attributed to the asymmetric and symmetric stretching of the methyl groups, whereas the signals of the -CH- linkages are almost negligible because their very low relative abundance. The symmetric and asymmetric bending modes of the same groups contribute with very intense bands at ca. 1240 and 815 cm^{-1}, respectively [8]. The low frequency region of the spectrum shows additional sharp bands, in analogy to the homologue $Cr[N(SiMe_3)_2]_3$ compound, already studied in the literature [7].

6.3 The properties of the Cr[CH(SiMe₃)₂]₃/SiO₂ catalysts

6.3.1. Electronic properties

All the $nCr[CH(SiMe_3)_2]_3/SiO_{2-600}$ samples appear bright green in color, with an intensity that depends on the Cr loading (more chromium, more green). The corresponding DR UV-Vis-NIR spectra are shown in Figure 6. 3a. All the spectra show the same spectroscopic features, and in particular: 1) a band centered at 30000 cm^{-1} with a charge-transfer character; 2) three main bands in the d-d region at ca. 22000, 16000 and 10000 cm^{-1}. However, the absolute intensity of the observed bands is different for each sample and roughly scales with the amount of chromium.
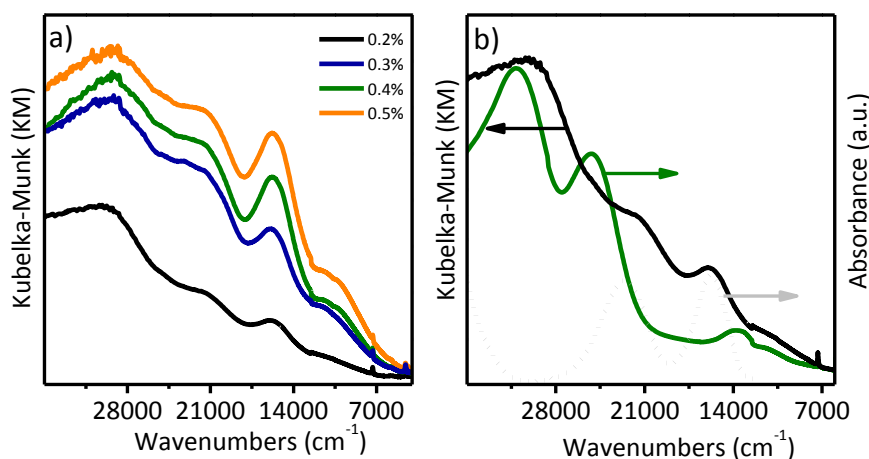
Figure 6. 3. Part a) DR UV-Vis spectra of the $nCr[CH(SiMe_3)_2]_3/SiO_{2-600}$ catalysts. Part b) The DR UV-Vis spectrum of $0.2Cr[CH(SiMe_3)_2]_3/SiO_{2-600}$ (black) is compared to the transmission UV-Vis spectra of $Cr[CH(SiMe_3)_2]_3$ in hexane (green) and $CrCl_3$ in H_2O (dotted grey).

In Figure 6. 3b the DR UV-Vis spectrum of $0.2Cr[CH(SiMe_3)_2]_3/SiO_{2-600}$ catalyst is compared to the transmission spectra of the $Cr[CH(SiMe_3)_2]_3$ precursor in hexane (green spectrum) and of $CrCl_3$ in aqueous solution (dotted grey spectrum), which is a reference for Cr(III) in an octahedral geometry. The spectrum of the $0.2Cr[CH(SiMe_3)_2]_3/SiO_{2-600}$ catalyst looks like a linear combination of the spectra of the two reference compounds. This result suggests the co-presence, in the catalyst, of two types of Cr sites: **1) Cr(III) sites in a low coordination environment (D₃ₕ symmetry), and 2) Cr(III) sites in a 6-fold coordination.** This is in good agreement with the hypothesis formulated by Monoi et al. [1] on the basis of the catalytic performances, postulating the existence of two types of Cr sites, those active in ethylene polymerization and those responsible for ethylene trimerization.

We anticipate here that **the first type of sites can be described as mono-grafted (≡SiO-)Cr[CH(SiMe$_3$)$_2$]$_2$ species, which maintain most of the structural and symmetric properties of the Cr[CH(SiMe$_3$)$_2$]$_3$ precursor**. According to the literature, mono-grafted Cr sites should be responsible for ethylene oligomerization to α-olefins, hence we will call these sites **Cr$_{oligom}$**. The second family of sites are tentatively described as **bis-grafted (≡SiO-)$_2$Cr[CH(SiMe$_3$)$_2$] sites, and are considered responsible for ethylene polymerization and co-polymerization with α-olefins**, hence they will be called hereafter **Cr$_{polym}$** sites.

6.3.2. Paramagnetic properties

Figure 6. 4 shows the EPR spectra of the nCr[CH(SiMe$_3$)$_2$]$_3$/SiO$_{2-600}$ catalysts, collected in continuous wave (CW) mode at the X-band energy. The spectra are divided into two main magnetic regions, the low field (part a) and the high field (part b). Cr(III) ions contribute in both fields, with a relative intensity that depends on the symmetry: Cr(III) species in a low coordination and distorted environment contribute mainly in the low field region (as discussed for the Cr[CH(SiMe$_3$)$_2$]$_3$ complex), while Cr(III) species in a highly symmetric coordination contribute mainly in the high field region [5, 9]. By looking at the sequence of spectra, it is evident that the signal at low field contributes mainly in the spectra of the samples with higher Cr loading, while the signal at high field mainly in the spectra of the samples with lower Cr loading.

Such an observation immediately indicates that the dominant Cr species in all the catalysts are characterized by a different symmetry.

Qualitatively, all the spectra equally present a remarkably structured in the low field region, although they differ in the intensity (inset in Figure 6. 4). This indicates that **the Cr species contributing mainly at low field are the same in the four catalysts, but they are more abundant at high Cr loading**. This signal can be assigned to mono-grafted (≡SiO-)Cr[CH(SiMe$_3$)$_2$]$_2$ species, **Cr$_{oligom}$**. In contrast, the shape of the signal in the high field region is different in the four cases, although the integrated area is quite similar (inset in Figure 6. 4). This means that **the Cr species contributing mainly at high field are structurally different in the four catalysts, but their amount is almost constant in the four cases**. The species responsible of this signal are tentatively described as the bis-grafted (≡SiO-)$_2$Cr[CH(SiMe$_3$)$_2$] sites, **Cr$_{polym}$**. The EPR data indicate that several Cr$_{polym}$ sites exist on the catalysts differing in the coordination environment. The different environment can be described in terms of different ligands nearby, such as weak siloxane ligands and/or CH(SiMe$_3$)$_2$ groups attached at the silica surface.

113
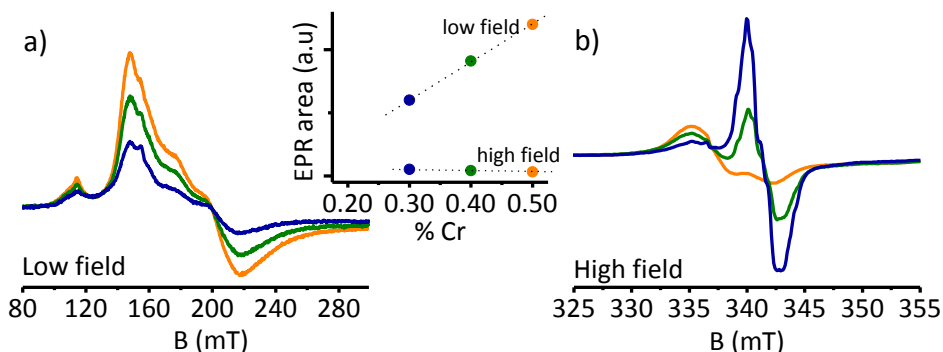
Figure 6. 4 X-band CW-EPR spectra of the nCr[CH(SiMe$_3$)$_2$]$_3$/SiO$_{2-600}$ catalysts, in both the low and the high magnetic field regions (parts a and b, respectively). The integrated areas of the EPR signals are reported in the inset.

6.3.3. Vibrational properties

Figure 6. 5a shows the FT-IR spectrum of the 0.2Cr[CH(SiMe$_3$)$_2$]$_3$/SiO$_{2-600}$ catalyst and that of pure silica activated in the same conditions (SiO$_{2-600}$). The spectrum of dehydroxylated SiO$_2$ is characterized by the same fingerprints already explained in the previous Chapters (Figure 4.2).
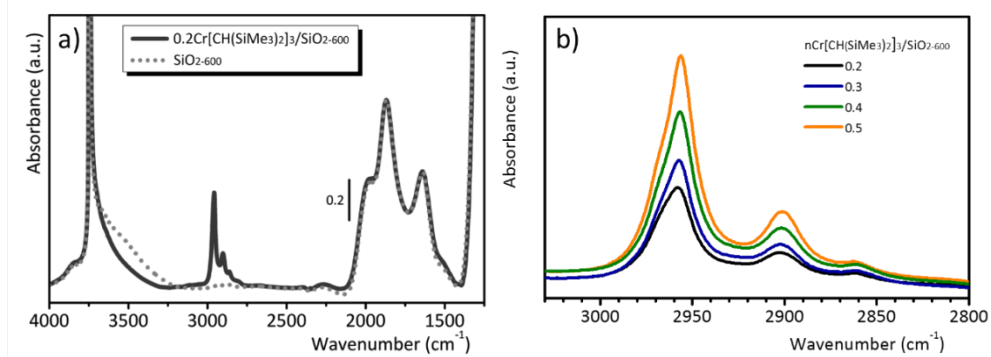
Figure 6. 5. Part a) FT-IR spectra of 0.2Cr[CH(SiMe$_3$)$_2$]$_3$/SiO$_{2-600}$ and of pure silica activated in the same conditions. Both spectra were flattened to allow a better comparison, and normalized to the thickness of the pellets. Part b) FT-IR spectra of the nCr[CH(SiMe$_3$)$_2$]$_3$/ SiO$_{2-600}$ catalysts in the v(CH$_x$) region. The spectra were normalized to the thickness of the pellets in order to allow a quantitative comparison.

The spectrum of the catalyst differs from that of the SiO$_{2-600}$ support in two main regions:

1. In the v(OH) region, the broad absorption band at 3700-3200 cm^{-1} due to H-bonded silanols is eroded, suggesting that **the chromium precursor is** (at least in part) **grafted to the silica surface through vicinal or nearby silanol groups**. Since the IR absorption band ascribed to the free silanols (at 3750 cm^{-1}) is out-

of-scale, it is difficult to evaluate the possible grafting of the chromium precursor to these surface species, though we can reasonably expect it.

2. In the 3000-2800 cm^{-1} region the sharp absorption bands due to $v(CH_3)$ vibrations of the methyl groups are observed. These bands are very similar to those observed in the spectrum of the $Cr[CH(SiMe_3)_2]_3$ precursor.

Figure 6. 5b shows the FT-IR spectra of all the $nCr[CH(SiMe_3)_2]_3/SiO_{2-600}$ catalysts in the $v(CH_3)$ region, normalized to the thickness of the pellets in order to allow a quantitative comparison. The intensity of the $v(CH_3)$ bands roughly scales with the amount of chromium. In general, the chemistry of "grafting" looks the same, since no changes in the relative intensity of the bands are observed irrespective of the amount of chromium. It is evident that FT-IR spectroscopy is not able to discriminate between Cr_{oligom} and Cr_{polym} sites, since the observable absorption bands are associated to the methyl groups, which are far from Cr and insensitive to structural variations.

6.4. Ethylene polymerization over nCr[CH(SiMe₃)₂]₃/SiO$_{2-600}$: a spectroscopic study

6.4.1. In situ DR UV-Vis spectroscopy

The time-resolved DR UV-Vis spectra collected during ethylene polymerization at room temperature on the 0.5Cr[CH(SiMe₃)₂]₃/SiO$_{2-600}$ and on the 0.2Cr[CH(SiMe₃)₂]₃/SiO$_{2-600}$ catalysts are shown in Figure 6. 6. In both cases, an immediate decrease in intensity overall the whole spectral region is observed, which indicates the formation of a large amount of polymer and the consequent modification of the scattering properties of the powder. The effect is more evident for the 0.2Cr[CH(SiMe₃)₂]₃/SiO$_{2-600}$ sample, which is the sample more active in ethylene polymerization, in well agreement with the literature [1]. The presence of the polymer is testified by the new absorption bands that appear in the NIR region (insets), which are related to the overtones and combination modes of the $\nu(CH_x)$ vibrational modes of the polymer chains.
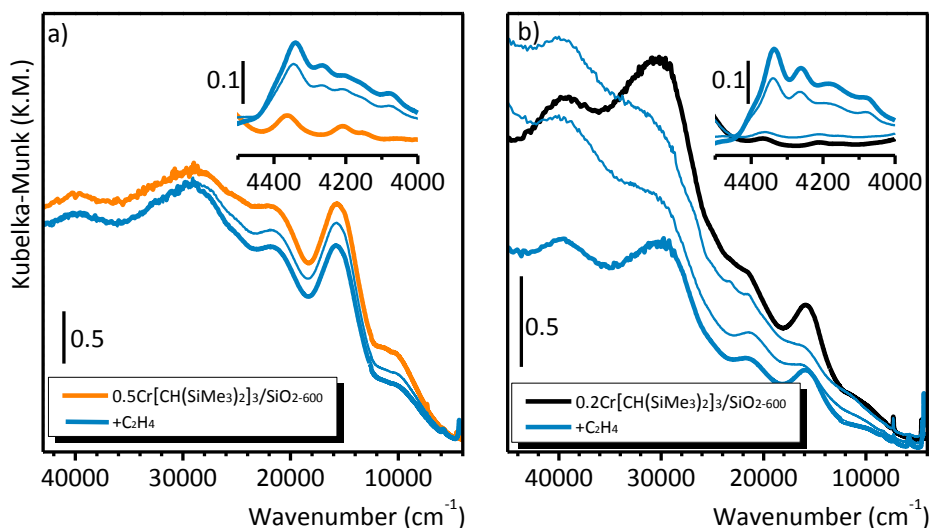
Figure 6. 6 Time resolved DR UV-Vis spectra collected during C₂H₄ polymerization at room temperature on 0.5Cr[CH(SiMe₃)₂]₃/SiO$_{2-600}$ (part a) and 0.2Cr[CH(SiMe₃)₂]₃/SiO$_{2-600}$ (part b) catalysts. The insets show a magnification of the NIR region.

In the case of 0.2Cr[CH(SiMe₃)₂]₃/SiO$_{2-600}$, the very first spectrum collected in the presence of ethylene clearly shows that the bands more affected by ethylene polymerization are those at 22000 and 16000 cm^{-1}, while that at 10000 cm^{-1} initially does not change. This observation is in agreement with the hypothesis that the first two bands are due to bis-grafted (≡SiO-)₂Cr[CH(SiMe₃)₂]

species, Cr$_{polym}$, responsible for ethylene polymerization, while the band at 10000 cm^{-1} is due to mono-grafted ($\equiv$SiO-)Cr[CH(SiMe$_3$)$_2$]$_2$ species, Cr$_{oligom}$, responsible for ethylene oligomerization.

6.4.2. In situ EPR spectroscopy

The EPR spectra collected for the 0.2Cr[CH(SiMe$_3$)$_2$]$_3$/SiO$_{2-600}$ and the 0.5Cr[CH(SiMe$_3$)$_2$]$_3$/SiO$_{2-600}$ catalysts after ethylene polymerization at room temperature are shown in Figure 6. 7. For both catalysts, no evident changes are observable in the high field region (parts a' and b'), i.e. where the main contribution is due to the bis-grafted ($\equiv$SiO-)$_2$Cr[CH(SiMe$_3$)$_2$] species. This means that during the ethylene polymerization the Cr sites do not change the oxidation state nor the coordination geometry. This is reasonable, if the Cossee-Arlman mechanism is assumed to explain the ethylene polymerization mechanism: the initiation site, ($\equiv$SiO-)$_2$Cr[CH(SiMe$_3$)$_2$], is very similar to the propagating site, ($\equiv$SiO-)$_2$Cr[polymer].
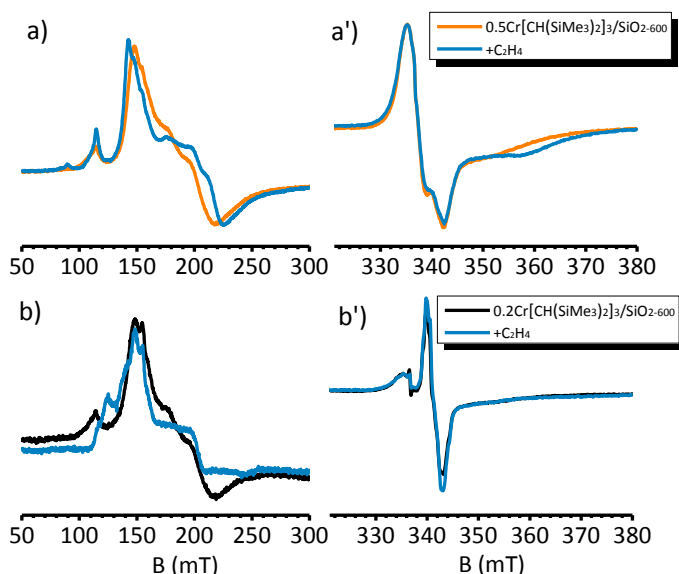
Figure 6. 7. X-band CW-EPR spectra of 0.5Cr[CH(SiMe$_3$)$_2$]$_3$/SiO$_{2-600}$ (parts a and a') and 0.2Cr[CH(SiMe$_3$)$_2$]$_3$/SiO$_{2-600}$ (parts b and b') catalysts, before and after ethylene polymerization at room temperature.

On the contrary, the signals in the low field region are slightly perturbed by the presence of ethylene (Figure 6. 7a and b). This suggests that the symmetry of the mono-grafted ($\equiv$SiO-)Cr[CH(SiMe$_3$)$_2$]$_2$ species changes in the presence of ethylene. This is again reasonable if a metallacycle mechanism is assumed to

explain ethylene oligomerization, as it has been demonstrated for many homogeneous Cr-based catalysts [10-12].

6.4.3. In situ FT-IR spectroscopy

The time-resolved FT-IR spectra collected during ethylene polymerization at room temperature on the $0.5Cr[CH(SiMe_3)_2]_3/SiO_{2-600}$ and on the $0.2Cr[CH(SiMe_3)_2]_3/SiO_{2-600}$ catalysts are shown in Figure 6. 8. Upon ethylene admission, ethylene polymerization readily occurs, as testified by the fast growth of several absorption bands in both $\nu(CH_x)$ and $\delta(CH_x)$ regions. In particular, four absorption bands are observed in the $\nu(CH_x)$ region, typical of a branched polyethylene. The two bands at 2925 and 2855 cm^{-1} are assigned to the asymmetric and symmetric stretching of the CH_2 moieties in the chains. The two bands at 2960 and 2875 cm^{-1} are assigned to the asymmetric and symmetric stretching of the terminations.
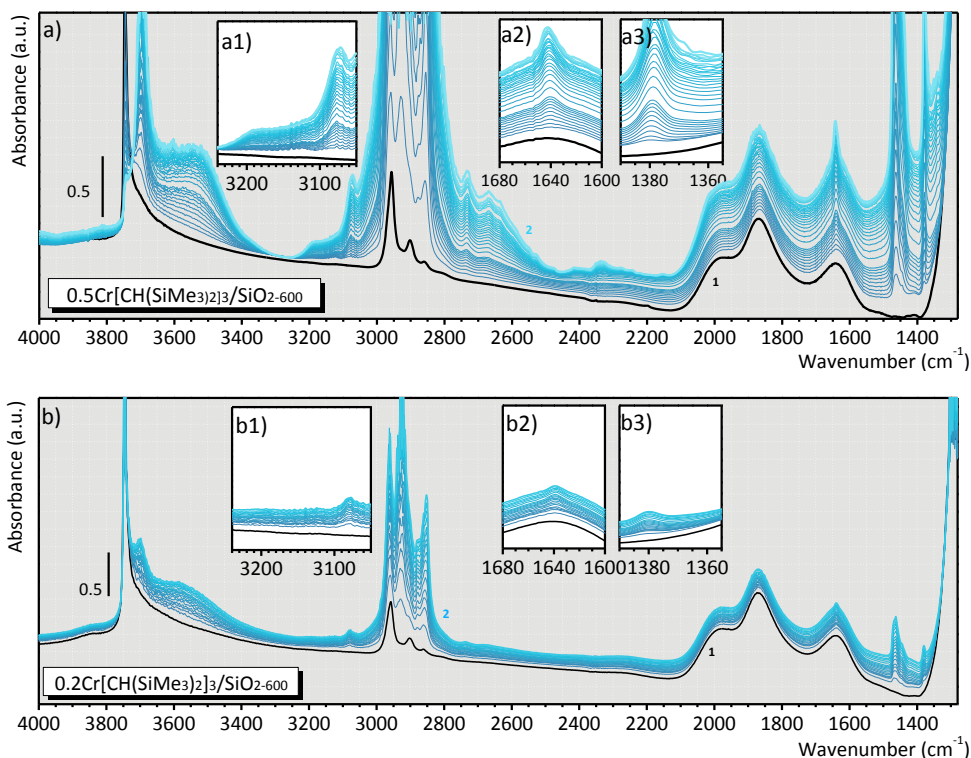
Figure 6. 8 Time resolved FT-IR spectra (from spectrum 1 to spectrum 2) collected during C_2H_4 polymerization at room temperature on $0.5Cr[CH(SiMe_3)_2]_3/SiO_{2-600}$ (part a) and on $0.2Cr[CH(SiMe_3)_2]_3/SiO_{2-600}$ (part b). Each spectrum was collected every 5 seconds; the whole sequence of spectra is collected in about 20 minutes. Insets a1), a2) and a3) report a magnification in the ($\nu(=CH_2)$), ($\nu(C=C)$), and $\delta(CH_3)$ regions, respectively. Insets b1), b2) and b3) the same for $0.2Cr[CH(SiMe_3)_2]_3/SiO_{2-600}$.

118

The simultaneous observation of the CH_3 groups and of two absorption bands at 3075 cm^{-1} ($v(=CH_2)$, insets a1 and b1) and 1641 cm^{-1} ($v(C=C)$, insets a2 and b2) indicate **the production of α-olefins, which are at first strongly physisorbed to the silanol groups at the silica surface** (as testified by the broad absorption band centered around 3600 cm^{-1}), **and then enchained in the growing polyethylene**, explaining the reason for the higher branching degree. These bands are much more evident for the polymerization conducted on the 0.5Cr[CH(SiMe$_3$)$_2$]$_3$/SiO$_{2-600}$ catalyst, while for the lower chromium loading they are scarcely observed, in well agreement with the analysis made on the polymer.

6.5 The accessibility of the Cr sites in the nCr[CH(SiMe$_3$)$_2$]$_3$/SiO$_2$ as probed by FT-IR spectroscopy of adsorbed CO.

On the basis of the results discussed so far, we can state that two types of Cr sites are co-present in the nCr[CH(SiMe$_3$)$_2$]$_3$/SiO$_{2-600}$ catalysts: those involved in the ethylene oligomerization process (Cr$_{oligom}$) and those involved in ethylene polymerization (Cr$_{polym}$). They differ in the coordination geometry (probably D$_{3h}$ and O$_h$, respectively) and ligands environment, but not in the oxidation state (+3). Furthermore, the proportion of the two sites varies as a function of the chromium loading. In order to highlight the structure at a molecular level of Cr$_{oligom}$ and Cr$_{polym}$ sites, we performed a series of FT-IR experiments in the presence of CO as molecular probe.

Figure 6. 9 shows the background subtracted FT-IR spectra of CO adsorbed at room temperature on the nCr[CH(SiMe$_3$)$_2$]$_3$/SiO$_{2-600}$ catalysts, at the maximum CO coverage. The spectra are reported after subtraction of those before CO adsorption. All the spectra are dominated by two main absorption bands in the ν(CO) region, characteristic of classical carbonyls (Figure 6. 9a). The first band, quite broad, is located at 2039 cm^{-1} (with a shoulder at 2050 cm^{-1}), and the second, extremely narrow, at 1993 cm^{-1}. A similar two-bands profile is characteristic of **highly symmetric tri-carbonyl metal complexes** [6]. The two bands are usually assigned to the non-degenerate total symmetric stretching and to the doubly degenerate total asymmetric stretching of the M(CO)$_3$ moiety. For example, the spectrum of (η^6-C$_6$H$_6$)Cr(CO)$_3$ shows two bands at 1966 and 1898 cm^{-1}. Generally speaking, the absolute intensity of these two bands is roughly proportional to the amount of chromium. This observation can have two different explanations: 1) at maximum θ$_{CO}$ it is not possible to distinguish Cr$_{polym}$ and Cr$_{oligom}$ sites by means of CO adsorption, because both sites form the same multi-carbonyl species; 2) CO probes only a family of sites, either Cr$_{polym}$ or Cr$_{oligom}$, whose amount is proportional to the Cr loading. However, the first hypothesis seems unlikely, especially on the basis of the results discussed in the previous Chapters. Indeed, CO has been demonstrated to be extremely sensitive to the mono-grafted or bis-grafted nature of the chromium species. Hence, we must accept that one of the two types of sites cannot be probed by CO at room temperature. The nature of the ν(CO) bands indicates that **the probed sites are the mono-grafted (≡SiO-)Cr[CH(SiMe$_3$)$_2$]$_2$ species, Cr$_{oligom}$,** that is reasonable on account of their low coordination. In contrast, **the bis-grafted (≡SiO-)$_2$Cr[CH(SiMe$_3$)$_2$] species, Cr$_{polym}$, do not coordinate CO in a molecular form**.
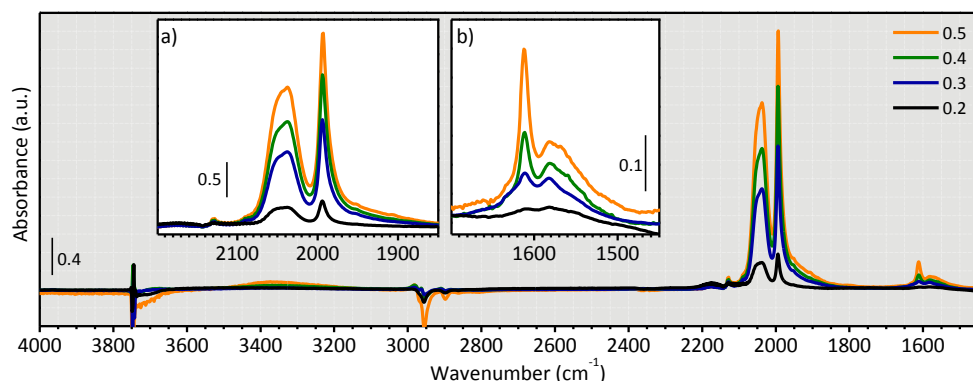
Figure 6. 9. FT-IR spectra of the nCr[CH(SiMe₃)₂]₃/ SiO₂₋₆₀₀ catalysts after adsorption of CO at room temperature (P = 30 mbar). The spectra were normalized to the thickness of the pellets, in order to allow a quantitative comparison.

A second series of weaker bands are observed in the $1700 - 1400$ cm^{-1} region (Figure 6. 9b). They are tentatively ascribed to **v(CO) of chromium acyl species, which are originated from CO insertion into the Cr-C bond** [13]. Indeed, it is known that CO has the capability to insert into metal-carbon bonds [14-16], and in olefin polymerization catalysis this is a strategy often adopted to quench the polymerization activity in case of reactor fouling. These bands are immediately formed when CO is admitted on the samples, and do not evolve in time. Moreover, their intensity is roughly proportional to the amount of chromium. This means that the insertion of CO in the Cr-C bond always interests a fraction of the chromium sites. Whether these sites are Cr_{polym} or Cr_{oligom} cannot be defined at this stage.

A very broad band is observed at ca. 3400 cm^{-1}, much more intense for $0.5Cr[CH(SiMe_3)_2]_3/SiO_{2-600}$ than for the other samples. This band is attributed to the presence of some OH groups in H-bonding interaction. It means that, for the higher chromium concentration, the $(\equiv SiO-)Cr[CH(SiMe_3)_2]_2(CO)_3$ carbonyls enter partially in interaction with the OH groups at the silica surface. Finally, weak negative bands are observed in the $v(CH_x)$ region, which indicate that a small fraction of the alkyl groups are perturbed by the interaction with CO. These two latter observation suggest that CO is not an innocent probe.

Figure 6. 10 shows the evolution of the FT-IR spectra in the v(CO) region upon decreasing the CO coverage (from red to green), for the $nCr[CH(SiMe_3)_2]_3/SiO_{2-600}$ catalysts. The two bands at 2039 and 1993 cm^{-1}, assigned to the $(\equiv SiO-)Cr[CH(SiMe_3)_2]_2(CO)_3$ tri-carbonyls at the mono-grafted Cr sites, gradually decrease in intensity. At the same time, a narrow band at 2069 cm^{-1}

gradually appears, which is tentatively assigned to a mono-carbonyl Cr species. The isosbestic point at ca. 2065 cm^{-1} indicates that the mono-carbonyl species derive, at least partially, from the transformation of the tri-carbonyls.
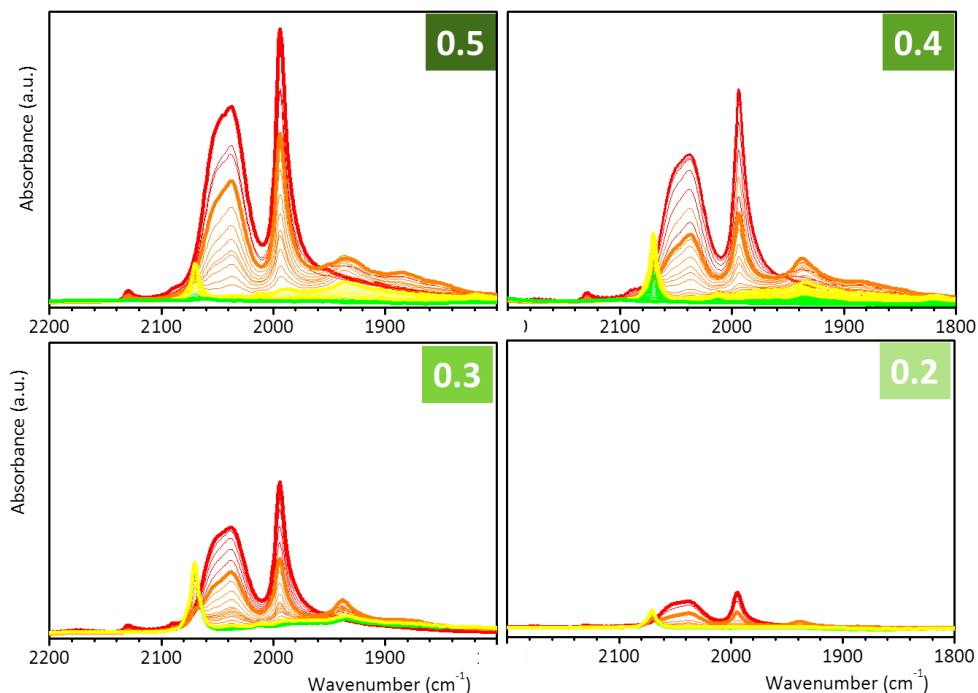
Figure 6. 10. Evolution of the background-subtracted FT-IR spectra of the nCr[CH(SiMe$_3$)$_2$]$_3$/SiO$_{2-600}$ catalysts in the v(CO) region as a function of CO coverage (θ_{max} = red, θ_{min} = green).

The evolution of the spectra as a function of θ_{CO} is qualitatively the same for all the Cr loadings. However, it has been noticed that the relative intensity of the absorption band at 2069 cm^{-1} (which appears only at low θ_{CO}) with respect to the bands at 2039 and 1993 cm^{-1} (which dominate the spectra at the maximum θ_{CO}) changes with the Cr loading. The band at 2069 cm^{-1} is relatively more intense for the 0.2Cr[CH(SiMe$_3$)$_2$]$_3$/SiO$_{2-600}$ catalysts. This behavior suggests that **there exist several types of mono-grafted ($\equiv$SiO-)Cr[CH(SiMe$_3$)$_2$]$_2$ species, which appear all the same at the maximum CO coverage (i.e. all of them form highly symmetric tri-carbonyls), but differentiate at low CO coverage.**

There are two additional observations that must be done at this step. The first one is that, upon degassing CO, a small but well observable amount of OH groups are consumed. At the same time, the absorption bands ascribed to v(CH$_x$) slightly decrease in intensity. The two phenomena appear correlated, and associated with the removal of CO. A possible explanation is that CO adsorption

122

compels the interaction of some mono-grafted ≡SiO-CrR$_2$ species with the OH groups at silica surface (as already observed in Figure 6. 9), and in some cases this situation can evolve into the reaction: ≡SiO-CrR$_2$(CO)$_3$ + ≡Si-OH → (≡SiO-)$_2$CrR(CO)$_3$ + RH, where the so formed RH compounds can be easily outgassed together with the CO molecules upon decreasing the gas pressure.

This means that **a small fraction of the mono-grafted (≡SiO-)Cr[CH(SiMe$_3$)$_2$]$_2$ species, originally close to isolated OH groups, are irreversibly transformed into bis-grafted (≡SiO-)$_2$Cr[CH(SiMe$_3$)$_2$] species after the interaction with CO**. This phenomenon is more probable at high Cr loading, where the probability to find a mono-grafted (≡SiO-)Cr[CH(SiMe$_3$)$_2$]$_2$ site in proximity of a OH group is greater.

The second important observation is that some changes are also observed in the 1700 – 1400 cm^{-1} region (not reported in Figure 6. 10) during the CO removal, but only in terms of position of the observed bands, and not of intensity. This means that the chromium acyl species change their symmetry, but are not removed during the CO evacuation.

6.6 A serendipitous discovery: CO selectively poisons the Cr$_{oligom}$ sites.

The experiments discussed above clearly demonstrate that CO is not an innocent probe towards the Cr sites. However, in the course of our experiments we realized that CO does not poison irreversibly the nCr[CH(SiMe$_3$)$_2$]$_3$/SiO$_{2-600}$ catalysts. **After interaction with CO all the catalysts still displayed a significant activity towards ethylene polymerization, while ethylene oligomerization was almost completely depressed**.
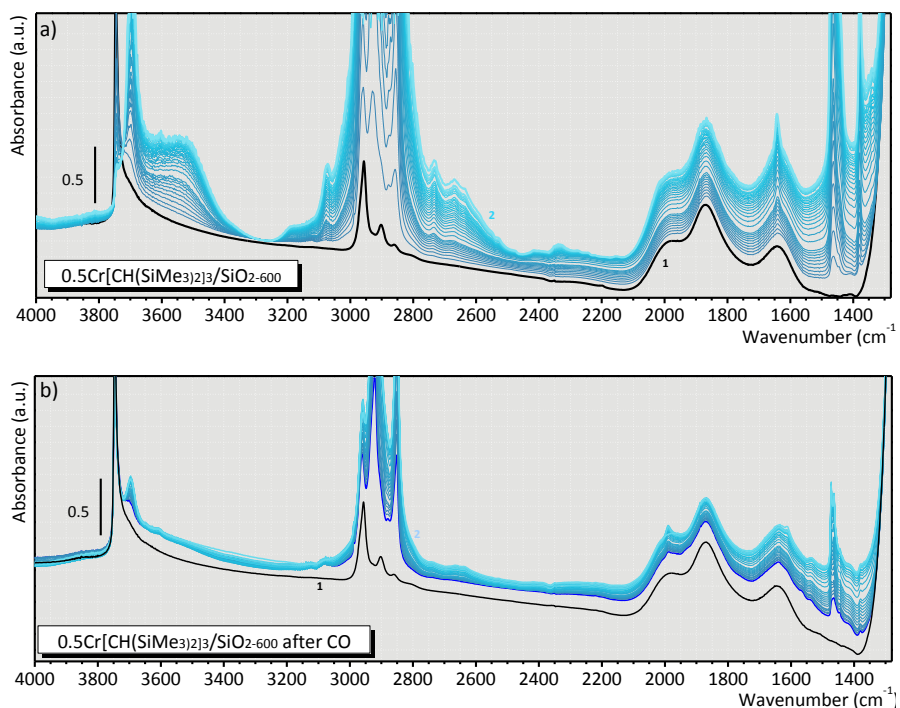
Figure 6. 11 Time resolved FT-IR spectra (from spectrum 1 to spectrum 2) collected during C$_2$H$_4$ polymerization on 0.5Cr[CH(SiMe$_3$)$_2$]$_3$/SiO$_{2-600}$ (part a) and on the same catalyst after CO poisoning (part b).

An example of this behavior is illustrated in Figure 6. 11, that shows the FT-IR spectra collected during ethylene polymerization on the 0.5Cr[CH(SiMe$_3$)$_2$]$_3$/SiO$_{2-600}$ catalyst before (part a) and after (part b) interaction with CO. The spectroscopic manifestation of the oligomers (v(=CH$_2$) at 3075 cm^{-1}, and v(C=C) at 1641 cm^{-1}) are very weak in the second case, but the catalyst still works for ethylene polymerization, although with a lower activity than before. This behaviour clearly indicates that **CO selectively poisons most of the Cr$_{oligom}$ sites,**

while the majority of the Cr$_{polym}$ sites are unaffected. This means **either that the Cr$_{polym}$ sites are completely inaccessible to CO or that the eventual insertion of CO into the Cr$_{polym}$-R bond is reversible in the presence of ethylene**.

To better understand this phenomenon, we repeated the experiment on the 0.5Cr[CH(SiMe$_3$)$_2$]$_3$/SiO$_{2-600}$ catalyst by dosing the same amount of CO (100 mbar) for four consecutive times, each time followed by complete evacuation. Figure 6. 12 shows the spectra in the ν(CO) region in the four cases. It is evident that the absolute intensity of the bands ascribed to mono-grafted ≡SiO-CrR$_2$(CO)$_3$ tri-carbonyls gradually decreases at each experiment, meaning that the mono-grafted ≡SiO-CrR$_2$ sites are progressively and irreversibly poisoned by CO. The above discussed reaction of the ≡SiO-CrR$_2$(CO)$_3$ carbonyls with the surface OH groups accounts only for a fraction of the lost ≡SiO-CrR$_2$ sites, and only the first time. From the second CO dosing onwards, no changes are observed in all the other spectral regions. **Additional deactivation mechanisms for the Cr$_{oligom}$ sites in the presence of CO should be invoked, although at the moment we cannot advance any hypothesis**. As a side note, by dosing ethylene at the end of the fourth CO dosing, a substantial polymerization activity was still observed, confirming that the Cr$_{polym}$ sites are only marginally affected by CO.
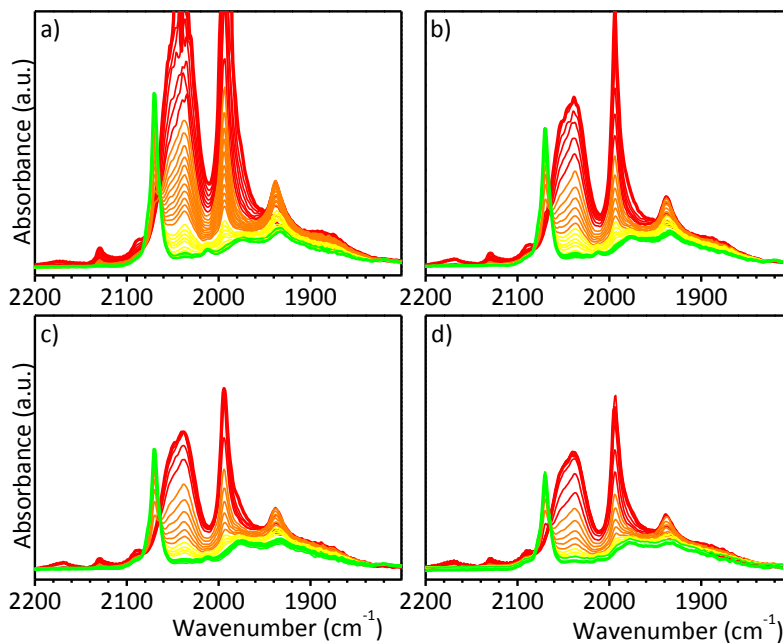
Figure 6. 12 Part a) Evolution of the background-subtracted FT-IR spectra in the ν(CO) region of CO adsorption on 0.5Cr[CH(SiMe$_3$)$_2$]$_3$/SiO$_{2-600}$ as a function of CO coverage (θ$_{max}$ = red, θ$_{min}$ = green). Parts b, c and d) Same as in part a after the second, the third and the fourth sending of CO, respectively.

6.7 A short summary on the properties of the nCr[CH(SiMe₃)₂]₃/SiO₂-₆₀₀ catalysts and some structural hypothesis.

The present paragraph summarizes the main results achieved by applying several complementary spectroscopic techniques to the investigation of nCr[CH(SiMe₃)₂]₃/SiO₂-₆₀₀ catalysts. Some hypothesis on the molecular structure of the Cr sites are also proposed.

6.7.1 The co-presence of two types of Cr(III) sites, their relative abundance and their role in ethylene polymerization

The whole set of spectroscopic measurements discussed so far, clearly pointed out the co-presence of two types of Cr(III) sites in the nCr[CH(SiMe₃)₂]₃/SiO₂-₆₀₀ catalysts, with a different behaviour in the presence of ethylene:

1. **Mono-grafted (≡SiO-)Cr[CH(SiMe₃)₂]₂ species in a low coordination environment** (Figure 6. 13a), which maintain most of the structural properties of the Cr[CH(SiMe₃)₂]₃ precursor and a symmetry close to D₃ₕ. These sites are responsible for ethylene oligomerization (**Cr_oligom** sites), as reported in the literature [17-19].

2. **Bis-grafted (≡SiO-)₂Cr[CH(SiMe₃)₂] species having a high coordination**, likely 6-fold coordinated (Figure 6. 13b), which are responsible for ethylene polymerization (**Cr_polym** sites).
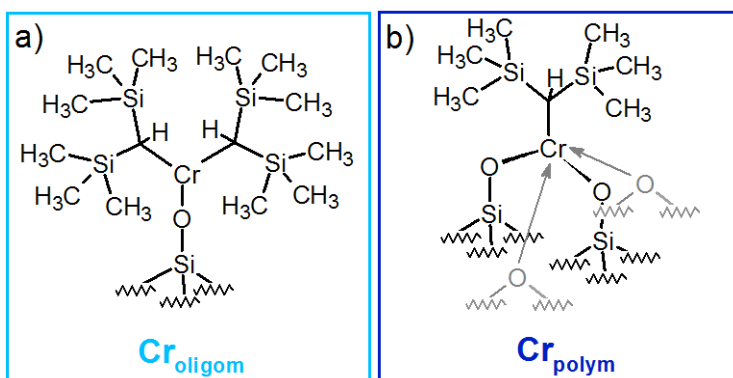
Figure 6. 13 Schematic representation of the local structure of Cr_oligom (part a) and Cr_polym sites (part b), as determined by several spectroscopic methods.

The concentration of the **Cr_polym** sites is almost constant irrespective of the Cr loading, although their local structure is slightly different. This result is quite intuitive. Indeed, bis-grafted (≡SiO-)₂Cr[CH(SiMe₃)₂] species can be formed

only if there are two OH species at the right distance on the silica surface, according to the reaction scheme shown in Figure 6. 14a. The OH population depends on the type of silica and on the activation temperature, which are the same for all the catalysts. A silica activated at 600 °C has only a limited fraction of OH species available for forming Cr_{polym} sites, which are completely occupied already at a Cr loading of 0.2 wt%.

Upon increasing the Cr concentration, only mono-grafted species can be formed. It is worth noticing that there are two routes for the formation of Cr_{oligom} sites, involving respectively an isolated silanol or a siloxane group, as schematically illustrated in Figure 6. 14b and b'. **The so formed sites are structurally identical, but differ in the ligand sphere.** Indeed, those formed following the second route are vicinal to a ≡Si-R group at the silica surface.
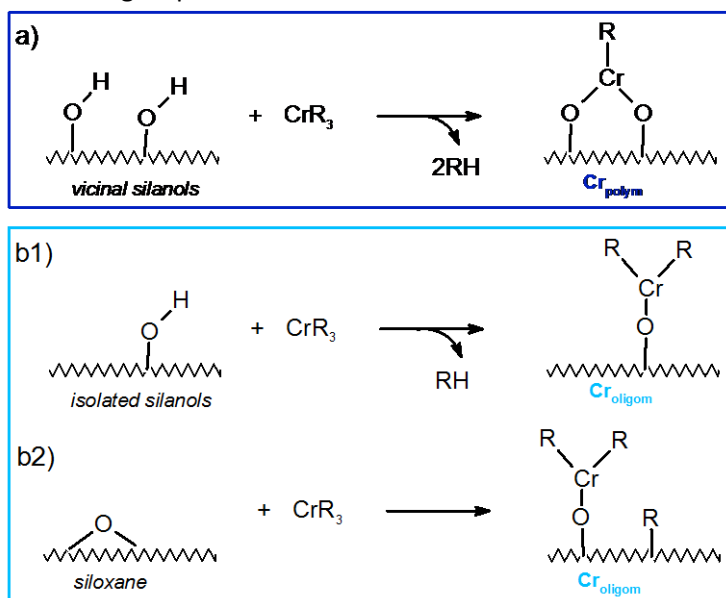
Figure 6. 14 Schematic representation of the possible routes leading to the formation of Cr_{polym} and Cr_{oligom} sites on silica surface. It is worth noticing that R stays for the $CH(SiMe_3)_2]_3$ group, which is a quite encumbering ligand.

It is also expected that at high Cr loading, the presence of many Cr_{oligom} sites adjacent to Cr_{polym} causes a change in the strain of the silica surface, which consequently slightly affects the local structure of the latter. Hence, we can conclude that by going from 0.2 to 0.5 wt% as a Cr loading the number of Cr_{oligom} sites gradually increases, while that of Cr_{polym} sites remains constant, although they slightly change their local structure.

6.7.2 Accessibility (and reactivity) of the Cr sites towards CO

The experiments performed in the presence of CO indicated that **the bis-grafted ($\equiv$SiO-)$_2$Cr[CH(SiMe$_3$)$_2$] species, Cr$_{polym}$, do not coordinate CO in a molecular form, but eventually only insert it into the Cr-R bond to give a Cr-acyl species**. Since ethylene polymerization is almost unaffected by CO, we might assume that the Cr-acyl species eventually formed on Cr$_{polym}$ sites are reversible in the presence of ethylene. In contrast, **the mono-grafted ($\equiv$SiO-)Cr[CH(SiMe$_3$)$_2$]$_2$ species, Cr$_{oligom}$, are accessible by CO and, at the maximum CO coverage, they all form highly symmetric tri-carbonyl metal complexes**. The behavior of these carbonyls upon decreasing the CO coverage, however, clearly indicates that there exist several types of mono-grafted ($\equiv$SiO-)Cr[CH(SiMe$_3$)$_2$]$_2$ species, that likely differ for the local environment, as already suggested in Figure 6. 14.
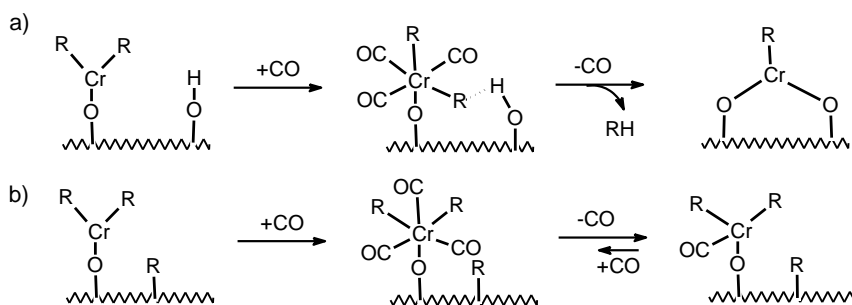
Figure 6. 15 Schematic representation of the reactivity of Cr$_{oligom}$ sites towards CO and some of the possible deactivation pathways that are compatible with the experimental observations.

Most of the Cr$_{oligom}$ sites are slowly and irreversibly poisoned by CO. Figure 6. 15 shows the reactivity of Cr$_{oligom}$ sites towards CO and some of the possible deactivation pathways, which are compatible with the experimental observations. Path a illustrates the case of the mono-grafted species originally in proximity of an isolated OH group. The formation upon CO adsorption of a highly symmetric ($\equiv$SiO-)Cr[CH(SiMe$_3$)$_2$]$_2$(CO)$_3$ tri-carbonyl species favors the interaction of an R ligand with a surface OH group. Upon degassing, RH is released and the Cr$_{oligom}$ sites is irreversibly transformed into a bis-grafted ($\equiv$SiO-)$_2$Cr[CH(SiMe$_3$)$_2$] species. This phenomenon is more feasible at high Cr loading, where the probability to find a mono-grafted ($\equiv$SiO-)Cr[CH(SiMe$_3$)$_2$]$_2$ site in proximity of a OH group is greater. The so-formed bis-grafted ($\equiv$SiO-)$_2$Cr[CH(SiMe$_3$)$_2$] species do not coordinate anymore CO in a molecular way, and the consequence is that the original Cr$_{oligom}$ site is no more visible by CO at a successive dosage.

Path b in Figure 6. 15 illustrates the case of a mono-grafted ($\equiv$SiO-)Cr[CH(SiMe$_3$)$_2$]$_2$ species originally close to a $\equiv$Si-R group (i.e., a Cr$_{oligom}$ site

originated from reaction of the precursor with a siloxane bridge). In presence of CO, a highly symmetric (≡SiO-)Cr[CH(SiMe$_3$)$_2$]$_2$(CO)$_3$ tri-carbonyl species is formed that, however, is much less incline to structural transformation because of the presence of the encumbering ≡Si-R group nearby. Hence, upon degassing CO, the tri-carbonyl is transformed into a (≡SiO-)Cr[CH(SiMe$_3$)$_2$]$_2$(CO) mono-carbonyl species. This process is only partially reversible upon adding/removing CO, that means that additional (slower) deactivation mechanisms for the ≡SiO-CrR$_2$ sites in the presence of CO should be invoked, although at the moment we cannot advance any hypothesis.

The neat result is that CO selectively poisons most of the Cr$_{oligom}$ sites, while the majority of the Cr$_{polym}$ sites are unaffected.

References

[1] Monoi, T., Ikeda, H., Sasaki, Y., Matsumoto, Y.,Polym. J., 35 (2003) 608-611.

[2] Monoi, T., Sasaki, Y.,J. Mol. Catal. A-Chem., 187 (2002) 135-141.

[3] Ikeda, H., Monoi, T., Sasaki, Y.,J. Polym. Sci.: Part A: Polym. Chem., 41 (2003) 413-419.

[4] Sheldrick, G.M., Sheldrick, W.S.,J. Chem. Soc. A, (1969) 2279-2282.

[5] Eller, P.G., Bradley, D.C., Hursthouse, M.B., Meek, D.W.,Coord. Chem. Rev., 24 (1977) 1-95.

[6] Miessler, G.L., Tarr, D.A., Inorganic Chemistry, St. Olaf College
Northfield, Minnesota.

[7] Aleya et al.,Journal of the Chemical Society, Dalton Transactions, (1973) 185-191.

[8] Colthup N.B., Daly H. L., E., W.S., INTRODUCTION TO INFRARED AND RAMAN SPECTROSCOPY, Harcourt Brace Jovanovich, Publishers, 1990.

[9] Hursthouse, M.B., Welch, A.J., Unpublished results.

[10] Delley, M.F., Núñez-Zarur, F., Conley, M.P., Comas-Vives, A., Siddiqi, G., Norsic, S., Monteil, V., Safonova, O.V., Copéret, C.,Proc. Natl. Acad. Sci. U. S. A., 111 (2014) 11624-11629.

[11] Brückner, A.,Physical Chemistry Chemical Physics, 5 (2003) 4461-4472.

[12] Brückner, A., Jabor, J.K., McConnell, A.E.C., Webb, P.B.,Organometallics, 27 (2008) 3849-3856.

[13] Barnett, K.W., Beach, D.L., Gaydos, S.P., Pollmann, T.G.,J. Organomet. Chemi., 69 (1974) 121-130.

[14] Calderazzo, F.,Pure Appl. Chem., 33 (1973) 453-474.

[15] Calderazzo, F.,Angew. Chem. Int. Ed. Engl., 16 (1977) 299-311.

[16] Calderazzo, F.,Pure Appl. Chem., 50 (1978) 49-53.

[17] McDaniel, M.P.,Adv. Catal., 53 (2010) 123-606.

[18] Barzan, C., Gianolio, D., Groppo, E., Lamberti, C., Monteil, V., Quadrelli, E.A., Bordiga, S.,Chem. Eur. J., 19 (2013) 17277-17282.

[19] Barzan, C., Groppo, E., Quadrelli, E.A., Monteil, V., Bordiga, S.,Phys.Chem.Chem.Phys., 14 (2012) 2239–2245.

Chapter 7
Conclusions and perspectives.

Polyolefins are one the most common plastic materials, used in every-day life because of their versatile applications in different fields. Polyethylene in particular has a crucial role and has recently demonstrated to be a direct competitor to much more expensive high performance polymers for advanced applications (like in medicine or automotive fields) [1, 2]. The industrial production of polyethylene relies mainly on catalytic polymerization processes. Heterogeneous Ziegler and Phillips catalysts are the catalysts mostly used in the industrial practice, thanks to their extremely low cost and because they offer a good control of the polymer morphology as a replica of the catalyst [3-9]. The physical and chemical properties of the produced polyethylene (e.g. density, level of branching, molecular weight distribution and architecture) are strictly connected with the structure of the catalysts. For this reason, a large fraction of the industrial research in this field has concentrated so far in changing the catalyst to tune the properties of the polymer.

Among ethylene polymerization catalysts, the Cr-based Phillips catalysts have the largest share in the HDPE market. Many variants of the Phillips catalyst have been developed and commercialized along the years, improving the catalyst activity, the polymer properties, and even the polymer processing. Nevertheless, despite more than fifty years of study, some fundamental questions about the structure of the chromium sites and the polymerization mechanism are still open

and far to be fully understood. In this context, although not resolutive, this PhD thesis represents a little step forward the understanding of the relationship between the molecular structure of the chromium sites and their activity, at least for what concern the analyzed systems.

The present PhD work has been focused on the investigation of the properties at a molecular level of the Cr sites in some variants of the heterogeneous Phillips catalyst employed in the industrial practice. A systematic approach was followed, based on the synergic application of different and complementary characterization techniques (mainly spectroscopic), coupled with a basic characterization of the polymer. The work was divided into three parts:

1) A fundamental study on the structure and the mechanism of formation of the Cr active sites in the classical Cr/SiO_2 catalyst, both in its oxidized ($Cr(VI)/SiO_2$) and reduced ($Cr(II)/SiO_2$) versions.
2) The examination of the effect of Al-alkyls (TEA and DEALE) as modifying agents for the Cr sites on both the $Cr(II)/SiO_2$ and the $Cr(VI)/SiO_2$ catalysts;
3) An in-depth study of a series of $Cr[CH(SiMe_3)_2]_3/SiO_{2-600}$ catalysts in order to find a correlation between the density of the produced polymer and the Cr loading.

The main results achieved within these three stories have been summarized in the previous Chapters. Herein, we will focus on the novelty of these results and on the perspectives that they open for future works in this field.

7.1 The relevance of Cr oxidation state in ethylene polymerization and some consideration on the discrepancies present in the literature

Currently, the literature on the Phillips catalyst is animated by a nervous debate on the oxidation state of the Cr sites active in ethylene polymerization. The measurements performed during my PhD add some small pieces to this complex story. To start, it is important to clarify the meaning of "active site". Scheme 1 summarizes the differences between Cr precursors, Cr intermediates and Cr active sites and also four different routes to form the active sites, all of them investigated in this work. During step 1 (the reduction), the Cr(VI) precursors are reduced to Cr(II) intermediates, either by ethylene at 100 °C (Route 1) or by CO at 350 °C (Route 2). In the former case, oxidized by-products are formed and retained by the Cr(II) sites [10], while in the latter CO_2 is released and leaves the sample at the reduction temperature. During step 2 (the alkylation), the Cr(II) intermediates are alkylated to Cr(?)-R sites by ethylene, whereby the question mark indicates that the oxidation state is still matter of discussion. These sites are those active in ethylene polymerization. Alternatively, the Cr(VI) reduction and alkylation can be achieved in a single step also by using Al-alkyls (Route 3). The same Al-alkyls can alkylate the Cr(II) precursors obtained during step 1 (Route 4), likely maintaining their oxidation state.
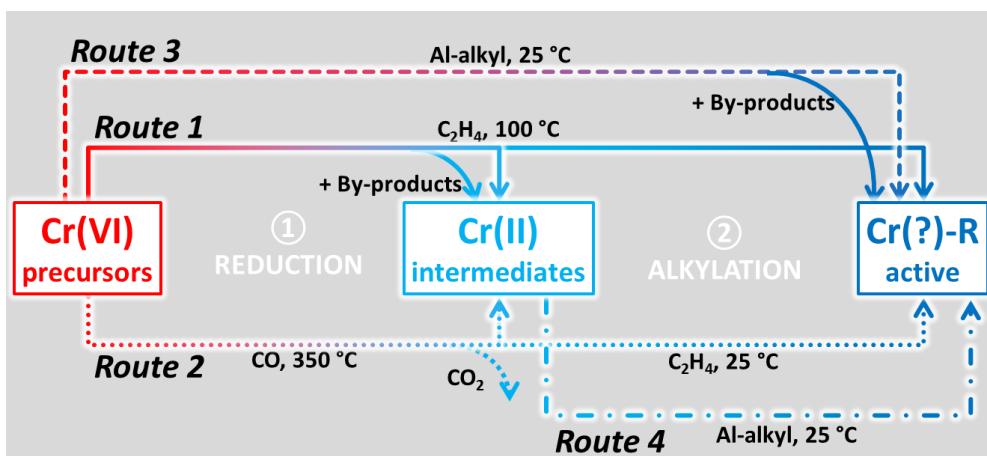
Scheme 1. Simplified scheme showing the four investigated routes to reduce and alkylate the Cr(VI) precursors, converting them into the chromium active sites.

Bis-grafted Cr(III)-R species are definitely active in ethylene polymerization, as demonstrated in the literature for some analogues of the

Phillips catalyst synthetized starting from organometallic precursors [11-13] and also by the work performed in this thesis on the $Cr[CH(SiMe_3)_2]_3/SiO_{2-600}$ catalysts (Chapter 6). This finding fostered the idea that similar Cr(III)-R sites would be the active sites also in the classical Cr/SiO_2 catalyst, and this was indeed the reason why I have been stimulated to work on the $Cr[CH(SiMe_3)_2]_3/SiO_{2-600}$ samples. However, the experiments performed within this PhD thesis clearly demonstrated that the situation is not so simple, and that the Cr(?)-R sites are structurally and electronically different depending on the route followed to generate them.

- For $Cr(II)/SiO_2$ reacting with ethylene (Chapter 3) no evidence for the formation of Cr(III) species was found, despite clear evidence of a consistent ethylene polymerization activity: the most likely hypothesis for the Cr(?)-R active sites are **Cr(IV)-R**.

- The same was found for $Cr(II)/SiO_2$ reacting with Al-alkyls (Chapter 4), that showed however an extraordinarily high activity in ethylene polymerization. In this case, a fraction of the active sites remain unmodified (and hence follow the same destiny as above), and another fraction is in the form of mono-grafted **Cr(II)-R** sites.

- When starting from $Cr(VI)/SiO_2$, both ethylene (Chapter 3) and Al-alkyls (Chapter 5) end up forming a reduced non-paramagnetic active state, probably **Cr(IV)-R**. In the former case, this is the result of a 2-electron oxidative addition of ethylene to the Cr(II) intermediate, whereas in the latter case Cr(IV)-R is the direct product of Cr(VI) reduction by Al-alkyls. Besides, also a small fraction of Cr(III) sites is actually formed in the presence of both ethylene and Al-alkyls. Those sites are detected by EPR spectroscopy (which is extremely sensitive to Cr(III)), but are almost invisible to all the other techniques, and appear mostly as the result of a 2-electron reduction of the Cr(V) species, which are ubiquitous in $Cr(VI)/SiO_2$ but generally considered not relevant for catalysis. Whether or not these Cr(III) sites are active in ethylene polymerization cannot be determined, but for sure they cannot be considered as the determining actors in the Phillips catalysis. Moreover, Al-alkyls can further reduce a fraction of Cr(VI) to Cr(II), which are detected by FT-IR spectroscopy of adsorbed CO, and appear very similar to those obtained by starting from $Cr(II)/SiO_2$ (i.e. **Cr(II)-R**).

- Nevertheless, when starting from $Cr(VI)/SiO_2$, there is always a fraction of Cr(VI) sites which are late in being reduced, both in the presence of ethylene and in the presence of Al-alkyls. Hence, ethylene polymerization starts in the presence

of residual Cr(VI) sites, that in some cases might be reduced by α-olefins eventually produced in situ.

Summing up all these observations, it is evident that, under the adopted experimental conditions, **isolated Cr(III)-R sites are not necessary for developing ethylene polymerization on the Cr/SiO₂ Phillips catalyst. Rather, a series of evidences converge towards Cr(IV)-R as the active species in most of the cases.** Unfortunately, these sites are quite elusive from a spectroscopic point of view, and so far their presence is supported mostly by indirect evidences.

This finding re-opens the question on the oxidation state of the propagating chromium sites, which was recently presented as a closed case [14], and also foster some consideration on the relevance of the chemical history of the investigated catalysts. During the three years of this PhD work (and on the basis of a long experience of the Torino's group in the field of the Phillips catalyst), I can affirm without hesitation that **the Phillips catalysts are among the most sensitive and touchy systems in catalysis. Subtle changes in the experimental set-up and/or in the activation protocol, leads to different and often misleading results**. I experienced directly this problem during my internship at LIKAT (Rostock), where I failed in performing reliable XPS experiments and I was not able to activate properly the Cr(VI)/SiO₂ catalyst, simply because the experimental set-up was different with respect to that present in our lab, optimized over decades of activity on the Phillips catalyst.

7.2 How do the local structure and the acidity of the Cr sites affect their reactivity towards ethylene?

Along this journey, I have encountered Cr sites characterized by very different local structures. The Cr sites can be **bis-grafted** (as in the classical Cr/SiO₂), **or mono-grafted to the silica surface**. This latter situation is generated during specific modification of the classical Cr/SiO₂ catalyst or as a consequence of the grafting of organochromium complexes on previously activated silica. According to McDaniel, the mono-grafted Cr species are often responsible of in situ α-olefin generation, i.e. they oligomerize ethylene rather than polymerize it [4]. Again, the results collected during this PhD work indicate that the situation is not as simple. As an example, I have found that Al-alkyls (and in particular TEA) transform a substantial fraction of the bis-grafted Cr species into mono-grafted ones, but the density of the obtained PE is not largely different from that obtained with a classical Cr/SiO₂. Hence, not all the mono-grafted Cr sites oligomerizes ethylene.

I have also realized that the **acid properties of the Cr sites strongly affect their behavior**. This is something well known in the industrial practice, and it is well documented that different supports can modulate the acidity of the Cr sites and hence their reactivity. However, what probably is not yet well established, is the role of the ligands in affecting the acid properties of the Cr sites, whereby with ligands we refer not only to those directly ligated to the Cr sites through a covalent bond, but also those interacting with them through non-bonding interactions.

According to our conclusions, **the presence of mono-grafted Cr sites is a necessary condition for ethylene oligomerization,** irrespective of their oxidation state (both Cr(II) and Cr(III) can oligomerizes ethylene). **However, this is not sufficient. The mono-grafted Cr sites must also behave as weak Lewis acid sites (W-LA sites). On the other hand, Cr sites with a strong Lewis acid (S-LA) character usually produce PE with a very high MW**, irrespective of their local structure. It is thus clear that, by tuning the structure and the acid character of the Cr sites, it is possible to move from a system which essentially oligomerizes ethylene, to one that polymerizes it to very long PE chains. I believe that these conclusions can be useful in the design of Cr-based catalysts, not only for ethylene polymerization but also for ethylene oligomerization.

7.3 The importance of the (ancillary) ligands

During this work, I have collected several examples of the important role played by the ligands surrounding the Cr sites. For example:

o For Cr(VI)/SiO$_2$ directly reduced in ethylene, we found that the nucleophilic by-products formed during the induction time (mostly methylformate) remain attached to the chromium sites during the initial steps of ethylene polymerization.

o The siloxane bridges at the silica surface stabilize the poorly coordinated Cr(II) sites, as well as many mono-grafted Cr species.

o For Cr/SiO$_2$ modified by Al-alkyls, it was demonstrated that the Lewis acidity of the modified Cr sites strongly depends on the number and the type of the ancillary ligands: AlR$_x$O$_y$ fragments at the silica surface generally increase the Lewis acidity.

All these examples reveal that, even for an apparently simple catalyst such as the Phillips catalyst, **the catalysis is strongly influenced by a complex network of cooperative effects that involve not only the active sites, but also the ligands nearby, and the support itself**. These phenomena, which are very much similar to those occurring in homogeneous catalysis (where for example the role of the

ligands, or the cooperation between two adjacent metal sites, are well recognized), are often neglected in heterogeneous catalysis.

7.4 Perspectives

Heterogeneous olefin polymerization catalysis is a still expanding research field, with great economic repercussions. The patent literature demonstrates that there are plenty of ways to manipulate the original Cr/SiO_2 catalyst in order to affect its performances (not only in terms of activity but also how efficiently it runs in the commercial reactor) and to finely tune the PE properties, which include the polymer MW, the breadth of the MW distribution, the incorporation degree of comonomer/macro monomer, and the subsequent distribution of short and long-chain branches within the MW distribution. The difficulty is to establish a correlation between the catalyst composition, the structure of the active sites, and the catalyst performances. For this reason, what observed during this PhD project could have **an interesting impact in the PO industry.** It was demonstrated that the use of a multi technical approach could be **the key for deciphering at a molecular scale the interconnections among all the components and rationally re-designing them for specific applications**. By analysing the effect of the several factors that can influence the catalytic activity of the Phillips catalyst (oxidations state, ancillary ligands, support and local structure of the sites), we started to rationalize the relationship between the Cr structures and their capacity to produce oligomers or polymers of different molecular weight. The results shown in this PhD thesis definitely demonstrate the potentials of a physico-chemical approach that, when applied to the investigation of a catalyst before and after a molecular modification, may open new perspectives in the rational development of innovative catalysts for ethylene conversion to polymers with widely adjustable properties.

References

[1] Peacock, A.J., Handbook of Polyethylene. Structures, properties and applications. , New York Basel 2000.

[2] Nowlin, T.E., Business and Technology of the Global Polyethylene Industry, Wiley-Scrivener, New York, 2014.

[3] McDaniel, M.P.,Adv. Catal., 33 (1985) 47-98.

[4] McDaniel, M.P.,Adv. Catal., 53 (2010) 123-606.

[5] McDaniel, M.P., A review of the Phillips Chromium Catalyst for Ethylene Polymerization, in: Handbook of Transition Metal Polymerization Catalysts: Second Edition, 2018, pp. 401-571.

[6] Cossee, P.,J. Catal., 3 (1964) 80-88.

[7] Arlman, E.J.,J. Catal., 3 (1964) 89-98.

[8] Arlman, E.J., Cossee, P.,J. Catal., 3 (1964) 99-104.

[9] Busico, V.,Mrs Bulletin, 38 (2013) 224-228.

[10] Barzan, C., Piovano, A., Braglia, L., Martino, G.A., Lamberti, C., Bordiga, S., Groppo, E.,JACS, 139 (2017) 17064-17073.

[11] Delley, M.F., Núñez-Zarur, F., Conley, M.P., Comas-Vives, A., Siddiqi, G., Norsic, S., Monteil, V., Safonova, O.V., Copéret, C.,Proc. Natl. Acad. Sci. U. S. A., 111 (2014) 11624-11629.

[12] Coperet, C., Basset, J.M.,Adv. Synth. Catal., 349 (2007) 78-92.

[13] Coperet, C., Chabanas, M., Saint-Arroman, R.P., Basset, J.M.,Angew. Chem.-Int. Edit., 42 (2003) 156-181 and references therein.

[14] Brown, C., Krzystek, J., Achey, R., Lita, A., Fu, R., Meulenberg, R.W., Polinski, M., Peek, N., Wang, Y., Van De Burgt, L.J., Profeta, S., Stiegman, A.E., Scott, S.L.,ACS Catal., 5 (2015) 5574-5583.

Chapter 8
Scientific publications.

Most of the results presented in Chapters 3 and 4 have already been published during my PhD project. In particular, following the list below Chapter 3 is related to articles 2, 5 and 6, while Chapter 4 to article 4.

The other data contained in the Thesis will be object of future publications.

The other articles listed below derived from side researches, to which I contributed because they are all part of the investigation of olefin polymerization catalysis, although not directly connected to my PhD project.

8.1 Articles published on international (ISI) journals

1. Alessandro Piovano, **Giorgia A. Martino**, Caterina Barzan, "A Spectroscopic Investigation of Silica-Supported $TiCl_x$ Species: a Case Study towards Ziegler-Natta Catalysis", 2016 *Rendiconti Lincei*

2. Caterina Barzan, Alessandro Piovano, Luca Braglia, **Giorgia A. Martino**, Carlo Lamberti, Silvia Bordiga and Elena Groppo ""Pursuing the Formation and Molecular Structure of the Cr sites active in ethylene polymerization in Cr^{VI}/SiO_2 Phillips catalyst." 2017 *Journal of the American Chemical Society*

3. **Giorgia A Martino**, Caterina Barzan, Alessandro Piovano, Andriy Budnyk, and Elena Groppo "Tracking the reasons for the uniqueness of Cr/Al_2O_3 catalyst in ethylene polymerization."2018 *Journal of Catalysis*

4. **Giorgia A. Martino**, Alessandro Piovano, Caterina Barzan, Silvia Bordiga, Elena Groppo "The effect of Al-alkyls on the Phillips catalyst for ethylene polymerization: the case of diethylaluminum ethoxide (DEALE)",2018 *Topics in Catalysis*

5. Elena Morra, **Giorgia A. Martino**, Alessandro Piovano, Caterina Barzan, Elena Groppo, and Mario Chiesa, "In Situ X- and Q-Band EPR Investigation of Ethylene Polymerization on Cr/SiO_2 Phillips Catalyst", 2018 *Journal of Physical Chemistry C*

6. Elena Groppo, **Giorgia A. Martino**, Alessandro Piovano, Caterina Barzan, "The active sites in the Phillips catalysts: origins of a lively debate and a vision for the future", 2018 *ACS Catalysis*

7. Lorenzo Mino, Caterina Barzan, **Giorgia A. Martino**, Alessandro Piovano, Giuseppe Spoto, Adriano Zecchina, and Elena Groppo "Photo-induced ethylene polymerization on the Cr^{VI}/SiO_2 Phillips catalyst", 2018 *Journal of Physical Chemistry C*

8. Giuseppe Leone, Elena Groppo, Giorgia Zanchin, **Giorgia A. Martino**, Alessandro Piovano, Fabio Bertini, Javier Marti-Rujas, Emilio Parisini, and Giovanni Ricci "Concerted Electron Transfer in Iminopyridine Chromium Complexes: Ligand Effects on the Polymerization of Various (Di)olefins", 2018 *Organometallics*

CrossMark

CONCEPTS IN CATALYSIS

A spectroscopic investigation of silica-supported TiCl$_x$ species: a case study towards Ziegler–Natta catalysis

Alessandro Piovano[1] · **Giorgia A. Martino**[1] · **Caterina Barzan**[1]

Abstract Since their discovery in the 1950s, several breakthroughs marked the evolution of Ziegler–Natta catalysts and contributed to improve their catalytic activity and selectivity, conditioning the whole polyolefin market. However, some fundamental questions are still open about the structural and functional properties of the active sites, whose understanding could open new perspectives in controlling the polymerization process. In this context, a SiO$_2$-supported Ziegler–Natta catalyst was prepared following a step by step approach, with the simultaneous goal of synthesis and characterization, to investigate with a surface science approach each step of the catalytic process.

Keywords Ziegler–Natta catalysts · In situ spectroscopy · Silica support · Surface science

1 Introduction

Polyethylene was first synthesized in 1933 in the research laboratories of the Imperial Chemical Company, but the polyolefins widespread commercial relevance started only after the discovery of Ziegler–Natta and Phillips catalysts in the early 1950s, which allowed the large scale production in mild conditions and with a good control of the

thermal and structural properties of the products. Successive breakthroughs modified these heterogeneous catalysts improving their activity, making the processes more efficient and enhancing the selectivity to specific products. Despite many efforts to rationally design new catalysts for olefin conversion, up to now these modifications have been mostly based on a trial and error approach. At the same time, in the last years the homogeneous catalysis has achieved a prominent role in this field too, mainly based on metallocene compounds (Kaminsky 1996). The great advantage of homogeneous catalysis is the possibility to tailor the synthesis of the catalysts according to the different needs, verging on the level of detail of enzymatic catalysis (Robert and Thomas 2013).

Ziegler-Natta catalysts can be placed at the contact point between heterogeneous and homogeneous catalysis. Indeed, on one side their composition from the first to the fourth generation has reached an almost molecular level of complexity and specificity (Terano 2004; Chang et al. 2006; Liu et al. 2015), and on the other side metallocene catalysts have been gradually undergoing a heterogenization process to exploit the widespread industrial technology for supported catalysts (Olabisi et al. 1997; Kaminsky and Winkelbach 1999; Fink et al. 2000; Tisse et al. 2014). Although this dualism may promote the transfer of the organometallic knowledge to the study of the mechanism of the traditional catalytic systems (Corradini et al. 2004), the research is still far from understanding the functions and mutual influence of each component in Ziegler–Natta catalysts. Despite some important progresses both in the experimental and theoretical characterization of the catalysts and in the development of specific tools for screening in real time the evolution of the reaction under operando conditions (Groppo et al. 2013; D'Amore et al. 2016; Busico et al. 2016), the complexity and the nonlinearity of

✉ Alessandro Piovano
  alessandro.piovano@unito.it

1   Department of Chemistry, NIS Centre and INSTM, University of Torino, via Quarello 15A, 10135 Turin, Italy

Springer

the physicochemical variables make Ziegler-Natta catalysts hard to be deeply investigated. In particular, some basic questions are still open about the structural and electronic properties of the active sites.

Broadly speaking the traditional Ziegler–Natta catalysts are constituted by an active phase ($TiCl_4$), a co-catalyst (an aluminum alkyl or an aluminum alkyl chloride) and a support material ($MgCl_2$) organic electron donors are usually further added to control the selectivity of the catalyst (Albizzati et al. 1996). All these components exerts different roles in the development of the catalysis, and this is the origin of the intrinsic complexity of Ziegler-Natta systems. This work is intended to demonstrate how the study of a simplified system, $TiCl_x$ species grafted on silica, can help in answering more general questions. Indeed the data presented hereafter, mainly collected by means of FT-IR and Diffuse Reflectance (DR) UV–Vis spectroscopies, can be used as a reference in the investigation of more complex systems. Silica was chosen as support material not only because it is particularly suitable for spectroscopic investigations, enabling in this case to isolate the signals of the $TiCl_x$ species, but also because its application in this field has already revealed to be successful for industries, offering advantages in terms of pore diffusion, steric accessibility, and particle fragmentation (Nowlin et al. 1991; Pullukat and Hoff 1999; Klapper et al. 2014). Moreover, $MgCl_2/SiO_2$ supported catalysts have been recently developed to control the polydispersity index and the molecular weight distribution by varying the [Si]/[Mg] ratio (Wang et al. 2006).

Finally, it is worth noticing that the characterization of the $TiCl_x$ species grafted on silica may capture the interest of a much larger scientific community, since this system is involved also in other catalytic fields. For instance, it is the precursor of dispersed titania for propylene epoxidation (Joustra 1989), and it has been recently employed as a catalyst in advanced organic syntheses (Mirjalili et al. 2012, 2014; Bamoniri et al. 2015).

2 Experimental

2.1 Sample preparation

An amorphous fumed silica (Aerosil®380), having a specific surface area of 380 m^2/g, was used as a support. Silica was thermally treated in dynamic vacuum at 600 °C for 2 h to significantly reduce the amount of surface OH groups to an approximate value of 1 OH/nm^2 (Groppo et al. 2005). In the following, the thermally activated silica will be referred to as $SiO_{2\text{-}600}$. Titanation of $SiO_{2\text{-}600}$ was achieved by dosing $TiCl_4$ (pure, Sigma-Aldrich) vapors at room temperature. The final amount of Ti in the $SiO_{2\text{-}600}$/

$TiCl_4$ pre-catalyst resulting from this procedure is expected to be about 4 wt%, by considering the involvement of all the surface OH groups (Schrijnemakers et al. 1999). Finally, $SiO_{2\text{-}600}/TiCl_4$ was activated by triethylaluminum (pure, from Sigma-Aldrich) vapors at room temperature. In the following, the activator agent will be referred to as TEA and the active catalyst as $SiO_{2\text{-}600}/TiCl_4/TEA$. All the synthesis steps were carried out directly inside the cell used for the spectroscopic measurements or inside the quartz reactor adopted for the catalytic tests, to avoid catalyst poisoning.

2.2 Analysis techniques

FT-IR spectroscopy FT-IR spectra were collected using a Bruker Vertex70 instrument equipped with a MCT detector, at a resolution of 2 cm^{-1}. The sample was characterized at each step of the preparation, in the form of a thin self-supporting pellet (surface density ca. 20 mg/cm^2) placed inside a quartz cell equipped with two KBr windows, which allows to perform thermal treatments and measurements in the presence of gases, both at room temperature and at liquid nitrogen temperature. To monitor in situ the spectra evolution during the reactions, the quartz cell interfaced with the spectrophotometer was directly connected to a vacuum line.

Diffuse reflectance UV–Vis spectroscopy DR UV–Vis spectra were collected in diffuse reflectance mode using a Varian Cary5000 spectrophotometer, equipped for reflectance measurements. The samples were prepared as very thick pellets (surface density ca. 200 mg/cm^2), and they were interfaced to the instrument using a cell with a window made of suprasil optical quartz. All the spectra were collected in reflectance and successively converted into Kubelka–Munk.

3 Results and discussion

3.1 Spectroscopic tools to monitor each step of the catalyst synthesis

The whole process of formation of the catalyst was monitored in situ by means of FT-IR and DR UV–Vis spectroscopies. In particular, Fig. 1 shows the sequence of spectra recorded during the titanation of the silica support, while Fig. 2 shows the spectra recorded during the activation of the pre-catalyst with TEA.

The FT-IR spectrum of $SiO_{2\text{-}600}$ (spectrum 1 in Fig. 1b) is characterized by an intense absorption band at 3750 cm^{-1}, which is due to ν(OH) of isolated silanol groups on the surface, and by the off-scale signals of the vibrational modes of silica bulk below 1280 cm^{-1}, whose

Fig. 1 **a** DR UV–Vis–NIR spectra of SiO_{2-600} support (spectrum 1) and of $SiO_{2-600}/TiCl_4$ pre-catalyst (spectrum 2). **b** FT-IR spectra as part **a**. The *insets* display a magnification of the $\nu(OH)$ spectral region (*left*) and of the window of transparency of silica (*right*). *Light grey* spectra have been collected during pre-catalyst formation (from spectrum 1 to spectrum 2)
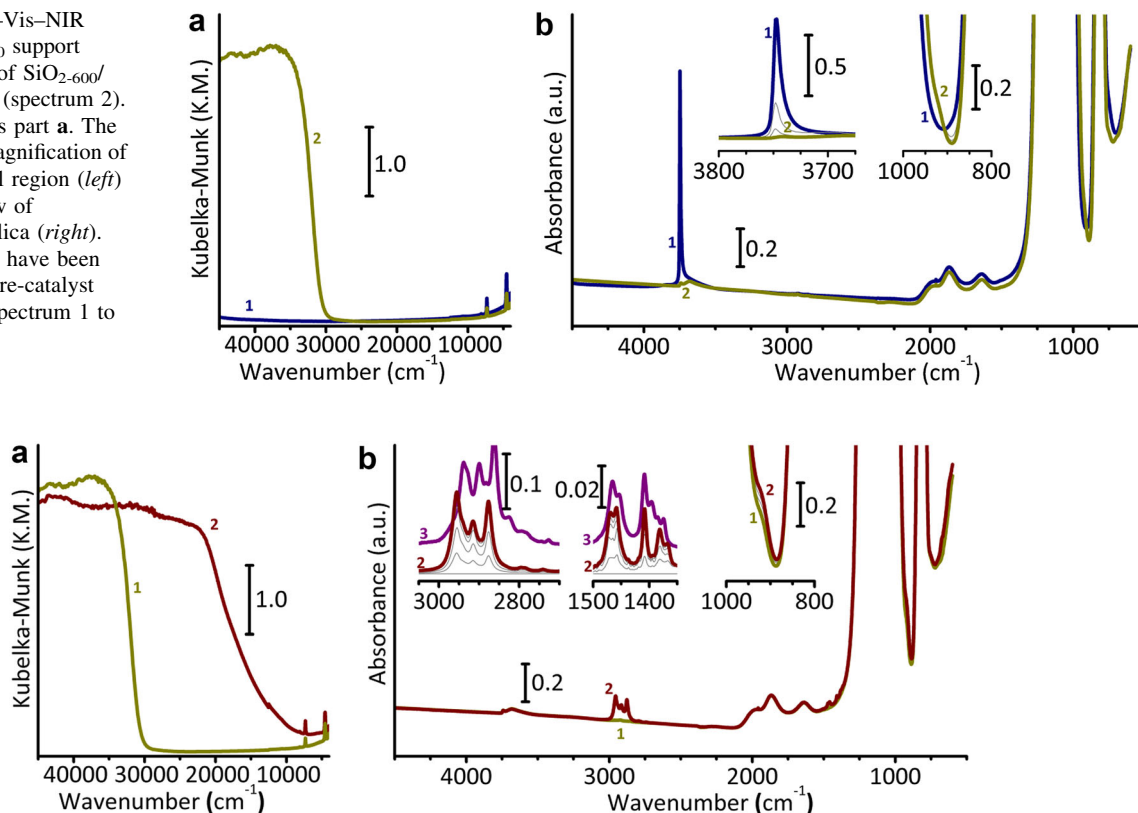
Fig. 2 **a** DR UV–Vis–NIR spectra of $SiO_{2-600}/TiCl_4$ pre-catalyst (spectrum 1) and of $SiO_{2-600}/TiCl_4/TEA$ catalyst (spectrum 2). **b** FT-IR spectra as part **a**. The *insets* display a magnification of $\nu(CH)$ (*left*) and $\delta(CH)$ spectral regions (*middle*), and of the window of transparency of silica (*right*): the spectra upon TEA dosage is compared with the FT-IR spectrum of TEA liquid recorded in ATR mode (spectrum 3). *Light grey* spectra have been collected during pre-catalyst formation (from spectrum 1 to spectrum 2)

overtones result in well defined bands at 1645, 1870 and 1986 cm^{-1}. In the region of the bulk vibrations, between 980 and 840 cm^{-1} there is the so-called "window of transparency" of silica, whose changes are often related to surface modifications.

As soon as $TiCl_4$ reaches the silica surface (spectrum 2 in Fig. 1b), the sharp absorption band at 3750 cm^{-1} is largely consumed because of the reaction between $TiCl_4$ and the surface hydroxy groups. During the reaction, evolution of gaseous HCl is observed (characteristic roto-vibrational profile centered at 2885 cm^{-1}). At the end of the reaction, a very small amount of residual Si–OH species is still observed, suggesting that a few hydroxy groups are not able to react with $TiCl_4$. At the same time, a new band appears inside the silica window of transparency (at 924 cm^{-1}), which is assigned to $\nu(SiO)$ vibrational modes of surface SiO_x moieties in interaction with $TiCl_3$ monodentate species (Schrijnemakers et al. 1999; Kinney and Staley 1983). The possible presence of SiO_x grafting $TiCl_2$ bidentate species cannot be confirmed since their $\nu(SiO)$ absorption band (at 995 cm^{-1}) is overlapped to the vibrational modes of the framework (Schrijnemakers et al. 1999; Kinney and Staley 1983).

Although the titanation does not involve a change in the sample color (which is white as the bare silica), the DR UV–Vis spectrum of the pre-catalyst (spectrum 2 in Fig. 1a) is dominated by two absorption bands in the UV region, at 36,500 and 42,000 cm^{-1}, which are assigned to $Cl \rightarrow Ti$ and $O \rightarrow Ti$ charge transfer transitions, respectively. The energy of a charge-transfer transition can be related to the properties of the metal and ligand according to the Jorgensen semi-empirical equation (Jorgensen 1962):

$$\nu(cm^{-1}) = 30{,}000\,(cm^{-1}) \times \left[\chi_{opt}(X) - \chi_{opt}(M)\right]$$

where $\chi_{opt}(M)$ is the optical electronegativity of the metal and has the character of the electron affinity of the orbital involved in the bond, decreasing with the fall in oxidation state and also with the reduction of the symmetry degree, whereas $\chi_{opt}(X)$ is the optical electronegativity of the ligand and is related with its ionization energy. The optical electronegativity values for many ions are reported in the literature. According to these literature data, $\chi_{opt}(Cl) = 3.0$ and $\chi_{opt}(O) = 3.2$ (Crouch et al. 1969; Duffy 1977), whereas $\chi_{opt}(Ti)$ depends on its coordination geometry and oxidation state (e.g., $\chi_{opt}(Ti^{4+}_{fourfold}) = 1.85$ and

S46

Rend. Fis. Acc. Lincei (2017) 28 (Suppl 1):S43–S49

$\chi_{opt}(Ti^{4+}_{sixfold}) = 2.06$) (Jorgensen 1970). Hence, both the absorption bands can be reasonably attributed to the presence of fourfold Ti^{4+} species (Seenivasan et al. 2011).

After activation with TEA, the catalyst appears dark brownish; this is the first clear evidence for the reduction of the titanium species. Indeed, the DR UV–Vis spectrum of $SiO_{2\text{-}600}/TiCl_4/TEA$ catalyst (spectrum 2 in Fig. 2a) is dominated by a very intense and large band at around 24,000 cm^{-1}. The intensity of this band is unusually high for a normal d–d transition and can be due to an intersite d–d transition taking place from a Ti^{3+} ion to another one through a Cl^- bridge, thus conferring a partial character of a charge transfer on the d–d transition. This phenomenon was already observed for bulk $TiCl_3$ (Clark 1964), and so it is taken here as the proof of the formation of clusters of reduced $TiCl_x$ species induced by TEA. Furthermore, another weaker absorption band can be individuated at ca. 13,000 cm^{-1}, although it is almost completely overlapped with the tail of the band at 24,000 cm^{-1}. This band can be compatible with a d–d transition for isolated Ti^{3+} sites in a sixfold coordination, having both O, Cl and alkyl groups as ligands (Piovano et al. 2016). The remaining features belonging to the charge-transfer spectral region (27,000–40,000 cm^{-1}) are not easily assignable due to the coexistence of several contributions, including the reduced Ti related charge-transfer transitions and the charge-transfer from the alkyl group R to the Ti centre.

In the FT-IR spectrum of $SiO_{2\text{-}600}/TiCl_4/TEA$ catalyst (spectrum 2 in Fig. 2b) the vibrational modes of the residual OH groups present in $SiO_{2\text{-}600}/TiCl_4$ pre-catalyst seems to be not affected either by TEA, meaning that the reaction likely involves only the grafted $TiCl_x$ species. Instead, a complex series of absorption bands gradually grows in both $\nu(CH_x)$ and $\delta(CH_x)$ regions. These bands are due to the alkyl groups deriving from TEA. Although the analysis of these bands is complicated by the coexistence of the alkylated $TiCl_xR_y$ species together with AlR_xCl_y by-products, some information about the species that are present on the catalyst surface can be drawn by comparing them with the FT-IR fingerprints of liquid TEA (spectrum 3), which were assigned in detail by Kvisle et al. (Kvisle and Rytter 1984). Previous works demonstrated that TEA in the liquid phase is a dimer (Benn et al. 1987), whose structure was determined by powder neutron diffraction at low temperature (McGrady 2000). The similar shapes of spectrum 2 and spectrum 3 suggest that TEA molecules are in the dimeric state in both cases. Although TEA is sent on the pre-catalyst in the gas phase, dimer species are mostly formed on the surface, because TEA molecules tend to accumulate and to aggregate on the surface, as already reported in the literature for TEA grafting on pure silica (Kerber et al. 2012). Moreover, it is worth noticing that $\nu(CH_x)$ bands in spectrum 2 are slightly shifted at higher
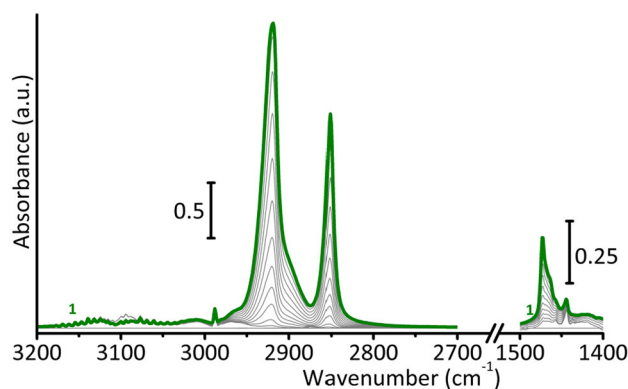
Fig. 3 Evolution of the FT-IR spectra (from baseline to spectrum 1) in the $\nu(CH)$ and $\delta(CH)$ regions during ethylene conversion on $SiO_{2\text{-}600}/TiCl_4/TEA$ catalyst

frequencies. This upward shift might be due to the fact that the alkyl chains feel a more polar environment, induced by the presence of chlorine in the surroundings.

Finally, the activity of the catalyst towards ethylene conversion was evaluated by spectroscopy and it proved to be very high even in very mild conditions (25 °C, $P_{C2H4} = 100$ mbar). Indeed, Fig. 3 shows the fast growth of two sharp absorption bands at 2920 and 2850 cm^{-1}, assigned to the asymmetric and symmetric $\nu(CH_2)$ modes characteristic of HDPE. Moreover, in the $\delta(CH_2)$ spectral region two absorption bands are visible at 1472 and 1463 cm^{-1}, which are related to the crystalline and to the amorphous phase of HDPE, respectively. Since the intensity of the band at 1472 cm^{-1} is much higher than the band at 1463 cm^{-1}, it can be stated that $SiO_{2\text{-}600}/TiCl_4/TEA$ mostly catalyses the production of a crystalline HDPE (Chelazzi et al. 2004).

3.2 Adsorption of carbon monoxide on the catalyst surface

CO adsorption at 100 K was used as a molecular probe to get information about the accessibility and the electronic properties of the functional sites on the surface at each step of the synthesis of the catalyst. Indeed, the $\nu(C\equiv O)$ is very sensitive to the properties of the adsorption sites. Figure 4 shows the sequence of FT-IR spectra, collected at decreasing CO coverage, for each of the three synthesis steps (SiO_2 activation, titanation, and activation of the pre-catalyst).

The spectrum of CO adsorbed on $SiO_{2\text{-}600}$ is characterized at the maximum coverage (spectrum 1) by two absorption bands at 2155 and 2137 cm^{-1}, which are assigned to CO in interaction with surface silanol groups and to physisorbed CO, respectively (Ghiotti et al. 1979; Zecchina and Otero Areán 1996). Since silanols are not strong Brønsted acid sites, their interaction with CO molecules is quite weak. This is testified by the easy
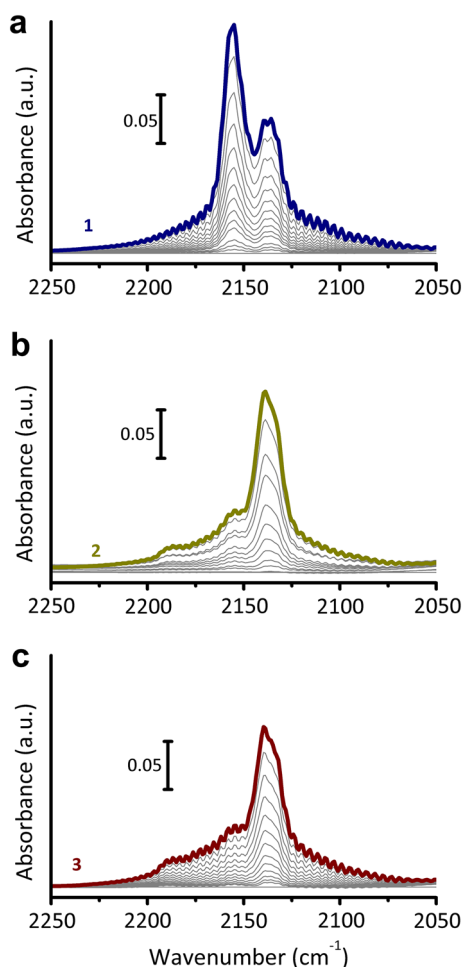
Fig. 4 Comparison between the evolution of the FT-IR spectra in the v(CO) region upon decreasing CO coverage (from the maximum coverage marked with colored spectra to zero coverage used as baselines) over SiO_{2-600} support (**a**), over $SiO_{2-600}/TiCl_4$ pre-catalyst (**b**), and over $SiO_{2-600}/TiCl_4/TEA$ catalyst (**c**)

reversibility of the corresponding absorption band, which is almost the same as for the physisorbed species.

The spectrum of CO adsorbed at the maximum coverage on the $SiO_{2-600}/TiCl_4$ sample (spectrum 2) is characterized by a modification in the relative intensities of the bands at 2155 and 2137 cm^{-1} and by the appearance of a new band at 2188 cm^{-1}. While the band at 2137 cm^{-1} is almost unaffected, the band at 2155 cm^{-1} is much less intense because most of the OH groups were consumed by $TiCl_4$ reaction. Besides, the new absorption band at 2188 cm^{-1} can be plausibly assigned to CO adsorbed on Ti^{4+}, since it is compatible with analogous values of v(CO) reported in the literature. For example, a band at 2180 cm^{-1} was assigned to CO adsorbed on Ti^{4+} within TS-1 (Zecchina et al. 1991), and a band at 2184 cm^{-1} was attributed to CO adsorbed on Ti^{4+} sites in TiO_2 nanoparticles (Xu et al. 2012). Since the position of the band depends on the polarizing power of Ti^{4+} sites, the shift of v(CO) up to 2188 cm^{-1} for CO adsorbed

on $SiO_{2-600}/TiCl_4$ pre-catalyst indicates that the Lewis acidity of Ti^{4+} is enhanced by the chloride ligands. In addition, the intensity of the band is quite low, may indicating that Ti^{4+} sites are scarcely accessible.

Surprisingly, the spectrum of CO adsorption after the activation of the catalyst (spectrum 3) is almost the same as that of CO adsorption on the pre-catalyst previously discussed (spectrum 2). While it is reasonable that the contributions of physisorbed CO and of CO adsorbed on residual hydroxy groups did not change after the reaction of the pre-catalyst with TEA, the fact that the band at 2188 cm^{-1} is still present is not straightforward. Indeed, it might be due either to a fraction of unreduced Ti^{4+} sites or to the unluckily concurrent signal of CO interacting with the Al^{3+} ions of TEA. Indeed, according to the literature, v(CO) in Al^{3+}–CO adducts can vary from 2180 up to 2230 cm^{-1} (Muddada et al. 2011). Moreover, no new bands ascribable to the interaction of CO with reduced Ti sites are observed. This may indicate that most of the reduced Ti species are not accessible by CO, either because of the formation of clusters (as indicated by DR UV–Vis spectroscopy) or because of the steric hindrance of the aluminum alkyls in close proximity to the active sites.

4 Conclusion

This work pointed out the potentials and the still present hurdles of a surface science approach for the characterization of heterogeneous polymerization catalysts. Complementary information can be achieved using other spectroscopic techniques, such as EPR spectroscopy, to unravel the nature and local coordinative environment of the unpaired electron of reduced Ti species (Morra et al. 2015), or NMR spectroscopy, to detect the interaction of the magnetically active nuclei involved in the catalytic process (as ^{27}Al, ^{13}C, ^{1}H and ^{35}Cl) (Kerber et al. 2012; Sormunen et al. 1990; Busico et al. 2008; Blaakmeer et al. 2016).

The $SiO_{2-600}/TiCl_4/TEA$ model catalyst turned out to be active in ethylene conversion, thus opening new perspectives in employing this system as the starting point for the synthesis of a catalyst suitable for industrial practice.

References

Albizzati E, Giannini U, Collina G, Noristi L, Resconi L (1996) Catalysts and polymerizations. In: Moore EPJ (ed)

S48

Rend. Fis. Acc. Lincei (2017) 28 (Suppl 1):S43–S49

Polypropylene Handbook. Hanser-Gardner Publications, Cincinnati, Chapter 2

Bamoniri A, Mirjalili BBF, Tarazian R (2015) Nano-TiCl$_4$/SiO$_2$: an efficient heterogeneous solid acid catalyst for the one pot cascade five-component synthesis of densely functionalized tetrahydropyridines. J Chem Sci 127(5):885–895

Benn R, Janssen E, Lehmkuhl H, Rufínska A (1987) 27Al-NMR-Spektroskopie zur Charakterisierung von Organoaluminium-Verbindungen. J Organomet Chem 333(2):155–168

Blaakmeer ES, Antinucci G, Busico V, Van Eck ERH, Kentgens APM (2016) Solid-state NMR investigations of MgCl$_2$ catalyst support. J Phys Chem C 120(11):6063–6074

Busico V, Causa M, Cipullo R, Credendino R, Cutillo F, Friederichs N, Lamanna R, Segre A, Castellit VV (2008) Periodic DFT and high-resolution magic-angle-spinning (HR-MAS) H-1 NMR investigation of the active surfaces of MgCl$_2$-supported Ziegler-Natta catalysts. The MgCl$_2$ matrix. J Phys Chem C 112(4):1081–1089

Busico V, Cipullo R, Mingione A, Rongo L (2016) Accelerating the research approach to Ziegler-Natta catalysts. Ind Eng Chem Res 55(10):2686–2695

Chang M, Liu X, Nelson PJ, Munzing GR, Gegan TA, Kissin YV (2006) Ziegler-Natta catalysts for propylene polymerization: Morphology and crystal structure of a fourth-generation catalyst. J Catal 239(2):347–353

Chelazzi D, Ceppatelli M, Santoro M, Bini R, Schettino V (2004) High-pressure synthesis of crystalline polyethylene using optical catalysis. Nat Mater 3(7):470–475

Clark RJH (1964) Diffuse reflectance spectra of some anhydrous transition-metal halides. J Chem Soc 417–425

Corradini P, Guerra G, Cavallo L (2004) Do new century catalysts unravel the mechanism of stereocontrol of old Ziegler-Natta catalysts? Acc Chem Res 37(4):231–241

Crouch PC, Fowles GWA, Walton RA (1969) Complex halides of transition metals. Part X. Reaction of molten diethylammonium chloride with titanium(III), vanadium(III), and chromium(III) chlorides: a spectroscopic and magnetic study of the TiCl$_6^{3-}$, Ti2Cl$_9^{3-}$, V2Cl$_9^{3-}$, and Cr2Cl$_9^{3-}$ anions. J Chem Soc A 972–976

D'Amore M, Thushara KS, Piovano A, Causà M, Bordiga S, Groppo E (2016) Surface investigation and morphological analysis of structurally disordered MgCl$_2$ and MgCl$_2$/TiCl$_4$ Ziegler–Natta catalysts. ACS Catal 6(9):5786–5796

Duffy JA (1977) Variable electronegativity of oxygen in binary oxides: possible relevance to molten fluorides. J Chem Phys 67(6):2930–2931

Fink G, Steinmetz B, Zechlin J, Przybyla C, Tesche B (2000) Propene polymerization with silica-supported metallocene/MAO catalysts. Chem Rev 100:1377–1390

Ghiotti G, Garrone E, Morterra C, Boccuzzi F (1979) Infrared study of low temperature adsorption. 1. CO on Aerosil. An interpretation of the hydrated silica spectrum. J Phys Chem 83(22):2863–2869

Groppo E, Lamberti C, Bordiga S, Spoto G, Zecchina A (2005) The structure of active centers and the ethylene polymerization mechanism on the Cr/SiO$_2$ catalyst: a frontier for the characterization methods. Chem Rev 105:115–183

Groppo E, Seenivasan K, Barzan C (2013) The potential of spectroscopic methods applied to heterogeneous catalysts for olefin polymerization. Catal Sci Technol 3:858–878

Jorgensen CK (1962) Electronegativity and chemical bonding. Orbitals in atoms and molecules, Academic Press, London and New York, vol 7, pp 80–100

Jorgensen CK (1970) Electron transfer spectra. Progr Inorg Chem 12:101–157

Joustra AH, De Bruijn W, Drent E, Reman WG (1989) A process for the preparation of an oxirane compound. EP0345856

Kaminsky W (1996) New polymers by metallocene catalysis. Macromol Chem Phys 197(12):3907–3945

Kaminsky W, Winkelbach H (1999) Influence of supported metallocene catalysts on polymer tacticity. Top Catal 7(1–4):61–67

Kerber RN, Kermagoret A, Callens E, Florian P, Massiot D, Lesage A, Coperet C, Delbecq F, Rozanska X, Sautet P (2012) Nature and structure of aluminum surface sites grafted on silica from a combination of high-field aluminum-27 solid-state NMR spectroscopy and first-principles calculations. J Am Chem Soc 134(15):6767–6775

Kinney JB, Staley RH (1983) Reactions of titanium tetrachloride and trimethylaluminum at silica surfaces studied by using infrared photoacoustic spectroscopy. J Phys Chem 87:3735–3740

Klapper M, Joe D, Nietzel S, Krumpfer JW, Müllen K (2014) Olefin polymerization with supported catalysts as an exercise in nanotechnology. Chem Mater 26(1):802–819

Kvisle S, Rytter E (1984) Infrared matrix isolation spectroscopy of trimethylgallium, trimethylaluminium and triethylaluminium. Spectrochim Acta A 40(10):939–951

Liu T, Li W, Xia X, Mao B (2015) Study of a novel fourth-generation supported Ziegler-Natta catalyst for propylene polymerization: Relationship between catalyst structure and polymerization properties. China Pet Process Pe. 17(1):39–47

McGrady GS (2000) Structure of the trimethylaluminum dimer as determined by powder neutron diffraction at low temperature. Organometallics 19(21):4398–4401

Mirjalili BBF, Bamoniri A, Zamania L (2012) Nano-TiCl$_4$/SiO$_2$: an efficient and reusable catalyst for the synthesis of tetrahydrobenzo[a]xanthenes-11-ones. Lett Org Chem 9(5):338–343

Mirjalili BBF, Zamani L, Afr S (2014) Nano-TiCl$_4$/SiO$_2$: a versatile and efficient catalyst for synthesis of dihydropyrimidones via biginelli condensation. J Chem 67:21–26

Morra E, Giamello E, Van Doorslaer S, Antinucci G, D'Amore M, Busico V, Chiesa M (2015) Probing the coordinative unsaturation and local environment of Ti^{3+} sites in an activated high-yield ziegler-natta catalyst. Angew Chem Int Ed 54(16):4857–4860

Muddada NB, Olsbye U, Fuglerud T, Vidotto S, Marsella A, Bordiga S, Gianolio D, Leofanti G, Lamberti C (2011) The role of chlorine and additives on the density and strength of Lewis and Bronsted acidic sites of gamma-Al$_2$O$_3$ support used in oxychlorination catalysis: A FTIR study. J Catal 284(2):236–246

Nowlin TE, Mink RI, Lo FY, Kumar T (1991) Ziegler-Natta catalysts on silica for ethylene polymerization. J Polym Sci Part A Polym Chem 29(8):1167–1173

Olabisi O, Atiqullah M, Kaminsky W (1997) Group 4 metallocenes: supported and unsupported. J Macromol Sci Rev Macromol Chem Phys 37(3):519–554

Piovano A, Thushara KS, Morra E, Chiesa M, Groppo E (2016) Unraveling the catalytic synergy between Ti^{3+} and Al^{3+} sites on a chlorinated Al$_2$O$_3$: a tandem approach to branched polyethylene. Angew Chem Int Ed 55(37):11203–11206

Pullukat TJ, Hoff RE (1999) Silica-based Ziegler-Natta catalysts: a patent review. Catal Rev Sci Eng 41(3–4):389–428

Robert C, Thomas CM (2013) Tandem catalysis: a new approach to polymers. Chem Soc Rev 42(24):9392–9402

Schrijnemakers K, Van Der Voort P, Vansant EF (1999) Characterization of a TiCl$_4$-modifed silica surface by means of quantitative surface analysis. Phys Chem Chem Phys 2569–2572

Seenivasan K, Sommazzi A, Bonino F, Bordiga S, Groppo E (2011) Spectroscopic investigation of heterogeneous Ziegler-Natta catalysts: Ti and Mg chloride tetrahydrofuranates, their interaction compound, and the role of the activator. Chem Eur J 17(31):8648–8656

Sormunen P, Hjertberg T, Iiskola E (1990) A solid-state ^{13}C NMR study on heterogeneous Ziegler-Natta catalyst components. Makromol Chem 191(11):2663–2673

Terano M (2004) Current achievements on heterogeneous olefin polymerization catalysts. Sankeisha & Co., Ltd, Nagoya

Tisse VF, Boisson C, McKenna TFL (2014) Activation and deactivation of the polymerization of ethylene over rac-EtInd$_2$ZrCl$_2$ and (nBuCp)$_2$ZrCl$_2$ on an activating silica support. Macromol Chem Phys 215(14):1358–1369

Wang J, Wang L, Gao H, Wang W, Zhao Z, Sun T, Feng L (2006) Ethylene polymerization using a novel MgCl$_2$/SiO$_2$-supported Ziegler-Natta catalyst. Polym Int 55(3):299–304

Xu MC, Noei H, Fink K, Muhler M, Wang YM, Woll C (2012) The surface science approach for understanding reactions on oxide powders: The importance of IR spectroscopy. Angew Chem Int Ed 51(19):4731–4734

Zecchina A, Otero Areán C (1996) Diatomic molecular probes for mid-IR studies of zeolites. Chem Soc Rev 25:187–197

Zecchina A, Spoto G, Bordiga S, Padovan M, Leofanti G, Petrini G (1991) IR Spectra of CO adsorbed at low temperature (77 K) on Titaniumsilicalite, H-ZSM5 and Silicalite. Stud Surf Sci Catal 65:671–680

Ligands Make the Difference! Molecular Insights into Cr^{VI}/SiO$_2$ Phillips Catalyst during Ethylene Polymerization

Caterina Barzan,*,[†] Alessandro Piovano,[†] Luca Braglia,[†,‡] Giorgia A. Martino,[†] Carlo Lamberti,[‡,§] Silvia Bordiga,[†] and Elena Groppo*,[†]

[†]Department of Chemistry, NIS Interdepartmental Center and INSTM Reference Center, University of Turin, Via G. Quarello 15A, Turin I10135, Italy

[‡]IRC "Smart Materials", Southern Federal University, Zorge Street 5, Rostov-on-Don 344090, Russia

[§]Department of Chemistry, CrisDi Interdepartmental Center, University of Turin, Via P. Giuria 7, Turin I10125, Italy

S *Supporting Information*

ABSTRACT: Operando-sensitive spectroscopic techniques were employed for investigating the changes in the molecular structure of the Cr sites in the Cr^{VI}/SiO$_2$ Phillips catalyst during ethylene polymerization. Practically, the most arduous barrier to be overcome was the separation of the chromates reduction carried out by ethylene from the subsequent polymerization. By carefully tuning the experimental parameters we succeeded in observing these two events separately. We found that the sites involved in ethylene polymerization are mainly divalent Cr ions in a 6-fold coordination, in interaction with the oxygenated byproduct (mostly methylformate, generated from the disproportionation of two formaldehyde molecules). Unreduced Cr^{VI} species are also present during ethylene polymerization as well as reduced Cr species (either Cr^{II} or Cr^{III}) acting as spectators. Our results challenge the old vision of "naked" chromium species (i.e., low coordinated) as the active sites and attribute a fundamental role to external (and flexible) oxygenated ligands that resemble the ancillary ligands in homogeneous polymerization catalysis.
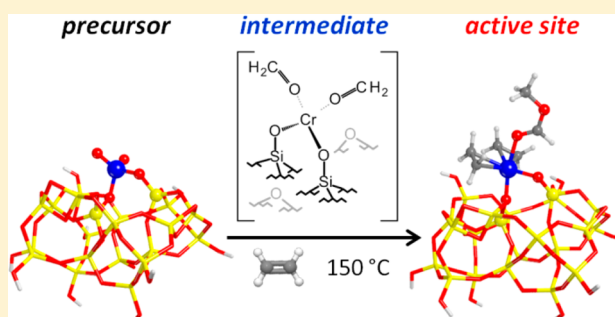
1. INTRODUCTION

Back in 1951, Hogan and Banks at Phillips Petroleum discovered a Cr-based catalyst for ethylene polymerization and named it after their company.[1] Since then the Phillips catalyst has been successfully used in the commercial production of high-density and linear low-density polyethylene (HDPE and LLDPE). Today the predictions of the global demand for polyethylene resins settles at 4.0% rise per year to 99.6 million tons in 2018, valued at $164 billion.[2] In this market the Phillips catalyst supplies almost 40% of the HDPE total world demand, thanks to its versatility in terms of hundreds of specialized PE grades produced, resulting in just as many specific applications ranging from packaging to medical and automotive sectors.[3−5] The catalyst synthesis consists in the impregnation of a polymer-grade porous silica with a Cr precursor (loadings lower than 1 wt %), followed by calcination at high temperature (>500 °C).[3,6−10] This procedure gives a highly dehydroxylated silica where the chromium ions are grafted mainly as isolated hexavalent chromates[6,9−20] (hereafter Cr^{VI}), although also mono-oxo CrO$_5$ species have been claimed in the recent literature.[21−29] These chromium species are just the precursors of the active sites. Indeed, once ethylene is introduced in the reactor at temperatures from 80 to 110 °C, it reduces the Cr^{VI} sites during a variable induction period,

forming reduced Cr species active in ethylene polymerization and some oxidation byproducts. Formaldehyde has been long claimed as the main ethylene oxidation byproduct and experimentally detected in a few cases.[7,8,30−33] In contrast, the nature of the reduced Cr sites (in terms of molecular structure, oxidation state, and local geometry) has been the subject of a long debate in the past[3,6−10,34] and has recently gained renewed attention in the high-level specialized literature, fostering a great number of experimental[22,23,35−40] and theoretical[24−29,41−44] studies. Most of the recent works are focused on the long-standing question of the chromium oxidation state. In fact, while Cr^{II} sites were invoked as the active sites since the early literature on the Phillips catalyst[45−49] and successively proved by many experimental studies,[3,6−9] Cr^{III} is coming back to researchers' attention after a series of papers by Coperet et al.,[35,36,43,44,50,51] who showed that Phillips-inspired Cr^{III}/SiO$_2$ catalysts obtained from well-defined Cr^{III} precursors are active in ethylene polymerization. These new results opened the way to the modeling of a large number of reaction pathways aimed at explaining the spontaneous self-
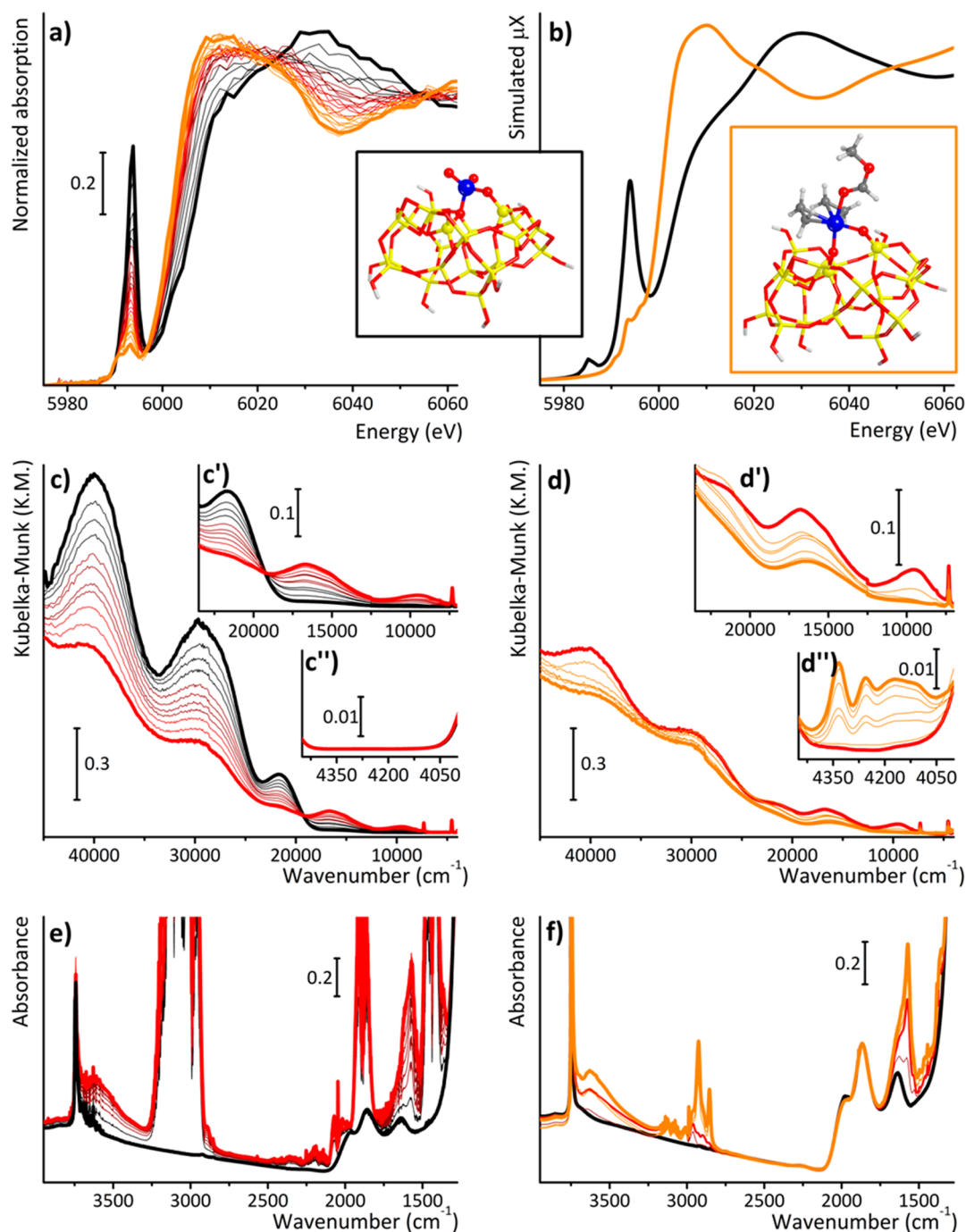
Figure 1. Time evolution of the spectra for the Cr^{VI}/SiO_2 catalyst (bold black) during reduction with ethylene (from black to bold red) and during ethylene polymerization at 150 °C (from red to bold orange). (a) Normalized Cr K-edge XANES spectra. (b) Simulated XANES spectra of Cr^{VI}/SiO_2 (black) and Cr^{II}/SiO_2 in interaction with methylformate and ethylene (orange), and corresponding structural models. (c and d) DR UV−vis−NIR spectra subdivided into the two reaction steps. Insets c′/d′ and c″/d″ show a magnification of the 24 000−7000 and 4400−4050 cm^{-1} regions in which the d−d absorption bands and the $\nu(CH_2)$ and $\delta(CH_2)$ combination modes of PE are present, respectively. (e) Operando FT-IR spectra. (f) FT-IR spectra collected in static conditions.

alkylation mechanism in the presence of ethylene[41,42,44,50] that has long remained unknown.

In this animated debate on the chromium oxidation state and polymerization mechanism, attention is distracted from the molecular structure of the active chromium sites. Traditionally, they have been considered as relatively "naked", irrespective of their oxidation state, and highly uncoordinated Cr sites have been indeed used to model the polymerization mechanism.[41−44] It is worth addressing the word "naked" as a vision

of extremely low-coordinated Cr sites, which are mostly represented as covalently bonded to two or three O−Si from the silica surface. At most, surrounding hemilabile siloxane groups have been considered to enter into the Cr coordination sphere.[41,52] While the vision of "naked" Cr sites might be plausible for the prereduced Phillips catalysts or for Cr-based catalysts derived from well-defined organometallic precursors, it appears less straightforward for Cr^{VI}/SiO_2 reduced in ethylene, where the active sites are formed at ca. 100 °C in the presence

of ethylene and of the oxidation byproducts. The present work has the intention to provide new insights into the molecular structure of Cr^{VI}/SiO_2 during ethylene polymerization. Achieving this goal not only would represent a scientific milestone but also would be the key for the development of new concepts and for the rational design of a new generation of olefin polymerization catalysts.[53]

To date, the main experimental difficulty was associated with the double role of ethylene as reducing agent and monomer. Several strategies were attempted to separate the formation of the active sites from the ethylene polymerization, e.g., using an external reducing agent prior to ethylene injection,[3,9,10,38−40,54,55] or synthesizing Cr/SiO_2 catalysts starting from well-defined $Cr^{VI−n}$ organometallic precursors.[35,36,51,56,57] Although these approaches gave a relevant contribution to the overall understanding of the Phillips catalyst, in most cases the obtained polyethylene is different with respect to that produced with the hexavalent Cr^{VI}/SiO_2 catalyst.[3] This implies that the molecular structure of the active Cr sites strongly depends on the prereducing process or synthesis methodology and that the only way to observe the real sites involved in ethylene-reduced Cr/SiO_2 is to look carefully at it under the actual reaction conditions. Large clusters are also important for the XANES simulation, because of the long mean free path of the photoelectron in the low kinetic energy region typical of the XANES region of the X-ray absorption spectrum. Operando spectroscopic techniques have this potential and nowadays have progressed enough to be applied with success also on very dilute systems.[58−63]

On these bases, we propose here a detailed investigation on the formation and structure of the active sites in Cr^{VI}/SiO_2 based on the synergic use of three operando spectroscopic techniques, namely, Cr K-edge XANES, diffuse reflectance (DR) UV−vis−NIR, and FT-IR spectroscopies (coupled with online MS), assisted by state-of-the-art theoretical calculation. Although the three techniques have been already used in the investigation of the Phillips catalyst by several research groups (including some of us), the novelties of the present work rely on (1) careful tuning of the experimental parameters that allowed us to distinguish between the formation of the active sites and the starting of the polymerization and (2) a multitechnique approach that allows monitoring at the same time the changes occurring at the Cr sites, the nature and location of the byproducts, and the occurrence of ethylene polymerization.

2. RESULTS AND DISCUSSION

A synthetic panning shot of the most relevant spectroscopic results is shown in Figure 1, which displays the spectra collected during Cr^{VI}/SiO_2 reduction in the presence of ethylene (from black to red) and subsequent polymerization (from red to orange) at 150 °C.[64] Both XANES (Figure 1a) and DR UV−vis−NIR (Figure 1c) indicate that the chromates[6,9,10,65,66] are gradually reduced. In the XANES spectra (i) the intense pre-edge peak centered at 5993.5 eV typical of pseudotetrahedral chromates[6,9,10,18,67−72] decreases in intensity and is gradually replaced by two very weak bands at 5989.8 and 5992.5 eV, (ii) the edge progressively downward shifts from 6006.7 to 6002.0 eV, and (iii) the white line increases in intensity (pronounced peak at about 6011 eV), while the maximum at 6032 eV is replaced by a profound minimum. At the end of the experiment, the occurrence of ethylene polymerization was indicated by the appearance of the

powder in the capillary: white and with a rubber consistence.[73] In the DR UV−vis−NIR spectra the intense band at 21 500 cm^{-1} (assigned to an O → Cr charge transfer transition localized mainly on the double bonded oxygen of the chromates)[6,9,10,15−20,65,66] gradually decreases in favor of two weaker bands at 9500 and 16 700 cm^{-1} (with a shoulder at 15 000 cm^{-1}) indicative of d−d transitions for $Cr^{VI−n}$ species (Figure 1c′).[6,9,10,24−29] After an induction time, the occurrence of ethylene polymerization on the reduced Cr sites is indicated by the appearance of a few narrow and weak bands in the 4400−4050 cm^{-1} region (Figure 1d″) due to the combination of the $\nu(CH_2)$ and $\delta(CH_2)$ vibrational modes of polyethylene.[35,43,74−80] The XANES and DR UV−vis−NIR spectra after ethylene reduction contain important indications on the local geometry and oxidation state of the reduced Cr sites. The weakness of the two bands at 5989.8 and 5992.5 eV in the pre-edge region of the XANES spectrum as well as the weak intensity of the d−d bands in the UV−vis spectrum point toward reduced Cr species characterized by a pseudo-octahedral coordination.[9,10,58,68,71,72]

A quick comparison of the XANES spectrum with that of a Cr^{III} reference compound might lead to the conclusion that the final oxidation state of the catalyst reduced in ethylene is +3. Indeed, at a first glance, the pre-edge features and edge position of Cr^{VI}/SiO_2 reduced in ethylene are very similar to those of Cr_2O_3 (Figure 2a), in which the Cr sites have an oxidation state of +3 and a 6-fold geometry. These (and similar) arguments have been used several times in the literature to set forth +3 as the main oxidation state of the Cr active sites.[35,36,43,51] However, Figure 2a demonstrates that the spectrum of Cr^{VI}/SiO_2 reduced in ethylene is also very similar to that of Cr^{VI}/SiO_2 reduced in cyclohexene at room temperature, where the Cr sites have an oxidation state of +2 in a 6-fold coordination environment due to the interaction with an ester (deriving from the oxidation of cyclohexene).[55] Notably, in that case EPR spectroscopy, which is selective toward Cr^{III}, incontrovertibly discarded the presence of Cr^{III}.[55] It clearly emerges that the assignment of the Cr oxidation state on the basis of *only* Cr K-edge XANES spectroscopy is not unambiguous. The same conclusion was reached several years ago by Tromp at al.,[72] who demonstrated that the position of the main absorption edge for a series of well-defined Cr^{III} complexes with different ligands and geometries can move as much as 8 eV (i.e., a shift comparable to that caused by a change in the oxidation state from +6 to 0).

Concerning the DR UV−vis−NIR spectra the bands at 9500 and 16 700 cm^{-1} could be assigned to Cr^{II} or to Cr^{III} or both. From a survey of the specialized literature, the salts of trivalent 6-fold-coordinated Cr ions give two bands around 17 000 and 24 000 cm^{-1} (and a third one, rather weak, at 37 000 cm^{-1}, which is however always masked by the intense charge transfer bands at high energy).[81] Cr^{II} ions in a perfect octahedral environment give a broad and weak band between ca. 10 000 and 20 000 cm^{-1} (e.g., $Cr^{2+}(H_2O)_6$ shows a single $^5E_g \rightarrow {}^5T_{2g}$ transition around ca. 14 000 cm^{-1}).[82] Upon distortion of the octahedral symmetry, this transition splits into multiple components. For Cr ions in a (largely) O-donor coordination sphere, d−d bands at wavenumbers as low as 9500 cm^{-1} are commonly assigned to Cr^{II} species. The presence of a band near 10 000 cm^{-1} in the UV−vis spectra of 6-fold-coordinated Cr^{II} complexes, especially discernible in DR mode, was noticed already in the 1960s.[81−83] According to these seminal works, the DR spectra of several octahedral distorted Cr^{II} salts show
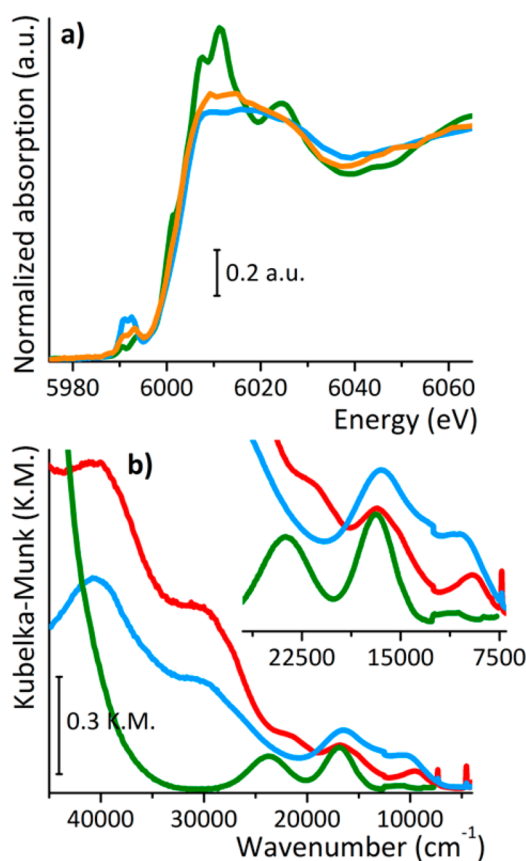
Figure 2. (a) XANES spectrum of the Cr^{VI}/SiO_2 catalyst upon reduction and polymerization in ethylene (orange) in comparison with the spectrum of the same catalyst reduced in cyclohexene at room temperature (light blue)[55] and with the spectrum of the reference Cr_2O_3 oxide (green). (b) DR UV−vis−NIR spectrum of the Cr^{VI}/SiO_2 catalyst upon reduction and before ethylene polymerization occurs (red) compared with the same catalyst reduced at room temperature in cyclohexene (light blue)[55] and of the a Cr^{III} reference ($CrCl_3 \cdot 6(H_2O)$ complex physisorbed on Aerosil SiO_2, green spectrum).

bands around 10 000, 13 100, 16 000, and 18 900 cm^{-1}. On these basis, our DR UV−vis−NIR measurements clearly indicate that a large fraction of the reduced Cr sites is in the divalent state and in a 6-fold coordination, although the copresence of also Cr^{III} species cannot be discarded. Further proof is given by a comparison of the DR UV−vis−NIR spectra shown in Figure 2b (and completely discussed in Section S1) of the Cr^{VI}/SiO_2 catalyst reduced in ethylene before polymerization starts (red) with that of the same catalyst reduced in cyclohexene at room temperature (light blue) and a reference for Cr^{III}/SiO_2 (green).

Also in this case the d−d bands of the ethylene-reduced Cr sites have positions and intensity ratios extremely similar to those obtained upon cyclohexene reduction, characterized by Cr^{II} 6-fold-coordinated species in interaction with an ester molecule.[55] We wish to underline here that this assignment has been possible because the DR UV−vis spectra have been collected in a wide energy region comprising also the NIR range, which is neglected in most of the recent literature.[84]

Hence, our working hypothesis to account for these results is that we are mainly detecting intermediate Cr^{II} species in 6-fold coordination because in interaction with formaldehyde molecules, which are the main ethylene oxidation byproducts

claimed in the literature.[7,8,30−33] However, to our surprise, only traces of masses diverse from ethylene were detected by online MS during both operando XANES and DR UV−vis−NIR measurements, also for long reaction times.

The lack of observation of formaldehyde or of any other volatile oxidation byproduct stimulated us to follow the same experiment by operando FT-IR spectroscopy, aimed at directly detecting possible oxygenated species released during the reduction of chromates and adsorbed at the catalyst surface. In the presence of ethylene at 150 °C (Figure 1e) a few IR absorption bands gradually grow at 2892 and 2865 cm^{-1} (typical IR region of $\nu(CH_x)$ modes), along with two more intense bands at 1617 and 1573 cm^{-1}. The assignment of these latter bands to vibrations involving oxygenated species is straightforward due to their extremely high intensity with respect to the $\nu(CH_x)$ modes. Indeed, only chemical groups with high extinction coefficient (such as organic carbonyls, formates, and others) can result in such intense manifestations.[85−89] In principle, also the $\nu(C=C)$ mode can be invoked; however, this group has a low extinction coefficient with respect to the $\nu(CH_x)$ modes and thus cannot be the guilty party.[74,77,90,91] A complete assignment of the IR absorption bands due to the adsorbed species can be done only by looking at the mid-IR spectral region in its totality. This is not feasible during the operando FT-IR measurements since the spectra are dominated by the absorption bands of gaseous ethylene and do not allow the observation of other spectroscopic fingerprints necessary for a complete assignment. To overcome this spectroscopic obstacle we performed a parallel FT-IR experiment in static conditions (150 °C, P_{C2H4} = 100 mbar, Figure 1f). Figure 3 shows the FT-IR spectra of Cr^{VI}/SiO_2 before and after reduction in ethylene at 150 °C. By removing the gaseous contribution of ethylene, the chromate reduction becomes visible and is testified by the gradual decrease in intensity of the band at 910 cm^{-1} and of the weak band at 1980 cm^{-1}, due to the fundamental $\nu(Cr=O)$
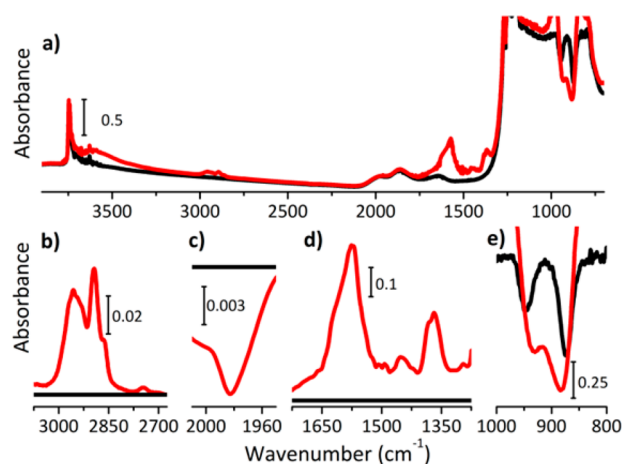
Figure 3. FT-IR spectra of Cr^{VI}/SiO_2 before (black) and after reduction in ethylene at 150 °C (red). (a) Spectra in the whole 3800−700 cm^{-1} wavenumber region; (b and d) magnifications in the spectral regions where the absorption bands characteristic of ethylene oxidation products give a contribution (spectra subtracted from that of Cr^{VI}/SiO_2); (c) magnification of the region in which the first overtone of the Cr=O mode of the chromate species contributes (subtracted spectra); (e) magnification of the region where the vibrational modes of silica perturbed by the presence of the chromates are visible.

vibrational mode and to its first overtone[9,10,69,70,78,92] (Figure 3c and 3e), respectively. At the same time, new absorption bands grow before ethylene polymerization starts at 2955, 2892, 2865, and 2747 cm^{-1} (Figure 3b) and 1617, 1573, 1455, 1383, and 1369 cm^{-1} (Figure 3d). The complete assignment of each IR absorption band is shown in Table 1, along with the

Table 1. Position (in wavenumbers, cm^{-1}) and Relative Intensity (vs = very strong, s = strong, m = medium, w = weak) of the IR Absorption Bands Attributed to Ethylene Oxidation Products in Interaction with the Ethylene-Reduced Cr^{VI}/SiO$_2$ Catalyst

observed bands (cm^{-1})	assignment
2955 (s)	$\nu_{asymm}(OCO) + \delta(CH)$
	$\nu_{asymm}(CH_3)$
2892 (s)	$\nu_{symm}(CH_3)$
2865 (s)	$\nu(CH)$
2747 (w)	$\nu_{symm}(OCO) + \delta(CH)$
1617, 1573 (vs)	$\nu_{asymm}(OCO)$
1455 (m)	$\delta(CH_3)$
1383 (s)	$\delta(CH)$
1369 (vs)	$\nu_{symm}(OCO)$

strength of the vibrational modes. These bands are assigned not to formaldehyde but rather to vibrations of oxygenated molecules derived from a disproportionation of formaldehyde on the Cr^{II} sites. In particular, our most accredited species is methylformate, which is formed through the Tischenko reaction[55,85,93−97] of two formaldehyde molecules at the same Cr^{II} site. It is important to notice that, according to the specialized literature,[85,98] the $\nu(C{=}O)$ vibrational mode of a methylformate molecule strongly bonded to Lewis acid sites may undergo an important red shift even larger than −100 cm^{-1} with respect to the free molecule ($\nu(C{=}O)$ = 1720 cm^{-1}).

To further prove our assignment and thus our hypothesis, we selectively dosed pure formaldehyde on SiO$_2$ and on a Cr^{II}/SiO$_2$ catalyst activated following the same route as the Cr^{VI}/SiO$_2$ catalyst. Details of surface reactions and assignment of the multiple products are largely discussed in Section S3.

The whole set of experimental data discussed so far and the comparison with the specialized literature point toward methylformate as the most probable oxygenated byproduct. However, we cannot exclude alternative reaction paths leading to the formation of adsorbed formate species and methoxy groups grafted at the silica surface that would lead to similar spectroscopic signatures in the IR spectrum. Notably, these oxygenated products are strongly bonded to the catalyst surface, since their IR absorption bands neither decrease in intensity in operando conditions (i.e., being removed by the ethylene flow) or during degassing at 150 °C in high vacuum, nor shift during ethylene polymerization (as it would be expected if they are displaced from the Cr site and adsorbed nearby at the silica surface). It is important to add to the discussion that *operando* FT-IR spectroscopy is a fundamental technique for identifying the oxidized byproducts. Indeed, attempts to extract the oxidized byproducts by means of several solvents failed for the simpler case of Cr^{VI}/SiO$_2$ reduced by cyclohexene,[55] owing to the extremely high reactivity of the reduced catalyst toward the solvents themselves (or pollutants). In the present case, the scenario is even more complicated due to the difficulty in stopping the reaction before the occurrence

of ethylene polymerization and hence to the possible copresence of polyethylene.

Having identified the main oxidation state of the reduced Cr sites (by DR UV−vis−NIR) and the main oxidation byproduct (by FT-IR), we went back to the XANES spectra with the aim of getting rid of the interpretation ambiguity. We simulated the XANES spectra of several DFT-optimized Cr structures relevant for the discussion by using the FDMNES code[99−101] (which uses the finite difference method to solve the Schrödinger equation) and self-consistent calculations (i.e., without imposing any restriction on the shape of the potential such as the *muffin-tin* approximation).[102−104] The experimental XANES spectra of Cr^{VI}/SiO$_2$, Cr^{II}/SiO$_2$, and Cr$_2$O$_3$ (Section S2) are well reproduced by our structural models,[105] demonstrating the reliability of our method. The XANES spectrum of Cr^{VI}/SiO$_2$ at the end of the reaction (orange in Figure 1a) was simulated by a model of Cr^{II}/SiO$_2$ in interaction with methylformate and two molecules of ethylene (orange in Figure 1b). The main experimental features are very well reproduced by the model, further supporting our previous conclusions.[106]

In summary, the first relevant result emerging from our spectroscopic study is the identification, during the reduction of Cr^{VI}/SiO$_2$ in ethylene, of 6-fold-coordinated Cr^{II} species in interaction with a methylformate molecule. This novel concept is in very good agreement with recent findings by McDaniel and co-workers, who demonstrated that under commercial ethylene polymerization conditions oxygenates may remain attached to the chromium sites.[107] The next questions are whether these hindered Cr^{II} sites are involved in ethylene polymerization and whether methylformate remains attached to the Cr sites during ethylene polymerization, participating in the whole reaction. DR UV−vis−NIR and FT-IR spectroscopies help in answering these questions.

In the DR UV−vis−NIR spectra (Figure 1d, from red to orange) the start of ethylene polymerization (appearance of absorption bands in the 4400−4050 cm^{-1} range) is accompanied by a visible change in the scattering properties of the catalyst powder and by the decrease in intensity of the two d−d bands at 9500 and 16 700 cm^{-1}. This concomitance clearly and strongly indicates *that the Cr^{II} species in interaction with the oxidized byproducts are the species involved in ethylene polymerization*. Interestingly, the decrease in intensity of the two d−d bands upon ethylene polymerization is not complemented by the growth of other bands. The reason is that polyethylene forms a white coating around the Cr/SiO$_2$ particles, which diffuses the incident light and shields the Cr sites involved in the ethylene polymerization from the DR UV−vis−NIR measurements. The effect is macroscopically visible in Figure 4, which shows the appearance of the activated Cr^{VI}/SiO$_2$ catalyst before, during reduction, and after ethylene polymerization (from left to right).

The final spectrum (bold orange in Figure 1d) is characterized by a general low intensity due to the presence of polyethylene at the catalyst surface. Two bands at 21 500 and 16 000 cm^{-1} are still detectable. The band at 21 500 cm^{-1} indicates the persistence of a few unreacted chromates, meaning that ethylene polymerization proceeds in the presence of residual—slowly reducible—chromates, in agreement with previous reports.[108,109] The band at 16 000 cm^{-1} could be assigned to a d−d transition of another reduced Cr species not involved in polyethylene formation. Its position is compatible with both 6-fold-coordinated Cr^{II} and Cr^{III} species.
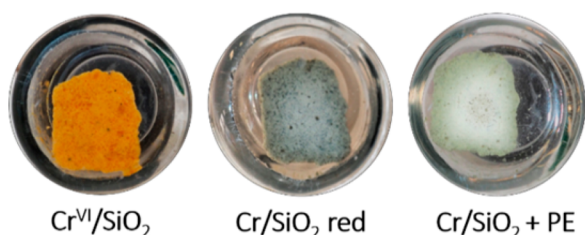
Figure 4. Pictures of the Cr^{VI}/SiO_2 catalyst pellet placed inside a quartz cell before, during reduction in ethylene, and after polymerization (from left to right). Gradual increase of the light diffusion of the pellet is macroscopic and proves the loss of KM units in the whole DR UV–vis–NIR spectra upon ethylene polymerization.

FT-IR spectroscopy (Figure 1f) reveals that ethylene polymerization (characteristic polyethylene bands: $\nu_{asymm}(CH_2)$ at 2924, $\nu_{symm}(CH_2)$ at 2853 cm^{-1}, and $\delta(CH_2)$ at 1472–1463 cm^{-1}) is consequent to the formation of methylformate. In addition, the absorption bands characteristic of methylformate are not affected by the polyethylene growth, testifying that the oxidized byproducts remain on the active Cr site also during ethylene polymerization and have to be considered important participants in the catalysis. As a side note, the IR absorption bands of methylformate keep on growing also during ethylene polymerization, confirming that the reaction starts in the presence of a residual fraction of Cr^{VI}.

As a final step, in Figure 5 we made an attempt to correlate the time evolution of all species detected with all techniques, which are involved in the reaction, namely, (i) the starting Cr^{VI}, (ii) the intermediate Cr^{II} in interaction with the oxygenated byproduct, (iii) a reduced Cr species acting as spectator, (iv) the polyethylene product, and (v) the oxygenated byproduct (methylformate). The spectroscopic fingerprints of Cr^{VI} were used to rescale the time vector for the three techniques. In the DR UV–vis–NIR and FT-IR spectra the absorption bands characteristic of each species were easily deconvoluted and their intensity plotted as a function of time. In contrast, for XANES a principal component analysis (PCA) followed by a multivariate curve resolution-alternating least squares (MCR-ALS) was applied to the whole sequence of spectra (Section S4). The analysis resulted in three principal components, corresponding to Cr^{VI}, Cr^{II} in interaction with the oxygenated byproduct, and a reduced Cr species behaving as a spectator. The border between the reduction and the polymerization steps was traced on the basis of the UV–vis–NIR and FT-IR results.

The data summarized in Figure 5 allow stating the following additional conclusions. (1) During the reduction step, Cr^{VI} are converted into Cr^{II} sites in interaction with the oxygenated byproduct (mostly methylformate) and into a reduced Cr species that does not participate in the reaction. (2) Ethylene polymerization starts on the Cr^{II} sites but in the presence of residual Cr^{VI} sites, which are slowly reduced in successive time. (3) The Cr^{II} sites involved in ethylene polymerization are rapidly buried in the produced polymer and become invisible for DR UV–vis–NIR spectroscopy but are still visible with XAS. These sites are continuously formed even during the polymerization to the expense of the residual Cr^{VI} and with the concomitant formation of methylformate.

3. CONCLUSIONS

Extremely focused spectroscopic investigations of the Cr^{VI}/SiO_2 Phillips catalyst in operando conditions have been the key
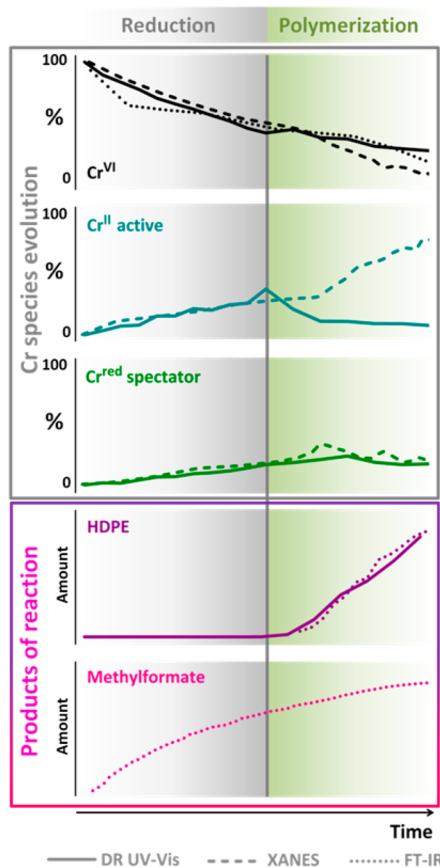
Figure 5. Time evolution of the DR UV–vis–NIR (solid lines), XANES (dashed lines), and FT-IR (dotted lines) spectroscopic fingerprints of (i) Cr^{VI} (21 500 cm^{-1} UV–vis; −1980 cm^{-1} FT-IR — first component in PCA XANES); (ii) Cr^{II} in interaction with methylformate and ethylene (9500 cm^{-1} UV–vis; second component in PCA XANES); (iii) spectator Cr (15 100 cm^{-1} UV–vis; third component in PCA XANES); (iv) HDPE (4400–4050 cm^{-1} UV–vis; −2853 cm^{-1} FT-IR); (v) methylformate (1573 cm^{-1} FT-IR).

to unravel the molecular structure of the Cr sites involved in ethylene polymerization. Our new spectroscopic evidence reveals that the chromium site involved in ethylene polymerization is a divalent ion, 6-fold coordinated, and in interaction with an external nucleophilic ligand (mostly methylformate). This study provides the first spectroscopic identification, at the molecular level, of the oxygenated species adsorbed on the catalyst during the induction period inferred by indirect TG, DSC, and MS experiments.[107] We also introduce the important concept that oxygenates remain in the Cr coordination sphere also *during* ethylene polymerization. Additionally, we demonstrate that ethylene polymerization occurs also if a fraction of the chromate sites is not reduced, implying that Cr^{VI} sites might have a role in the first steps of the catalysis in cooperation with the active Cr^{II} sites, as already proposed in the literature.[108,109] A possible role of the residual Cr^{VI} sites (but most probably of residual Cr^{V} as well, which have been detected by EPR spectroscopy)[110] might be to alter the strain at the silica surface[111] and in particular at the Cr-reduced species formed nearby.

We wish to underline that each technique employed in this work, if taken as a single measurement, cannot lead to safe statements on the molecular structure of the Cr sites. On the other hand, the totality of the results collected with each

spectroscopic technique converge to a single picture in which the Cr^{II} sites 6-fold coordinated are those involved in the reaction, while a fraction of reduced Cr sites acts as spectator. This is valid for Cr^{VI}/SiO$_2$ directly reduced in ethylene. We reiterate that in our opinion both "naked" Cr^{II} and Cr^{III} sites may be active in ethylene polymerization, as for ad-hoc-reduced catalysts and ad-hoc-synthesized catalytic systems, respectively.[29,35,37,51] The aim of the present work was not to enter into the debate on the formal oxidation state of the Cr sites active in ethylene polymerization, which is inflaming the literature on the Phillips catalyst in recent times. Rather, we want to shed light on the products of chromates reduction, which remain in the coordination sphere of the reduced Cr sites and participate in the polymerization reaction. We believe that the molecular structure and the ligand sphere of the Cr sites, irrespective of their formal oxidation state, are key players behind the activity toward ethylene and might also explain their tendency toward ethylene polymerization vs oligomerization (i.e., the preference toward propagation vs termination). In fact, the literature on heterogeneous Cr-based catalysts contains examples of (i) catalysts based on a different Cr oxidation state (Cr^{II} [29,37,75,76] or Cr^{III} [35,36,43,51]) giving a similar polyethylene and (ii) catalysts based on the same Cr oxidation state (either Cr^{II} [90,112,113] or Cr^{III} [51,114,115])[38–40] which either polymerize or oligomerize ethylene. This is true also for homogeneous Cr-based catalysts.[34,116–119] Thus, the scientific debate of the Phillips community cannot accommodate a short-sighted discussion centered only on the oxidation state of the active species.

The emerging panorama from this work should set aside the "old" vision of the Phillips catalyst active site constituted by a *naked* (i.e., low-coordinated) chromium species, which now appears unrealistic of the reaction taking place in industrial conditions. Rather, external (and flexible) oxygenated ligands seem to be fundamental actors in the polymerization reaction, very much like the ancillary ligands in homogeneous polymerization catalysis. On these basis, external nucleophilic ligands are surely suitable candidates in the *ab initio* design of Phillips-related olefin polymerization catalysts. It is worth mentioning that the picture resulting from this work might be extendible also to most of the prereducing agents (e.g., Al-alkyls, B-alkyls, etc.) employed on the Cr^{VI}/SiO$_2$ catalyst to shorten the induction time and modify the polymer properties. It is predicted that also in those cases the oxidized byproducts remain in the coordination sphere of the reduced Cr sites (whichever is the formal oxidation state), affecting their catalytic properties. The different nature of the oxidized byproducts might be one of the reasons why each prereducing agent gives rise to extremely different catalytic behavior and consequently to different polyethylene products.

4. EXPERIMENTAL SECTION

4.1. Catalyst Synthesis and Activation. The Cr/SiO$_2$ catalyst was prepared by wet impregnation of SiO$_2$ (aerosol, surface area ca. 360 m^2 g^{-1}) with an aqueous solution of CrO$_3$ having a chromium loading of 1.0 wt %.[9] The chromium loading was kept low enough to avoid segregation of CrO$_x$ during the activation treatments but sufficiently high to guarantee a good sensitivity with all techniques. The Cr^{VI}/SiO$_2$ catalyst was obtained by treating the impregnated sample in the presence of oxygen at 650 °C either in static conditions (two cycles of 30 min in pure oxygen, equilibrium pressure 100 mbar) for DR UV–vis–NIR and FT-IR measurements or in dynamic conditions (10% O$_2$ in He, total flow 10 mL/min) for XAS measurements. Reduction of Cr^{VI}/SiO$_2$ by means of ethylene and subsequent polymerization was

achieved by flowing ethylene (pure ethylene 20 mL/min for DR UV–vis–NIR and FT-IR measurements and pure ethylene in He 10 mL/min for XAS) in the reaction cells at 150 °C. Complementary FT-IR experiments were performed in static conditions (P_{C2H4} = 100 mbar). The reference Cr^{II}/SiO$_2$ catalyst was obtained by reducing the activated Cr^{VI}/SiO$_2$ sample by means of CO at 350 °C (two cycles of 30 min in pure carbon monoxide, equilibrium pressure 100 mbar) and subsequent outgassing at the same temperature.

4.2. Cr K-Edge XANES spectroscopy. Cr K-edge XAS spectra were collected at the BM23 beamline[120] at the European Synchrotron Radiation Facility (ESRF, Grenoble, F). The white beam was monochromatized using a Si(111) double crystal, and harmonic rejection was performed by using silicon mirrors (4 mrad). The intensity of the incident beam was monitored by an ionization chamber and was vertically focused to a few micrometers. Due to Cr dilution, EXAFS spectra were collected in fluorescence mode by means of a 12-element Ge detector. To minimize the elastic scattering a 45° geometry between the incoming X-ray beam and the detector nose was adopted. The samples were measured in the form of powder inside a quartz capillary 1.5 mm in diameter having upstream and downstream two small pieces of quartz wool. The capillary was connected to a gas-dosing system with mass-flow controllers to flow different gas mixtures and inserted inside a half-circular oven allowing treating the sample up to 650 °C in the presence of different reagents, simultaneously collecting the XAS spectra. XANES spectra were acquired with an energy step of 0.4 eV and an integration time of 2 s/point up to k = 5 Å^{-1} to allow a confident normalization. Each XANES spectrum required an acquisition time of about 12 min as a compromise between fast acquisition and quality of the spectra. The XANES spectra were normalized using the Athena program.[121] The evolution of gaseous products of reaction are monitored with online mass spectroscopy at the end of the capillary by sampling a fraction of the exit flow. The PCA MCR-ALS analysis of the series of XANES spectra has been performed as detailed in Section S4 and elsewhere.[122]

4.3. DR UV–vis–NIR Spectroscopy. Diffuse reflectance (DR) UV–vis–NIR spectra were recorded on a Varian Cary5000 instrument on samples in the form of powder placed inside a cell made in Suprasil quartz. Sample activation was performed in quartz cylinders in static conditions (two cycles of 30 min in pure O$_2$, ep = 100 mbar). The activated sample was stocked in a glovebox and in a second moment transferred inside a DR UV–vis–NIR cell made in optical quartz (Suprasil) and allowing reactions in flow of different gaseous mixtures. The reaction in ethylene was performed by connecting the cell to a gas-dosing system with mass-flow controllers to flow different gas mixtures and inserting the cell inside a circular oven. The spectra were collected in reflectance mode and successively converted in Kubelka–Munk units. Also, in this case we followed the downstream evolution of gaseous products of reaction with online mass spectroscopy by sampling a fraction of the exit flow.

4.4. FT-IR Spectroscopy. Transmission FT-IR spectra were recorded on a Bruker Vertex70 instrument at 2 cm^{-1} resolution. The catalysts were measured inside a quartz cell equipped with two KBr windows and in the form of thin self-supported pellets. The activation treatments were performed directly in the IR measurement cell in static conditions (two cycles of 30 min in pure O$_2$, equilibrium pressure = 100 mbar). The measurements during ethylene reduction/polymerization were performed by connecting the cell to a gas-dosing system with mass-flow controllers to flow different gas mixtures. The cell was heated with two glowplugs immersed in silicon carbide powder.

■ ASSOCIATED CONTENT

ⓢ Supporting Information

The Supporting Information is available free of charge on the ACS Publications website at DOI: 10.1021/jacs.7b07437.

Detailed assignment and discussion of the DR UV–vis–NIR and FT-IR spectra, along with XANES simulations and DFT-optimized clusters (PDF)

■ AUTHOR INFORMATION

Corresponding Authors

*caterinabarzan@unito.it
*elenagroppo@unito.it

ORCID Ⓘ

Carlo Lamberti: 0000-0001-8004-2312
Silvia Bordiga: 0000-0003-2371-4156
Elena Groppo: 0000-0003-4153-5709

Notes

The authors declare no competing financial interest.

■ REFERENCES

(1) Hogan, J. P.; Banks, R. L. US. Patent 2.825.721, 1958.
(2) *World Polyethylene, Industry Study with Forecast for 2018 & 2023*; The Freedonia Group: Cleveland, 2014; Study 3210.
(3) McDaniel, M. P. *Adv. Catal.* **2010**, *53*, 123−606.
(4) Nowlin, T. E. *Business and Technology of the Global Polyethylene Industry*; Wiley-Scrivener: New York, 2014.
(5) *Market Report: Global Catalyst Market*; 3rd ed.; Acmite Market Intelligence: Ratingen, Germany, 2015.
(6) Weckhuysen, B. M.; Wachs, I. E.; Schoonheydt, R. A. *Chem. Rev.* **1996**, *96*, 3327−3349.
(7) Cheng, R.; Liu, Z.; Zhong, L.; He, X.; Qiu, P.; Terano, M.; Eisen, M. S.; Scott, S. L.; Liu, B. In *Polyolefins: 50 Years after Ziegler and Natta I: Polyethylene and Polypropylene*; Kaminsky, W., Ed.; Spinger-Verlag: Berlin Heidelberg, 2013; Vol. *257*, pp 135−202.
(8) Liu, Z.; He, X.; Cheng, R.; Eisen, M. S.; Terano, M.; Scott, S. L.; Liu, B. *Adv. Chem. Eng.* **2014**, *44*, 127−191.
(9) Groppo, E.; Lamberti, C.; Bordiga, S.; Spoto, G.; Zecchina, A. *Chem. Rev.* **2005**, *105*, 115−183.
(10) Groppo, E.; Seenivasan, K.; Barzan, C. *Catal. Sci. Technol.* **2013**, *3*, 858−878.
(11) McDaniel, M. P. *J. Catal.* **1981**, *67*, 71−76.
(12) McDaniel, M. P. *J. Catal.* **1982**, *76*, 29−36.
(13) McDaniel, M. P. *J. Catal.* **1982**, *76*, 37−47.
(14) McDaniel, M. P. *J. Catal.* **1982**, *76*, 17−28.
(15) Weckhuysen, B. M.; Deridder, L. M.; Schoonheydt, R. A. *J. Phys. Chem.* **1993**, *97*, 4756−4763.
(16) Weckhuysen, B. M.; Verberckmoes, A. A.; Buttiens, A. L.; Schoonheydt, R. A. *J. Phys. Chem.* **1994**, *98*, 579−584.
(17) Weckhuysen, B. M.; Deridder, L. M.; Grobet, P. J.; Schoonheydt, R. A. *J. Phys. Chem.* **1995**, *99*, 320−326.
(18) Weckhuysen, B. M.; Schoonheydt, R. A.; Jehng, J. M.; Wachs, I. E.; Cho, S. J.; Ryoo, R.; Kijlstra, S.; Poels, E. *J. Chem. Soc., Faraday Trans.* **1995**, *91*, 3245−3253.
(19) Weckhuysen, B. M.; Verberckmoes, A. A.; Baets, A. R.bD.; Schoonheydt, R. A. *J. Catal.* **1997**, *166*, 160−171.
(20) Weckhuysen, B. M.; Verberckmoes, A. A.; Debaere, J.; Ooms, K.; Langhans, I.; Schoonheydt, R. A. *J. Mol. Catal. A: Chem.* **2000**, *151*, 115−131.
(21) Wachs, I. E.; Roberts, C. A. *Chem. Soc. Rev.* **2010**, *39*, 5002−5017.
(22) Chakrabarti, A.; Gierada, M.; Handzlik, J.; Wachs, I. E. *Top. Catal.* **2016**, *59*, 725−739.
(23) Chakrabarti, A.; Wachs, I. E. *Catal. Lett.* **2015**, *145*, 985−994.
(24) Guesmi, H.; Tielens, F. *J. Phys. Chem. C* **2012**, *116*, 994−1001.
(25) Tielens, F.; Islam, M. M.; Skara, G.; De Proft, F.; Shishido, T.; Dzwigaj, S. *Microporous Mesoporous Mater.* **2012**, *159*, 66−73.
(26) Handzlik, J.; Grybos, R.; Tielens, F. *J. Phys. Chem. C* **2013**, *117*, 8138−8149.
(27) Gao, J.; Zheng, Y.; Tang, Y.; Jehng, J.-M.; Grybos, R.; Handzlik, J.; Wachs, I. E.; Podkolzin, S. G. *ACS Catal.* **2015**, *5*, 3078−3092.
(28) Handzlik, J.; Grybos, R.; Tielens, F. *J. Phys. Chem. C* **2016**, *120*, 17594−17603.
(29) Gierada, M.; Michorczyk, P.; Tielens, F.; Handzlik, J. *J. Catal.* **2016**, *340*, 122−135.
(30) Liu, B.; Nakatani, H.; Terano, M. *J. Mol. Catal. A: Chem.* **2002**, *184*, 387−398.
(31) Liu, B. P.; Nakatani, H.; Terano, M. *J. Mol. Catal. A: Chem.* **2003**, *201*, 189−197.
(32) Xia, W.; Liu, B. P.; Fang, Y. W.; Hasebe, K.; Terano, M. *J. Mol. Catal. A: Chem.* **2006**, *256*, 301−308.
(33) Zhong, L.; Liu, Z.; Cheng, R. H.; Tang, S. Y.; Qiu, P. Y.; He, X. L.; Terano, M.; Liu, B. P. *ChemCatChem* **2012**, *4*, 872−881.
(34) McGuinness, D. S. *Chem. Rev.* **2011**, *111*, 2321−2341.
(35) Delley, M. F.; Nunez-Zarur, F.; Conley, M. P.; Comas-Vives, A.; Siddiqi, G.; Norsic, S.; Monteil, V.; Safonova, O. V.; Coperet, C. *Proc. Natl. Acad. Sci. U. S. A.* **2014**, *111*, 11624−11629.
(36) Conley, M. P.; Delley, M. F.; Siddiqi, G.; Lapadula, G.; Norsic, S.; Monteil, V.; Safonova, O. V.; Coperet, C. *Angew. Chem., Int. Ed.* **2014**, *53*, 1872−1876.
(37) Brown, C.; Krzystek, J.; Achey, R.; Lita, A.; Fu, R.; Meulenberg, R. W.; Polinski, M.; Peek, N.; Wang, Y.; van de Burgt, L. J.; Profeta, S. J.; Stiegman, A. E.; Scott, S. L. *ACS Catal.* **2015**, *5*, 5574−5583.
(38) Cicmil, D.; Meeuwissen, J.; Vantomme, A.; Wang, J.; van Ravenhorst, I. K.; van der Bij, H. E.; Munoz-Murillo, A.; Weckhuysen, B. M. *Angew. Chem., Int. Ed.* **2015**, *54*, 13073−13079.
(39) Cicmil, D.; Meeuwissen, J.; Vantomme, A.; Weckhuysen, B. M. *ChemCatChem* **2016**, *8*, 1937−1944.
(40) Cicmil, D.; van Ravenhorst, I. K.; Meeuwissen, J.; Vantomme, A.; Weckhuysen, B. M. *Catal. Sci. Technol.* **2016**, *6*, 731−743.
(41) Fong, A.; Peters, B.; Scott, S. L. *ACS Catal.* **2016**, *6*, 6073−6085.
(42) Fong, A.; Yuan, Y.; Ivry, S. L.; Scott, S. L.; Peters, B. *ACS Catal.* **2015**, *5*, 3360−3374.
(43) Conley, M. P.; Delley, M. F.; Nunez-Zarur, F.; Comas-Vives, A.; Coperet, C. *Inorg. Chem.* **2015**, *54*, 5065−5078.
(44) Floryan, L.; Borosy, A. P.; Nunez-Zarur, F.; Comas-Vives, A.; Coperet, C. *J. Catal.* **2017**, *346*, 50−56.
(45) Krauss, H. L.; Stach, H. *Inorg. Nucl. Chem. Lett.* **1968**, *4*, 393.
(46) Krauss, H. L.; Stach, H. *Z. Anorg. Allg. Chem.* **1969**, *366*, 34−42.
(47) Finch, J. N. *J. Catal.* **1976**, *43*, 111.
(48) Zecchina, A.; Garrone, E.; Ghiotti, G.; Morterra, C.; Borello, E. *J. Phys. Chem.* **1975**, *79*, 966−972.
(49) McDaniel, M. P. *Adv. Catal.* **1985**, *33*, 47−98.
(50) Coperet, C.; Allouche, F.; Chang, K. W.; Conley, M. P.; Delley, M. F.; Fedorov, A.; Moroz, I. B.; Mougel, V.; Pucino, M.; Searles, K.; Yamamoto, K.; Zhizhko, P. A. *Angew. Chem., Int. Ed.* **2017**, DOI:10.1002/anie.201702387.
(51) Delley, M. F.; Lapadula, G.; Nunez-Zarur, F.; Comas-Vives, A.; Kalendra, V.; Jeschke, G.; Baabe, D.; Walter, M. D.; Rossini, A. J.; Lesage, A.; Emsley, L.; Maury, O.; Coperet, C. *J. Am. Chem. Soc.* **2017**, *139*, 8855−8867.
(52) Gianolio, D.; Groppo, E.; Vitillo, J. G.; Damin, A.; Bordiga, S.; Zecchina, A.; Lamberti, C. *Chem. Commun.* **2010**, *46*, 976−978.
(53) Corma, A. *Angew. Chem., Int. Ed.* **2016**, *55*, 6112−6113.

(54) Schwerdtfeger, E.; Buck, R.; McDaniel, M. *Appl. Catal., A* **2012**, *423-424*, 91−99.

(55) Barzan, C.; Damin, A. A.; Budnyk, A.; Zecchina, A.; Bordiga, S.; Groppo, E. *J. Catal.* **2016**, *337*, 45−51.

(56) Amor Nait Ajjou, J.; Scott, S. L. *J. Am. Chem. Soc.* **2000**, *122*, 8968−8976.

(57) Amor Nait Ajjou, J.; Scott, S. L.; Paquet, V. *J. Am. Chem. Soc.* **1998**, *120*, 415−416.

(58) Bordiga, S.; Groppo, E.; Agostini, G.; van Bokhoven, J. A.; Lamberti, C. *Chem. Rev.* **2013**, *113*, 1736−1850.

(59) Lamberti, C.; Zecchina, A.; Groppo, E.; Bordiga, S. *Chem. Soc. Rev.* **2010**, *39*, 4951−5001.

(60) Singh, J.; Lamberti, C.; van Bokhoven, J. A. *Chem. Soc. Rev.* **2010**, *39*, 4754−4766.

(61) Chakrabarti, A.; Ford, M. E.; Gregory, D.; Hu, R.; Keturakis, C. J.; Lwin, S.; Tang, Y.; Yang, Z.; Zhu, M.; Banares, M. A.; Wachs, I. E. *Catal. Today* **2017**, *283*, 27−53.

(62) Vimont, A.; Thibault-Starzyk, F.; Daturi, M. *Chem. Soc. Rev.* **2010**, *39*, 4928−4950.

(63) Dou, J.; Sun, Z.; Opalade, A. A.; Wang, N.; Fu, W.; Tao, F. *Chem. Soc. Rev.* **2017**, *46*, 2001−2027.

(64) The temperature of 150 °C adopted in this work is slightly higher with respect that used in industrial conditions. This correction was necessary to compensate for the low ethylene pressure employed in our experimental conditions.

(65) Fubini, B.; Ghiotti, G.; Stradella, L.; Garrone, E.; Morterra, C. *J. Catal.* **1980**, *66*, 200−213.

(66) Weckhuysen, B. M.; Schoonheydt, R. A. *Catal. Today* **1999**, *49*, 441−451.

(67) Engemann, C.; Hormes, J.; Longen, A.; Dotz, K. H. *Chem. Phys.* **1998**, *237*, 471−481.

(68) Pantelouris, A.; Modrow, H.; Pantelouris, M.; Hormes, J.; Reinen, D. *Chem. Phys.* **2004**, *300*, 13−22.

(69) Demmelmaier, C. A.; White, R. E.; van Bokhoven, J. A.; Scott, S. L. *J. Phys. Chem. C* **2008**, *112*, 6439−6449.

(70) Demmelmaier, C. A.; White, R. E.; van Bokhoven, J. A.; Scott, S. L. *J. Catal.* **2009**, *262*, 44−56.

(71) Groppo, E.; Prestipino, C.; Cesano, F.; Bonino, F.; Bordiga, S.; Lamberti, C.; Thüne, P. C.; Niemantsverdriet, J. W.; Zecchina, A. *J. Catal.* **2005**, *230*, 98−108.

(72) Tromp, M.; Moulin, J. O.; Reid, G.; Evans, J. *AIP Conf. Proc.* **2006**, *882*, 699−701.

(73) Heating the catalyst/polymer composite in O_2 gave CO and CO_2 as the main oxidation byproducts, as revealed by online MS.

(74) Groppo, E.; Lamberti, C.; Bordiga, S.; Spoto, G.; Damin, A.; Zecchina, A. *J. Phys. Chem. B* **2005**, *109*, 15024−15031.

(75) Groppo, E.; Lamberti, C.; Cesano, F.; Zecchina, A. *Phys. Chem. Chem. Phys.* **2006**, *8*, 2453−2456.

(76) Groppo, E.; Lamberti, C.; Bordiga, S.; Spoto, G.; Zecchina, A. *J. Catal.* **2006**, *240*, 172−181.

(77) Groppo, E.; Estephane, J.; Lamberti, C.; Spoto, G.; Zecchina, A. *Catal. Today* **2007**, *126*, 228−234.

(78) Groppo, E.; Damin, A.; Otero Arean, C.; Zecchina, A. *Chem. - Eur. J.* **2011**, *17*, 11110−11114.

(79) Chelazzi, D.; Ceppatelli, M.; Santoro, M.; Bini, R.; Schettino, V. *Nat. Mater.* **2004**, *3*, 470−475.

(80) Delley, M. F.; Conley, M. P.; Coperet, C. *Catal. Lett.* **2014**, *144*, 805−808.

(81) Fackler, J.; Holah, D. *Inorg. Chem.* **1965**, *4*, 954−958.

(82) Figgis, B. N. *Introduction to ligand fields*; John Wiley & Sons: New York, 1966.

(83) Clark, R. J. H. *J. Chem. Soc.* **1964**, *0*, 417−425.

(84) Note that the band centered at ca. 9500 cm^{-1} corresponds to a very broad band centered at 1050 nm. Since most of the literature spectra are shown in the 200−800 nm range, this band and similar ones cannot be measured. In addition, reporting the spectra in wavenumbers (which is the most correct way, with wavenumbers being directly proportional to the energy of the transition) allows one

to define the maximum of d−d bands which would be too broad in wavelength.

(85) Crocella, V.; Cerrato, G.; Magnacca, G.; Morterra, C.; Cavani, F.; Maselli, L.; Passeri, S. *Dalt. Trans.* **2010**, *39*, 8527−8537.

(86) Busca, G.; Lorenzelli, V. *J. Catal.* **1980**, *66*, 155−161.

(87) Busca, G.; Lamotte, J.; Lavalley, J. C.; Lorenzelli, V. *J. Am. Chem. Soc.* **1987**, *109*, 5197−5202.

(88) Vijayaraj, M.; Gopinath, C. S. *J. Catal.* **2004**, *226*, 230−234.

(89) Busca, G. *Catal. Today* **1996**, *27*, 457−496.

(90) Barzan, C.; Groppo, E.; Quadrelli, E. A.; Monteil, V.; Bordiga, S. *Phys. Chem. Chem. Phys.* **2012**, *14*, 2239−2245.

(91) Spoto, G.; Bordiga, S.; Ricchiardi, G.; Scarano, D.; Zecchina, A.; Borello, E. *J. Chem. Soc., Faraday Trans.* **1994**, *90*, 2827−2835.

(92) Cieslak-Golonka, M. *Coord. Chem. Rev.* **1991**, *109*, 223−249.

(93) Ooi, T.; Miura, T.; Itagaki, Y.; Ichikawa, I.; Maruoka, K. *Synthesis* **2002**, *2002*, 279−291.

(94) Mojtahedi, M. M.; Akbarzadeh, E.; Sharifi, R.; Abaee, M. S. *Org. Lett.* **2007**, *9*, 2791−2793.

(95) Gnanadesikan, V.; Horiuchi, Y.; Ohshima, T.; Shibasaki, M. *J. Am. Chem. Soc.* **2004**, *126*, 7782−7783.

(96) Hoshimoto, Y.; Ohashi, M.; Ogoshi, S. *J. Am. Chem. Soc.* **2011**, *133*, 4668−4671.

(97) Curran, S. P.; Connon, S. J. *Angew. Chem., Int. Ed.* **2012**, *51*, 10866−10870.

(98) Lochar, V. *Appl. Catal., A* **2006**, *309*, 33−36.

(99) Joly, Y. *Phys. Rev. B: Condens. Matter Mater. Phys.* **2001**, *63*, 125120.

(100) Guda, S. A.; Guda, A. A.; Soldatov, M. A.; Lomachenko, K. A.; Bugaev, A. L.; Lamberti, C.; Gawelda, W.; Bressler, C.; Smolentsev, G.; Soldatov, A. V.; Joly, Y. *J. Chem. Theory Comput.* **2015**, *11*, 4512−4521.

(101) Guda, A. A.; Guda, S. A.; Soldatov, M. A.; Lomachenko, K. A.; Bugaev, A. L.; Lamberti, C.; Gawelda, W.; Bressler, C.; Smolentsev, G.; Soldatov, A. V.; Joly, Y. *J. Phys.: Conf. Ser.* **2016**, *712*, 012004.

(102) Bunau, O.; Joly, Y. *J. Phys.: Condens. Matter* **2009**, *21*, 345501.

(103) Smolentsev, G.; Soldatov, A. V.; Joly, Y.; Pascarelli, S.; Aquilanti, G. *Radiat. Phys. Chem.* **2006**, *75*, 1571−1573.

(104) Joly, Y.; Greiner, S. Theory of X-Ray Absorption Near Edge Structure in *X-Ray Absorption and X-ray Emission Spectroscopy: Theory and Applications*, van Bokhoven, J. A.; Lamberti, C. (Eds.), Wiley and Sons: Chichester, UK, 2016; Vol. I, pp 73−97.

(105) Note that the employed models contain more than 80 atoms in order to simulate a substantial portion of the silica support, which is known to affect the strain at the Cr sites.

(106) Notably, the main message coming from XANES spectral comparison and simulation is that the assignment of the Cr oxidation state by XANES spectroscopy is not unambiguous, as pointed in the past (ref 72) but often neglected, and it should be assisted by theoretical calculation and taking into account any additional information obtained by complementary characterization techniques.

(107) Potter, K. C.; Beckerle, C. W.; Jentoft, F. C.; Schwerdtfeger, E.; McDaniel, M. P. *J. Catal.* **2016**, *344*, 657−668.

(108) Liu, B. P.; Sindelar, P.; Fang, Y. W.; Hasebe, K.; Terano, M. *J. Mol. Catal. A: Chem.* **2005**, *238*, 142−150.

(109) Cheng, R. H.; Xu, C.; Liu, Z.; Dong, Q.; He, X. L.; Fang, Y. W.; Terano, M.; Hu, Y. T.; Pullukat, T. J.; Liu, B. P. *J. Catal.* **2010**, *273*, 103−115.

(110) Weckhuysen, B. M.; Schoonheydt, R. A.; Mabbs, F. E.; Collison, D. *J. Chem. Soc., Faraday Trans.* **1996**, *92*, 2431−2436.

(111) Amakawa, K.; Sun, L.; Guo, C.; Hävecker, M.; Kube, P.; Wachs, I. E.; Lwin, S.; Frenkel, A. I.; Patlolla, A.; Hermann, K.; Schlögl, R.; Trunschke, A. *Angew. Chem., Int. Ed.* **2013**, *52*, 13553−13557.

(112) Barzan, C.; Gianolio, D.; Groppo, E.; Lamberti, C.; Monteil, V.; Quadrelli, E. A.; Bordiga, S. *Chem. - Eur. J.* **2013**, *19*, 17277−17282.

(113) Monoi, T.; Sasaki, Y. *J. Mol. Catal. A: Chem.* **2002**, *187*, 135−141.

(114) Monoi, T.; Ikeda, H.; Ohira, H.; Sasaki, Y. *Polym. J.* **2002**, *34*, 461−465.

(115) Nenu, C. N.; Bodart, P.; Weckhuysen, B. M. European Patent 2005050565, 2005.

(116) Vidyaratne, I.; Nikiforov, G. B.; Gorelsky, S. I.; Gambarotta, S.; Duchateau, R.; Korobkov, I. *Angew. Chem., Int. Ed.* **2009**, *48*, 6552.

(117) Jabri, A.; Mason, C. B.; Sim, Y.; Gambarotta, S.; Burchell, T. J.; Duchateau, R. *Angew. Chem., Int. Ed.* **2008**, *47*, 9717−9721.

(118) Albahily, K.; Koc, E.; Al-Baldawi, D.; Savard, D.; Gambarotta, S.; Burchell, T. J.; Duchateau, R. *Angew. Chem., Int. Ed.* **2008**, *47*, 5816−5819.

(119) Yang, Y.; Gurnham, J.; Liu, B. P.; Duchateau, R.; Gambarotta, S.; Korobkov, I. *Organometallics* **2014**, *33*, 5749−5757.

(120) Mathon, O.; Beteva, A.; Borrel, J.; Bugnazet, D.; Gatla, S.; Hino, R.; Kantor, I.; Mairs, T.; Munoz, M.; Pasternak, S.; Perrin, F.; Pascarelli, S. *J. Synchrotron Radiat.* **2015**, *22*, 1548−1554.

(121) Ravel, B.; Newville, M. *J. Synchrotron Radiat.* **2005**, *12*, 537−541.

(122) Martini, A.; Borfecchia, E.; Lomachenko, K. A.; Pankin, I. A.; Negri, C.; Berlier, G.; Beato, P.; Falsig, H.; Bordiga, S.; Lamberti, C. *Chem. Sci.* **2017**, DOI: 10.1039/C7SC02266B.

Ligands make the difference! Molecular insights into Cr^{VI}/SiO_2 Phillips catalyst during ethylene polymerization.

Caterina Barzan,[a]* Alessandro Piovano,[a] Luca Braglia,[ab] Giorgia A. Martino,[a] Carlo Lamberti,[ab] Silvia Bordiga[a] and Elena Groppo[a]*

[a] Department of Chemistry and NIS Centre, University of Torino, via G. Quarello 15A, I-10135 Torino, Italy

[b] IRC "Smart Materials", Southern Federal University, Zorge Street 5, 344090 Rostov-on-Don, Russia

S1. Oxidation state and coordination geometry of the Cr sites active in ethylene polymerization: DR UV-Vis-NIR spectroscopy

The DR UV-Vis-NIR spectrum of the Cr^{VI}/SiO_2 catalyst reduced in ethylene prior polymerization is compared with those of Cr^{II} and Cr^{III} references in Figure S1a.

- The spectrum of the CO-reduced Cr^{II}/SiO_2 catalyst (dark blue) is dominated by two well defined d-d bands at 7500 and 12000 cm^{-1} assigned to Cr^{II} ions having a +2 oxidation state and a 4-folded coordination.[1-5] These bands blue shift when the Cr^{II} ions expand their ligand field up to a distorted octahedral coordination. For example, in the presence of CO the d-d bands shift up to 20000 cm^{-1}.[1, 3]

- The spectrum of $CrCl_3*6(H_2O)$ physisorbed on Aerosil SiO_2 (bold green) is that typical of 6-fold coordinated Cr^{III} ions, i.e. it shows two equally intense bands in the 15000–17000 cm^{-1} and 20000–25000 cm^{-1} regions attributed to the $^4A_2 \rightarrow ^4T_2$ and $^4A_2 \rightarrow ^4T_1$ transitions, respectively.[5-8]

- The spectrum of the Cr^{VI}/SiO_2 catalyst reduced in ethylene (red) is characterized by two d-d bands at 9500 cm^{-1} and 16700 cm^{-1} (having a shoulder at 15100 cm^{-1}) and three charge-transfer bands at 21500 cm^{-1}, 29500 and 40000 cm^{-1}. The assignment of this spectrum is not straightforward, also due to the fact that the catalyst is not yet completely reduced. Nevertheless, the d-d band at 9500 cm^{-1} is assigned to the first d-d transition of a Cr^{II} species, being too low in energy to be attributed to Cr^{III} ions. The band at 16700 cm^{-1} is assigned to the second d-d transition of Cr^{II} species in a distorted 6-fold geometry. Indeed, Cr^{II} ions in a perfect octahedral geometry, as for $Cr(H_2O)_6^{2+}$, show a single $^5E_g \rightarrow ^5T_{2g}$ transition around ~14000 cm^{-1}.[9] A vertical distortion of the octahedral geometry results in the splitting of the transition in four separate contributions.[9] However, this is true in

solution, in which the distortion is completely symmetrical; in the solid state and in a system governed by amorphous silica, the distortions of the octahedral metal sites cannot be ad symmetrical, thus might result in a lower number of transitions, characterized by heterogeneity and thus resulting in a broadening of the bands. Finally, we coupled the two d-d bands at 9500 and 16700 cm^{-1} also because they display a similar behavior as a function of the reaction time.

The ambiguity in the full assignment of the UV-Vis bands is due to the overlap of the low-energy charge-transfer region (i.e. O=Cr LMCT) and the high-energy d-d region (Cr^{III} $^4A_2 \rightarrow ^4T_1$). This is the reason why the UV-Vis data require the XANES data counterpart in order to overcome possible wrong assignments (and VICEVERSA).

Figure S1b compares the spectrum of Cr^{VI}/SiO_2 catalyst reduced in ethylene at 150 °C (bold red) with that of the same catalyst reduced in cyclohexene at room temperature (light blue).[11] Cyclohexene is considered a model molecule that can simulate what is happening during the reduction of chromate species in the presence of an olefin (induction period), but without taking part to the subsequent polymerization reaction. Reduction of Cr^{VI} species in cyclohexene leads to 6-fold coordinated Cr^{II} sites in interaction with an ester molecule.[11] We wish to underline once more that this catalyst does not display Cr^{III} species, as verified by EPR spectroscopy (highly selective for Cr^{III} ions) The corresponding UV-Vis spectrum is characterized by two d-d bands at 10000 and 16500 cm^{-1}, very similar to those observed for Cr^{VI}/SiO_2 catalyst reduced in ethylene. Interestingly, the spectrum of Cr^{VI}/SiO_2 catalyst reduced in cyclohexene (light blue) does not show the shoulder at 15100 cm^{-1}, which might be attributed to a d-d transition of another reduced Cr species.
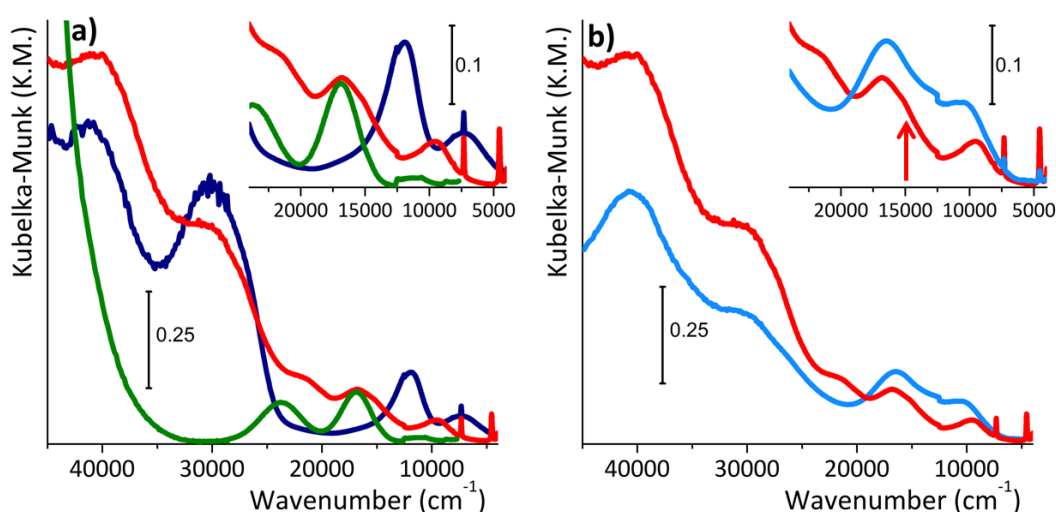
Figure S1: Part (a): DR UV-Vis-NIR spectra of Cr^{VI}/SiO_2 catalyst upon reduction in ethylene at 150 °C (bold red), upon reduction in CO at 350 °C (blue) and of the $CrCl_3*6(H_2O)$ complex physisorbed on Aerosil SiO_2 (green). Part (b): DR UV-Vis-NIR spectra of Cr^{VI}/SiO_2 catalyst reduced in ethylene at 150 °C (bold red), and after reduction in cyclohexene at room temperature (light blue). In both cases the insets show the magnification of the d-d spectral region.

S2. XANES spectroscopy: simulations

At first, we simulated the XANES spectra of a few DFT-optimized clusters representing Cr^{VI}/SiO_2, Cr^{II}/SiO_2 and Cr_2O_3 in order to validate our theoretical method. Calculations were performed by adopting a cluster approach[10] and Gaussian 09 software.[11] To model Cr^{VI}/SiO_2 and Cr^{II}/SiO_2 (in their highly dehydroxylated form), we adopted clusters having a brutto formula of $H_{10}O_{48+2}Si_{21}Cr$ (see the graphical representation in Figure S2 A and B). The chromium sites can be grafted on the silica surface in various positions. However, it was found that their geometry does not significantly influence the position of the main XANES features. For Cr_2O_3, the geometry of a small cluster (12 Å large) cut from the periodic structure of Cr_2O_3 and terminated with H atoms, was optimized at the same level of theory. In all the cases the computational cost was reduced by employing the ONIOM embedding approach[12] as already shown in our previous work.[4]

High-level calculations were performed by adopting the ωB97xD long-range corrected hybrid functional.[13] H atoms were described through a standard Pople-type 6-311++G(2d,2p) basis set;[14] Cr by an Ahlrichs TZVp (triple zeta valence plus polarization) basis set;[14] Si atoms through LanL2DZ pseudo-potential and the associated basis-set;[15] TZV2p Ahlrichs basis set was adopted to describe O atoms.[14] Low level is defined by employing the B97D functional;[16] H, Cr, and Si atoms are described with a 6-31G(d,p) basis set;[17] 6-31+G(d,p) basis set[18] was employed for O and C atoms. As dealing with open shell species [Cr(II)], the unrestricted formalism was adopted.

The XANES spectra of the Cr^{VI}/SiO_2, Cr^{II}/SiO_2 and Cr_2O_3 models discussed above were simulated using the sped up version of the FDMNES code[19,20] that uses the finite-difference method to solve the Schrödinger equation.[21] The cluster radius included in the calculation process was 5 Å from the Cr absorber. Hedin–Lundquist exchange and correlation potential were applied. XANES absorption spectra were modelled in the dipole and quadrupole approximation. Moreover, self-consistent calculations were performed, i.e. without imposing any restriction to the shape of the potential (i.e. beyond the *muffin-thin* approximation).[22] The theoretical spectra were convoluted by using an arctangent shape of the line broadening. Figure S2 compares the experimental and simulated XANES spectra for Cr^{VI}/SiO_2, Cr^{II}/SiO_2 and Cr_2O_3. The three experimental spectra are very well reproduced by our structural models, demonstrating the reliability of our method.

On the basis of the experimental results obtained with *operando* FT-IR and DR UV-Vis spectroscopies, the XANES spectrum of Cr^{II}/SiO_2 in interaction with methylformate and ethylene was also simulated. In the DFT-optimized cluster the methylformate ligand is arranged with the sp² oxygen of the O=C bond in interaction with the divalent Cr ion (see the graphical representation in Figure S3C). The simulated XANES spectrum (Figure S3, middle) perfectly matches the main features of the experimental one (Figure S3, left), confirming the results obtained with the other spectroscopic techniques.
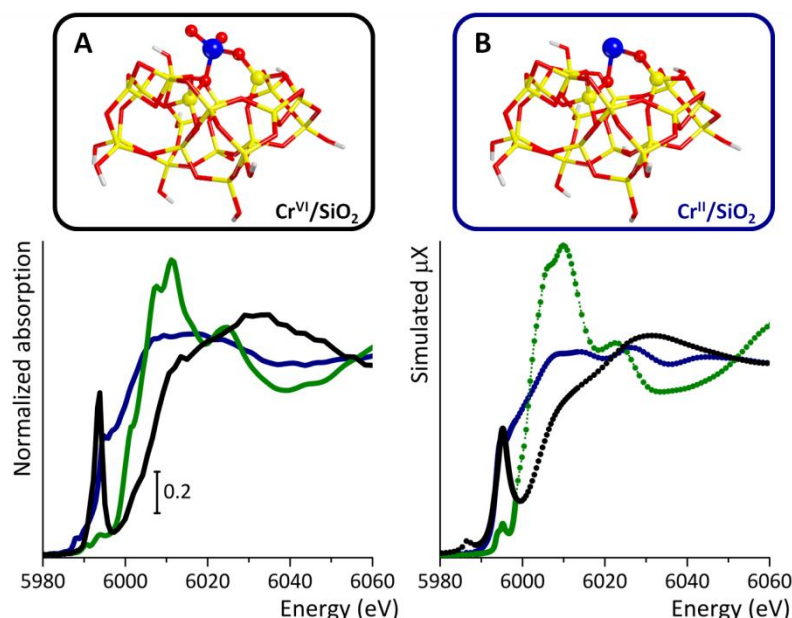
Figure S2: Top: Graphical representation of the clusters adopted to model Cr^{VI}/SiO_2 (A) and Cr^{II}/SiO_2 (B). The color code of the atoms is: white for H, yellow for Si, red for O, blue for Cr. Bottom: Experimental (left) and simulated (right) XANES spectra of Cr^{VI}/SiO_2 (black), Cr^{II}/SiO_2 (blue) and Cr_2O_3 (green).
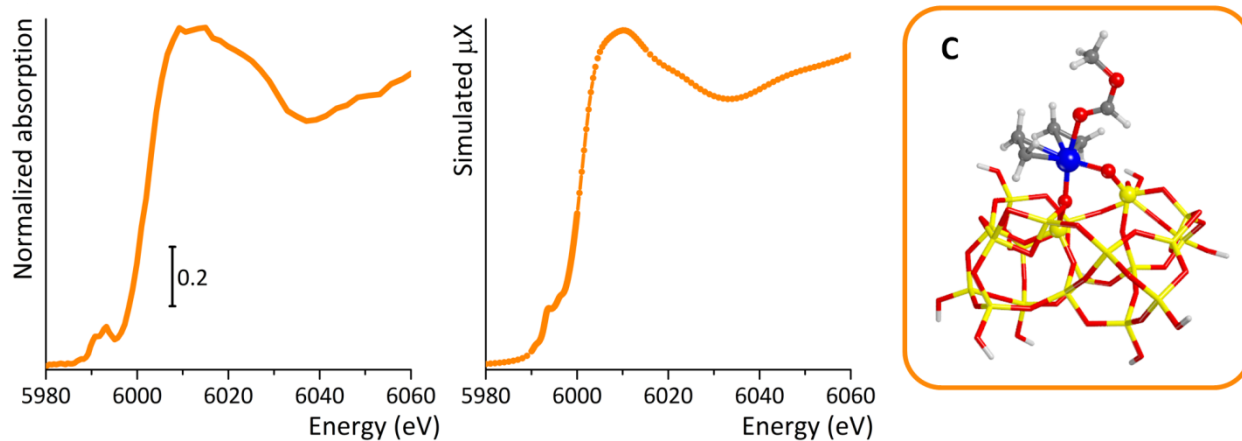
Figure S3: Experimental (left) and simulated (middle) XANES spectra of Cr[VI]/SiO$_2$ reduced in ethylene. Right: Graphical representation of the clusters adopted to model Cr[II]/SiO$_2$ in interaction with two molecules of ethylene and one of methylformate. The color code of the atoms is: white for H, yellow for Si, red for O, blue for Cr.

Last but not least, a remarkable achievement is given from the comparison of the calculated charge of the Cr ion in the mentioned models. The ionic charge is figured out with FDMNES code from the atomic number of the absorber less the number of electrons, which is calculated by integration of the density of electron up to the ionic radius (0.8 Å). In these cases, it is not important to consider the absolute value of ion charge but the relative value in the systems [23,24]: 3.2 in Cr[VI]/SiO$_2$, 2.3 Cr$_2$O$_3$, 1.2 in Cr[II]/SiO$_2$, and 0.9 in Cr[II]/SiO$_2$ in interaction with methylformate. This result strengthens the hypothesis that we detect an intermediate Cr[II] species in interaction with methylformate during the ethylene polymerization.

S3. Characterization of the ethylene oxidation by-products: FT-IR spectroscopy

Figure 3 in the main text (here proposed again for clarity as Figure S4) shows the FT-IR spectra of the Cr^{VI}/SiO_2 catalyst before (black) and after reduction in ethylene at 150 °C and removal of gaseous ethylene (red). The spectrum of Cr^{VI}/SiO_2 is that typical of an highly dehydroxilated silica, with in addition the two fingerprints of grafted chromates at 1980 cm^{-1} and 910 cm^{-1} (the latter in part e). When the catalyst is reduced in ethylene, new absorption bands appear in the 3050-2700 cm^{-1} region (part b, $v(CH_x)$), in the 1750-1500 cm^{-1} range (part d, $v(CO)$ due to the extremely high extinction coefficient, as already discussed in the main text) and in the 1500-1300 cm^{-1} region (part d, $\delta(CH_x)$). The partial reduction of the chromates is testified by the decrease of the two bands at 1980 cm^{-1} and 910 cm^{-1} (parts c –subtracted spectrum - and e, respectively).

The assignment of the IR absorption bands in the 3050-2700 and 1750-1300 cm^{-1} regions is not straightforward. Being two molecules of formaldehyde and a bare Cr^{II} site the most claimed product of ethylene oxidation on the Phillips catalyst during the induction time, efforts were devoted to understand whether these bands might be related to formaldehyde (HCHO) molecules adsorbed on Cr^{II} sites or on SiO_2. To this aim, formaldehyde was dosed at room temperature on a highly dehydroxlated SiO_2 (the same Aerosil used for the synthesis of Cr^{VI}/SiO_2) calcined at the same temperature that Cr^{VI}/SiO_2 (650 °C) and on Cr^{II}/SiO_2. The resulting spectra are shown in Figure S5. It must be noticed that pure formaldehyde is not available because it is highly reactive. Thus we obtained it by the direct decomposition of paraformaldehyde at temperatures higher than 200 °C in vacuum.[25-28] Being also H_2O a side product of paraformaldehyde decomposition, the gas phase was passed through a trap containing anhydrous Na_2SO_4.

Parts A1 and A2 – Formaldehyde adsorbed on dehydroxylated silica

When formaldehyde is dosed on pure SiO_2 (light grey spectrum in Figure S5, A1 and A2) a sharp IR band is observed at 1730 cm^{-1}, which is assigned to the $v(C=O)$ of formaldehyde in interaction with the silica surface. The FT-IR spectra gradually change as a function of time (from light to dark grey). The band at 1730 cm^{-1} decreases in intensity, concomitantly to the growth of a series of IR absorption bands, assigned to polyoxymethylene (Table S1). [26, 28]

Table S1: Position (in wavenumbers, cm^{-1}) and assignment of the absorption bands in the FT-IR spectra of formaldehyde adsorbed on pure silica dehydroxylated at 650 °C.

assignment	Polyoxymethylene on SiO_2	Formaldehyde on SiO_2
$v_{asymm}(CH_2)$	2980	
$v_{symm}(CH_2)$	2915	
$2w(CH_2)$	2797	
$v(CO)$		1730
$\delta(CH_2)$	1478	
$w(CH_2)$	1427	
$w(CH_2)$	1383	
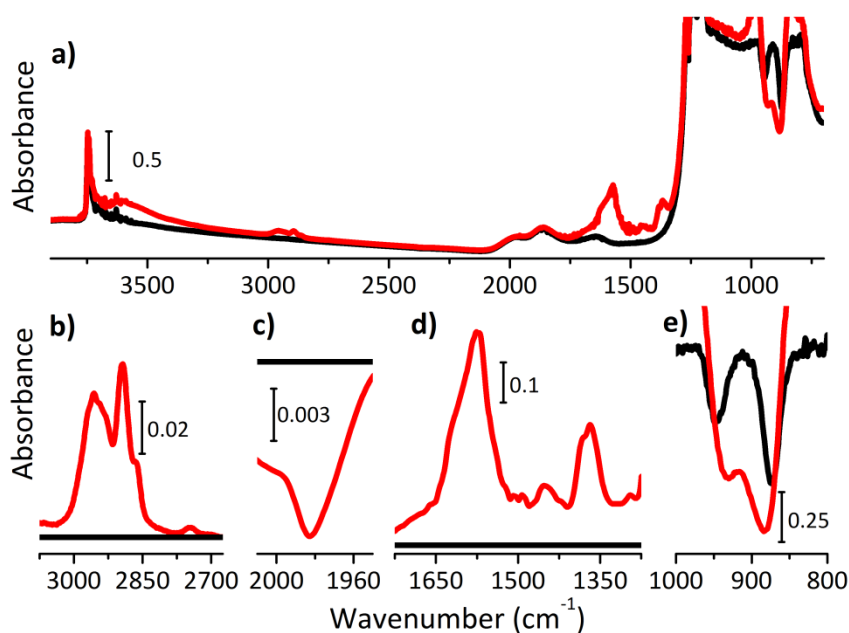
Figure S4: FT-IR spectra of Cr^{VI}/SiO_2 before (black) and after reduction in ethylene at 150 °C (red). Part (a) shows the spectra in the whole 3800–700 cm^{-1} wavenumber region; parts (b) and (d) show magnifications in the spectral regions where the absorption bands characteristic of ethylene oxidation products give a contribution (spectra subtracted from that of Cr^{VI}/SiO_2); part (c) shows the magnification of the region in which the first overtone of the Cr=O mode of the chromate species contributes (subtracted spectra); part (e) reports a magnification of the region where the vibrational modes of silica perturbed by the presence of the chromates are visible.
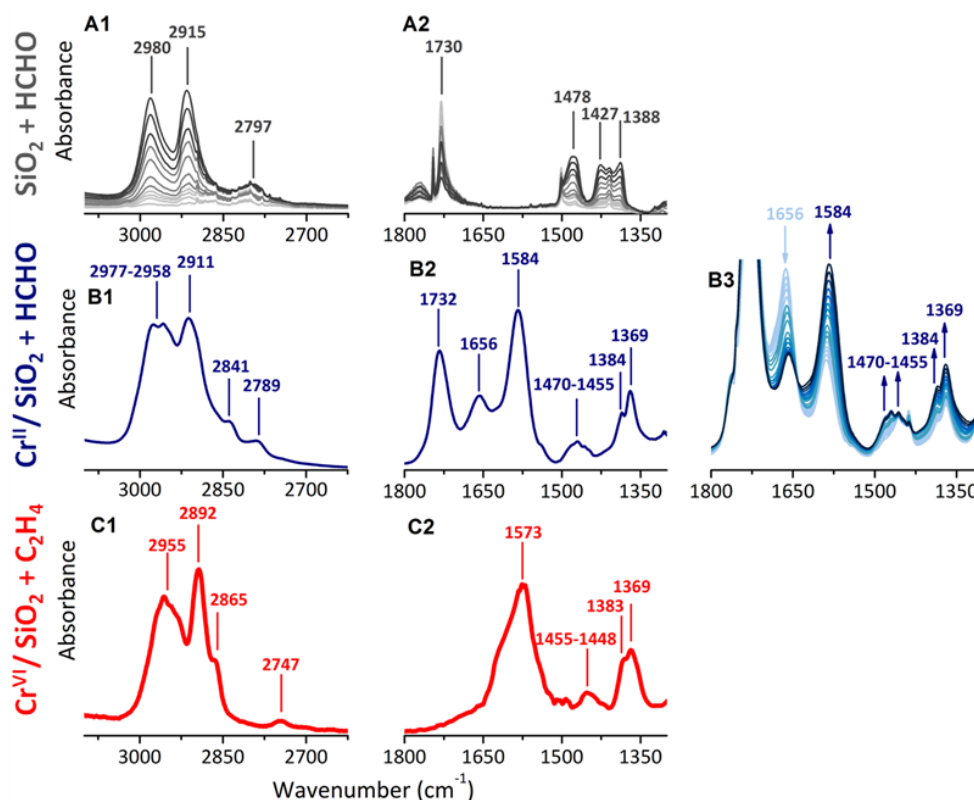
Figure S5: Parts A1 and A2: Time-resolved FT-IR spectra of highly dehydroxylated silica in interaction/reaction with an excess of formaldehyde. Parts B1-B3: FT-IR spectra of Cr^{II}/SiO_2 after reaction with formaldehyde and removal of the excess from the IR cell. The whole sequence of spectra collected during reaction of formaldehyde with Cr^{II}/SiO_2 are shown in part B3 (from light blue to blue). Parts C1 and C2: FT-IR spectra of Cr^{VI}/SiO_2 after reduction in ethylene. Column 1 shows the 3100-2600 cm^{-1} range where $v(CH_x)$ bands are expected, while column 2 shows the 1800-1500 cm^{-1} range, where the bands due to $v(C=O)$, $\delta(CH)$ modes give a contribution.

Table S2: : Position (in wavenumbers, cm^{-1}) and assignment of the absorption bands in the FT-IR spectra of formaldehyde adsorbed on the CO-reduced Cr^{II}/SiO_2 catalyst and of its products of reaction.

assignment	polyoxymethylene	formaldehyde on SiO_2	formaldehyde on Cr^{II}	methylformate on Cr^{II}
$v_{asymm}(CH_2)$	2977			
$v_{asymm}(OCO) + \delta(CH)$				2958
$v_{asymm}(CH_3)$				
$v_{symm}(CH_2)$	2911			
$v_{symm}(CH_3)$				2893 (shoulder)
$v(CH)$				2865 (shoulder)
$v_{symm}(CH_2)$		2841	2841	
$2w(CH_2)$	2789			
$v_{symm}(OCO) + \delta(CH)$				2745
$v(CO)$		1732		
$v(CO)$			1656	
$v_{asymm}(OCO)$				1584
$\delta(CH_2)$	1470			
$\delta(CH_3)$				1455
$\delta(CH_2)$			1455	
$\delta(CH)$				1384
$v_{symm}(OCO)$				1369

When formaldehyde is dosed on Cr^{II}/SiO$_2$, the FT-IR spectra evolve as a function of time (Figure S5 part B3 from light blue to blue) until an equilibrium is reached. The complexity of the spectra is due to the concomitance of the polymerization of formaldehyde on silica and of the reaction/interaction of formaldehyde with the Cr^{II} sites. The IR bands at 1732 and 1656 cm^{-1} have been assigned to the ν(C=O) of formaldehyde in interaction with SiO$_2$ and Cr^{II} sites, respectively. The growth of the IR bands at 1584, 1470, 1455, 1384 and 1369 cm^{-1} and the simultaneous decrease of that at 1656 cm^{-1} testifies that HCHO on the Cr^{II} sites is not stable, but it undergoes a molecular disproportionation leading to products more similar to formate or carboxylate species in which the ν(C=O) vibration is lower than 1600 cm^{-1} due to a weak C=O and C-O resonance. When formaldehyde is removed from the cell the IR band at 1732 cm^{-1} decreases in intensity testifying that the excess of HCHO is partially removed from the silica surface. The multitude of IR bands remaining upon outgassing has been assigned in Table S2 (based on the literature).[26, 29, 30] Moreover, based on our previous work involving the reaction of aldehydes with Cr^{II} species,[31] we have assigned the IR bands at 2958, 2745, 1584, 1455, 1384 and 1369 cm^{-1} to

methylformate generated from the Tishchenko reaction occurring between two molecules of formaldehyde on the Cr^{II} Lewis acid site.

Parts C1 and C2 – Cr^{VI}/SiO$_2$ catalyst reduced by ethylene at 150 °C

The spectrum of the ethylene reduced Cr^{VI}/SiO$_2$ catalyst is characterized by IR bands not easily attributable to formaldehyde in interaction with the catalyst surface or with reduced Cr sites. The vibrational manifestations are similar to those of formates or carboxylates, being the intense IR bands in the ν(CO) region lower than 1600 cm^{-1} (as discussed before). Based on the above assignment, we came to the conclusion that the main product of ethylene oxidation are two molecules of formaldehyde which are immediately converted to one methylformate molecule remaining in interaction with the just reduced Cr^{II} site. The extreme simplicity of the IR spectrum upon ethylene reduction leaves few doubts on the possibility that other products of oxidation, rather than methylformate, remain adsorbed on the catalyst surface. The assignment of all the IR bands is shown in Table 1 in the main text and is proposed again here in Table S3, along with a schematic representation of the reaction occurring during the induction period is shown in Scheme S1.
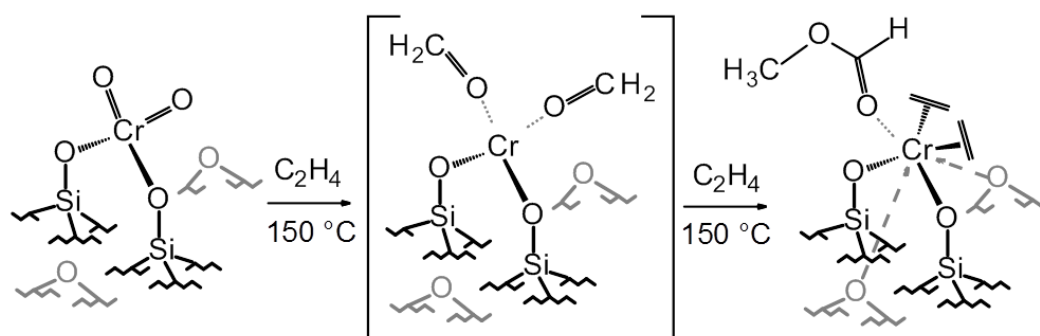
Scheme S1: Possible reaction pathway occurring between Cr^{VI}/SiO$_2$ Phillips catalyst and ethylene at 423 K during the induction period. The reduced Cr site is in interaction with methylformate and results in a Cr^{II} ion 6-fold coordinated.

Table S3: Position (in wavenumbers, cm^{-1}) and relative intensity (vs = very strong, s = strong, m = medium, w = weak) of the IR absorption bands attributed to ethylene oxidation products in interaction with the ethylene reduced Cr^{VI}/SiO$_2$ catalyst

Assignment	Methylformate on Cr^{II}
ν_{asymm}(OCO) + δ(CH) $\Big\}$	2955 (s)
ν_{asymm}(CH$_3$)	
ν_{symm}(CH$_3$)	2892 (s)
ν(CH)	2865 (s)
ν_{symm}(OCO) + δ(CH)	2747 (w)
ν_{asymm}(OCO)	1617, 1573 (vs)
δ(CH$_3$)	1455 (m)
δ(CH)	1383 (s)
ν_{symm}(OCO)	1369 (vs)

S4. Application of Multivariate Curve Resolution – Alterning Least Squares (MCR-ALS) on the XANES spectra

Multivariate Curve Resolution - Alterning Least Squares (MCR-ALS) is a powerful chemometric algorithm that permits to decompose an experimental set of spectra into pure contributions, allowing to deriving the concentration profiles and the corresponding pure spectra of different species contributing to the experimental signals. Herein we applied the MCR-ALS algorithms in MATLAB, as described in Joaquim Jaumot *et al.*[32] Practically, it is recommended to introduce a set of constraints in order to suppress the ambiguity related to the algorithm solutions.[33] In this case, we imposed that the concentrations and the spectra of the pure components must be positive. Starting from this statement we run the PCA on the series of XANES spectra shown in Figure 1a in the main text. The analysis gave three main components, which their plot reconstruction with MCR-ALS is shown in Figure S6.

i) **Component 1**: the spectrum is the same as that of Cr^{VI}/SiO_2. We assign this component to monochromates.

ii) **Component 2**: the spectrum is similar to that collected at the end of the reaction (i.e. that of Cr^{VI}/SiO_2 after ethylene polymerization) and to the simulated XANES spectrum of cluster C in Figure S4. Consequently, this component is assigned to Cr^{II} in interaction with methylformate, which is the species active in ethylene polymerization.

iii) **Component 3**: this components is similar to Component 2 in terms of edge position and white line contribution, while it differs in terms of pre-edge features. This spectrum is assigned to the Cr species defined from the UV-Vis measurements as the spectator ones.
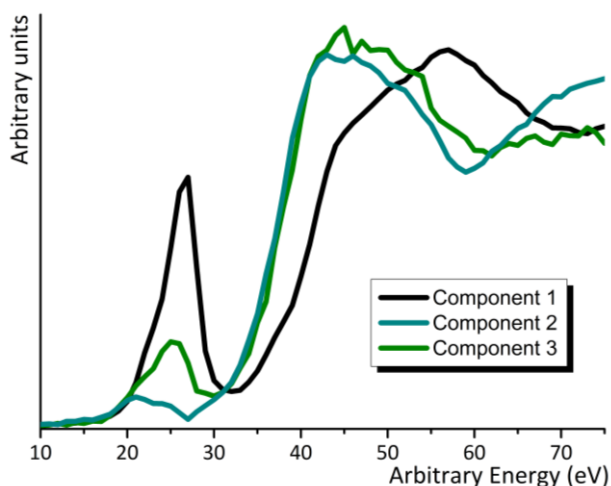
Figure S6: Principal Components resulting from the MCR-ALS

Figure S7 shows the evolution of the three Components during time (same color code). The same results are shown in the main text in Figure 2 (dashed curves). Component 1, assigned to the Cr^{VI} monochromate species, is the only present at the

beginning and slowly decreases in concentration during the reaction. Component 2, assigned to the reduced active sites, keeps on growing in concentration, while Component 3, assigned to the reduced Cr sites acting as spectators, reaches a plateaux.
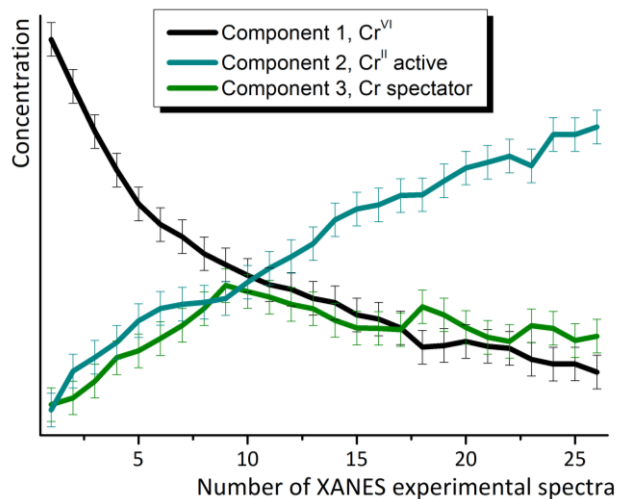
Figure S7: Evolution of Principal Component concentrations during time (the x-axis shows the number of spectra, each one collected in 12 minutes). The error bar is also introduced.

References

[1] E. Groppo, C. Lamberti, S. Bordiga, G. Spoto, A. Zecchina, *Chem. Rev.* **2005**, *105*, 115.

[2] E. Groppo, K. Seenivasan, C. Barzan, *Catal. Sci. Technol.* **2013**, *3*, 858.

[3] A. Budnyk, A. Damin, C. Barzan, E. Groppo, C. Lamberti, S. Bordiga, A. Zecchina, *J. Catal.* **2013**, *308*, 319.

[4] A. Budnyk, A. Damin, E. Groppo, A. Zecchina, S. Bordiga, *J. Catal.* **2015**, *324*, 79.

[5] B. M. Weckhuysen, L. M. Deridder, R. A. Schoonheydt, *J. Phys. Chem.* **1993**, *97*, 4756.

[6] B. M. Weckhuysen, I. E. Wachs, R. A. Schoonheydt, *Chem. Rev.* **1996**, *96*, 3327.

[7] A. Zecchina, E. Garrone, G. Ghiotti, C. Morterra, E. Borello, *J. Phys. Chem.* **1975**, *79*, 966.

[8] M. Cieslak-Golonka, *Coordin. Chem. Rev.* **1991**, *109*, 223.

[9] B. N. Figgis, *Introduction to ligand fields*, John Wiley & Sons, New York, **1966**.

[10] J. Sauer, P. Ugliengo, E. Garrone, V. R. Saunders, *Chem. Rev.* **1994**, *94*, 2095.

[11] M. J. Frisch, G. W. Trucks, H. B. Schlegel, G. E. Scuseria, M. A. Robb, J. R. Cheeseman, J. Montgomery, J. A., T. Vreven, K. N. Kudin, J. C. Burant, J. M. Millam, S. S. Iyengar, J. Tomasi, V. Barone, B. Mennucci, M. Cossi, G. Scalmani, N. Rega, G. A. Petersson, H. Nakatsuji, M. Hada, M. Ehara, K. Toyota, R. Fukuda, J. Hasegawa, M. Ishida, T. Nakajima, Y. Honda, O. Kitao, H. Nakai, M. Klene, X. Li, J. E. Knox, H. P. Hratchian, J. B. Cross, V. Bakken, C. Adamo, J. Jaramillo, R. Gomperts, R. E. Stratmann, O. Yazyev, A. J. Austin, R. Cammi, C. Pomelli, J. W. Ochterski, P. Y. Ayala, K. Morokuma, G. A. Voth, P. Salvador, J. J. Dannenberg, V. G. Zakrzewski, S. Dapprich, A. D. Daniels, M. C. Strain, O. Farkas, D. K. Malick, A. D. Rabuck, K. Raghavachari, J. B. Foresman, J. V. Ortiz, Q. Cui, A. G. Baboul, S. Clifford, J. Cioslowski, B. B. Stefanov, G. Liu, A. Liashenko, P. Piskorz, I. Komaromi, R. L. Martin, D. J. Fox, T. Keith, M. A. Al-Laham, C. Y. Peng, A. Nanayakkara, M. Challacombe, P. M. W. Gill, B. Johnson, W. Chen, M. W. Wong, C. Gonzalez, J. A. Pople, Revision B.05 ed., Gaussian, Inc., Wallingford CT, **2004**.

[12] S. Dapprich, I. Komaromi, K. S. Byun, K. Morokuma, M. J. Frisch, *J. Mol. Struct.-THEOCHEM* **1999**, *461*, 1.

[13] J.-D. Chai, M. Head-Gordon, *Phys. Chem. Chem. Phys.* **2008**, *10*, 6615.

[14] P. C. Hariharan, J. A. Pople, *Theor. Chim. Acta* **1973**, *28*, 213.

[15] J. P. Hay, W. R. Wadt, *J. Chem. Phys.* **1985**, *82*, 270.

[16] S. Grimme, *J. Comput. Chem.* **2006**, *27*, 1787.

[17] R. Ditchfield, W. J. Hehre, J. A. Pople, *J. Chem. Phys.* **1971**, *54*, 724.

[18] W. J. Hehre, R. Ditchfield, J. A. Pople, *J. Chem. Phys.* **1972**, *56*, 2257.

[19] S. A. Guda, A. A. Guda, M. A. Soldatov, K. A. Lomachenko, A. L. Bugaev, C. Lamberti, W. Gawelda, C. Bressler, G. Smolentsev, A. V. Soldatov, Y. Joly, *J. Chem. Theory Comput.* **2015**, *11*, 4512.

[20] A. A. Guda, S. A. Guda, M. A. Soldatov, K. A. Lomachenko, A. L. Bugaev, C. Lamberti, W. Gawelda, C. Bressler, G. Smolentsev, A. V. Soldatov, Y. Joly, *J. Phys.: Conf. Ser.* **2016**, *712*, Article N. 012004.

[21] Y. Joly, *Phys. Rev. B* **2001**, *63*, art. no. 125120.

[22] O. Bunau, Y. Joly, *J. Phys.-Condes. Matter* **2009**, *21*.

[23] G. Aullón, S. Alvarez, *Theor. Chem. Acc.*, **2009**, *123*, 67.

[24] F. Jensen, Introduction to Computational Chemistry, ISBN-13: 978-0-470-01186-7

[25] G. Busca, V. Lorenzelli, *J. Catal.* **1980**, *66*, 155.

[26] G. Busca, J. Lamotte, J. C. Lavalley, V. Lorenzelli, *J. Am. Chem. Soc.* **1987**, *109*, 5197.

[27] J. C. Lavalley, J. Lamotte, G. Busca, V. Lorenzelli, *J. Chem. Soc., Chem. Commun.* **1985**, 1006.

[28] F. Xamena, C. O. Arean, S. Spera, E. Merlo, A. Zecchina, *Catal. Lett.* **2004**, *95*, 51.

[29] J. F. Edwards, G. L. Schrader, *J. Phys. Chem.* **1985**, *89*, 782.

[30] V. Crocella, G. Cerrato, G. Magnacca, C. Morterra, F. Cavani, L. Maselli, S. Passeri, *Dalt. Trans.* **2010**, *39*, 8527.

[31] C. Barzan, A. A. Damin, A. Budnyk, A. Zecchina, S. Bordiga, E. Groppo, *J. Catal.* **2016**, *337*, 45.

[32] J. Jaumot, R. Gargallo, A. de Juan, R. Tauler, *Chemometr. Intell. Lab.* **2005**, *76*, 101.

[33] K. A. Lomachenko, E. Borfecchia, C. Negri, G. Berlier, C. Lamberti, P. Beato, H. Falsig, S. Bordiga, *J. Am. Chem. Soc.* **2016**, *138*, 12025.

Tracking the reasons for the peculiarity of Cr/Al$_2$O$_3$ catalyst in ethylene polymerization

Giorgia A. Martino [a], Caterina Barzan [a], Alessandro Piovano [a], Andriy Budnyk [a,b], Elena Groppo [a,*]

[a] University of Torino, Department of Chemistry, NIS Centre and INSTM, Via G. Quarello 15A, I10135, Italy
[b] Southern Federal University, International Research Center "Smart Materials", Zorge 5, Rostov-on-Don 344000, Russia

ARTICLE INFO

ABSTRACT

Looking to the past, heading to the future. In this contribution we explain the reasons why the Cr/Al$_2$O$_3$ Phillips catalysts exhibit a faster kinetics profile in ethylene polymerization reaction with respect to Cr/SiO$_2$. Diffuse reflectance UV–Vis and FT-IR spectroscopies unequivocally demonstrate that, albeit several types of reduced Cr sites are stabilized by the Al$_2$O$_3$ support, only the 4-fold coordinated Cr^{2+} sites are active precursors in ethylene polymerization, as for Cr^{2+}/SiO$_2$. Nevertheless, kinetic experiments indicate that ethylene polymerization is 15 times faster on CO-reduced Cr/Al$_2$O$_3$ than on CO-reduced Cr/SiO$_2$. The difference is even more striking (two order of magnitude) when the reaction rates per active Cr sites are compared. Our experimental results suggest two reasons behind the faster polymerization kinetic of Cr/Al$_2$O$_3$: (1) the higher ionic character of the Cr—O—Al bond with respect to the Cr—O—Si one; (2) the nature of the ancillary ligands in the coordination sphere of the Cr active sites (which are mainly carbonates for CO-reduced Cr/Al$_2$O$_3$ and siloxane bridges for CO-reduced Cr/SiO$_2$).

© 2017 Elsevier Inc. All rights reserved.

1. Introduction

The Cr-based Phillips catalyst is among the most important heterogeneous catalysts for ethylene polymerization. It accounts for about 50% of the high density polyethylene (HDPE) world's demand, owning also a large share of linear low density polyethylene (LLDPE) market [1–3]. Generally speaking, the active phase is constituted by a highly dispersed chromium oxide supported on a high surface area material [4]. Porous silica has been traditionally employed, due to its tendency to fragment during the polymer growing. The smaller silica fragments generated in this process provide new chromium sites accessible for ethylene polymerization. Besides silica, almost all the high surface area oxides have been tested as supports, and some of them also found practical applications [5–9]. In this context, also alumina (Al$_2$O$_3$) was tested, but the resulting Cr/Al$_2$O$_3$ catalyst was left aside due to its tendency to fast deactivation, providing only 10–20% of the polymerization activity of Cr/SiO$_2$. Noticeably, alumina does not fulfil the fragility, porosity and high surface area standards required for boosting polymerization. Nevertheless, the Cr/Al$_2$O$_3$ catalysts do show some unique features compared to Cr/SiO$_2$, that could make them extremely appealing [5]: (1) a much faster kinetic profile (i.e.

rapid development of polymerization upon ethylene addition); (2) a lower tendency to β-hydride elimination (the polyethylene produced in the absence of H$_2$ has an extremely high molecular weight, approaching the ultra-high classification); (3) an unusual tendency to distribute the branching evenly throughout the molecular weight distribution (nearly all the physical properties of the polymer are improved); (4) a much higher H$_2$ sensitivity as chain transfer agent (which implies the possibility of controlling the molecular weight distribution). The reasons behind these peculiar features must be searched in the molecular structure of the Cr sites.

The singular properties of Cr/Al$_2$O$_3$ stimulated us to carry out a complete spectroscopic investigation at a molecular level of the Cr sites, aimed at tracking the reasons behind the unusual features of Cr/Al$_2$O$_3$ in ethylene polymerization. The literature on the spectroscopic properties of Cr^{6+}/Al$_2$O$_3$ is wide, since this is one of the most used catalysts for propene dehydrogenation [10–25]. Opposite to the case of Cr^{6+}/SiO$_2$, for which the aggregation state and the structure of the grafted Cr^{6+} sites is still debated [5,7–9,20,22–24,26–35], there is a general consensus on that Cr^{6+} on Al$_2$O$_3$ exists primarily as (tetrahedrally coordinated) monochromate species [9,10,19–24]. Much less was done on reduced Cr/Al$_2$O$_3$, and the reference works remain those of Weckhuysen et al. dating back to the middle of 1990s [9,10,19–24]. More recently, Airaksinen et al. [25] studied the reduction of alumina-supported chromia containing 13 wt%

chromium, by X-ray photoelectron and absorption spectroscopies, in situ temperature-programmed Raman and Diffuse Reflectance FT-IR spectroscopies, combined with mass spectrometry. According to these seminal works, after reduction by carbon monoxide or hydrogen mainly Cr^{3+} is formed, although the formation of Cr^{2+} in carbon monoxide reduction was also observed. In the last years spectroscopic methods have progressed enormously. For this reason, it is timely a systematic spectroscopic investigation on reduced Cr/Al_2O_3 catalysts, with the specific purpose to determine the structure of the reduced Cr sites and to correlate it with its unusual behaviour in ethylene polymerization with respect to Cr/SiO_2. Both H_2 and CO have been used as reducing agents as indicated by the literature [5]. Transmission FT-IR and Diffuse Reflectance UV–Vis-NIR spectroscopies coupled with molecular probes have been employed to confirm the presence of different Cr reduced species at the catalyst surface and to clarify which are those involved in the ethylene polymerization reaction.

2. Experimental section

2.1. Materials

The alumina-supported Phillips catalysts were prepared by wet-impregnation, using as a support a transition-Al_2O_3 (Aeroxide Alu C, Evonik-Degussa) characterized by a specific surface area of 100 m^2/g, and CrO_3 (Sigma-Aldrich) as Cr precursor, according to the procedure already adopted for the synthesis of Cr/SiO_2 [8]. Two Cr/Al_2O_3 samples differing in the Cr loading (1 wt% and 0.5 wt%, hereafter referred to as $0.5Cr/Al_2O_3$ and $1.0Cr/Al_2O_3$, respectively) were prepared: the former was used for the FT-IR measurement and the latter for DR-UV–Vis-NIR and kinetics experiments. The choice was done to optimize the spectral quality. Cross-checking experiments demonstrated that the spectroscopic properties are the same irrespective of the Cr loading, as already demonstrated in the past for the similar Cr/SiO_2 catalyst [8].

The catalysts were activated directly inside the measurement cells, that can be connected to a vacuum line allowing activations and gas dosages. The activation procedure was very similar to that well optimized for Cr/SiO_2 catalysts [8]. Briefly, the main steps are: (i) degassing in dynamic vacuum at increasing temperature up to 650 °C to dehydroxylate the alumina surface; (ii) oxidation at the same temperature in the presence of O_2, resulting in the grafting of the Cr species at the alumina surface; (iii) reduction in the presence of CO or H_2 at 350 °C, followed by removal of the gaseous phase at the same temperature; (iv) cooling down at room temperature. For probing the accessible Cr sites, CO was dosed at room temperature (equilibrium pressure P_{CO} = 100 mbar), followed by step-by-step expansions. The kinetics of ethylene polymerization was studied by sending 200 mbar of ethylene at room temperature over 0.5 g of catalyst inside a quartz reactor of known volume, and recording the ethylene pressure as a function of time. Similar experiments were repeated for the catalyst inside the FT-IR and DR UV–Vis cells, collecting the spectra as a function of time.

2.2. Methods

Transmission FT-IR spectra were collected at 2 cm^{-1} resolution with a Bruker Vertex70 instrument equipped with a MCT detector. The experiments were performed in situ and in controlled atmosphere within a quartz cell equipped with two KBr windows, allowing performing thermal treatments and measurements in the presence of gases. The FT-IR spectra were normalized to the optical thickness of the pellet.

Diffuse reflectance (DR) UV–Vis-NIR spectra were collected using a Varian Cary5000 spectrophotometer with a diffuse reflec-

tance accessory. The samples were measured in the powder form, inside a cell made of optical quartz, allowing performing thermal treatments and measurements in the presence of gases. The reflectance (%R) signal was later converted into Kubelka-Munk values.

3. Results and discussion

3.1. The role of CO and H_2 as reducing agents for Cr^{6+}/Al_2O_3

The spectroscopic properties of Cr^{6+} on Al_2O_3 are well known in the specialized literature. While for Cr^{6+} on SiO_2 there is still a debate on the aggregation state of the Cr^{6+} species (both mono- and dichromates have been proposed [5,7–9,20,22–24,26,34,35], or even mono-oxo CrO_5 [27–33]), Cr^{6+} exist primarily as monochromate species on Al_2O_3 [9,10,19–24] (the corresponding DR UV–Vis-NIR spectrum is shown in Fig. S1a). Temperature-programmed reduction measurements have demonstrated that Cr^{6+} on Al_2O_3 are more reducible than Cr^{6+} on SiO_2 (i.e. their reduction is achieved at lower temperature), both in CO and in H_2 [5,36]. DR UV–Vis-NIR spectroscopy has been traditionally used to determine the final valence state of the reduced Cr sites in Cr/Al_2O_3, Cr/SiO_2 and variant thereof [8–10,19–24,36–40]. Although DR UV–Vis-NIR is often disused in favour of other methods (such as XANES or EPR), it remains one of the techniques most informative on the electronic properties of heterogeneous catalysts. In the specific case of Cr^{n+} sites on inorganic support, the literature on the topic is well assessed. DR UV–Vis-NIR spectroscopy has been used since the early 1990s not only to discriminate among various oxidation states and coordination geometries, but also to quantify the amount of each species as a function of the sample composition and treatment. For this reason, we started our investigation by collecting the DR UV–Vis-NIR spectra of Cr/Al_2O_3 reduced in CO and in H_2 at 350 °C (Fig. 1, spectra 1 and 1′, respectively).

The DR UV–Vis-NIR spectra demonstrate that in the adopted experimental conditions most of the Cr^{6+} species have been reduced in both cases. Indeed, the intense charge-transfer band at 27000 cm^{-1} characteristic of mono-chromates [9,10,19–24,41] is no longer observed. Both spectra are dominated by an intense band centred at 39000 cm^{-1}, which is straightforwardly assigned to an oxygen to chromium (O → Cr) charge transfer transition [9,10,19–24,42,43]. In the low wavenumbers region, a multitude of bands are observed and assigned to d-d transitions of several types of reduced Cr sites, differing in the oxidation state and coordination geometry. In particular, a very broad envelop of d-d bands is observed in the spectrum of the CO-reduced catalyst, while that of the H_2-reduced catalyst displays more defined bands centred at 26,000, 16,000 and 10,500 cm^{-1}. The presence of a multitude of d-d bands suggests a larger heterogeneity of reduced Cr sites with respect of those obtained on Cr/SiO_2 systems [8], comprising both +3 and +2 oxidation states and different coordination geometries. It is worth noticing that the spectrum of the CO-reduced catalyst is comparable to those previously reported by Weckhuysen et al. for similar systems [9,10,19–24], which are unanimously considered as the reference spectra in this field.

The assignment of the d-d bands is straightforward on the basis of the specialized literature [9,10,19–24]. The UV–Vis spectra of 6-fold coordinated Cr^{3+} species (Cr_{6c}^{3+}) are expected to show two equally intense d-d bands centred at around 17,000 cm^{-1} ($^4A_{2g} \rightarrow ^4T_{2g}$ transition) and 25,000 cm^{-1} ($^4A_{2g} \rightarrow ^4T_{1g}$ transition) and a third one, rather weak, at 37,000 cm^{-1} (which is however always masked by the intense charge-transfer band at high energy) [20,23,44]. On the other hand, the spectra of undistorted 6-fold coordinated Cr^{2+} ions (Cr_{6c}^{2+}) in high-spin $3d^4$ complexes are known to show a single d-d band centred between ca. 10,000 and 20,000 cm^{-1}, which is ascribed to the $^5E_g \rightarrow ^5T_{2g}$ transition [44]. For example, the hexa-
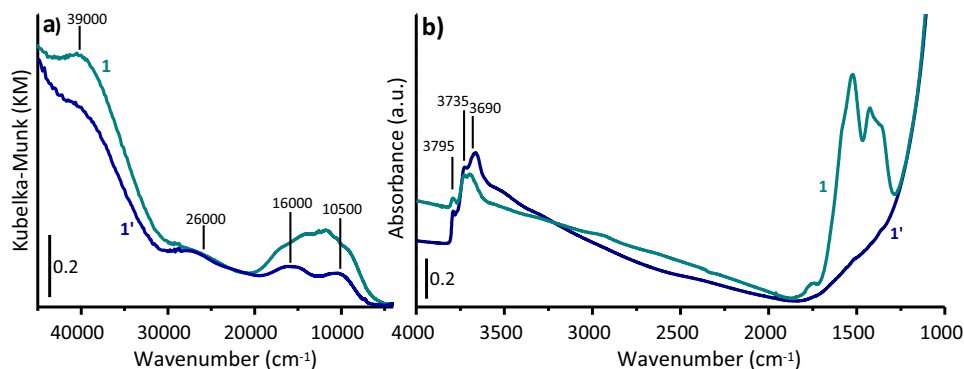
Fig. 1. Part (a) DR UV–Vis-NIR of the 0.5Cr/Al$_2$O$_3$ catalyst reduced in CO at 350 °C (curves 1) and in H$_2$ at 350 °C (curves 1′). Part b) FT-IR spectra of the 1.0Cr/Al$_2$O$_3$ catalyst reduced in CO at 350 °C (curves 1) and in H$_2$ at 350 °C (curves 1′). The FT-IR spectra are normalized to the thickness of the pellet.

aquo Cr^{2+}(H$_2$O)$_6$ complex shows a single transition around ca. 14000 cm^{-1} [44]. The DR UV–Vis-NIR spectra of the two reduced Cr/Al$_2$O$_3$ catalysts are characterized by bands around 26000 and 16000 cm^{-1}, which are compatible with the presence of both Cr$_{6c}^{3+}$ and Cr$_{6c}^{2+}$ species. However, in both cases an additional d-d band is observed around 10500 cm^{-1}, that univocally demonstrates the presence of Cr^{2+} species in a lower symmetry. Indeed, bands at wavenumbers as low as 10,000 cm^{-1} have been reported since 1960s for several distorted tetrahedral complexes of Cr^{2+} [45–47], and are commonly observed in the UV–Vis spectra of the CO-reduced Cr/SiO$_2$ catalysts, where 4-fold (pseudo-tetrahedral) coordinated Cr^{2+} sites (Cr$_{4c}^{2+}$) are cleanly and selectively obtained.

On these basis, the DR UV–Vis-NIR spectra in Fig. 1 allow concluding that the reduction of Cr^{6+}/Al$_2$O$_3$ catalyst leads to the formation of at least three types of reduced chromium sites, differing in the oxidation state and coordination geometry, in close agreement with the seminal works of Weckhuysen et al. [9,10,19–24]. The relative concentration of the Cr$_{4c}^{2+}$, Cr$_{6c}^{2+}$ and Cr$_{6c}^{3+}$ sites is a function of the reduction conditions and can be roughly estimated by deconvolving the DR UV–Vis-NIR spectra in the d-d region with four Gaussian curves centred at ca. 10500, 14000, 16,000 and 26,000 cm^{-1} (Fig. S2), and considering that the molar extinction coefficient of spin-allowed/Laporte partially allowed (by p-d mixing) transitions (as for tetrahedral complexes) is usually ten times larger than that of spin-allowed/Laporte forbidden transitions (as for octahedral complexes) [44,48]. We found that reduction in H$_2$ at 350 °C leads to the preferential formation of Cr$_{6c}^{3+}$ sites (ca. 98%), with a small amount of Cr$_{4c}^{2+}$ species (ca. 2%). Whereas reduction in CO at the same temperature leads to a larger heterogeneity of sites, with Cr$_{6c}^{3+}$, Cr$_{6c}^{2+}$, Cr$_{4c}^{2+}$ sites accounting for about 70%, 22% and 8% of the total, respectively.

The preferential formation of Cr$_{6c}^{3+}$ species differentiates Cr/Al$_2$O$_3$ from Cr/SiO$_2$, where mainly Cr$_{4c}^{2+}$ species are formed upon reduction in CO and only a small amount of Cr$_{6c}^{3+}$ species are obtained after reduction in H$_2$ [8,33,49]. This difference has been explained by Weckhuysen et al. [23] considering the different "hardness" of the two supports, where a harder support – according to the definition first introduced by Pearson [50] – means that it is less susceptible to electron fluctuations [51]. Silica is "softer" and this facilitates the reduction of Cr^{6+} in Cr^{2+}, whereas alumina is "harder" and retards the reduction (leading to Cr^{3+} formation) [9]. Moreover, the so formed Cr^{3+} species are quite stable on the alumina surface because of the similarity in size and charge with Al^{3+} (r(Cr$_{Oh}^{3+}$) = 0.615 Å and r(Al$_{Oh}^{3+}$) = 0.53 Å) [52], that makes relatively easy to diffuse into vacant octahedral Al^{3+} sites. The Cr^{3+} sites occupying the octahedral interstices in the Al$_2$O$_3$ lattice are clearly not accessible to incoming molecules. A similar structure is believed for Cr$_{6c}^{2+}$, whose formation implies a slight distortion of the crystalline struc-

ture because of the bigger dimension of the Cr^{2+} ions. On the other hand, the 4-fold coordinated Cr^{2+} sites stay on the surface, covalently bonded to the alumina through two oxygen atoms and with two other additional weaker ligands in the coordination sphere, in analogy to the Cr/SiO$_2$ catalyst.

The FT-IR spectra of the reduced Cr/Al$_2$O$_3$ catalysts (Fig. 1b) are dominated by the intense (and out of scale) absorption due to the vibrational modes of the framework (below 1200 cm^{-1}) and by several weak absorption bands in the 3800–3500 cm^{-1} region (with maxima at 3795, 3735, 3690 cm^{-1}), due to the ν(OH) modes of various surface OH groups. The large amount of surface OH groups characterized by a slightly different acidity [53–61] in contrast with the presence of isolated, well-defined, silanol groups at the SiO$_2$ surface, is a direct consequence of the Lewis acidity of Al$_2$O$_3$ [53,54]. The higher intensity of the ν(OH) bands in the spectrum of the H$_2$-reduced catalyst indicates a larger amount of OH species. This was already reported in the literature [25] and is expected, since the by-product of chromates reduction is water that, at 350 °C, partially re-hydrates the silica surface. On the other side, the spectrum of the CO-reduced catalyst shows a series of broad absorption bands in the 1800–1100 cm^{-1} region which have been attributed in the specialized literature to pseudo-carbonate species [25,55,62–65]. The presence of these species is a direct consequence of the tendency of some metal oxides (including alumina) to reactively adsorb CO$_2$ on their basic surface sites with the consequent formation of different kinds of carbonates [66]. In the present case, CO$_2$ is produced in situ during the reduction of the chromate species in CO at 350 °C. This is observed also for reduction of Cr^{6+}/SiO$_2$ in CO [65,67], although the absence of basic sites at the silica surface allows for a complete removal of CO$_2$ at the reduction temperature [8]. Interestingly, a small amount of surface carbonates are also formed when pure Al$_2$O$_3$ is treated in the same conditions (Fig. S2), indicating that a surface reduction occurs at some extent, although alumina is usually considered a not reducible metal-oxide. The process likely involves the formation of oxygen vacancies on a few defective sites.

3.2. Accessibility of the reduced Cr sites

The abundant literature on Cr/SiO$_2$ catalysts demonstrates that CO is an excellent molecular probe for reduced chromium species [8,9,68]. Fig. 2 shows the evolution of the DR UV–Vis-NIR and FT-IR spectra of CO- and H$_2$-reduced Cr/Al$_2$O$_3$ catalysts as a function of the CO coverage at room temperature. The DR UV–Vis-NIR spectra of both catalysts change in the presence of CO (spectra 2 and 2′ in Fig. 2a, c) mainly in the d-d region. In particular, the absorption bands attributed to Cr$_{4c}^{2+}$ originally at around 10,000 cm^{-1} drastically decreases in intensity, while simultaneously a new band appears
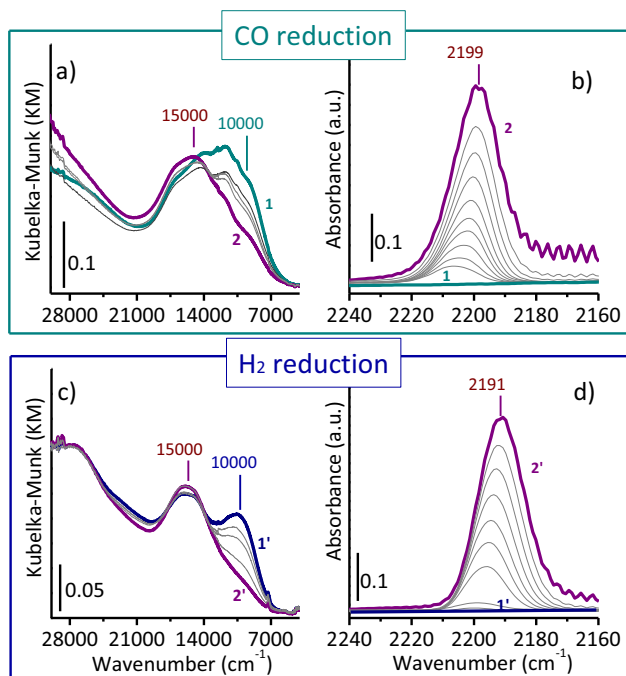
Fig. 2. Part (a) DR UV–Vis-NIR spectra in the d-d region of the CO-reduced 0.5Cr/Al$_2$O$_3$ catalyst (spectrum 1), and of the same sample in the presence of CO (P$_{CO}$ = 100 mbar) at room temperature (spectrum 2). Grey spectra show the effect of gradual CO desorption at room temperature. Part (b) Evolution of the FT-IR spectra (magnification of the ν(CO) region) upon CO adsorption at room temperature on the CO-reduced 1.0Cr/Al$_2$O$_3$ catalyst as a function of P$_{CO}$ coverage, from P$_{CO}$ = 100 mbar (spectrum 2) to zero (spectrum 1). Parts (b) and (d): as part (a) and (c) for H$_2$-reduced 0.5Cr/Al$_2$O$_3$ and 1.0Cr/Al$_2$O$_3$, respectively.

around 15,000 cm^{-1} typical of Cr$_{6c}^{2+}$ species. The phenomenon is more evident when looking to the difference spectra (Fig. S4). The presence of an isosbestic point at ca. 13,000 cm^{-1} indicates that the Cr$_{4c}^{2+}$ species are converted into Cr$_{6c}^{2+}$ species, due to CO coordination [8]. The weaker intensity of the newly formed band is in agreement with the expected lower extinction coefficient for transitions involving 6-fold coordinated sites [44]. Upon degassing CO, the original spectra are restored, indicating that CO adsorption on Cr$_{4c}^{2+}$ sites is a reversible process. On the other hand, the bands attributed to Cr$_{6c}^{3+}$ and Cr$_{6c}^{2+}$ sites are not influenced by the presence of CO, unequivocally demonstrating that these sites are mostly inaccessible to the CO molecule, as expected since their coordination sphere is fully occupied. Supplementary experiments of re-oxidation in the presence of O$_2$ (Fig. S5) verified that all the reduced Cr sites are re-oxidized to Cr^{6+}, thus excluding that Cr$_{6c}^{3+}$ and Cr$_{6c}^{2+}$ are completely buried in the Al$_2$O$_3$ lattice. It is worth noticing that the spectroscopic behaviour is the same whether or not carbonates are present at the catalyst surface.

Fig. 2b, d show the FT-IR spectra, in the ν(CO) region, of CO adsorbed on the two catalysts as a function of the CO coverage. At the maximum coverage, the spectra are dominated by an intense and quite broad absorption band, centred at 2199 cm^{-1} for CO-reduced Cr/Al$_2$O$_3$ and at 2191 cm^{-1} for H$_2$-reduced Cr/Al$_2$O$_3$. The observation of a single (although broad) absorption band for all the CO coverage indicates the formation of mono-carbonyl Cr complexes. This differentiates again reduced Cr/Al$_2$O$_3$ from Cr^{2+}/SiO$_2$, where a fraction of very low-coordinated Cr^{2+} sites are able to adsorb up to two CO molecules in the same experimental conditions [8]. In principle, both Cr^{n+} and surface Al^{3+} sites could be available for CO adsorption. CO adsorbed on unsaturated Al^{3+} sites has been reported to contribute in this wavenumber region, but with very weak bands at room temperature [55,69],

opposite to what observed herein. Hence, both bands observed in Fig. 2b, d are ascribed to mono-carbonyl adducts formed on reduced Cr sites. The shift of the ν(CO) bands at higher frequencies upon decreasing the CO coverage, observed in both cases, reveals the occurrence of inter-molecular interactions between CO molecules adsorbed nearby. This phenomenon is typically observed on ordered surfaces [68–71]. In the present case, it might reflect the proximity of several available adsorption sites for CO, comprising not only the reduced Cr sites, where CO is strongly bonded, but also the unsaturated Al^{3+} sites.

The position of both bands indicates that the interaction of CO with the reduced Cr sites is dominated by σ-donation/polarization effects, while π-back donation is negligible. Similar "non classic" carbonyls are formed on Cr^{2+}/SiO$_2$, which account for ν(CO) bands around 2180 cm^{-1} [8]. The much higher ν(CO) values observed for CO adsorbed on Cr/Al$_2$O$_3$ reduced in CO and in H$_2$ (+10 and + 20 cm^{-1}, respectively) could be attributed, in principle, to a higher oxidation state of the accessible Cr sites. For instance, bands at very similar ν(CO) values (2188 and 2202 cm^{-1}) were assigned by Copéret et al. [72] to CO adsorbed on well-defined Cr^{3+} sites at the silica surface. However, in our case the DR UV–Vis results discussed above unequivocally show that only the Cr$_{4c}^{2+}$ sites are accessible to CO at room temperature. Hence, the absorption band in Fig. 2b, d is attributed to mono-carbonyl adducts formed on Cr$_{4c}^{2+}$ sites. The position of the ν(CO) band can be explained by considering the more ionic character of alumina with respect to silica. Indeed, according to Busca [53,54,57], semi-metal oxides, such as silicas, are constituted by essentially covalent network structures (i.e. the Si—O bond is classifiable as a covalent bond), while typical metal oxides (such as titania, zirconia, and alumina) are essentially ionic network structures (i.e. the Al—O bond has the characteristics of an ionic bond). Hence, a Cr^{2+} site grafted at the alumina surface feels a lower electronic density than a Cr^{2+} site at the surface of silica, because of the more ionic character of the Al—O bond with respect to the Si—O bond. The difference in 10 cm^{-1} observed in the position of the ν(CO) absorption bands for the two catalysts can be explained by considering the different local environment of the Cr$_{4c}^{2+}$ sites in CO- and H$_2$-reduced Cr/Al$_2$O$_3$. Indeed, in the H$_2$-reduced sample a fraction of the Cr$_{4c}^{2+}$ sites might be partially in interaction with surface —OH groups, which are by far more abundant than in the CO-reduced sample (Fig. 1b). In the CO-reduced sample, at least a fraction of the Cr$_{4c}^{2+}$ sites are in proximity of surface carbonates (Fig. 1b), i.e. of electronegative groups. A similar induction effect was reported in the early 1990s for CO adsorbed on Cr$_2$O$_3$ in the presence of carbonates [73]. In this respect, it is worth noticing that CO adsorption on CO-reduced Cr/Al$_2$O$_3$ causes a perturbation of the absorption bands associated to surface carbonates-like species (Fig. S6), which is largely reversible upon decreasing the CO pressure.

Summarizing, in contrast to the Cr$_{4c}^{2+}$ sites present at the surface of the CO-reduced Cr^{2+}/SiO$_2$ catalyst (where the ancillary ligands are, at most, the strained siloxane bridges), the CO- and H$_2$-reduced Cr/Al$_2$O$_3$ catalysts display accessible surface Cr$_{4c}^{2+}$ sites at least partially surrounded by carbonates and hydroxyl groups, respectively. The presence of these ancillary ligands might influence the reactivity of the reduced Cr/Al$_2$O$_3$ catalysts towards ethylene.

3.3. Ethylene polymerization

Kinetic experiments were performed on both the CO- and H$_2$-reduced Cr/Al$_2$O$_3$ catalysts to evaluate the ethylene polymerization rate in comparison with the CO-reduced Cr^{2+}/SiO$_2$ catalyst [74,75]. Fig. 3a shows the decrease of ethylene pressure as a function of time for the three catalysts, monitored in the same experimental conditions and at a constant Cr loading. The data indicate that the CO-reduced Cr/Al$_2$O$_3$ catalyst is almost 15 times faster than
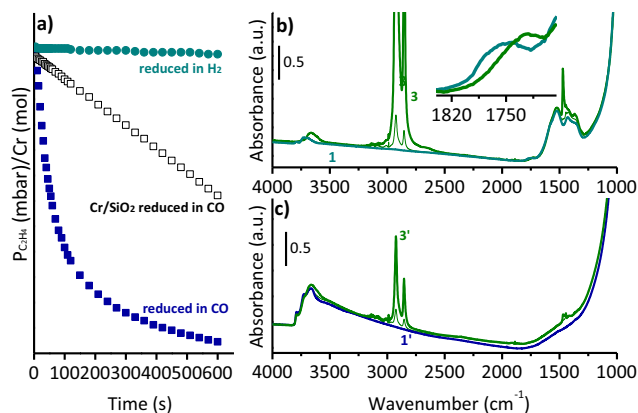
Fig. 3. Part (a) Kinetics of ethylene polymerization on CO- and H$_2$-reduced 1.0Cr/ Al$_2$O$_3$ catalysts, compared to that of CO-reduced Cr/SiO$_2$ obtained by recording the ethylene pressure as a function of time. Parts (b) and (c) Time resolved FT-IR spectra collected during the C$_2$H$_4$ polymerization at room temperature on the 1.0Cr/Al$_2$O$_3$ catalyst reduced in CO after 35 s of polymerization (spectrum 3) and on the same catalyst reduced in H$_2$ after 30 min of polymerization (spectrum 3′), respectively. Grey spectra are collected at intermediate times. The inset in part (b) shows a magnification of the spectral region where only the carbonates contribute, to highlight the effect of ethylene polymerization on the absorption bands ascribed to carbonates.

the Cr^{2+}/SiO$_2$ catalyst and even 350 times faster than the H$_2$-reduced Cr/Al$_2$O$_3$ catalyst. The ethylene polymerization rate observed for the Cr/Al$_2$O$_3$ catalyst reduced in CO is in good agreement with the "fast kinetics" of the chromia alumina reported by McDaniel [5]. By plotting the natural logaritm of the ethylene pressure versus time (that is, under the usual approximation of a first-order reaction), rate constants of 0.6 and 210 s^{-1}molCr^{-1} were obtained for H$_2$- and CO-reduced Cr/Al$_2$O$_3$, to be compared with the value of 15 s^{-1}molCr^{-1} obtained for Cr/SiO$_2$ in the same reaction conditions.

In situ time-resolved FT-IR spectroscopy is in qualitative agreement with the kinetic experiments. Fig. 3b, c show the time-resolved FT-IR spectra collected during ethylene polymerization (P$_{C2H4}$ = 100 mbar) at room temperature on both the CO- and H$_2$-reduced Cr/Al$_2$O$_3$ catalysts. The occurrence of ethylene polymerization is indicated by the growth of the IR absorption bands characteristic of polyethylene, in both ν(CH$_2$) and δ(CH$_2$) vibrational ranges (at 3000–2800 and 1500–1350 cm^{-1}, respectively). The much faster ethylene polymerization rate of CO-reduced Cr/Al$_2$O$_3$ is demonstrated by the rapid saturation of the ν(CH$_2$) absorption bands (after 35 s only), while the same bands reach a lower intensity even after 30 min of ethylene reaction on H$_2$-reduced Cr/Al$_2$O$_3$ (lower amount of polyethylene formed).

Additional information can be obtained by a closer inspection of the FT-IR spectra in Fig. 3b, c: (1) the formed polyethylene is highly crystalline also at short polymerization time, as evidenced by the intensity ratio between the two δ(CH$_2$) bands at 1472 and 1463 cm^{-1} [76]; (2) the absorption bands assigned to surface pseudo-carbonates in the spectrum of the CO-reduced catalyst are slightly perturbed immediately after ethylene dosage (inset in Fig. 3b). The effect is similar to that observed in the presence of CO, validating the previous conclusion on the close proximity of carbonates to a fraction of the reduced Cr$^{2+}_{4c}$ sites; (3) at long polymerization time, i.e. for high polyethylene content, also the ν(OH) bands are perturbed, as a consequence of the interaction with the polyethylene chains [8].

In order to understand which reduced Cr site is active in ethylene polymerization, we followed the reaction at room temperature by means of DR UV–Vis-NIR spectroscopy on both the CO- and H$_2$-reduced Cr/Al$_2$O$_3$ catalysts. The resulting spectra are shown
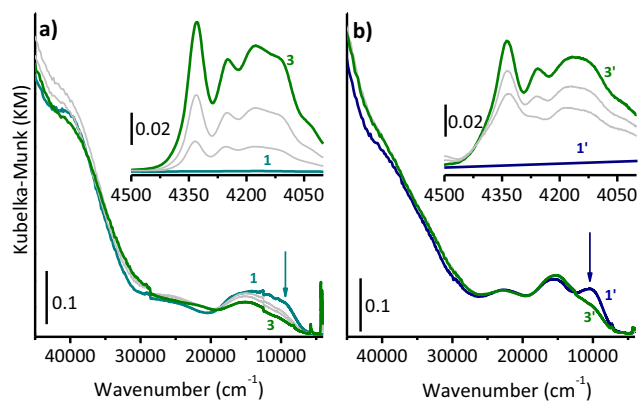

Fig. 4. Part (a): DR UV–Vis-NIR spectrum of 0.5Cr/Al$_2$O$_3$ reduced in CO at 350 °C (spectrum 1) and during ethylene polymerization at room temperature (grey); the last spectrum (spectrum 3) is collected at the end of the reaction. The arrow highlights the band more affected by ethylene polymerization. The inset shows a magnification in the region where the combination of polyethylene stretching and bending modes are observable. Part (b): as part (a) for the 0.5Cr/Al$_2$O$_3$ reduced in H$_2$ at 350 °C.

in Fig. 4. Upon ethylene dosage, the DR UV–Vis-NIR spectra of both catalysts change mainly in the d-d region, where the d-d bands previously ascribed to Cr$^{2+}_{4c}$ sites are gradually eroded (see arrows in Fig. 4). Meanwhile, weak bands grow in the 4500–4000 cm^{-1} region, where overtones and combinations of the stretching and bending vibrational modes of polyethylene are located (see insets in Fig. 4). These results provide a strong evidence that the Cr$^{2+}_{4c}$ sites are those mainly involved in ethylene polymerization, whereas the other reduced chromium species (Cr$^{2+}_{6c}$ and to Cr$^{3+}_{6c}$ sites) are mostly inactive, because inaccessible to ethylene (as for CO, Fig. 2). Interestingly, the disappearance of the spectroscopic fingerprints of Cr$^{2+}_{4c}$ is not accompanied by the appearance of any additional band that could reveal the destiny of the active sites. Likely, the Cr active sites remain buried into a layer of polyethylene and become rapidly invisible to DR UV–Vis-NIR. This is a limitation intrinsic to the physical method with which the UV–Vis spectra are collected. Indeed, in the reflectance mode, the spectrophotometer collects the light scattered by the sample. As soon as a coating of polyethylene is formed around the Cr/Al$_2$O$_3$ particles, their size rapidly approaches the nanometer range, and they become strong light scatterers, thus preventing the light from penetrating deeply into the sample (i.e. where there are the Cr sites). This is macroscopically visible in the aspect of the sample that progressively becomes white. The white colour is not the colour of polyethylene (which is transparent in the whole UV–Vis region), neither that of Cr/Al$_2$O$_3$ (whichever is the oxidation state, Cr ions give always a colour different than white). Rather, the white colour is the result of the scattering of the light from the combination polyethylene + catalyst particles. In these conditions, no information on the active Cr sites can be obtained anymore. However, collecting the UV–Vis spectra in the early stages of ethylene polymerization allows following the process. The first spectroscopic manifestation of Cr/Al$_2$O$_3$ that disappear during the formation of polyethylene are those associated to the active sites (i.e. where the polymer is forming).

The results summarized above converge in indicating that, in our experimental conditions, the 4-fold coordinated Cr^{2+} sites are those acting as precursors in ethylene polymerization, although we cannot solve (for the moment) the long-standing question about the mechanism of ethylene polymerization [74,77–79]. This is in agreement with a part of the specialized literature (citing Max McDaniel, Cr(II) is at least an active precursor, but whether the chromium remains divalent during olefin polymerization is doubtful [5]). This statement does not exclude that also Cr^{3+} sites may be active in ethylene polymerization to some extent, as for ad-hoc

synthesized catalytic systems reported in recent literature [72,80,81].

Once determined which are the Cr sites mainly involved in the ethylene polymerization reaction (Cr_{4c}^{2+}) and knowing their approximate concentration (as assessed by DR UV–Vis-NIR spectroscopy), it is possible to estimate the reaction rates per active site. Values of 30 and 2625 $s^{-1}[mol(Cr_{4c}^{2+})]^{-1}$ have been obtained for H_2- and CO-reduced Cr/Al_2O_3, to be compared with 15 $s^{-1}molCr^{-1}$ of Cr/SiO_2 (since the totality of Cr sites in Cr/SiO_2 are Cr_{4c}^{2+}). Although approximated, these values clearly indicate that Cr_{4c}^{2+} sites on Al_2O_3 are intrinsically more active than the same sites on SiO_2 (effect of the support). Moreover, the Cr_{4c}^{2+} sites on CO-reduced Cr/Al_2O_3 are ca. two orders of magnitude more active than those on H_2-reduced Cr/Al_2O_3 (effect of the ancillary ligands). It emerges that both the electronic and the local structure of the chromium sites play a major role in affecting their catalytic performances. The support is decisive in influencing both properties, but also the preparation and activation steps are important instruments to tune the properties of the Cr active sites. This explains why, at the present, there is still a controversy on the oxidation state of the active Cr sites. Considering all the variables in the catalyst synthesis and activation, we believe that the two main hypothesis (+2 and +3) may coexist.

4. Conclusions

In this work we thoroughly investigated the physical-chemical properties of the Cr/Al_2O_3 catalyst, aiming to understand the reasons behind its incredibly fast kinetic profile in ethylene polymerization. We demonstrated that a heterogeneity of Cr reduced sites are formed when Cr^{6+}/Al_2O_3 is reduced either in CO or in H_2, differing in the oxidation state (+3 or +2), in the local structure (6-fold or 4-fold coordination) and surroundings (types of ancillary ligands). The relative amount of the reduced Cr sites is a function of the reduction procedure. Among these sites, the 4-fold coordinated Cr^{2+} ones revealed to be those involved in ethylene polymerization, while both 6-fold coordinated Cr^{2+} and Cr^{3+} sites are just spectators, being almost inaccessible to the incoming molecules. The Cr_{4c}^{2+} sites are relatively more abundant in the CO-reduced Cr/Al_2O_3 (accounting for about 8% of the total) than in the H_2-reduced Cr/Al_2O_3 (ca. 2% of the total), and they are the dominating species in Cr^{2+}/SiO_2. Nevertheless, the CO-reduced Cr/Al_2O_3 catalyst is 15 times faster in ethylene polymerization than the Cr^{2+}/SiO_2 catalyst. The estimated reaction rates indicate that the Cr_{4c}^{2+} sites on CO-reduced Cr/Al_2O_3 are two order of magnitude more active than the same sites on SiO_2 or on H_2-reduced Al_2O_3.

The results discussed above demonstrate that there are at least two reasons behind the faster polymerization profile of the CO-reduced Cr/Al_2O_3 catalyst. The first one is the higher ionicity of the Cr—O—Al bond with respect to the Cr—O—Si bond evidenced by the strong perturbation of the CO probe adsorbed at the accessible Cr sites. As a consequence, the Cr_{4c}^{2+} sites at the alumina surface experience a lower electronic density than those at the silica surface. The second reason lies in the nature of the ancillary ligands around the Cr_{4c}^{2+} sites. Beside the strained Al—O—Al bridges, carbonates are found in the CO-reduced Cr/Al_2O_3 and hydroxyl groups are present in the H_2-reduced Cr/Al_2O_3, while strained siloxane bridges complete the coordination sphere of Cr^{2+} sites in Cr^{2+}/SiO_2. The three types of ancillary ligands are characterized by a different strength of interaction with the Cr_{4c}^{2+} sites (i.e. they are more or less displaceable by the incoming ethylene monomer) and exert a different electronic influence. It is reasonable to assume that the same two reasons might explain also the other peculiar features of Cr/Al_2O_3 in ethylene polymerization (i.e. the lower tendency to β-hydride elimination, the even distribution of branches throughout the whole molecular weight distribution and the H_2 sensitivity). Hence, these results indi-

cate a strategy for the development of Cr-based catalysts with improved efficiency, which relies on the increase of the support ionicity and on the selection of the right ancillary ligands, a practice that is common in Ziegler-Natta catalysis but less employed in the field of the Phillips catalyst. Last, but not least, the new data shown in this contribution strengthen the hypothesis that, in Cr-based catalysts, ethylene polymerization occurs on divalent Cr species in interaction with suitable ancillary ligands, as we showed in our previous works [82–84].

Acknowledgments

Appendix A. Supplementary material

Supplementary data associated with this article can be found, in the online version, at https://doi.org/10.1016/j.jcat.2017.11.007.

References

[1] T.E. Nowlin. In Business and Technology of the Global Polyethylene Industry, Ed., Wiley-Scrivener, New York, 2014.
[2] In Market Report: Global Catalyst Market, Ed., Acmite Market Intelligence, Ratingen, Germany, 2015.
[3] T.J. Hutley, M. Ouederni, Polyolefins – the history and economic impact, in: M. A.-A. AlMa'adeed, I. Krupa (Ed.), Polyolefin Compounds and Materials, Springer, Switzerland, 2016, pp. 13–50.
[4] J.P. Hogan, R.L. Banks, U.S. Patent 2, 825, 721, 1958.
[5] M.P. McDaniel, Adv. Catal. 53 (2010) 123–606.
[6] A. Clark, Catal. Rev. 3 (1970) 145–173.
[7] R. Cheng, Z. Liu, L. Zhong, X. He, P. Qiu, M. Terano, et al., Phillips Cr/silica catalyst for ethylene polymerization, in: W. Kaminsky (Ed.), Polyolefins: 50 Years after Ziegler and Natta I: Polyethylene and Polypropylene, Spinger-Verlag, Berlin Heidelberg, 2013, 257, pp. 135-202.
[8] E. Groppo, C. Lamberti, S. Bordiga, G. Spoto, A. Zecchina, Chem. Rev. 105 (2005) 115–183.
[9] B.M. Weckhuysen, I.E. Wachs, R.A. Shoonheydt, Chem. Rev. 96 (1996) 3327–3349.
[10] B.M. Weckhuysen, R.A. Schoonheydt, Catal. Today 51 (1999) 223–232.
[11] V.Z. Fridman, R. Xing, M. Severance, Appl. Catal., A 523 (2016) 39–53.
[12] V.Z. Fridman, R. Xing, Appl. Catal., A 530 (2017) 154–165.
[13] H.J. Lugo, J.H. Lunsford, J. Catal. 91 (1985) 155–166.
[14] L.R. Mentasty, O.F. Gorriz, L.E. Cadus, Ind. Eng. Chem. Res 38 (1999) 396–404.
[15] M.A. Vuurman, I.E. Wachs, D.J. Stufkens, A. Oskam, J. Mol. Catal. 80 (1993) 209–227.
[16] M.A. Vuurman, I.E. Wachs, J. Phys. Chem. 96 (1992) 5008–5016.
[17] F.D. Hardcastle, I.E. Wachs, J. Mol. Catal. 46 (1988) 173–186.
[18] M.A. Vuurman, F.D. Hardcastle, I.E. Wachs, J. Mol. Catal. 84 (1993) 193–205.
[19] B.M. Weckhuysen, L.M. Deridder, P.J. Grobet, R.A. Schoonheydt, J. Phys. Chem. 99 (1995) 320–326.
[20] B.M. Weckhuysen, L.M. Deridder, R.A. Schoonheydt, J. Phys. Chem. 97 (1993) 4756–4763.
[21] B.M. Weckhuysen, R.A. Schoonheydt, Catal. Today 51 (1999) 215–221.
[22] B.M. Weckhuysen, R.A. Schoonheydt, J.M. Jehng, I.E. Wachs, S.J. Cho, R. Ryoo, et al., J. Chem. Soc. Faraday Trans. 91 (1995) 3245–3253.
[23] B.M. Weckhuysen, A.A. Verberckmoes, A.L. Buttiens, R.A. Schoonheydt, J. Phys. Chem. 98 (1994) 579–584.
[24] B.M. Weckhuysen, A.A. Verberckmoes, A.R. DeBaets, R.A. Schoonheydt, J. Catal. 166 (1997) 160–171.
[25] S.M.K. Airaksinen, A.O.I. Krause, J. Sainio, J. Lahtinen, K.J. Chao, M.O. Guerrero-Pérez, et al., Phys. Chem. Chem. Phys. 5 (2003) 4371–4377.
[26] E. Groppo, K. Seenivasan, C. Barzan, Catal. Sci. Technol. 3 (2013) 858–878.
[27] I.E. Wachs, C.A. Roberts, Chem. Soc. Rev. 39 (2010) 5002–5017.
[28] A. Chakrabarti, M. Gierada, J. Handzlik, I.E. Wachs, Top. Catal. 59 (2016) 725–739.
[29] A. Chakrabarti, I.E. Wachs, Catal. Lett. 145 (2015) 985–994.
[30] H. Guesmi, F. Tielens, J. Phys. Chem. C 116 (2012) 994–1001.
[31] J. Handzlik, R. Grybos, F. Tielens, J. Phys. Chem. C 117 (2013) 8138–8149.
[32] J. Gao, Y. Zheng, Y. Tang, J.-M. Jehng, R. Grybos, J. Handzlik, et al., ACS Catal. 5 (2015) 3078–3092.
[33] M. Gierada, P. Michorczyk, F. Tielens, J. Handzlik, J. Catal. 340 (2016) 122–135.
[34] B.P. Liu, M. Terano, J. Mol. Catal. A 172 (2001) 227–240.

[35] C.A. Demmelmaier, R.E. White, J.A. van Bokhoven, S.L. Scott, J. Phys. Chem. C 112 (2008) 6439–6449.
[36] A. Iannibello, S. Marengo, P. Tittarelli, G. Morelli, A. Zecchina, J. Chem. Soc., Faraday Trans. 1 (80) (1984) 2209–2223.
[37] A. Zecchina, E. Garrone, G. Ghiotti, S. Coluccia, J. Phys. Chem. 79 (1975) 972–978.
[38] H.-L. Krauss, H. Stach, Z. Anorg, Allg. Chem. 414 (1975) 97–108.
[39] B. Fubini, G. Ghiotti, L. Stradella, E. Garrone, C. Morterra, J. Catal. 66 (1980) 200–213.
[40] G. Ghiotti, E. Garrone, G. Della Gatta, B. Fubini, E. Giamello, J. Catal. 80 (1983) 249–262.
[41] Z.G. Szabó, K. Kamarás, S. Szebeni, I. Ruff, Spectrochim. Acta Part A Mol. Spectrosc. 34 (1978) 607–612.
[42] B.M. Weckhuysen, B. Schoofs, R.A. Schoonheydt, J. Chem. Soc. Faraday Trans. 93 (1997) 2117–2120.
[43] B.M. Weckhuysen, R.A. Schoonheydt, Stud. Surface Sci. Catal. 84 (1994) 965–972.
[44] B.N. Figgis, Introduction to Ligand Fields, John Wiley & Sons, New York, 1966.
[45] R.J.H. Clark, J. Chem. Soc. (1964) 417–425.
[46] J. Fackler, D. Holan, Inorg. Chem. 4 (1964) 954–958.
[47] A.B.P. Lever, Inorganic electronic spectroscopy, Elsevier, Amsterdam, 1984.
[48] C.K. Jorgensen, Progr. Inorg. Chem. 12 (1970) 101–157.
[49] A.B. Gaspar, R.L. Martins, M. Schmal, L.C. Dieguez, J. Mol. Catal. A 169 (2001) 105–112.
[50] R.G. Pearson, J. Am. Chem. Soc. 85 (1963) 3533.
[51] A. Corma, G. Sastre, R. Viruela, C. Zicovich-Wilson, J. Catal. 136 (1992) 521–530.
[52] R.D. Shannon, C.T. Prewitt, Acta Crystall. B25 (1969).
[53] G. Busca, Catal. Today 226 (2014) 2–13.
[54] G. Busca, Chem. Rev. 107 (2007) 5366–5410.
[55] C. Morterra, G. Magnacca, Catal. Today 27 (1996) 497–532.
[56] G. Busca, V. Lorenzelli, V.S. Escribano, R. Guidetti, J. Catal. 131 (1991) 167–177.
[57] G. Busca, Phys. Chem. Chem. Phys. 1 (1999) 723–736.
[58] H. Knoezinger, P. Ratnasamy, Cat. Rev.-Sci. Eng. 17 (1978) 31–70.
[59] M. Digne, P. Sautet, P. Raybaud, P. Euzen, H. Toulhoat, J. Catal. 211 (2002) 1–5.
[60] M. Digne, P. Sautet, P. Raybaud, P. Euzen, H. Toulhoat, J. Catal. 226 (2004) 54–68.
[61] A.A. Tsyganenko, V.N. Filimonov, J. Mol. Struct. 19 (1973) 579–589.

[62] K. Nakamoto, Infrared and Raman spectra of inorganic and coordination compounds, in: Handbook of Vibrational Spectroscopy, L. John Wiley & Sons, 2006, pp. 1872–1892.
[63] T. Montanari, L. Castoldi, L. Lietti, G. Busca, Appl. Catal., A 400 (2011) 61–69.
[64] G. Ramis, G. Busca, V. Lorenzelli, Mater. Chem. Phys. 29 (1991) 425–435.
[65] A. Bensalem, B.M. Weckhuysen, R.A. Schoonheydt, J. Chem. Soc. Faraday Trans. 93 (1997) 4065–4069.
[66] J.C. Lavalley, Catal. Today 27 (1996) 377–401.
[67] A. Bensalem, B.M. Weckhuysen, R.A. Schoonheydt, J. Phys. Chem. B 101 (1997) 2824–2829.
[68] C. Lamberti, A. Zecchina, E. Groppo, S. Bordiga, Chem. Soc. Rev. 39 (2010) 4951–5001.
[69] E.N. Gribov, O. Zavorotynska, G. Agostini, J.G. Vitillo, G. Ricchiardi, G. Spoto, et al., Phys. Chem. Chem. Phys. 12 (2010) 6474–6482.
[70] A. Zecchina, D. Scarano, S. Bordiga, G. Spoto, C. Lamberti, Adv. Catal. 46 (2001) 265–397.
[71] D. Scarano, G. Ricchiardi, S. Bordiga, P. Galletto, C. Lamberti, G. Spoto, et al., Faraday Discuss. 105 (1996) 119–138.
[72] M.F. Delley, F. Núñez-Zarur, M.P. Conley, A. Comas-Vives, G. Siddiqi, S. Norsic, et al., Proc. Natl. Acad. Sci. U.S.A. 111 (2014) 11624–11629.
[73] K. Hadjiivanov, G. Busca, Langmuir 10 (1994) 4534–4541.
[74] E. Groppo, A. Damin, C. Otero Arean, A. Zecchina, Chem. Eur. J. 17 (2011) 11110–11114.
[75] C. Barzan, E. Groppo, E.A. Quadrelli, V. Monteil, S. Bordiga, Phys. Chem. Chem. Phys. 14 (2012) 2239–2245.
[76] D. Chelazzi, M. Ceppatelli, M. Santoro, R. Bini, V. Schettino, Nat. Mater. 3 (2004) 470–475.
[77] A. Fong, Y. Yuan, S.L. Ivry, S.L. Scott, B. Peters, ACS Catal. 5 (2015) 3360–3374.
[78] A. Fong, B. Peters, S.L. Scott, ACS Catal. 6 (2016) 6073–6085.
[79] C. Brown, J. Krzystek, R. Achey, A. Lita, R. Fu, R.W. Meulenberg, et al., ACS Catal. 5 (2015) 5574–5583.
[80] M.P. Conley, M.F. Delley, G. Siddiqi, G. Lapadula, S. Norsic, V. Monteil, et al., Angew. Chem. Int. Ed. 53 (2014) 1872–1876.
[81] M.F. Delley, M.P. Conley, C. Copéret, Catal. Lett. 144 (2014) 805–808.
[82] C. Barzan, S. Bordiga, E. Groppo, ACS Catal. 6 (2016) 2918–2922.
[83] C. Barzan, A.A. Damin, A. Budnyk, A. Zecchina, S. Bordiga, E. Groppo, J. Catal. 337 (2016) 45–51.
[84] C. Barzan, A. Piovano, L. Braglia, G. Martino, C. Lamberti, S. Bordiga, E. Groppo, J. Am. Chem. Soc. (2017), https://doi.org/10.1021/jacs.7b07437 (in press).

Tracking the reasons for the uniqueness of Cr/Al_2O_3 catalyst in ethylene polymerization.

Giorgia A. Martino, Caterina Barzan, Alessandro Piovano, Andriy Budnyk and Elena Groppo*
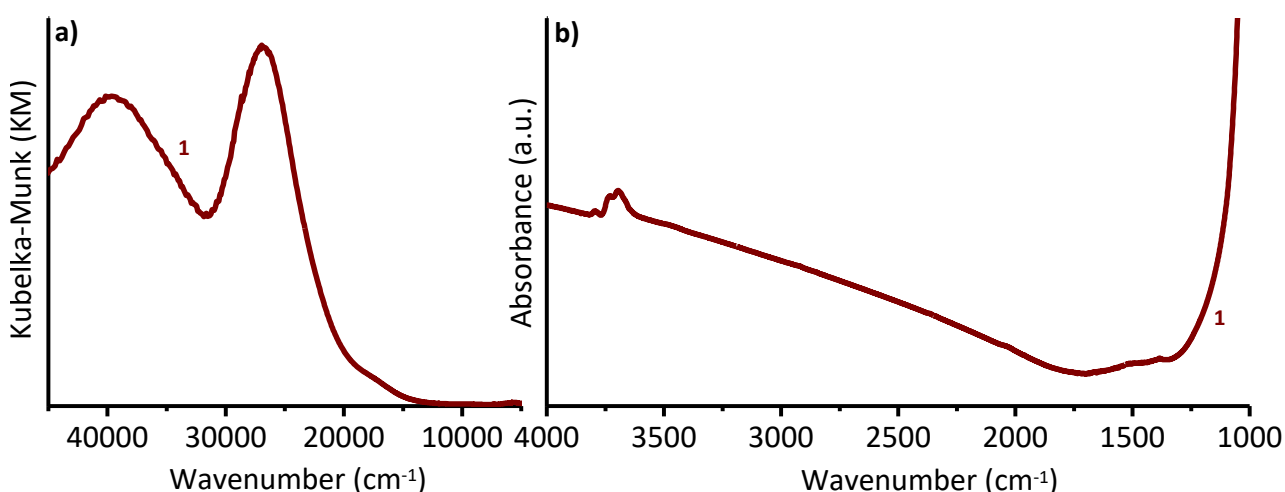
Figure S1 DR UV-Vis (part a) and FT-IR (part b) spectra of the Cr^{6+}/Al_2O_3 catalyst calcined at 650 °C.

Figure S1 shows the DR UV-Vis (part a) and FT-IR (part b) spectra of Cr^{6+}/Al_2O_3. Starting from the UV-Vis measurements, two intense absorption bands at about 27000 cm^{-1} and 41000 cm^{-1} dominate the spectrum, in well agreement with the fundamental works of Weckhuysen et al. [1-8]. These bands are assigned to O $\rightarrow$ Cr(VI) charge-transfer transitions for well dispersed monochromate species [1-8]. No additional bands are present in the d-d transition region, being Cr^{6+} a d^0 transition metal ion. The FT-IR spectrum of Cr^{6+}/Al_2O_3 is characterized by the intense and out-of-scale absorption due to the framework modes of

alumina (below 1200 cm^{-1}), and by the weak absorption bands in the v(OH) region (3800-3500 cm^{-1}) assigned to different Al-OH surface species [9-14].
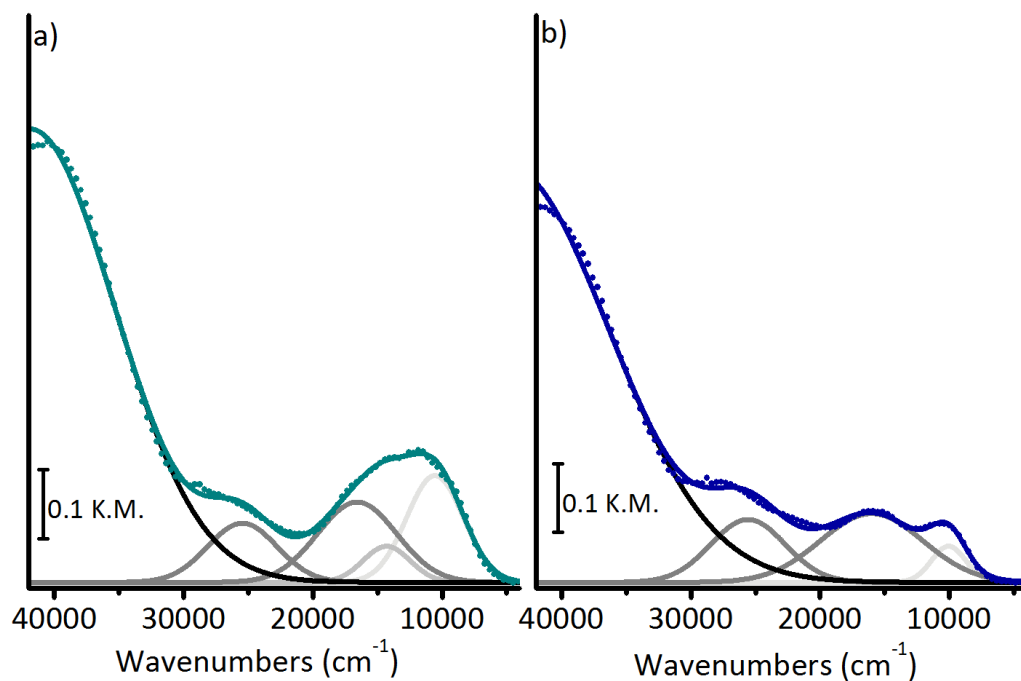
Figure S2 DR UV-Vis-NIR spectra of CO-reduced Cr/Al$_2$O$_3$ (part a) and H$_2$-reduced Cr/Al$_2$O$_3$ and spectral deconvolution to determine the relative concentration of Cr$^{2+}_{4c}$ (light grey), Cr$^{2+}_{6c}$ (intermediate grey) and Cr$^{3+}_{6c}$ (dark grey).
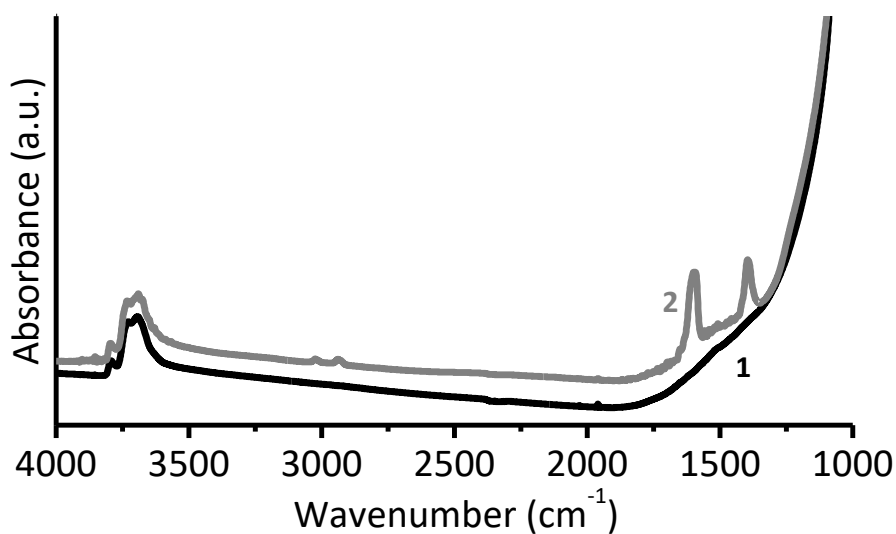
Figure S3 FT-IR spectra of alumina dehydroxylated and calcined at 650 °C (curve 1), and after reduction in CO at 350 °C and outgassing at the same temperature (curve 2).

Figure S3 shows the FT-IR spectrum of alumina dehydroxylated and calcined at 650 °C (curve 1) and upon treatment in CO at 350 °C (curve 2). The spectrum of activated Al_2O_3 is evidently analogous to that of the Cr^{6+}/Al_2O_3 sample, while the CO-reduced alumina is characterized by the presence of two additional absorption bands at 1600 and 1395 cm^{-1}. According to Morterra [15], these bands can be attributed to pseudo-carbonate species. The presence of these species can be traced back to the formation of CO_2 resulting from CO oxidation at the alumina surface; this means that CO reduces also the bare alumina, likely at some defective sites where oxygen vacancies are created, leading to CO_2 formation and its successive stabilization at the alumina surface in the form of carbonates.
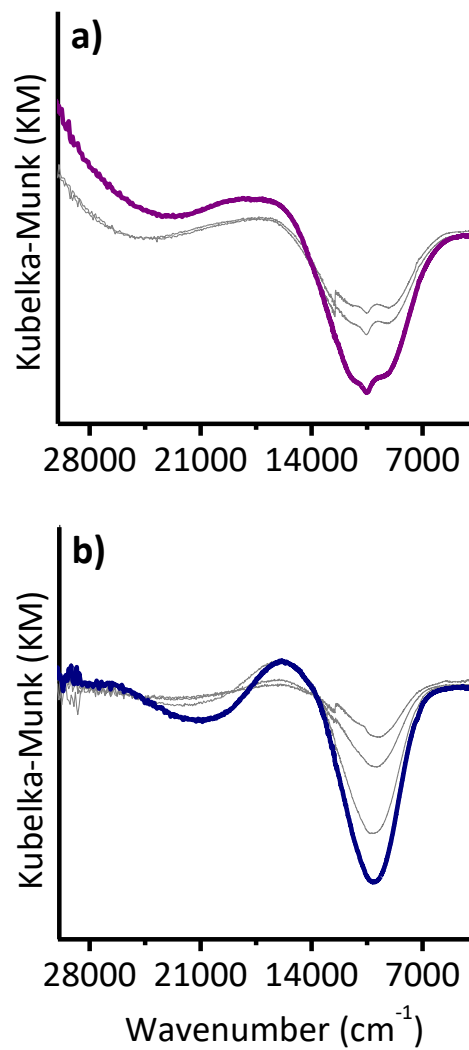
Figure S4. Difference DR UV-Vis-NIR spectra in the d-d region of the Cr/Al$_2$O$_3$ catalyst reduced in CO (part a) and in H$_2$ (part b), in the presence of increasing amount of CO. The spectra have been obtained after subtraction of the spectrum prior CO dosage (spectra 1 and 1' shown in Figure 2 in the main text).
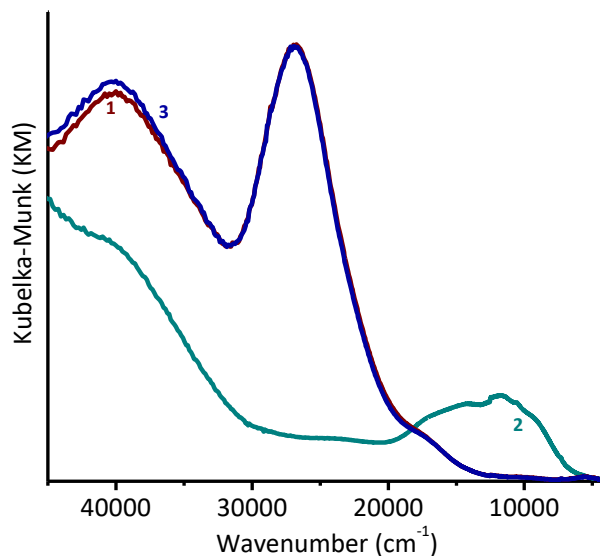
Figure S5 DR UV-Vis-NIR spectra of Cr^{6+}/Al_2O_3 (curve 1), of the same sample reduced in CO at 350°C (curve 2) and upon re-oxidation at 650 °C (curve 3).

Our UV-Vis spectroscopic investigation revealed that three main Cr reduce sites are formed upon reduction in H_2 or CO at 350 °C. Since the only sites available for CO adsorption and ethylene reaction are the Cr^{2+}_{4c}, we tried to understand whether the other Cr^{2+}_{6c} and Cr^{3+}_{6c} sites were not available because buried into the Al_2O_3 lattice. We thus performed a supplementary experiment in which Cr^{6+}/Al_2O_3 (curve 1 in Figure S5) was reduced in CO at 350 °C (curve 2 in Figure S5) and re-oxidized back with two dosages of oxygen at 650 °C (curve 3 in Figure S5). If the Cr^{2+}_{6c} and Cr^{3+}_{6c} sites were buried into the alumina, these sites would not be accessible to O_2. The perfect match between curves 1 and 3 in Figure S5 indicates that all the reduced Cr sites were re-oxidized to Cr^{6+}, demonstrating that all the reduced Cr sites are accessible to O_2 and thus are not buried into the alumina lattice.
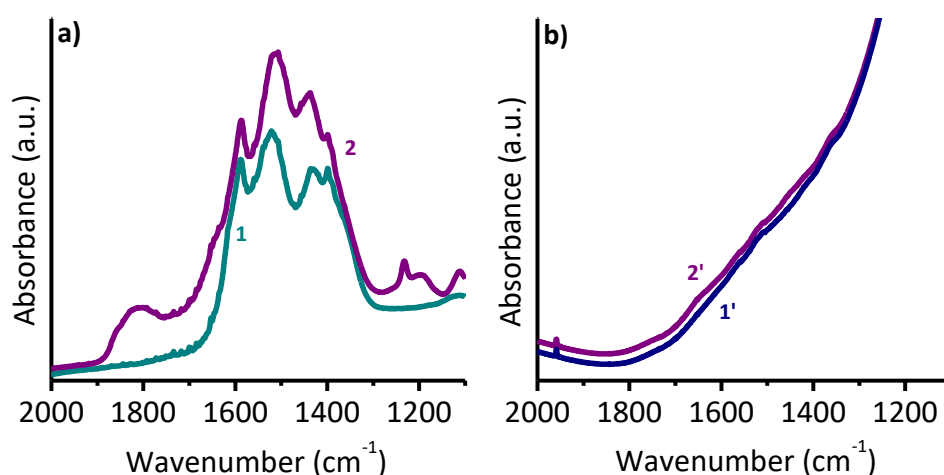
Figure S6 FT-IR spectra (magnification of the pseudo-carbonates region) upon CO adsorption at room temperature on CO- and H_2-reduced Cr/Al_2O_3 (parts a and b, respectively), maximum coverage (spectra 2 and 2') and zero (spectra 1 and 1').

Figure S6 shows the spectrum of CO- and H_2-reduced Cr/Al_2O_3 catalysts (curves 1 and 1' in parts a and b, respectively) and upon CO adsorption at room temperature (curves 2 and 2') in the carbonates stretching region (1900-1100 cm^{-1}). For the H_2-reduced sample (Figure S6b), the spectrum does not show significant changes upon CO adsorption. For the CO-reduced sample (Figure S6a) CO adsorption causes a perturbation of the absorption bands assigned to carbonates (suggesting that CO displaces a fraction of the carbonates from the Cr^{2+}_{4c} sites) and the appearance of new IR adsorption bands around 1800 and 1200 cm^{-1} (new and different carbonate species are formed).

References

[1] B.M. Weckhuysen, L.M. Deridder, P.J. Grobet, R.A. Schoonheydt, J. Phys. Chem., 99 (1995) 320-326.

[2] B.M. Weckhuysen, L.M. Deridder, R.A. Schoonheydt, J. Phys. Chem., 97 (1993) 4756-4763.

[3] B.M. Weckhuysen, R.A. Schoonheydt, Catal.Today, 51 (1999) 223-232.

[4] B.M. Weckhuysen, R.A. Schoonheydt, J.M. Jehng, I.E. Wachs, S.J. Cho, R. Ryoo, S. Kijlstra, E. Poels, J. Chem. Soc. Faraday Trans., 91 (1995) 3245-3253.

[5] B.M. Weckhuysen, A.A. Verberckmoes, A.L. Buttiens, R.A. Schoonheydt, J. Phys. Chem., 98 (1994) 579-584.

[6] B.M. Weckhuysen, A.A. Verberckmoes, J. Debaere, K. Ooms, I. Langhans, R.A. Schoonheydt, J. Mol. Catal. A, 151 (2000) 115-131.

[7] B.M. Weckhuysen, A.A. Verberckmoes, A.R. DeBaets, R.A. Schoonheydt, J. Catal., 166 (1997) 160-171.

[8] B.M. Weckhuysen, I.E. Wachs, R.A. Shoonheydt, Chem. Rev., 96 (1996) 3327-3349.

[9] G. Busca, Physical Chemistry Chemical Physics, 1 (1999) 723-736.

[10] G. Busca, Catal. Today, 226 (2014) 2-13.

[11] H. Knoezinger, P. Ratnasamy, Cat. Rev. - Sci. Eng., 17 (1978) 31-70.

[12] M. Digne, P. Sautet, P. Raybaud, P. Euzen, H. Toulhoat, J. Catal., 211 (2002) 1-5.

[13] M. Digne, P. Sautet, P. Raybaud, P. Euzen, H. Toulhoat, J. Catal., 226 (2004) 54-68.

[14] A.A. Tsyganenko, V.N. Filimonov, J. Mol. Struct., 19 (1973) 579-589.

[15] C. Morterra, G. Magnacca, Catal. Today, 27 (1996) 497-532.

ORIGINAL PAPER

CrossMark

The Effect of Al-Alkyls on the Phillips Catalyst for Ethylene Polymerization: The Case of Diethylaluminum Ethoxide (DEALE)

Giorgia A. Martino[1] · Alessandro Piovano[1] · Caterina Barzan[1] · Silvia Bordiga[1] · Elena Groppo[1]

Abstract
Al-alkyls are often used in the industrial practice for modifying the Phillips catalysts for polyethylene production: they are not necessary to develop the activity, but they have relevant effects on the catalysis, decreasing the induction time, promoting the in situ branching, and enhancing the H_2 sensitivity for the molecular weight regulation. Herein we investigate the effect of diethylaluminum ethoxide (DEALE) on $Cr(II)/SiO_2$ (in a stoichiometric amount of Al:Cr = 2:1), focusing the attention on the modification of the Cr(II) sites at a molecular level. Diffuse reflectance UV–Vis and FT-IR spectroscopies, applied in the presence of CO and CD_3CN as molecular probes, unequivocally demonstrate that: (1) DEALE modifies only a fraction of the Cr(II) sites (ca. 30%) even if dosed in excess with respect to the Cr sites; (2) DEALE reacts with the silica surface, forming Al-grafted species which are at least partially in interaction with the Cr(II) sites and hence act as ancillary ligands; (3) the modified Cr(II) sites are more acidic and likely mono-grafted to the silica surface; the presence of Al-grafted species nearby is essential for their stabilization. Finally, kinetic experiments indicate that the modified Cr(II) sites are ca. 60 times faster in inserting ethylene than the unmodified Cr(II) sites. The intrinsic higher activity of the modified Cr(II) sites is a consequence not only of their molecular structure, but of the whole series of effects listed above.

1 Introduction

Polyolefins (POs) are ubiquitous materials in the modern economy, combining unrivalled functional properties with low cost, low weight and excellent barrier properties. In this market the Phillips catalyst produces hundreds of specialized PE grades, supplying almost 50% of the total HDPE world demand [1–3]. Since its discovery in 1951 [4], the Cr/SiO_2 Phillips catalyst was modified and evolved mainly following trial and error approaches or serendipitous discoveries. One of these discoveries was the possibility of introducing Al-alkyls in the catalytic process. Indeed, opposite to Ziegler–Natta catalysts, the Phillips catalysts do not require any

co-catalysts (or activators) to develop an activity, but they are used to enhance it and to modify the produced polymer [5]. The idea of using Al-alkyls to change the performances of the Phillips catalyst originated from an accident occurred at an industrial plant running a Phillips catalyst, that was accidentally contaminated with the aluminium alkyls employed in a Ziegler–Natta polymerization line nearby. This "mistake" led to the unexpected production of a short-chain branched polyethylene with remarkable properties for technological applications [6]. Further investigations driven by the industrial curiosity revealed that many metal-alkyls bearing at least one M–R bond (hereafter referred to as MR) affect the Cr active sites distribution, promote the in situ branching, and enhance the sensitivity to H_2 [5, 7]. This latter aspect is particularly interesting because the un-modified Phillips catalyst is not sensitive to the presence of hydrogen during the polymerization process, which is among the easiest methods for the regulation of the molecular weight. The modification of the Phillips catalysts by metal-alkyls can be carried out both on the oxidized form ($Cr(VI)/SiO_2$) and on the CO-reduced form ($Cr(II)/SiO_2$). According to McDaniel [5], the $Cr(II)/SiO_2$ Phillips catalyst is more readily subject


✉ Elena Groppo
elena.groppo@unito.it

1 Department of Chemistry, NIS Centre and INSTM, University of Torino, via G. Quarello 15A, 10135 Turin, Italy
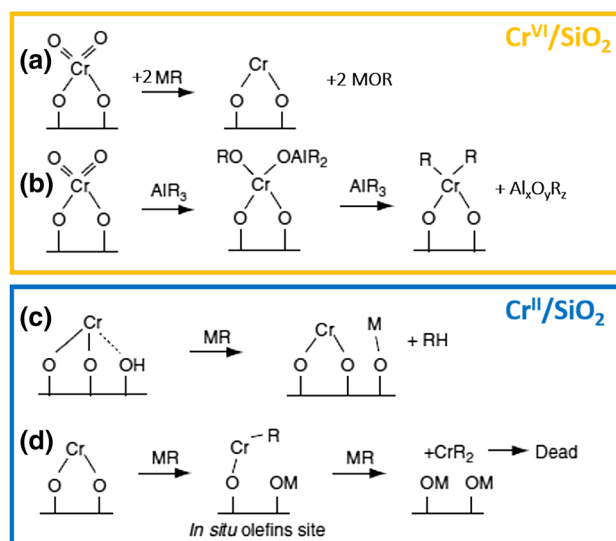
to attack by metal-alkyls, and by combining the catalyst activation with suitable reaction variables it is possible to increase enormously its H_2 sensitivity.

Metal-alkyls can potentially interact/react with both the silica support and the Cr sites. As far as the modification of the silica surface by MR is concerned, extensive studies can be found in the literature, since this is a really versatile approach for the surface functionalization [8–12]. MR can react with surface OH groups and/or with the strained siloxane bridges, whose relative amount is a function of the de-hydroxylation conditions [13, 14]. Several concomitant reaction pathways were identified [10–12], such as the M grafting by the protonolysis of one (Scheme 1a) or two silanols and the M grafting by the opening of a siloxane bridge through the nucleophilic attack of an alkyl group (Scheme 1b). Further rearrangements of the grafted M with other siloxane bridges nearby are also possible.

In contrast, the reactivity of Al-alkyls with the Cr sites in Cr/SiO$_2$ was much less explored, and a wide range of possible products can be envisaged, depending on the reaction conditions, on the amount and type of co-catalyst, and on the pre-treatment of the catalyst [5]. The scientific literature in this field is very poor, with just a few articles and a few research groups working on this system [6, 15–22]. The few hypothesis that have been formulated are summarized in Scheme 2, considering the reaction of a generic MR with the Phillips catalysts either in the oxidized (parts a and b) or in the reduced (parts b and c) forms. Among the various possibilities, the MR can: (a) reduce Cr(VI) to lower-valent active species, thus accelerating the development of the polymerization rate; (b) alkylate the chromium, similarly to the role of the co-catalyst in Ziegler–Natta catalysis; (c) react with the chromium site itself, or with neighbouring OH or siloxane groups, to modify the site or become part of its environment, thus influencing its behaviour; (d) attack the Cr-support bonds, thus initially converting di-grafted
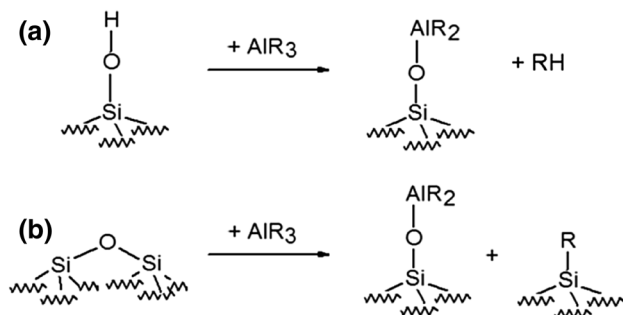
Scheme 2 Mechanisms proposed in the literature [5, 6, 15–22] for the reaction of AlR$_3$ with Cr(VI)/SiO$_2$ (**a** and **b**) and Cr(II)/SiO$_2$ (**c** and **d**)

chromium species into mono-grafted ones, and eventually destroying the sites and causing a loss of activity. Most of these hypotheses are not confirmed yet by direct experimental evidence on the structure of the active sites at molecular level.

In this work we propose for the first time an in-depth investigation on the effect of an Al-alkyl on the CO-reduced form of the Phillips catalyst, Cr(II)/SiO$_2$. We decided to focus our attention on Cr(II)/SiO$_2$ in order to limit the number of working hypothesis (formally only paths c and d in Scheme 2 are possible). Among all the possible Al-alkyls, we choose diethylaluminum ethoxide (DEALE = ROAlR$_2$, with R = ethyl), that is known to have a very pronounced influence on the H_2 sensitivity [5]. We adopted DR UV–Vis and FT-IR spectroscopies (the latter also in the presence of probe molecules), since these techniques have been demonstrated to be extremely sensitive and able to discriminate among several Cr sites differing in the coordination geometry, much more than other more sophisticated methods. Our spectroscopic investigation allowed us to get information on the fraction of the Cr sites modified by DEALE and on their structure at a molecular level.

2 Experimental Section

2.1 Catalyst Activation and Modification

The Phillips catalysts were prepared by wet-impregnation of a SiO$_2$ (Aerosil®380) with a solution of chromic acid (Sigma-Aldrich) as Cr precursor, according to the procedure

Scheme 1 Mechanisms proposed in the literature for the reaction of a metal alkyl (MR) with the surface of dehydroxylated silica [10–12]: grafting of M by protonolysis of one silanol group (**a**); grafting of M by siloxane bridge opening through the nucleophilic attack of an alkyl group (**b**)

widely adopted in the past [23]. Two Cr/SiO$_2$ samples differing in the Cr loading (1 wt% and 0.5 wt%) were prepared: the former was used for the FT-IR measurement and the latter for DR-UV–Vis-NIR. The choice was done to optimize the spectral quality. We have previously demonstrated that the properties of the Cr sites in the two catalysts are the same [23]. The catalysts were activated directly inside the measurement cells, to avoid any type of contamination. The activation procedure can be resumed in four main steps: (i) degassing in dynamic vacuum at increasing temperature up to 650 °C to dehydroxylate the silica surface; (ii) calcination at the same temperature, resulting in the grafting of the Cr species at the silica surface in the form of monochromates; (iii) reduction in the presence of CO at 350 °C, followed by degassing at the same temperature; (iv) cooling down at room temperature. The obtained material will be called hereafter Cr(II)/SiO$_2$.

The modification of Cr(II)/SiO$_2$ with DEALE was accomplished by impregnating Cr(II)/SiO$_2$ in the glove-box with a well-defined amount of DEALE in hexane, calculated considering a stoichiometric Al/Cr ratio of 2/1. In all the experiments, the DEALE/hexane mixture was left in contact with the catalyst for ca. 15–20 min, followed by removal of hexane immediately before the experiment. Hence, our procedure mimics the catalyst pre-treatment stage employed in commercial operations, where the catalyst is treated with the Al-alkyl for about 30 min directly in the polymerization reactor before the introduction of the monomer. This procedure is known to give a much more pronounced response than introducing the Al-Alkyl at the polymerization stage, i.e. in the presence of the monomer [5]. The Al/Cr stoichiometry is known to strongly influence the Cr speciation [24, 25], and the maximum activity is usually achieved at a ratio near 1/1 or 2/1. The resulting sample will be labelled as Cr(II)/SiO$_2$ + DEALE in the following.

Finally, a series of blank experiments were performed on a bare SiO$_2$ activated with the same procedure as for Cr(II)/SiO$_2$ and successively reacted with DEALE in the same amount as for Cr(II)/SiO$_2$ + DEALE. This sample will be labelled as SiO$_2$ + DEALE.

2.2 Methods

Diffuse reflectance (DR) UV–Vis-NIR spectra were collected using a Varian Cary5000 spectrophotometer with a diffuse reflectance accessory. The samples were measured in the form of thick self-supported pellets (surface density ca. 200 mg/cm^2), placed inside a cell equipped with a quartz suprasil window, that allows performing thermal treatments and measurements in the presence of gases. The reflectance (R%) signal was later converted into Kubelka–Munk values F(R).

Transmission FT-IR spectra were collected at 2 cm^{-1} resolution with a Bruker Vertex70 instrument equipped with a MCT detector. The experiments were performed on samples in the form of thin self-supported pellets (surface density ca. 30 mg/cm^2), placed inside a quartz cell equipped with two KBr windows, which allows performing thermal treatments and measurements in the presence of gases. All the FT-IR spectra were normalized to the optical thickness of the pellet, in order to allow quantitative comparisons to be done.

The kinetics of ethylene polymerization was studied by sending 200 mbar of ethylene at room temperature over 0.2 g of catalyst inside a quartz reactor of known volume, and recording the ethylene pressure as a function of time, as already done in the past [26, 27]. A similar experiment was repeated for the catalyst inside the FT-IR cell, collecting the spectra as a function of time.

For probing the accessible Cr sites after modification with DEALE, FT-IR experiments of adsorbed carbon monoxide (CO) and d-acetonitrile (CD$_3$CN) were performed. CO was dosed in the gas phase (equilibrium pressure P_{CO} = 100 mbar) at room temperature. CD$_3$CN was dosed in the vapour phase (from the liquid vapour tension) at room temperature. A FT-IR spectrum was collected at the maximum CO (or CD$_3$CN) coverage, followed by step-by-step expansions to diminish the equilibrium pressure in a controlled way.

3 Results and Discussion

3.1 Reactivity of DEALE with Cr(II)/SiO$_2$

Figure 1 displays the DR UV–Vis-NIR (part a) and the FT-IR spectra (part b) of the CO-reduced Cr(II)/SiO$_2$ catalyst before (black spectra) and after the reaction with DEALE in the stoichiometric ratio of Al/Cr = 2/1 (grey spectra). The spectra of Cr(II)/SiO$_2$ were deeply discussed in the past [23], and will be just commented briefly here. In the UV–Vis-NIR region, the two intense bands centred at ca. 41,000 and 30,000 cm^{-1} are attributed to O→Cr charge-transfer transitions, while the two bands at 12,000 and 7500 cm^{-1} are assigned to the d–d transitions characteristic of 4-coordinated d^4 Cr(II) sites in a distorted tetrahedral environment. In the Mid-IR region, the spectrum is dominated by the fingerprints of a highly dehydroxylated silica, i.e. a very narrow absorption band centred at 3745 cm^{-1} due to the ν(OH) of isolated silanol groups, the out-of-scale absorption below 1100 cm^{-1} due to the vibrations of the silica lattice and a triplet of bands in the 2100–1500 cm^{-1} region due to the overtones and combinations of the SiO$_2$ lattice vibrations.

After reaction with DEALE, both the DR UV–Vis and FT-IR spectra greatly change. In the UV–Vis region the bands characteristic of Cr(II) sites decrease in intensity, and at the
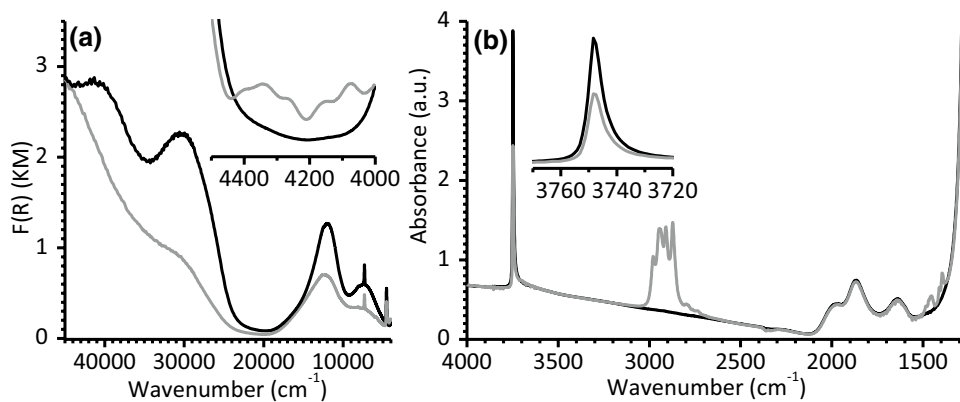
same time also the ν(OH) absorption band in the Mid-IR spectrum is consumed (inset in Fig. 1b), indicating that DEALE reacts with both the Cr(II) sites and the silica surface. Simultaneously, new absorption bands appear in the 3000–2700 cm^{-1} and 1500–1350 cm^{-1} regions, which are straightforwardly assigned to ν(CH$_x$) and δ(CH$_x$) vibrations. The corresponding overtones and combinations are observed in the NIR region (inset in Fig. 1a). These bands are related to the alkyl groups derived from DEALE, although it is not possible to distinguish among all the putative species depicted in Scheme 1c and d, namely the alkylated Cr-R sites and the AlR(OR) species grafted on silica. Indeed, the same bands are observed in the spectrum of SiO$_2$ + DEALE (Fig. S1). This implies that the fraction of modified Cr sites is very small and/or that the vibrational fingerprints of the modified Cr sites do not differ from those of the Al species grafted on silica.

In addition, two important observations must be done. Although the amount of DEALE is the double of the Cr(II) sites, only ca. 30% of the Cr(II) sites seem involved in the reaction. Indeed, the two bands in the DR UV–Vis spectrum at 12,000 and 7500 cm^{-1} decrease of roughly 1/3. At the same time, no specific features associable with the modified Cr sites are observed neither in the UV–Vis nor in the FT-IR spectra. The absence of peculiar spectroscopic fingerprints makes it difficult to unravel the molecular structure of the modified Cr sites. Nevertheless, the observation that the modified Cr sites are almost invisible by UV–Vis spectroscopy might suggest that they have prevalently an octahedral coordination. Indeed, d–d transitions are formally Laporte forbidden for transition metals in octahedral symmetry [28]. Hence, the corresponding bands are expected to have a very low intensity compared to those of the unmodified Cr(II) sites.

3.2 Testing the Cr(II)/SiO$_2$ + DEALE Catalyst in Ethylene Polymerization

The Cr(II)/SiO$_2$ + DEALE catalyst was very active towards ethylene polymerization, even at room temperature and

at mild ethylene pressure. Figure 2a shows the evolution of the FT-IR spectra collected every 12 s during ethylene polymerization, after subtraction of the spectrum before ethylene admission into the cell. Two absorption bands at 2920 and 2855 cm^{-1} rapidly grow and go out of scale in less than 1 min. Simultaneously, in the δ(CH$_2$) region (inset in Fig. 2a), two bands are observed. The first, at 1442 cm^{-1} dominates the spectra at short polymerization times and is assigned to the δ(CH$_2$) vibrational mode of ethylene coordinated to Cr(II) sites [29–32]. The corresponding ν(=CH$_2$) mode is observed at 3004 cm^{-1}. It gives an indication of the existence of a fraction of sites that do coordinate ethylene but are slow to start working (dormant sites) or do not start at all in the experimental conditions (spectators). The same band was previously reported for ethylene coordinated to the unmodified Cr(II)/SiO$_2$ catalyst [29]. The second band, initially at 1463 cm^{-1}, is due to the δ(CH$_2$) vibrational mode of the polyethylene chains. At longer polymerization times a third band appears at ca. 1472 cm^{-1}, which indicates the formation of crystalline polyethylene [33].

Kinetic experiments were performed to evaluate the ethylene polymerization rate on the Cr(II)/SiO$_2$ + DEALE catalyst in comparison with the Cr(II)/SiO$_2$ catalyst. Figure 2b shows the decrease of ethylene pressure as a function of time for the two catalysts, monitored in the same experimental conditions and at a constant Cr loading. The data clearly demonstrate that Cr(II)/SiO$_2$ + DEALE is much faster than the unmodified Cr(II)/SiO$_2$ catalyst. In particular, the reaction rate constant is 14 s^{-1} molCr^{-1} for the unmodified system, and 270 s^{-1} molCr^{-1} for the modified one (20 times higher). Considering that only ca. 30% of the total Cr(II) sites have been modified by DEALE, this means that they are approximately 60 times faster than the unmodified Cr(II) sites in inserting ethylene.

3.3 Probing the Cr(II) Sites Modified by DEALE

Successively, the accessibility of the Cr sites in Cr(II)/ SiO$_2$ + DEALE were investigated by means of FT-IR
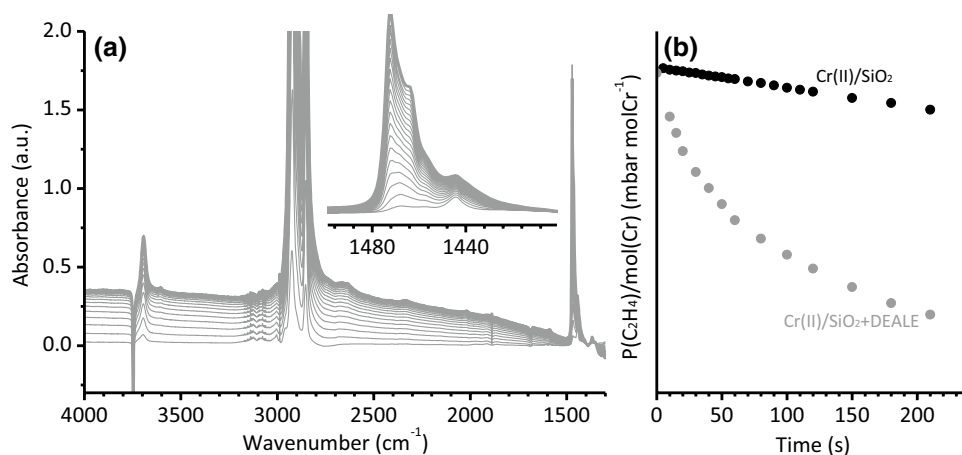
Fig. 2 a FT-IR spectra collected during ethylene polymerization on the Cr(II)/SiO$_2$ + DEALE catalyst (PC$_2$H$_4$ = 100 mbar), after subtraction of the spectrum prior ethylene admission in the cell. The spectra were collected every 12 s. The last spectrum was collected after 4 min of reaction. The inset shows a magnification of the δ(CH$_2$) region. **b** Kinetics of ethylene polymerisation on the Cr(II)/SiO$_2$ + DEALE catalyst in comparison to that on Cr(II)/SiO$_2$, obtained by recording the ethylene equilibrium pressure as a function of time

spectroscopy of adsorbed probe molecules. CO and CD$_3$CN were selected as suitable probes.

3.3.1 CO as a Molecular Probe

Figure 3 shows the evolution of the background subtracted FT-IR spectra, in the ν(CO) region, for CO adsorbed at room temperature on Cr(II)/SiO$_2$ + DEALE (part a) as a function of the CO coverage, compared to the same sequence of spectra collected for CO adsorbed on the unmodified Cr(II)/SiO$_2$ (part b). The same experiment was also performed for SiO$_2$ + DEALE and the corresponding spectra are reported in Fig. S2.

The spectra of CO adsorbed on Cr(II)/SiO$_2$ + DEALE show several absorption bands in two distinct spectral regions. At the maximum CO coverage, a triplet of bands is observed at 2191, 2184 and 2178 cm^{-1}, exactly the same as those observed for CO adsorbed on unmodified Cr(II)/SiO$_2$ (Fig. 2b). In the pioneering works of Zecchina et al. [34–37] they are ascribed to mono- and di-carbonyl species formed on two types of Cr(II) sites grafted on the silica surface through two monoanionic [≡SiO–] siloxy ligands and in interaction with a different number of adjacent siloxane bridges, respectively labelled as Cr$_B$ and Cr$_A$ [23, 38]. Upon decreasing the CO coverage, the 2184 and 2178 cm^{-1} doublet of the di-carbonyl species on Cr$_A$ evolves into a single band at 2180 cm^{-1} due to mono-carbonyl species [23, 38]. The tendency of the Cr(II) sites in unmodified Cr(II)/SiO$_2$ to form non-classical carbonyls (i.e. where the Cr←CO σ donation prevails over the Cr→CO π back-donation) was largely documented in the past and was attributed to the unique nature of the silica support, that acts as a macro- and

Fig. 3 Evolution of the background subtracted FT-IR spectra, in the ν(CO) region, for CO adsorbed at room temperature on Cr(II)/SiO$_2$ + DEALE as a function of the CO coverage (part **a**), compared to the same sequence of spectra collected for CO adsorbed on unmodified Cr(II)/SiO$_2$ (part **b**). All the spectra are reported after subtraction of that collected before CO dosing. Spectra in parts **a** and **b** are normalized for the optical thickness of the pellet. Bold spectra: maximum CO coverage; dotted spectra: irreversible fraction of adsorbed CO. The inset in part **a** shows a magnification of the 2050–1900 cm^{-1} region

multi-dentate ligand able to stabilize Cr(II) sites in geometries which are unlikely for homogeneous complexes [39]. The integrated absorbance of the "triplet" (ca. 20 a.u.) is roughly 70% of that observed for CO adsorbed on unmodified Cr(II)/SiO$_2$ (ca. 29 a.u.). This indicates that approximately 70% of the original Cr(II) sites are not modified by DEALE, a value which is in very good agreement with that estimated by the analysis of the UV–Vis spectra (Fig. 1a).

A second set of bands is observed in the 2100–1900 cm^{-1} region (inset of Fig. 3a), which indicates the formation of classical Cr carbonyls (i.e. of carbonyls where the prevalent contribution is the Cr→CO π back-donation) [40, 41]. In particular, at the maximum CO coverage the main absorption band is centred at 1987 cm^{-1}, with a shoulder at 2014 cm^{-1}. Upon decreasing the CO pressure the former gradually diminishes in intensity and the latter shifts at 2017 cm^{-1}. While classical carbonyls are typically formed on homogeneous Cr complexes [42–45], they are much more rare for Cr species grafted on support materials. One of the very few examples reported in the literature for classical Cr carbonyls on heterogeneous Cr-based systems is represented by CO adsorption on the CO-reduced Cr(II)/SiO$_2$ catalyst modified by hydrosilanes (SiH$_4$ or R$_3$SiH) [46, 47]. In that case, the modifying agents were demonstrated to transform the bis-grafted Cr(II) sites into mono-grafted ones, having a character similar to that of homogeneous Cr complexes, and forming prevalently di-carbonyl species in the presence of CO. The ν(CO) bands observed in the 2100–1900 cm^{-1} region and their evolution upon decreasing the CO coverage are very similar to those reported by Barzan et al. [46], strongly suggesting that they are related to di-carbonyl species formed on mono-grafted Cr sites. It is worth noticing that the bands in the 2100–1900 cm^{-1} region are very weak in comparison to those observed in the "triplet" region. Considering that the molar extinction coefficient for a ν(CO) band increases upon decreasing ν, the fraction of the modified Cr(II) sites accessible by CO should be very small and surely not accounting for the 30% of sites as expected on the basis of the analysis of the triplet region. Notably, when the same experiment is conducted on SiO$_2$ + DEALE (Fig. S2), no absorption bands are observed in the whole spectral region, but only the roto-vibrational spectrum of gaseous CO. The obvious conclusion is that CO molecules at room temperature interacts only with the Cr sites.

Summarizing, the FT-IR spectra reported in Fig. 3 point out the co-presence of at least three types of Cr sites in Cr(II)/SiO$_2$ + DEALE:

(a) a fraction of unmodified Cr(II) sites, accounting for ca. 70% of the originally accessible Cr sites (a value determined by integrating the area behind the "CO triplet");

(b) a first type of modified Cr(II) sites, which are accessible to CO, and are likely mono-grafted to silica, as previ-

ously demonstrated for the sites obtained upon reacting Cr(II)/SiO$_2$ with hydrosilanes;

(c) a second type of modified Cr(II) sites, which are not accessible by CO, probably because shielded by sterically encumbering ligands nearby.

3.3.2 CD$_3$CN as a Molecular Probe

To obtain a more complete description of the Cr(II)/SiO$_2$ + DEALE system, the accessibility of the Cr sites was successively probed by the adsorption of CD$_3$CN at room temperature. This molecule has been largely employed to probe both acid and basic sites on metal oxides and zeolites [48–57]. Curiously it was never used in the characterization of the Phillips catalyst. Since both Cr(II) and Al(III) sites are Lewis acids (i.e. prone to accept electrons), acetonitrile is expected to interact with both of them as a soft Lewis base by sharing the nitrogen lone-pair, according to Eq. (1):

$$CD_3CN : + M(surf) \rightarrow [CD_3CN : \cdots M(surf)]_{ads} \quad (1)$$

where M(surf) = Cr(II) or Al(III).

As a consequence of this interaction, the ν(C≡N) vibration is expected to increase, proportionally to the strength of the Lewis acid-base couple. In general, d-acetonitrile (CD$_3$CN) is employed to avoid the occurrence of an annoying Fermi resonance effect [58].
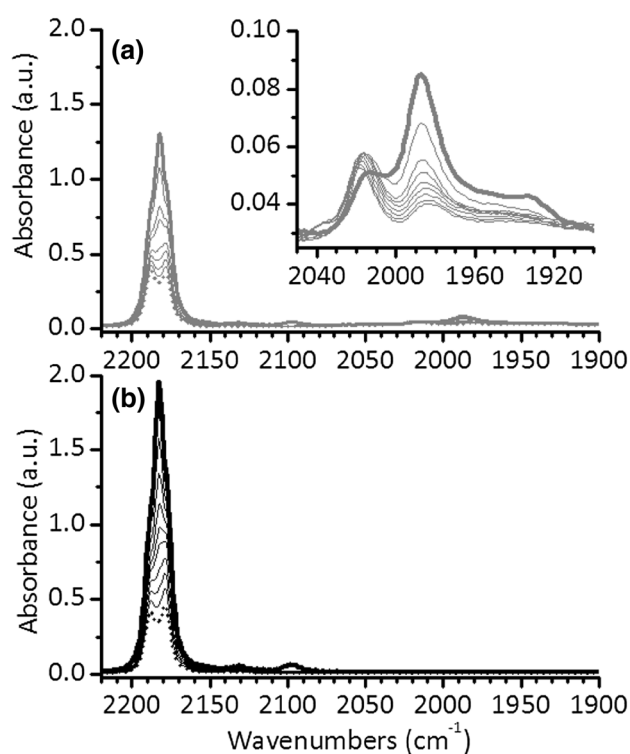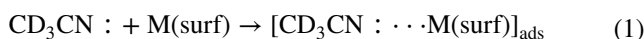
Figure 4 shows the evolution of the background subtracted FT-IR spectra in the ν(C≡N) region for CD$_3$CN adsorbed at room temperature on Cr(II)/SiO$_2$ + DEALE (part a), Cr(II)/SiO$_2$ (part b) and SiO$_2$ + DEALE (part c), as a function of the CD$_3$CN coverage. The data in all the spectral range are reported in Fig. S3. Differently from CO, CD$_3$CN interacts not only with the Cr sites, but also with the silica surface. This is clearly evident by looking to the spectra of CD$_3$CN adsorbed on SiO$_2$ + DEALE (Fig. 4c). Two bands are observed in the ν(C≡N) region, at 2276 and 2267 cm^{-1}, which are assigned to CD$_3$CN adsorbed on the OH groups and to liquid-like acetonitrile, respectively [48, 50, 51, 57]. Both bands decrease rapidly in intensity upon degassing up to disappear, indicating that the interaction of CD$_3$CN with the silica surface is quite weak and fully reversible. A minor band is hardly observable at ca. 2318 cm^{-1}, which is due to CD$_3$CN in interaction with an almost negligible amount of Al(III) species. The majority of Al(III) sites are inaccessible to the probe probably because of steric reasons. In this respect it is worth mentioning that most of the Al-alkyls have the tendency to dimerize [59], and this is likely to happen also between the AlR$_x$ species grafted at the silica surface and the DEALE in excess. The same two bands at 2275 and 2265 cm^{-1} are observed when CD$_3$CN is dosed on Cr(II)/SiO$_2$ (Fig. 3b), although with a reversed intensity. However, this time the spectra are dominated by an intense and broad band centred at ca. 2305 cm^{-1} (integrated absorbance of ca.
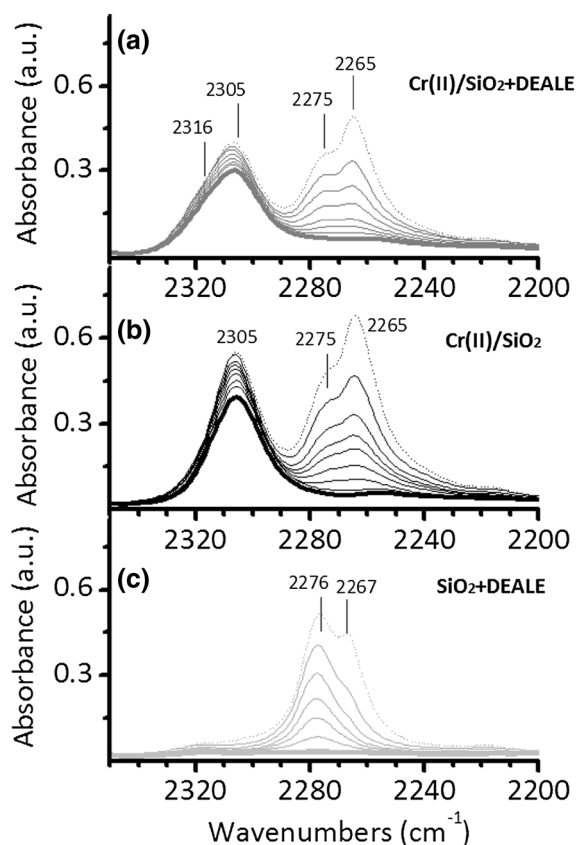
Fig. 4 Evolution of the background subtracted FT-IR spectra, in the $\nu(C{\equiv}N)$ region, for CD_3CN adsorbed at room temperature on Cr(II)/SiO_2 + DEALE as a function of the CO coverage (part **a**), compared to the same sequence of spectra collected for CD_3CN adsorbed on unmodified Cr(II)/SiO_2 (part **b**), and on SiO_2 + DEALE (part **c**). All the spectra are reported after subtraction of that collected before CD_3CN dosing. The spectra are all normalized for the optical thickness of the pellet. Dotted spectra: maximum CD_3CN coverage; bold spectra: irreversible fraction of adsorbed CD_3CN

8.9 a.u.), which is straightforwardly ascribed to CD_3CN in interaction with the Cr(II) sites. This band is only slightly affected by degassing, indicating that the interaction is very strong. The strength of that interaction is the reason why CD_3CN does not discriminate between the Cr_A and Cr_B sites, as done by CO, which is a much weaker (and hence more selective) probe.

The spectra of CD_3CN adsorbed on Cr(II)/SiO_2 + DEALE (Fig. 4a) are very similar to those of CD_3CN adsorbed on Cr(II)/SiO_2 (Fig. 4b), except that the absorption band ascribed to CD_3CN in interaction with Cr(II) sites is even broader and with an evident shoulder at ca. 2316 cm^{-1}. By deconvolving this absorption band two contributions can be found, the first centred at 2305 cm^{-1} (integrated absorbance of ca. 5.8 a.u.), and the second at 2316 cm^{-1} (integrated absorbance of ca. 1.6 a.u.). The former is ascribed to CD_3CN adsorbed on the fraction of unmodified Cr(II) sites, and accounts for about 65% of the total Cr(II) sites, in

excellent agreement with the values determined by the previous analysis. The latter is assigned to CD_3CN adsorbed on the modified Cr(II) sites. Opposite to CO, CD_3CN is able to probe a larger number of modified Cr(II) sites, although perhaps not all of them, but it is unable to discriminate among them. The position of the $\nu(C{\equiv}N)$ band indicates that these sites are more acidic than the unmodified ones.

4 Conclusions

The whole set of spectroscopic data discussed so far allowed to make the following conclusions regarding the reactivity of Cr(II)/SiO_2 with DEALE.

1. DEALE reacts both with the Cr(II) sites and the silica surface, involving both isolated silanols and siloxane bridges.
2. Even when DEALE is used in excess with respect to the Cr sites (stoichiometric ratio Al/Cr = 2/1), only a fraction of the Cr(II) sites are modified, accounting for about 30–35% of the total. This finding has two important consequences. The first is that in Cr(II)/SiO_2 + DEALE a substantial fraction of unmodified Cr(II) sites are always co-present with the modified ones, creating the premises for the development of a tandem catalysis. The second consequence is that there is an abundance of DEALE-derived species at the silica surface, that become part of the environment of the modified Cr(II) sites, affecting their properties in a similar way as the ancillary ligands do in homogeneous catalysis.
3. The modified Cr(II) sites are scarcely accessible by CO, that is notoriously a weak probe, while they are more accessible to CD_3CN, which is a stronger Lewis base. As already demonstrated in the past, the information conveyed by a certain probe molecule is often a compromise between the ability to probe as many sites as possible and the sensibility of discriminating their small differences.
4. Neither CO nor CD_3CN interact with the Al(III) of the DEALE-derived species grafted at the silica surface. This suggests that the Al-grafted species are in the form of small clusters.
5. As far as the modified Cr(II) sites are concerned, they look more acidic than the unmodified Cr(II) sites, and they are likely mono-grafted to the silica surface, i.e. of the type ≡Si–O–Cr–L, where L stands either for an alkyl (R) or an alkoxy group (OR). The presence of the Al-grafted species nearby is essential for their stabilization.
6. Finally, kinetic experiments indicate that the modified Cr(II) sites are ca. 60 times faster in inserting ethylene than the unmodified Cr(II) sites. Several reasons might account for their faster activity, among which the sim-

plest is that they are already alkylated (i.e. the first Cr–C bond is already present). However, it should be noticed that a similar fast kinetic profile is shown also by CO-reduced Cr/Al$_2$O$_3$ in the absence of any activator [5], and recently ascribed to the presence of Al(III) sites in close proximity to the Cr(II) sites [27], a situation very similar to that found for Cr(II)/SiO$_2$ + DEALE.

As a general conclusion, the results discussed in this work demonstrate once more that the intrinsic activity of the Cr sites in Phillips-type catalysts depends not only on their molecular structure, but also on the concurrence of several other phenomena involving the support and the surroundings of the active sites [60].

References

1. Nowlin TE (2014) Business and technology of the global polyethylene industry. Wiley, New York
2. Market Report (2015) Global catalyst market. Acmite Market Intelligence, Ratingen
3. Hutley TJ, Ouederni M (2016) "Polyolefins—the history and economic impact" in polyolefin compounds and materials. Springer, Cham
4. Hogan JP (1958) Banks RL U.S. Patent 2,825,721
5. McDaniel MP (2010) Adv Catal 53:123–606
6. Cicmil D, Meeuwissen J, Vantomme A, Wang J, van Ravenhorst IK, van der Bij HE, Munoz-Murillo A, Weckhuysen BM (2015) Angew Chem 54:13073–13079
7. Schwerdtfeger E, Buck R, McDaniel M (2012) Appl Catal A 423–424:491
8. Bent BE, Nuzzo RG, Dubois LH (1989) J Am Chem Soc 111:1634
9. Klepper KB, Nilsen O, Fjellvåg H (2010) Dalton Trans 39:11628
10. Kerber RN, Kermagoret A, Callens E, Florian P, Massiot D, Lesage A, Coperet C, Delbecq F, Rozanska X, Sautet P (2012) J Am Chem Soc 134:6767–6775
11. Li JH, DiVerdi JA, Maciel GE (2006) J Am Chem Soc 128:17093–17101
12. Pelletier J, Espinas J, Vu N, Norsic S, Baudouin A, Delevoye L, Trebosc J, Le Roux E, Santini C, Basset J-M, Gauvin RM, Taoufik M (2011) Chem Commun 47:2979
13. Sauer J, Ugliengo P, Garrone E, Saunders VR (1994) Chem Rev 94:2095–2160
14. Zhuravlev LT (2000) Colloid Surf A 173:1–38
15. Barzan C, Bordiga S, Groppo E (2016) ACS Catal 6:2918–2922
16. Liu BP, Terano M (2001) J Mol Catal A 172:227–240
17. Liu B, Šindelář P, Fang Y, Hasebe K, Terano M (2005) J Mol Catal A 238:142–150
18. Liu H, Fang Y, Nakatani H, Terano M (2004) Macromol Symp 213:37–46
19. Xia W, Liu B, Fang Y, Hasebe K, Terano M (2006) J Mol Catal A 256:301–308
20. Cicmil D, Meeuwissen J, Vantomme A, Weckhuysen BM (2016) ChemCatChem 8:1937–1944
21. Cicmil D, van Ravenhorst IK, Meeuwissen J, Vantomme A, Weckhuysen BM (2016) Catal Sci Technol 6:731–743
22. Xia W, Tonosaki K, Taniike T, Terano M, Fujitani T, Liu BP (2009) J Appl Polym Sci 111:1869–1877
23. Groppo E, Lamberti C, Bordiga S, Spoto G, Zecchina A (2005) Chem Rev 105:115–183
24. McDaniel M, Welch MB, Dreiling MJ (1983) J Catal 82:118–126
25. Liu B, Šindelář P, Hasebe FangY, Terano K M (2005) J Mol Catal A 238:142–150
26. Groppo E, Damin A, Otero Arean C, Zecchina A (2011) Chem Eur J 17:11110–11114
27. Martino GA, Barzan C, Piovano A, Budnyk A, Groppo E (2018) J Catal 357:206–212
28. Figgis BN (1966) Introduction to ligand fields. Wiley, New York
29. Groppo E, Lamberti C, Bordiga S, Spoto G, Zecchina A (2005) J Phys Chem B 109:15024–15031
30. Ghiotti G, Garrone E, Zecchina A (1991) J Mol Catal 65:73–83
31. Vikulov K, Spoto G, Coluccia S, Zecchina A (1992) Catal Lett 16:117–122
32. Bade OM, Blom R, Dahl IM, Karlsson A (1998) J Catal 173:460–469
33. Chelazzi D, Ceppatelli M, Santoro M, Bini R, Schettino V (2004) Nat Mater 3:470–475
34. Spoto G, Bordiga S, Garrone E, Ghiotti G, Zecchina A, Petrini G, Leofanti G (1992) J Mol Catal 74:175–184
35. Zecchina A, Bordiga S, Spoto G, Marchese L, Petrini G, Leofanti G, Padovan M (1992) J Phys Chem 96:4991–4997
36. Zecchina A, Garrone E, Ghiotti G, Coluccia S (1975) J Phys Chem 79:972–978
37. Zecchina A, Groppo E (2012) Proc R Soc A 468:2087–2098
38. Lamberti C, Zecchina A, Groppo E, Bordiga S (2010) Chem Soc Rev 39:4951–5001
39. Gianolio D, Groppo E, Vitillo JG, Damin A, Bordiga S, Lamberti C (2010) Chem Commun 46:976–978
40. Lupinetti AJ, Frenking G, Strauss SH (1998) Angew Chem Int Ed 37:2113–2116
41. Lupinetti AJ, Strauss SH, Frenking G (2001) Prog Inorg Chem 49:1–112
42. Braterman PS (1975) Metal carbonyl spectra. Academic Press, London
43. Zhou MF, Andrews L, Bauschlicher CW (2001) Chem Rev 101:1931–1961
44. Estephane J, Groppo E, Vitillo JG, Damin A, Gianolio D, Lamberti C, Bordiga S, Quadrelli EA, Basset JM, Kervern G, Emsley L, Pintacuda G, Zecchina A (2010) J Phys Chem C 114:4451–4458
45. Estephane J, Groppo E, Vitillo JG, Damin A, Lamberti C, Bordiga S, Zecchina A (2009) Phys Chem Chem Phys 11:2218–2227
46. Barzan C, Gianolio D, Groppo E, Lamberti C, Monteil V, Quadrelli EA, Bordiga S (2013) Chem Eur J 19:17277–17282
47. Barzan C, Groppo E, Quadrelli EA, Monteil V, Bordiga S (2012) Phys Chem Chem Phys 14:2239–2245
48. Morterra C, Mentruit MP, Cerrato G (2002) Phys Chem Chem Phys 4:676–687
49. Cerruti M, Morterra C, Ugliengo P (2005) Chem Mater 17:1416–1423
50. Morterra C, Cerrato G, Novarino E, Mentruit MP (2003) Langmuir 19:5708–5721
51. Platero EE, Mentruit MP, Morterra C (1999) Langmuir 15:5079–5087
52. Arean CO, Platero EE, Mentruit MP, Delgado MR, Xamena F, Garcia-Raso A, Morterra C (2000) Microporous Mesoporous Mater 34:55–60
53. Sempels RE, Rouxhet PG (1976) J Colloid Interface Sci 55:263–273
54. Pelmenschikov AG, Van Santen RA, Jänchen J, Meijer E (1993) J Phys Chem 97:11071–11074

55. Chen J, Thomas JM, Sankar G (1994) J Chem Soc Faraday Trans 90:3455–3459
56. Aboulayt A, Binet C, Lavalley J (1995) J Chem Soc Faraday Trans 91:2913–2920
57. Cerruti M, Bolis V, Magnacca G, Morterra C (2004) Phys Chem Chem Phys 6:2468–2479
58. Knoezinger H, Krietenbrink H (1975) J Chem Soc Faraday Trans 71:2421–2430
59. Jeffery EA, Mole T (1968) Aust J Chem 21:2683–2686
60. Barzan C, Piovano A, Braglia L, Martino GA, Lamberti C, Bordiga S, Groppo E (2017) J Am Chem Soc 139:17064–17073

The effect of Al-alkyls on the Phillips catalyst for ethylene polymerization: the case of diethylaluminum ethoxide (DEALE)

Giorgia A. Martino, Alessandro Piovano, Caterina Barzan, Silvia Bordiga, Elena Groppo*
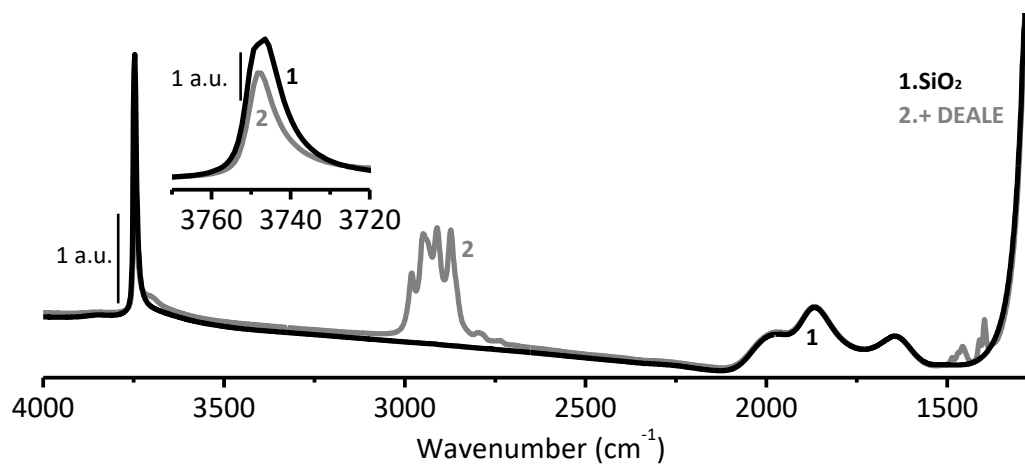
Figure S1 FT-IR spectra of SiO_2 (black spectrum), and of the same sample reacted with DEALE, Al/Cr = 2/1 (grey spectrum). The inset shows a magnification of the ν(OH) absorption band.
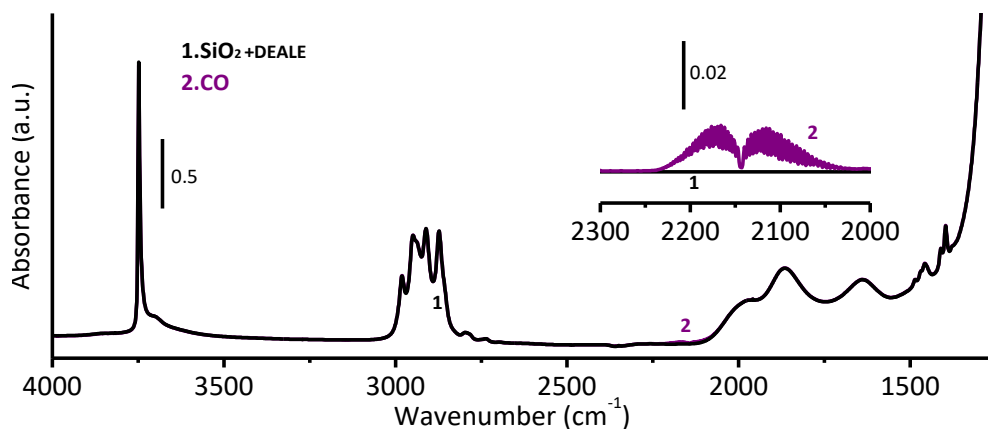
Figure S2 FT-IR spectra of a SiO_2/DEALE before (black spectrum) and after the interaction with CO (purple spectrum). The inset shows a magnification of the $\nu(CO)$ region.
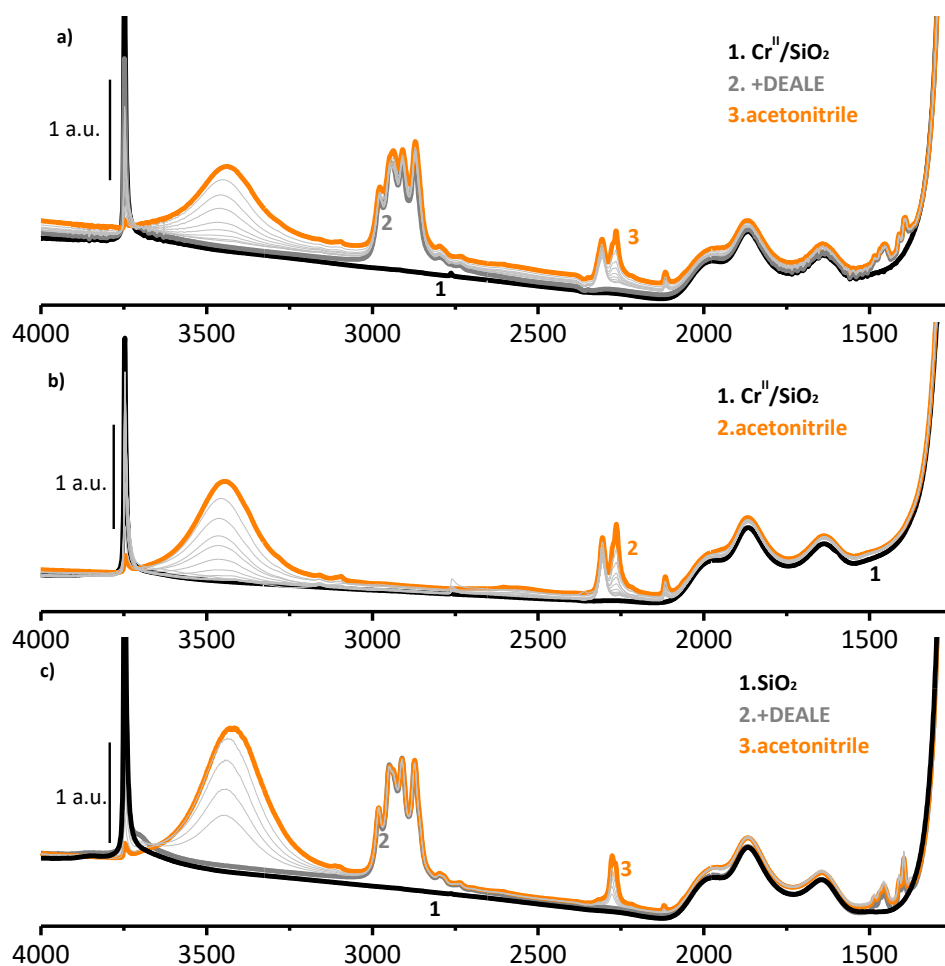
Figure S3 Evolution of the FT-IR spectra for CD_3CN adsorbed at room temperature on $Cr(II)/SiO_2$+DEALE as a function of the CD_3CN coverage (part a), compared to the same sequence of spectra collected for CD_3CN adsorbed on unmodified $Cr(II)/SiO_2$ (part b), and on SiO_2+DEALE (part c). The spectra are all normalized for the optical thickness of the pellet. Orange spectra: maximum CD_3CN coverage.

In Situ X- and Q-Band EPR Investigation of Ethylene Polymerization on Cr/SiO$_2$ Phillips Catalyst

Elena Morra, Giorgia A. Martino, Alessandro Piovano, Caterina Barzan, Elena Groppo,*[ID] and Mario Chiesa*[ID]

Department of Chemistry, INSTM and NIS Centre, University of Torino, via Giuria 7, I-10125 Torino (Italy)

S *Supporting Information*

ABSTRACT: We present an X- and Q-band electron paramagnetic resonance (EPR) investigation of a 0.5 wt % Cr/SiO$_2$ Phillips catalyst, aimed at establishing the Cr oxidation and spin state under different ethylene polymerization conditions. Our data indicate the formation of different Cr(III) species upon reaction of Cr(VI)/SiO$_2$ with ethylene at 150 °C, which is correlated to the disappearance of Cr(V) sites originally present in the catalyst. These species are characterized by unusually large zero field splitting (ZFS). No EPR active species are formed when ethylene is reacted at room temperature with Cr(II)/SiO$_2$, despite clear evidence of a consistent ethylene polymerization activity.
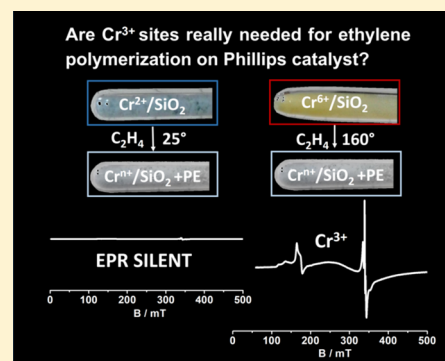
1. INTRODUCTION

Producing annually more than 40% of all high density polyethylene (HDPE), the Cr/SiO$_2$ Phillips catalyst is one of the World's most important industrial catalysts.[1−3] It is also among the most investigated and yet controversial catalytic systems.[3−6] Developed in the 1950s at Phillips Petroleum and industrially used since 1956,[7] it has been the object of both industrial and academic research since its early history. Industrial research was driven by the need of constantly improving the catalytic performances and expanding the portfolio of accessible polymeric products. Academic research was concentrated to solve some fundamental questions.[8−10] Indeed, despite the apparent simplicity of its chemical formulation (Cr ions at the surface of amorphous silica), the Phillips catalyst remains largely mysterious.

A crucial point of debate concerns the initiation mechanism for ethylene polymerization at the Cr sites. This question is strictly connected to the Cr oxidation states, and conflicting views are present in the literature. Unlike other widely used olefin polymerization catalysts, such as the Ziegler−Natta and metallocene ones, the Phillips catalyst does not require the use of any alkylating cocatalyst to trigger the catalytic activity. In the industrial practice, the active sites are directly formed in the polymerization reactor at ca. 100 °C, as a consequence of two subsequent events. During the first step, ethylene slowly reduces the Cr(VI) sites initially present in the precatalyst to low valent Cr(II) sites (step 1 in Scheme 1),[9,11−15] with the concomitant formation of oxygenated byproducts.[2−4,16−22] The initial reduction step is followed by a steady increase in the polymerization activity within the next 1−2 h,[3] associated with the formation of the active alkyl−Cr sites by ethylene itself (step 2 in Scheme 1).[23−25] Alternatively, the Cr(VI) →

Scheme 1. Schematic Representation of the Redox Processes Leading to the Formation of the Active Cr Sites in the Phillips Catalyst[a]
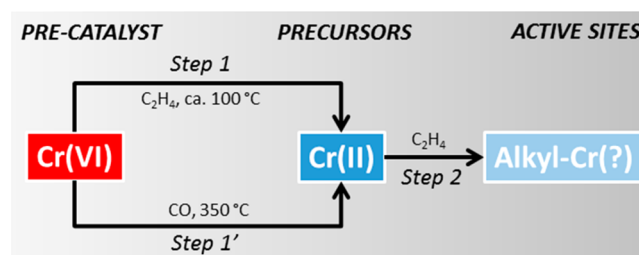
[a]In Step 1 ethylene reduces the Cr(VI) sites to Cr(II) precursors. During the subsequent Step 2 the Cr(II) sites are alkylated and re-oxidized, either to Cr(III) or to Cr(IV). Step 1 and 1′ have a general consensus in the specialized literature, while Step 2 is still debated.

Cr(II) prereduction can be accomplished by using CO at 350 °C as a reducing agent (step 1′ in Scheme 1).[9,14,15] In this case, the induction period is eliminated, but the subsequent development of full polymerization activity follows the same behavior.[3]

It is clear that, whatever the reduction step, the so-formed Cr(II) species are just precursors of the active sites since they do not present the Cr−alkyl bonds required by the Cossee−Arlman polymerization mechanism.[26,27] Hence, the question arises as to how the first Cr−C bond is formed in the presence

of ethylene (step 2 in Scheme 1). Most of the initiation mechanisms proposed in the past involved a two-electron redox step in which Cr(II) is oxidized to Cr(IV) by oxidative addition of ethylene. A similar mechanism is well documented for homogeneous Cr complexes that selectively oligomerize ethylene to α-olefins.[28−30] Several two-electron redox mechanisms have been proposed so far.[3,9,16] Some of them have been supported by (not conclusive) experimental evidence, but most of them have been strongly criticized in the recent literature, mainly based on exceedingly high activation energies predicted by theoretical calculations.[23−25,31−33]

Recently Cr(III) has become the most popular oxidation state for the putative active species in the Phillips catalyst. This is due to the concomitance of two main experimental evidences. The first one is the observation of a high catalytic activity for Cr(III) molecularly defined analogues of the Phillips catalyst obtained by surface organometallic chemistry by the group of Coperet.[34−38] The second experimental evidence is reported by Scott and co-workers and is based on electron paramagnetic resonance (EPR) spectroscopic experiments performed on Cr-doped porous silica xerogels, which suggest the rapid reoxidation of Cr(II) sites to Cr(III) in the presence of diluted amounts of ethylene.[15,39] Based on these EPR results the same authors proposed two possible mechanisms that can explain the formation of the organo-Cr(III) propagating sites starting from Cr(II) and ethylene.[24,25]

The above-mentioned results and the associated proposed mechanisms[15,24,25,34,36,39−42] are of great interest but need to be extended and validated for the classical Cr/SiO$_2$ Phillips catalyst in the presence of an excess of ethylene. In fact, although there are no doubts that Cr(III)-based catalysts can efficiently polymerize ethylene,[43,44] these systems are not necessarily representative of the active Cr sites in the classical Phillips catalyst. To do so, we performed a detailed X- and Q-band EPR investigation of a 0.5 wt % Cr/SiO$_2$ Phillips catalyst, with systematic simulation of the experimental spectra, aimed at establishing the Cr oxidation state under different ethylene polymerization conditions. The EPR spectroscopy of Cr/SiO$_2$ Phillips catalysts is particularly delicate because of the possible copresence of several Cr oxidation and spin states, not always detectable at conventional frequencies and temperatures. Cr(III) (d^3, $S = 3/2$) and Cr(V) (d^1, $S = 1/2$) are the typical EPR-active species observed on Cr/SiO$_2$ catalysts at conventional frequencies.[45,46] Interestingly Cr(III) in a low spin $S = 1/2$ state has also been reported recently.[47] EPR evidence for the formation of Cr(II) in model Phillips catalysts has also been recently provided by Scott and co-workers, operating at 106 GHz.[15]

2. EXPERIMENTAL SECTION

Sample Preparation. The Cr(VI)/SiO$_2$ sample (Cr loading 1 wt %) was prepared by wet impregnation of a pyrogenic silica (Aerosil, surface area ca. 380 m^2 g^{-1}) employing CrO$_3$ as the chromium precursor. The catalyst was activated directly inside the EPR cell, to avoid any type of contamination. The activation procedure consisted of two main steps: (i) activation at 650 °C in dynamic vacuum (residual pressure <10^{-4} mbar) in order to dehydroxylate the silica surface and (ii) subsequent oxidation in O$_2$ (equilibrium pressure ca. 100 mbar, twice) at the same temperature to graft the Cr species in the form of monochromates.[9] The Cr(II)/SiO$_2$ sample was obtained from Cr(VI)/SiO$_2$ after further

reduction in CO (equilibrium pressure ca. 100 mbar, twice) at 350 °C, followed by degassing at the same temperature.[9]

Ethylene Polymerization. Ethylene polymerization on Cr(VI)/SiO$_2$ was performed by contacting the activated catalyst with ethylene, at an equilibrium pressure of 100 mbar and at a temperature of 150 °C, for increasing time. X-band EPR spectra were collected at 77 K at four subsequent steps (10 min, 30 min, 1 h, and 2 h). Ethylene polymerization on Cr(II)/SiO$_2$ was performed by dosing ethylene at room temperature. The reaction was quenched after 10 min by cooling the sample with liquid nitrogen, and the X-band EPR spectrum was collected.

EPR Measurements. X-band (microwave frequency 9.76 GHz) and Q-band (microwave frequency 33.7 GHz) CW-EPR experiments were carried out on a Bruker ELEXYS 580 EPR spectrometer, equipped with a SHQ cavity (X-band) and a flexline dielectric ring Q-band EPR and ENDOR resonator (Bruker EN 5107D2). Low-temperature measurements were performed at Q-band with an Oxford Instruments CF935 continuous flow helium cryostat. X-band measurements at 77 K were performed using a finger dewar, filled with liquid nitrogen. The magnetic field was measured with a Bruker ER035 M NMR gaussmeter. The temperature at which different experiments were carried out is specified in the figure captions. All simulations of the EPR spectra were done using Easyspin.[48]

3. RESULTS AND DISCUSSION

3.1. Ethylene Polymerization on Cr(II)/SiO$_2$. After the oxidative treatment at 650 °C, most of the Cr sites in the Cr/SiO$_2$ catalyst are in the form of diamagnetic Cr(VI) monochromates, hence EPR inactive. The X-Band EPR spectrum of such an oxidized sample (hereafter indicated as Cr(VI)/SiO$_2$) is characterized by pseudo axial resonances in the g region, 1.895−1.979 (spectrum 1 in Figure 1a), which is due to residual Cr(V) species, always present in this system and usually considered as spectators.[3,45,46] The amount of Cr(V) is typically lower than 2% of the total Cr sites.[46]
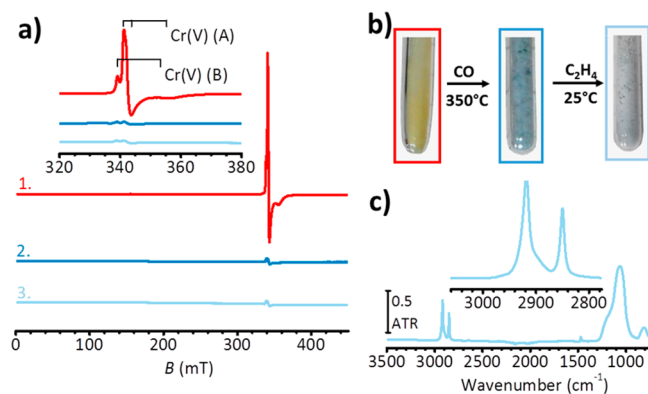
Figure 1. (a) X-band CW-EPR spectra of oxidized Cr(VI)/SiO$_2$ (1), CO-reduced Cr(II)/SiO$_2$ (2), and Cr(II)/SiO$_2$ after reaction with ethylene ($P = 100$ mbar) at room temperature (3). The enlargement of the $g = 2$ resonant-field region is shown in the inset. The spectra were recorded at $T = 77$ K, with microwave power of 1 mW. (b) Pictures of the Cr/SiO$_2$ catalyst upon the different treatments. The colors correspond to those of the EPR spectra in panel (a). (c) ATR FT-IR spectrum of the Cr(II)/SiO$_2$ catalyst after ethylene polymerization. The inset shows a magnification of the $\nu_{asym}(CH_2)$ and $\nu_{sym}(CH_2)$ bands of polyethylene.

Table 1. Spin-Hamiltonian Parameters Extracted from Computer Simulation of the Spectra Reported in Figures 3, S1, and S4[a]

system	species	%	g_1	g_2	g_3	$\lvert D \rvert$	$\lvert E/D \rvert$
Cr(VI)/SiO$_2$	Cr(V) (A)	90	1.978	1.968	1.89		
	Cr(V) (B)	10	1.988		1.91		
Cr(VI)/SiO$_2$ + C$_2$H$_4$@160 °C	Cr(III) (C)	45	1.98			70	0.02
	Cr(III) (D)	45	1.98			70	0.2
	Cr(III) (E)	4	2.010	2.000	1.98		
	Cr(V) (A)	6	1.978	1.968	1.89		

[a]The zero-field splitting terms are given in GHz. The spectral deconvolutions are presented in Figures S1 and S5.

Computer simulation (Figure S1, Supporting Information) indicates the presence of two different species (labeled A and B in Figure 1a) with different spin Hamiltonian parameters (Table 1), reflecting different local symmetries.

Reaction of the Cr(VI)/SiO$_2$ with CO at 350 °C leads to a change in the sample color (from orange to light blue in Figure 1b) associated with the reduction of Cr to low valent Cr(II) species (hereafter indicated as Cr(II)/SiO$_2$ catalyst). Such species, characterized by a non-Kramer spin state ($S = 2$), are EPR silent at conventional frequency-field conditions; therefore, only the disappearance of the Cr(V) signal is monitored at the X-band (spectrum 2 in Figure 1a). After reduction with CO (Figure 1a1) the integrated area of the Cr(V) peak decreases by ca. 97% with respect to the starting Cr(VI)/SiO$_2$, indicating that almost all the Cr(V) sites have been reduced by CO at 350 °C.

At this stage, ethylene ($P = 100$ mbar) was admitted to the sample at room temperature. Ethylene polymerization rapidly occurred, as testified by the decrease of the ethylene pressure, by the rapid change of the powder appearance (from light blue to whitish in Figure 1b), and finally by the ATR-IR spectrum collected (a posteriori) on the catalyst (Figure 1c). After 10 min, the reaction was quenched with liquid nitrogen, and an EPR spectrum was collected (spectrum 3 in Figure 1a). We do not observe any change in the EPR spectrum before and after ethylene polymerization. These results unequivocally indicate that, under our experimental conditions, the active Cr-alkyl sites originated by reacting Cr(II)/SiO$_2$ with an excess of ethylene at room temperature are not EPR active. These results greatly differ from those reported by Scott and co-workers,[39] who observed the formation of a significantly intense signal at $g = 1.981$ after ethylene polymerization on Cr(II)/SiO$_2$, which was assigned to Cr(III)-alkyl species originated from the one-electron oxidation of Cr(II) by ethylene. Although the absence of an EPR signal does not necessarily imply that no Cr(III) is present in the sample, considering the EPR detection limit, this should be much below 10 ppm, which is much less than 0.2% of the total Cr sites. It seems thus unrealistic that such a small amount of Cr(III), if present, is only responsible for the catalytic activity of the catalyst. In this respect, we notice that one of the most reliable methods for determining the fraction of active Cr sites in the Phillips catalyst is titration by poisons. Depending on the type of poisons, values comprised between 10% and 60% have been estimated,[3] which are more than an order of magnitude larger than the detection limit of EPR.

3.2. Ethylene Polymerization on Cr(VI)/SiO$_2$. As a complementary experiment, the oxidized Cr(VI)/SiO$_2$ sample was reacted directly with ethylene at 150 °C,[49] for increasing time lengths. Also in this case the occurrence of the polymerization was indicated by the decrease in ethylene pressure and univocally proven by the whitish coverage around

the catalyst particles (Figure 2b) and by FT-IR spectroscopy in ATR mode at the end of the experiment (Figure 2c). The
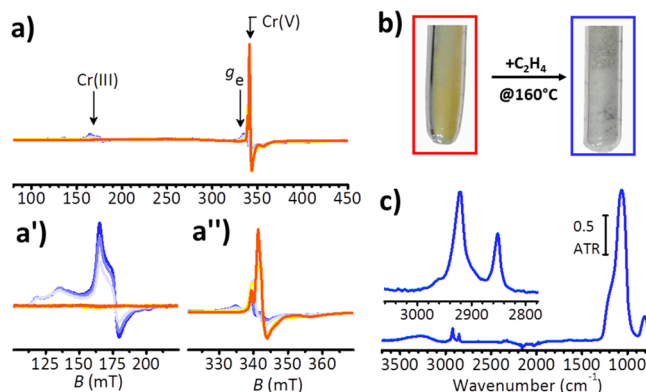
Figure 2. (a) X-band CW-EPR spectra of Cr(VI)/SiO$_2$ (red trace) and upon reaction with ethylene at 150 °C for 10 min, 30 min, 1 h, and 2 h (blue trace). Panels (a′) and (a″) show the enlargements of the low-field and $g = 2$ resonant-field spectral regions. The spectra were recorded at $T = 77$ K, with microwave power of 1 mW. (b) Pictures of the Cr(VI)/SiO$_2$ before and after reaction with C$_2$H$_4$. (c) ATR FT-IR spectra of the Cr/SiO$_2$ catalyst after ethylene polymerization.

corresponding EPR results are reported in Figure 2a. Upon reaction with ethylene, a marked change in the EPR spectrum occurs in both the low-field (100−225 mT) and $g = 2$ resonant-field (320−370 mT) spectral regions of both X- (Figure 2a′ and Figure 2a″) and Q-band (Figure S2). After 10 min of reaction with ethylene the EPR signals associated with Cr(V) species decrease in intensity. After 30 min of reaction a further decrease in intensity, accompanied by a g shift and a change in the spectral profile in the g_e region, is observed, together with the appearance of a new complex signal in the low-field region (Figure 2a′) at $g \approx 4.3$. This signal, which is not detected when ethylene is reacted with Cr(II)/SiO$_2$ catalyst (Figure 1a), is the fingerprint of Cr(III) (d^3, $S = 3/2$) species and further increases in intensity for prolonged reaction times.

Simulation of the spectra taken at different reaction steps (before reaction, after 30 min, and after 2 h of reaction with ethylene) allows estimating the relative contribution of the different species as a function of the reaction evolution (Figure S3). The overall contribution of Cr(V) is found to decrease from 99 ± 1% to 13 ± 2% after 30 min of reaction to 4 ± 3% at the end of the reaction, while the corresponding contribution of the overall Cr(III) species (see Table 1) is found to increase from 1 ± 1% up to 96 ± 3%. Although it is not possible to exclude that a fraction of the Cr(III) sites is derived from the reduction of Cr(VI), a clear correlation between the disappearance of the Cr(V) signal and the onset

of the Cr(III) signal is found. Moreover, we note that reduction of Cr(V) to Cr(III) is also consistent with the absence of Cr(III) in the EPR spectrum of Cr(II)/SiO$_2$ after ethylene polymerization, where no Cr(V) was present.

Unfortunately, a quantitative evaluation of the total Cr(III) species is hampered by the lack of a suitable standard. From the simulation of the EPR spectra of Cr(III) we find evidence of a ZFS term D larger than the X- and Q-band mw quantum (0.32 and 1.1 cm^{-1}). Under these circumstances some transitions may fall beyond the magnetic field range of the spectrometer, preventing the determination of a spin number via integration of the spectral area. Moreover, the two species have different spin states. It has been demonstrated[50] that the integrated EPR signal intensity is proportional to $S(S + 1)$ and that this must be taken into account in comparing the relative concentrations of paramagnetic species with different spins. In our case, considering two species Cr(V) and Cr(III) with $S = 1/2$ and $S = 3/2$, respectively, the number of spins of the two species will be given by $N_{Cr(V)} = N_{Cr(III)} \frac{g_{Cr(III)}}{g_{Cr(V)}} \frac{(S_{Cr(III)}(S_{Cr(III)} + 1))}{(S_{Cr(V)}(S_{Cr(V)} + 1))} \frac{A_{Cr(V)}}{A_{(Cr(III))}}$ where A is the integrated area, g the average g value, and S the spin. Assuming the same average g factor (which is a reasonable approximation) two signals with the same integrated area will correspond to a spin population $N_{cr(V)} = 5N_{Cr(III)}$. It is clear therefore that, the spin states being different, direct comparison between the integrated areas of the two signals cannot be made.

Computer simulation at both X- (Figure 3) and Q-band (Figure S4) frequencies was carried out on the basis of the
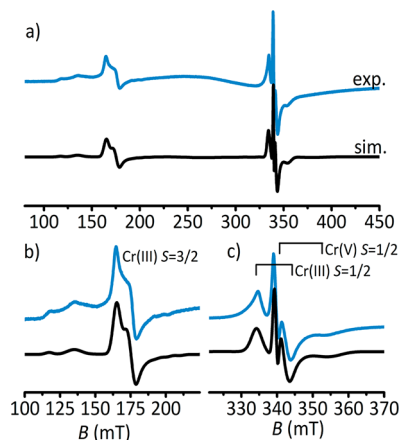

Figure 3. (a) Experimental (blue) and simulated (black) CW-EPR spectra of Cr(VI)/SiO$_2$ reacted with ethylene at 150 °C for 2 h, recorded at X-band. The X-band spectrum was recorded at $T = 77$ K, with microwave power of 1 mW. Panels (b) and (c) show the enlargements of the low-field and $g = 2$ resonant-field spectral regions. The corresponding experimental and simulated Q-band spectra are shown in Figure S3 of the Supporting Information.

following overall spin Hamiltonian: $\hat{\mathcal{H}} = \mu_B \mathbf{Bg\hat{S}} + \hat{S}\mathbf{D}\hat{S}$, where $\mathbf{D}$ is the zero field splitting (ZFS) tensor, which is usually expressed in term of the parameters $D = \frac{2D_z - (D_x + D_y)}{2}$ and $E = \frac{(D_x - D_y)}{2}$, with D_x, D_y, and D_z being the principal elements of the traceless $\mathbf{D}$ tensor. The ZFS is very sensitive to structural changes, its magnitude reflecting deviations from high (cubic) symmetry.[51] The spin Hamiltonian parameters

used in the simulation are reported in Table 1 and were used to fit the X- and Q-band spectra simultaneously. The best fit of the spectra was obtained by assuming the presence of three different types of Cr(III) species (species C, D, and E) featuring different |D| values and |E/D| ratios, which reflect different local symmetries. Species C was perfectly reproducible over a number of experiments, while the intensity of the spectral components associated with species D was found to be erratic. In any case for both species an unusually high value of $D = 70$ GHz (2.3 cm^{-1}) was needed in order to reproduce the low-field spectral features at both frequencies. This value is larger than those reported by Weckhuysen et al.[45] for Cr(III) on a Cr/SiO$_2$ catalyst oxidized at 550 °C and CO-reduced at 200 °C and by Coperet and co-workers for Cr(III) molecular precursors grafted on SiO$_2$,[47] but consistent with values for three-coordinated Cr(III) molecular complexes, subjected to a large trigonal crystal field,[52] although a comparison with homogeneous systems must be done with caution as surface Cr species on amorphous silica are often stabilized in geometries unconventional for homogeneous complexes. We remark, however, that such a large ZFS can be determined only approximately at these microwave frequencies, and further high-field EPR experiments will be needed.

A relatively sharp resonance component is also present in the $g = 2.0$ region of the spectrum. This signal can be explained only assuming a third Cr(III) species (species E), which, based on the comparison between X- and Q-band experiments, can be simulated assuming an $S = 1/2$ species with ($g_1 = 2.010$, $g_2 = 2.000$. $g_3 = 1.98$). Similar spectra have been reported for frozen solutions of unsaturated 13-electron Cr(III)-alkyl complexes[53] and more recently for Cr(III) species grafted on SiO$_2$.[47] Based on the spectral simulation these features represent however a small fraction of the overall spectral intensity not exceeding the 1% of the EPR active Cr.

4. CONCLUSIONS

The above-reported EPR experiments unambiguously show the formation of different Cr(III) species characterized by high ZFS, together with a minority of low-spin Cr(III), upon reaction of the Cr(VI)/SiO$_2$ catalyst with ethylene at 150 °C. The formation of these Cr(III) sites is correlated to the disappearance of the Cr(V) sites originally present in the oxidized catalyst, suggesting a two-electron reduction process. The unusually large ZFS term points to low-symmetry Cr(III) sites, and further work is needed to relate the spin Hamiltonian parameters to specific structures. Whether or not these sites are involved in ethylene polymerization cannot be affirmed yet. However, no evidence for the formation of Cr(III) species is found when ethylene is reacted at room temperature with the Cr(II)/SiO$_2$ catalyst, despite clear evidence of a consistent ethylene polymerization activity. Hence, under the adopted experimental conditions, it seems that isolated Cr(III) sites are not necessary for developing ethylene polymerization on the Cr/SiO$_2$ Phillips catalyst. This is in stark contrast with the results recently published by Scott and co-workers,[39] who showed the appearance of an intense signal at $g = 1.981$ during ethylene polymerization on Cr(II)/SiO$_2$ and assigned it to Cr(III)-alkyl sites. It is essential to stress at this stage the importance of the specific experimental conditions and sample chemical history, which can critically influence the reaction pathway of the catalyst. The differences in the experimental conditions may explain the discrepancies between our results and those reported in ref 39 where the reaction was performed

with diluted ethylene and in the presence of a self-sealing porous silica xerogel as a support. In summary, although we do not solve yet the problem of the nature of the active sites in the Phillips catalyst, our results reopen the question on the oxidation (and spin) state of the propagating Cr-alkyl sites that was recently presented as a closed case. Rather, these results give new life to the mechanistic proposal involving Cr(IV)-dialkyls species (EPR silent at conventional frequency field) proposed in the past.[9,24]

ASSOCIATED CONTENT

Ⓢ Supporting Information

The Supporting Information is available free of charge on the ACS Publications website at DOI: 10.1021/acs.jpcc.8b07699.

EPR simulation and spectral deconvolution for Cr(V) species detected on the Cr(VI)/SiO$_2$ catalyst; comparison of X- and Q-band spectra recorded on the Cr(VI)/SiO$_2$ catalyst after reaction with ethylene at 150 °C for 2 h; experimental and simulated X-band and Q-band EPR spectra of the Cr(VI)/SiO$_2$ catalyst at different stages of reaction with ethylene (PDF)

AUTHOR INFORMATION

Corresponding Authors
*E-mail: elena.groppo@unito.it.
*E-mail: mario.chiesa@unito.it.

ORCID Ⓘ
Elena Groppo: 0000-0003-4153-5709
Mario Chiesa: 0000-0001-8128-8031

Notes
The authors declare no competing financial interest.

REFERENCES

(1) Nowlin, T. E. *Business and Technology of the Global Polyethylene Industry*; Scrivener Publishing LLC: New York, 2014.

(2) Cheng, R.; Liu, Z.; Zhong, L.; He, X.; Qiu, P.; Terano, M.; Eisen, M. S.; Scott, S. L.; Liu, B. Phillips Cr/Silica Catalyst for Ethylene Polymerization. *Adv. Polym. Sci.* **2013**, *257*, 135−202.

(3) McDaniel, M. P. A Review of the Phillips Supported Chromium Catalyst and its Commercial Use for Ethylene Polymerization. *Adv. Catal.* **2010**, *53*, 123−606.

(4) McDaniel, M. P. Supported Chromium Catalysts for Ethylene Polymerization. *Adv. Catal.* **1985**, *33*, 47−98.

(5) McDaniel, M. P. Handbook of heterogeneous catalysis. In *Handbook of Heterogeneous Catalysis*; Ertl, G., Knözinger, H., Weitkamp, J., Ed.; VHC: Weinheim, 1997; Vol. 5, p 2400.

(6) McDaniel, M. Some Reflections on the Current State of Cr-based Polymerization Catalysts. *MRS Bull.* **2013**, *38*, 234−238.

(7) Hogan, J. P.; Banks, R. L. U.S. Patent 2,825,721, 1958.

(8) Weckhuysen, B. M.; Wachs, I. E.; Shoonheydt, R. A. Surface Chemistry and Spectroscopy of Chromium in Inorganic Oxides. *Chem. Rev.* **1996**, *96*, 3327−3349.

(9) Groppo, E.; Lamberti, C.; Bordiga, S.; Spoto, G.; Zecchina, A. The Structure of Active Centers and the Ethylene Polymerization Mechanism on the Cr/SiO$_2$ Catalyst: a Frontier for the Characterization Methods. *Chem. Rev.* **2005**, *105*, 115−183.

(10) Groppo, E.; Seenivasan, K.; Barzan, C. The Potential of Spectroscopic Methods Applied to Heterogeneous Catalysts for Olefin Polymerization. *Catal. Sci. Technol.* **2013**, *3*, 858−878.

(11) Krauss, v. H. L.; Stach, H. Chrom(II) Als Wirksamer Bestandteil des Phillips Katalysators zur Äthylenpolymerisation. *Inorg. Nucl. Chem. Lett.* **1968**, *4*, 393−397.

(12) Krauss, H. L.; Stach, H. Über Oberflächenverbindungen von Übergangsmetallen, III. Reaktionen Reduzierter PHILLIPS-Kontakte. *Z. Anorg. Allg. Chem.* **1969**, *366*, 34−42.

(13) Finch, J. N. Reduction Studies on Supported Chromic Anhydride Catalysts. *J. Catal.* **1976**, *43*, 111.

(14) Zecchina, A.; Garrone, E.; Ghiotti, G.; Morterra, C.; Borello, E. On the Chemistry of Silica Supported Chromium Ions. I. Characterization of the Samples. *J. Phys. Chem.* **1975**, *79*, 966−972.

(15) Brown, C.; Krzystek, J.; Achey, R.; Lita, A.; Fu, R.; Meulenberg, R. W.; Polinski, M.; Peek, N.; Wang, Y.; Van De Burgt, L. J.; Profeta, S.; Stiegman, A. E.; Scott, S. L. Mechanism of Initiation in the Phillips Ethylene Polymerization Catalyst: Redox Processes Leading to the Active Site. *ACS Catal.* **2015**, *5*, 5574−5583.

(16) Liu, Z.; He, X.; Cheng, R.; Eisen, M. S.; Terano, M.; Scott, S. L.; Liu, B. Chromium Catalysts for Ethylene Polymerization and Oligomerization. *Adv. Chem. Eng.* **2014**, *44*, 127−191.

(17) Liu, B.; Nakatani, H.; Terano, M. New Aspects of the Induction Period of Ethene Polymerization Using Phillips CrO$_x$/SiO$_2$ Catalyst Probed by XPS, TPD and EPMA. *J. Mol. Catal. A: Chem.* **2002**, *184*, 387−398.

(18) Liu, B. P.; Nakatani, H.; Terano, M. Mechanistic Implications of the Unprecedented Transformations of Ethene into Propene and Butene over Phillips CrO$_x$/SiO$_2$ Catalyst During Induction Period. *J. Mol. Catal. A: Chem.* **2003**, *201*, 189−197.

(19) Xia, W.; Liu, B.; Fang, Y.; Hasebe, K.; Terano, M. Unique Polymerization Kinetics Obtained from Simultaneous Interaction of Phillips Cr(VI)Ox/SiO$_2$ Catalyst with Al-alkyl Cocatalyst and Ethylene Monomer. *J. Mol. Catal. A: Chem.* **2006**, *256*, 301−308.

(20) Zhong, L.; Liu, Z.; Cheng, R.; Tang, S.; Qiu, P.; He, X.; Terano, M.; Liu, B. Active Site Transformation During the Induction Period of Ethylene Polymerization over the Phillips CrOx/SiO$_2$ Catalyst. *ChemCatChem* **2012**, *4*, 872−881.

(21) Potter, K. C.; Beckerle, C. W.; Jentoft, F. C.; Schwerdtfeger, E.; Mcdaniel, M. P. Reduction of the Phillips Catalyst by Various Olefins: Stoichiometry, Thermochemistry, Reaction Products and Polymerization Activity. *J. Catal.* **2016**, *344*, 657−668.

(22) Barzan, C.; Piovano, A.; Braglia, L.; Martino, G. A.; Lamberti, C.; Bordiga, S.; Groppo, E. Ligands Make the Difference! Molecular Insights into CrVI/SiO$_2$ Phillips Catalyst During Ethylene Polymerization. *J. Am. Chem. Soc.* **2017**, *139*, 17064−17073.

(23) Fong, A.; Yuan, Y.; Ivry, S. L.; Scott, S. L.; Peters, B. Computational Kinetic Discrimination of Ethylene Polymerization Mechanisms for the Phillips (Cr/SiO$_2$) Catalyst. *ACS Catal.* **2015**, *5*, 3360−3374.

(24) Fong, A.; Peters, B.; Scott, S. L. One-Electron-Redox Activation of the Reduced Phillips Polymerization Catalyst, via Alkylchromium-(IV) Homolysis: A Computational Assessment. *ACS Catal.* **2016**, *6*, 6073−6085.

(25) Fong, A.; Vandervelden, C.; Scott, S. L.; Peters, B. Computational Support for Phillips Catalyst Initiation via Cr-C Bond Homolysis in a Chromacyclopentane Site. *ACS Catal.* **2018**, *8*, 1728−1733.

(26) Cossee, P. Ziegler-Natta catalysis I. Mechanism of Polymerization of α-olefins with Ziegler-Natta Catalysts. *J. Catal.* **1964**, *3*, 80−88.

(27) McGuinness, D. S.; Davies, N. W.; Horne, J.; Ivanov, I. Unraveling the Mechanism of Polymerization with the Phillips Catalyst. *Organometallics* **2010**, *29*, 6111−6116.

(28) McGuinness, D. S. Olefin Oligomerization via Metallacycles: Dimerization, Trimerization, Tetramerization, and Beyond. *Chem. Rev.* **2011**, *111*, 2321−2341.

(29) Jabri, A.; Mason, C. B.; Sim, Y.; Gambarotta, S.; Burchell, T. J.; Duchateau, R. Isolation of Single-Component Trimerization and Polymerization Chromium Catalysts: The Role of the Metal Oxidation State. *Angew. Chem., Int. Ed.* **2008**, *47*, 9717−9721.

(30) Thapa, I.; Gambarotta, S.; Korobkov, I.; Murugesu, M.; Budzelaar, P. Isolation and Characterization of a Class II Mixed-Valence Chromium(I)/(II) Self-Activating Ethylene Trimerization Catalyst. *Organometallics* **2012**, *31*, 486−494.

(31) Gierada, M.; Handzlik, J. Active Sites Formation and their Transformations During Ethylene Polymerization by the Phillips CrOx/SiO2 Catalyst. *J. Catal.* **2017**, *352*, 314−328.

(32) Gierada, M.; Handzlik, J. Computational Insights into Reduction of the Phillips CrOx/SiO2 catalyst by Ethylene and CO. *J. Catal.* **2018**, *359*, 261−271.

(33) Chakrabarti, A.; Gierada, M.; Handzlik, J.; Wachs, I. E. Operando Molecular Spectroscopy During Ethylene Polymerization by Supported CrOx/SiO2 Catalysts: Active Sites, Reaction Intermediates, and Structure-Activity Relationship. *Top. Catal.* **2016**, *59*, 725−739.

(34) Conley, M. P.; Delley, M. F.; Siddiqi, G.; Lapadula, G.; Norsic, S.; Monteil, V.; Safonova, O. V.; Copéret, C. Polymerization of Ethylene by Silica-Supported Dinuclear Cr[III] Sites Through an Initiation Step Involving C = H Bond Activation. *Angew. Chem., Int. Ed.* **2014**, *53*, 1872−1876.

(35) Conley, M. P.; Delley, M. F.; Núñez-Zarur, F.; Comas-Vives, A.; Copéret, C. Heterolytic Activation of C-H Bonds on Cr[III]-O Surface Sites is a Key Step in Catalytic Polymerization of Ethylene and Dehydrogenation of Propane. *Inorg. Chem.* **2015**, *54*, 5065−5078.

(36) Delley, M. F.; Núñez-Zarur, F.; Conley, M. P.; Comas-Vives, A.; Siddiqi, G.; Norsic, S.; Monteil, V.; Safonova, O. V.; Copéret, C. Proton Transfers Are Key Elementary Steps in Ethylene Polymerization on Isolated Chromium(III) Silicates. *Proc. Natl. Acad. Sci. U. S. A.* **2014**, *111*, 11624−11629.

(37) Delley, M. F.; Praveen, C. S.; Borosy, A. P.; Núñez-Zarur, F.; Comas-Vives, A.; Copéret, C. Olefin Polymerization on Cr(III)/SiO2: Mechanistic Insights from the Differences in Reactivity Between Ethene and Propene. *J. Catal.* **2017**, *354*, 223−230.

(38) Liu, H. J.; Cai, I. C.; Fedorov, A.; Ziegler, M. S.; Copéret, C.; Tilley, T. D. Tricoordinate Organochromium(III) Complexes Supported by a Bulky Silylamido Ligand Produce Ultra-High-Molecular Weight Polyethylene in the Absence of Activators. *Helv. Chim. Acta* **2016**, *99*, 859−867.

(39) Brown, C.; Lita, A.; Tao, Y.; Peek, N.; Crosswhite, M.; Mileham, M.; Krzystek, J.; Achey, R.; Fu, R.; Bindra, J. K.; Polinski, M.; Wang, Y.; Van De Burgt, L. J.; Jeffcoat, D.; Profeta, S.; Stiegman, A. E.; Scott, S. L. Mechanism of Initiation in the Phillips Ethylene Polymerization Catalyst: Ethylene Activation by Cr(II) and the Structure of the Resulting Active Site. *ACS Catal.* **2017**, *7*, 7442−7455.

(40) Peters, B.; Scott, S. L.; Fong, A.; Wang, Y.; Stiegman, A. E. Reexamining the Evidence for Proton Transfers in Ethylene Polymerization. *Proc. Natl. Acad. Sci. U. S. A.* **2015**, *112*, E4160−E4161.

(41) Conley, M. P.; Delley, M. F.; Siddiqi, G.; Lapadula, G.; Norsic, S.; Monteil, V.; Safonova, O. V.; Copéret, C. Erratum: Polymerization of Ethylene by Silica-Supported Dinuclear Cr[III] Sites through an Initiation Step Involving C-H Bond Activation. *Angew. Chem., Int. Ed.* **2015**, *54*, 6670.

(42) Delley, M. F.; Nuñez-Zarura, F.; Conley, M. P.; Comas-Vivesa, A.; Siddiqia, G.; Norsic, S.; Monteil, V.; Safonova, O. V.; Copéret, C. Reply to Peters et al.: Proton Transfers Are Plausible Initiation and Termination Steps on Cr(III) Sites in Ethylene Polymerization. *Proc. Natl. Acad. Sci. U. S. A.* **2015**, *112*, E4162−E4163.

(43) Theopold, K. H. Understanding chromium-based olefin polymerization catalyst. *CHEMTECH* **1997**, *27*, 26−32.

(44) Theopold, K. H. Homogeneous Chromium Catalysts for Olefin Polymerization. *Eur. J. Inorg. Chem.* **1998**, *1998*, 15−24.

(45) Weckhuysen, B. M.; Schoonheydt, R. A.; Mabbs, F. E.; Collison, D. Electron Paramagnetic Resonance of Heterogeneous Chromium Catalysts. *J. Chem. Soc., Faraday Trans.* **1996**, *92*, 2431−2436.

(46) Weckhuysen, B. M.; Deridder, L. M.; Grobet, P. J.; Schoonheydt, R. A. Redox Behavior and Dispersion of Supported Chromium Catalysts. *J. Phys. Chem.* **1995**, *99*, 320−326.

(47) Delley, M. F.; Lapadula, G.; Núñez-Zarur, F.; Comas-Vives, A.; Kalendra, V.; Jeschke, G.; Baabe, D.; Walter, M. D.; Rossini, A. J.; Lesage, A.; Emsley, L.; Maury, O.; Copéret, C. Local Structures and Heterogeneity of Silica-Supported M(III) Sites Evidenced by EPR, IR, NMR, and Luminescence Spectroscopies. *J. Am. Chem. Soc.* **2017**, *139*, 8855−8867.

(48) Stoll, S.; Schweiger, A. EasySpin, a Comprehensive Software Package for Spectral Simulation and Analysis in EPR. *J. Magn. Reson.* **2006**, *178*, 42−55.

(49) The temperature of 150 °C adopted in this work is slightly higher with respect to that used in industrial conditions. This correction was necessary to compensate for the low ethylene pressure employed in our experimental conditions.

(50) Carrington, A.; Luckhurst, G. R. Electron Spin Resonance Line Widths of Transition Metal Ions in Solution. Relaxation Through Zero-Field Splitting. *Mol. Phys.* **1964**, *8*, 125−132.

(51) Telser, J. EPR Interactions - Zero-Field Splittings. In *eMagRes*; Harris, R. K., Wasylishen, R. L., Eds.; John Wiley & Sons, Ltd., 2017; Vol. 6, pp 207−234.

(52) Bradley, D. C.; Copperthwaite, R. G.; Cotton, S. A.; Sales, K. D.; Gibson, J. F. Three-co-ordinated Transition-Metal Compounds. Part III. Electron Spin Resonance Studies on tris-(bistrimethylsilylamido) Derivatives of Titanium, Chromium, and Iron. *J. Chem. Soc., Dalton Trans.* **1973**, 191−194.

(53) Barrera, J. A.; Wilcox, D. E. EPR Study of the Toluene Solution Properties of the Chromium(III)-alkyl Complexes [CpCrMeCl]2, [Cp*CrRCl]2 (R = Me, Et, CH2SiMe3) and [Cp*CrMeBr]2: Dimer-Monomer Equilibria in Solution. *Inorg. Chem.* **1992**, *31*, 1745−1752.

SUPPORTING INFORMATION

In situ X- and Q-band EPR Investigation of Ethylene Polymerization on Cr/SiO$_2$ Phillips Catalyst

Elena Morra, Giorgia A. Martino, Alessandro Piovano, Caterina Barzan, Elena Groppo*, Mario Chiesa*

[1] Department of Chemistry, INSTM and NIS Centre, University of Torino, via Quarello 15, I-10135 Torino (Italy)

e-mail: elena.groppo@unito.it, mario.chiesa@unito.it
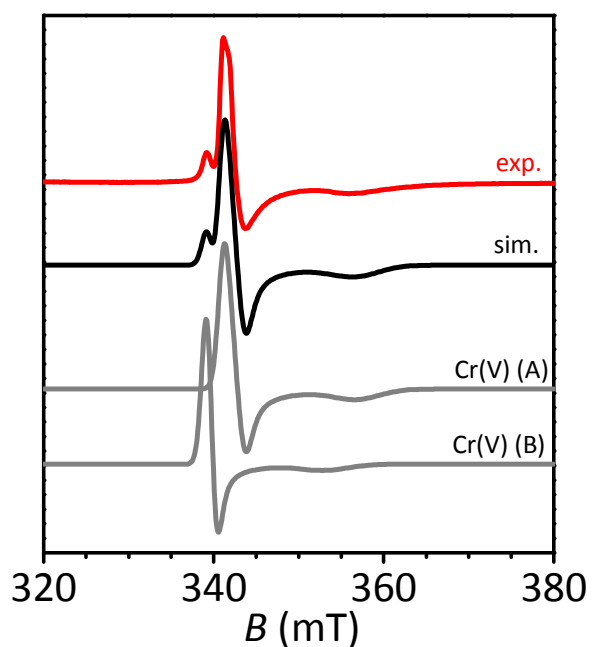
Figure S1 Experimental (red) and simulated (black) X-band EPR spectra of Cr(V) species detected on the Cr(VI)/SiO$_2$ catalyst. In grey the spectral deconvolution is shown. The spin Hamiltonian parameters employed in the simulation are reported in Table 1 of the main text.
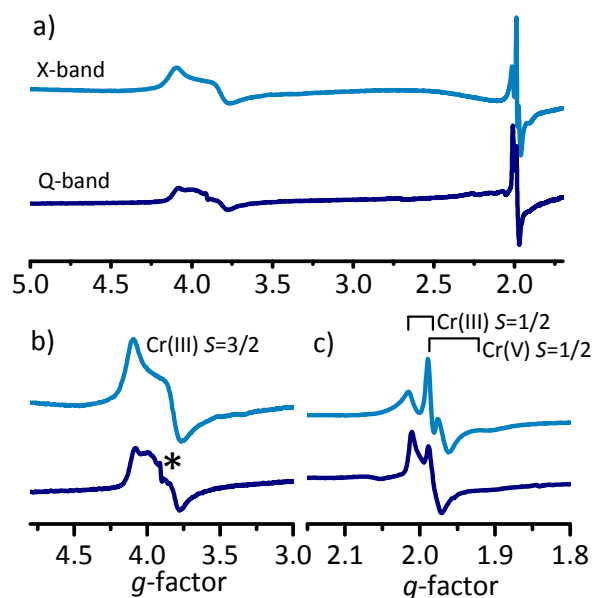
Figure S2 Comparison of the X- and –Q-band spectra recorded on the of the Cr(VI)/SiO₂ sample reacted with ethylene at 150 °C for 2 h. The Q-band spectrum was recorded at T = 5 K, with microwave power of 0.2 mW. The asterisk in panel b) indicates a cavity impurity signal. Panels b) and c) are enlargements of the signal in panel a).
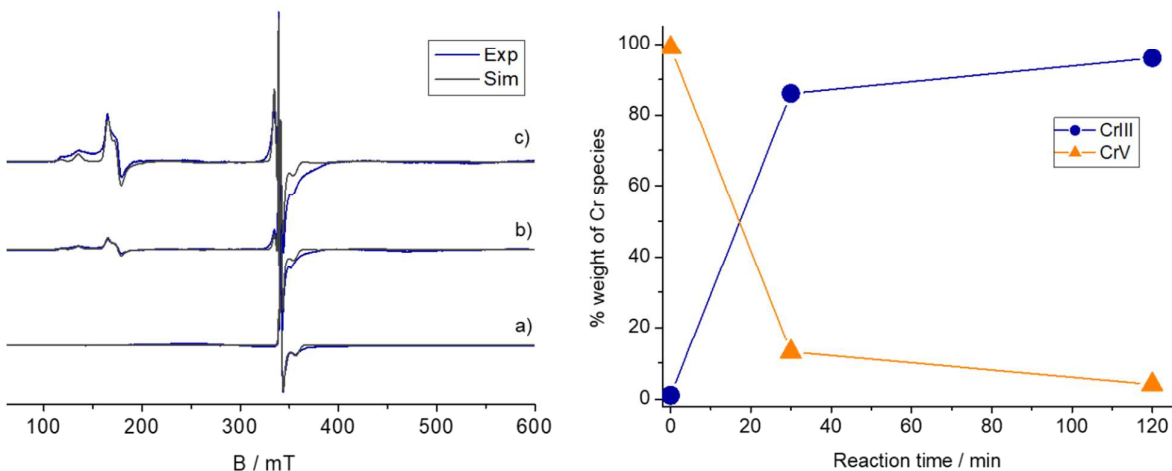
Figure S3 Experimental (blue) and simulated (grey) X-band EPR spectra of the Cr(VI)/SiO$_2$ sample at different stages of reaction with ethylene. a) oxidized sample before reaction; b) after reaction with ethylene at 150 °C for 30 min, c) after reaction with ethylene for 2h. All spectra were recorded at 77K. The simulation was carried out using the same spin Hamiltonian parameters reported in Table 1 of the main text and varying the relative abundance of the different species. The % of the total Cr(III) and Cr(V) species at the different stages of reaction is plotted on the right hand side of the figure.
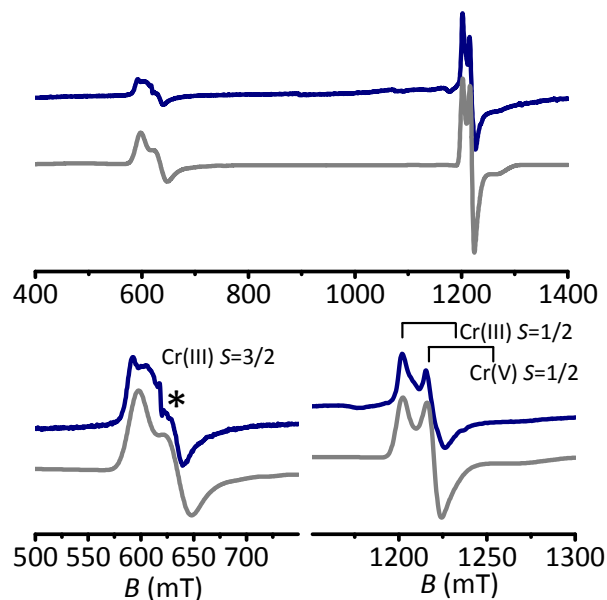
Figure S4. Experimental (blue) and computer simulation (grey) of the Q-band EPR spectra of the Cr(VI)/SiO$_2$ sample reacted with ethylene at 150 °C for 2 h. Panels b) and c) are enlargements of the signal in panel a). Spectral features related to species Cr(III)(D) (See Figure S5) are not observed in the Q-band spectrum, probably due to strain effects.
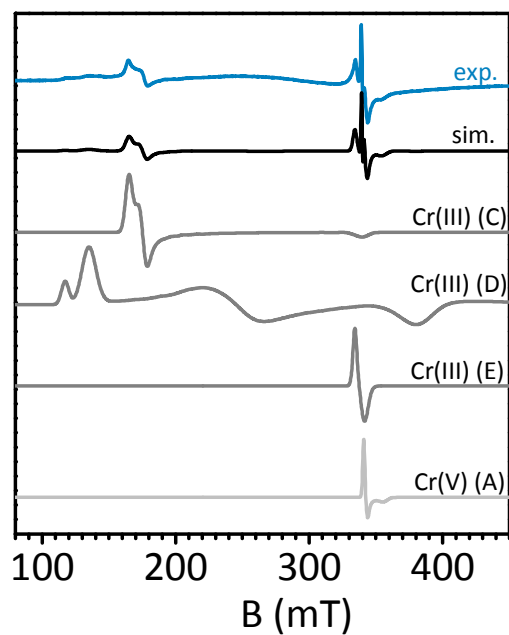
Figure S5 Deconvolution of the different Cr species employed in the simulation of the X-band EPR spectrum of the Cr(VI)/SiO$_2$ sample reacted with ethylene at 150 °C for 2 h. The spin Hamiltonian parameters are listed in Table 1 of the main text.

The Active Sites in the Phillips Catalysts: Origins of a Lively Debate and a Vision for the Future

Elena Groppo,*[ID] Giorgia Antonina Martino, Alessandro Piovano, and Caterina Barzan

Department of Chemistry, NIS Centre and INSTM, University of Torino, Via Quarello 15/A, 10125 Torino, Italy

ABSTRACT: In this work, we summarize and critically compare some of the experimental results recently published on the Phillips catalyst, in the attempt to make the point on a few particularly debated questions that have recently animated the specialized literature; in particular, we discuss the structure of the active chromium sites and how ethylene polymerization initiates on them. The data collected in this article unequivocally demonstrate that the structural and electronic properties of the chromium sites strongly depend on the strain of the silica surface, which in turns is affected by both the activation treatment and the chromium loading. This explains, at least partially, the differences of results obtained in different research groups. Another fundamental message is the need of applying the largest possible set of characterization methods, including theoretical calculation on large and flexible models. Our final purpose (and hope) is to promote a positive and constructing discussion on this catalyst, as a premise to create a solid scientific base useful to both the young researchers approaching this field and the industrial researchers who daily work with it.

The multi-faces of the Phillips catalyst

KEYWORDS: Phillips catalyst, chromium, silica, spectroscopies, ethylene polymerization, polyethylene, heterogeneous catalysis
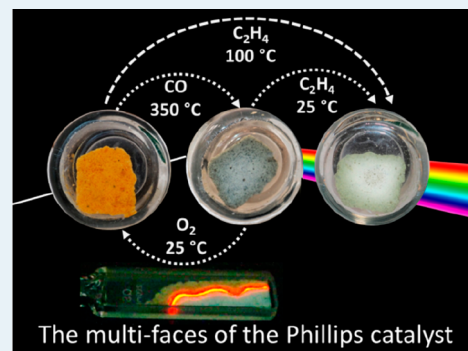
1. INTRODUCTION

Producing annually more than 30 million tons of high density polyethylene (HDPE) (i.e., about one-third of the poly-ethylene global production capacity), the Phillips catalyst has been one of the world's most important industrial catalysts for more than half a century.[1,2] It is also among the most investigated and yet controversial catalytic systems.[2−7] Developed in the 1950s at Phillips Petroleum and industrially used since 1956,[8] it has been the object of both industrial and academic research since its early history. Industrial innovation is constantly driven by the need to improve the catalytic performances, reducing the costs and increasing the quality of the produced polymers, at the same time expanding the portfolio of accessible polymeric products. More than 65 years of industrial research led to the evolution of the original formulation and to the development of hundreds of variants, which make the Phillips catalyst among the most versatile catalytic system in industry. Only part of these industrial discoveries are disclosed in patents and even fewer are easily accessible in the form of scientific papers, the latter mainly due to the prolific activity of Max McDaniel.[9]

On the other hand, academic research has been concentrated since the beginning to solve some fundamental questions, such as the structure of the active sites and the polymerization mechanism.[10−12] The first spectroscopic studies on model systems date back to the 1970s.[13−16] The apparent simplicity of its chemical formulation—highly diluted chromium ions at the surface of an optically transparent amorphous silica—and its unique ability to polymerize ethylene even in the absence of an activator were the two main factors that elevated the Phillips catalyst to a workhorse for optical spectroscopies, such as FT-IR and UV−vis at first, later followed by Raman. For several generations of researchers, not necessarily involved in olefin polymerization, the study of this catalyst was a stimulus to push further the limits of several characterization techniques. As a matter of fact, the Phillips catalyst embodied most of the difficulties encountered in the molecular-level characterization of a heterogeneous catalyst, such as the dilution of the metal centers, the extreme air sensitivity, the low fraction of the active sites, and the exceptionally high speed of the catalytic event. These difficulties fostered the development of characterization methods more sensitive, cleaner, able to discriminate between active sites and spectators, and faster.[10−12] As recently pointed out by McDaniel,[17] most of these spectroscopic studies were conducted on model systems and under experimental conditions (e.g., vacuum lines) far from the pressure−temperature conditions typical of the industrial process. For this reason, extrapolations of the results to the industrial catalyst should be made with caution. Nevertheless, a certain number of achievements have been accumulated along more than 60 years of academic research, and we are confident that at least part of them have been and still are useful for industrial researchers. Only recently, and quite late in comparison to other fields in catalysis,[18−24] the operando approach (i.e., measurements performed in conditions as close

as possible to the industrial process) showed its appearance in the investigation of the Phillips catalyst.[25−28] Although still at its infancy, this approach has already led to important discoveries.

With ups and downs, the scientific literature on the topic is constantly alive and, despite decades of academic research, the Phillips catalyst still remains largely mysterious. The goal of this perspective article is not to cover all the aspects of this interesting catalytic system (on which there are already several extensive review articles),[3,5,6,11,29,30] but rather to make the point on a few particularly debated questions that have recently animated the specialized literature, and in particular: (1) the structure of the Cr(VI) and Cr(II) sites and the role of silica as a macro-ligand; (2) the mechanism of chromium alkylation by ethylene and the nature of the chromium active sites (strictly connected with their oxidation state). A relatively small number of research groups are currently active on this topic, as emerging from a simple search on the scientific databases. Beside Max McDaniel at Chevron Phillips, who is the direct successor of the catalyst discoverers and perhaps the person who better knows the intimate secrets of this system, in the last two decades (period 1998−2018) the research groups who contributed mostly in this field are (in random order) those of Bert Weckhuysen (Utrecht University, NL), Susannah Scott (University of Santa Barbara, US), Boping Liu (East China University of Science and Technology, China), Israel Wachs (Leigh University, U.S.A.), and most recently, Cristophe Coperet (ETH Zurich, CH) and Jarosław Handzlic (Cracow University of Technology, Poland). Our group (Torino University, I) also contributed a lot, carrying on the tradition of Adriano Zecchina, who is one of the pioneers in the application of spectroscopic methods to the Phillips catalyst. Of course, this list is not exhaustive and surely does not include the large number of industrial contributions in the form of patents. Notwithstanding the small number of researchers involved in this field, the debate is often intense,[31,32] and controversial results can be found in the literature. We will try to analyze the reasons for these controversies, when possible comparing the results obtained by our research group with those published by others.

This Perspective is organized as follows. Chapter 2 gives a concise overview of the composition of the Phillips catalyst, to set the scene for readers not expert in this field. Chapter 3 is entirely devoted to discussing the main debates on the Phillips catalyst and is divided into four subchapters: section 3.1 is devoted to discuss the structure of the chromium sites and the reaction mechanisms on the oxidized form of the catalyst ($Cr(VI)/SiO_2$); section 3.2 discusses the structure of the chromium sites and the reaction mechanism on the reduced form ($Cr(II)/SiO_2$); section 3.3 tries to give a unified picture of the two systems; and section 3.4 describes the role of theoretical calculation. Chapter 4 gives a flavor of an almost virgin area to explore from a fundamental point of view, which is the role of cocatalysts. Finally, Chapter 5 offers some conclusions and provides a (personal) vision for the future.

2. THE COMPOSITION OF THE PHILLIPS CATALYST: ONLY SEEMINGLY SIMPLE

2.1. Chromium Precursors, Supports, and Activation Procedures. Strictly speaking, the Phillips catalyst constitutes hexavalent chromium ions (hereafter labeled as Cr(VI)) highly dispersed on the surface of a porous inorganic material.[3−5] Several types of _chromium precursors_ can be used, although

Cr(III) salts are preferred for governmental regulations. In the United States and Europe, in fact, Cr(VI) has been considered as potentially carcinogenic, and regulations have become increasingly severe. Before entering into the polymerization reactor, the catalyst needs to be calcined at a temperature higher than 600 °C in an oxidizing atmosphere. During this treatment, which is called "activation" in the commercial practice (a term that will be used throughout this Perspective), the chromium ions are stabilized in the hexavalent state irrespective of the starting chromium precursor. During the activation step, which consists of a treatment at a temperature higher than 600 °C in an oxidizing atmosphere, the chromium ions are stabilized in the hexavalent state irrespective of the starting chromium precursor. However, the activation must be conducted in the proper way; otherwise, the chromium ions easily segregate to form Cr_2O_3 particles. This phenomenon is more probable for high chromium loadings (typically higher than 1.0 wt %) and for high activation temperatures, or in the presence of an excess of water vapor. The activation step is one of the most powerful methods commercially used to modify the performances of the catalyst and to tailor the polyethylene (PE) architecture and therefore its molding and mechanical properties.[17] The activation procedure influences the amount of surface −OH groups, the type and distribution of the chromium centers, and through them the activity of the catalyst and many properties of the PE, such as the melt index, the shear response, the molecular weight, the polydispersity, and the amount of long chain branching.[17] Hence, a first complication arises from the _control of the activation procedure_.

Concerning the _support_, amorphous silica has been traditionally employed, due to its tendency to fragment during the polymer growth. The smaller silica fragments generated in this process provide new chromium sites accessible for ethylene polymerization. Besides silica, almost all the high surface area oxides have been tested as supports, and some of them also found practical applications.[2,3,5,10,33−35] For example, silica−alumina, silica−titania, aluminophosphates, aluminosulfates, and various types of doped silicas are industrially employed. The support has a pivotal role in affecting the catalyst activity and in determining the properties of the produced PE. The support's properties such as the acidity, the surface tension, the porosity, and others, are all important. For example, adding titanium tends to broaden the molecular weight (M_w) distribution, whereas doping silica with fluorine tends to narrow it.[5,36] This means that the support influences the properties of the chromium sites (i.e., where the polymer is formed).

2.2. Heterogeneity of Chromium Sites. The amorphous nature of the inorganic support materials implies that _the dispersed chromium sites are not all the same_, and each one produces its own characteristic type of polymer. This property distinguishes the Phillips catalysts from many other industrially employed olefin polymerization catalysts and, industrially speaking, is one of the major strength of this catalyst in comparison to its competitors. Indeed, the Phillips catalysts are extremely versatile, affording an array of polymer grades much wider than any other catalyst currently in use, with molecular weight distributions (M_w/M_n) ranging from 5 to 100.[5] For comparison, Ziegler−Natta catalysts (which are also heterogeneous in nature), typically produce PEs with a much narrower molecular weight distribution (M_w/M_n of ca. 4), mainly as a consequence of the crystalline nature of the $MgCl_2$ support.

For this reason, the Phillips catalysts dominate the market of some specific HDPE applications, such as pipe, blow molding, sheet, and geomembrane films.[5,6] On the other hand, the heterogeneity of sites is one of the major weakness in terms of their characterization. Discriminating among several types of chromium sites characterized by slightly different properties remains a great challenge.[11,12,29] Many characterization techniques give an average picture over the totality of chromium sites. Also those techniques which are able to discriminate among similar (but not the same) chromium sites (such as FT-IR spectroscopy of adsorbed probe molecules, vide infra), lack in correlating the spectroscopic data with the molecular architecture of the produced polymer.

In this respect, it is a widespread opinion that *only a small percentage of the chromium sites are active*, while the others are just spectators, or develop activity much later. The fraction of the active sites is one of the controversial questions, and numbers in the 60%−1% range have been proposed, depending on the evaluation method.[5] This issue has often raised the problem of what can be probed by spectroscopic methods, whether it is the active chromium site or the spectator one. Citing Jensen's work,[37] this has led to the widely quoted adage in industry: "If you can see it, it is probably not catalyst".

3. OPEN DEBATES CURRENTLY INFLAMING THE SCIENTIFIC COMMUNITY

3.1. The Phillips Catalyst in Its Oxidized Form: Cr(VI)/SiO₂. 3.1.1. Monochromates, Dichromates, Mono-Oxo Cr(VI), and Cr(V): Which One and in Which Amount? The oxidized form of the Phillips catalyst (i.e., the system after the activation treatment, hereafter defined as $Cr(VI)/SiO_2$ catalyst) and its variants have been characterized by a large variety of spectroscopic methods providing information on the vibrational (FT-IR, Raman), electronic (UV−vis, XANES), structural (EXAFS), and magnetic (EPR) properties of the chromium sites. Along the years, monochromates, dichromates and mono-oxochromate sites have been proposed to exist,[2,5,10,11,38−62] as well as a small fraction of Cr(V), whose distribution and relative abundance depend on the sample composition (chromium loading, support, etc.) and treatment.[48] In this respect, it is important to mention that the Cr(VI) species are highly mobile during calcination, moving not only within the silica particle (in average 100 μm large) but also between one particle and another.[5,17,63] This process, which is now used industrially to add chromium to silica, occurs through direct particle-to-particle contact during fluidization, rather than through a movement of the Cr(VI) via gas-phase.

Among all the cited techniques, Raman[39,45−47,49−55,57−59] and EXAFS[38,40,43,56,57] spectroscopies have been fundamental to clarify the aggregation state of the Cr(VI) species. Indeed, dichromates and polynuclear chromium oxides display characteristic vibrational modes that do not overlap with those of monochromates and are characterized by specific Cr−O−Cr contributions at long scattering distances.[11,12] Most of the studies concluded that at low chromium loading, the majority of the Cr(VI) sites are monochromates with a dioxochromate structure, although the relative importance of dichromates increases at high chromium loadings and activation temperature.

Diffuse reflectance (DR) UV−vis-NIR spectroscopy has been used since the early 1990s not only to discriminate among various chromates but also to quantify the amount of each species.[10,41−44,64−66] The latter is the most critical (and sometimes criticized) aspect for two reasons. The first one is the notorious invalidity of the Lambert−Beer law for spectra collected in reflectance mode, while the second reason is that the bands assigned to oligomeric Cr(VI) species are very similar to those of monomeric Cr(VI) species. This is not to say that DR UV−vis spectroscopy cannot be used for this purpose, but the analysis must be conducted accurately on the basis of a well-assessed calibration.[41] A quantitative analysis is much safer for UV−vis spectra collected in transmission mode on optically transparent silica glasses. Transmission UV−vis spectra of low loaded $Cr(VI)/SiO_2$ catalyst in the form of transparent monoliths were first reported by Stiegman and co-workers,[57] followed by Budnyk et al.[67] More recently, Stiegman and co-workers re-examined the electronic structure of Cr(VI) sites by coupling UV−vis spectroscopy with time-dependent density functional theory (TD-DFT).[68] This work is a remarkable example of the potential of UV−vis spectroscopy in discriminating among different monomeric Cr(VI) structures. For example, the authors demonstrated that all the monomeric Cr(VI) sites on strained siloxane rings (having a C_{2v} or slightly lower symmetry) have essentially the same primary coordination environment and hence a very similar electronic structure, while distinguishable differences are observed for monomeric Cr(VI) sites grafted on larger (less strained) siloxane rings.

Figure 1a shows the UV−vis spectrum reported by Stiegman and co-workers[68] for a 0.008 wt % $Cr(VI)/SiO_2$ monolith activated at 500 °C, which is characterized by four main absorption bands centered at 41 500, 36 900, 29 100, and 22 800 cm^{-1}, all of them ascribed to O → Cr(VI) charge-transfer transitions. The spectrum is compared to that published by Budnyk et al.[67] (Figure 1b, yellow) for a $Cr(VI)/SiO_2$ monolith having a very similar chromium loading (0.01 wt %), but activated at a different temperature (650 °C). Although similar, the two spectra are not the same. In particular, a single band is observed at high energy (41 500 cm^{-1}), and two bands are present at ca. 31 400 and 21 700 cm^{-1}. Interestingly, once the $Cr(VI)/SiO_2$ sample giving the yellow spectrum in Figure 1b is exposed to air at room temperature, its spectrum gradually changes and turns out to be the same as that reported by Stiegman and co-workers (compare red spectrum in Figure 1b with the spectrum in Figure 1a): a second band is observed in the high-energy region at 36 900 cm^{-1}, and the bands at 31 400 and 21 700 cm^{-1} shift to 29 100 and 22 800 cm^{-1}, respectively. Exposure of $Cr(VI)/SiO_2$ to air at room temperature does not affect the oxidation state of the chromium sites, but leads to the gradual rehydroxylation of the silica surface. As a matter of fact, the final UV−vis spectrum is the same as that of a similar sample dehydroxylated at lower temperature (500 °C, Figure 1a). This clearly demonstrates that the electronic properties of the Cr(VI) sites are strongly influenced by the degree of silica hydroxylation, that is, by the activation treatment. It is well-known that the degree of dehydroxylation strongly affects the stress/strain at the silica surface: the higher the temperature of the treatment, the greater the strain induced at the surface.[69,70] Hence, the UV−vis data shown in Figure 1ab indicate that the electronic structure of the Cr(VI) sites ultimately depends on
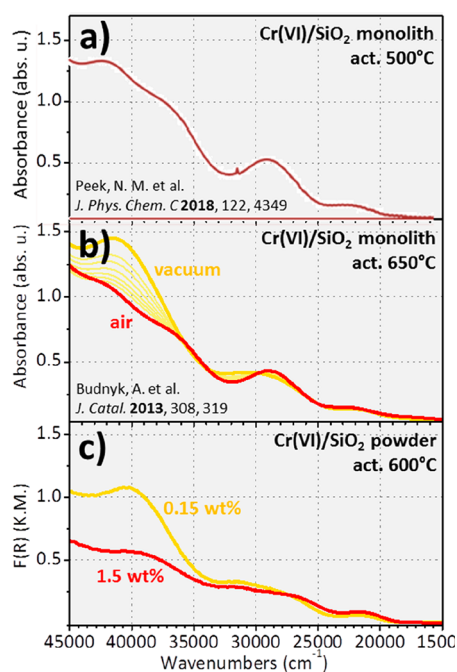
Figure 1. (a) UV−vis spectrum (collected in transmission mode) of a Cr(VI)/SiO$_2$ monolith (Cr loading 0.008 wt %) activated at 500 °C, as reported in ref 68. (b) UV−vis spectra (collected in transmission mode) of a Cr(VI)/SiO$_2$ monolith (Cr loading 0.01 wt %) activated at 650 °C and measured in vacuum (yellow) and after exposure to air (light yellow spectra, up to red). Spectrum yellow was reported in ref 67, and spectrum red is unpublished. (c) DR UV−vis spectra (collected in reflectance mode after dilution in dehydroxylated silica) of two commercial Cr(VI)/SiO$_2$ catalysts (Cr loading 0.15 and 1.5 wt %, respectively) activated at 600 °C and measured in vacuum. The dilution was adapted in order to normalize the spectra in the low wavenumbers region. The samples were kindly provided by Dr. T. Monoi at Japan Polychem Corporation. The spectra are unpublished.

the strain at the silica surface, in good agreement with the theoretical results obtained by Stiegman and co-workers.[57]

The practical relevance of this finding is discussed in Figure 1c, which displays the DR UV−vis spectra of two commercial Cr(VI)/SiO$_2$ catalysts activated at 600 °C, measured in reflectance mode after appropriate dilution (using dehydroxylated silica as a diluent). The spectrum of the 0.15 wt % Cr(VI)/SiO$_2$ catalyst (yellow in Figure 1c) is very similar to that reported by Budnyk et al. for the 0.01 wt % Cr(VI)/SiO$_2$ monolith activated at a similar temperature (yellow in Figure 1b). In contrast, the spectrum of the 1.5 wt % Cr(VI)/SiO$_2$ catalyst (red in Figure 1c) differs from the previous one and has some analogies with that of the hydrated 0.01 wt % Cr(VI)/SiO$_2$ monolith (red in Figure 1b).

The important message emerging from these comparisons is that *the electronic properties of the Cr(VI) sites are strongly influenced by the stress/strain at the silica surface, which in turn can be tailored by acting on the activation treatment (i.e., on the dehydroxilation degree of the silica surface), on the chromium loading, or both.* Lowering the chromium loading has an effect similar to increasing the activation temperature. The influence of these parameters is often neglected and may explain, at least partially, the variability in experimental results achieved by different research groups. More important, this could be the key to understand some industrial observation, such as the higher per-site activity at low chromium loadings,[5] or the exceptionally high activity of Cr(VI)/SiO$_2$ catalysts highly dehydroxylated by chemical methods.[3−5,17,36] Notably, DR UV−vis measurements are easily accessible also in industrial laboratories and can be used as screening methods for testing the properties of new catalyst formulations, provided that the correct methodology is set in advance. It is worth noticing that these results have important implications that go beyond the Phillips catalyst. They demonstrate that the electronic properties (and hence the reactivity) of single-metal-sites at amorphous silica can be tuned "simply" by acting on the activation temperature and/or on the surface density of the metal sites, in perfect agreement with the recent conclusions of Trunschke and co-workers on the similar MoO$_x$/SiO$_2$ system.[70]

Finally, in this context, it is relevant to mention that a small amount of Cr(V) is always copresent with Cr(VI) in the oxidized form of the Phillips catalyst. Cr(V) (d^1) was detected in the X-band EPR spectrum of Cr(VI)/SiO$_2$ since the early 1990s,[71−74] and is the only EPR detectable species if the activation is correctly done. The typical EPR spectrum of Cr(V) is characterized by pseudo axial resonances in the region g = 1.895−1.979.[74] It is a common opinion that Cr(V) sites are not involved in the catalysis, although they are accessible to reactants including reducing agents and hence can be regarded as possible parents for traces of Cr(III) species when Cr(VI)/SiO$_2$ is reduced by CO or by ethylene.

3.1.2. Cr(VI) Reduction by Ethylene and the Identity of the Active Species. One of the main debate has always concerned the mechanism through which the ethylene polymerization reaction is initiated at the Cr(VI) sites. Unlike other widely used olefin polymerization catalysts, such as the Ziegler−Natta and metallocene catalysts, the Phillips catalyst does not require the use of any alkylating cocatalyst to develop activity. In the industrial practice, the active sites are directly formed in the polymerization reactor at ca. 100 °C, as a consequence of two subsequent events, namely, the reduction and the alkylation (Scheme 1).

During an induction time that can last from minutes to hours depending on the catalyst treatment and the reaction conditions, ethylene slowly reduces the Cr(VI) precursors initially present in the precatalyst to low valent chromium sites, with the concomitant formation of oxygenated byproducts

Scheme 1. Simplified Scheme Showing the Two Fundamental Steps in the Transformation of the Cr(VI) Precursors into the Chromium Active Sites[a]
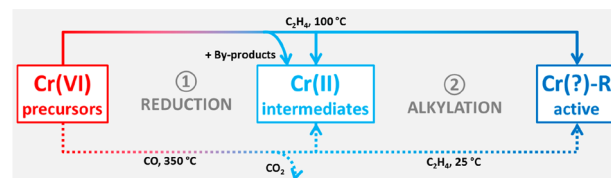
[a]During step 1 (the reduction), the Cr(VI) precursors are reduced to Cr(II) intermediates, either by ethylene at 100 °C (full line) or by CO at 350 °C (dotted line). In the former case, oxidized by-products are formed and retained by the Ct(II) sites, while in the latter, CO$_2$ is released and leaves the sample at the reduction temperature. During step 2 (the alkylation), the Cr(II) intermediates are alkylated to Cr(?)-R sites by ethylene, where the question mark indicates that the oxidation state is still matter of discussion. These sites are those active in ethylene polymerization.

D

(step 1 in Scheme 1, top).[3,5] As far as the chromium oxidation state is concerned, there is a general consensus on that Cr(II) sites are mainly formed during this step.[5,11,14,75−78] Concerning the oxygenated byproducts, formaldehyde has been long claimed as the most probable one,[2,79−83] but recent experiments performed in *operando* conditions pointed out that more complex species (such as ketones, carboxylic acids, or esters) are actually formed and, more important, retained on the chromium sites (and likely also at the silica surface), at least during the first steps of the ethylene polymerization reaction.[28,84] This finding is particularly relevant, since it turns upside down the long-standing vision of the active site as a *naked* (i.e., low coordinated) chromium species, and it conveys an active role to the external oxygenated ligands, like the ancillary ligands in homogeneous catalysis.

The initial reduction step is followed by a steady increase in the polymerization activity within the next 1−2 h.[5] This behavior has been ascribed to the slow activation of the Cr(II) sites by ethylene itself, leading to the formation of the alkyl-Cr sites (step 2 in Scheme 1, top) that initiate the ethylene polymerization, following the standard Cossee−Arlman mechanism.[85−87] That the polymer chain growth at the Phillips catalyst proceeds mainly via a Cossee−Arlman process was demonstrated by Mc Guinness et al.[88] through the analysis of low molecular weight oligomers/polymers formed during ethylene/α-olefin copolymerization with labeled monomers. In contrast, the nature of the Cr-alkyl active species and the way through which they are formed starting from Cr(II) in the presence of ethylene is not clarified yet. A Cr(III)-alkyl was advocated by Theopold[89,90] based on comparison with homogeneous catalysts,[91,92] recently reproposed by the groups of Coperet for Phillips-inspired Cr(III)/SiO$_2$ catalysts obtained from well-defined Cr(III) precursors,[93−97] and finally considered as firmly established by Scott and co-workers based on EPR data.[87,98] However, the experimental evidence supporting the formation of Cr(III)-alkyl species in the industrial Phillips catalyst are poor at best. Alternatively, a Cr(IV)-dialky was also proposed in the past,[99] on the basis of an organometallic approach. Therefore, the question on the initiation mechanism is still controversial, and more details will be given in Section 3.2.2.

3.2. The Phillips Catalyst in Its Reduced form: Cr(II)/SiO$_2$. *3.2.1. Structure of the Cr(II) Sites and the Role of Surface Hemilabile Ligands.* The Cr(VI) → Cr(II) reduction step can be accomplished before the precatalyst enters the polymerization reactor by using CO at 350 °C.[5,11,14,78] When done correctly, this treatment converts the Cr(VI) almost quantitatively to Cr(II), as established quite early through actual titration.[3,13,75,76] In this case, the induction period is eliminated, but the subsequent development of full polymerization activity follows the same behavior. This is the reason why the CO-reduced Phillips catalyst (hereafter defined as Cr(II)/SiO$_2$) has been widely adopted as a model system to investigate the initiation mechanism.

In this regard, there are however at least two false myths to be dispelled. The first one is the idea, largely diffuse in the academic laboratories, that the CO-reduction is not used in the industrial practice. This concept fostered the nomenclature of "model catalyst" referred to Cr(II)/SiO$_2$ and of "industrial catalyst" referred to Cr(VI)/SiO$_2$. This is not completely true. Although nowadays there are no more companies using CO for activation, in the past CO-reduction was employed in commercial practice to shorten the induction time,[33] especially

when low polymerization temperatures were necessary, for example, when the target polymer product was the ultrahigh molecular weight PE (UHMWPE). The second false myth is that the polyethylene produced by Cr(II)/SiO$_2$ is the same as that obtained with Cr(VI)/SiO$_2$. The two products are actually similar, but not the same. As clearly reviewed by McDaniel,[5,17] Cr(II)/SiO$_2$ produces a polymer with slightly higher M$_W$ and displays a better comonomer incorporation efficiency. These differences, which are enhanced by changing the support (for example, with SiO$_2$−TiO$_2$), indicate that the Cr(II) intermediates are actually different in the two cases. The presence (or the absence) of the oxidized byproducts in the chromium coordination sphere may account for this difference, as suggested in Scheme 1. It is also interesting to recall here the finding by Budnyk et al.,[100] that the activity of Cr(II)/SiO$_2$ increases upon decreasing the activation temperature. This result is apparently in contradiction with the opposite trend reported in the literature for the Cr(VI)/SiO$_2$ catalyst[5] and indicates once more that the two systems are not the same.

The structure of the Cr(II) sites in Cr(II)/SiO$_2$ has been investigated since the early 1960s with a multitude of spectroscopic methods. The presence of low-coordinated Cr(II) sites with multiple coordination vacancies available for adsorption of probe molecules has been of great stimulus for the development of the method known as "spectroscopy of adsorbed probe molecules",[11,101,102] of which Zecchina was the pioneer.[13] The method, which has been applied universally since the 1960s in conjunction with both DR UV−vis and FT-IR spectroscopies, and later also with XAS, provides indirect information on the electronic and structural properties of the Cr(II) sites.[12] In association with the right molecular probe (not too strong, neither too weak), FT-IR spectroscopy is perhaps the best technique to discriminate among Cr(II) sites having very similar properties. For example, on the traditional Cr(II)/SiO$_2$ catalyst, carbon monoxide (CO) at room temperature discriminates among two different Cr(II) sites (Cr$_A$ and Cr$_B$), differing in the number of coordination vacancies available for CO insertion (Figure 2, spectrum b):[11] Cr$_A$ coordinates two CO molecules (absorption bands at 2180 and 2178 cm^{-1}) and Cr$_B$ coordinates one CO molecule (absorption band at 2191 cm^{-1}). For Cr(II) on Al$_2$O$_3$, only one type of site is probed by CO, giving a broad absorption band at 2199 cm^{-1} (Figure 2, spectrum a).[103] For both Cr(II)/SiO$_2$ and Cr(II)/Al$_2$O$_3$, the interaction of CO with Cr(II) is dominated by a transfer of electron density from the σ(CO) molecular orbital (bonding character) to 3d(Cr) molecular orbitals having an antibonding character. In addition, a Cr(II) site grafted at the alumina surface feels a lower electronic density than a Cr(II) site at the surface of silica because of the more ionic character of the Al−O bond with respect to the Si−O bond. This explains why the $\tilde{\nu}$(CO) band is observed at higher wavenumbers for CO adsorbed on Cr(II)/Al$_2$O$_3$ than for CO adsorbed on Cr(II)/SiO$_2$.[103]

FT-IR spectroscopy of adsorbed CO had the merit of highlighting an important feature of the Cr(II)/SiO$_2$ catalyst, that is, the presence of a variable number of weak siloxane ligands in the Cr(II) coordination sphere, which are visible only under certain circumstances, but play a fundamental role in determining the properties of the Cr(II) sites. These hemilabile ligands can be displaced from the Cr(II) sites in the presence of competitive species, including the ethylene monomer.[11,29,106] The most representative example is the adsorption of carbon monoxide at 100 K. The formation of
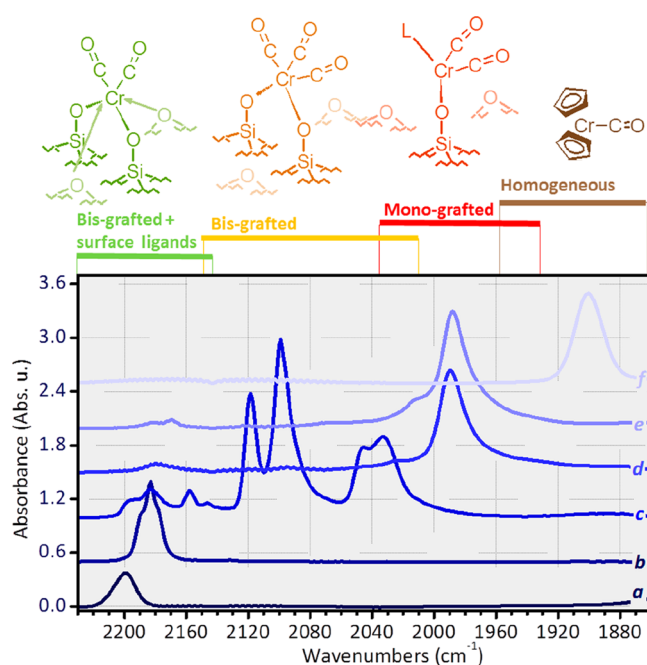
Figure 2. FT-IR spectra of CO adsorbed on different Cr(II) containing catalysts: Cr(II)/Al$_2$O$_3$ (spectrum a),[103] Cr(II)/SiO$_2$ (spectra b and c, collected at room temperature and 100 K, respectively),[11] Cr(II)/SiO$_2$ after reaction with triethylsilane (spectrum d),[104] Cr(II)/SiO$_2$ after reaction with triethylaluminum (spectrum e), and Cp$_2$Cr(II)(CO) (spectrum f).[105] Spectrum e is unpublished. All the spectra (which are translated for clarity) are collected at a comparable CO equilibrium pressure (ca. 50 mbar) and at room temperature, except spectrum c, which is collected at 100 K. On the top of the figure, are indicated the spectroscopic ranges characteristic of the following: Cr(II) carbonyls bis-grafted to the support and in interaction with hemilabile surface ligands (green), Cr(II) carbonyls bis-grafted to the support but not in interaction with surface ligands (yellow), Cr(II) carbonyls monografted to the support (red), and homogeneous Cr(II) carbonyls (brown).

Cr(II) multicarbonyls (characterized by absorption bands in the 2130−2000 cm^{-1} range, Figure 2, spectrum c and second structure on the top) occurs through π back-donation from 3d(Cr) molecular orbitals having a bonding character to the π(CO) molecular orbital (antibonding),[107,108] and causes a consistent elongation of the Cr−O bond, as determined by EXAFS spectroscopy.[109] The resulting scenario is that *silica (perhaps more than any other inorganic oxide) plays an active role in stabilizing Cr(II) sites in geometries which are unlikely for homogeneous complexes.* In other words, it acts as a macroligand for the Cr(II) sites. This explains why the Phillips catalyst is unique among the silica-supported olefin polymerization catalysts, providing polymers with a very broad M$_W$ distribution. For example, metallocene/MAO/SiO$_2$ or TiCl$_x$/MgCl$_2$/donor/SiO$_2$ produce polymers with a narrow M$_W$ distribution. However, both metallocene and titanium do not have direct interaction with silica, while chromium sites in the Phillips catalyst do. This direct interaction does not mean that the Cr(II) sites are rigidly attached to the support, but *rather they are structurally flexible in the presence of the adsorbates and have the capability to expand their coordination sphere at the expenses of the hemilabile siloxane ligands belonging to the silica surface.* This *cooperative effect*, similar to that characteristic of certain homogeneous catalysts and of the enzymes, is often neglected by researchers who aim at modeling the properties of the Cr(II) sites by means of rather small and rigid cluster models. This choice is questionable because the presence of the hemilabile siloxane ligands certainly affects the energy of adsorption/desorption for several molecules, including ethylene. The role of the siloxane ligands in lowering the energetic barriers involved in the initiation mechanism for ethylene polymerization on Cr(II)/SiO$_2$ has been recently recognized.[85,97]

The flexibility of the Cr(II) sites increases when the Cr(II)/SiO$_2$ catalyst is reacted with the so-called activators, such as hydrosilanes and aluminum alkyls. It has been proposed that the cocatalyst attacks one of the Cr−O−Si anchoring links, generating a modified Cr(II) site which is monografted to the silica surface (third structure on top in Figure 2). These sites have been advocated as responsible for in situ α-olefin generation and explain why the use of cocatalysts introduces short chain branches in PE, up to the formation of LLDPE in the presence of ethylene as the only feed.[5] These modified Cr(II) sites are able to coordinate two CO molecules, forming "classical" chromium carbonyl species[104] (i.e., characterized by a strong Cr → CO π back-donation contribution that overcomes the Cr ← CO σ donation and leads to the weakening of the C−O bond),[107,108] contributing in the 2050−1950 cm^{-1} region, as typically observed in homogeneous organometallic carbonyl complexes, including chromium complexes.[105,110−112] Two examples are reported in Figure 2, which shows the FT-IR spectra of Cr(II)/SiO$_2$ reacted with excess of triethylsilane[104] (spectrum d) and with excess of triethylaluminum (spectrum e). As a term of comparison, also the spectrum of the Cp$_2$Cr(CO) homogeneous complex[105,112] is reported (Figure 2, spectrum f and fourth structure on the top).

The selection of FT-IR spectra reported in Figure 2 demonstrates that *FT-IR spectroscopy of adsorbed CO is a powerful method to discriminate among different Cr(II) sites,* being able to differentiate between mono- and bis-grafted Cr(II) sites, either with or without hemilabile surface ligands. There are however two issues to consider. The first one is that not all the Cr(II) sites detected by CO are necessarily those involved in ethylene polymerization. In this regard, an elegant approach to distinguish the active sites from the spectators consists in performing the CO adsorption experiment twice, before and after ethylene polymerization. The difference in the CO adsorption corresponds to the active chromium sites. However, the method works well only by keeping the polymerization time short enough; otherwise, too much PE does not allow the diffusion of CO to the chromium centers.[113] The second issue to consider is that in some cases the Cr(II) sites might be not accessible by CO, but accessible to ethylene. This is the case, for example, of the Cr(II) sites modified by AlR$_3$ and similar activators. We have recently demonstrated that most of the chromium sites modified by diethylaluminoethoxide are not reached by CO, likely because they are shielded by the modifier and/or by some reaction byproducts.[114] In these cases, a possible solution is to make use of stronger probes, which are molecules interacting strongly with the chromium sites (such as acetonitrile).

3.2.2. The Mechanism for Cr(II) Self-Alkylation: One-Electron or Two-Electron Oxidation? As anticipated in the previous section, the question on how the first Cr−C bond is formed starting from Cr(II) and ethylene is strictly connected to the identification of the oxidation state of the active

Scheme 2. Path (a): The Non-Redox Initiation Mechanism Proposed by the Coperet Group Involves the Heterolytic C−H Activation of Ethylene on One of the Three Cr(III)−O Bonds, with the Formation of a Cr(III)-Vinyl Species and a Surface OH;[93−95,97,118] Paths (b) and (c): The Two Neat One-Electron Redox Processes Proposed by the Scott Group[86,87] Consisting of Two Steps[a]
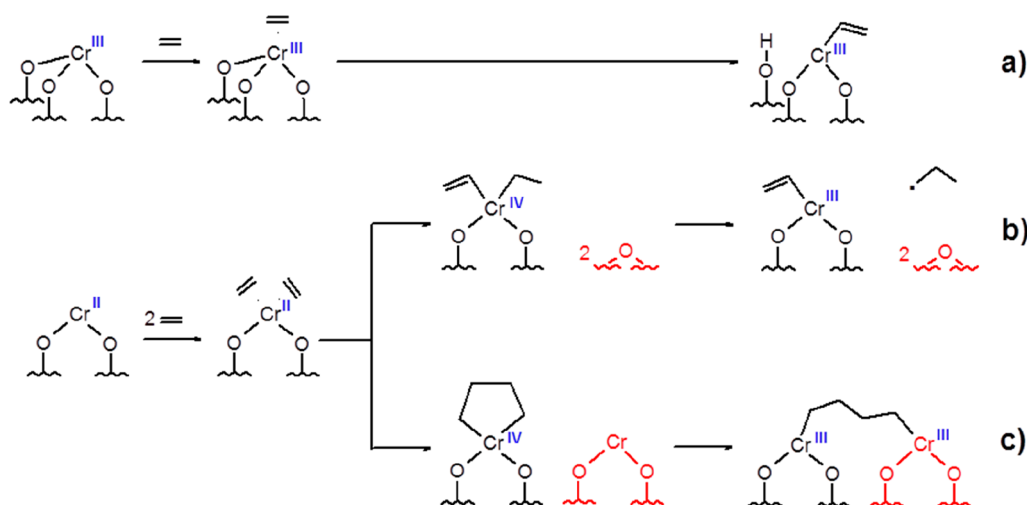
[a](1) The oxidative addition of two ethylene molecules to Cr(II) to give a Cr(IV) intermediate (either a Cr-vinyl-ethyl or a chromacyclopentane); (2) followed by a Cr−C bond homolysis assisted by a second participant on the surface (either the siloxane ligands, path (b), or a second Cr(II) site, part (c)), which are depicted in red. In both cases, during step 2) the intermediate Cr(IV) is reduced to Cr(III), with generation of an organic radical. The radical leaves the system in path (b), while it reacts with the second Cr(II) in path (c), generating a second Cr(III).

chromium sites (i.e., the nature of the question mark in Scheme 1). Most of the initiation mechanisms proposed in the past involved a two-electron redox step in which Cr(II) is oxidized to Cr(IV) by oxidative addition of ethylene. A similar mechanism is well-documented for homogeneous chromium complexes that selectively oligomerizes ethylene to α-olefins.[115−117] Several two-electrons redox mechanisms have been proposed so far.[11,79] Some of them have been supported by (not conclusive) experimental evidence, but most of them have been strongly criticized in the recent literature, mainly because theoretical calculation predicted unfeasible high propagation barriers.[85−87]

At the same time, Cr(III) has become gradually the most popular putative species accounting for ethylene polymerization. This is due to the concomitance of two main experimental evidence. The group of Scott found, by EPR spectroscopy, that exposure of a CO-reduced Phillips-like precatalyst to pulses of ethylene causes the rapid reoxidation of the Cr(II) sites to Cr(III), even below room temperature.[78,98] At the same time, Coperet and co-workers demonstrated that silica-supported Cr(III) molecularly defined analogues of the Phillips catalyst obtained by Surface Organometallic Chemistry are extremely active in ethylene polymerization, while the Cr(II) analogues are almost inactive.[93−95,97,118] The two experimental evidence together prompted the computational investigation of initiation mechanisms leading to a Cr(III)-alkyl propagating site. A nonredox initiation mechanism, involving the heterolytic C−H activation of ethylene on one of the three Cr(III)−O bonds (path a in Scheme 2) was initially proposed by the Coperet group,[93,94] but later on refuted by the Scott group.[31,32,119] The latter is perhaps the most prolific team in this field and recently proposed two possible mechanisms that can explain the formation of the Cr(III)-alkyl propagating site starting from Cr(II) and ethylene (paths b and c in Scheme 2).[86,87] Both mechanisms are neat one-electron redox processes, consisting of two consecutive

steps: the oxidative addition of two ethylene molecules to Cr(II), followed by a Cr−C bond homolysis, which causes Cr(IV) to be reduced to Cr(III) and the generation of an organic radical. The two mechanisms differ in the nature of the intermediate Cr(IV) species and in the destiny of the organic radical, while both of them require the participation of external "actors" (either the siloxane bridges or a second Cr(II) site). Both mechanisms are kinetically viable and account for most of the known reactivity properties of the catalyst, although they do not explain all of them. For example, they do not account for the increased per site activity at low chromium loading, or for the observation that ethylene polymerization on a CO-reduced precatalyst initiates even at room temperature or below.[87]

3.2.3. The Question of the Chromium Oxidation State: The Use and Misuse of UV−vis, XANES, and EPR Spectroscopies. The assessment of the oxidation state for the active chromium sites is perhaps the most debated topic in recent times and is strongly related to the problem of the self-alkylation mechanism. For this reason, it is useful to review some relevant observations accumulated over years of research based on the use of three main characterization techniques, which are UV−vis, XANES, and EPR spectroscopies. These three techniques have been largely used (and often misused) to determine the oxidation state of the chromium sites during ethylene polymerization or immediately after.

Among the three techniques, UV−vis spectroscopy is perhaps the least preferred, based on the following two arguments: (i) electronic transitions give rise to broad and overlapping bands, (ii) whose position depends on both the oxidation state and the coordination geometry of the chromium sites, which are difficult to disentangle.[120] There is a third problem, neglected by most of the literature, which is a limitation intrinsic to the physical method for collecting the UV−vis spectra.[28] The PE coating formed around the Cr/SiO$_2$ particles diffuses the incident light and shields the active
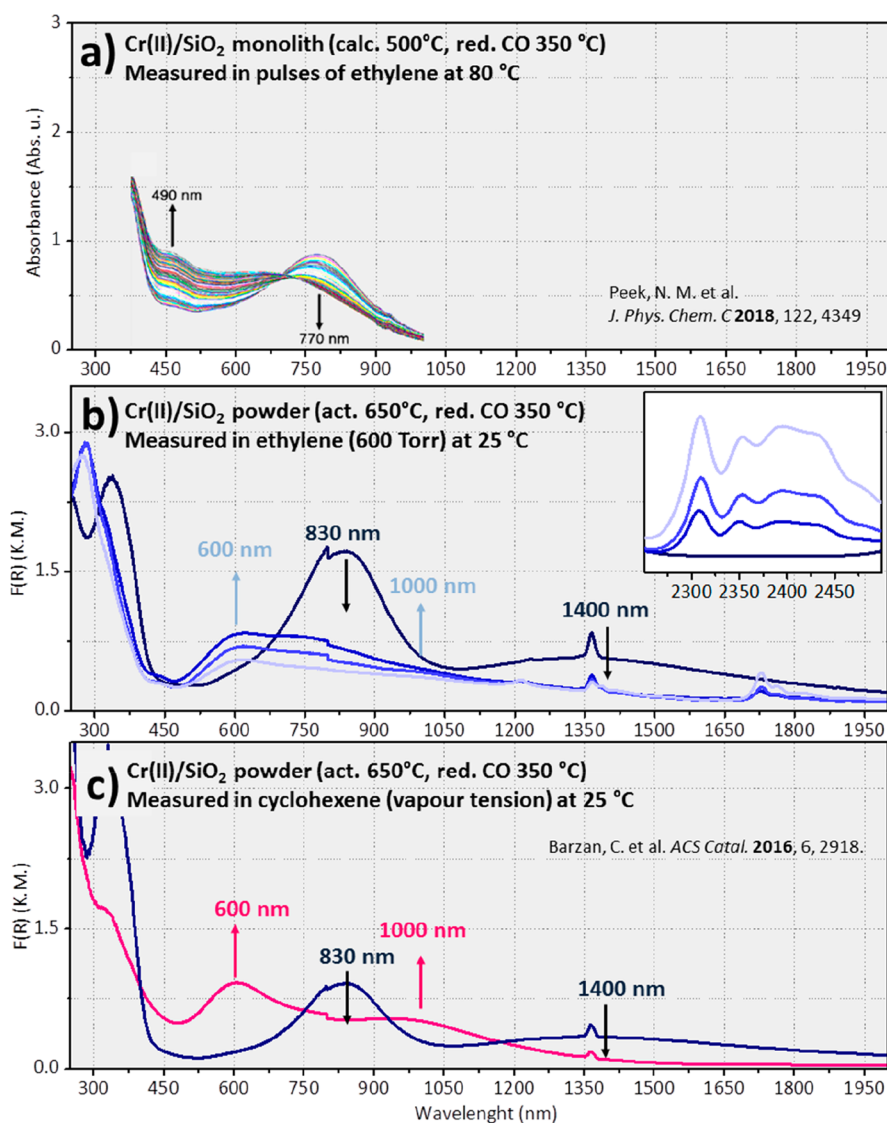
Figure 3. (a) Transmission UV−vis spectra of a Cr(II)/SiO$_2$ monolith (calcined at 500 °C and reduced in CO at 350 °C) titrated with pulses of ethylene at 80 °C, as reported in ref 98. (b) DR UV−vis spectra of a powdered Cr(II)/SiO$_2$ catalyst (activated at 650 °C and reduced in CO at 350 °C, black) and its time evolution in the presence of ethylene (600 Torr) at room temperature (from dark to light blue). The inset shows a magnification of the NIR region, where appear the vibrational features of PE. (c) DR UV−vis of the same Cr(II)/SiO$_2$ catalyst reported in panel b before (black) and after (pink) interaction with cyclohexene at room temperature.[122] In all three panels, up and down arrows highlight the bands that appear and disappear as a function of the experimental conditions.

chromium sites (i.e., the sites where the polymer is formed). This is macroscopically visible in the aspect of the sample that progressively becomes white during the polymerization. The white color is not the color of PE (which is transparent in the whole UV−vis region), neither that of the catalyst, but is the result of the scattering of the visible light from the combination PE + catalyst particles. In these conditions, no information on the active chromium sites can be obtained anymore. The situation, critical in diffuse reflectance, is even worse when collecting UV−vis spectra in transmission mode on transparent, highly diluted, Cr/SiO$_2$ monoliths. Indeed, as demonstrated by Budnyk et al.,[67] as soon as the silica pores are filled with the polymer, the monoliths become opaque, and the incident light is no longer transmitted.

Hence, only by collecting the UV−vis spectra in the presence of ethylene pulses and/or in the very early stages of ethylene polymerization is it possible to obtain relevant information on the active chromium sites. An example of the first case has been reported recently by Scott and co-workers[78,98] and is reproduced in Figure 3a, which shows a sequence of transmission UV−vis spectra collected for a diluted Cr(II)/SiO$_2$ monolith in the presence of pulses of ethylene at 80 °C. An example of the second case is shown in Figure 3b, displaying a sequence of DR UV−vis spectra collected by our research group for a 0.5 wt % Cr(II)/SiO$_2$ catalyst in the presence of ethylene at room temperature. For sake of comparison, the two sequences have been reproduced in the same scale, although unfortunately a very limited wavelength region is reported by the Scott group, which does not allow a full comparison. The two experiments shown in Figure 3 lead to two different conclusions and effectively represent the kind of variability in results that is found in the specialized literature and that somehow generates confusion on the topic. During titration with highly dilute aliquots of ethylene (Figure 3a), the spectrum of the Cr(II)/SiO$_2$ monolith slowly changes, with the band at 770 nm

709 disappearing and a new band at 490 nm emerging. The authors
710 ascribe the new band to the formation of Cr(III) species with
711 coordination numbers higher than four but with a symmetry
712 lower than octahedral. Quantitative analysis yielded an average
713 C/Cr ratio of 1.9 ± 0.2, suggesting that at the end point of the
714 titration, the material has taken up on average one ethylene per
715 Cr(III) site, consistent with the formation of organo-Cr(III)
716 sites but not with the development of a real polymerization.[98]
717 As a matter of fact, if polymer is formed, the silica monolith
718 would have become opaque for transmission.[67]

719   During the early stages of ethylene polymerization at room
720 temperature, the DR UV−vis spectrum of the 0.5 wt % Cr(II)/
721 SiO$_2$ catalyst changes in a different way (Figure 3b).[121] Since
722 the very first spectrum, the two d−d bands at 830 and 1400
723 nm, characteristic of highly uncoordinated Cr(II) sites,[11]
724 decrease in intensity and shift to 650 and 1000 nm, while the
725 intense charge-transfer band initially at 335 nm shifts at 275
726 nm. These changes simply reveal that all the Cr(II) sites get in
727 contact with ethylene, increasing the number of ligands in their
728 coordination sphere.[11] Indeed, very similar spectra have been
729 reported for Cr(II)/SiO$_2$ in interaction with nonreactive
730 (probe) molecules, such as CO[11] or cyclohexene.[122] The
731 case of cyclohexene, which is reported in Figure 3c for a direct
732 comparison, is particularly interesting because it mimics the
733 coordination effect of ethylene on the Cr(II) sites, without
734 polymerizing. The change in the DR UV−vis spectrum is
735 extraordinarily similar to that observed in the presence of
736 ethylene, except for the fact that it does not evolve with time.
737 In contrast, as soon as PE is formed (Figure 3b), the whole
738 spectrum decreases in intensity. At the same time, a complex
739 series of bands grow in the NIR region due to the
740 combinations and overtones of the vibrational modes of PE
741 (inset in Figure 3b).

742   In conclusion, both experiments discussed in Figure 3
743 actually fail in observing the active chromium sites. No
744 polymer is formed in the first case (Figure 3a). Hence, the
745 question arises whether the experiment is really representative
746 of the oxidation state of the active chromium sites, or rather it
747 provides a picture of deactivated chromium species. Indeed,
748 the alkylated chromium species should be rather unstable in
749 the absence of the monomer. On the other hand, when PE is
750 formed (such as in the experiment reported in Figure 3b), it
751 obscures the active chromium species, and only the spectator
752 sites (or those slower to start) remain visible. This does not
753 mean that UV−vis spectroscopy is not useful in the
754 investigation of these systems, but that the results must be
755 interpreted with caution and in combination with other
756 methods.

757   XANES spectroscopy is more popular (and less criticized)
758 than DR UV−vis spectroscopy and has been often adopted to
759 claim the oxidation state of the chromium sites. This is curious
760 because actually it suffers of exactly the same problems of UV−
761 vis spectroscopy. Indeed, the edge position of a Cr K-edge
762 XANES spectrum is a function of both the oxidation state and
763 the coordination geometry, and it is hard to disentangle the
764 two factors without knowing at least one of them. An example
765 of the possible mistakes that can be made by relying on
766 XANES data alone is given in Figure 4, which shows the
767 XANES spectra of a Cr(VI)/SiO$_2$ catalyst after ethylene
768 polymerization (spectrum a) in comparison to that of Cr$_2$O$_3$
769 (spectrum c), used as a reference for Cr(III). A quick
770 comparison of the two XANES spectra might lead to the
771 conclusion that the final oxidation state of the catalyst reduced
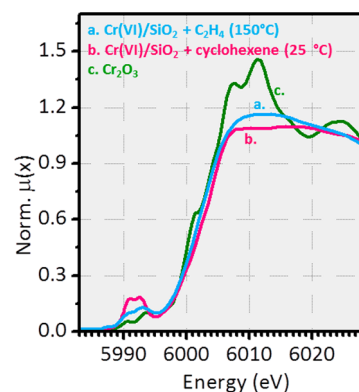
Figure 4. Cr K-edge normalized XANES spectra of (a) Cr(VI)/SiO$_2$ catalyst after ethylene polymerization at 150 °C and (b) after reduction with cyclohexene at room temperature, in comparison to that of Cr$_2$O$_3$ (spectrum c), used as a reference for Cr(III).[28]

772 in ethylene is +3. Indeed, at a first glance, the pre-edge features
773 and the edge position are very similar in the two cases.[28] These
774 (and similar) arguments have been used several times in the
775 literature to set forth +3 as the main oxidation state of the
776 chromium active sites.[93−96] However, Figure 4 shows that the
777 spectrum of Cr(VI)/SiO$_2$ after ethylene polymerization is also
778 very similar to that of Cr(VI)/SiO$_2$ reduced in cyclohexene at
779 room temperature (spectrum b), where the chromium sites
780 have an oxidation state of +2 in a 6-fold coordination
781 environment due to the interaction with an ester (deriving
782 from the oxidation of cyclohexene).[123] Notably, in that case,
783 EPR spectroscopy incontrovertibly discarded the presence of
784 Cr(III).[123] It clearly emerges that the assignment of the
785 chromium oxidation state on the basis of *only* Cr K-edge
786 XANES spectroscopy is not unambiguous. The same
787 conclusion was reached several years ago by Tromp et al.,[124]
788 who demonstrated that the position of the main absorption
789 edge for a series of well-defined Cr(III) complexes with
790 different ligands and geometries can move as much as 8 eV
791 (i.e., a shift comparable to that caused by a change in the
792 oxidation state from +6 to 0).

793   With respect to DR UV−vis spectroscopy, XANES spec-
794 troscopy does not have problems associated with the formation
795 of the polymer, and hence, in principle it probes all the
796 chromium species in the catalyst before, during, and after
797 ethylene polymerization.[125] This is an advantage of the
798 method, but turns out to be a disadvantage when considering
799 that the information is always averaged on the total chromium
800 sites. Moreover, the sensitivity of XANES is limited to about
801 10% of the total chromium sites, meaning that a species
802 present in a percent below ca. 10% could escape detection with
803 this technique.[40] This opens the question whether XANES
804 spectroscopy might convey information on the active
805 chromium sites or it detects only the spectators, being that
806 the active sites are too small a fraction of the total.

807   The sensitivity is not an issue for EPR spectroscopy, which is
808 notoriously a technique sensitive even to traces of para-
809 magnetic species. This is why EPR spectroscopy has been used
810 to assess the oxidation (and spin) states of the chromium sites
811 in Cr(II)/SiO$_2$ after (or during) ethylene polymerization,
812 under the assumption that it is one among the few methods
813 able to reveal a few percent of sites.[78,98] However, the
814 oxidation (and spin) states that can be probed by EPR at
815 conventional fields are Cr(V) (d^1) and Cr(III) (d^3) only, while

I

the technique is normally silent toward Cr(IV) (d^2) and Cr(II) (d^4), which are other putative actors in catalysis.[126] In other words, the main issues of EPR spectroscopy are exactly the opposite of those raised for XANES spectroscopy: it is an extremely sensitive technique, but blind toward specific spin states. Hence, the question of the significance of the species detected by EPR arises, that is, whether they are involved or not in the reaction and how much they account for the total chromium present in the catalyst.

3.3. Cr(VI)/SiO$_2$ and Cr(II)/SiO$_2$: A Unified Picture of the Chromium Active Sites.
In the attempt to summarize the potentials and the limits of the three techniques discussed above in the investigation of the active chromium sites, Figure 5 shows the evolution of the DR UV−vis, XANES, and EPR
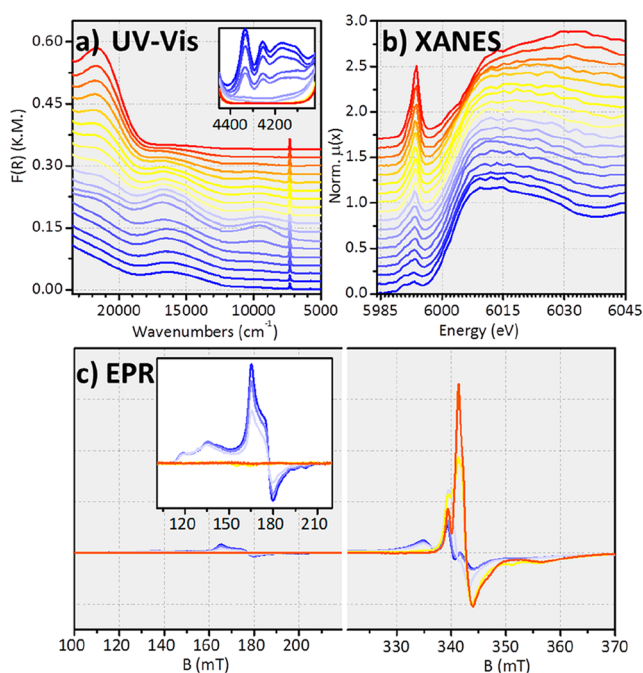
Figure 5. Time evolution (from red to blue) of the DR UV−vis (a),[28] Cr K-edge normalized XANES (b),[28] and EPR (c)[128] spectra of Cr(VI)/SiO$_2$ in the presence of ethylene at 150 °C. From red to yellow: induction time; from yellow to blue: onset of ethylene polymerization. The inset in panel a shows a magnification of the NIR region, where appear the vibrational features of PE. The inset in panel c shows a magnification of the low field signal, attributed to Cr(III) species. The spectra in panels a and b have been vertically translated for clarity. The DR UV−vis and XANES spectra are vertically translated for clarity.

spectra for Cr(VI)/SiO$_2$ in the presence of ethylene at 150 °C,[127] while Figure 6 shows the same for Cr(II)/SiO$_2$ in the presence of ethylene at room temperature. Most of these spectra, obtained by our research group on the same catalyst and using the same experimental approach, have been already published and separately discussed in previous works, but they have been never discussed together with a unifying vision. It is worth noticing that the whole sets of data are fully comparable each-others, a situation that is rather uncommon.

As far as Cr(VI)/SiO$_2$ is concerned, the whole set of data shown in Figure 5 clearly indicates the existence of two subsequent regimes, which have been distinguished with red−yellow and light blue−blue spectra. Initially, a fraction of the chromates are slowly reduced by ethylene (from red to yellow

spectra in Figure 5) to intermediate species, which are characterized by peculiar and distinguishable d−d bands at 16 700 and 9500 cm^{-1} in the DR UV−vis-NIR spectrum (Figure 5a), falling in a spectral region where the original chromates (d^0 species) do not contribute. The corresponding spectrum is extraordinarily similar to that obtained by interacting Cr(II)/SiO$_2$ with cyclohexene (Figure 3c).[122] Hence, the intermediate chromium species have been identified as 6-fold coordinated Cr(II).[28] The 6-fold coordination of these Cr(II) sites is determined by the presence of the oxidized byproducts, which have been detected by parallel FT-IR measurements.[28] XANES spectra are compatible with this interpretation, but they cannot be used to define univocally the nature of the reduced chromium species because their spectroscopic fingerprints overlap to those of the chromates, which are copresent at this stage. EPR spectroscopy at conventional frequency-field conditions is silent toward Cr(II) species, and in fact, the EPR spectra do not reveal the formation of additional EPR active chromium species during this period (Figure 5c). The few Cr(V) sites initially present in the oxidized Cr(VI)/SiO$_2$ (resonance in the high field region) are almost unaltered.[128] After the induction time, and in the presence of a residual amount of Cr(VI) species, ethylene polymerization takes place (from yellow to blue spectra in Figure 5). DR UV−vis-NIR spectra are fundamental to reveal the onset of the polymerization, but only when collected in an extended spectral range, because the polymer contributes in the NIR region with a series of complex bands attributed to the overtones and combination of the fundamental CH$_2$ vibrations (inset in Figure 5a). During the polymerization, the bands associated to the 6-fold coordinated Cr(II) intermediates disappear, which unambiguously indicate that these sites are involved in the reaction.[28] Indeed, these sites are the first sites to be shielded by the growing polymer that they have produced themselves. However, no new bands are observed in the spectra that can reveal the nature of the propagating chromium sites, for the same reasons discussed above (see Figure 3b). At the same time, the residual Cr(VI) sites are also reduced, as indicated by both UV−vis (decrease of the charge-transfer band at 22000 cm^{-1}, Figure 5a) and XANES (disappearance of the peak at 5993.5 eV, Figure 5b) spectra. According to the EPR spectra (Figure 5c), the Cr(V) sites have the same destiny and most of them are converted into Cr(III) species (appearance of the resonance characteristic of Cr(III) in the low field range, inset in Figure 5c).

Summarizing, the three sets of spectra shown in Figure 5 reveal the existence of at least two types of Cr(VI) in Cr(VI)/SiO$_2$ and a small amount of Cr(V), differing in their reducibility at 150 °C in the presence of ethylene. The most reducible Cr(VI) sites are converted into 6-fold coordinated Cr(II) (EPR inactive) in interaction with the oxidized byproducts. These sites appear to be intermediates involved in ethylene polymerization. A second type of Cr(VI) sites are reduced by ethylene only later, concurrently to the reduction of Cr(V), and most likely converted into Cr(III) sites (EPR active). It is important to notice that, by considering the EPR results only, one could be tempted to consider the Cr(III) species as the active sites in ethylene polymerization. Although this cannot be excluded, there are two sets of experimental evidence that point toward a different interpretation. The first one is conveyed by UV−vis spectroscopy, which unambiguously indicates the 6-fold coordinated Cr(II) intermediates as those involved in ethylene polymerization. The second

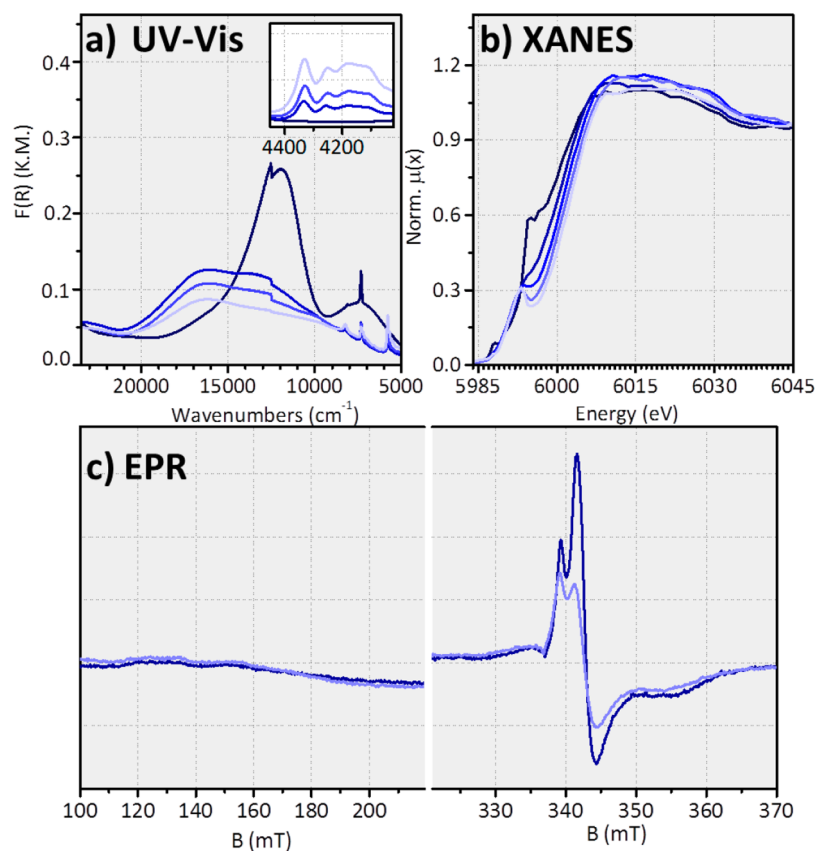**Figure 6.** Time evolution (from dark to light blue) of the DR UV−vis (a), Cr K-edge normalized XANES (b), and EPR[128] (c) spectra of Cr(II)/SiO$_2$ in the presence of ethylene at room temperature. The inset in panel a shows a magnification of the NIR region, where appear the vibrational features of PE.

907 evidence is provided by the complementary experiment
908 performed on Cr(II)/SiO$_2$, which is summarized in Figure 6
909 and discussed here below.
910   The DR UV−vis, XANES, and EPR spectra of Cr(II)/SiO$_2$
911 rapidly change in the presence of ethylene at room
912 temperature, concurrently with the fast ethylene polymer-
913 ization (inset in Figure 6a). The DR UV−vis spectra reported
914 in Figure 6a are the same commented above (Figure 3b), but
915 reported this time in wavenumbers instead of wavelengths.[129]
916 As discussed above, the DR UV−vis spectra simply tell us that
917 the majority of the Cr(II) sites interact with ethylene, but they
918 are scarcely useful to assess the properties of the active
919 chromium sites, which are rapidly shielded by the formed PE.
920 In the Cr K-edge XANES spectra (Figure 6b), the edge
921 (determined at 0.75 of the edge jump) upward shifts from
922 6000.0 to 6003.6 eV, which is compatible with an oxidation of
923 the Cr(II) sites. At the same time, the intense and well
924 resolved pre-edge peak at 5994.8 eV, assigned to a Cr 1s → Cr
925 4p transition and considered the fingerprint of isolated Cr(II)
926 sites,[109] decreases in intensity, and a new peak appears at
927 5993.0 eV. Although it is not possible to exactly determine the
928 average oxidation state of the chromium sites for the reasons
929 discussed above, the presence of this pre-edge peak (intense
930 0.3 in normalized absorbance units) indicates that during
931 ethylene polymerization, at least a fraction of the chromium
932 sites have a symmetry characterized by the almost complete
933 absence of the inversion center (typically, a tetrahedral
934 symmetry). Indeed, the electronic transition responsible for
935 the pre-edge peak is subjected to the Laporte selection

936 rule.[11,38,40,124] For comparison, the XANES spectrum of the
937 almost perfect tetrahedral monochromates in Cr(VI)/SiO$_2$
938 (Figure 5b, red) displays a pre-edge peak as intense as 0.8,
939 while those of the perfectly tetrahedral Cr(Np)$_4$ and Cr(Ns)$_4$
940 (Np = neopentyl, Ns = neosylil) homogeneous complexes are
941 characterized by a pre-edge peak as intense as 1.0. Curiously,
942 and at a difference with respect to what published by S. Scott
943 and co-workers,[98] we do not observe any change in the EPR
944 spectrum before and after ethylene polymerization (Figure 6c),
945 despite the formation of abundant PE. These results indicate
946 that, in our experimental conditions, the active chromium sites
947 originated by reacting Cr(II)/SiO$_2$ with an excess of ethylene
948 at room temperature are not EPR active.
949   Altogether, the experiments reported in Figure 5 and Figure
950 6 converge in indicating that, under the experimental
951 conditions typically adopted in our lab, isolated Cr(III) sites
952 are not necessary for developing ethylene polymerization on
953 the Cr/SiO$_2$ Phillips catalyst. There are no doubts that Cr(III)-
954 based catalysts can efficiently polymerize ethylene, as largely
955 demonstrated for both homogeneous[89,90] and heterogene-
956 ous[93−97] Cr(III) catalysts, but these systems are not necessarily
957 representative of the active chromium sites in the classical
958 Phillips catalyst. The discrepancies of our results with respect
959 to those obtained by different research groups, can be
960 explained by considering the different experimental conditions,
961 as discussed above, for instance the use of diluted pulses of
962 ethylene, as well as of a silica xerogel having a large amount of
963 micropores, might promote termination mechanisms which are
964 unlikely to occur in large excess of the monomer and on

polymer-grade silica supported chromium sites. Although we are not able yet to describe in details the structure of the active chromium sites in the Phillips catalysts, the data discussed above support the occurrence of a two-electron oxidation of the Cr(II) intermediates to Cr(IV) sites, having a tetrahedral-like symmetry (most likely dialkyl Cr(IV) sites).

3.4. The Role of Theoretical Calculations: Predictive, Explanative, or Both? In this complex and controversial scenario, theoretical calculations play a fundamental role and have also some responsibility. In the past decade, in particular, the number of papers on the Phillips catalyst relying entirely on theoretical calculations is increasing exponentially. This is probably a consequence of not only the improved speed and reliability of the computational methods but also the increasing frustration in obtaining definitive results from experimental methods. Indeed, most theoretical papers on the Phillips catalyst have been concentrated on the reaction mechanism, mainly on Cr(II)/SiO$_2$,[30,31,85−87,130] but also on Cr(III)/SiO$_2$,[93−95,130] and Cr(VI)/SiO$_2$,[131] which is probably the question most difficult to tackle by means of experimental methods.

One of the main problems of theoretical calculations is the choice of the model, wherein we include the dimension of the cluster and its termination, the position of the chromium sites within the cluster and their relation with other surface species, and the oxidation state of the chromium sites. Modeling of amorphous silica is per se a challenging task, although several attempts have been made to develop realistic models of this material.[132−135] Most of the works are based on rather small and rigid cluster models of reduced Cr(II) and Cr(III) species supported on a silica fragment,[31,32,85−87,93−95,136−141] which assume only minimal information on the local environment around the chromium sites. In most of the recent works, the silica clusters are terminated with OH capping groups, but also fluorine and hydrogen termination have been used. These models enable effective computations of many complex reaction pathways[32,85−87,93−95,119,141] at a reasonable computational cost, and in some cases, they were found to provide results similar to larger, more detailed, models.[130] However, as admitted by most of the authors, they cannot fully reproduce neither the complexity and the strain of the silica surface nor the heterogeneity of the chromium sites.

Only a few works employed larger SiO$_2$ clusters having an amorphous structure,[100,130,131] or periodic models of amorphous silica.[97,142−145] Larger and/or periodic models are usually more flexible and account for the presence of siloxane ligands nearby the chromium sites. Both properties are very important in affecting the structure of the chromium sites and, consequently, their reactivity and the type of polymer they produce. For example, Handzlik and co-workers[144] found that, for periodic models of Cr(II)/SiO$_2$, the interaction between Cr(II) and surface siloxane bridges affects the O−Cr−O angle, relaxing the strain effect induced by the small size of the chromasiloxane ring. Concerning the effect of the siloxane ligands on the reactivity of the chromium sites, the group of Scott and Peters[86] suggested that the activation barrier for Cr−C bond homolysis of an organo-Cr(IV), to give the active Cr(III)-alkyl and an alkyl radical, might be reduced for chromium sites in interaction with hemilabile siloxane ligands. Similarly, according to Coperet and co-workers, the energetics of the initial steps in ethylene polymerization over Cr(III)/SiO$_2$ are different when evaluated either at the cluster[94,95] or at the periodic level.[145] Finally, Taniike and co-workers[146]

demonstrated that monoalkyl-Cr(III) species on SiO$_2$ with a different coordination environment showed remarkable variations for both the ethylene insertion and the chain transfer energies, resulting in a broad range of polyethylene molecular weights. These results highlight the importance of conducting calculation on sufficiently large and flexible models.

Once that the model has been selected and the calculations performed, some questions arise about how to distinguish between different outcomes—which ones can be considered feasible and which others must be rejected. In most of the cases, the selection is done exclusively on the basis of the computed energies. Reaction paths with very high energy barriers, or with unstable intermediates, are considered infeasible. Unfortunately, this is not sufficient, as recently pointed out by Peters et al.,[31] who suggested that any computational result must be evaluated according to three guidelines: one related to the structure of the sites (i.e., there should be a viable pathway to obtain the sites proposed in the models) and other two related to the reaction mechanism (i.e., the complete catalytic cycle should be considered, and computations should distinguish between possible and impossible). In our opinion, there is a fourth condition that must be fulfilled to validate a theoretical model, which however is rarely taken into account. Before providing realistic energetic barriers for the investigated reaction, a good model should be able to reproduce some properties of the chromium sites that can be measured experimentally, such as vibrational or electronic properties. Indeed, the energetics of the adsorption/desorption of reactants, as well as the barriers associated with the initiation, propagation, and termination steps, strongly depend on the properties of the chromium sites. Unfortunately, in most of the cases only the structural details and the stability of the models are provided, with rare exceptions.

Another issue that is rarely considered by the computational works, is the fact that ethylene polymerization is a strongly exothermic reaction. Although the temperature of a fluidized bed reactor is kept under control for example operating in the condensed mode,[147] the local temperature at each active chromium site might increase several tens of degrees, making it possible to overcome the energetic barriers evaluated as too high at the polymerization temperature.

4. BEYOND THE EXISTING DEBATES: THE ROLE OF THE COCATALYST AS AN EXAMPLE OF AN ALMOST VIRGIN AREA TO EXPLORE

The Phillips catalysts can be further tailored by adding modifying agents[148−151] or cocatalysts in the right amount.[25−27,82,152−154] Opposite to Ziegler−Natta catalysts, the Phillips catalysts do not require any cocatalysts (or activators) to achieve activity, while they are used to enhance it and to modify the produced polymer.[5] For example, Cr/SiO$_2$ heterogeneous Phillips catalysts modified by hydrosilanes account for the production of several unique low-density PEs, manufactured through an in situ branching process (i.e., without the use of external α-olefins as comonomers) and commercially introduced during the early 1990s.[155−158] This comonomer-free industrial technology presents several commercial advantages with respect to the copolymerization route (i.e., the use of a comonomer, typically 1-hexene, in the ethylene feed),[5,115,159] such as (i) lower feedstock cost (ethylene is cheaper than the typical comonomers); (ii) feasibility of overcoming the lack of appropriate comonomers;

and (iii) reduced cost of loading, purification, storage, feeding, or downstream recycling in absence of comonomers.

We have recently investigated the effect of triethylsilane (TES) on the structure of the Cr(II) sites in Cr(II)/SiO$_2$, by synergically coupling FT-IR spectroscopy of adsorbed CO, DR UV−vis-NIR, XANES, and EXAFS spectroscopies.[104,160,161] The results are summarized in Figure 7 and will be briefly
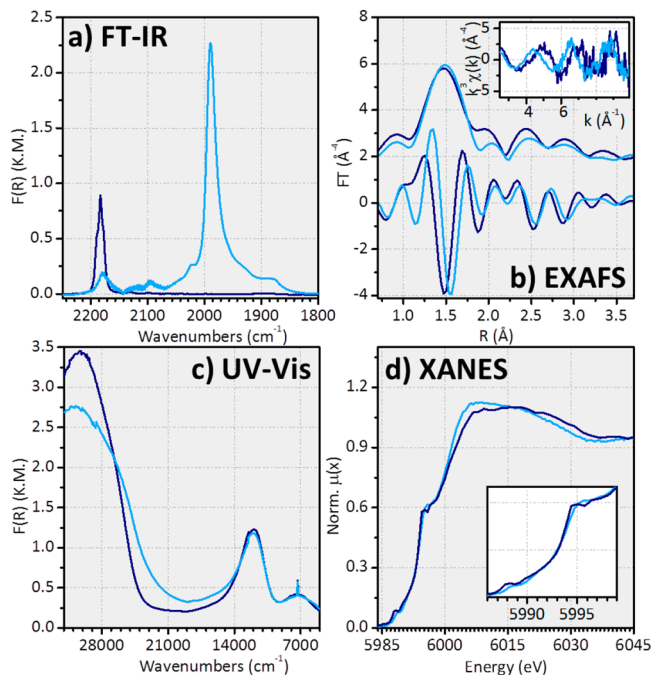
Figure 7. FT-IR spectra of CO adsorbed at room temperature (a), k^3-weighted FT of the EXAFS signals (b) in both modulus (top) and imaginary part (bottom), DR UV−vis-NIR spectra (c), and Cr K-edge normalized XANES spectra (d) of Cr(II)/SiO$_2$ before (dark blue) and after reaction with triethylsilane (TES, cyan).[104] The inset in panel b shows the k^3-weighted $\chi(k)$ functions; the inset in panel d shows a magnification of the XANES edge.

discussed in the following, also because they nicely demonstrate the complementarity of the above-mentioned characterization techniques in the investigation of such a complex system. According to the FT-IR results (Figure 7a), a substantial fraction (over 85%) of the Cr(II) sites are modified by TES: indeed, the IR absorption band around 2180 cm^{-1}, ascribed to CO coordinated to Cr$_A$ and Cr$_B$ sites, drastically decreases, in favor of a new absorption band around 2000 cm^{-1}, which is the fingerprint of CO coordinated to the modified sites. As anticipated in Section 3.2.1, the modified Cr sites have a homogeneous behavior[162] and show up to two coordination vacancies available at room temperature. The EXAFS data are in well agreement with this picture. The k$^3\chi(k)$ EXAFS signal of Cr(II)/SiO$_2$ drastically changes after reaction with TES (inset in Figure 7b), indicating that the majority of the Cr(II) sites are affected. The Fourier-Transform of the EXAFS signals (Figure 7b) look similar in modulus (Figure 7b, top), while the imaginary parts (Figure 7b, bottom) are clearly shifted. According to the analysis of the EXAFS data, on average, the modified chromium sites are surrounded by two oxygen atoms in the first (covalent) coordination shell, as in Cr(II)/SiO$_2$, but at a longer distance (1.95 Å vs 1.86 Å). Their "homogeneous" nature is testified by the small σ^2 value (0.004 Å^{-2} vs 0.015 Å^{-2}). Despite that most

of the Cr(II) sites are modified by TES, the DR UV−vis-NIR (Figure 7c) and the XANES (Figure 7d) spectra of Cr(II)/SiO$_2$ are almost unaffected. Since both spectra are very sensitive to the chromium oxidation state and type of ligands[12] their invariance has been considered as an evidence that no substantial changes in the chromium oxidation state, nor in the type of ligands (namely, siloxy [≡SiO−] monoanionic ligands and adjacent siloxanes [−SiOSi−] neutral ligands) occur in the chromium coordination sphere, in good agreement with the EXAFS data analysis.

Overall, the whole set of spectroscopic data reported in Figure 7 (and largely commented in ref 104) demonstrate the copresence of two different Cr(II) sites on Cr(II)/SiO$_2$+TES. A large fraction of modified Cr(II) sites, having a "homogenous-like" character and displaying a flexible ligand sphere of general formula, [O−Cr(II)-OSiR$_3$] (with R = H or Et), account for the oligomerization of ethylene. The remaining unmodified Cr(II) sites, highly unsaturated and less flexible, copolymerize the in situ produced comonomers and ethylene, to give LLDPE in the presence of ethylene as the only feed. Such a dual catalytic system explains the bimodal mass weight distribution observed in the resulting products.

Not only hydrosilanes but also many other compounds bearing at least one metal−alkyl bond (such as AlR$_3$, BR$_3$, and ZnR$_2$) can be employed to affect the distribution of chromium active sites, promote in situ branching, and enhance the sensitivity to hydrogen.[5,163] This latter aspect is particularly interesting because the unmodified Phillips catalyst is not sensitive to the presence of hydrogen during the polymerization process, which is among the easiest methods for the regulation of the molecular weight. Although the cocatalysts are commonly employed in industry and their influence on the polymer properties is well assessed, the effect of the cocatalyst on the chromium sites was rarely investigated with spectroscopic methods,[25−27,104,114,160,161] likely as a consequence of the difficulty in manipulating metal−alkyls in the proper way. Preliminary spectroscopic data collected in our lab indicate that triethylaluminum and diethylaluminum-ethoxide have an effect similar to that of TES on Cr(II)/SiO$_2$: only a fraction of the Cr(II) sites are modified (even when an excess of cocatalyst is used), and at least a fraction of the modified sites are more "homogeneous" in nature.[114] This is still a largely unexplored area, where spectroscopic methods may help in understanding and hence in tuning the properties of the catalyst, and ultimately, of the PE products.

5. CONCLUSIONS AND A VISION FOR THE FUTURE

We have summarized and critically compared some of the experimental results recently published on the Phillips catalyst, in the attempt to clarify the reasons for the lively debate that is animating a small, but rather active, scientific community. Most of the attention has been devoted so far to clarify the mechanism of initiation of ethylene polymerization, which is a problem strictly connected with the chromium oxidation state. According to part of the literature, Cr(II) sites are the precursors, while Cr(III)-alkyl are the active sites. However, we have recently demonstrated that ethylene polymerization on Cr(II)/SiO$_2$ takes place without forming any paramagnetic chromium species detectable by EPR, including Cr(III), in contrast to the experimental evidence provided by Scott and her group. These data not only reopen the question on the oxidation state of the propagating chromium sites (which was recently presented as a closed case) but also foster some

consideration on the reasons why different research groups obtain different results on apparently the same system.

At least in part, these discrepancies can be explained in terms of the different history of the investigated samples. In particular, the whole set of data summarized in this work unequivocally demonstrate that both the activation treatment and the chromium loading have a strong influence on the stress/strain of the silica surface, which in turns affects the structural and electronic properties of the chromium sites. This is something well-known by industrial researchers, who are used to act on both parameters to tune the catalytic performances. Some of the results present in the literature are obtained on samples activated at rather low temperature (e.g., 500 °C) with respect to that suggested by the industrial practice, or CO-reduced at a temperature higher than the conventional one (350 °C). The reactivity of the chromium sites activated following different protocols is obviously not the same and any extrapolation of the reaction paths should be done with caution.

Another message clearly emerging by our analysis is that there is no a single experimental method better than others in clarifying the properties of the active chromium sites. In order to avoid misleading conclusions, the best strategy is to collect the largest set of data with as many techniques as possible, on the same catalyst and with the same experimental setup. The example reported in Figure 7 is emblematic: by looking to the DR UV−vis and XANES results only, one might conclude that most of the original Cr(II) sites were not modified by the cocatalyst. This is, however, not true, as indicated by FT-IR spectroscopy of adsorbed CO and EXAFS spectroscopy. Hence, the latter two techniques were fundamental to unravel the fraction of modified sites. On the other hand, FT-IR and EXAFS spectroscopy alone could hardly define univocally the oxidation state of the modified chromium sites without DR UV−vis and XANES. Finally, as far as theoretical calculation, they can distinguish between feasible and unfeasible reaction paths, but the adopted models should be validated by reproducing some properties of the chromium sites that can be experimentally measured, while often only the energetics of the process are computed. The results present in the literature and summarized in this work demonstrate that only large and/ or periodic models are able to account for the flexibility of the silica surface, although they clearly have a much higher computational cost than small and rigid clusters. These are very general conclusions that go beyond the single case of the Phillips catalysts and can be useful for other important catalysts involving isolated metal ions dispersed on high surface area amorphous or disordered supports, such as MoO_x/Al_2O_3, WO_x/SiO_2, and ReO_x/Al_2O_3, which have long been used for the industrial production of polyolefins and in large-scale continuous alkene metathesis.

The overall conclusion is that a complete experimental and computational investigation on the Phillips catalyst is affordable only by those research groups having manpower, working time, and money to be spent in a long-term project on olefin polymerization catalysis. This is quite hard in recent times, which are marked by a global shortage of resources. For academic researchers willing to undertake this route, there are two options: either applying for public money or finding an industrial sponsor. Unfortunately, the accessibility to public money based on competitive projects is rather limited if not impossible, as in other fields of research. This is mainly a consequence of the widespread opinion that olefin polymer-ization catalysis is a mature field of research. This opinion has been fostered along the years by the same scientific community working in this field (who literally coined the term "mature"), but is largely unmotivated. Innovations in the field of polyolefins are not only possible, but rather desirable, and are driven by improvements in the catalyst process as well as in the polyolefins applications. On the other hand, with rare exceptions that are driven by the personal curiosity of single researchers, apparently polyolefins companies are not inter-ested in the Phillips catalysts. The general perception is that the system is so complex that it is hard to fine-tune its properties to obtain new PE products with a high added value, and this limits the attractiveness to invest in further basic research in comparison to its competitors. It must be noticed, however, that this complexity is not at all a prerogative of the Phillips catalyst. Also the heterogeneous Ziegler−Natta catalysts are extremely complex systems, if not more so, because they are multicomponent, nanocrystalline, and thus intrinsically highly defective.[164] For these reasons, they present exactly the same problems of the Phillips catalyst when looking at a rational manipulation of the active sites. Indeed, the industrial development of both families of catalysts followed the same trial-and-error strategy.

Opposite to the general belief, the patent literature demonstrates that there are plenty of ways to manipulate the original Cr/SiO_2 catalyst in order to affect its performances (not only in terms of activity but also how efficiently it runs in the commercial reactor) and to finely tune the PE properties, which include the polymer MW, the breadth of the MW distribution, the incorporation degree of comonomer/macro-mer, and the subsequent distribution of short and long-chain branches within the MW distribution. The difficulty is to establish a correlation between the catalyst composition, the structure of the active sites, and the catalyst performances. However, the data summarized in this work demonstrate that it is possible, although challenging. There are still many aspects of the Phillips catalysts that have not yet received much attention by academic researchers, but at the same time, they are surely topics of interest for polyolefin companies. For example, the influence of supports[165] or the effect of activators (such as aluminum-alkyls) on the properties of the chromium sites have been rarely investigated at a molecular level, and only a few (mostly unproven) hypotheses have been formulated. Nevertheless, a multitude of supports and activators are normally used in practical application of the Phillips catalyst to tune the properties of the produced polyethylene. The characterization methods are now estab-lished enough to tackle these questions, as mentioned in this Perspective. A strong cooperation between academic and industrial researchers on these and other topics would be desirable for the foreseeable future, and it might lead to unexpected revolutions in olefin polymerization catalysis. We, as academic researchers, have the responsibility to promote a positive and constructing discussion on this catalyst. This is the premise for creating a solid scientific base that will serve both young researchers at the beginning of their career and at the same time the industrial researchers who daily work with it. This is a challenging target that requires dedication, passion, and scientific maturity.

■ AUTHOR INFORMATION

Corresponding Author

*E-mail: elena.groppo@unito.it.

ORCID

Elena Groppo: 0000-0003-4153-5709

Notes

The authors declare no competing financial interest.

■ REFERENCES

(1) Nowlin, T. E. *Business And Technology Of The Global Polyethylene Industry*; Scrivener Publishing LLC: New York, 2014.

(2) Cheng, R.; Liu, Z.; Zhong, L.; He, X.; Qiu, P.; Terano, M.; Eisen, M. S.; Scott, S. L.; Liu, B. Phillips Cr/Silica Catalyst For Ethylene Polymerization. *Advances In Polymer Science*; Springer: Berlin, 2013; Vol. 257, pp 135−202.

(3) Mcdaniel, M. P. Supported Chromium Catalysts For Ethylene Polymerization. *Adv. Catal.* **1985**, *33*, 47−98.

(4) Mcdaniel, M. P. In *Handbook Of Heterogeneous Catalysis*; Ertl, G., Knözinger, H., Weitkamp, J., Eds.; Wiley-VCH: Weinheim, 1997; Vol. 5, p 2400.

(5) Mcdaniel, M. P. A Review Of The Phillips Supported Chromium Catalyst And Its Commercial Use For Ethylene Polymerization. *Adv. Catal.* **2010**, *53*, 123−606.

(6) Mcdaniel, M. Some Reflections On The Current State Of Cr-Based Polymerization Catalysts. *MRS Bull.* **2013**, *38*, 234−238.

(7) Weckhuysen, B. M.; Schoonheydt, R. A. Olefin Polymerization Over Supported Chromium Oxide Catalysts. *Catal. Today* **1999**, *51*, 215−221.

(8) Hogan, J. P.; Banks, R. L. Polymers And Production Thereof. U.S. Patent 2, 825, 721, Mar. 4, 1958.

(9) Jayaratne, K. C.; Cymbaluk, T. H.; Jensen, M. D. A Career In Catalysis: Max Mcdaniel. *ACS Catal.* **2018**, *8*, 602−614.

(10) Weckhuysen, B. M.; Wachs, I. E.; Schoonheydt, R. A. Surface Chemistry And Spectroscopy Of Chromium In Inorganic Oxides. *Chem. Rev.* **1996**, *96*, 3327−3350.

(11) Groppo, E.; Lamberti, C.; Bordiga, S.; Spoto, G.; Zecchina, A. The Structure Of Active Centers And The Ethylene Polymerization Mechanism On The Cr/SiO$_2$ Catalyst: A Frontier For The Characterization Methods. *Chem. Rev.* **2005**, *105*, 115−183.

(12) Groppo, E.; Seenivasan, K.; Barzan, C. The Potential Of Spectroscopic Methods Applied To Heterogeneous Catalysts For Olefin Polymerization. *Catal. Sci. Technol.* **2013**, *3*, 858−878.

(13) Zecchina, A.; Garrone, E.; Ghiotti, G.; Coluccia, S. On The Chemistry Of Silica Supported Chromium Ions. II. One-Ligand Complexes. Adsorption Of Carbon Monoxide, Carbon Dioxide And Pyridine. *J. Phys. Chem.* **1975**, *79*, 972−978.

(14) Zecchina, A.; Garrone, E.; Ghiotti, G.; Morterra, C.; Borello, E. On The Chemistry Of Silica Supported Chromium Ions. I. Characterization Of The Samples. *J. Phys. Chem.* **1975**, *79*, 966−972.

(15) Zecchina, A.; Garrone, E.; Morterra, C.; Coluccia, S. On The Chemistry Of Silica Supported Chromium Ions. III Two-Ligand Complexes. Nitric Oxide Adsorption. *J. Phys. Chem.* **1975**, *79*, 978−983.

(16) Ghiotti, G.; Garrone, E.; Zecchina, A. IR Investigation Of Polymerization Centres Of The Phillips Catalyst. *J. Mol. Catal.* **1988**, *46*, 61−77.

(17) Mcdaniel, M. Manipulating Polymerization Chemistry Of Cr/Silica Catalysts Through Calcination. *Appl. Catal., A* **2017**, *542*, 392−410.

(18) Tromp, M. Catalysis Seen In Action. *Philos. Trans. R. Soc., A* **2015**, *373*, 20130152.

(19) Weckhuysen, B. M. Determining The Active Site In A Catalytic Process: Operando Spectroscopy Is More Than A Buzzword. *Phys. Chem. Chem. Phys.* **2003**, *5*, 4351−4360.

(20) Topsøe, H. Developments In Operando Studies And In Situ Characterization Of Heterogeneous Catalysts. *J. Catal.* **2003**, *216*, 155−164.

(21) Tinnemans, S. J.; Mesu, J. G.; Kervinen, K.; Visser, T.; Nijhuis, T. A.; Beale, A. M.; Keller, D. E.; Van Der Eerden, A. M. J.; Weckhuysen, B. M. Combining Operando Techniques In One Spectroscopic-Reaction Cell: New Opportunities For Elucidating The Active Site And Related Reaction Mechanism In Catalysis. *Catal. Today* **2006**, *113*, 3−15.

(22) Bañares, M. A. Operando Methodology: Combination Of In Situ Spectroscopy And Simultaneous Activity Measurements Under Catalytic Reaction Conditions. *Catal. Today* **2005**, *100*, 71−77.

(23) Bañares, M. A. Operando Spectroscopy: The Knowledge Bridge To Assessing Structure−Performance Relationships In Catalyst Nanoparticles. *Adv. Mater.* **2011**, *23*, 5293−5301.

(24) Arean, C. O.; Weckhuysen, B. M.; Zecchina, A. Operando Surface Spectroscopy-Placing Catalytic Solids At Work Under The Spotlight. *Phys. Chem. Chem. Phys.* **2012**, *14*, 2125−2127.

(25) Cicmil, D.; Meeuwissen, J.; Vantomme, A.; Wang, J.; Van Ravenhorst, I. K.; Van Der Bij, H. E.; Munoz-Murillo, A.; Weckhuysen, B. M. Polyethylene With Reverse Co-Monomer Incorporation: From An Industrial Serendipitous Discovery To Fundamental Understanding. *Angew. Chem., Int. Ed.* **2015**, *54*, 13073−13079.

(26) Cicmil, D.; Meeuwissen, J.; Vantomme, A.; Weckhuysen, B. M. Real-Time Analysis Of A Working Triethylaluminium-Modified Cr/Ti/SiO2 Ethylene Polymerization Catalyst With In Situ Infrared Spectroscopy. *ChemCatChem* **2016**, *8*, 1937−1944.

(27) Cicmil, D.; Van Ravenhorst, I. K.; Meeuwissen, J.; Vantomme, A.; Weckhuysen, B. M. Structure-Performance Relationships Of Cr/Ti/SiO2 Catalysts Modified With Teal For Oligomerisation Of Ethylene: Tuning The Selectivity Towards 1-Hexene. *Catal. Sci. Technol.* **2016**, *6*, 731−743.

(28) Barzan, C.; Piovano, A.; Braglia, L.; Martino, G. A.; Lamberti, C.; Bordiga, S.; Groppo, E. Ligands Make The Difference! Molecular Insights Into Cr^{VI}/SiO$_2$ Phillips Catalyst During Ethylene Polymerization. *J. Am. Chem. Soc.* **2017**, *139*, 17064−17073.

(29) Zecchina, A.; Groppo, E. Surface Chromium Single Sites: Open Problems And Recent Advances. *Proc. R. Soc. London, Ser. A* **2012**, *468*, 2087−2098.

(30) Chakrabarti, A.; Gierada, M.; Handzlik, J.; Wachs, I. E. Operando Molecular Spectroscopy During Ethylene Polymerization By Supported Crox/SiO2 Catalysts: Active Sites, Reaction Inter-

mediates, And Structure-Activity Relationship. *Top. Catal.* **2016**, *59*, 725−739.

(31) Peters, B.; Scott, S. L.; Fong, A.; Wang, Y.; Stiegman, A. E. Reexamining The Evidence For Proton Transfers In Ethylene Polymerization. *Proc. Natl. Acad. Sci. U. S. A.* **2015**, *112*, E4160− E4161.

(32) Delley, M. F.; Nuñez-Zarur, F.; Conley, M. P.; Comas-Vives, A.; Siddiqi, G.; Norsic, S.; Monteil, V.; Safonova, O. V.; Copéret, C. Reply To Peters Et Al.: Proton Transfers Are Plausible Initiation And Termination Steps On Cr(III) Sites In Ethylene Polymerization. *Proc. Natl. Acad. Sci. U. S. A.* **2015**, *112*, E4162−E4163.

(33) Clark, A. Olefyn Polymerization On Supported Cr Oxide Catalysts. *Catal. Rev.: Sci. Eng.* **1970**, *3*, 145−173.

(34) Mcdaniel, M. P.; Johnson, M. M. A Comparison Of Cr/Sio$_2$ And Cr/Alpo$_4$ Polymerization Catalysts: I. Kinetics. *J. Catal.* **1986**, *101*, 446−457.

(35) Mcdaniel, M. P.; Johnson, M. M. A Comparison Of Cr/Sio$_2$ And Cr/Alpo$_4$ Polymerization Catalysts 2. Chain Transfer. *Macromolecules* **1987**, *20*, 773−778.

(36) Mcdaniel, M. P.; Welch, M. B. Activation Of The Phillips Polymerization Catalyst. Influence Of The Hydroxyl Population. *J. Catal.* **1983**, *82*, 98−109.

(37) Jensen, M. D.; Yang, Q.; Yu, Y.; Mcdaniel, M. P. Kinetics Of Long-Chain Branch Formation In Polyethylene. *ACS Catal.* **2018**, *8*, 725−737.

(38) Groppo, E.; Prestipino, C.; Cesano, F.; Bonino, F.; Bordiga, S.; Lamberti, C.; Thüne, P. C.; Niemantsverdriet, J. W.; Zecchina, A. In Situ, Cr K-Edge XAS Study On The Phillips Catalyst: Activation And Ethylene Polymerization. *J. Catal.* **2005**, *230*, 98−108.

(39) Groppo, E.; Damin, A.; Bonino, F.; Zecchina, A.; Bordiga, S.; Lamberti, C. New Strategies In The Raman Study Of The Cr/Sio$_2$ Phillips Catalyst: Observation Of Molecular Adducts On Cr(II) Sites. *Chem. Mater.* **2005**, *17*, 2019−2027.

(40) Bordiga, S.; Groppo, E.; Agostini, G.; Van Bokhoven, J. A.; Lamberti, C. Reactivity Of Surface Species In Heterogeneous Catalysts Probed By In Situ X-Ray Absorption Techniques. *Chem. Rev.* **2013**, *113*, 1736−1850.

(41) Weckhuysen, B. M.; Deridder, L. M.; Schoonheydt, R. A. A Quantitative Diffuse Reflectance Spectroscopy Study Of Supported Chromium Catalysts. *J. Phys. Chem.* **1993**, *97*, 4756−4763.

(42) Weckhuysen, B. M.; Verberckmoes, A. A.; Buttiens, A. L.; Schoonheydt, R. A. Diffuse-Reflectance Spectroscopy Study Of The Thermal Genesis And Molecular Structure Of Chromium Supported Catalysts. *J. Phys. Chem.* **1994**, *98*, 579−584.

(43) Weckhuysen, B. M.; Schoonheydt, R. A.; Jehng, J. M.; Wachs, I. E.; Cho, S. J.; Ryoo, R.; Kijlstra, S.; Poels, E. Combined DRS-RS-EXAFS-XANES-TPR Study Of Supported Chromium Catalysts. *J. Chem. Soc., Faraday Trans.* **1995**, *91*, 3245−3253.

(44) Weckhuysen, B. M.; Verberckmoes, A. A.; Debaets, A. R.; Schoonheydt, R. A. Diffuse Reflectance Spectroscopy Of Supported Chromium Oxide Catalysts: A Self-Modeling Mixture Analysis. *J. Catal.* **1997**, *166*, 160−171.

(45) Weckhuysen, B. M.; Wachs, I. E. In Situ Raman Spectroscopy Of Supported Chromium Oxide Catalysts: Reactivity Studies With Methanol And Butane. *J. Phys. Chem.* **1996**, *100*, 14437−14442.

(46) Weckhuysen, B. M.; Wachs, I. E. Raman Spectroscopy Of Supported Chromium Oxide Catalysts - Determination Of Chromium-Oxygen Bond Distances And Bond Orders. *J. Chem. Soc., Faraday Trans.* **1996**, *92*, 1969−1973.

(47) Weckhuysen, B. M.; Wachs, I. E. In Situ Raman Spectroscopy Of Supported Chromium Oxide Catalysts: $^{18}O_2$-$^{16}O_2$ Isotopic Labeling Studies. *J. Phys. Chem. B* **1997**, *101*, 2793−2796.

(48) Weckhuysen, B. M.; Schoonheydt, R. A.; Mabbs, F. E.; Collison, D. Electron Paramagnetic Resonance Of Heterogeneous Chromium Catalysts. *J. Chem. Soc., Faraday Trans.* **1996**, *92*, 2431− 2436.

(49) Vuurman, M. A.; Stufkens, D. J.; Oskam, A.; Moulijn, J. A.; Kapteijn, F. Raman Spectra Of Chromium-Oxide Species In Cro$_3$/ Al$_2$O$_3$ Catalysts. *J. Mol. Catal.* **1990**, *60*, 83−98.

(50) Vuurman, M. A.; Wachs, I. E. In Situ Raman-Spectroscopy Of Alumina-Supported Metal-Oxide Catalysts. *J. Phys. Chem.* **1992**, *96*, 5008−5016.

(51) Vuurman, M. A.; Wachs, I. E.; Stufkens, D. J.; Oskam, A. Characterization Of Chromium-Oxide Supported On Al$_2$O$_3$, Zro$_2$, Tio$_2$, And Sio$_2$ Under Dehydrated Conditions. *J. Mol. Catal.* **1993**, *80*, 209−227.

(52) Vuurman, M. A.; Hardcastle, F. D.; Wachs, I. E. Characterization Of Cro$_3$/Al$_2$O$_3$ Catalysts Under Ambient Conditions - Influence Of Coverage And Calcination Temperature. *J. Mol. Catal.* **1993**, *84*, 193−205.

(53) Wachs, I. E. Raman And IR Studies Of Surface Metal Oxide Species On Oxide Supports: Supported Metal Oxide Catalysts. *Catal. Today* **1996**, *27*, 437−455.

(54) Wachs, I. E.; Roberts, C. A. Monitoring Surface Metal Oxide Catalytic Active Sites With Raman Spectroscopy. *Chem. Soc. Rev.* **2010**, *39*, 5002−5017.

(55) Lee, E. L.; Wachs, I. E. In Situ Raman Spectroscopy Of Sio2-Supported Transition Metal Oxide Catalysts: An Isotopic O-18-O-16 Exchange Study. *J. Phys. Chem. C* **2008**, *112*, 6487−6498.

(56) Demmelmaier, C. A.; White, R. E.; Van Bokhoven, J. A.; Scott, S. L. Nature Of Siocr$_2$cl And (Sio)$_2$cr$_2$ Sites Prepared By Grafting Cro$_2$cl$_2$ Onto Silica. *J. Phys. Chem. C* **2008**, *112*, 6439−6449.

(57) Moisii, C.; Deguns, E. W.; Lita, A.; Callahan, S. D.; Van De Burgt, L. J.; Magana, D.; Stiegman, A. E. Coordination Environment And Vibrational Spectroscopy Of Cr(VI) Sites Supported On Amorphous Silica. *Chem. Mater.* **2006**, *18*, 3965−3975.

(58) Cieslak-Golonka, M. Spectroscopy Of Chromium(VI) Species. *Coord. Chem. Rev.* **1991**, *109*, 223−249.

(59) Dines, T. J.; Inglis, S. Raman Spectroscopic Study Of Supported Chromium(VI) Oxide Catalysts. *Phys. Chem. Chem. Phys.* **2003**, *5*, 1320−1328.

(60) Thune, P. C.; Verhagen, C. P. J.; Van Den Boer, M. J. G.; Niemantsverdriet, J. W. Working Surface Science Model For The Phillips Ethylene Polymerization Catalyst: Preparation And Testing. *J. Phys. Chem. B* **1997**, *101*, 8559−8563.

(61) Thune, P. C.; Linke, R.; Van Gennip, W. J. H.; De Jong, A. M.; Niemantsverdriet, J. W. Bonding Of Supported Chromium During Thermal Activation Of The Cro$_x$/Sio$_2$ (Phillips) Ethylene Polymerization Catalyst. *J. Phys. Chem. B* **2001**, *105*, 3073−3078.

(62) Liu, B. P.; Terano, M. Investigation Of The Physico-Chemical State And Aggregation Mechanism Of Surface Cr Species On A Phillips Cro$_x$/Sio$_2$ Catalyst By XPS And EPMA. *J. Mol. Catal. A: Chem.* **2001**, *172*, 227−240.

(63) Mcdaniel, M. P.; Collins, K. S.; Benham, E. A. Activation Of Phillips Cr/Silica Catalysts IV. Mobility Of Cr(VI). *J. Catal.* **2007**, *252*, 281−295.

(64) Weckhuysen, B. M.; Deridder, L. M.; Grobet, P. J.; Schoonheydt, R. A. Redox Behavior And Dispersion Of Supported Chromium Catalysts. *J. Phys. Chem.* **1995**, *99*, 320−326.

(65) Weckhuysen, B. M.; Schoonheydt, R. A. Recent Progresses In Diffuse Reflectance Spectroscopy Of Supported Metal Oxide Catalysts. *Catal. Today* **1999**, *49*, 441−451.

(66) Weckhuysen, B. M.; Verberckmoes, A. A.; Debaere, J.; Ooms, K.; Langhans, I.; Schoonheydt, R. A. In Situ UV-Vis Diffuse-Reflectance Spectroscopy-On Line Activity Measurements Of Supported Chromium Oxide Catalysts: Relating Isobutane Dehydrogenation Activity With Cr Speciation Via Experimental Design. *J. Mol. Catal. A: Chem.* **2000**, *151*, 115−131.

(67) Budnyk, A.; Damin, A.; Barzan, C.; Groppo, E.; Lamberti, C.; Bordiga, S.; Zecchina, A. Cr-Doped Porous Silica Glass As A Model Material To Describe Phillips Catalyst Properties. *J. Catal.* **2013**, *308*, 319−327.

(68) Peek, N. M.; Jeffcoat, D. B.; Moisii, C.; Van De Burgt, L.; Profeta, S.; Scott, S. L.; Stiegman, A. E. Reassessment Of The Electronic Structure Of Cr(VI) Sites Supported On Amorphous Silica And Implications For Cr Coordination Number. *J. Phys. Chem. C* **2018**, *122*, 4349−4358.

(69) Goldsmith, B. R.; Peters, B.; Johnson, J. K.; Gates, B. C.; Scott, S. L. Beyond Ordered Materials: Understanding Catalytic Sites On Amorphous Solids. *ACS Catal.* **2017**, *7*, 7543−7557.

(70) Amakawa, K.; Sun, L.; Guo, C.; Havecker, M.; Kube, P.; Wachs, I. E.; Lwin, S.; Frenkel, A. I.; Patlolla, A.; Hermann, K.; Schlogl, R.; Trunschke, A. How Strain Affects The Reactivity Of Surface Metal Oxide Catalysts. *Angew. Chem., Int. Ed.* **2013**, *52*, 13553−13557.

(71) Cordischi, D.; Indovina, V.; Occhiuzzi, M. Exchange-Coupled Cr(V) And Mo(V) Ions On The Surface Of Cro$_x$ Zro$_2$ And Moo$_x$ Zro$_2$ - An Electron-Paramagnetic Resonance Study. *J. Chem. Soc., Faraday Trans.* **1991**, *87*, 3443−3447.

(72) Cordischi, D.; Indovina, V.; Occhiuzzi, M. The Dispersion Of Cr(V) And Mo(V) On The Surface Of Various Oxides, As Investigated By ESR Spectroscopy. *Appl. Surf. Sci.* **1992**, *55*, 233−237.

(73) Cordischi, D.; Campa, M. C.; Indovina, V.; Occhiuzzi, M. Structure Of Cr-V Species On The Surface Of Various Oxides - Reactivity With NH$_3$ And H$_2$O, As Investigated By EPR Spectroscopy. *J. Chem. Soc., Faraday Trans.* **1994**, *90*, 207−212.

(74) Groeneveld, C.; Wittgen, P. P. M. M.; van Kersbergen, A. M.; Mestrom, P. L. M.; Nuijten, C. E.; Schuit, G. C. A. *J. Catal.* **1979**, *59*, 153.

(75) Krauss, V. H. L.; Stach, H. Chrom(II) Als Wirksamer Bestandteil Des Phillips Katalysators Zur Äthylenpolymerisation. *Inorg. Nucl. Chem. Lett.* **1968**, *4*, 393−397.

(76) Krauss, H. L.; Stach, H. Z. *Z. Anorg. Allg. Chem.* **1969**, *366*, 34−42.

(77) Finch, J. N. *J. Catal.* **1976**, *43*, 111.

(78) Brown, C.; Krzystek, J.; Achey, R.; Lita, A.; Fu, R.; Meulenberg, R. W.; Polinski, M.; Peek, N.; Wang, Y.; Van De Burgt, L. J.; Profeta, S.; Stiegman, A. E.; Scott, S. L. Mechanism Of Initiation In The Phillips Ethylene Polymerization Catalyst: Redox Processes Leading To The Active Site. *ACS Catal.* **2015**, *5*, 5574−5583.

(79) Liu, Z.; He, X.; Cheng, R.; Eisen, M. S.; Terano, M.; Scott, S. L.; Liu, B. Chromium Catalysts For Ethylene Polymerization And Oligomerization. *Advances in Chemical Engineering*; Elsevier: Amsterdam, 2014; Vol. *44*, pp 126−191.

(80) Liu, B.; Nakatani, H.; Terano, M. New Aspects Of The Induction Period Of Ethene Polymerization Using Phillips Cro$_x$/Sio$_2$ Catalyst Probed By XPS, TPD And EPMA. *J. Mol. Catal. A: Chem.* **2002**, *184*, 387−398.

(81) Liu, B. P.; Nakatani, H.; Terano, M. Mechanistic Implications Of The Unprecedented Transformations Of Ethene Into Propene And Butene Over Phillips Cro$_x$/Sio$_2$ Catalyst During Induction Period. *J. Mol. Catal. A: Chem.* **2003**, *201*, 189−197.

(82) Xia, W.; Liu, B.; Fang, Y.; Hasebe, K.; Terano, M. Unique Polymerization Kinetics Obtained From Simultaneous Interaction Of Phillips Cr(VI)Ox/Sio2 Catalyst With Al-Alkyl Cocatalyst And Ethylene Monomer. *J. Mol. Catal. A: Chem.* **2006**, *256*, 301−308.

(83) Zhong, L.; Liu, Z.; Cheng, R.; Tang, S.; Qiu, P.; He, X.; Terano, M.; Liu, B. Active Site Transformation During The Induction Period Of Ethylene Polymerization Over The Phillips Crox/Sio2 Catalyst. *ChemCatChem* **2012**, *4*, 872−881.

(84) Potter, K. C.; Beckerle, C. W.; Jentoft, F. C.; Schwerdtfeger, E.; Mcdaniel, M. P. Reduction Of The Phillips Catalyst By Various Olefins: Stoichiometry, Thermochemistry, Reaction Products And Polymerization Activity. *J. Catal.* **2016**, *344*, 657−668.

(85) Fong, A.; Yuan, Y.; Ivry, S. L.; Scott, S. L.; Peters, B. Computational Kinetic Discrimination Of Ethylene Polymerization Mechanisms For The Phillips (Cr/Sio2) Catalyst. *ACS Catal.* **2015**, *5*, 3360−3374.

(86) Fong, A.; Peters, B.; Scott, S. L. One-Electron-Redox Activation Of The Reduced Phillips Polymerization Catalyst, Via Alkylchromium(IV) Homolysis: A Computational Assessment. *ACS Catal.* **2016**, *6*, 6073−6085.

(87) Fong, A.; Vandervelden, C.; Scott, S. L.; Peters, B. Computational Support For Phillips Catalyst Initiation Via Cr-C Bond Homolysis In A Chromacyclopentane Site. *ACS Catal.* **2018**, *8*, 1728−1733.

(88) Mcguinness, D. S.; Davies, N. W.; Horne, J.; Ivanov, I. Unraveling The Mechanism Of Polymerization With The Phillips Catalyst. *Organometallics* **2010**, *29*, 6111−6116.

(89) Theopold, K. H. Understanding Chromium-Based Olefin Polymerization Catalyst. *CHEMTECH* **1997**, *27*, 26−32.

(90) Theopold, K. H. Homogeneous Chromium Catalysts For Olefin Polymerization. *Eur. J. Inorg. Chem.* **1998**, *1998*, 15−24.

(91) Kohn, R. D.; Haufe, M.; Mihan, S.; Lilge, D. Triazacyclohexane Complexes Of Chromium As Highly Active Homogeneous Model Systems For The Phillips Catalyst. *Chem. Commun.* **2000**, 1927−1928.

(92) Macadams, L. A.; Buffone, G. P.; Incarvito, C. D.; Rheingold, A. L.; Theopold, K. H. A Chromium Catalyst For The Polymerization Of Ethylene As A Homogeneous Model For The Phillips Catalyst. *J. Am. Chem. Soc.* **2005**, *127*, 1082−1083.

(93) Conley, M. P.; Delley, M. F.; Siddiqi, G.; Lapadula, G.; Norsic, S.; Monteil, V.; Safonova, O. V.; Copéret, C. Polymerization Of Ethylene By Silica-Supported Dinuclear Cr^{iii} Sites Through An Initiation Step Involving C-H Bond Activation. *Angew. Chem., Int. Ed.* **2014**, *53*, 1872−1876.

(94) Delley, M. F.; Núñez-Zarur, F.; Conley, M. P.; Comas-Vives, A.; Siddiqi, G.; Norsic, S.; Monteil, V.; Safonova, O. V.; Copéret, C. Proton Transfers Are Key Elementary Steps In Ethylene Polymerization On Isolated Chromium(III) Silicates. *Proc. Natl. Acad. Sci. U. S. A.* **2014**, *111*, 11624−11629.

(95) Conley, M. P.; Delley, M. F.; Núñez-Zarur, F.; Comas-Vives, A.; Copéret, C. Heterolytic Activation Of C-H Bonds On Cr^{ii}-O Surface Sites Is A Key Step In Catalytic Polymerization Of Ethylene And Dehydrogenation Of Propane. *Inorg. Chem.* **2015**, *54*, 5065−5078.

(96) Delley, M. F.; Lapadula, G.; Núñez-Zarur, F.; Comas-Vives, A.; Kalendra, V.; Jeschke, G.; Baabe, D.; Walter, M. D.; Rossini, A. J.; Lesage, A.; Emsley, L.; Maury, O.; Copéret, C. Local Structures And Heterogeneity Of Silica-Supported M(III) Sites Evidenced By EPR, IR, NMR, And Luminescence Spectroscopies. *J. Am. Chem. Soc.* **2017**, *139*, 8855−8867.

(97) Delley, M. F.; Praveen, C. S.; Borosy, A. P.; Núñez-Zarur, F.; Comas-Vives, A.; Copéret, C. Olefin Polymerization On Cr(III)/Sio2: Mechanistic Insights From The Differences In Reactivity Between Ethene And Propene. *J. Catal.* **2017**, *354*, 223−230.

(98) Brown, C.; Lita, A.; Tao, Y.; Peek, N.; Crosswhite, M.; Mileham, M.; Krzystek, J.; Achey, R.; Fu, R.; Bindra, J. K.; Polinski, M.; Wang, Y.; Van De Burgt, L. J.; Jeffcoat, D.; Profeta, S.; Stiegman, A. E.; Scott, S. L. Mechanism Of Initiation In The Phillips Ethylene Polymerization Catalyst: Ethylene Activation By Cr(II) And The Structure Of The Resulting Active Site. *ACS Catal.* **2017**, *7*, 7442−7455.

(99) Amor Nait Ajjou, J.; Scott, S. L. A Kinetic Study Of Ethylene And 1-Hexene Homo- And Copolymerization Catalyzed By A Silica-Supported Cr(IV) Complex: Evidence For Propagation By A Migratory Insertion Mechanism. *J. Am. Chem. Soc.* **2000**, *122*, 8968−8976.

(100) Budnyk, A.; Damin, A.; Groppo, E.; Zecchina, A.; Bordiga, S. Effect Of Surface Hydroxylation On The Catalytic Activity Of A Cr(II)/SiO2Model System Of Phillips Catalyst. *J. Catal.* **2015**, *324*, 79−87.

(101) Lamberti, C.; Groppo, E.; Spoto, G.; Bordiga, S.; Zecchina, A. Infrared Spectroscopy Of Surface Transient Species. *Adv. Catal.* **2007**, *51*, 1−74.

(102) Lamberti, C.; Zecchina, A.; Groppo, E.; Bordiga, S. Probing The Surfaces Of Heterogeneous Catalysts By In Situ IR Spectroscopy. *Chem. Soc. Rev.* **2010**, *39*, 4951−5001.

(103) Martino, G. A.; Barzan, C.; Piovano, A.; Budnyk, A.; Groppo, E. Tracking The Reasons For The Peculiarity Of Cr/Al$_2$O$_3$ Catalyst In Ethylene Polymerization. *J. Catal.* **2018**, *357*, 206−212.

(104) Barzan, C.; Gianolio, D.; Groppo, E.; Lamberti, C.; Monteil, V.; Quadrelli, E. A.; Bordiga, S. The Effect Of Hydrosilanes On The Active Sites Of The Phillips Catalyst: The Secret For In Situ Olefin Generation. *Chem. - Eur. J.* **2013**, *19*, 17277−17282.

(105) Estephane, J.; Groppo, E.; Vitillo, J. G.; Damin, A.; Lamberti, C.; Bordiga, S.; Zecchina, A. Chromocene In Porous Polystyrene: An Example Of Organometallic Chemistry In Confined Spaces. *Phys. Chem. Chem. Phys.* **2009**, *11*, 2218−2227.

(106) Spoto, G.; Bordiga, S.; Garrone, E.; Ghiotti, G.; Zecchina, A.; Petrini, G.; Leofanti, G. Cr(II) And Cr(III) Ions Grafted At Internal Nests Of A Pentasilic Zeolite (Silicalite) - Characterization And Formation Of Polycarbonylic, Polynitrosylic, And Mixed Species By Interaction With CO And NO. *J. Mol. Catal.* **1992**, *74*, 175−184.

(107) Lupinetti, A. J.; Frenking, G.; Strauss, S. H. Nonclassical Metal Carbonyls: Appropriate Definitions With A Theoretical Justification. *Angew. Chem., Int. Ed.* **1998**, *37*, 2113−2116.

(108) Lupinetti, A. J.; Strauss, S. H.; Frenking, G. Nonclassical Metal Carbonyls. *Prog. Inorg. Chem.* **2007**, *49*, 1−112.

(109) Gianolio, D.; Groppo, E.; Vitillo, J. G.; Damin, A.; Bordiga, S.; Zecchina, A.; Lamberti, C. Direct Evidence Of Adsorption Induced Crii Mobility On The Sio2 Surface Upon Complexation By CO. *Chem. Commun.* **2010**, *46*, 976−978.

(110) Zhou, M. F.; Andrews, L.; Bauschlicher, C. W. Spectroscopic And Theoretical Investigations Of Vibrational Frequencies In Binary Unsaturated Transition-Metal Carbonyl Cations, Neutrals, And Anions. *Chem. Rev.* **2001**, *101*, 1931−1961.

(111) Braterman, P. S. *Metal Carbonyl Spectra*; Academic Press: London, 1975.

(112) Estephane, J.; Groppo, E.; Damin, A.; Vitillo, J. G.; Gianolio, D.; Lamberti, C.; Bordiga, S.; Prestipino, C.; Nikitenko, S.; Quadrelli, E. A.; Taoufik, M.; Basset, J. M.; Zecchina, A. Structure And Enhanced Reactivity Of Chromocene Carbonyl Confined Inside The Cavities Of Nay Zeolite. *J. Phys. Chem. C* **2009**, *113*, 7305−7315.

(113) Groppo, E.; Lamberti, C.; Cesano, F.; Zecchina, A. On The Fraction Of Crii Sites Involved In The C2H4 Polymerization On The Cr/Sio2 Phillips Catalyst: A Quantification By FTIR Spectroscopy. *Phys. Chem. Chem. Phys.* **2006**, *8*, 2453−2456.

(114) Martino, G. A.; Piovano, A.; Barzan, C.; Bordiga, S.; Groppo, E. The Effect Of Al-Alkyls On The Phillips Catalyst For Ethylene Polymerization: The Case Of Diethylaluminum Ethoxide (DEALE). *Top. Catal.* **2018**, *61*, 1465.

(115) Mcguinness, D. S. Olefin Oligomerization Via Metallacycles: Dimerization, Trimerization, Tetramerization, And Beyond. *Chem. Rev.* **2011**, *111*, 2321−2341.

(116) Jabri, A.; Mason, C. B.; Sim, Y.; Gambarotta, S.; Burchell, T. J.; Duchateau, R. Isolation Of Single-Component Trimerization And Polymerization Chromium Catalysts: The Role Of The Metal Oxidation State. *Angew. Chem., Int. Ed.* **2008**, *47*, 9717−9721.

(117) Thapa, I.; Gambarotta, S.; Korobkov, I.; Murugesu, M.; Budzelaar, P. Isolation And Characterization Of A Class II Mixed-Valence Chromium(I)/(II) Self-Activating Ethylene Trimerization Catalyst. *Organometallics* **2012**, *31*, 486−494.

(118) Liu, H. J.; Cai, I. C.; Fedorov, A.; Ziegler, M. S.; Copéret, C.; Tilley, T. D. Tricoordinate Organochromium(III) Complexes Supported By A Bulky Silylamido Ligand Produce Ultra-High-Molecular Weight Polyethylene In The Absence Of Activators. *Helv. Chim. Acta* **2016**, *99*, 859−867.

(119) Conley, M. P.; Delley, M. F.; Siddiqi, G.; Lapadula, G.; Norsic, S.; Monteil, V.; Safonova, O. V.; Copéret, C. Erratum: Polymerization Of Ethylene By Silica-Supported Dinuclear Crii Sites Through An Initiation Step Involving C-H Bond Activation (Angewandte Chemie - International Edition (2014) (53)). *Angew. Chem., Int. Ed.* **2015**, *54*, 6670.

(120) Figgis, B. N. *Introduction To Ligand Fields*; John Wiley & Sons: New York, 1966.

(121) Note that the initial spectrum in the two experiments is not the same, although in both cases the samples are formally described as Cr(II)/SiO2. Indeed, the d−d band characteristic of Cr(II) is observed at 770 nm (13 000 cm^{-1}) in the first case and at 830 nm (12 000 cm^{-1}) in the second case. This difference can be easily explained by considering the different activation treatments (calcination At 550 °C and 650 °C, respectively) and indicates once more that the activation strongly affects the properties of the chromium sites.

(122) Barzan, C.; Bordiga, S.; Groppo, E. Toward The Understanding Of The Comonomer Effect On Crii/Sio2 Phillips Catalyst. *ACS Catal.* **2016**, *6*, 2918−2922.

(123) Barzan, C.; Damin, A. A.; Budnyk, A.; Zecchina, A.; Bordiga, S.; Groppo, E. Pre-Reduction Of The Phillips Crvi/Sio2 Catalyst By Cyclohexene: A Model For The Induction Period Of Ethylene Polymerization. *J. Catal.* **2016**, *337*, 45−51.

(124) Tromp, M.; Moulin, J. O.; Reid, G.; Evans, J. Cr K-Edge XANES Spectroscopy: Ligand And Oxidation State Dependence - What Is Oxidation State? *AIP Conf. Proc.* **2006**, *882*, 699−701.

(125) Note that the XANES spectra are always normalized to the edge jump. The normalization procedure accounts for the dilution of the chromium absorbing centers due to the formation of the polymer.

(126) Cr(II) has been detected by Scott and co-workers using EPR operating at 106 Ghz.[78]

(127) The temperature of 150 °C is slightly higher with respect to that used in industrial conditions. This correction was necessary to compensate for the low ethylene pressure employed in our experimental conditions.

(128) Morra, E.; Martino, G. A.; Piovano, A.; Barzan, C.; Groppo, E.; Chiesa, M. In Situ X- And Q-Band EPR Investigation Of Ethylene Polymerization On Cr/SiO2 Phillips Catalyst. *J. Phys. Chem. C* **2018**, *122*, 21531.

(129) This is the most correct way to show UV−vis spectra, because wavenumbers are directly proportional to the energy of the electronic transition.

(130) Gierada, M.; Handzlik, J. Active Sites Formation And Their Transformations During Ethylene Polymerization By The Phillips Crox/Sio2 Catalyst. *J. Catal.* **2017**, *352*, 314−328.

(131) Gierada, M.; Handzlik, J. Computational Insights Into Reduction Of The Phillips Crox/Sio2 catalyst By Ethylene And CO. *J. Catal.* **2018**, *359*, 261−271.

(132) Schumacher, C.; Gonzalez, J.; Wright, P. A.; Seaton, N. A. Generation Of Atomistic Models Of Periodic Mesoporous Silica By Kinetic Monte Carlo Simulation Of The Synthesis Of The Material. *J. Phys. Chem. B* **2006**, *110*, 319−333.

(133) Ugliengo, P.; Sodupe, M.; Musso, F.; Bush, I. J.; Orlando, R.; Dovesi, R. Realistic Models Of Hydroxylated Amorphous Silica Surfaces And MCM-41 Mesoporous Material Simulated By Large-Scale Periodic B3LYP Calculations. *Adv. Mater.* **2008**, *20*, 4579−4583.

(134) Tielens, F.; Gervais, C.; Lambert, J. F.; Mauri, F.; Costa, D. Ab Initio Study Of The Hydroxylated Surface Of Amorphous Silica: A Representative Model. *Chem. Mater.* **2008**, *20*, 3336−3344.

(135) Ewing, C. S.; Bhavsar, S.; Veser, G.; Mccarthy, J. J.; Johnson, J. K. Accurate Amorphous Silica Surface Models From First-Principles Thermodynamics Of Surface Dehydroxylation. *Langmuir* **2014**, *30*, 5133−5141.

(136) Espelid, O.; Borve, K. J. Theoretical Models Of Ethylene Polymerization Over A Mononuclear Chromium(II)/Silica Site. *J. Catal.* **2000**, *195*, 125−139.

(137) Espelid, O. Theoretical Models Of Active Sites At Cr/Silica Phillips-Type Catalysts For Ethylene Polymerization. Ph.D. Thesis, 2001.

(138) Espelid, O.; Borve, K. J. Molecular-Level Insight Into Cr/Silica Phillips-Type Catalysts: Polymerization-Active Dinuclear Chromium Sites. *J. Catal.* **2002**, *206*, 331−338.

(139) Espelid, O.; Borve, K. J. Molecular-Level Insight Into Cr/Silica Phillips-Type Catalysts: Polymerization-Active Mononuclear Chromium Sites. *J. Catal.* **2002**, *205*, 366−374.

(140) Damin, A.; Vitillo, J. G.; Ricchiardi, G.; Bordiga, S.; Lamberti, C.; Groppo, E.; Zecchina, A. Modeling CO And N2 Adsorption At Cr Surface Species Of Phillips Catalyst By Hybrid Density Functionals: Effect Of Hartree-Fock Exchange Percentage. *J. Phys. Chem. A* **2009**, *113*, 14261−14269.

(141) Liu, Z.; Cheng, R.; He, X.; Wu, X.; Liu, B. DFT Functional Benchmarking On The Energy Splitting Of Chromium Spin States

And Mechanistic Study Of Acetylene Cyclotrimerization Over The Phillips Cr(II)/Silica Catalyst. *J. Phys. Chem. A* **2012**, *116*, 7538−7549.

(142) Guesmi, H.; Tielens, F. Chromium Oxide Species Supported On Silica: A Representative Periodic DFT Model. *J. Phys. Chem. C* **2012**, *116*, 994−1001.

(143) Handzlik, J.; Grybos, R.; Tielens, F. Structure Of Monomeric Chromium(VI) Oxide Species Supported On Silica: Periodic And Cluster DFT Studies. *J. Phys. Chem. C* **2013**, *117*, 8138−8149.

(144) Gierada, M.; Michorczyk, P.; Tielens, F.; Handzlik, J. Reduction Of Chromia-Silica Catalysts: A Molecular Picture. *J. Catal.* **2016**, *340*, 122−135.

(145) Floryan, L.; Borosy, A. P.; Núñez-Zarur, F.; Comas-Vives, A.; Copéret, C. Strain Effect And Dual Initiation Pathway In Criii/Sio2 Polymerization Catalysts From Amorphous Periodic Models. *J. Catal.* **2017**, *346*, 50−56.

(146) Tonosaki, K.; Taniike, T.; Terano, M. Origin Of Broad Molecular Weight Distribution Of Polyethylene Produced By Phillips-Type Silica-Supported Chromium Catalyst. *J. Mol. Catal. A: Chem.* **2011**, *340*, 33−38.

(147) Jenkins, J. M.; Jones, R. L.; Jones, T. M. Fluidized Bed Reaction Systems. U.S. Patent US 4,543,399, Sept. 24, 1985.

(148) Nenu, C. N.; Weckhuysen, B. M. Single-Site Heterogeneous Cr-Based Catalyst For The Selective Trimerisation Of Ethylene. *Chem. Commun.* **2005**, 1865−1867.

(149) Nenu, C. N.; Van Lingen, J. N.; De Groot, F. M. F.; Koningsberger, D. C.; Weckhuysen, B. M. Controlled Assembly Of A Heterogeneous Single-Site Ethylene Trimerization Catalyst As Probed By X-Ray Absorption Spectroscopy. *Chem. - Eur. J.* **2006**, *12*, 4756−4763.

(150) Nenu, C. N.; Groppo, E.; Lamberti, C.; Beale, A. M.; Visser, T.; Zecchina, A.; Weckhuysen, B. M. Dichloromethane As A Selective Modifying Agent To Create A Family Of Highly Reactive Chromium Polymerization Sites. *Angew. Chem., Int. Ed.* **2007**, *46*, 1465−1468.

(151) Groppo, E.; Damin, A.; Otero Arean, C.; Zecchina, A. Enhancing The Initial Rate Of Polymerisation Of The Reduced Phillips Catalyst By One Order Of Magnitude. *Chem. - Eur. J.* **2011**, *17*, 11110−11114.

(152) Liu, B.; Šindelář, P.; Fang, Y.; Hasebe, K.; Terano, M. Correlation Of Oxidation States Of Surface Chromium Species With Ethylene Polymerization Activity For Phillips Crox/Sio2 Catalysts Modified By Al-Alkyl Cocatalyst. *J. Mol. Catal. A: Chem.* **2005**, *238*, 142−150.

(153) Liu, B.; Fang, Y.; Nakatani, H.; Terano, M. Surface Physico-Chemical State Of CO-Prereduced Phillips Crox/Sio2 Catalyst And Unique Polymerization Behavior In The Presence Of Al-Alkyl Cocatalyst. *Macromol. Symp.* **2004**, *213*, 37−46.

(154) Xia, W.; Tonosaki, K.; Taniike, T.; Terano, M.; Fujitani, T.; Liu, B. P. Copolymerization Of Ethylene And Cyclopentene With The Phillips Crox/Sio2 Catalyst In The Presence Of An Aluminum Alkyl Cocatalyst. *J. Appl. Polym. Sci.* **2009**, *111*, 1869−1877.

(155) Benham, E. A.; McDaniel, M. P.; Bailey, F. W. High Strength Linear, Low Density Polyethylene Polymerization Process. U.S. Patent 4,966,951, Oct. 30, 1990.

(156) Benham, E. A.; McDaniel, M. P.; Mcelvain, R. R.; Schneider, R. O. High-Temperature Slurry Polymerization Of Ethylene. U.S. Patent 5,071,927, Dec. 10, 1991.

(157) Benham, E. A.; McDaniel, M. P.; Bailey, F. W. High Strength Linear, Low Density Ethylene Copolymer. U.S. Patent 5,115,068, May 19, 1992.

(158) Mcdaniel, M. P.; Benham, E. A. Linear, Very Low Density Polyethylene Polymerization Process And Products Thereof. U.S. Patent 5,274,056, Dec. 28, 1993.

(159) Komon, Z. J. A.; Bazan, G. C. *Macromol. Rapid Commun.* **2001**, *22*, 467.

(160) Barzan, C.; Groppo, E.; Quadrelli, E. A.; Monteil, V.; Bordiga, S. Ethylene Polymerization On A Sih4-Modified Phillips Catalyst: Detection Of In Situ Produced A-Olefins By Operando FT-IR Spectroscopy. *Phys. Chem. Chem. Phys.* **2012**, *14*, 2239−2245.

(161) Barzan, C.; Bordiga, S.; Quadrelli, E. A.; Groppo, E. Reactivity Of Hydrosilanes With The Crii/Sio2 Phillips Catalyst: Observation Of Intermediates And Properties Of The Modified Criisites. *Top. Catal.* **2016**, *59*, 1732−1739.

(162) Note that the term "homogeneous" has a double meaning here: (1) ability to form carbonyl complexes having a strong metal p-back-donation contribution and (2) all the sites have relatively uniform structure.

(163) Schwerdtfeger, E.; Buck, R.; Mcdaniel, M. Reduction Of Cr(VI) Polymerization Catalysts By Non-Olefinic Hydrocarbons. *Appl. Catal., A* **2012**, *423−424*, 91−99.

(164) Zecchina, A.; Groppo, E.; Bordiga, S. Selective Catalysis And Nanoscience: An Inseparable Pair. *Chem. - Eur. J.* **2007**, *13*, 2440−2460.

(165) Mcdaniel, M. P. Influence Of Catalyst Porosity On Ethylene Polymerization. *ACS Catal.* **2011**, *1*, 1394−1407.

THE JOURNAL OF
PHYSICAL CHEMISTRY C

Photoinduced Ethylene Polymerization on the Cr^{VI}/SiO$_2$ Phillips Catalyst

Lorenzo Mino,*[ORCID] Caterina Barzan, Giorgia A. Martino, Alessandro Piovano, Giuseppe Spoto, Adriano Zecchina,* and Elena Groppo[ORCID]

Department of Chemistry, NIS Centre and INSTM, University of Torino, via Pietro Giuria 7, Torino, Italy

ABSTRACT: Herein we report on two photoinduced reactions occurring at the surface of the Cr^{VI}/SiO$_2$ Phillips catalyst. The first is the photoreduction of Cr^{VI}/SiO$_2$ in CO at room temperature, that leads to the reduction of a fraction of the Cr^{VI} sites to Cr^{IV}(=O) intermediates and then to Cr^{II}. With respect to the thermal reduction of Cr^{VI}/SiO$_2$ in CO, the relative amount of highly uncoordinated Cr^{II} sites is larger, suggesting that the relaxation of the Cr^{II} sites at the silica surface strongly depends on the temperature at which they are formed. The second is the photoinduced ethylene polymerization on Cr^{VI}/SiO$_2$ at room temperature that is reported here for the first time. We demonstrate that UV−vis light has the potential to trigger the reduction of chromates by ethylene and the successive ethylene polymerization. Diffuse reflectance (DR) UV−vis and FT-IR spectroscopies allowed us to identify the nature of the Cr sites involved in the polymerization (i.e., 6-fold coordinated Cr^{II}) and of the oxidized byproducts remaining in their coordination sphere, which are methylformate and ethylene oxide. While the former was previously observed during the thermally induced ethylene polymerization on Cr^{VI}/SiO$_2$, the latter was never observed.
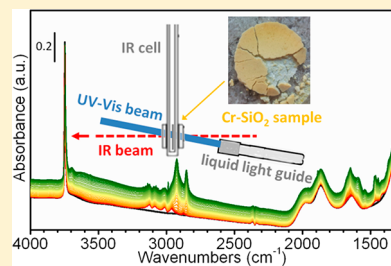
1. INTRODUCTION

Chromium(VI) supported on amorphous silica is one of the most used catalysts in the petrochemical industry, affording more than one-third of all the high-density polyethylene (HDPE) produced worldwide and also a large fraction of linear low-density polyethylene (LLDPE).[1−3] Due to its apparent simplicity, it has been the object of fundamental studies for more than half a century. Since the beginning, most of the efforts have been devoted to correlate the structural and electronic properties of the chromium sites to the peculiar performances of this catalyst in ethylene polymerization,[4−10] such as its ability to polymerize ethylene without any activator or the very broad molecular weight distribution of the produced HDPE. These properties place the Phillips catalyst in a unique position in the polyethylene market when compared to its competitors.[1] Direct spectroscopic methods applied on model versions of the catalyst, such as the CO-reduced form (Cr^{II}/SiO$_2$),[6,8,11−17] or systems obtained from well-defined Cr$^{VI−n}$ organometallic precursors,[18−24] or even planar models suitable for surface science investigation,[25−33] have played the major role in the characterization of the active sites at a molecular level, while the mechanism of ethylene polymerization has been mainly investigated by means of theoretical calculation.[23,34−43]

A crucial feature that distinguishes the Phillips catalyst from most of its competitors in olefin polymerization is its capability to start the polymerization reaction in the absence of any Al-alkyl activator, a fact that simplifies its handling in the polymerization reactor, but also opens some questions on the polymerization mechanism and on the nature of the active sites. The Phillips catalyst enters the polymerization reactor after being activated in oxidizing conditions at a temperature higher than 600 °C. This procedure mainly gives isolated hexavalent chromates[6,8,11,44−48] (hereafter Cr^{VI}), and possibly also a small amount of mono-oxo CrO$_5$,[40,49−54] grafted on the surface of a highly dehydroxylated silica. Hence, the catalyst is not alkylated when it goes into the reactor; that is, it has no Cr−alkyl bond into which ethylene may be inserted. The Cr^{VI} sites are slowly reduced by ethylene at the reaction temperature (ca. 100 °C) during a variable induction time that can also last some hours and are successively transformed into the (alkylated) active sites. Although the two steps (reduction and alkylation) cannot be separated in the industrial reactor, much experimental evidence has been accumulated in academic laboratories indicating that, during the reduction step, the Cr^{VI} sites are reduced to Cr^{II} precursors.[1,4,6,9,10,55−58] For a long time it was considered that the oxidized byproducts derived from ethylene oxidation left the surface of the catalyst at the reaction temperature and that therefore the precursors of the active sites were low-coordinated Cr^{II} species, similar to those obtained by reducing the Cr^{VI}/SiO$_2$ in CO at 350 °C.[59−62] Only recently, this concept has been revolutionized, due to the observation that the oxidized byproducts (ketones, aldehydes, carboxylates, or esters) do not desorb into the gas phase at temperatures below 250 °C, which suggests that under commercial polymerization
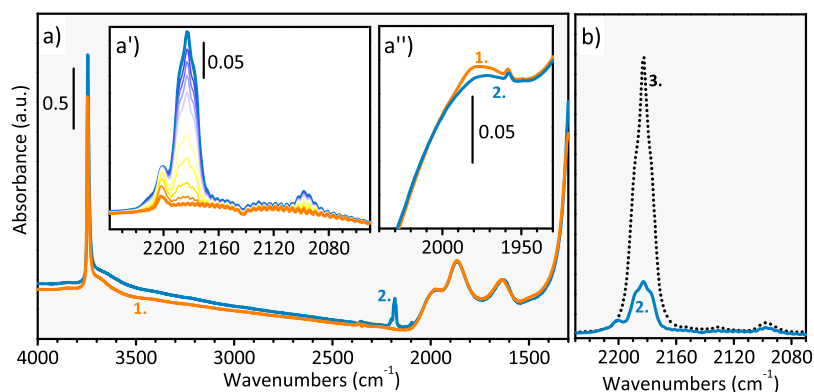
A

Figure 1. (a) FT-IR spectra of Cr^{VI}/SiO_2 before (spectrum 1) and after 60 min of *in situ* UV irradiation in CO (spectrum 2) at room temperature ($P_{CO} = 100$ mbar). Inset a' shows the whole sequence of FT-IR spectra collected at intermediate irradiation time after subtraction of spectrum 1. Inset a" shows a magnification of the spectral region where the only spectroscopic fingerprint of the Cr^{VI} sites appears. (b) The same spectrum 2 as in part a, compared to the FT-IR spectrum, in the $\nu(CO)$ region, of CO adsorbed on a Cr^{II}/SiO_2 sample obtained upon thermal reduction in CO at 350 °C (spectrum 3).

75 conditions oxygenates may remain attached to the chromium
76 sites.[63,64]

77 On the whole, it is clear that the reducing ability of ethylene
78 toward the chromates is quite poor. This is one of the reasons
79 why often, in the industrial practice, specific reducing agents
80 are added in the reactor before or together with the ethylene
81 injection, aimed at shortening (or even eliminating) the
82 induction time, and/or at performing ethylene polymerization
83 at lower temperature.[1,65−69] In this work we explore, for the
84 first time, the use of UV−vis light to trigger the ethylene
85 polymerization on the Cr^{VI}/SiO_2 catalyst at room temperature,
86 without the addition of any activator. The idea had the
87 inception from the documented knowledge that highly
88 dispersed and isolated Cr^{VI} sites in the form of monochromates
89 supported on silica can operate as efficient photocatalysts for a
90 wide range of reactions under visible-light irradiation, such as
91 for the decomposition of NO, for the partial oxidation of
92 propane with molecular oxygen, and for the selective oxidation
93 of CO in the presence of H_2.[70−74] In particular, it has been
94 demonstrated that visible-light irradiation of tetrahedrally
95 coordinated $Cr^{VI}(=O)_2$ species produces the excited triplet
96 state $Cr^{V}(=O)(O^-)^*$, which behaves as an active site for
97 oxidation. Moreover, more than 20 years ago, Kohler and
98 Ekerdt demonstrated the possibility to photoreduce the $Cr^{VI}/$
99 SiO_2 catalyst in CO.[75] These examples prompted us to develop
100 an experimental setup to monitor the Cr^{VI}/SiO_2 catalyst *during*
101 the UV−vis light irradiation in the presence of ethylene at
102 room temperature, by means of FT-IR and diffuse reflectance
103 (DR) UV−vis spectroscopies. By combining these two
104 sensitive methods, we have been able to (1) observe the
105 gradual reduction of the chromates, (2) investigate the
106 properties of the reduced chromium sites, (3) detect the
107 byproducts of ethylene oxidation, and (4) demonstrate the
108 occurrence of ethylene polymerization at room temperature.

2. EXPERIMENTAL SECTION

109 The Cr^{VI}/SiO_2 sample (Cr loading 1 wt %) was prepared by
110 wet-impregnation of a pyrogenic silica (Aerosil, surface area ca.
111 380 m^2g^{-1}) employing CrO_3 as chromium precursor. The
112 catalyst was activated directly inside the measurement cells, to
113 avoid any type of contamination. The activation procedure
114 consisted of two main steps: (i) activation at 650 °C in
115 dynamic vacuum (residual pressure $<10^{-4}$ mbar) in order to

116 dehydroxylate the silica surface and (ii) subsequent oxidation
117 in O_2 (equilibrium pressure ca. 100 mbar, twice) at the same
118 temperature to graft the Cr species in the form of
119 monochromates.[6,8,11,44−46] The Cr^{II}/SiO_2 reference sample
120 was obtained from Cr^{VI}/SiO_2 after further reduction in CO
121 (equilibrium pressure ca. 100 mbar, twice) at 350 °C, followed
122 by degassing at the same temperature.[6] For both FT-IR and
123 DR UV−vis−NIR measurements the sample was prepared in
124 the form of a self-supporting pellet, having a surface density of
125 ca. 10 and 60 mg cm^{-2}, respectively.

126 The FT-IR spectra were recorded on a Bruker IFS 28 FT-IR
127 spectrometer, equipped with a MCT cryogenic detector,
128 averaging 64 interferograms recorded at 2 cm^{-1} resolution.
129 Diffuse reflectance (DR) UV−vis−NIR spectra were recorded
130 on a Cary 5000 Varian spectrophotometer equipped with a
131 reflectance sphere. In both cases, UV−vis irradiation was
132 performed using a Newport 500 W Hg(Xe) arc lamp, equipped
133 with a water filter to eliminate the infrared portion of the
134 spectrum. For *in situ* UV−vis irradiation during the FT-IR
135 experiments, the radiation was focused on the sample using an
136 aspherical fiber bundle focusing assembly and a large core
137 liquid light guide.[76−78] This experimental setup reduces the
138 amount of photons reaching the sample but allows collecting
139 FT-IR spectra during continuous UV−vis irradiation. In
140 contrast, for UV−vis irradiation during the DR UV−vis−
141 NIR experiments, the radiation was not focused. This
142 experimental setup maximizes the number of photons reaching
143 the sample but does not allow collecting DR UV−vis−NIR
144 spectra simultaneously with the irradiation.

3. RESULTS AND DISCUSSION

145 **3.1. Photoreduction of Cr^{VI}/SiO_2 in CO at Room**
146 **Temperature.** Initially, we followed by *in situ* FT-IR
147 spectroscopy the photoreduction of Cr^{VI}/SiO_2 under UV−vis
148 irradiation in the presence of CO ($P_{CO} = 100$ mbar) at room
149 temperature, aimed at validating our experimental setup.
150 Figure 1a shows the FT-IR spectrum of Cr^{VI}/SiO_2 before
151 (spectrum 1) and after (spectrum 2) 60 min of irradiation in
152 CO, while Figure 1a' shows all the spectra collected at
153 intermediate irradiation time, in the $\nu(CO)$ region and after
154 subtraction of spectrum 1. The spectrum of Cr^{VI}/SiO_2 is
155 characterized by a narrow band at 3745 cm^{-1} ascribed to the
156 $\nu(OH)$ vibration of isolated silanols, and three broad bands at

ca. 1980, 1870, and 1635 cm^{-1} which are due to the overtones and combinations of the fundamental vibrational modes of silica, contributing below 1300 cm^{-1}. The only spectroscopic manifestation of the Cr^{VI} sites is a weak absorption band at 1980 cm^{-1} (Figure 1a″), assigned to the first overtone of the $\nu(Cr\!=\!O)$ modes,[8,47,48,63,79,80] which are obscured in the IR by the intense absorption due to the silica framework vibrations, but were detected at 982−990 cm^{-1} by Raman spectroscopy.[5,12,49,81−85]

During UV−vis irradiation in CO a series of bands slowly appear in the $\nu(CO)$ region (Figure 1a′), concurrently with the disappearance of the band at 1980 cm^{-1} (Figure 1a″), which indicates the slow reduction of the Cr^{VI} sites and the formation of Cr-carbonyls on the reduced Cr sites. The first band to appear is centered at 2201 cm^{-1} and reaches the maximum intensity after about 10 min of irradiation. A similar absorption band was previously observed by Kohler and Ekerdt during the photoreduction of a 2 wt % Cr^{VI}/SiO$_2$ in CO,[75] and by some of us upon adsorption of CO on a Cr^{II}/SiO$_2$ sample selectively modified by N$_2$O.[79] In both cases it was ascribed to monocarbonyl species formed on Cr$^{IV}\!=\!O$ (chromyl) sites. After a few minutes of UV−vis irradiation, a triplet of bands at 2189, 2183, and 2177 cm^{-1} also starts growing, which is known to arise from the vibrational modes of monocarbonyls and dicarbonyls (symmetric and asymmetric modes) formed on two types of coordinatively unsaturated Cr^{II} sites (Cr$^{II}_B$ and Cr$^{II}_A$, respectively).[6−8,58] A weak band is also visible at 2096 cm^{-1}, and assigned to multicarbonyls formed on a small fraction of even more uncoordinated Cr^{II} sites.[6,8,86]

The experiment reported in Figure 1a demonstrates that when Cr^{VI}/SiO$_2$ is irradiated by UV−vis light in the presence of CO at room temperature, the Cr^{VI} sites are gradually reduced, initially to Cr^{IV} and successively to Cr^{II}, in good agreement with the pioneering work of Kohler and Ekerdt.[75] The photoreduction in CO is less efficient than the thermal reduction in CO at 350 °C. This is evident by looking at Figure 1b, that compares the FT-IR spectrum of Cr^{VI}/SiO$_2$ photoreduced in the presence of CO (spectrum 2), to that of CO adsorbed at room temperature on a Cr^{II}/SiO$_2$ sample (i.e., obtained upon thermal reduction of Cr^{VI}/SiO$_2$ in CO at 350 °C, spectrum 3). The spectra have been normalized to the optical thickness of the pellets; hence, their total intensity can be quantitatively compared. Spectrum 2 is ca. 4 times less intense than spectrum 3. Since it has been demonstrated that the thermal reduction of Cr^{VI}/SiO$_2$ in CO at 350 °C leads to the stoichiometric conversion of all the Cr^{VI} sites to Cr^{II},[1] Figure 1b indicates that only ca. 1/4 of the total Cr^{VI} sites are reduced after 60 min of UV−vis irradiation in the presence of CO, partially to Cr^{IV} and partially to Cr^{II}.

The observation that the intensity of the weak band at 2096 cm^{-1} with respect to the triplet centered at 2180 cm^{-1} is higher for spectrum 2 than for spectrum 3 is also of interest. This means that the relative amount of highly uncoordinated Cr^{II} sites capable of forming multicarbonyls in the presence of CO at room temperature is much higher when the Cr^{II} sites are obtained by photoreduction of Cr^{VI}. This is probably a consequence of a different strain at the silica surface.[87] When the reduction of Cr^{VI}/SiO$_2$ is accomplished at high temperature (350 °C), the obtained Cr^{II} sites have the possibility to relax. Reduction of Cr^{VI}/SiO$_2$ in milder conditions does not permit the relaxation of the Cr^{II} sites, that remain more accessible to the incoming molecules. This might have important consequences in terms of catalytic performances.

Indeed, it has been recently demonstrated that the Cr coordination environment influences both the ethylene insertion and the chain transfer energies, with immediate consequences on the molecular weight distribution of the obtained polyethylene.[43,88]

3.2. Photoinduced Ethylene Polymerization on Cr^{VI}/SiO$_2$.

Also, ethylene (i.e., the monomer of the polymerization reaction) may act as reducing agent for Cr^{VI}/SiO$_2$. However, as for CO, the reaction does not occur at room temperature but needs ca. 100 °C, and also at that temperature it requires a certain induction time that can vary from minutes to hours, depending on the experimental conditions.[1] Ethylene polymerization starts on these reduced Cr sites, and the steady state is reached only after several hours. Inspired by the results discussed above for the photoinduced CO-reduction of Cr^{VI}/SiO$_2$, we decided to investigate whether UV−vis light irradiation can be exploited for performing ethylene polymerization on Cr^{VI}/SiO$_2$ at room temperature. The experiments were performed in static conditions, at room temperature and low ethylene pressure (P_{C2H4} = 100 mbar), and were followed by means of both DR UV−vis−NIR and FT-IR spectroscopies.

Figure 2 shows the DR UV−vis−NIR spectra of the Cr^{VI}/SiO$_2$ sample before (spectrum 0) and after (spectra 1−6) UV−
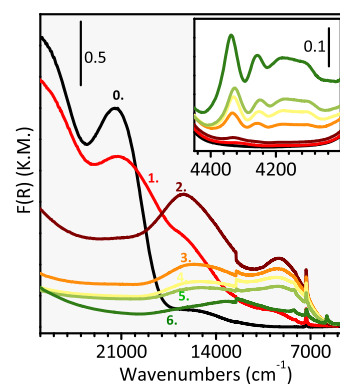
Figure 2. DR UV−vis spectra of Cr^{VI}/SiO$_2$ before (spectrum 0, black) and after UV irradiation in the presence of ethylene (P_{C2H4} = 100 mbar) at room temperature for increasing times (1 = 20 s, 2 = 40 s, 3 = 50 s, 4 = 1 min, 5 = 2 min, 6 = 5 min). The inset shows a magnification of the NIR region, where polyethylene contributes with a series of bands due to the overtones and combinations of the $\nu(CH_2)$ and $\delta(CH_2)$ vibrational modes.

vis irradiation in the presence of ethylene at room temperature for increasing times. The spectrum of Cr^{VI}/SiO$_2$ (spectrum 0) is dominated by two intense bands at ca. 28 000 and 21 500 cm^{-1}, due to the O → Cr^{VI} charge-transfer transitions characteristic of monochromates.[5,8,11,44,45] The spectra rapidly change upon UV−vis irradiation in the presence of ethylene, and two subsequent events can be distinguished. After less than 50 s of irradiation (spectra 1 and 2), the spectroscopic fingerprints of the monochromates decrease in intensity, concurrently with the appearance of two bands at ca. 16 500 and 9500 cm^{-1}, which indicate the reduction of the Cr^{VI} sites (d^0 species) to low-valent Cr sites (d^n species). The same bands were observed during the thermal reduction of Cr^{VI}/SiO$_2$ in ethylene, and ascribed to d−d transitions of Cr^{II} sites having a 6-fold coordination geometry, determined by the presence of oxidized byproducts in their coordination sphere.[63] The assignment was corroborated by the observation of very similar spectra for Cr^{VI}/SiO$_2$ reduced by cyclohexene, a cyclic

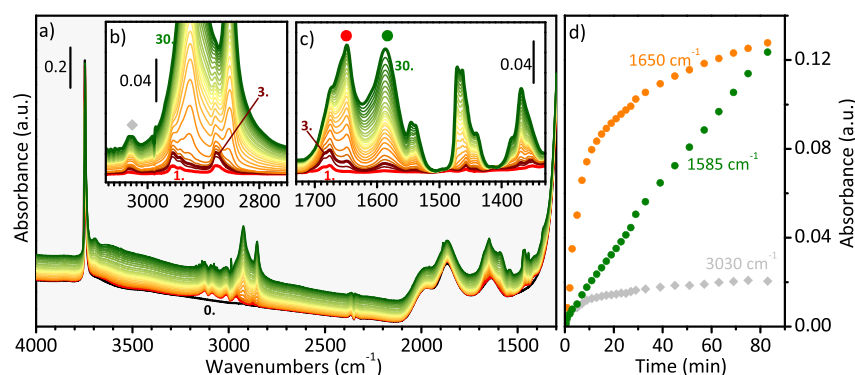**Figure 3.** (a) FT-IR spectra of Cr^{VI}/SiO_2 (spectrum 0, black) and of the same sample during continuous UV irradiation in the presence of ethylene (P_{C2H4} = 100 mbar) at room temperature for increasing times (1 = 30 s, 3 = 1 min, 30 = 90 min). (b) Magnification of the same spectra reported in part a, after subtraction of spectrum 0 and of the contribution due to gaseous ethylene, in the $\nu(CH_x)$ region. (c) Same as part b in the 1730−1330 cm^{-1} region. (d) Time evolution of the intensity of the absorption bands at 3030 cm^{-1} (ethylene oxide), 1650 cm^{-1} (methylformate ligated through the C=O moiety), and 1585 cm^{-1} (methylformate ligated in a bidentate fashion).
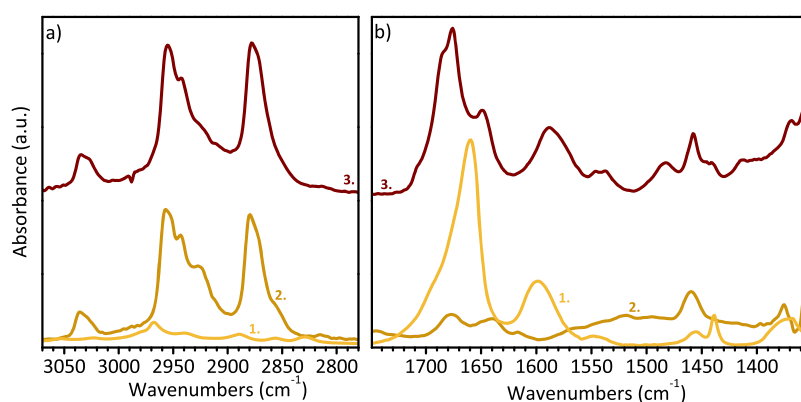

Figure 4. FT-IR spectra of methylformate adsorbed on Cr^{II}/SiO_2 (spectrum 1), the product of reacting a limited amount of O_2 on a Cr^{II}/SiO_2 catalyst at the very beginning of the ethylene polymerization, previously ascribed to ethylene oxide on Cr^{II}/SiO_2 (spectrum 2), compared to the spectrum collected after 1 min of UV−vis irradiation of Cr^{VI}/SiO_2 in the presence of ethylene (spectrum 3, the same as in Figure 3). Parts a and b show the $\nu(CH_x)$ and $\nu(C=O)$ regions, respectively.

olefin that mimics the reactivity of ethylene without polymerizing.[69] During this step no ethylene polymerization occurs, as demonstrated by the absence of any absorption bands in the 4400−4050 cm^{-1} range (inset in Figure 2), which is where polyethylene contributes to a series of bands due to the overtones and combinations of the $\nu(CH_2)$ and $\delta(CH_2)$ vibrational modes. Ethylene polymerization is observed after only 50 s of UV−vis irradiation (spectrum 3), and efficiently proceeds for a longer irradiation time. The global effect is the decrease in intensity of the d−d bands at 16 500 and 9500 cm^{-1}, and in general of the whole spectrum. The same phenomenon was observed during the thermally induced ethylene polymerization on Cr^{VI}/SiO_2 and explained in terms of formation of a layer of polymer on the surface of the catalyst particles, which diffuses the incident light preventing the observation of the active Cr sites.[63]

The DR UV−vis−NIR experiment discussed above clearly indicates that ethylene has the potential to reduce the Cr^{VI} sites at room temperature under UV−vis irradiation and is then polymerized in mild conditions. Figure 3a shows the complementary experiment performed by FT-IR spectroscopy, aimed at monitoring the formation of polyethylene and of the oxidized byproducts to identify their nature. The FT-IR spectrum of Cr^{VI}/SiO_2 before reaction with ethylene (Figure 3, spectrum 0) has been discussed above. During the first minute

of UV−vis irradiation, a series of well-defined IR absorption bands appear in the $\nu(CH_x)$ stretching region (Figure 3b, spectra 1−3) and in the 1750−1300 cm^{-1} range (Figure 3c, spectra 1−3). In particular, the most evident bands are observed at ca. 3030, 2955, and 2877 cm^{-1} (Figure 3b) and at 1677, 1650, and 1585 cm^{-1} (Figure 3c). These bands are clearly not attributable to polyethylene and reveal the formation of surface byproducts resulting from the oxidation of ethylene by monochromates. According to the UV−vis−NIR spectra (Figure 2) these byproducts remain in the coordination sphere of the reduced Cr^{II} sites. The onset of ethylene polymerization occurs after ca. 2 min of continuous UV−vis irradiation in the presence of ethylene, as testified by the constant growth of two bands at 2922 and 2853 cm^{-1} (Figure 3b, spectra 4−30), which are due to the $\nu_{asymm}(CH_2)$ and $\nu_{symm}(CH_2)$ modes of polyethylene, and of the corresponding $\delta(CH_2)$ band at ca. 1470 cm^{-1} (Figure 3c, spectra 4−30).

A closer inspection of the spectra collected prior the onset of ethylene polymerization (spectra 1−3) might give an indication of the nature of the byproducts, and hence of the mechanism of initiation of ethylene polymerization under UV−vis irradiation. In this respect, it is useful to recall here that methylformate (formed through the Tischenko reaction of two formaldehyde molecules at the same Cr^{II} site) has been

identified as the main byproduct of ethylene oxidation during the thermally induced ethylene polymerization on Cr^{VI}/SiO_2.[63] For this reason, in Figure 4 we have compared the spectrum collected after 1 min of UV–vis irradiation of Cr^{VI}/SiO_2 in the presence of ethylene (spectrum 3, the same as in Figure 3) with two reference spectra collected with independent experiments. Spectrum 1 corresponds to methylformate adsorbed on Cr^{II}/SiO_2 (after removal of the physisorbed molecules). The spectrum is characterized by very weak bands in the $\nu(CH_x)$ region (Figure 4a), whereas it is dominated by two intense bands at ca. 1660 cm^{-1} (with a pronounced tail at high wavenumbers) and 1597 cm^{-1} (Figure 4b). On the basis of the literature of methylformate adsorbed on other systems,[89,90] both bands are assigned to the $\nu(C=O)$ vibration of methylformate adsorbed on Cr^{II} sites differing in their adsorption geometry: the former is ascribed to methylformate ligated through the $C=O$ moiety, whereas the latter is due to methylformate ligated in a bidentate fashion. The similarity of spectrum 3 to spectrum 1 in this spectral region suggests that also in this case methylformate is one of the byproducts of chromate reduction. As already discussed for the thermally induced ethylene polymerization, methylformate originates from the disproportion of two formaldehyde molecules formed at the same Cr site.[63] On the other hand, spectrum 2 was obtained by dosing a limited amount of O_2 on a Cr^{II}/SiO_2 catalyst at the very beginning of the ethylene polymerization. This spectrum, which is characterized by quite intense absorption bands in the 3050–2800 cm^{-1} region (Figure 4a) but shows negligible features at lower wavenumbers (Figure 4b), was assigned to ethylene oxide adsorbed on partially oxidized $Cr^{IV}(=O)/SiO_2$.[91] The close similarity of spectrum 1 to spectrum 3 in the $\nu(CH_x)$ region indicates that a second reaction is taking place during the UV–vis irradiation of Cr^{VI}/SiO_2 in ethylene, involving the formation of ethylene oxide.

In summary, the FT-IR data shown in Figures 3 and 4 indicate the formation of two different oxidized byproducts during the initial steps of photoinduced ethylene polymerization on Cr^{VI}/SiO_2 at room temperature: ethylene oxide and methylformate. Interestingly, the absorption bands associated with methylformate keep on growing also during ethylene polymerization (Figure 3d, orange and green circles), although with a different relative intensity. In particular, the band at ca. 1585 cm^{-1} (green circles) grows faster than that at ca. 1650 cm^{-1} (orange circles) and becomes the dominant one at longer irradiation/reaction time. This behavior suggests a slow conversion of the methylformate species ligated to the Cr^{II} sites through the $C=O$ moiety into the most stable bidentate species. In contrast, the absorption bands associated with ethylene oxide apparently do not increase in intensity during ethylene polymerization. This is evident by looking to the band at ca. 3030 cm^{-1} (Figure 3d, gray diamond), which does not overlap with any bands due to the growing polyethylene. As a final comment, the evolution of the FT-IR spectra reported in Figure 3 clearly indicates that (1) ethylene polymerization is photoinitiated on Cr^{VI}/SiO_2 in the presence of a substantial amount of Cr^{VI} sites which are slower to be reduced, as already reported for the thermally induced ethylene polymerization,[63] and (2) ethylene polymerization starts and proceeds in the presence of both types of oxidized byproducts, that evidently remain adsorbed at the catalyst surface during the initiation of the reaction, contributing to define the ligands sphere around the active Cr sites.

4. CONCLUSIONS

In this work we have presented two examples of photoinduced reactions on the Cr^{VI}/SiO_2 Phillips catalyst. At first, we found that irradiation of Cr^{VI}/SiO_2 with UV–vis light in the presence of CO leads to its partial reduction already at room temperature, first to a $Cr^{IV}(=O)$ intermediate, and then further to Cr^{II}, in good agreement with the pioneering work of Kohler and Ekerdt.[75] Although the photoreduction is less efficient than the thermal one (i.e., a lower fraction of Cr^{VI} sites is reduced), notably it brings about the formation of a larger amount of highly uncoordinated Cr^{II} sites able to form multicarbonyls in the presence of CO. This finding highlights the role of the strain at the silica surface in affecting the properties of the Cr sites and might have important consequences in terms of catalytic performances.

Second, we demonstrated the novel observation that UV–vis light efficiently triggers the ethylene polymerization on the Cr^{VI}/SiO_2 catalyst already at room temperature. By means of DR UV–vis–NIR and FT-IR spectroscopies, we have been able to discriminate between the two fundamental steps involved in the initiation of the reaction, namely, the Cr^{VI} reduction by ethylene and the successive polymerization. With respect to the thermally induced ethylene polymerization, the induction time is drastically reduced. Moreover, two types of oxidized byproducts derived from the oxidation of ethylene by chromates have been detected: methylformate and ethylene oxide. While the former was found also during the thermally induced ethylene polymerization, the latter was never observed. The reason might be due to the specific photo-activation mechanism for Cr^{VI} that, according to the literature, involves a single oxygen per time passing through the formation of a $Cr^{V}(=O)(O^-)^*$ excited state. Alternatively, we might consider the possibility that ethylene oxide is formed also during the thermally induced ethylene polymerization but not detected because it desorbs from the Cr sites at the reaction temperature. This different polymerization mechanism with respect to the thermally induced process could also result in a polymer with peculiar characteristics. However, the limited amount of polyethylene produced in our setup prevented at the moment a more thorough *ex situ* characterization of the products by differential scanning calorimetry or size exclusion chromatography, which will be the object of a future study.

■ AUTHOR INFORMATION

Corresponding Authors
*E-mail: lorenzo.mino@unito.it.
*E-mail: adriano.zecchina@unito.it.

ORCID ⊙

Lorenzo Mino: 0000-0002-9882-8361
Elena Groppo: 0000-0003-4153-5709

Notes

The authors declare no competing financial interest.

■ REFERENCES

(1) McDaniel, M. P. A Review of the Phillips Supported Chromium Catalyst and Its Commercial Use for Ethylene Polymerization. *Adv. Catal.* **2010**, 53, 123–606.
(2) McDaniel, M. P. Organic Reactions. In *Handbook of Heterogeneous Catalysis*; Ertl, G., Knözinger, H., Weitkamp, J., Eds.; VHC: Weinheim, 1997; Vol. 5, p 2400.

(3) Nowlin, T. E. *Business and Technology of the Global Polyethylene Industry*; Scrivener Publishing LLC: New York, 2014.

(4) McDaniel, M. P. Supported Chromium Catalysts for Ethylene Polymerization. *Adv. Catal.* **1985**, *33*, 47−98.

(5) Weckhuysen, B. M.; Wachs, I. E.; Schoonheydt, R. A. Surface Chemistry and Spectroscopy of Chromium in Inorganic Oxides. *Chem. Rev.* **1996**, *96*, 3327−3350.

(6) Groppo, E.; Lamberti, C.; Bordiga, S.; Spoto, G.; Zecchina, A. The Structure of Active Centers and the Ethylene Polymerization Mechanism on the Cr/SiO₂ Catalyst: A Frontier for the Characterization Methods. *Chem. Rev.* **2005**, *105*, 115−183.

(7) Zecchina, A.; Groppo, E. Surface Chromium Single Sites: Open Problems and Recent Advances. *Proc. R. Soc. London, Ser. A* **2012**, *468*, 2087−2098.

(8) Groppo, E.; Seenivasan, K.; Barzan, C. The Potential of Spectroscopic Methods Applied to Heterogeneous Catalysts for Olefin Ppolymerization. *Catal. Sci. Technol.* **2013**, *3*, 858−878.

(9) Cheng, R.; Liu, Z.; Zhong, L.; He, X.; Qiu, P.; Terano, M.; Eisen, M. S.; Scott, S. L.; Liu, B. Phillips Cr/Silica Catalyst for Ethylene Polymerization. *Adv. Polym. Sci.* **2013**, *257*, 135−202.

(10) Liu, Z.; He, X.; Cheng, R.; Eisen, M. S.; Terano, M.; Scott, S. L.; Liu, B. Chromium Catalysts for Ethylene Polymerization and Oligomerization. *Adv. Chem. Eng.* **2014**, *44*, 127−191.

(11) Weckhuysen, B. M.; Schoonheydt, R. A.; Jehng, J. M.; Wachs, I. E.; Cho, S. J.; Ryoo, R.; Kijlstra, S.; Poels, E. Combined DRS-RS-EXAFS-XANES-TPR Study of Supported Chromium Catalysts. *J. Chem. Soc., Faraday Trans.* **1995**, *91*, 3245−3253.

(12) Groppo, E.; Damin, A.; Bonino, F.; Zecchina, A.; Bordiga, S.; Lamberti, C. New Strategies in the Raman Study of the Cr/SiO₂ Phillips Catalyst: Observation of Molecular Adducts on Cr(II) Sites. *Chem. Mater.* **2005**, *17*, 2019−2027.

(13) Groppo, E.; Lamberti, C.; Bordiga, S.; Spoto, G.; Zecchina, A.; Damin, A. FTIR Investigation of the H₂, N₂ and C₂H₄ Molecular Complexes Formed on the Cr(II) Sites in the Phillips Catalyst: a Preliminary Step in the Understanding of a Complex System. *J. Phys. Chem. B* **2005**, *109*, 15024−15031.

(14) Groppo, E.; Lamberti, C.; Spoto, G.; Bordiga, S.; Magnacca, G.; Zecchina, A. Tuning the Structure, Distribution and Reactivity of Polymerization Centres of Cr(II)/SiO₂ Phillips Catalyst by Controlled Annealing. *J. Catal.* **2005**, *236*, 233−244.

(15) Zhong, L.; Lee, M.-Y.; Liu, Z.; Wanglee, Y.-J.; Liu, B.; Scott, S. L. Spectroscopic and Structural Characterization of Cr(II)/SiO₂ Active Site Precursors in Model Phillips Polymerization Catalysts. *J. Catal.* **2012**, *293*, 1−12.

(16) Brown, C.; Krzystek, J.; Achey, R.; Lita, A.; Fu, R.; Meulenberg, R. W.; Polinski, M.; Peek, N.; Wang, Y.; Van De Burgt, L. J.; et al. Mechanism of Initiation in the Phillips Ethylene Polymerization Catalyst: Redox Processes Leading to the Active Site. *ACS Catal.* **2015**, *5*, 5574−5583.

(17) Brown, C.; Lita, A.; Tao, Y.; Peek, N.; Crosswhite, M.; Mileham, M.; Krzystek, J.; Achey, R.; Fu, R.; Bindra, J. K.; et al. Mechanism of Initiation in the Phillips Ethylene Polymerization Catalyst: Ethylene Activation by Cr(II) and the Structure of the Resulting Active Site. *ACS Catal.* **2017**, *7*, 7442−7455.

(18) Amor Nait Ajjou, J.; Scott, S. L. Reactions of Tetraalkylchromium(IV) with Silica: Mechanism of Grafting and Characterization of Surface Organometallic Complexes. *Organometallics* **1997**, *16*, 86−92.

(19) Amor Nait Ajjou, J.; Scott, S. L. A Kinetic Study of Ethylene and 1-Hexene Homo- and Copolymerization Catalyzed by a Silica-Supported Cr(IV) Complex: Evidence for Propagation by a Migratory Insertion Mechanism. *J. Am. Chem. Soc.* **2000**, *122*, 8968−8976.

(20) Amor Nait Ajjou, J.; Scott, S. L.; Paquet, V. Synthesis and Characterization of Silica-Stabilized Chromium(IV) Alkylidene Complexes. *J. Am. Chem. Soc.* **1998**, *120*, 415−416.

(21) Delley, M. F.; Núñez-Zarur, F.; Conley, M. P.; Comas-Vives, A.; Siddiqi, G.; Norsic, S.; Monteil, V.; Safonova, O. V.; Copéret, C. Proton Transfers Are Key Elementary Steps in Ethylene Polymerization on Isolated Chromium(III) Silicates. *Proc. Natl. Acad. Sci. U. S. A.* **2014**, *111*, 11624−11629.

(22) Conley, M. P.; Delley, M. F.; Siddiqi, G.; Lapadula, G.; Norsic, S.; Monteil, V.; Safonova, O. V.; Copéret, C. Polymerization of Ethylene by Silica-Supported Dinuclear CrIII Sites Through an Initiation Step Involving C = H Bond Activation. *Angew. Chem., Int. Ed.* **2014**, *53*, 1872−1876.

(23) Conley, M. P.; Delley, M. F.; Núñez-Zarur, F.; Comas-Vives, A.; Copéret, C. Heterolytic Activation of C-H Bonds on CrIII-O Surface Sites Is a Key Step in Catalytic Polymerization of Ethylene and Dehydrogenation of Propane. *Inorg. Chem.* **2015**, *54*, 5065−5078.

(24) Delley, M. F.; Praveen, C. S.; Borosy, A. P.; Núñez-Zarur, F.; Comas-Vives, A.; Copéret, C. Olefin Polymerization on Cr(III)/SiO₂: Mechanistic Insights from the Differences in Reactivity Between Ethene and Propene. *J. Catal.* **2017**, *354*, 223−230.

(25) Thune, P. C.; Verhagen, C. P. J.; van den Boer, M. J. G.; Niemantsverdriet, J. W. Working Surface Science Model for the Phillips Ethylene Polymerization Catalyst: Preparation and Testing. *J. Phys. Chem. B* **1997**, *101*, 8559−8563.

(26) Thune, P. C.; Loos, J.; Lemstra, P. J.; Niemantsverdriet, J. W. Polyethylene Formation on a Planar Surface Science Model of a Chromium Oxide Polymerization Catalyst. *J. Catal.* **1999**, *183*, 1−5.

(27) Thune, P. C.; Loos, J.; de Jong, A. M.; Lemstra, P. J.; Niemantsverdriet, J. W. Planar Model System for Olefin Polymerization: the Phillips CrOₓ/SiO₂ Catalyst. *Top. Catal.* **2000**, *13*, 67−74.

(28) Thune, P. C.; Linke, R.; van Gennip, W. J. H.; de Jong, A. M.; Niemantsverdriet, J. W. Bonding of Supported Chromium During Thermal Activation of the CrOₓ/SiO₂ (Phillips) Ethylene Polymerization Catalyst. *J. Phys. Chem. B* **2001**, *105*, 3073−3078.

(29) Thune, P. C.; Loos, J.; Wouters, D.; Lemstra, P. J.; Niemantsverdriet, J. W. The CrOₓ/SiO₂/Si(100) catalyst - A surface science approach to supported olefin polymerization catalysis. *Macromol. Symp.* **2001**, *173*, 37−52.

(30) Thune, P. C.; Loos, J.; Chen, X. H.; van Kimmenade, E. M. E.; Kong, B.; Niemantsverdriet, J. W. H. Visualization of Local Ethylene Polymerization Activity on a Flat CrOx/SiO₂/Si(100) Model Catalyst. *Top. Catal.* **2007**, *46*, 239−245.

(31) van Kimmenade, E. M. E.; Kuiper, A. E. T.; Tamminga, Y.; Thune, P. C.; Niemantsverdriet, J. W. A Surface Science Model for the Phillips Ethylene Polymerization Catalyst: Thermal Activation and Polymerization Activity. *J. Catal.* **2004**, *223*, 134−141.

(32) van Kimmenade, E. M. E.; Loos, J.; Niemantsverdriet, J. W.; Thune, P. C. The Effect of Temperature on Ethylene Polymerization over Flat Phillips Model Catalysts. *J. Catal.* **2006**, *240*, 39−46.

(33) Pan, Q.; Li, L.; Shaikhutdinov, S.; Freund, H. J. Planar Model System of the Phillips (Cr/SiO₂) Catalyst Based on a Well-Defined Thin Silicate Film. *J. Catal.* **2018**, *357*, 12−19.

(34) Fong, A.; Yuan, Y.; Ivry, S. L.; Scott, S. L.; Peters, B. Computational Kinetic Discrimination of Ethylene Polymerization Mechanisms for the Phillips (Cr/SiO₂) Catalyst. *ACS Catal.* **2015**, *5*, 3360−3374.

(35) Fong, A.; Peters, B.; Scott, S. L. One-Electron-Redox Activation of the Reduced Phillips Polymerization Catalyst, via Alkylchromium-(IV) Homolysis: A Computational Assessment. *ACS Catal.* **2016**, *6*, 6073−6085.

(36) Fong, A.; Vandervelden, C.; Scott, S. L.; Peters, B. Computational Support for Phillips Catalyst Initiation via Cr-C Bond Homolysis in a Chromacyclopentane Site. *ACS Catal.* **2018**, *8*, 1728−1733.

(37) Gierada, M.; Handzlik, J. Active Sites Formation and Their Transformations During Ethylene Polymerization by the Phillips CrOx/SiO₂ Catalyst. *J. Catal.* **2017**, *352*, 314−328.

(38) Gierada, M.; Handzlik, J. Computational Insights into Reduction of the Phillips CrOₓ/SiO₂ Catalyst by Ethylene and CO. *J. Catal.* **2018**, *359*, 261−271.

(39) Chakrabarti, A.; Gierada, M.; Handzlik, J.; Wachs, I. E. Operando Molecular Spectroscopy During Ethylene Polymerization by Supported CrOₓ/SiO₂ Catalysts: Active Sites, Reaction Inter-

mediates, and Structure-Activity Relationship. *Top. Catal.* **2016**, *59*, 725−739.

(40) Gao, J.; Zheng, Y.; Tang, Y.; Jehng, J. M.; Grybos, R.; Handzlik, J.; Wachs, I. E.; Podkolzin, S. G. Spectroscopic and Computational Study of Cr Oxide tructures and Their Anchoring Sites on ZSM-5 Zeolites. *ACS Catal.* **2015**, *5*, 3078−3092.

(41) Handzlik, J.; Grybos, R.; Tielens, F. Structure of Monomeric Chromium(VI) Oxide Species Supported on Silica: Periodic and Cluster DFT Studies. *J. Phys. Chem. C* **2013**, *117*, 8138−8149.

(42) Handzlik, J.; Grybos, R.; Tielens, F. Isolated Chromium(VI) Oxide Species Supported on Al-Modified Silica: A Molecular Description. *J. Phys. Chem. C* **2016**, *120*, 17594−17603.

(43) Floryan, L.; Borosy, A. P.; Núñez-Zarur, F.; Comas-Vives, A.; Copéret, C. Strain Effect and Dual Initiation Pathway in CrIII/SiO2 Polymerization Catalysts From Amorphous Periodic Models. *J. Catal.* **2017**, *346*, 50−56.

(44) Weckhuysen, B. M.; Deridder, L. M.; Schoonheydt, R. A. A Quantitative Diffuse Reflectance Spectroscopy Study of Supported Chromium Catalysts. *J. Phys. Chem.* **1993**, *97*, 4756−4763.

(45) Weckhuysen, B. M.; Verberckmoes, A. A.; Buttiens, A. L.; Schoonheydt, R. A. Diffuse-Reflectance Spectroscopy Study of the Thermal Genesis and Molecular Structure of Chromium Supported Catalysts. *J. Phys. Chem.* **1994**, *98*, 579−584.

(46) Groppo, E.; Prestipino, C.; Cesano, F.; Bonino, F.; Bordiga, S.; Lamberti, C.; Thüne, P. C.; Niemantsverdriet, J. W.; Zecchina, A. In Situ, Cr K-Edge XAS Study on the Phillips Catalyst: Activation and Ethylene Polymerization. *J. Catal.* **2005**, *230*, 98−108.

(47) Demmelmaier, C. A.; White, R. E.; van Bokhoven, J. A.; Scott, S. L. Evidence for a Chromasiloxane Ring Size Effect in Phillips (Cr/SiO2) Polymerization Catalysts. *J. Catal.* **2009**, *262*, 44−56.

(48) Demmelmaier, C. A.; White, R. E.; van Bokhoven, J. A.; Scott, S. L. Nature of SiOCrO2Cl and (SiO)2CrO2 Sites Prepared by Grafting CrO2Cl2 Onto Silica. *J. Phys. Chem. C* **2008**, *112*, 6439−6449.

(49) Wachs, I. E.; Roberts, C. A. Monitoring Surface Metal Oxide Catalytic Active Sites with Raman Spectroscopy. *Chem. Soc. Rev.* **2010**, *39*, 5002−5017.

(50) Chakrabarti, A.; Gierada, M.; Handzlik, J.; Wachs, I. E. Operando Molecular Spectroscopy During Ethylene Polymerization by Supported CrOx/SiO2 Catalysts: Active Sites, Reaction Intermediates, and Structure-Activity Relationship. *Top. Catal.* **2016**, *59*, 725−739.

(51) Chakrabarti, A.; Wachs, I. E. The Nature of Surface CrOx Sites on SiO2 in Different Environments. *Catal. Lett.* **2015**, *145*, 985−994.

(52) Guesmi, H.; Tielens, F. Chromium Oxide Species Supported on Silica: A Representative Periodic DFT Model. *J. Phys. Chem. C* **2012**, *116*, 994−1001.

(53) Gierada, M.; Michorczyk, P.; Tielens, F.; Handzlik, J. Reduction of Chromia-Silica Catalysts: A Molecular Picture. *J. Catal.* **2016**, *340*, 122−135.

(54) Handzlik, J.; Grybos, R.; Tielens, F. Isolated Chromium(VI) Oxide Species Supported on Al-Modified Silica: A Molecular Description. *J. Phys. Chem. C* **2016**, *120*, 17594−17603.

(55) Krauss, H. L.; Stach, H. Über Oberflächenverbindungen von Übergangsmetallen. IV*. Polymerisationsreaktionen an Oberflächen-Chrom(II)-Verbindungen. *Z. Anorg. Allg. Chem.* **1969**, *366*, 34−42.

(56) Krauss, v. H. L.; Stach, H. Chrom(II) als wirksamer bestandteil des Phillips Katalysators zur Äthylenpolymerisation. *Inorg. Nucl. Chem. Lett.* **1968**, *4*, 393−397.

(57) Finch, J. N. Reduction Studies on Supported Chromic Anhydride Catalysts. *J. Catal.* **1976**, *43*, 111.

(58) Zecchina, A.; Garrone, E.; Ghiotti, G.; Coluccia, S. On the Chemistry of Silica Supported Chromium Ions. II. One-Ligand Complexes. Adsorption of Carbon Monoxide, Carbon Dioxide and Pyridine. *J. Phys. Chem.* **1975**, *79*, 972−978.

(59) Liu, B.; Nakatani, H.; Terano, M. New Aspects of the Induction Period of Ethene Polymerization Using Phillips CrOx/SiO2 Catalyst Probed by XPS, TPD and EPMA. *J. Mol. Catal. A: Chem.* **2002**, *184*, 387−398.

(60) Liu, B. P.; Nakatani, H.; Terano, M. Mechanistic mplications of the Unprecedented Transformations of Ethene Into Propene and Butene over Phillips CrOx/SiO2 Catalyst During Induction Period. *J. Mol. Catal. A: Chem.* **2003**, *201*, 189−197.

(61) Xia, W.; Liu, B.; Fang, Y.; Hasebe, K.; Terano, M. Unique Polymerization Kinetics Obtained fromSsimultaneous Interaction of Phillips Cr(VI)Ox/SiO2 Catalyst With Al-Alkyl Cocatalyst and Ethylene Monomer. *J. Mol. Catal. A: Chem.* **2006**, *256*, 301−308.

(62) Zhong, L.; Liu, Z.; Cheng, R.; Tang, S.; Qiu, P.; He, X.; Terano, M.; Liu, B. Active Site Transformation During the Induction Period of Ethylene Polymerization over the Phillips CrOx/SiO2 Catalyst. *ChemCatChem* **2012**, *4*, 872.

(63) Barzan, C.; Piovano, A.; Braglia, L.; Martino, G. A.; Lamberti, C.; Bordiga, S.; Groppo, E. Ligands Make the Difference! Molecular Insights into Cr-VI/SiO2 Phillips Catalyst during Ethylene Polymerization. *J. Am. Chem. Soc.* **2017**, *139*, 17064−17073.

(64) Potter, K. C.; Beckerle, C. W.; Jentoft, F. C.; Schwerdtfeger, E.; McDaniel, M. P. Reduction of the Phillips Catalyst by Various Olefins: Stoichiometry, Thermochemistry, Reaction Products and Polymerization Activity. *J. Catal.* **2016**, *344*, 657−668.

(65) Cicmil, D.; Meeuwissen, J.; Vantomme, A.; Wang, J.; van Ravenhorst, I. K.; van der Bij, H. E.; Munoz-Murillo, A.; Weckhuysen, B. M. Polyethylene with Reverse Co-Monomer Incorporation: From an Industrial Serendipitous Discovery to Fundamental Understanding. *Angew. Chem., Int. Ed.* **2015**, *54*, 13073−13079.

(66) Cicmil, D.; Meeuwissen, J.; Vantomme, A.; Weckhuysen, B. M. Real-time Analysis of a Working Triethylaluminium-Modified Cr/Ti/SiO2 Ethylene Polymerization Catalyst with In Situ Infrared Spectroscopy. *ChemCatChem* **2016**, *8*, 1937−1944.

(67) Cicmil, D.; van Ravenhorst, I. K.; Meeuwissen, J.; Vantomme, A.; Weckhuysen, B. M. Structure-Performance Relationships of Cr/Ti/SiO2 Catalysts Modified with TEAl for Oligomerisation of Ethylene: Tuning the Selectivity towards 1-Hexene. *Catal. Sci. Technol.* **2016**, *6*, 731−743.

(68) Schwerdtfeger, E.; Buck, R.; McDaniel, M. Reduction of Cr(VI) Polymerization Catalysts by Non-Olefinic Hydrocarbons. *Appl. Catal., A* **2012**, *423−424*, 91−99.

(69) Barzan, C.; Damin, A. A.; Budnyk, A.; Zecchina, A.; Bordiga, S.; Groppo, E. Pre-Reduction of the Phillips CrVI/SiO2 Catalyst by Cyclohexene: A Model for the Induction Period of Ethylene Polymerization. *J. Catal.* **2016**, *337*, 45−51.

(70) Anpo, M.; Thomas, J. M. Single-Site Photocatalytic Solids for the Decomposition of Undesirable Molecules. *Chem. Commun.* **2006**, 3273−3278.

(71) Anpo, M.; Kim, T. H.; Matsuoka, M. The Design of Ti-, V-, Cr-Oxide Single-Site Catalysts within Zeolite Frameworks and Their Photocatalytic Reactivity for the Decomposition of Undesirable Molecules-The Role of Their Excited States and Reaction Mechanisms. *Catal. Today* **2009**, *142*, 114−124.

(72) Kamegawa, T.; Morishima, J.; Matsuoka, M.; Thomas, J. M.; Anpo, M. Eliminating Traces of Carbon Monoxide Photocatalytically from Hydrogen with a Single-Site, Non-Noble Metal Catalyst. *J. Phys. Chem. C* **2007**, *111*, 1076−1078.

(73) Berg, O.; Hamdy, M. S.; Maschmeyer, T.; Moulijn, J. A.; Bonn, M.; Mul, G. On the Wavelength-Dependent Performance of Cr-Doped Silica in Selective Photo-Oxidation. *J. Phys. Chem. C* **2008**, *112*, 5471−5475.

(74) Tsukamoto, D.; Shiro, A.; Shiraishi, Y.; Hirai, T. Visible-Light-Induced Partial Oxidation of Cyclohexane by Cr/Ti/Si Ternary Mixed Oxides with Molecular Oxygen. *J. Phys. Chem. C* **2011**, *115*, 19782−19788.

(75) Kohler, S. D.; Ekerdt, J. G. Infrared Spectroscopic Characterization of Chromium Carbonyl Species Formed by Ultraviolet Photoreduction of Silica-Supported Chromium(vi) in Carbon-Monoxide. *J. Phys. Chem.* **1994**, *98*, 4336−4342.

(76) Mino, L.; Zecchina, A.; Martra, G.; Rossi, A. M.; Spoto, G. A Surface Science Approach to TiO2 P25 Photocatalysis: An in Situ FTIR Study of Phenol Photodegradation at Controlled Water

Coverages from Sub-Monolayer to Multilayer. *Appl. Catal., B* **2016**, *196*, 135−141.

(77) Mino, L.; Negri, C.; Zecchina, A.; Spoto, G. Photodegradation of Organic Pollutants on TiO$_2$ P25 Surfaces Investigated by Transmission FTIR Spectroscopy Under in Situ UV-Vis Irradiation. *Z. Phys. Chem.* **2016**, *230*, 1441−1451.

(78) Barzan, C.; Mino, L.; Morra, E.; Groppo, E.; Chiesa, M.; Spoto, G. Photoinduced Ethylene Polymerization on Titania Nanoparticles. *ChemCatChem* **2017**, *9*, 4324−4327.

(79) Groppo, E.; Damin, A.; Otero Arean, C.; Zecchina, A. Enhancing the Initial Rate of Polymerisation of the Reduced Phillips Catalyst by One Order of Magnitude. *Chem. - Eur. J.* **2011**, *17*, 11110−11114.

(80) Cieslak-Golonka, M. Spectroscopy of chromium(VI) species. *Coord. Chem. Rev.* **1991**, *109*, 223−249.

(81) Weckhuysen, B. M.; Wachs, I. E. Raman Spectroscopy of Supported Chromium Oxide Catalysts - Determination of Chromium-Oxygen Bond Distances and Bond Orders. *J. Chem. Soc., Faraday Trans.* **1996**, *92*, 1969−1973.

(82) Weckhuysen, B. M.; Wachs, I. E. In Situ Raman Spectroscopy of Supported Chromium Oxide Catalysts: $^{18}O_2$-$^{16}O_2$ Isotopic Labeling Studies. *J. Phys. Chem. B* **1997**, *101*, 2793−2796.

(83) Vuurman, M. A.; Wachs, I. E.; Stufkens, D. J.; Oskam, A. Characterization of Chromium-Oxide Supported on Al$_2$O$_3$, ZrO$_2$, TiO$_2$, and SiO$_2$ under Dehydrated Conditions. *J. Mol. Catal.* **1993**, *80*, 209−227.

(84) Wachs, I. E. Raman and IR Studies of Surface Metal Oxide Species on Oxide Supports: Supported Metal Oxide Catalysts. *Catal. Today* **1996**, *27*, 437−455.

(85) Lee, E. L.; Wachs, I. E. In Situ Raman Spectroscopy of SiO$_2$-Supported Transition Metal Oxide Catalysts: An Isotopic O-18-O-16 Exchange Study. *J. Phys. Chem. C* **2008**, *112*, 6487−6498.

(86) Spoto, G.; Bordiga, S.; Garrone, E.; Ghiotti, G.; Zecchina, A.; Petrini, G.; Leofanti, G. Cr(II) and Cr(III) Ions Grafted at Internal Nests of a Pentasilic Zeolite (Silicalite) - Characterization and Formation of Polycarbonylic, Polynitrosylic, and Mixed Species by Interaction with CO and NO. *J. Mol. Catal.* **1992**, *74*, 175−184.

(87) Amakawa, K.; Sun, L.; Guo, C.; Hävecker, M.; Kube, P.; Wachs, I. E.; Lwin, S.; Frenkel, A. I.; Patlolla, A.; Hermann, K.; et al. How Strain Affects the Reactivity of Surface Metal Oxide Catalysts. *Angew. Chem., Int. Ed.* **2013**, *52*, 13553−13557.

(88) Tonosaki, K.; Taniike, T.; Terano, M. Origin of Broad Molecular Weight Distribution of Polyethylene Produced by Phillips-Type Silica-Supported Chromium Catalyst. *J. Mol. Catal. A: Chem.* **2011**, *340*, 33−38.

(89) Millar, G. J.; Rochester, C. H.; Waugh, K. C. Infrared Study of Methyl Formate and Formaldehyde Adsorption on educed and Oxidised Silica-Supported Copper Catalysts. *J. Chem. Soc., Faraday Trans.* **1991**, *87*, 2785−2793.

(90) Millar, G. J.; Rochester, C. H.; Waugh, K. C. Evidence for the Adsorption of Molecules at Special Sites Located at Copper/Zinc Oxide Interfaces. Part 3.—Fourier-Transform Infrared Study of Methyl Formate Adsorption on Reduced and Oxidised Cu/ZnO/SiO$_2$ Catalysts. *J. Chem. Soc., Faraday Trans.* **1992**, *88*, 3497−3503.

(91) Groppo, E.; Lamberti, C.; Bordiga, S.; Spoto, G.; Zecchina, A. In-Situ FTIR Spectroscopy of Key Intermediates in the First Stages of Ethylene Polymerization on the Cr/SiO$_2$ Phillips Catalyst: Solved the Puzzle of the Initiation Mechanism? *J. Catal.* **2006**, *240*, 172−181.

Concerted Electron Transfer in Iminopyridine Chromium Complexes: Ligand Effects on the Polymerization of Various (Di)olefins

Giuseppe Leone,[*,†] Elena Groppo,[*,‡] Giorgia Zanchin,[†] Giorgia A. Martino,[‡] Alessandro Piovano,[‡] Fabio Bertini,[†] Javier Martí-Rujas,[§,∥] Emilio Parisini,[§] and Giovanni Ricci[†]

†CNR-Istituto per lo Studio delle Macromolecole (ISMAC), via A. Corti 12, I-20133 Milano, Italy

‡Dipartimento di Chimica, NIS Interdepartmental Research Center and INSTM Reference Center, Università degli Studi di Torino, Via G. Quarello 15A, I-10135 Torino, Italy

§Center for Nano Science and Technology at Polimi, Istituto Italiano di Tecnologia, Via Pascoli 70/3, I-20133 Milano, Italy

S *Supporting Information*

ABSTRACT: A study of reactions among $CrCl_2$, $CrCl_3(THF)_3$, and iminopyridine ligands differing in the nature of the substituents at the iminic carbon and at the ortho positions of the aryl ring ($2,6\text{-}R^1{}_2C_6H_3N=CR^2(C_5H_3N)$) ($R^1 = R^2 = H$ (**L1**); $R^1 = iPr$, $R^2 = H$ (**L2**); $R^1 = H$, $R^2 = CH_3$ (**L3**)) but featuring close electron-accepting properties has provided a new example of the redox chemistry of chromium complexes. The reactions of unsubstituted aniline **L1** and of **L3** with $CrCl_2$ give rise to $[(L1^{\bullet})\text{-}Cr^{III}Cl_2(THF)]^-$ (**Cr1**) and $[(L3^{\bullet})Cr^{III}Cl_2(THF)]^-$ (**Cr3**) complexes, respectively, containing chromium in the *physical* trivalent oxidation state and the ligand in the monoanionic radical state $(L^{\bullet})^-$ as a result of a one-electron transfer from the metal to the ligand. In contrast, the reactions of $CrCl_2$ with the ortho-substituted **L2** and of $CrCl_3(THF)_3$ with the unsubstituted **L1** give rise to $[(L2)Cr^{II}Cl_2(THF)]^0$ (**Cr2**) and $[(L1)\text{-}Cr^{III}Cl_3(THF)]^0$ (**Cr4**) having the chromium in the divalent and trivalent oxidation states, respectively, and the unperturbed ligand in the neutral state. All four complexes were used, in combination with methylaluminoxane (MAO), as catalyst precursors for the polymerization of ethylene, cyclic olefins (i.e., norbornene and dicyclopentadiene), and 1,3-butadiene. A chromium to ligand synergy, coupled with a good stability of the active intermediate in the presence of the Al activator, proven particularly effective in the polymerization of ethylene, especially for **Cr1**, giving high molecular weight linear poly(ethylene)s. The formalism in the metal oxidation state does not affect the reactivity toward the cyclic olefins and 1,3-butadiene, while ligand steric effects emerge clearly. The use of bulky ortho substituents shuts down the activity in the polymerization of cyclic olefins, particularly for the bulkier dicyclopentadiene, and reverses the catalyst chemoselectivity in the polymerization of 1,3-butadiene.
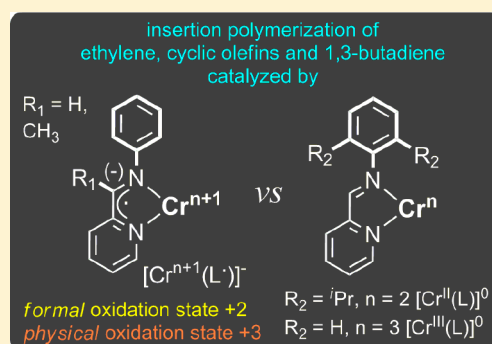
1. INTRODUCTION

Poly(olefin)s are an integral part of everyday life, and the insertion polymerization of olefins is one of the most industrially relevant synthetic reactions.[1−6] Chromium catalysts play a key role in this field, prompted by the extensive use of Phillips[7] and Union Carbide[8] catalysts for the synthesis of more than one-third of the high-density poly(ethylene) (HDPE) produced worldwide.[9,10] Moreover, from the year 2000 onward, several molecular chromium complexes have been developed and used for the selective oligomerization and polymerization of ethylene.[11−14] Most of the recently reported chromium complexes are enveloped by non-cyclopentadienyl ligands,[15] namely multidentate ligands with phosphine, amine, ether, and thioether donors, because of their easy tuning of steric and electronic properties.[16] Notable examples are chromium complexes ligated by tetradentate N_2P_2,[17] tridentate $S^{\wedge}N^{\wedge}S$,[18,19] $P^{\wedge}N^{\wedge}P$,[20] $O^{\wedge}N^{\wedge}N$,[21] and $N^{\wedge}N^{\wedge}N$,[22−25] and bidentate $N^{\wedge}N$ ligands.[26−29] Generally, these complexes involve trivalent chromium, with a few exceptions.[30−33]

However, some unsolved issues in all of the chromium systems (either homogeneous or heterogeneous) and related catalytic mechanism remain, for which scientists have not yet come to a consensus.[34−38] As recently reported by Sydora, Caruthers, and Abu-Omar,[36] these include (i) the oxidation state of intermediates and active sites, (ii) the kinetic order of the reaction in ethylene, (iii) the elementary mechanistic steps, and (iv) the polymerization mechanism of ethylene. One of the main inconsistences is the chromium oxidation state responsible for either polymerization or oligomerization of ethylene, which has been the subject of a long debate in the past[37,38] and has recently gained renewed attention in high-level specialized literature, fostering a great number of experimental[36,39−43] and theoretical studies.[44−47]

In the present work, we aim at increasing the knowledge of chromium-catalyzed (di)olefin polymerization and related

mechanistic aspects by focusing our attention on iminopyridine chromium complexes. Iminopyridines have recently received particular consideration as ancillary ligands in coordination chemistry by virtue of their low cost, easy preparation, and fine-tunability of their steric and electronic properties.[48,49] Iminopyridines generate interesting chemistry when they are bound to a variety of metal ions: iron, cobalt, palladium, and nickel complexes with iminopyridines have been extensively employed as catalyst precursors for the oligomerization and polymerization of olefins and conjugated dienes.[50−54] Iminopyridines belong to the family of redox-active ligands, among which diimines are perhaps the most famous analogues. Redox-active ligands are those that participate in redox chemistry with a metal, rather than existing as spectators. They have gone from being of marginal concern to the forefront of inorganic and organometallic chemistry.[55,56] These ligands serve as electron reservoirs working in concert with metal ions and providing an unexpected utility in a wide range of catalytic molecular conversions. Generally, diimine complexes of a certain metal (Mt) can be classified in terms of their electronic structures as $[Mt^n(L)]^0$, $[Mt^{n+1}(L^\bullet)]^-$ and $[Mt^{n+2}(L^{red})]^{2-}$ (Scheme 1).

Scheme 1. Different Redox States of a Diimine Ligand and Possible Electronic Structures of Their Complexes[a]
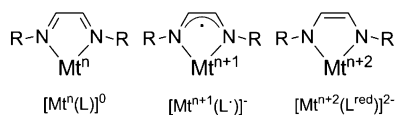

[a]Mt = metal; R = usually a different *o*- and *p*-aryl-substituted group.

Among them, $[Mt^n(L)]^0$ is the most common: the ligand is neutral and is structurally unperturbed.[44] Transfer of one electron from the metal to the ligand gives rise to the monoanion radical $(L^\bullet)^-$, while transfer of a second electron gives the doubly reduced dianion $(L^{red})^{2-}$. To the best of our knowledge, iminopyridine complexes have been much less investigated than their diimine analogues, and metal complexes ligated by $(L^\bullet)^-$ and $(L^{red})^{2-}$ iminopyridines are rare.

Herein, we report the synthesis and characterization of a series of iminopyridine chromium complexes with chromium in the oxidation states of +2 by reaction of CrCl$_2$ with three ligands of the type 2,6-R$_2^1$C$_6$H$_3$N=CR^2(C$_5$H$_3$N) (R^1 = R^2 = H (**L1**); R^1 = *i*Pr, R^2 = H (**L2**); R^1 = H, R^2 = CH$_3$ (**L3**)) (**Cr1−Cr3**) and +3 by reaction of CrCl$_3$(THF)$_3$ with **L1** (**Cr4**). The iminopyridines differ in the nature of substituents at the iminic carbon and at the ortho positions of the aryl ring (Scheme 2) but feature close electron-accepting properties. Upon activation with MAO, **Cr1−Cr4** were evaluated as catalyst precursors for the polymerization of ethylene, the cyclic olefins norbornene (NB) and dicyclopentadiene (DCPD), and 1,3-butadiene. We disclose the role of the ligand and the effects of the monomer type and of some

Scheme 2. Structure and Numbering of the Iminopyridine Ligands Employed in This Work

L1   **L2**   **L3**
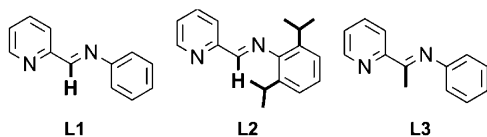
polymerization conditions on the overall productivity, selectivity, and polymer properties. Furthermore, since the redox-active ligands impart additional complexity to the electronic structures of the complexes, UV−vis−NIR spectroscopy has been applied to discriminate between the *formal* and the *physical* (or *spectroscopic*) chromium oxidation state.[57] Although some questions remain unresolved, this study (i) expands the range of electronically characterized chromium complexes of non-innocent ligands, (ii) demonstrates that iminopyridine chromium complexes are efficient and versatile catalysts, and (iii) suggests a relationship between the electronic/steric properties of these complexes and their catalytic behavior, which is at the basis of a future rational design of chromium catalysts for (di)olefin conversion.

2. RESULTS AND DISCUSSION

2.1. Synthesis and Characterization of Chromium Complexes. The iminopyridine ligands **L1−L3** (Scheme 2) were synthesized according to the literature.[49] **Cr1−Cr3** were synthesized by the reaction of CrCl$_2$ with a stoichiometric amount of the corresponding **L1−L3** ligand in THF at room temperature. The complexes formed immediately and rapidly precipitated from an initially clear solution. By this procedure, the solids were isolated in high yield, ranging from 70 to 94%. **Cr4** was prepared by the reaction of CrCl$_3$(THF)$_3$ with the stoichiometric amount of **L1** in THF at room temperature. The complex was isolated as a green powder in good yield (77%). All of the complexes were highly air and moisture sensitive, thus requiring characterization under strictly inert conditions. Each complex was characterized by elemental analysis, attenuated total reflection (ATR) FT-IR, and ^{1}H NMR spectroscopy, the elemental analysis being consistent with the formation of complexes of (L)CrCl$_n$(THF) composition (n = 2, **Cr1−Cr3**; n = 3, **Cr4**). The electronic properties of all the investigated complexes were determined by UV−vis−NIR spectroscopy, which has been demonstrated to be a sensitive tool for discriminating between neutral and charged redox ligands,[58,59] the latter being characterized by extremely intense electronic transitions in the visible range.

As expected, isolation of single crystals of **Cr1−Cr4**, suitable for X-ray diffraction, proved problematic. The use of CrCl$_3$(THF)$_3$ was crucial to the successful isolation of a microcrystalline, characterizable product. Single crystals, suitable for X-ray diffraction, were obtained only for **Cr4** from a concentrated dichloromethane solution cooled to −18 °C for days. The crystal structure of **Cr4** is provided in Figure 1, along with a selection of its main structural details (bond lengths (Å) and angles (deg)). Table S1 gives the main crystal data and structural refinement statistics.

The X-ray diffraction analysis of **Cr4** shows that the Cr atom is six-coordinated and that a hydroxide anion completes the octahedral coordination sphere of the metal by binding to the chromium atom trans to the N1 atom of the **L1** ligand (Cr1−O1 = 2.014(8) Å, Cr1−N1 = 2.07(1) Å, O1−Cr1−N1 = 172.9(4)°). Traces of adventitious water during the workup for the single-crystal growth are the likely source of the formation of the unexpected coordination of oxygen, whose binding to the chromium atom likely occurs with the simultaneous dissociation of a coordinated THF molecule. Consistent with this hypothesis, the ATR-IR spectrum of pristine solid **Cr4** did not show any band associable to the presence of a hydroxide anion (Figure S1), while it shows bands due to THF (vide infra Figure 2a'). The **Cr4**·OH complex crystallizes in the
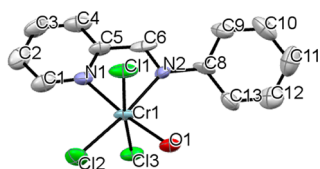
Figure 1. X-ray crystal structure view of **Cr4·OH** (thermal ellipsoids set at 50% probability). Hydrogen atoms have been omitted for clarity. Selected bond lengths (Å) and angles (deg): Cr1–N1, 2.07(1); Cr1–N2, 2.09(1); Cr1–Cl2, 2.283(4); Ni1–C5, 1.34(2); Ni2–C6, 1.28(2); C5–C6, 1.42(3) Cl1–Cr1–Cl2, 93.2(1); Cl1–Cr1–Cl3, 172.8(1); Cl1–Cr1–N1, 91.2(3); Cl1–Cr1–N2, 86.6(3); Cl2–Cr1–Cl3, 93.9(1); Cl2–Cr1–N1, 95.6(3); Cl2–Cr1–N2, 173.4(3); Cl3–Cr1–N1, 88.6(3); Cl3–Cr1–N2, 86.4(3); N1–Cr1–N2, 77.8(4).

orthorhombic $P2_12_12_1$ space group. **L1** chelates the Cr atom, forming a nearly planar five-membered ring, with an angle of 0.43° between the plane passing through the N1–Cr1–N2 atoms and the mean plane passing through the five atoms of the ring. The distances to the metal of the two Cl atoms that are trans to each other are 2.331(4) and 2.316(4) Å, with Cl1–Cr1–Cl3 = 172.8(1)°. The third Cl atom is trans to the N2 atom of the chelating ligand (Cr1–Cl2 = 2.283(4) Å, Cr1–N2 = 2.09(1) Å, Cl2–Cr1–N2 = 173.4(3)°). In the structure, the angle between the planes of the two aromatic rings of **L1** is 51.63°.

Unfortunately, despite numerous attempts, single crystals of **Cr1–Cr3** suitable for X-ray diffraction analysis were not obtained, thus preventing their structural characterization. In addition, the paramagnetism of the complexes made uncertain any structural characterization via NMR. The difficulties encountered in obtaining single crystals for **Cr1–Cr3** could

be due to their unsaturated coordination and electronic structures. Indeed, on the basis of elemental analysis and by analogy with **Cr4**, we speculate that **Cr1–Cr3** have a five-coordinate structure with a bidentate chelating ligand, one THF, and two chloride ions binding to the chromium atom. Nonetheless, the question regarding the metal oxidation state remains open also by virtue of the redox properties of iminopyridines. In addition, it is well established that a Cr(II) complex may be reoxidized to Cr(III) by disproportionation.[38] All of these arguments imply that the exact assignment of the chromium oxidation state is highly desirable and useful also because the metal oxidation state is expected to play a fundamental role in determining the selectivity toward the polymerization or oligomerization of ethylene. Keeping this in mind, in an effort to access the ligand electronic structure and the associated chromium oxidation state, we collected UV–vis–NIR absorption spectra for **Cr1–Cr4** and pristine **L1–L3** (Figure 2a–c).

The UV–vis–NIR spectra of all the chromium complexes are dominated by the π–π^* transitions characteristic of the ligand above 24000–28000 cm^{-1}. In addition, very weak absorption bands ($\varepsilon \approx 5 \times 10^2$ M^{-1}cm^{-1}) were observed at 22000 and 16500 cm^{-1} for **Cr4** (red in Figure 2a) and at about 15400 cm^{-1} for **Cr2** (red in Figure 2c). The position and the intensity of these bands are those expected for d–d transitions of highly coordinated Cr(III) and Cr(II) ions, respectively,[60,61] consistent with the expected complex stoichiometry.

The ATR-IR spectra of **Cr4** and **Cr2** (red in Figure 2a′,c′, respectively) closely resemble those of the corresponding ligands (**L1** and **L2**, respectively) except for the absorption bands associated with the vibrations localized around the C═N iminic bond, which shift and/or split into multiple
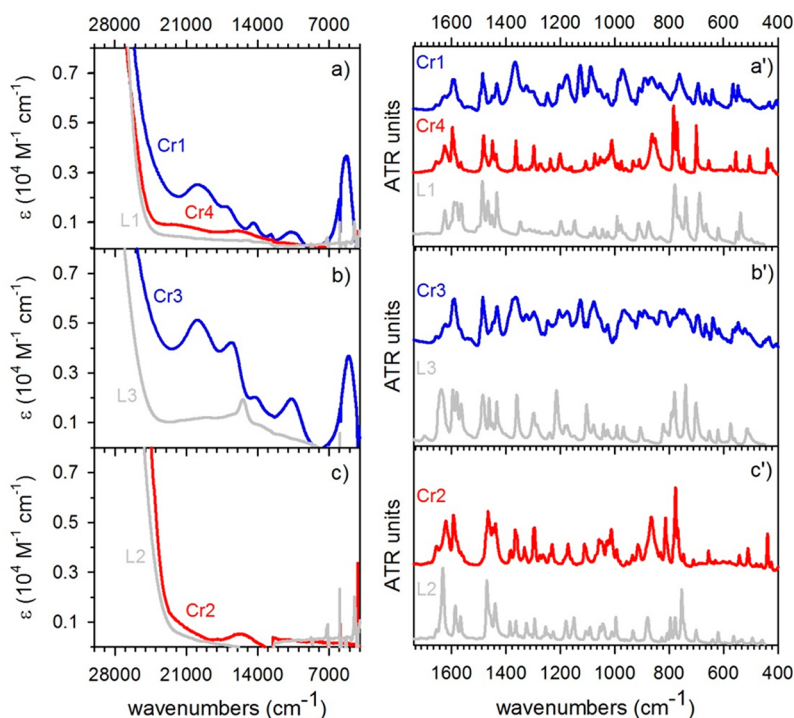
Figure 2. UV–vis–NIR absorption spectra and ATR-IR spectra of **Cr1** and **Cr4** (blue and red in (a) and (a′)), **Cr3** (blue in (b) and (b′)), and **Cr2** (red in (c) and (c′)), in comparison to those of the corresponding ligands (gray). All of the UV–vis–NIR spectra have been measured in chloroform and reported after subtraction of the spectrum of the solvent. The ATR-IR spectra have been collected on the samples in the powder form.

components due to the coordination of the chromium ion. For example, the $\nu(C=N)$ band observed at 1623 and 1632 cm^{-1} for **L1** and **L2**, respectively, splits into two components at about 1655 and 1600 cm^{-1} in the spectrum of **Cr4** and at about 1654 and 1620 cm^{-1} in the spectrum of **Cr2**. Moreover, in both cases, additional bands are observed around 1010 and 850 cm^{-1}, which are assigned to the asymmetric and symmetric $\nu(C-O-C)$ modes of coordinated THF, in agreement with the expected composition.

In contrast to **Cr2** and **Cr4**, the UV−vis−NIR spectra of **Cr1** (blue in Figure 2a) and **Cr3** (blue in Figure 2b) are characterized by much more intense absorption bands in the 21000−4000 cm^{-1} region (maxima observed at about 20000, 16500, 14000, 10500, and 5050 cm^{-1}), which are too intense ($\varepsilon \approx 10^3 - 10^4$ M^{-1} cm^{-1}) to be classified as d−d transitions associated with the Cr(II) ions. The first four bands are very similar to those observed in the spectra of π-radical monoanionic ligands of the type $(bpy^{\bullet})^-$ or $(tpy^{\bullet})^-$ (bpy = bipyridine, tpy = terpyridine).[62−64] For example, intense ($\sim 10^4$ M^{-1} cm^{-1}) bands have been reported at 22220, 16130, 14200, and 10640 cm^{-1} for $(tpy^{\bullet})^-$ and assigned to intraligand $\pi-\pi^*$ transitions.[65] The presence of these bands in the spectra of **Cr1** and **Cr3** clearly indicates that **L1** and **L3** are redox-noninnocent ligands[66,67] and that **Cr1** and **Cr3** should be formulated as $[(\mathbf{L1^{\bullet}})Cr^{III}Cl_2(THF)]^-$ and $[(\mathbf{L3^{\bullet}})Cr^{III}Cl_2(THF)]^-$ species, rather than $(\mathbf{L1})Cr^{II}Cl_2(THF)$ and $(\mathbf{L3})Cr^{II}Cl_2(THF)$. In other words, **Cr1** and **Cr3** are only *formally* divalent chromium complexes, while the metal is better described as adopting the trivalent oxidation state (Scheme 3).

Scheme 3. Synthesis of Cr1 and Cr3 and Formalism in the Chromium Oxidation State As Determined by UV−Vis−NIR Spectroscopy
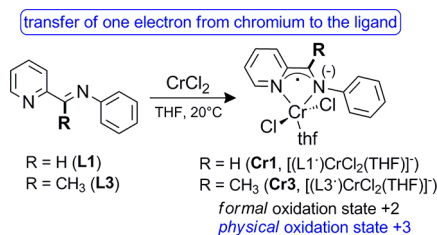

This is a quite common phenomenon for chromium complexes of N-, S-, and O-donor ligands, due to the low covalence of their bonding and the high stability of the high-spin Cr(III) ion. Indeed, it has been reported that several formally low spin Cr(II) complexes actually contain Cr(III) antiferromagnetically coupled to a π-radical anion and that their redox chemistry is entirely ligand centered.[62,68−75] This picture is confirmed by the ATR-IR spectra of **Cr1** and **Cr3** (blue in Figure 2a′,b′), which are sensibly different from those of the corresponding **L1** and **L3** ligands, respectively. In particular, most of the absorption bands in the 1400−800 cm^{-1} region are enhanced in intensity and broadened, a fact that is well documented for radical anions of conjugated molecules.[76,77]

The origin of the intense band centered at 5050 cm^{-1} that can be observed both in the UV−vis−NIR spectra and in the ATR-IR spectra of **Cr1** and **Cr3** is less straightforward. An electronic absorption band in the near-infrared region has been often reported for ligand mixed-valent species and assigned as a

ligand to ligand intervalence charge transfer (LLIVCT) band, diagnostic of the copresence of two equal ligands in a different redox state.[62−64] However, this assignment is not compatible with our situation, because it implies a Cr:L = 1:2 ratio, which does not match with the expected stoichiometry. On the other hand, a few examples can be found in the literature about bpy complexes of the type $[Mt^n(bpy)]^0$, where the transition of an electron from the metal to the ligand to give $[Mt^{n+1}(bpy^{\bullet})]^-$ originates a similar band in the NIR region.[78] Hence, in our case, we can tentatively ascribe the band at 5050 cm^{-1} to the specular electronic transition from the $[(\mathbf{L1^{\bullet}})Cr^{III}Cl_2(THF)]^-$ and $[(\mathbf{L3^{\bullet}})Cr^{III}Cl_2(THF)]^-$ ground states to the respective $(\mathbf{L1})Cr^{II}Cl_2(THF)$ and $(\mathbf{L3})Cr^{II}Cl_2(THF)$ excited states.

In summary, the UV−vis−NIR and ATR-IR spectra shown in Figure 2 clearly reveal that **Cr1** and **Cr3** differ from **Cr4** and **Cr2**, in that the former have a marked tendency to undergo an electron transfer from the metal to the ligand (either **L1** or **L3**), while such electron transfer does not take place in **Cr4** or in **Cr2**. The reason for the inhibition of chromium to **L1** electron transfer in **Cr4** may be due to the fact that the oxidation of a Cr(III) ion to Cr(IV) is thermodynamically unfavorable, but also to a lower chance of a close approach between the metal and the ligand as a consequence of the metal ion size decrease in the case of a Cr(III)/Cr(IV) oxidation. Similarly, the reticence of **Cr2** to undergo chromium to **L2** electron transfer is proposed to be a consequence of the steric demand of the *o*-isopropyl substituents, which weakens the chromium−ligand interaction and prevents an efficient electronic delocalization. As a whole, **Cr4** and **Cr2** can be formulated as $[(\mathbf{L1})Cr^{III}Cl_3(THF)]^0$ and $[(\mathbf{L2})Cr^{II}Cl_2(THF)]^0$ species, respectively, with the ligand in the neutral state (Scheme 4).

Scheme 4. Synthesis of Cr2 and Cr4 and Formalism in the Chromium Oxidation State As Determined by UV−Vis−NIR Spectroscopy
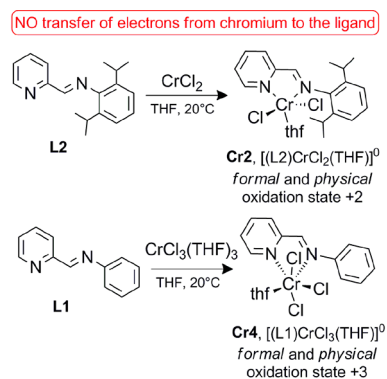
The interpretation that emerged from the UV−vis−NIR absorption spectrum of **Cr4** is in good agreement with the X-ray diffraction data (Figure 1). In the ligand N−C−C−N backbone for **Cr4**, the C−C, C−N$_{imine}$, and C−N$_{pyridine}$ bond lengths are 1.42(3), 1.28(2), and 1.34(2) Å, respectively. These metric parameters are consistent with those expected for the ligand in the neutral state. The bond lengths fall in a close range of those formerly reported for related compounds coordinated by a neutral iminopyridine ligand.[79] With respect to the ligand electronic structures and oxidation state formalism, the UV−vis−NIR and X-ray diffraction studies both corroborate our hypothesis that **Cr4** should be

Table 1. Polymerization of Ethylene Catalyzed by Cr1−Cr4[a]

entry	Cr	Al/Cr	aging time[b] (min)	PE yield (g)	activity[c] (×10⁵)	M_w[d] (×10³)	M_w/M_n	T_m[e](°C)
1	**Cr1**	250		1.86	5.58	131.6	35.6	103/113/127
2	**Cr2**	250		none				
3	**Cr3**	250		none				
4	**Cr4**	250		none				
5	**Cr1**	250	1	0.45	1.35	26.7	18.4	89/103/123
6	**Cr1**	250	3	0.40	1.21	18.6	11.3	105/124
7	**Cr4**	1000		0.10	0.30	68.4	3.8	130
8	CrCl₂	250		none				
9	CrCl₃(THF)₃	250		0.17	0.51	_f_		_f_
10	CrCl₃(THF)₃	1000		traces				
11	Cr(acac)₃	250		none				

[a]Polymerization conditions: ethylene pressure, 1.01 bar; total volume, 20 mL (toluene); Cr, 10 μmol; MAO as cocatalyst; time, 20 min; temperature, 20 °C. [b]Precontact between **Cr1** and MAO (Al/Cr = 200). This treatment acts in two ways: it helps to solubilize the poorly soluble complex, and it preforms the active species. [c]Activity in g of PE mol_{Cr}^{-1} h^{-1}. [d]Average molecular weight (M_w) and molecular weight distribution (M_w/M_n) by SEC. [e]Melting temperature at the maximum (T_m) by DSC (second heating). [f]Not determined.

formulated as $[(\mathbf{L1})Cr^{III}Cl_3(THF)]^0$ with trivalent chromium ligated by the iminopyridine ligand in the neutral state. As described below, all of these electronic features have significant consequences on the course of the ethylene polymerization.

2.2. Polymerization of Ethylene. *2.2.1. Rationalizing the Important Parameters for Cr−Iminopyridines To Polymerize Ethylene.* Most active ethylene polymerization catalysts contain multidentate ligands,[80−82] while a large range of N^N bidentate ligands, in combination with various chromium sources, have been reported to be active for ethylene trimerization and tetramerization.[14] In comparison to the well-known tridentate N^N^N ligands,[21−25] iminopyridines were expected to provide a less efficient shielding to stabilize the chromium active species and suppress chain transfer in the polymerization of olefins. Nonetheless, quite surprisingly, **Cr1**, in combination with MAO (250 equiv with respect to Cr), afforded a highly active catalyst for the polymerization of ethylene under mild conditions. A solid PE, on the order of grams, was obtained (Table 1, entry 1, activity = 5.58 × 10⁵ g of PE mol_{Cr}^{-1} h^{-1}). In contrast, **Cr2−Cr4** did not exhibit any polymerization activity under the same conditions (Table 1, entries 2−4). The lack of polymerization activity by **Cr2−Cr4** may likely be due to faster ethylene displacement or faster termination paths involving either β-H elimination or transfer to monomer and subsequent chain transfer rather than chain propagation. The latter reductive elimination paths are commonly observed for insertion ethylene (or growing chain) intermediates, their relative stability determining the selectivity toward oligomerization or polymerization products. It is worth noting that the formation of liquid oligomers is intentionally not factored in Table 1.

Before discussing in detail the performance of the iminopyridine chromium complexes, we should also mention that the polymerization of ethylene catalyzed by *naked* CrCl₂, CrCl₃(THF)₃, and Cr(acac)₃ was also investigated for comparison (*naked* because it is assumed that the metal is only surrounded by the growing polymer chain, the new incoming monomer, and the weakly coordinating anion, with no ancillary ligands) (Table 1, entries 8−11). Under our polymerization conditions, a small amount of PE was obtained only with CrCl₃(THF)₃/MAO at Al/Cr = 250 (entry 9). Given the inclination of trivalent chromium complexes toward reduction upon the addition of the Al activator,[36] it can be inferred that reduction takes place at chromium, forming

divalent chromium, which is active to afford solid PE. Nonetheless, with an increase in Al/Cr up to 1000, only traces of polymer were recovered, suggesting that CrCl₃(THF)₃ decomposes in the presence of an excess of MAO (entry 10). At the moment we are not able to confidently explain this behavior. A possibility that could be taken into consideration is the formation of lower valent chromium species in this latter case as well as in the case of CrCl₂. In comparison with these results, the **L1** ligand strongly increased the overall PE productivity.

Given the structural similarity between **Cr1** and **Cr4**, which are both ligated by **L1**, the activity exhibited by **Cr1** is ascribed to the pristine radical anion $(\mathbf{L1}^{\bullet})^-$ ligand state, while in the case of **Cr4** the same ligand is neutral and essentially unperturbed. It can be inferred that the presence of an intermediate akin to $[(L^{\bullet})Cr^{III}]^-$ is the *necessary condition* for iminopyridine chromium complexes to exhibit ethylene polymerization activity.

As far as **Cr2** is concerned, in addition to the absence of the necessary $[(L^{\bullet})Cr^{III}]^-$ intermediate, we must also consider that the sterically demanding isopropyl substituents at the ortho positions of the aniline, perpendicular to the coordination plane, might hinder olefin binding and insertion at the metal, accelerating chain transfer over the chain propagation.[53,81,83] Related arguments have been invoked by Sun et al. to rationalize the unique behavior of chromium complexes, where sterically demanding alkyl substituents at the ligand weaken the interaction between the metal and the π electrons of ethylene, increasing the nucleophilicity of the metal and simultaneously decreasing the rate of monomer insertion.[80]

However, the presence of an intermediate of the type $[(L^{\bullet})Cr^{III}]^-$ is *not sufficient*, as demonstrated by the lack of activity of **Cr3** (entry 3), which is also of the type $[(L^{\bullet})Cr^{III}]^-$ as **Cr1** (Scheme 3). The different catalytic behavior exhibited by **Cr1** and **Cr3** indicates that the *physical* oxidation state of chromium and the redox state of the ligand in the precursor are not the *only* factors influencing their reactivity, which probably depends also on further transformations undergone in the presence of MAO, including further metal reduction or different deactivation paths. A possibility is the rearrangement of ketimine **L3**, where the lability of hydrogen atoms of methyl groups attached to the imine moiety is well established.[84]

To provide insight into the unusual features of **Cr1** and **Cr3**, UV−vis−NIR absorption spectra were acquired upon the
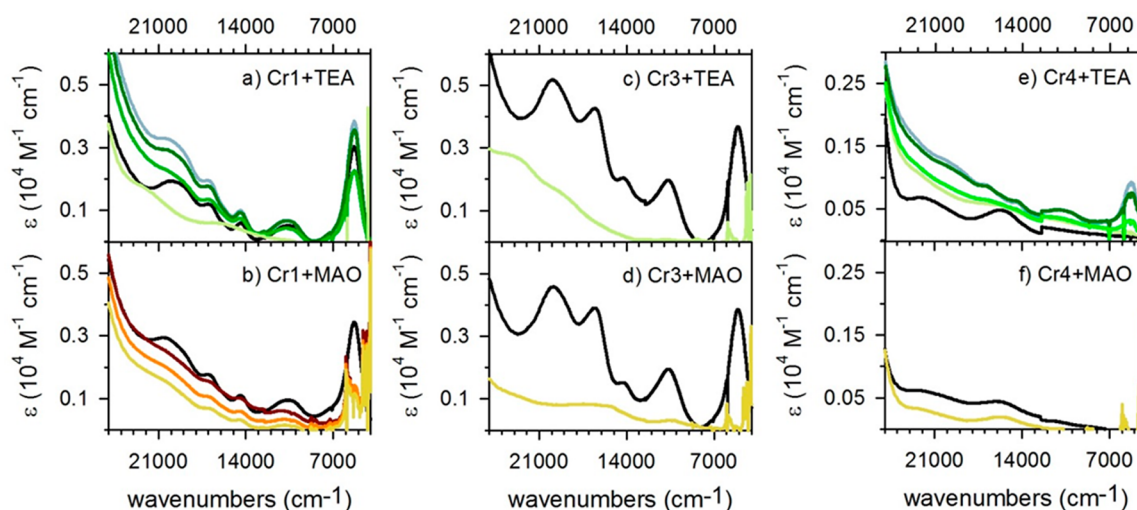
Figure 3. (a) UV−vis−NIR absorption spectra of **Cr1** in chloroform before (black) and after addition of TEA (from blue to green). (b) UV−vis−NIR absorption spectra of the **Cr1** complex in chloroform before (black) and after addition of MAO (from dark red to yellow). The spectrum of chloroform has been subtracted to all the spectra. (c, d) As in (a) and (b) for **Cr3**. (e, f) As in (a) and (b) for **Cr4**.

addition of the Al activator (Figure 3a−d). To keep the conditions as close as possible to those employed for the polymerization tests, both triethylaluminum (TEA),[85] and MAO were evaluated. Due to the available experimental setup, the first spectra were collected a few minutes after the addition of the activator and in the absence of the monomer; hence, they are representative of the phenomena occurring during the aging of the chromium complexes in the presence of the activator rather than of the activation process itself. The spectra of the two complexes greatly change after the addition of TEA and MAO. In all of the cases, the absorption bands characteristic of the initial complexes, diagnostic for the presence of π-radical monoanionic $(L^\bullet)^-$ ligands, disappear. This evidence univocally indicates that, at the end of the aging process, **L1** and **L3** are no longer π-radicals. Moreover, the following comments can be made.

(i) The transformation is very fast for **Cr3**, for which the first spectra collected after the precontact with TEA or MAO no longer contain the fingerprints of the π-radical $(L3^\bullet)^-$ (Figure 3c,3d). In contrast, the spectral evolution is much slower for **Cr1**, suggesting a slower rearrangement of this complex in the presence of both of the Al activators (Figure 3a,b).

(ii) The spectra collected at the end of the aging process are different for the four complex−activator combinations. This indicates that the final oxidation states/coordination geometries of the two chromium complexes are different. However, more detailed information is required to untangle the effect of the symmetry from that of the oxidation state, which is far beyond the scope of this work.

Once **Cr1** in the presence of MAO is transformed into a *formal* and *physical* Cr(II) complex with neutral **L1**, the polymerization of ethylene is strongly inhibited. This is evident by looking at entries 5 and 6 in Table 1. In these two experiments, **Cr1** was previously dissolved and preactivated with MAO at different times. We observed that the activities were more than 4 times lower with respect to the same run without the precontact between **Cr1** and MAO (entry 1). Altogether, the spectroscopic data discussed in Figure 3a−d and the catalytic studies indicate that the active species (or intermediates) involved in the polymerization of ethylene, of

the type $[(L^\bullet)Cr^{III}]^-$, are not very robust in the presence of MAO and are even less robust in the absence of the monomer. These species are rapidly transformed into new species with neutral ligands, no longer active in the ethylene conversion to high-M_w PE. Whether the catalyst deactivation involves instability of the Cr-alkyl moiety or further chromium reduction with or without ligand involvement cannot be established at this moment.

In addition, it is interesting to note that traces of solid PE were recovered with **Cr4** by increasing the amount of MAO up to Al/Cr = 1000 (entry 7). This intriguing behavior was investigated following the evolution of the UV−vis−NIR spectra of **Cr4** in the presence of TEA and MAO (Figure 3e,f). The addition of an excess of TEA causes the appearance of the absorption bands characteristic of the $(L1^\bullet)^-$ radical anion (Figure 3e). This suggests that TEA has the capability to reduce **Cr4**, the reduction being ligand centered. However, the reduced complex has only a transient character, and the successive evolution of the spectra is the same as for **Cr1** (Figure 3a,b). The same phenomenon was not observed in the presence of MAO (Figure 3f), likely due to the low Al/Cr ratio used for the spectroscopic experiments and to the fact that MAO is a mild reducing and alkylating agent in comparison to TEA. Nonetheless, the close similarity of the UV−vis−NIR spectra of pristine **Cr1** with those of **Cr4** upon the addition of the Al activator substantiates our hypothesis that the polymerization of ethylene might be mediated by $[(L^\bullet)Cr^{III}]^-$ species or, in any case, takes place through this intermediate.

The tendency of chromium to undergo one-electron transfer to the iminopyridine ligands is claimed to be fundamental in the catalytic transformation of ethylene to high-M_w PE. Both **Cr1** and **Cr4** in the formal oxidation states +2 and +3, respectively, contain the ligand in the $(L^\bullet)^-$ form as a result of a formal one-electron oxidation of the chromium ion along with ligand reduction to the radical anionic state. However, for the *formal* and *physical* trivalent **Cr4**, this transformation occurs only when the Al activator is added. Given the inclination of trivalent chromium complexes toward reduction upon the addition of the Al activator,[36] we speculate that the reduction initially takes place at the chromium, forming divalent chromium, followed by a further rapid transfer of one

Table 2. Polymerization of Ethylene Catalyzed by Cr1/MAO[a]

entry	solvent	T (°C)	Al/Cr	PE yield (g)	activity[b] (×10⁵)	$M_w{}^c$ (×10³)	$M_w/M_n{}^c$	$^{HF}M_p{}^d$ (×10³)	$^{LF}M_p{}^d$ (×10³)	$T_m{}^e$ (°C)
1[f]	PhMe	20	250	1.86	5.58	131.6	35.6	broad tail	2.4	103/113/127
12	PhMe	20	1000	1.41	4.23	2.2	1.5			93/103/119
13	PhMe	20	50	1.20	3.60	569.5	18.7	648.1	44.7	134
14	PhMe	0	250	0.39	1.16	275.3	20.7	57.8[g]	3.5	135
15	PhMe	40	250	0.86	2.57	3.6	1.8			105/113/123
16	CH₂Cl₂	20	1000	1.77	5.36	59.3	10.1	66.2	4.7	130

[a]Polymerization conditions: ethylene pressure, 1.01 bar; total volume, 20 mL; Cr, 10 μmol; MAO as cocatalyst; time, 20 min. [b]Activity in g of PE $mol_{Cr}{}^{-1}$ h⁻¹. [c]Average molecular weight (M_w) and molecular weight distribution (M_w/M_n) by SEC. [d]$^{HF}M_p$ and $^{LF}M_p$ are the peak molecular weights of the high-M_w and low-M_w fractions, respectively. [e]Melting temperature at the maximum (T_m) by DSC (second heating). [f]First reported in Table 1. [g]The $^{HF}M_p$ peak broadened to its high-molecular-weight side (see Figure 4b).

electron from the metal to the ligand, forming the ligand radical anion. For the *physical* trivalent **Cr1** and **Cr3**, which contain the ligand in the radical anion state from the beginning, the important parameter that discriminates their catalytic behavior in the polymerization of ethylene is the stability of the complex in the presence of the Al activator.

On the whole, although these results provide a reasonably realistic picture of the complexity of what happens in the polymerization of ethylene mediated by **Cr1**−**Cr4**, they cannot be generalized at such an early stage. However, new and attractive hypotheses for the design of iminopyridine chromium complexes emerge.

2.2.2. Effects of Polymerization Conditions on the Catalytic Behavior of Cr1/MAO and Properties of PE. The effect of some different polymerization conditions (i.e., Al/Cr ratio, temperature, and solvent) were explored in detail for **Cr1**. The results are summarized in Table 2.

Generally, all of the obtained PEs are fully saturated, semicrystalline polymers with a low amount of branching (i.e., an average of 10 branches/1000 carbon atoms as determined by the ¹H NMR) (Figures S2 and S3). The formation of saturated PEs can be accounted for by a termination path involving chain transfer to the aluminum. Their general properties resemble those of PEs by heterogeneous chromium catalysts[9] and some pyridinebis(imino)[32] and bis-(pyridylmethyl)amine chromium complexes.[80] **Cr1**/MAO produces PEs with molecular weights (M_w) ranging from 569500 to 2000 g/mol and molecular weight distributions (M_w/M_n) in the range 1.5−35.6 with the shape depending on the polymerization conditions. This clearly indicates the presence of several active species under certain polymerization conditions. Multicomponent M_w/M_n values cannot be meaningfully described by the average molecular weight value only; most of the SEC curves are dominated by two components: a low-molecular-weight and a high-molecular-weight fraction. The peak molecular weight (M_p) for each of these two fractions (i.e., $^{LF}M_p$ and $^{HF}M_p$, respectively) are also reported in Table 2.

A series of polymerizations with **Cr1**/MAO were performed over the range of Al/Cr from 50 to 1000. A low excess of MAO (Al/Cr = 50) was sufficient for exhibiting activity as high as 3.60×10^5 g of PE $mol_{Cr}{}^{-1}$ h⁻¹ (Table 2, entry 13), whereas the maximum value of 5.58×10^5 g of PE $mol_{Cr}{}^{-1}$ h⁻¹ was reached at Al/Cr = 250 (entry 1). The Al/Cr ratio significantly affects both the polymer molecular weight and the molecular weight distribution. First, as the Al/Cr value increases, the molecular weight of the resulting PEs drops from 569500 to 2200 g/mol, likely due to the chain transfer of the growing polymer chain to the free AlMe₃ present in MAO. Second, the

relative amounts of the low-M_w ($^{LF}M_p$) and the high-M_w ($^{HF}M_p$) fractions significantly change. The SEC traces in Figure 4a clearly show a dramatic increase in the high-M_w PE
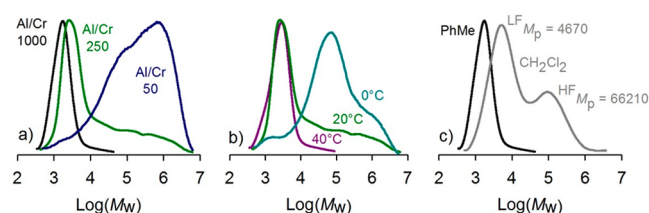

Figure 4. SEC traces (refractive index plots) for the PEs obtained by **Cr1**/MAO at different Al/Cr ratios (a) and polymerization temperatures (b) and with different solvents (c).

fraction as the Al/Cr ratio decreases. This result is reminiscent of the well-known behavior of Fe(II)-based catalysts[86] and Cr(II) and Cr(III) complexes bearing tridentate pyridine ligands.[32]

With a feed of 250 equiv of MAO, a series of polymerizations were carried out at different temperatures from 0 to 40 °C (Table 2, entries 1, 14, and 15). When the polymerization temperature was increased from 0 to 20 °C, the activity strongly increased from 1.16 to 5.58×10^5 g of PE $mol_{Cr}{}^{-1}$ h⁻¹ (entries 14 and 1, respectively). A further increase to 40 °C leads to a decreased activity while a high level of productivity is maintained (entry 15). This may be due to the increased instability of the Cr−alkyl bond and the lower solubility of ethylene in the reaction medium at higher temperatures. The same trend was also encountered for chromium complexes bearing 2-benzimidazolyl-*N*-phenylquinoline-8-carboxamide[83] and 2-benzimidazolyl-6-aryliminopyridine ligands,[87] which exhibited the best productivity at room temperature. This strong reduction in activity with an increase in the polymerization temperature correlates with the dominant chain transfer.[80] The molecular weight of the resulting PEs decreases from 275300 to 3600 g/mol with an increase in the polymerization temperature, an effect that is common to most metallocene and post-metallocene catalysts as well.[88,89] This effect may be likely due to the higher tendency to give β-H elimination at a last enchained ethylene unit followed by chain transfer, and it is explained by a lower activation energy of β-H elimination in comparison to that for chain propagation with an increase in the reaction temperature. Moreover, the relative amounts of the low-M_w and the high-M_w fractions change significantly. The SEC traces in Figure 4b clearly show a dramatic increase in the high-M_w PE fraction as the polymerization temperature is decreased.

We have also attempted to utilize dichloromethane as a solvent, since toluene is known to occasionally have a poisoning effect (Table 2, entry 16).[38,90] The choice of medium solvent does not dramatically affect the activity (entry 16 vs entry 12). In contrast, the use of dichloromethane has a strong effect on the polymer molecular weight and molecular weight distribution. The SEC trace of the polymer generated in dichloromethane clearly shows a bimodal character, with the low-M_w and high-M_w components centered at 4670 and 66210 g/mol, respectively (Figure 4c, gray line). In contrast, for the polymer generated in toluene under the same conditions, a large fraction of the molecular weight distribution can be described by a single component with a low molecular weight ($M_w = 2200$, $M_p = 1700$, and $M_w/M_n = 1.5$) and the peak was only slightly broadened at its low-molecular-weight side (Figure 4c, black line).

The heterogeneous composition of the obtained polymers is reflected in their thermal properties. The DSC heating curves of the PEs crystallized from the melt at 20 °C/min are reported in Figure 5. The PEs with higher molecular weight,
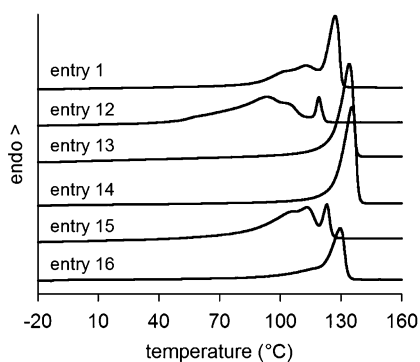

Figure 5. DSC profile of selected PEs obtained with **Cr1**/MAO.

regardless of their molecular weight distribution, show a single melting event with a maximum at about 135 °C (Table 2, entries 13 and 14). In contrast, the PEs with a low molecular weight, and even more those with a broad molecular weight distribution, exhibit multiple endotherms upon heating (entries 1, 5, and 6 in Table 1, and entries 12 and 15 in Table 2). The enthalpy of fusion, which ranges from 210 to 230 J/g, denotes a bulk crystallinity higher than 70%, in agreement with the crystallinity determined by XRD (Figure S4).

2.3. Polymerization of Norbornene and Dicyclopentadiene. We investigated the ability of **Cr1**–**Cr4** to polymerize the two different cyclic olefins NB and DCPD. Unlike ethylene, the insertion of these cyclic olefins at the Cr–alkyl bond prevents β-H elimination for stereoelectronic reasons, avoiding the alignment in a syn coplanar arrangement of the metal–C_α and C_β–H bonds, according to Bredt's rule. The results are summarized in Table 3.

All of the complexes, upon activation with MAO, proved to be active, affording solid NB and DCPD oligomers with molecular weights from 970 to 6590 g/mol. In particular, **Cr1** and **Cr4**, both ligated by the aldimine **L1**, were highly and almost equally active. In contrast, the ketimine **L3** shuts down the activity of **Cr3**, particularly for DCPD. Likewise, a detrimental effect on the activity was observed for **Cr2** ligated by the aldimine **L2** having bulky substituents at the aniline. We speculate that steric effects play a fundamental role because of

Table 3. Polymerization of NB and DCPD Catalyzed by Cr1–Cr4[a]

| entry	Cr	monomer	yield (g)	yield (%)	M_w[b]	M_w/M_n[b]
17	**Cr1**	NB	1.14	84	970	1.2
18		DCPD	1.10	46	1600	1.1
19	**Cr2**	NB	0.45	33	6590	3.9
20		DCPD	0.10	10	c	c
21	**Cr3**	NB	0.58	42	1270	1.5
22		DCPD	traces			
23	**Cr4**	NB	1.10	81	1410	1.1
24		DCPD	0.99	43	1400	1.1

[a]Polymerization conditions: NB, 1.35 g; DCPD, 2.36 g; total volume, 18 mL (toluene); Cr, 10 μmol; MAO as cocatalyst; Al/Cr = 1000; time, 24 h. [b]Average molecular weight (M_w) and molecular weight distribution (M_w/M_n) by SEC. [c]Not determined.

enhanced repulsion between the increased bulkiness of the ortho substituents and the monomer, particularly for bulkier DCPD, reducing the propagation rate.[83,91,92]

Overall, regardless of the ligand electronic structure and the chromium oxidation state, all the complexes are, albeit to a different extent, active for the polymerization of NB and DCPD, while **Cr2**–**Cr4** were not active in the polymerization of ethylene (Table 1). This nicely corroborates the hypothesis about the poor stability of the catalytically active intermediate upon the ethylene insertion for **Cr2**–**Cr4**. As also illustrated in Figure 3c,d, in the case of **Cr3** this may be the consequence of the rapid transformation (or ligand rearrangement) of $[(\mathbf{L3}^\bullet)CrCl_2(THF)]^-$ species when it reacts with MAO, which seems to favor faster chain termination over chain propagation. Otherwise, in the case of **Cr2** and **Cr4** the *lack of communication* between chromium and the ligand may disadvantage the polymer chain growth and may facilitate ethylene displacement or faster termination paths involving β-H elimination, which is prohibited in the case of cyclic olefin polymerization.

The FT-IR spectra of NB oligomers show characteristic absorption bands at 2942 (s), 2865 (m), 1451 (m), 1294 (w), 1110 (w), and 891 (w) cm^{-1} (Figure S5). The absence of any band at 1680–1620 cm^{-1}, characteristic of the unsaturated NB ring, demonstrates that the oligomerization of NB occurs by a 2,3-vinyl type addition (Scheme 5).[93] The FT-IR spectra of

Scheme 5. Vinyl-Type Addition Polymerization of NB and DCPD

cis 2,3-exo vinyl addition
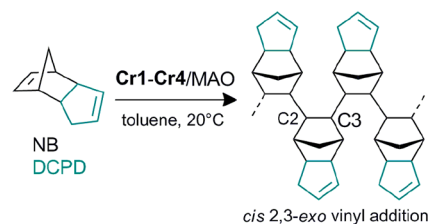
DCPD oligomers show characteristic absorption bands at 3038 (s), 2933–2865 (s), 1613 (w), 1457 (m), 942 (m), 737 (s), and 696 (s) cm^{-1} (Figure S6). The presence of bands at 3038 and 1613 cm^{-1} and the absence of any band at about 1580 cm^{-1} indicate that all of the bicycloheptene double bonds were consumed during the oligomerization.[94] The remaining unsaturations are entirely due to the cyclopentene double bond: the bands at 3038 and 1613 cm^{-1} are characteristic of

Table 4. Polymerization of 1,3-Butadiene Catalyzed by Cr1−Cr4[a]

entry	Cr	yield (g)	yield (%)	M_w^b (×10³)	M_w/M_n^b	microstructure (%)[c] cis-1,4/trans-1,4/1,2	T_g^d (°C)
25	**Cr1**	1.37	98	428.9	2.0	52/12/36	−85
26	**Cr2**	1.40	100	323.0	1.5	2/66/32	−64
27[e]	**Cr3**	0.13	10	248.7	2.0	16/17/67	−56
28[f]	**Cr4**	1.20	90	503.8	1.9	54/13/33	−85

[a]Polymerization conditions unless specified otherwise: 1,3-butadiene, 1.4 g; total volume, 18 mL (toluene); Cr, 10 μmol; MAO as cocatalyst; Al/Cr = 1000; time, 2 h. [b]Average molecular weight (M_w) and molecular weight distribution (M_w/M_n) by SEC. [c]By ¹³C NMR and ATR-IR in the case of entry 27. [d]Glass transition temperature (T_g) by DSC. [e]Polymerization time 4.5 h. [f]Polymerization time 1 h.

the olefinic =C−H and C=C stretching vibrations, respectively. The absorption band at 942 cm⁻¹ is assigned to the bending of the C−H bonds in the ring system of NB, thus confirming that also the oligomerization of DCPD occurs through a 2,3-addition rather than via ROMP (Scheme 5).[95]

The obtained products were characterized by thermal analysis. DSC scans carried out from −40 to 200 °C did not show any thermal event. TGA performed under inert atmosphere evidenced that NB and DCPD oligomers are thermally stable up to about 220 °C (Figure S7).

2.4. Polymerization of 1,3-Butadiene. We also attempted to use 1,3-butadiene as a monomer for the catalytic run. The results are summarized in Table 4. Despite the different ligand redox states and structures, **Cr1**, **Cr2**, and **Cr4**, ligated by the aldimine **L1** and **L2**, gave an almost quantitative conversion in less than 2 h, affording high-molecular-weight poly(1,3-butadiene)s with a mixed 1,4/1,2 structure. It can be inferred that such a different behavior among the polymerizations of 1,3-butadiene and ethylene for **Cr1** (the only catalyst active in the polymerization of ethylene), **Cr2**, and **Cr4** is reasonably ascribed to the enhanced stability of chromium−monomer (or growing chain) interactions, which are of the allylic type in the case of the more electron rich 1,3-butadiene while of the σ type in the case of ethylene.

Cr1 and **Cr4**, bearing the same ligand **L1**, produced polymers with almost the same microstructure, the 1,4/1,2 ratios being in the range from 64/36 to 67/33 (Table 4, entries 25 and 28, respectively) (¹H and ¹³C NMR spectra are reported in Figure S8). This suggests that the different ligand redox states found for these two complexes did not significantly affect the chemoselectivity: i.e., the formation of 1,4- or 1,2-units. Interestingly, for the aniline-substituted **Cr2**, a strong inversion in cis-1,4/trans-1,4 selectivity was observed, the trans-1,4 content increasing with respect to the substituent-free **Cr1** and **Cr4**. This intriguing behavior could be attributed to a preferred trans-η^2 coordination of 1,3-butadiene in the presence of the bulky **L2**, with the consequent formation of a syn allylic unit, giving rise to a trans-1,4- or 1,2-unit, depending on the insertion of the monomer at C1 or C3 of the allylic unit, respectively (Scheme 6).[96] A faster anti−syn isomerization of the last polymerized unit, with respect to the insertion of the new incoming monomer on the allylic group, could be also responsible for the preferred formation of trans-1,4 units. Generally, the anti−syn isomerization occurs with a significant decrease in the polymerization rate, as reported, for instance, for the polymerization of isoprene by V(acac)₃/MAO.[97] In our case we do not observe such a reduction, and that is why we tend to favor the first hypothesis.

In contrast, for **Cr3**, ligated by the substituent-free methylketimine **L3**, the reactivity strongly decreased with respect to the analogous aldimine compounds (Table 4, entry 27). The substitution of hydrogen by a methyl group at the imine

Scheme 6. Simplified Scheme for the Formation of a cis- or trans-1,4 Monomeric Unit[a]
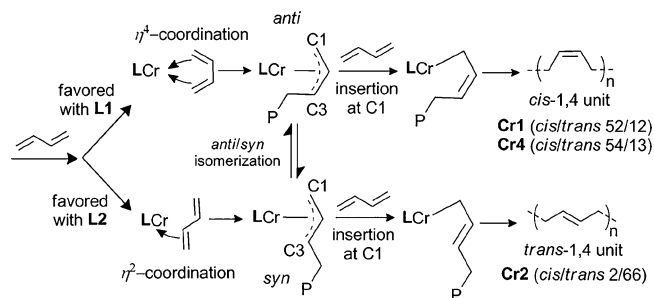
[a]P = polymer chain.

moiety shuts down the activity. This different behavior exhibited by aldimine and ketimine compounds in the polymerization of 1,3-butadiene was not surprising; Bai and Hu have previously attributed this poisoning effect of ketimine ligands to a different ligand reorganization in the presence of the Al activator.[50] Moreover, it is tempting to attribute this result to the evolution product of **Cr3** in the presence of MAO, as shown by UV−vis−NIR spectroscopy (Figure 3c,d).

Glass transition temperatures (T_g values) of the obtained polymers varied from −85 to −56 °C, depending on their microstructure. Samples in Table 4, entries 25 and 28, with the highest content of cis-1,4 units show the lowest T_g value, while the sample in entry 27, the polymer richest in 1,2-units, has the highest value (Figure S9).

3. CONCLUSIONS

In this paper, we report the synthesis and the characterization of a series of chromium-iminopyridine complexes with the metal in the *formal* oxidation states +2 by reaction of CrCl₂ with ligands of the type 2,6-R¹₂C₆H₃N=CR²(C₅H₃N) (R¹ = R² = H (**L1**); R¹ = iPr, R² = H (**L2**); R¹ = H, R² = CH₃ (**L3**)) and +3 by reaction of CrCl₃(THF)₃ with **L1**. The iminopyridines differ in the nature of substituents at the iminic carbon and at the ortho positions of the aryl ring, but feature similar electron-accepting properties. UV−vis−NIR absorption spectroscopy showed that a redistribution of the electron density from the chromium ion to the ligand takes place through a concerted one-electron transfer. This phenomenon occurs for CrCl₂ ligated by unsubstituted aldimine **L1** (**Cr1**) and ketimine **L3** (**Cr3**) and gives rise to the formation of *physical* trivalent chromium complexes with the ligand in the monoanionic radical (L•)⁻ state. In contrast, metal to ligand electron transfer does not occur with CrCl₂ ligated by the ortho-substituted aldimine **L2** (**Cr2**), because bulky isopropyl substituents prevent an efficient electronic delocalization, nor with CrCl₃(THF)₃ ligated by **L1** (**Cr4**).

The redox-active ligand and the chromium to ligand synergy have a significant influence on the reactivity of chromium-iminopyridine complexes (Scheme 7). The occurrence of a

Scheme 7. Simplified Scheme Summarizing the Results from the Polymerization of Ethylene Catalyzed by Cr1–Cr4/MAO[a]
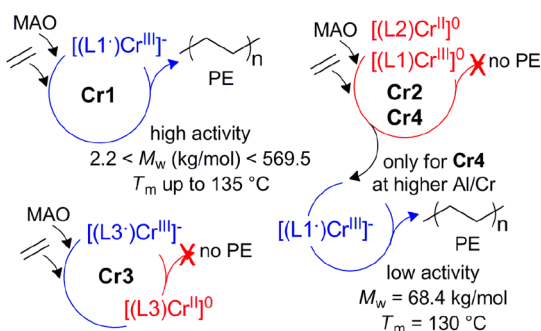
[a]**Cr1** and **Cr4** are both ligated by **L1**.

concerted chromium to ligand electron transfer, coupled with a good stability of the $[(L^{\bullet})Cr^{III}]^{-}$ species in the presence of the Al activator—both investigable by UV−vis−NIR spectroscopy—were proved to be two essential conditions in facilitating the polymerization of ethylene. Both conditions are fulfilled only by **Cr1**. For **Cr3**, only the first condition is fulfilled, while the $[(L3^{\bullet})Cr^{III}]^{-}$ intermediate is too unstable in the presence of the aluminum alkyl and is quickly deactivated. **Cr2** and **Cr4** do not satisfy the first requirement, although **Cr4** displays a low activity with an increase in the Al/Cr ratio, which has been associated with its reduction to the transient $[(L1^{\bullet})Cr^{III}]^{-}$ "active" intermediate. The ability of **Cr1** to give high-M_w PEs was completely unexpected, since iminopyridine ligands were believed to have the right "structural" motif to generate complexes for the oligomerization of ethylene but not for its polymerization.[14]

The concerted cooperation between the metal and the ligand has proven to be particularly fruitful in the polymerization of ethylene, while the chromium to ligand synergy does not affect the reactivity toward cyclic olefins and 1,3-butadiene. This is explainable by considering that (i) unlike the case for ethylene, the cyclic olefin insertion prevents β-H elimination for stereoelectronic reasons and (ii) the chromium−monomer (or growing chain) interactions have different natures, of the σ type in the case of ethylene but of the allylic type in the case of 1,3-butadiene. In contrast, steric ligand effects play a key role: the presence of bulky ortho substituents shuts down the activity, particularly for the bulkier DCPD, and reverses the catalyst chemoselectivity in the polymerization of 1,3-butadiene.

In conclusion, the tendency of chromium to foster one-electron transfer to the iminopyridine ligand and the ligand/monomer steric factors are claimed to be central in the polymerization of (di)olefins. The great versatility of the iminopyridine chromium complexes in terms of structure of the ligands and electronic properties of the metal centers makes them a powerful tool for tuning the polymer properties, depending on the specific application. Furthermore, with these starting compounds and data about their electronic structures in hand, we plan to extend our study to other chromium derivatives and to employ a variety of computational and

experimental techniques. These would be introduced in the future.

4. EXPERIMENTAL SECTION

4.1. General Procedures and Materials. Manipulations of air- and/or moisture-sensitive materials were carried out under an inert atmosphere using a dual vacuum/nitrogen line and standard Schlenk-line techniques with oven-dried glassware. Nitrogen and ethylene were purified by passage over columns of $CaCl_2$, molecular sieves, and BTS catalysts. THF (Aldrich ≥99.9%) was refluxed over Na/benzophenone alloy for 8 h and then distilled and stored over molecular sieves. Toluene (Aldrich >99.5%) was refluxed over Na for 8 h and then distilled and stored over molecular sieves. Pentane (Aldrich >99%) was refluxed over Na/K alloy for 8 h and then distilled and stored over molecular sieves. Diethyl ether (Aldrich ≥99.8%) was refluxed over Na for 8 h and then distilled. Dichloromethane (Aldrich ≥99.9%) was degassed under vacuum and then by bubbling nitrogen, kept over molecular sieves, and used without any further purification. NB (Sigma-Aldrich 99% pure) was stirred over molten potassium at 80 °C under nitrogen for 4 h and then distilled. A stock solution was prepared by dissolving 50 g of freshly distilled NB in 86.2 mL of toluene. DCPD (Aldrich 95% pure) was dried over CaH_2 at 60 °C under nitrogen for 4 h and then distilled under reduced pressure. 1,3-Butadiene (Aldrich ≥99%) was evaporated from the container prior to each run, dried by passing through a column packed with molecular sieves, and condensed into the reactor which had been precooled to −20 °C. MAO (Aldrich, 10 wt % solution in toluene), $CrCl_2$ (Aldrich 99.99%), $Cr(acac)_3$ (acac = acetylacetonate, Aldrich 99.99%), and deuterated solvent for NMR measurements $(C_2D_2Cl_4)$ (Aldrich, >99.5% atom D) were used as received. $CrCl_3(THF)_3$ was prepared through the Soxhlet extraction of anhydrous $CrCl_3$ with boiling THF and the aid of Zn dust. The iminopyridine ligands were synthesized following a methodology previously reported.[48]

4.2. Synthesis of Chromium Complexes. All of the chromium complexes were synthesized following the method reported in the literature for analogous compounds.[44] The general procedure is reported for **Cr1**.

4.2.1. Dichloro(N-(pyridin-2-ylmethylene)aniline)chromium−THF (Cr1). To a stirred suspension of $CrCl_2$ (0.24 g, 2.0 mmol) in 25 mL of THF at room temperature was added **L1** ligand (0.44 g, 2.4 mmol). The suspension was stirred for 24 h and then filtered. The residue on the filter was thoroughly washed with pentane (3 × 25 mL), dried under vacuum, and stored under nitrogen in a Schlenk tube. The dark brown solid **Cr1** was dried overnight in vacuo. Yield (based on $CrCl_2$): 92%. FT-IR ν (cm^{-1}): 1592 (w), 1485 (m), 1433 (w), 1366 (s), 1246 (w), 1174 (m), 1126 (s), 1087 (s), 971 (s), 887 (s), 864 (s), 761 (s), 692 (m), 666 (m), 640 (m), 564 (s), 545 (s). Anal. Calcd for $C_{16}H_{18}Cl_2CrN_2O$: C, 50.94; H, 4.81; N, 7.43. Found: C, 49.68; H, 4.17; N, 7.25. The differences between C, H found and C, H calculated values are likely due to the volatile THF and the incomplete combustion that can cause inaccurate results. Such deviation from the calculated values has been reported for many other chromium complexes.[32,44]

4.2.2. Dichloro(2,6-diisopropyl-N-(pyridin-2-ylmethylene)-aniline)chromium−THF (Cr2). Dark green solid, yield 70%. FTIR ν (cm^{-1}): 1592 (m), 1465 (m), 1365 (m), 1294 (m), 1230 (w), 1171 (w), 1110 (w), 1057 (m), 1012 (m), 913 (m), 865 (s), 813 (s), 777 (vs), 767 (m), 654 (w), 541 (w), 509 (m). Anal. Calcd for $C_{22}H_{30}Cl_2CrN_2O$: C, 57.27; H, 6.55; N, 6.07. Found: C, 57.0; H, 6.20; N, 6.35.

4.2.3. Dichloro(N-(1-(pyridin-2-ylethylidene)aniline)chromium−THF (Cr3). Dark gray solid, yield 94%. FT-IR ν (cm^{-1})L 1592 (m), 1486 (m), 1437 (m), 1387 (m), 1377 (m), 1351 (w), 1290 (m), 1213 (s), 1140 (s), 1075 (m), 932 (s), 909 (vs), 814 (vs), 789 (s), 732 (s), 700 (s), 666 (m), 636 (s), 616 (m), 551 (m), 522 (m). Anal. Calcd for $C_{17}H_{20}Cl_2CrN_2O$: C, 52.19; H, 5.15; N, 7.16. Found: C, 52.26; H, 5.15; N, 7.15.

4.2.4. Trichloro(N-(pyridin-2-ylmethylene)aniline)chromium−THF (Cr4). The same complexation procedure as for **Cr1** was

employed for **Cr4** but using a $CrCl_3(THF)_3$ source. After drying, a light green solid was isolated. Yield (based on $CrCl_3(THF)_3$): 77%. FT-IR ν (cm^{-1}): 1595 (m), 1481 (m), 1448 (m), 1361 (m), 1296 (w), 1272 (w), 1235 (w), 1200 (m), 1105 (w), 1072 (w), 1010 (m), 931 (w), 908 (w), 861 (s), 782 (vs), 770 (s), 745 (w), 699 (s), 653 (w), 574 (w), 554 (m), 503 (m). Anal. Calcd for $C_{16}H_{18}Cl_3CrN_2O$: C, 46.57; H, 4.40; N, 6.79. Found: C, 46.25; H, 4.35; N, 6.90. ^1H NMR ($C_2D_2Cl_4$) broad peaks δ (ppm): 5.211 (1H), 3.142 (2H), 1.299 (2H).

4.3. Polymerization Procedures. Polymerization of ethylene was carried out in a 50 mL round-bottomed Schlenk flask, while the polymerization of NB, DCPD, and 1,3-butadiene was carried out in a 25 mL Schlenk tube. Prior to the start of polymerization, the reactor was heated to 110 °C under vacuum for 1 h and back-filled with nitrogen. For the ethylene polymerization, the reactor was charged at room temperature with toluene and MAO in that order. After thermal equilibration at the desired temperature, the solution was degassed, and ethylene was added until saturation. Polymerization was started by adding a fine toluene slurry (2 mg mL^{-1}) of the chromium complex via syringe under a continuous flow of ethylene. For the polymerization of NB, DCPD, and 1,3-butadiene, the monomer and toluene were transferred into the reactor, the solution was brought to the desired polymerization temperature, and then MAO and a toluene solution (2 mg mL^{-1}) of the chromium complex were added in that order. In the case of 1,3-butadiene, it was first condensed into the 25 mL Schlenk tube kept at −20 °C. Polymerizations were stopped with methanol containing a small amount of hydrochloric acid; the precipitated polymers were collected by filtration, repeatedly washed with fresh methanol, and finally dried under vacuum at room temperature to constant weight.

In all of the reactions investigated, no polymerization activity was observed in the absence of a chromium source.

4.4. Characterization Methods. Elemental analyses were performed by using a Perkin-Elmer CHN Analyzer 2400 Series II instrument.

NMR spectra were recorded on a Bruker NMR Advance 400 spectrometer equipped with a SEX 10 mm probe with automatic matching and tuning, operating at 400 MHz (^1H) and 100.58 MHz (^{13}C) in the PFT mode at 103 °C. Experiments were performed by dissolving 70 mg of polymer in $C_2D_2Cl_4$ in a 10 mm tube and referenced to HMDS as internal standard.

FT-IR spectra were acquired in attenuated total reflectance (ATR) mode, in the spectral range of 7000−400 cm^{-1}, using a Bruker Alpha spectrophotometer equipped with a diamond ATR crystal. The instrument was placed inside the glovebox to avoid sample contamination.

UV−vis−NIR absorption spectra were collected using a Cary5000 spectrophotometer. Both the pure ligands and the chromium complexes were dissolved in chloroform, and the solutions were measured inside homemade cells equipped with windows in optical quartz (Suprasil), which were filled inside the glovebox and closed with Teflon plugs. The spectrum of the solvent was measured under the same conditions and subtracted from those of the samples.

Single-crystal X-ray diffraction data were recorded at room temperature using a Bruker X8 Prospector APEX-II/CCD diffractometer equipped with a focusing mirror (Cu Kα radiation, λ = 1.54056 Å). The structures were determined using direct methods and refined (based on F^2 using all independent data) by full-matrix least-squares methods (SHELXTL 97).[98,99] All non-hydrogen atoms were located from different Fourier maps and refined with anisotropic displacement parameters. Hydrogen atoms were added in riding positions. Specific structure determination details are included in the Supporting Information.

Molecular weight (M_w) and molecular weight distribution (M_w/M_n) were obtained by a high-temperature Waters GPCV2000 size exclusion chromatography (SEC) system using an online refractometer detector. The experimental conditions consisted of three PL Gel Olexis columns, o-dichlorobenzene as the mobile phase, 0.8 mL/min flow rate, and 145 °C temperature. The calibration of the SEC system was constructed using 18 narrow M_w/M_n PS standards with

M_w values ranging from 162 to 5.6×10^6 g/mol. For SEC analysis, about 12 mg of polymer was dissolved in 5 mL of o-dichlorobenzene.

Wide-angle X-ray diffraction (XRD) experiments were performed at 25 °C under nitrogen flux, using a Siemens D-500 diffractometer equipped with Soller slits (2°) placed before the sample, 0.3° aperture and divergence windows, and a VORTEX detector with extreme energy resolution specific for thinner films. Cu Kα radiation at 40 kV × 40 mA power was adopted; each pattern was carried out with steps of 0.05° (2θ) and 6 s measurement time.

Differential scanning calorimetry (DSC) measurements were performed on a Perkin-Elmer DSC 8000 instrument equipped with a liquid nitrogen device. The scans were carried out from −100 to 200 °C under a nitrogen atmosphere using heating and cooling rates of 20 °C/min.

Thermogravimetric analysis (TGA) was performed on a Perkin-Elmer TGA-7 instrument under a nitrogen atmosphere. Before the TGA run was performed, the sample (2−3 mg) was held at 50 °C for 30 min; the scan was carried out from 50 to 700 °C at a heating rate of 10 °C/min.

■ ASSOCIATED CONTENT

Ⓢ Supporting Information

The Supporting Information is available free of charge on the ACS Publications website at DOI: 10.1021/acs.organomet.8b00812.

    FT−IR, NMR, XRD, TGA, and DSC spectra (PDF)

    Three-dimensional structure of **Cr4** (XYZ)

Accession Codes

CCDC 1538683 contains the supplementary crystallographic data for this paper. These data can be obtained free of charge via www.ccdc.cam.ac.uk/data_request/cif, or by emailing data_request@ccdc.cam.ac.uk, or by contacting The Cambridge Crystallographic Data Centre, 12 Union Road, Cambridge CB2 1EZ, UK; fax: +44 1223 336033.

■ AUTHOR INFORMATION

Corresponding Authors

*E-mail for G.L.: giuseppe.leone@ismac.cnr.it.
*E-mail for E.G.: elena.groppo@unito.it.

ORCID ⓘ

Giuseppe Leone: 0000-0001-6977-2920
Elena Groppo: 0000-0003-4153-5709
Giorgia Zanchin: 0000-0003-0161-4963
Emilio Parisini: 0000-0002-5529-0039
Giovanni Ricci: 0000-0001-8586-9829

Present Address

‖J.M.-R.: Dipartimento di Chimica Materiali e Ingegneria Chimica "Giulio Natta", Politecnico di Milano, Via Luigi Mancinelli 7, 20131 Milan, Italy.

Notes

The authors declare no competing financial interest.

■ REFERENCES

(1) Eagan, J. M.; Xu, J.; Di Girolamo, R.; Thurber, C. M.; Macosko, C. W.; LaPointe, A. M.; Bates, F. S.; Coates, G. W. Combining Polyethylene and Polypropylene: Enhanced Performance with PE/iPP Multiblock Polymers. *Science* **2017**, *355*, 814−816.

(2) Peng, D.; Yan, X.; Yu, C.; Zhang, S.; Li, X. Transition Metal Complexes Bearing Tridentate Ligands for Precise Olefin Polymerization. *Polym. Chem.* **2016**, *7*, 2601−2634.

(3) Stürzel, M.; Mihan, S.; Mülhaupt, R. From Multisite Polymerization Catalysis to Sustainable Materials and All-Polyolefin Composites. *Chem. Rev.* **2016**, *116*, 1398−1433.

(4) Busico, V. Ziegler-Natta Catalysis: Forever Young. *MRS Bull.* **2013**, *38*, 224−228.

(5) Small, B. L. Discovery and Development of Pyridine-bis(imine) and Related Catalysts for Olefin Polymerization and Oligomerization. *Acc. Chem. Res.* **2015**, *48*, 2599−2611.

(6) Baier, M. C.; Zuideveld, M. A.; Mecking, S. Post-Metallocenes in the Industrial Production of Polyolefins. *Angew. Chem., Int. Ed.* **2014**, *53*, 9722−9744.

(7) Hogan, J. P.; Banks, R. L. U.S. Patent No. 2825721 (Phillips Petroleum Co.), 1954.

(8) Karapinka, G. L. US Patent No. 3709853 (Union Carbide Corp.), 1973.

(9) McDaniel, M. P. A Review of the Phillips Supported Chromium Catalyst and Its Commercial Use for Ethylene Polymerization. *Adv. Catal.* **2010**, *53*, 123−606.

(10) Groppo, E.; Lamberti, C.; Bordiga, S.; Spoto, G.; Zecchina, A. The Structure of Active Centers and the Ethylene Polymerization Mechanism on the Cr/SiO2 Catalyst: A Frontier for the Characterization Methods. *Chem. Rev.* **2005**, *105*, 115−183.

(11) Tomov, A. K.; Nobbs, J. D.; Chirinos, J. J.; Saini, P. K.; Malinowski, R.; Ho, S. K. Y.; Young, C. T.; McGuinness, D. S.; White, A. J. P.; Elsegood, M. R. J.; Britovsek, G. J. P. Alternating α-Olefin Distributions via Single and Double Insertions in Chromium-Catalyzed Ethylene Oligomerization. *Organometallics* **2017**, *36*, 510−522.

(12) Peulecke, N.; Müller, B. H.; Spannenberg, A.; Höhne, M.; Rosenthal, U.; Wöhl, A.; Müller, W.; Alqahtani, A.; Al Hazmi, M. Ligands with an NPNPN-Framework and Their Application in Chromium Catalysed Ethene Tri-/Tetramerization. *Dalton Trans.* **2016**, *45*, 8869−8874.

(13) Sydora, O. L.; Jones, T. C.; Small, B. L.; Nett, A. J.; Fischer, A. A.; Carney, M. J. Selective Ethylene Tri-/Tetramerization Catalysts. *ACS Catal.* **2012**, *2*, 2452−2455.

(14) McGuinness, D. S. Olefin Oligomerization via Metallacycles: Dimerization, Trimerization, Tetramerization, and Beyond. *Chem. Rev.* **2011**, *111*, 2321−2341.

(15) Gibson, V. C.; Spitzmesser, S. K. Advances in Non-Metallocene Olefin Polymerization Catalysis. *Chem. Rev.* **2003**, *103*, 283−315.

(16) Agapie, T.; Labinger, J. A.; Bercaw, J. Mechanistic Studies of Olefin and Alkyne Trimerization with Chromium Catalysts: Deuterium Labeling and Studies of Regiochemistry Using a Model Chromacyclopentane Complex. *J. Am. Chem. Soc.* **2007**, *129*, 14281−14295.

(17) Rozenel, S. S.; Chomitz, W. A.; Arnold, J. Chromium Complexes Supported by the Multidentate Monoanionic N₂P₂ Ligand: Reduction Chemistry and Reactivity with Ethylene. *Organometallics* **2009**, *28*, 6243−6253.

(18) McGuinness, D. S.; Wasserscheid, P.; Keim, W.; Morgan, D.; Dixon, J. T.; Bollmann, A.; Maumela, H.; Hess, F.; Englert, U. First Cr(III)−SNS Complexes and Their Use as Highly Efficient Catalysts for the Trimerization of Ethylene to 1-Hexene. *J. Am. Chem. Soc.* **2003**, *125*, 5272−5273.

(19) Agapie, T.; Schofer, S. J.; Labinger, J. A.; Bercaw, J. E. Mechanistic Studies of the Ethylene Trimerization Reaction with Chromium−Diphosphine Catalysts: Experimental Evidence for a Mechanism Involving Metallacyclic Intermediates. *J. Am. Chem. Soc.* **2004**, *126*, 1304−1305.

(20) McGuinness, D. S.; Wasserscheid, P.; Morgan, D. H.; Dixon, J. T. Ethylene Trimerization with Mixed-Donor Ligand (N,P,S) Chromium Complexes: Effect of Ligand Structure on Activity and Selectivity. *Organometallics* **2005**, *24*, 552−556.

(21) Jones, D. J.; Gibson, V. C.; Green, S. M.; Maddox, P. J. Discovery of a New Family of Chromium Ethylene Polymerisation Catalysts Using High Throughput Screening Methodology. *Chem. Commun.* **2002**, 1038−1039.

(22) Hao, Z.; Xu, B.; Gao, W.; Han, Y.; Zeng, G.; Zhang, J.; Liand, G.; Mu, Y. Chromium Complexes with N,N,N-Tridentate Quinolinyl Anilido-Imine Ligand: Synthesis, Characterization, and Catalysis in Ethylene Polymerization. *Organometallics* **2015**, *34*, 2783−2790.

(23) Köhn, R. D.; Haufe, M.; Kociok-Köhn, G.; Grimm, S.; Wasserscheid, P.; Keim, W. Selective Trimerization of α-Olefins with Triazacyclohexane Complexes of Chromium as Catalysts. *Angew. Chem., Int. Ed.* **2000**, *39*, 4337−4339.

(24) Rüther, T.; Cavell, K. J.; Braussaud, N. C.; Skelton, B. W.; White, A. H. Synthesis, Characterisation and Catalytic Behaviour of a Novel Class of Chromium(III) and Vanadium(III) Complexes Containing Bi- And Tri-Dentate Imidazole Chelating Ligands: A Comparative Study. *Dalton Trans.* **2002**, 4684−4693.

(25) Wasserscheid, P.; Grimm, S.; Köhn, R. D.; Haufe, M. Synthesis of Synthetic Lubricants by Trimerization of 1-Decene and 1-Dodecene with Homogeneous Chromium Catalysts. *Adv. Synth. Catal.* **2001**, *343*, 814−818.

(26) Ackerman, L. J.; Bei, X.; Boussie, T. R.; Diamond, G. M.; Hall, K. A.; Lapointe, A. M.; Longmire, J. M.; Murphy, V. J.; Sun, P.; Verdugo, D.; Schofer, S.; Dias, E.; McConville, D. H.; Li, R. T.; Walzer, J.; Rix, F.; Kuchta, M. WO 2006/096881 (Exxon-Mobil), 2006.

(27) MacAdams, L. A.; Buffone, G. P.; Incarvito, C. D.; Rheingold, A. L.; Theopold, K. H. A Chromium Catalyst for the Polymerization of Ethylene as a Homogeneous Model for the Phillips Catalyst. *J. Am. Chem. Soc.* **2005**, *127*, 1082−1083.

(28) Gibson, V. C.; Newton, C.; Redshaw, C.; Solan, G. A.; White, A. J. P.; Williams, D. J.; Maddox, P. J. Chromium(III) Complexes Bearing N,N-Chelate Ligands As Ethene Polymerization Catalysts. *Chem. Commun.* **1998**, 1651−1652.

(29) Albahily, K.; Al-Baldawi, D.; Gambarotta, S.; Duchateau, R.; Koç, E.; Burchell, T. J. Preparation and Characterization of a Switchable Single-Component Chromium Trimerization Catalyst. *Organometallics* **2008**, *27*, 5708−5711.

(30) Reagan, W. K. EP 0417477 (Phillips Petroleum Co.), 1991.

(31) Emrich, R.; Heinemann, O.; Jolly, P. W.; Krüger, C.; Verhovnik, G. P. J. The Role of Metallacycles in the Chromium-Catalyzed Trimerization of Ethylene. *Organometallics* **1997**, *16*, 1511−1513.

(32) Small, B. L.; Carney, M. J.; Holman, D. M.; O'Rourke, C. E.; Halfen, J. A. New Chromium Complexes for Ethylene Oligomerization: Extended Use of Tridentate Ligands in Metal-Catalyzed Olefin Polymerization. *Macromolecules* **2004**, *37*, 4375−4386.

(33) Turki, T.; Guerfel, T.; Bouachir, F. Synthesis, Characterization and Crystal Structure of Diamagnetic Tetracoordinated Chromium (II) Complexes Supported by α-Diimine Ligands. *Inorg. Chem. Commun.* **2006**, *9*, 1023−1025.

(34) Barzan, C.; Piovano, A.; Braglia, L.; Martino, G. A.; Lamberti, C.; Bordiga, S.; Groppo, E. Ligands Make the Difference! Molecular Insights into Cr^{VI}/SiO$_2$ Phillips Catalyst during Ethylene Polymerization. *J. Am. Chem. Soc.* **2017**, *139*, 17064−17073.

(35) Groppo, E.; Martino, G. A.; Piovano, A.; Barzan, C. The active sites in the Phillips catalysts: origins of a lively debate and a vision for the future. *ACS Catal.* **2018**, *8*, 10846.

(36) Gunasekara, T.; Kim, J.; Preston, A.; Steelman, D. K.; Medvedev, G. A.; Delgass, W. N.; Sydora, O. L.; Caruthers, J. M.; Abu-Omar, M. M. Mechanistic Insights into Chromium-Catalyzed Ethylene Trimerization. *ACS Catal.* **2018**, *8*, 6810−6819.

(37) Temple, C.; Jabri, A.; Crewdson, P.; Gambarotta, S.; Korobkov, I.; Duchateau, R. The Question of the Cr Oxidation State in the {Cr(SNS)} Catalyst for Selective Ethylene Trimerization: An Unanticipated Re-Oxidation Pathway. *Angew. Chem.* **2006**, *118*, 7208−7211.

(38) Jabri, A.; Mson, C. B.; Sim, Y.; Gambarotta, S.; Burchell, T. J.; Duchateau, R. Isolation of Single-Component Trimerization and Polymerization Chromium Catalysts: The Role of the Metal Oxidation State. *Angew. Chem., Int. Ed.* **2008**, *47*, 9717−9721.

(39) Jabri, A.; Temple, C.; Crewdson, P.; Gambarotta, S.; Korobkov, I.; Duchateau, R. Role of the Metal Oxidation State in the SNS−Cr Catalyst for Ethylene Trimerization: Isolation of Di- and Trivalent Cationic Intermediates. *J. Am. Chem. Soc.* **2006**, *128*, 9238−9247.

(40) Conley, M. C.; Delley, M. F.; Siddiqi, G.; Lapadula, G.; Norsic, S.; Monteil, V.; Safonova, O. V.; Copéret, C. Polymerization of Ethylene by Silica-Supported Dinuclear Cr^{III} Sites through an Initiation Step Involving C−H Bond Activation. *Angew. Chem., Int. Ed.* **2014**, *53*, 1872−1876.

(41) Chakrabarti, A.; Gierada, M.; Handzlik, J.; Wachs, I. E. Operando Molecular Spectroscopy During Ethylene Polymerization by Supported CrO$_x$/SiO$_2$ Catalysts: Active Sites, Reaction Intermediates, and Structure-Activity Relationship. *Top. Catal.* **2016**, *59*, 725−739.

(42) Cicmil, D.; Meeuwissen, J.; Vantomme, A.; Weckhuysen, B. M. Real-time Analysis of a Working Triethylaluminium-Modified Cr/Ti/ SiO$_2$ Ethylene Polymerization Catalyst with In Situ Infrared Spectroscopy. *ChemCatChem* **2016**, *8*, 1937−1944.

(43) Morra, E.; Martino, G. A.; Piovano, A.; Barzan, C.; Groppo, E.; Chiesa, M. In Situ X- and Q-Band EPR Investigation of Ethylene Polymerization on Cr/SiO$_2$ Phillips Catalyst. *J. Phys. Chem. C* **2018**, *122*, 21531.

(44) Kreisel, K. A.; Yap, G. P. A.; Theopold, K. H. Synthesis, Characterization, and Electronic Structure of Diimine Complexes of Chromium. *Inorg. Chem.* **2008**, *47*, 5293−5303.

(45) Gao, J.; Zheng, Y.; Tang, Y.; Jehng, J.-M.; Grybos, R.; Handzlik, J.; Wachs, I. E.; Podkolzin, S. G. Spectroscopic and Computational Study of Cr Oxide Structures and Their Anchoring Sites on ZSM-5 Zeolites. *ACS Catal.* **2015**, *5*, 3078−3092.

(46) Fong, A.; Peters, B.; Scott, S. L. One-Electron-Redox Activation of the Reduced Phillips Polymerization Catalyst, via Alkylchromium-(IV) Homolysis: A Computational Assessment. *ACS Catal.* **2016**, *6*, 6073−6085.

(47) Fong, A.; Yuan, Y.; Ivry, S. L.; Scott, S. L.; Peters, B. Computational Kinetic Discrimination of Ethylene Polymerization Mechanisms for the Phillips (Cr/SiO$_2$) Catalyst. *ACS Catal.* **2015**, *5*, 3360−3374.

(48) Takahashi, T.; Tsai, F.-Y.; Li, Y.; Wang, H.; Kondo, Y.; Yamanaka, M.; Nakajima, K.; Kotora, M. Selective Preparation of Pyridines, Pyridones, and Iminopyridines from Two Different Alkynes via Azazirconacycles. *J. Am. Chem. Soc.* **2002**, *124*, 5059−5067.

(49) Köppl, A.; Alt, H. G. Substituted 1-(2-pyridyl)-2-azaethene-(N,N)-nickel dibromide complexes as catalyst precursors for homogeneous and heterogeneous ethylene polymerization. *J. Mol. Catal. A: Chem.* **2000**, *154*, 45−53.

(50) Dai, Q.; Jia, X.; Yang, F.; Bai, C.; Hu, Y.; Zhang, X. Iminopyridine-Based Cobalt(II) and Nickel(II) Complexes: Synthesis, Characterization, and Their Catalytic Behaviors for 1,3-Butadiene Polymerization. *Polymers* **2016**, *8*, 12−27.

(51) Boudier, A.; Breuil, P.-A. R.; Magna, L.; Olivier-Bourbigou, H.; Braunstein, P. Ethylene Oligomerization Using Iron Complexes: Beyond the Discovery of Bis(Imino)Pyridine Ligands. *Chem. Commun.* **2014**, *50*, 1398−1407.

(52) Kuwabara, J.; Takeuchi, D.; Osakada, K. Early−Late Heterobimetallic Complexes as Initiator for Ethylene Polymerization. Cooperative Effect of Two Metal Centers to Afford Highly Branched Polyethylene. *Chem. Commun.* **2006**, 3815−3817.

(53) Bianchini, C.; Giambastiani, G.; Mantovani, G.; Meli, A.; Mimeau, D. Oligomerisation of Ethylene to Linear α-Olefins by Tetrahedral Cobalt(II) Precursors Stabilised by Benzo[b]thiophen-2-yl-Substituted (Imino)Pyridine Ligands. *J. Organomet. Chem.* **2004**, *689*, 1356−1361.

(54) Britovsek, G. J. P.; Baugh, S. P. D.; Hoarau, O.; Gibson, V. C.; Wass, D. F.; White, A. J. P.; Williams, D. J. The Role of Bulky Substituents in the Polymerization of Ethylene Using Late Transition Metal Catalysts: A Comparative Study of Nickel and Iron Catalyst Systems. *Inorg. Chim. Acta* **2003**, *345*, 279−291.

(55) Luca, O. R.; Crabtree, R. H. Redox-Active Ligands in Catalysis. *Chem. Soc. Rev.* **2013**, *42*, 1440−1459.

(56) Eisenberg, R.; Gray, H. B. Noninnocence in Metal Complexes: A Dithiolene Dawn. *Inorg. Chem.* **2011**, *50*, 9741−9751.

(57) The formal oxidation number (state) of a given metal ion in a mononuclear coordination compound is an unmeasurable integer which is commonly defined as "the charge left on the metal after all ligands have been removed in their normal, closed-shell configuration-that is with their electron pair". In contrast, the physical (or spectroscopic) oxidation numbers refers to a quantity that can be measured by various spectroscopic methods. Hegedus, L. S. In *Transition Metals in the Synthesis of Complex Organic Molecules*; University Science Books: Mill Valley, CA, 1994; p 3.

(58) Ward, M. D.; McCleverty, J. A. Non-Innocent Behaviour in Mononuclear and Polynuclear Complexes: Consequences for Redox and Electronic Spectroscopic Properties. *J. Chem. Soc., Dalton Trans.* **2002**, *3*, 275−288.

(59) Ray, K.; Petrenko, T.; Wieghardt, K.; Neese, F. Joint Spectroscopic and Theoretical Investigations of Transition Metal Complexes Involving Non-Innocent Ligands. *Dalton Trans.* **2007**, *16*, 1552−1566.

(60) Fackler, J.; Holah, D. Properties of Chromium(II) Complexes. I. Electronic Spectra of the Simple Salt Hydrates. *Inorg. Chem.* **1965**, *4*, 954−958.

(61) Figgis, B. N. *Introduction to ligand fields*; Wiley: New York, 1966.

(62) Scarborough, C. C.; Lancaster, K. M.; DeBeer, S.; Weyhermüller, T.; Sproules, S.; Wieghardt, K. Experimental Fingerprints for Redox-Active Terpyridine in $[Cr(tpy)_2](PF_6)_n$ ($n = 3−0$), and the Remarkable Electronic Structure of $[Cr(tpy)_2]^{1−}$. *Inorg. Chem.* **2012**, *51*, 3718−3732.

(63) Wang, M.; England, J.; Weyhermüller, T.; Kokatam, S.-L.; Pollock, C. J.; DeBeer, S.; Shen, J.; Yap, G. P. A.; Theopold, K. H.; Wieghardt, K. New Complexes of Chromium(III) Containing Organic π-Radical Ligands: An Experimental and Density Functional Theory Study. *Inorg. Chem.* **2013**, *52*, 4472−4487.

(64) Scarborough, C. C.; Sproules, S.; Doonan, C. J.; Hagen, K. S.; Weyhermüller, T.; Wieghardt, K. Scrutinizing Low-Spin Cr(II) Complexes. *Inorg. Chem.* **2012**, *51*, 6969−6982.

(65) Braterman, P. S.; Song, J. L.; Peacock, R. D. Electronic Absorption Spectra of the Iron(II) Complexes of 2,2′-Bipyridine, 2,2′-Bipyrimidine, 1,10-Phenanthroline, And 2,2′:6′,2″-Terpyridine and Their Reduction Products. *Inorg. Chem.* **1992**, *31*, 555−559.

(66) Kaim, W. Manifestations of Noninnocent Ligand Behavior. *Inorg. Chem.* **2011**, *50*, 9752−9765.

(67) Kaim, W. Concepts for Metal Complex Chromophores Absorbing in the Near Infrared. *Coord. Chem. Rev.* **2011**, *255*, 2503−2513.

(68) Scarborough, C. C.; Sproules, S.; Weyhermüller, T.; DeBeer, S.; Wieghardt, K. Electronic and Molecular Structures of the Members of the Electron Transfer Series $[Cr(^tbpy)_3]^n$ ($n = 3+, 2+, 1+, 0$): An X-ray Absorption Spectroscopic and Density Functional Theoretical Study. *Inorg. Chem.* **2011**, *50*, 12446−12462.

(69) Banerjee, P.; Sproules, S.; Weyhermüller, T.; DeBeer George, S.; Wieghardt, K. Electronic Structure of the $[Tris(dithiolene)-chromium]^z$ ($z = 0, 1−, 2−, 3−$) Electron Transfer Series and Their Manganese(IV) Analogues. An X-ray Absorption Spectroscopic and Density Functional Theoretical Study. *Inorg. Chem.* **2009**, *48*, 5829−5847.

(70) Buchanan, R. M.; Downs, H. H.; Shorthill, W. B.; Pierpont, C. G.; Kessel, S. L.; Hendrickson, D. N. Intramolecular Antiferromagnetic Exchange in Tris(o-Semiquinone) Complexes of Vanadium(III), Chromium(III), and Iron(III). *J. Am. Chem. Soc.* **1978**, *100*, 4318−4320.

(71) Buchanan, R. M.; Kessel, S. L.; Downs, H. H.; Pierpont, C. G.; Hendrickson, D. N. Structural and Magnetic Properties of Tris(o-Semiquinone) Complexes of Iron(III) and Chromium(III). *J. Am. Chem. Soc.* **1978**, *100*, 7894−7900.

(72) Chun, H.; Nazari Verani, C.; Chaudhuri, P.; Bothe, E.; Bill, E.; Weyhermüller, T.; Wieghardt, K. Molecular and Electronic Structure of Octahedral o-Aminophenolato and o-Iminobenzosemiquinonato

Complexes of V(V), Cr(III), Fe(III), and Co(III). Experimental Determination of Oxidation Levels of Ligands and Metal Ions. *Inorg. Chem.* **2001**, *40*, 4157−4166.

(73) Joy, S.; Krämer, T.; Paul, N. D.; Banerjee, P.; McGrady, J. E.; Goswami, S. Isolation and Assessment of the Molecular and Electronic Structures of Azo-Anion-Radical Complexes of Chromium and Molybdenum. Experimental and Theoretical Characterization of Complete Electron-Transfer Series. *Inorg. Chem.* **2011**, *50*, 9993−10004.

(74) Sproules, S.; Wieghardt, K. Dithiolene Radicals: Sulfur K-edge X-ray Absorption Spectroscopy and Harry's Intuition. *Coord. Chem. Rev.* **2011**, *255*, 837−860.

(75) Kapre, R. R.; Bothe, E.; Weyhermüller, T.; DeBeer, G. S.; Muresan, N.; Wieghardt, K. Electronic Structures of Tris(dioxolene)-chromium and Tris(dithiolene)chromium Complexes of the Electron-Transfer Series $[Cr(dioxolene)_3]^z$ and $[Cr(dithiolene)_3]^z$ ($z = 0, 1-, 2-, 3-$). A Combined Experimental and Density Functional Theoretical Study. *Inorg. Chem.* **2007**, *46*, 7827−7839.

(76) Brienne, S. H. R.; Boyd, P. D. W.; Schwerdtfeger, P.; Bowmaker, G. A.; Cooney, R. P. Intensity Enhancements in the IR Spectra of Organic Radical Ions. A Theoretical Study. *J. Chem. Soc., Faraday Trans.* **1993**, *89*, 3015−3020.

(77) Zamadar, M.; Asaoka, S.; Grills, D. C.; Miller, J. R. Giant infrared absorption bands of electrons and holes in conjugated molecules. *Nat. Commun.* **2013**, DOI: 10.1038/ncomms3818.

(78) Kaim, W.; Reinhardt, R.; Sieger, M. Chemical and Electro-chemical Generation of Hydride-Forming Catalytic Intermediates $(bpy)M(C_nR_n)$: M = Rh, Ir ($n = 5$); M = Ru, Os ($n = 6$). Coordinatively Unsaturated Ground State Models of MLCT Excited States? *Inorg. Chem.* **1994**, *33*, 4453−4459.

(79) Lu, C. C.; Bill, E.; Weyhermüller, T.; Bothe, E.; Wieghardt, K. Neutral Bis(α-iminopyridine)metal Complexes of the First-Row Transition Ions (Cr, Mn, Fe, Co, Ni, Zn) and Their Monocationic Analogues: Mixed Valency Involving a Redox Noninnocent Ligand System. *J. Am. Chem. Soc.* **2008**, *130*, 3181−3197.

(80) Zhang, W.; Sun, W.-H.; Zhang, S.; Hou, J.; Wedeking, K.; Schultz, S.; Fröhlich, R.; Song, H. Synthesis, Characterization, and Ethylene Oligomerization and Polymerization of [2,6-Bis(2-benzimidazolyl)pyridyl]chromium Chlorides. *Organometallics* **2006**, *25*, 1961−1969.

(81) Esteruelas, M. A.; López, A. M.; Méndez, L.; Oliván, M.; Oñate, E. Preparation, Structure, and Ethylene Polymerization Behavior of Bis(imino)pyridyl Chromium(III) Complexes. *Organometallics* **2003**, *22*, 395−406.

(82) Carney, M. J.; Robertson, N. J.; Halfen, J. A.; Zakharov, L. N.; Rheongold, A. L. Octahedral Chromium(III) Complexes Supported by Bis(2-pyridylmethyl)amines: Ligand Influence on Coordination Geometry and Ethylene Polymerization Activity. *Organometallics* **2004**, *23*, 6184−6190.

(83) Wang, D.; Liu, S.; Zeng, Y.; Sun, W.-S.; Redshaw, C. 2-Benzimidazolyl-N-phenylquinoline-8-carboxamide Chromium(III) Trichlorides: Synthesis and Application for Ethylene Oligomerization and Polymerization. *Organometallics* **2011**, *30*, 3001−3009.

(84) Sugiyama, H.; Aharonian, G.; Gambarotta, S.; Yap, G. P. A.; Budzelaar, P. H. M. Participation of the α,α'-Diiminopyridine Ligand System in Reduction of the Metal Center during Alkylation. *J. Am. Chem. Soc.* **2002**, *124*, 12268−12274.

(85) The use of TEA resembles the trimethylaluminum alkyl free in the commercial MAO solution.

(86) Zhang, Y.; Suo, H.; Huang, F.; Liang, T.; Hu, X.; Sun, W.-H. Thermo-Stable 2-(Arylimino)benzylidene-9-arylimino-5,6,7,8-tetrahy-dro Cyclohepta[b]pyridyliron(II) Precatalysts Toward Ethylene Polymerization and Highly Linear Polyethylenes. *J. Polym. Sci., Part A: Polym. Chem.* **2017**, *55*, 830−842.

(87) Chen, Y.; Zuo, W.; Hao, P.; Zhang, S.; Gao, K.; Sun, W.-H. Chromium(III) Complexes Ligated by 2-(1-Isopropyl-2-benzimida-zolyl)-6-(1-(arylimino)ethyl)pyridines: Synthesis, Characterization and Their Ethylene Oligomerization and Polymerization. *J. Organo-met. Chem.* **2008**, *693*, 750−762.

(88) Talsi, E. P.; Babushkin, D. E.; Semikolenova, N. V.; Zudin, V. N.; Panchenko, V. N.; Zakharov, V. A. Polymerization of Ethylene Catalyzed by Iron Complex Bearing 2,6-Bis(imine)pyridyl Ligand: ^{1}H and ^{2}H NMR Monitoring of Ferrous Species Formed via Catalyst Activation with $AlMe_3$, MAO, $AlMe_3/B(C_6F_5)_3$ and $AlMe_3/CPh_3(C_6F_5)_4$. *Macromol. Chem. Phys.* **2001**, *202*, 2046−2051.

(89) Leone, G.; Pierro, I.; Zanchin, G.; Forni, A.; Bertini, F.; Rapallo, A.; Ricci, G. Vanadium(III)−Catalyzed Copolymerization of Ethylene with Norbornene: Microstructure at Tetrad Level and Reactivity Ratios. *J. Mol. Catal. A: Chem.* **2016**, *424*, 220−231.

(90) Sun, W.-H.; Tang, X.; Gao, T.; Wu, B.; Zhang, W.; Ma, H. Synthesis, Characterization, and Ethylene Oligomerization and Polymerization of Ferrous and Cobaltous 2-(Ethylcarboxylato)-6-iminopyridyl Complexes. *Organometallics* **2004**, *23*, 5037−5047.

(91) Small, B. L.; Brookhart, M.; Bennett, A. M. A. Highly Active Iron and Cobalt Catalysts for the Polymerization of Ethylene. *J. Am. Chem. Soc.* **1998**, *120*, 4049−4050.

(92) Pierro, I.; Zanchin, G.; Parisini, E.; Martí-Rujas, J.; Canetti, M.; Ricci, G.; Bertini, F.; Leone, G. Chain-Walking Polymerization of α-Olefins by α-Diimine Ni(II) Complexes: Effect of Reducing the Steric Hindrance of *Ortho-* and *Para*-Aryl Substituents on the Catalytic Behavior, Monomer Enchainment, and Polymer Properties. *Macromolecules* **2018**, *51*, 801−814.

(93) Ricci, G.; Leone, G.; Rapallo, A.; Biagini, P.; Guglielmetti, G.; Porri, L. Syndiospecific Oligomerization and Polymerization of Norbornene with Titanium Catalysts. *Polymer* **2011**, *52*, 5708−5715.

(94) Rapallo, A.; Ricci, G.; Porzio, W.; Arrighetti, G.; Leone, G. A Crystalline 2,3-*exo*-Disyndiotactic Dicyclopentadiene Tetramer. *Cryst. Growth Des.* **2014**, *14*, 5767−5772.

(95) Zanchin, G.; Leone, G.; Pierro, I.; Rapallo, A.; Porzio, W.; Bertini, F.; Ricci, G. Addition Oligomerization of Dicyclopentadiene: Reactivity of *Endo* and *Exo* Isomers and Postmodification. *Macromol. Chem. Phys.* **2017**, *218*, 1600602.

(96) Ricci, G.; Sommazzi, A.; Masi, F.; Ricci, M.; Boglia, A.; Leone, G. Well-Defined Transition Metal Complexes with Phosphorus and Nitrogen Ligands for 1,3-Dienes Polymerization. *Coord. Chem. Rev.* **2010**, *254*, 661−676.

(97) Ricci, G.; Italia, S.; Porri, L. Polymerization of 1,3-dienes with methylaluminoxane-triacetyl-acetonatovanadium. *Macromol. Chem. Phys.* **1994**, *195*, 1389−1397.

(98) Sheldrick, G. M. *SHELXTL Reference Manual*; Siemens Analytical X-ray Systems, Inc., Madison, WI, USA, 1996.

(99) Sheldrick, G. M. *Acta Crystallogr., Sect. A: Found. Crystallogr.* **2008**, *64*, 112−122.

Supporting Information

Concerted Electron Transfer in Iminopyridine Chromium Complexes: Ligand Effects on the Polymerization of Various (Di)olefins

Giuseppe Leone,[1,*] Elena Groppo,[2,*] Giorgia Zanchin,[1] Giorgia A. Martino,[2] Alessandro Piovano,[2] Fabio Bertini,[1] Javier Martí-Rujas,[3,Ŧ] Emilio Parisini,[3] and Giovanni Ricci[1]

[1] CNR-Istituto per lo Studio delle Macromolecole (ISMAC), via A. Corti 12, I-20133 Milano, Italy.

[2] Dipartimento di Chimica, NIS Interdepartmental Research Center and INSTM Reference Center, Università degli Studi di Torino, Via G. Quarello 15A, I-10135 Torino, Italy.

[3] Center for Nano Science and Technology at Polimi, Istituto Italiano di Tecnologia, Via Pascoli 70/3, I-20133 Milano, Italy.

[Ŧ] Current address: Dipartimento di Chimica Materiali e Ingegneria Chimica "Giulio Natta", Politecnico di Milano, Via Luigi Mancinelli 7, 20131 Milan, Italy.

Table of contents

Additional Files

The supplemental file "complex.xyz" contains the computed Cartesian coordinates of **Cr4**.

Table S1. Summary of X-ray crystallographic data for compound **Cr4**.

Complex	Cr4·OH
Molecular formula	$C_{12}H_{11}Cl_3CrN_2O$
Temperature (°K)	296(2)
Wavelength (Å)	1.54178
Crystal system, space group	Orthorhombic, P2(1)2(1)2(1)
Unit cell dimensions (Å, °)	$a = 8.8887(9)$ $b = 9.0834(9)$ $c = 18.756(2)$
Volume (Å^3)	1514.3(3)
Z, calculated density (g cm^{-3})	4, 1.568
Absorption coefficient (mm^{-1})	11.029
$F(000)$	720
Crystal size (mm)	0.05 x 0.05 x 0.03
θ range	4.715 ÷ 65.817
Reflections collected/unique	4846 / 2330
R_{int}[a]	0.1117
Absorption correction	Sadabs
Data/restraints/parameters	2330 / 0 /173
Goodness-of-fit on F^2	1.001
Final R indices [$I > 2\sigma(I)$][b]	R1=0.1071, wR2 = 0.2082
R indices (all data)[b]	R1=0.1802, wR2 = 0.2379
Largest diff. peak and hole (e Å^{-3})	1.564 and -1.085
Completeness (%)	96.9

[a] $R\text{int} = \Sigma|Fo^2 – Fo^2(\text{mean})|/\Sigma Fo^2$; $R\sigma = \Sigma\sigma(Fo^2)/\Sigma Fo^2$.

[b] $R1 = \Sigma||Fo| – |Fc||/\Sigma|Fo|$; $wR2 = \{\Sigma[w(Fo^2 – Fc^2)^2]/\Sigma[w(Fo^2)^2]\}^{0.5}$. $\text{GoF} = \{S/(n – p)\}^{0.5} = \{\Sigma[w(Fo^2 – Fc^2)^2]/(n – p)\}^{0.5}$.

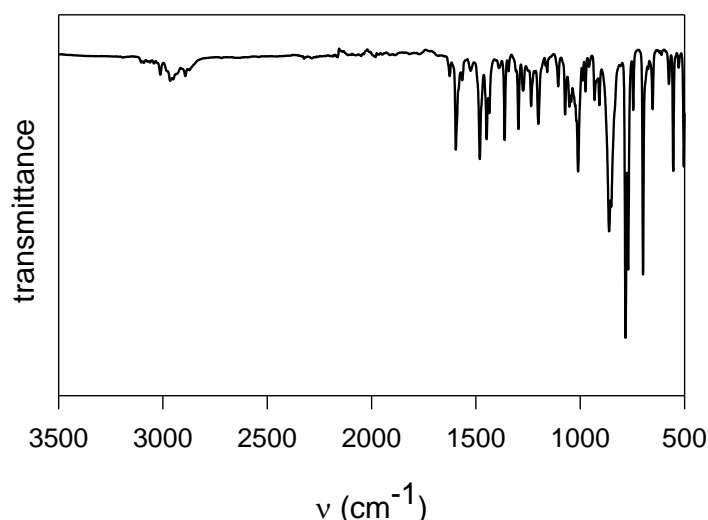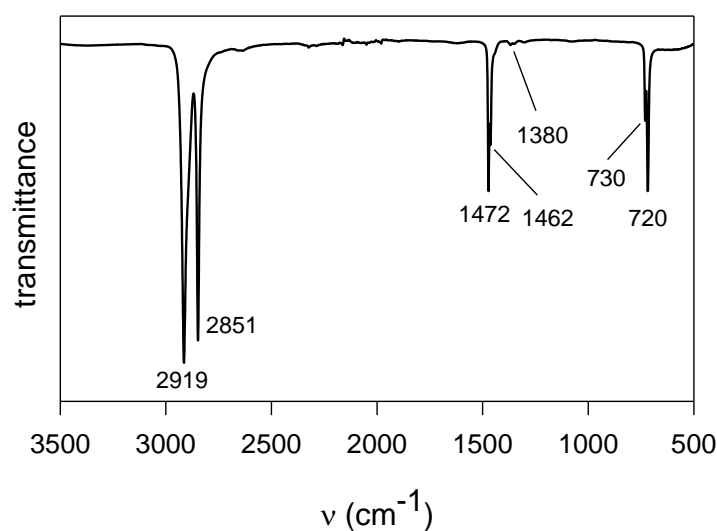**Figure S1**. FTIR spectra of as-prepared **Cr4**.

Figure S2. ATR–IR spectra of poly(ethylene) obtained by **Cr1** (entry 1 of Table 1 in the manuscript).

The ATR–IR spectra in Figure S2 show three sets of peaks characteristic of poly(ethylene): strong absorbances due to the C–H stretching (very strong peaks at 2919 and 2851 cm^{-1}), C–H bending (two strong peaks at 1472 and 1462 cm^{-1}) and C–H rocking (two medium-strong peaks at 730 and 720 cm^{-1}). These two last bands are representative of the ethylene crystallinity and correspond to long methylene sequences. In all the spectra a weak signal at 1380 cm^{-1} was detected; this peak is attributed to the C–H bending of a CH$_3$ group, revealing the presence of branches.

Figure S3. ^{1}H (top) and ^{13}C NMR (bottom) spectra of poly(ethylene) obtained by **Cr1** (entry 1 of Table 1 in the manuscript).
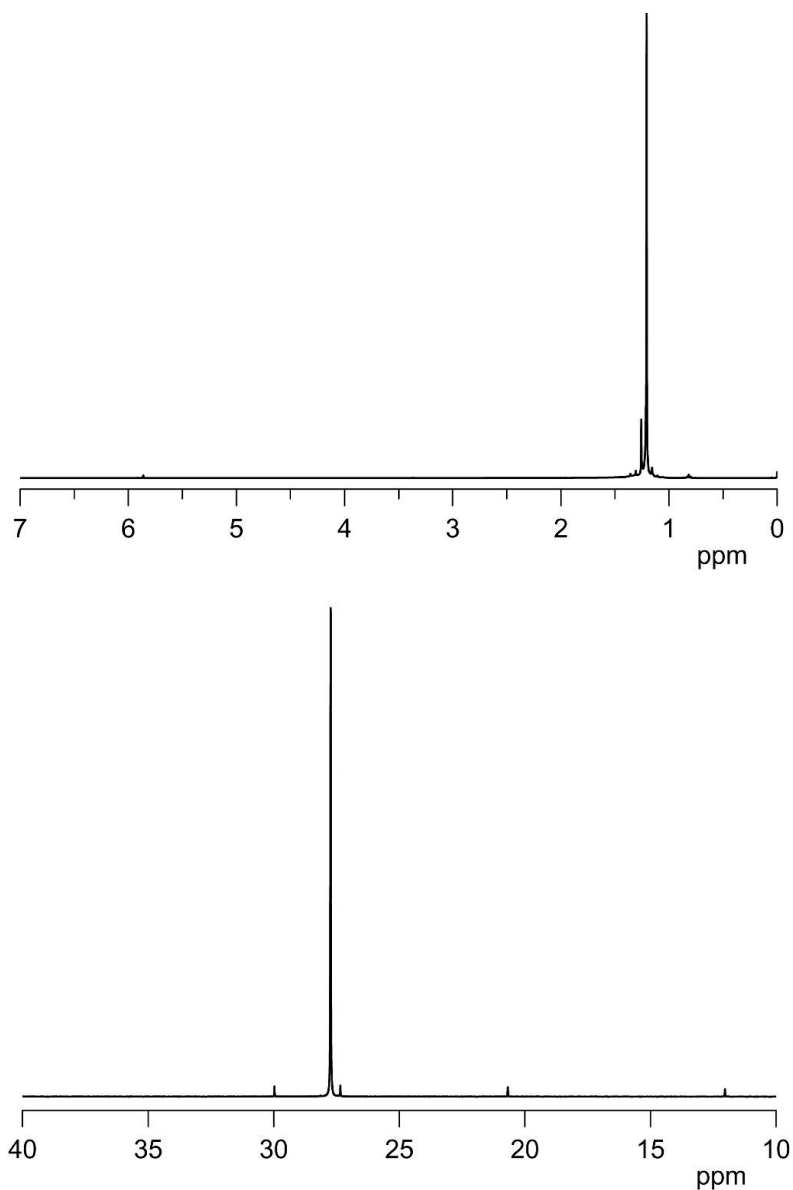
Consistent the ATR–IR (Figure S2), ^{13}C NMR spectra also showed resonances attributed to carbon atoms of alkyl branches, namely at 12.02 ppm (1B$_n$), 20.70 ppm (2B$_n$), 27.30 ppm (3B$_n$), and 29.95 ppm (4B$_n$). However, the amount of branches is relatively low: calculations from the ^{1}H NMR spectrum revealed a number of methyl groups per 1000 carbon atoms which is around 10.

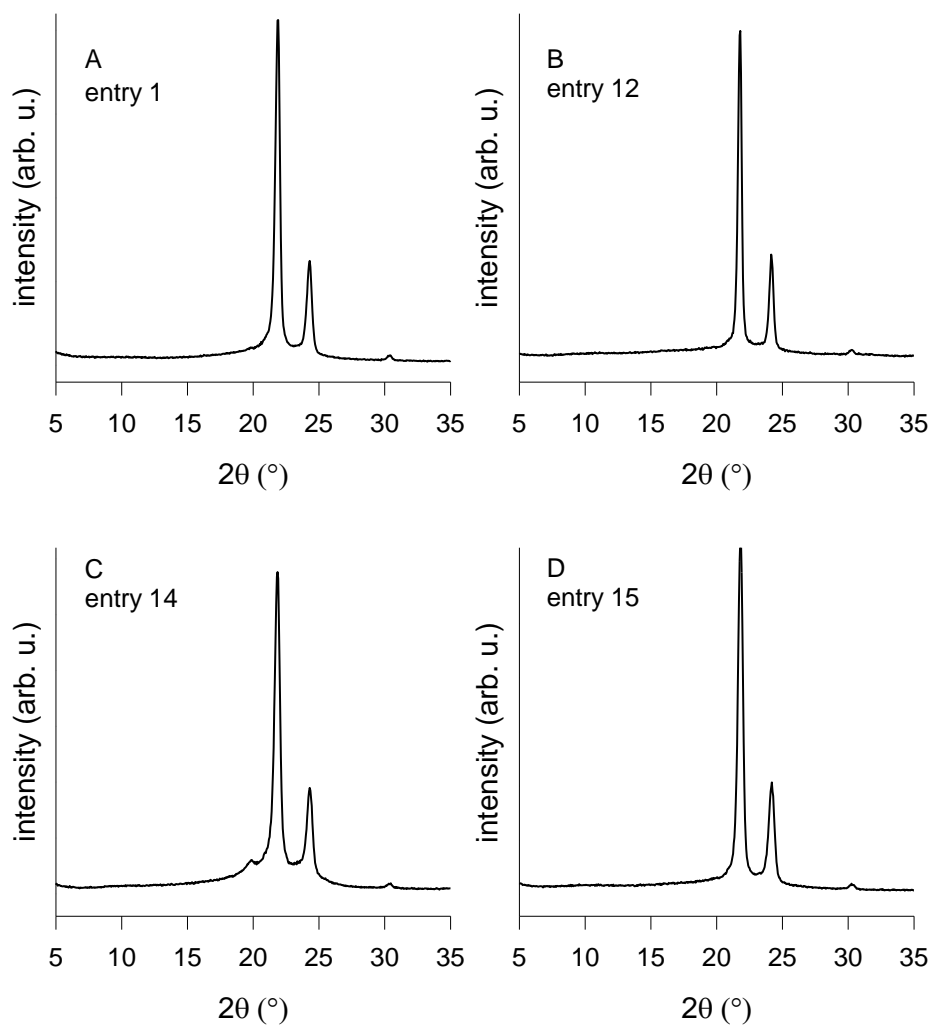**Figure S4.** XRD spectrum of the obtained poly(ethylene)s with complex **Cr1** (see Table 2 in the manuscript).

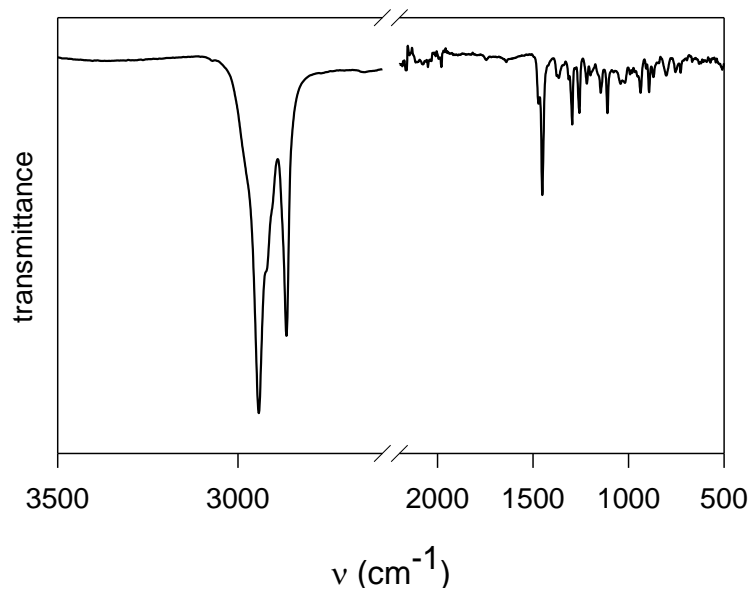**Figure S5.** FTIR spectra of NB polymer (entry 17, Table 3 in the manuscript).

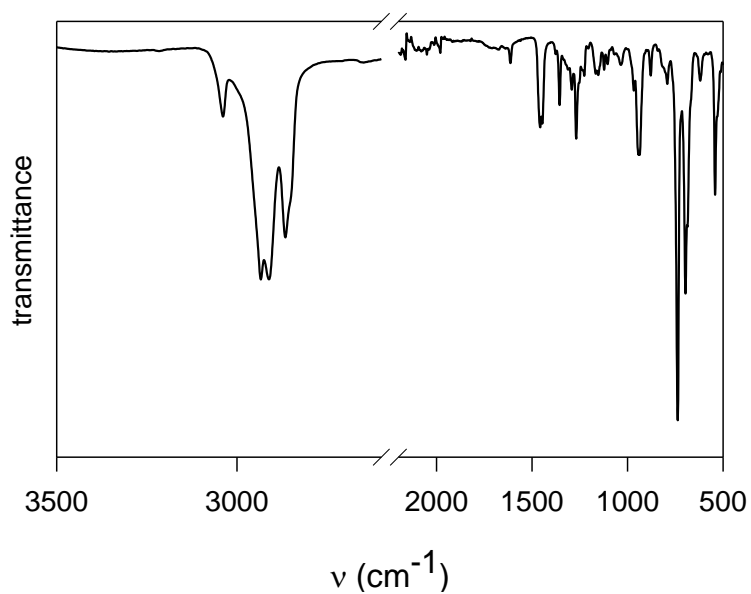**Figure S6.** FTIR spectra of DCPD polymer (entry 18, Table 3 in the manuscript).

Figure S7. TGA (A) and DTG (B) curves under nitrogen flow of: entry 17 in blue, and entry 18 in red (see Table 3 of the manuscript).
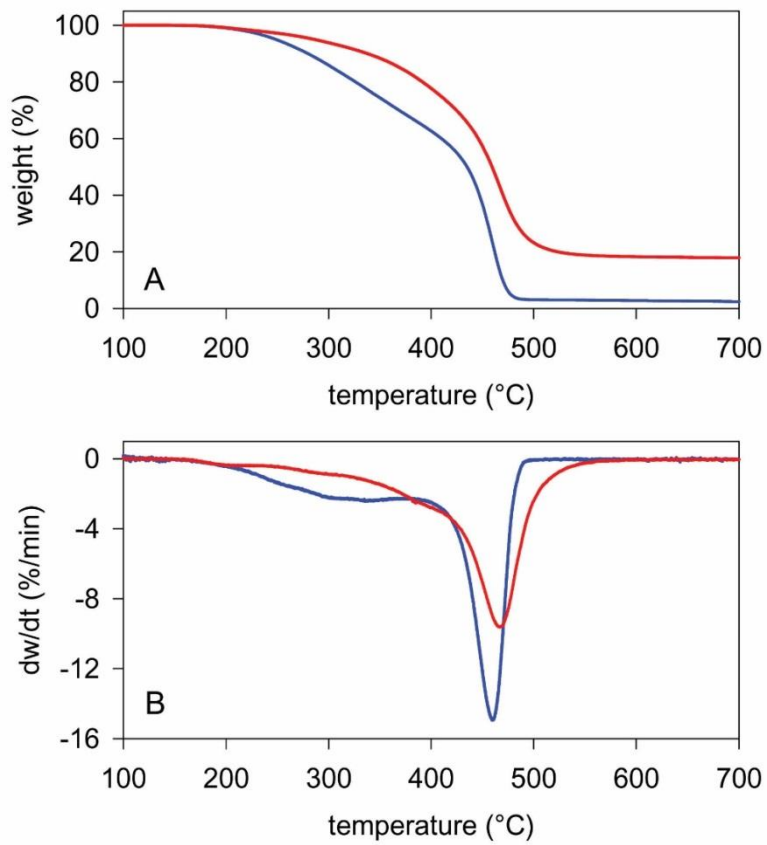
Figure S8. ^{1}H (top) and ^{13}C NMR (bottom) spectra of poly(1,3-butadiene)s (Table 4 in the manuscript); (a) entry 25, (b) entry 26 and (c) entry 28.
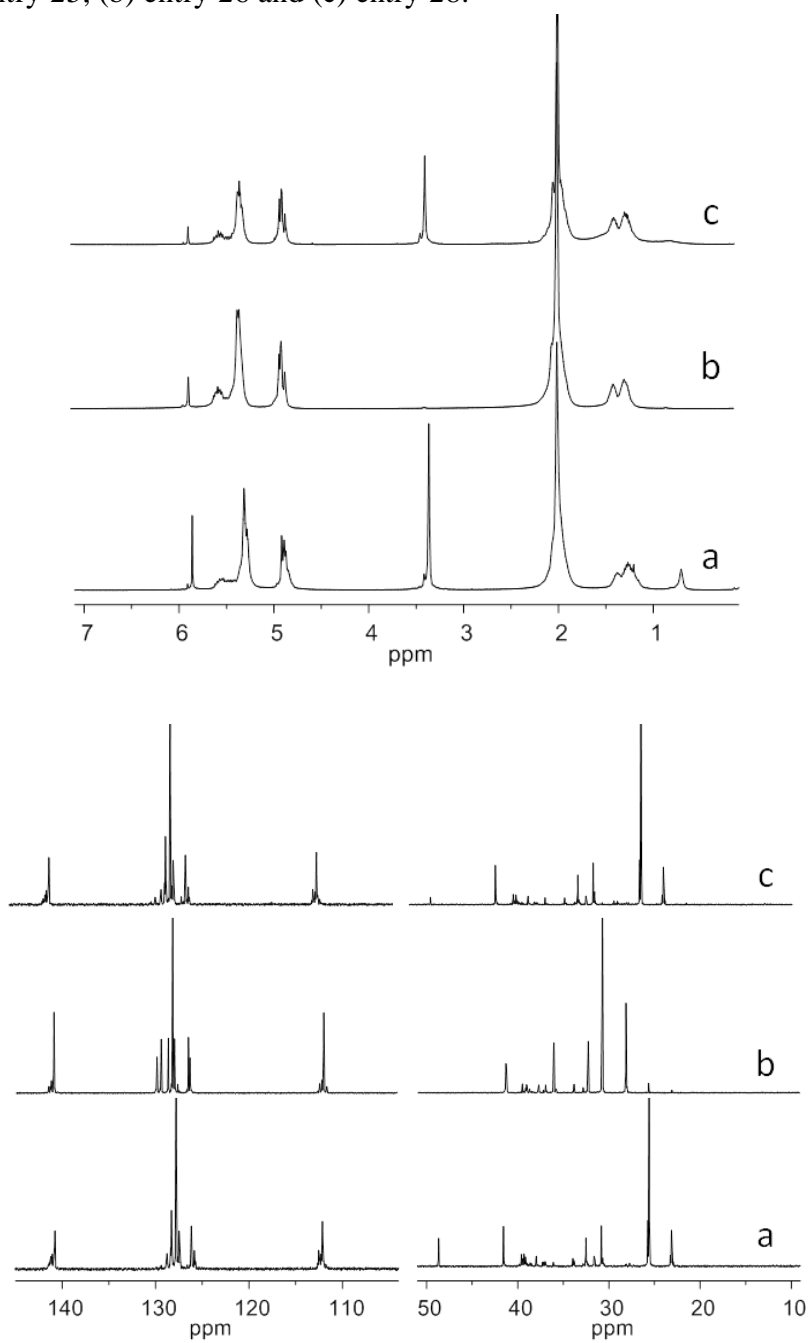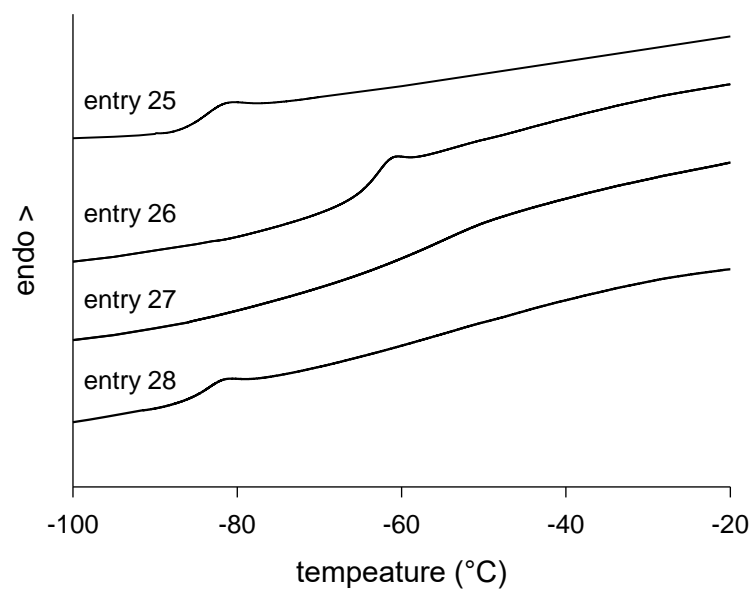
Figure S9. DSC profile of poly(1,3-butadiene)s obtained with complex **Cr1**–**Cr4** (entry 25–28 of Table 4 in the manuscript).

Ringraziamenti

Arrivata al termine di questo lungo percorso è doveroso ringraziare le persone che mi sono state accanto e considerando che non ho mai scritto dei ringraziamenti, potrei dovermi dilungare un po'…ma o lo faccio adesso o non lo faccio più!

In primis non posso non ringraziare Il CAPO! Grazie per la meravigliosa opportunità che mi hai dato di intraprendere questo percorso, difficile ma stimolante, che mi ha fatto superare insicurezze e paure (soprattutto quella di parlare in pubblico). Grazie per essere stato un supervisor così attento e presente durante questi anni, aiutandomi sempre con la tua passione straripante e sostenendomi anche nei momenti di profonda depressione. Dovrei ringraziarti per altri mille motivi, ma mi dilungherei troppo quindi ti dico solo GRAZIE GRAZIE e ancora GRAZIE!

In secundis, come non ringraziare il mio fantastico mentore Caterina! Tu non solo hai provato a trasmettermi tutta la tua sapienza scientifica (ahimè non sarò mai al tuo livello), ma mi hai insegnato che volere è potere anche con tutte le difficoltà che il mondo ci pone davanti. Sei un modello di donna da imitare: indipendente, ambiziosa e sempre positiva. Per me sei stata un mentore, un'amica e sei un esempio da seguire.

Volevo poi ringraziare il santo Dottor Piovano, una delle persone più pazienti e gentili che conosca, doti molto utili quando si è così fortunati da lavorare in un gruppo di sole donne! Grazie per aver sopportato giornalmente i miei sproloqui e i miei deliri cercando sempre di rincuorarmi e aiutarmi quando ne avevo bisogno. Sei il miglior collega, compagno di laboratorio e limitrofo di ufficio della storia!

Come ci sono i "ragazzi di via Panisperna" a Roma, qui ci sono i "ragazzi di via Quarello", vecchi e nuovi, i miei compagni giornalieri di avventura che hanno condiviso gioie e dolori di questo percorso, che mi hanno continuamente spronata ad affrontare le difficoltà al suon di "fatti furba", e che sono stati sempre presenti quando chiedevo il loro aiuto, dal riparare la bici al discutere di scienza. Non posso ringraziarvi uno alla volta perché altrimenti dovrei scrivere un'altra tesi solo per voi, ma voglio comunque dirvi che siete stati preziosi per la mia crescita umana e scientifica e che probabilmente senza di voi questi tre anni non sarebbero stati così belli e pieni.

Parallelamente ai "ragazzi di via Quarello" ci sono i "ragazzi di via Giuria", con voi ho meno discusso di scienza, e più di "altro" in momenti ricreativi più o meno

alcolici. Innumerevoli sono i viaggi, gli aperitivi, gli eventi sportivi (con aperitivi) e le risate che abbiamo condiviso. Avete reso questi tre anni splendidi, ho trovato in voi degli amici e da terrona lontana da casa non mi sono sentita mai sola. Eh beh che dire! (cit. Cutini) Grazie!

I have to thank two fantastic people that I met last winter during my period in Germany! Giovanni and Christian without you I would have probably started a massive production of knitted sweaters. You have been my lifeline and I will never thank you enough. I hope we will meet soon in some part of the world... maybe in our beloved smiling Rostock (or maybe not)!

Anche se in ritardo di tre anni, voglio approfittare di questa tesi per ringraziare anche i miei amici e compagni di studio Michelotta e Riccardo (in arte Totò). Nonostante le nostre litigate durante lo studio "matto e disperatissimo" avete reso la magistrale più leggera del previsto. Eravamo proprio un bel trio. Spero di venirvi a trovare presto in Francia. Je vous aime, mes chéries.

Devo poi ringraziare tutti i miei amici di Palermo e non (Gibi, Marzia, Sullo, Giulia, Carogna, Battaglia, Ciattaglia, Lulina, Dilla, Carol, Gae, Foffa, Flacca, Reno,) che mi sopportano loro malgrado da tanto tempo, so di non essere sempre una persona piacevole, ma vi voglio bene! Grazie per la pazienza, il sostegno e l'affetto dimostratomi in questi anni.

Ma soprattutto voglio ringraziare il Dott. Luca Mastrandrea, continua fonte d'ispirazione nei miei momenti bui, il tuo esempio è stato formativo e fondamentale per la scrittura di questa tesi.

Un grazie particolare va alle mie amiche storiche, Elena, Ilaria e Virginia, con le quali da sempre (l'anno prossimo sono dieci anni dalla maturità, tanto per ricordarvi che ci conosciamo da più della metà della nostra vita) ho condiviso tantissimi splendidi e terribili momenti, e alle quali nonostante la distanza mi sento sempre vicina. Sebbene con qualche pausa più o meno lunga siete le mie amiche più care e spero di condividere con voi ancora tantissimi bellissimi momenti delle nostre vite.
Vi voglio un gran bene.

Parlando di amiche non posso che non spendere due parole in più per te Fallucca…Un proverbio siciliano dice "Solo i veri amici ti diranno quando il tuo viso è sporco" e tu me ne hai dette di tutti i colori partendo da "ma come sei combinata?" "truccati" "sistemati meglio" e mille altre ancora. Ci conosciamo dal liceo e per tua fortuna e mia malaugurata sorte siamo amiche da allora, mentre aspettavamo l'autobus ore infinite dopo scuola e ancora adesso quando

riusciamo a ritagliarci solo mezz'ora per prenderci un caffè e raccontarci come stanno evolvendo le nostre vite. Grazie per esserci stata praticamente in ogni momento della mia vita e grazie perché so che se voglio posso anche chiamarti alle 4 del mattino (ammesso e non concesso che tu senta il telefono). Ora la smetto perché sai che non mi piace essere smielata, ma probabilmente questa è l'unica occasione che avrò mai per dirti quanto sei importante per me e quanto ti voglio bene. Cerca di non piangere. Ciao Fallucchide.

Finalmente è arrivato il momento di ringraziare la FAMIGGHIA! Ma assai siamo e sperando che nessuno me ne voglia ringrazierò solo i pezzi da 90, altrimenti non finisco più.

Si parte dagli anziani…quindi si inizia da mia Zia Francesca! Zi zi tra le tante ragioni per cui dovrei ringraziarti, una mi viene prima di tutto in mente: la musica. Tu sei quella che mi ha avvicinato a questo mondo, che ormai è parte di me e di cui non posso fare più a meno. Volevo anche ringraziarti perché fin da quando abbiamo iniziato a leggere, hai sempre instillato in me e Martina l'idea che la conoscenza è potere, e che per poter essere persone utili alla società in cui viviamo dovessimo studiare e istruirci. Per questo e molto altro non ti ringrazierò mai abbastanza.

Genitori, voi al suon di "ti mannu a lavari i scali" volenti o nolenti mi avete sostenuta durante tutto questo percorso, anche se probabilmente non avete ancora capito appieno cosa è un dottorato. E proprio per questo vi ringrazio, perché nonostante tutto vi siete sempre fidati di me e del mio giudizio, limitandovi solo a dare dei consigli senza provare mai a imporre la vostra opinione (almeno in ambito scolastico, non si può dire lo stesso in altri ambiti, tipo l'ordine cromatico con cui stendere la biancheria). Grazie per essere stati sempre presenti, per avermi sempre seguita alle partite di pallavolo, per essere venuti a vedere tutti i concerti (anche se vi annoiavate a morte) e per tutto il cibo che mi avete spedito.
La vostra perla di Labuan.

Devo poi ringraziare la più meravigliosa delle sorelle, che ha organizzato 1285 feste di compleanno a sorpresa, ha trasportato una quantità illegale di bottiglie di salsa pronta in valigia e si è fatta 1829 Km solo per venir ad ascoltare il mio pessimo inglese. Grazie per tutto quello che hai sempre fatto per me e che sono certa continuerai a fare nonostante io sia un tantino "s****za". Probabilmente non ti merito come tu non ti meriti quel nome. Ti voglio bene sorella.

Dulcis in fundo…devo ringraziare Francesco, che più di tutti ha da sempre creduto in me, incoraggiandomi nei momenti di difficoltà e smorzando i miei momenti di eccessiva euforia, spingendomi sempre a superare i miei limiti e le mie paure, esortandomi a impegnarmi a fondo in tutto quello che faccio che sia scienza canto o altro, commuovendosi per la discussione nonostante l'avesse ascoltata diverse volte. Senza di te non so se avrei avuto la forza di lasciare la mia amata e odiata Palermo e di arrivare a questo punto. Sono felice di averti reso fiero di me. Grazie…